UNIVERSIDADE FEDERAL DE SÃO CARLOS
CENTRO DE CIÊNCIAS EXATAS E DE TECNOLOGIA
DEPARTAMENTO DE QUÍMICA
PROGRAMA DE PÓS-GRADUAÇÃO EM QUÍMICA

PHOTOREDOX-MEDIATED AMINOALKYLATION AND CARBAMOYLATION OF AZOMETHINE IMINES

Bianca Taeko Matsuo*

Tese apresentada como parte dos requisitos para obtenção do título de DOUTORA EM CIÊNCIAS, área de concentração: QUÍMICA ORGÂNICA.

Orientador: Prof. Dr. Márcio Weber Paixão

*** bolsista CNPq**

São Carlos - SP
2021

UNIVERSIDADE FEDERAL DE SÃO CARLOS

Centro de Ciências Exatas e de Tecnologia
Programa de Pós-Graduação em Química

Folha de Aprovação

Defesa de Tese de Doutorado da candidata Bianca Taeko Matsuo, realizada em 25/08/2021.

Comissão Julgadora:

Prof. Dr. Márcio Weber Paixão (UFSCar)

Profa. Dra. Rose Maria Carlos (UFSCar)

Profa. Dra. Fernanda Gadini Finelli (UFRJ)

Prof. Dr. Leandro Helgueira de Andrade (USP)

Prof. Dr. Carlos Roque Duarte Correia (UNICAMP)

O presente trabalho foi realizado com apoio da Coordenação de Aperfeiçoamento de Pessoal de Nível Superior - Brasil (CAPES) - Código de Financiamento 001.
O Relatório de Defesa assinado pelos membros da Comissão Julgadora encontra-se arquivado junto ao Programa de Pós-Graduação em Química.

PHOTOREDOX-MEDIATED AMINOALKYLATION AND CARBAMOYLATION OF AZOMETHINE IMINES

Bianca Taeko Matsuo

A THESIS

in

Chemistry

Presented to the Federal University of São Carlos

In

Partial Fulfillment of the Requirements for the

Degree of Doctor of Philosophy

2021

Supervisor

_____

Prof. Dr. Márcio Weber Paixão

Dissertation Committee

_____

Profa. Dra. Rose Maria Carlos (DQ – UFSCar)

Profa. Dra. Fernanda Gadini Finelli (UFRJ – UFRJ)

Prof. Dr. Leandro Helgueira de Andrade (IQ – USP)

Prof. Dr. Carlos Roque Duarte Correia (IQ – UNICAMP)

“Don't let anyone rob you of your imagination, your creativity, or your curiosity. It's your place in the world; it's your life. Go on and do all you can with it and make it the life you want to live.”

Mae Jemison.

ACKNOWLEDGEMENTS

I am grateful for the support and guidance of my PhD supervisor, professor Dr. Márcio Weber Paixão. Over the past 10 years, he has supported my career and inspired me with his creativity and dedication to his work as researcher. I could not be more grateful for all the years of work and collaboration I have been under his guidance. I am grateful for all the opportunity I had, aiming at my professional growth and for the professional I have become. I will always appreciate how Dr. Paixão has supported my research, my career aspirations, and future endeavors.

Moreover, I would like to thank the committee members, professors Rose Maria Carlos, Fernanda Gadini Finelli, Leandro Helgueira de Andrade and Carlos Roque Duarte Correia for their availability to participate in my thesis defense and for their useful contributions to my thesis. In addition, I would like to acknowledge:

The funding agency CNPq for the scholarship granted during my PhD course and CAPES for the granting of the scholarship abroad during the period.

The Federal University of São Carlos, where I have completed my entire education since graduation. It was an honor to be at this prestigious university.

The Department of Chemistry for all the resources invested and for all excellent professors who shared their knowledge with me and certainly inspired me throughout my trajectory.

I must thank all the past and present members of the LSPN lab and Márcio's group for the collaboration, inspiration, and friendship. In particular, Marilia, Lorena, Natália, Wanderson, José Tiago and Pedro for their friendship, guidance and for motivating me. I am thankful for the incredible time we shared together in the lab. Certainly, there are many good moments that I will remember with profound gratitude.

My parents and sisters (Michele and Thaíssa) for their support and understanding.

ABBREVIATIONS

AIBN: azobisisobutyronitrile

BDE: bond dissociation energy

CT: charge transfer

CV: cyclic voltammetry

DCM: dichloromethane

DHP: dihydropyridine

DMA: dimethylacetamide

DMF: dimethylformamide

DMSO: dimethyl sulfoxide

EDA: electron donor-acceptor

EnT: energy transfer

HAT: hydrogen atom transfer

HOMO: highest occupied molecular orbital

IC: internal conversion

ISC: intersystem crossing

LED: light-emitting diode

LUMO: lower occupied molecular orbital

MeCN: acetonitrile

MLCT: metal to ligand charge transfer

MS: mass spectrometry

NMR: nuclear magnetic resonance

PCET: proton-coupled electron transfer

RT: room temperature

SCS: spin center shift

SET: single-electron transfer

TMS: tetramethylsilane

UV: ultraviolet

UV-Vis: ultraviolet-visible

TABLES

FIGURES

FIGURE 2.9 – ^{1}H NMR ($CDCl_3$, 400 MHz) spectra of the carbamoyl dimer. ^{1}H NMR (400 MHz, CDCl3) δ 3.47 (ddd, *J* = 14.5, 10.5, 3.9 Hz, 2H), 1.95 – 1.91 (m, 4H), 1.72 – 1.67 (m, 4H), 1.62 – 1.58 (m, 2H), 1.39 – 1.25 (m, 4H), 1.19 – 1.07 (m, 6H).

SCHEMES

ABSTRACT

PHOTOREDOX-MEDIATED AMINOALKYLATION AND CARBAMOYLATION OF AZOMETHINE IMINES. Over the past decade, the organic synthetic community has witnessed the emergence of a new and complementary approach to the conventional radical chemistry. Photochemistry has proven to be a powerful and more sustainable tool through the photoredox catalysis concepts, which are based on the use of organic and metallic photocatalysts capable of absorbing visible light irradiation and converting it into electrochemical potential, promoting the rationalization of new disconnections that are not viable or difficult to be achieved by conventional methods.

Nitrogen-centered 1,3-dipoles are considered key building blocks for the preparation of five-membered heterocyclic compounds and are widely explored in (3 + 2) cycloaddition reactions. Despite the advances in translating these reactions under photocatalytic conditions, the use of such dipoles - except for nitrones and azides - remains scarcely explored. Among this class of versatile compounds, azomethine imines presents a zwitterionic nature that have been mainly explored in 1,3-dipolar cycloadditions and only few reports involving photoisomerization and photocyclization promoted by ultraviolet irradiation were disclosed in the literature.

In this scenario, we initially became interested in exploring the reactivity of azomethine imines under visible-light irradiation. To this end, we envisioned that the easily generated and reactive *α*-aminoalkyl radicals would be ideal coupling partners for the development of a new photoredox functionalization strategy of azomethine ions leading to the synthesis of *N*-(*β*-aminoalkyl) pyrazolidinones under mild reaction conditions.

Having proven the reactive potential of these species under the photoredox catalysis, we then challenged them in a one-electron approach for amide bond installation in the presence of readily available and stable 4-carbamoyl-1,4-dihydropyridines as carbamoyl radical source. The principal relevance of the developed protocol relies on the rich nature of the accessed compounds, as a library of diversified amino acid derivatives, including more complex substrates and drug derivatives.

We demonstrated that photoredox catalysis is an excellent strategy for the α-functionalization of azomethine imines, leading to an easy access to high functionalized compounds through a new α-amino functionalization protocol and by installing amide bonds. The potential of the developed methods was demonstrated preparing complex examples involving peptides, pharmaceutical ingredients, and sterically hindered amides.

RESUMO

AMINOALQUILAÇÃO E CARBAMOILAÇÃO FOTORREDOX DE AZOMETINA IMINAS. Ao longo da última década, a comunidade sintética orgânica tem observado o surgimento de uma nova abordagem complementar à química radicalar convencional. A fotoquímica tem se mostrado uma ferramenta poderosa e mais sustentável através dos conceitos da catálise fotorredox, que se baseiam na utilização de fotocatalisadores orgânicos e metálicos capazes de absorverem irradiação de luz visível e convertê-la em potencial eletroquímico, promovendo a racionalização de novas desconexões que são inviáveis ou difícil de serem alcançadas por métodos convencionais.

1,3-dipolos centrados no átomo de nitrogênio são considerados blocos de construção chave para a preparação de compostos heterocíclicos de cinco membros e são amplamente explorados em reações de cicloadição (3 + 2). Apesar dos avanços transladando essas reações sob condições fotocatalíticas, o uso de tais dipolos, exceto para nitronas e azidas, ainda é pouco explorado. Dentre essa classe de compostos versáteis, as azometina iminas apresentam uma natureza zwitteriônica que tem sido explorada principalmente em cicloadições 1,3-dipolares e existem apenas poucos relatos na literatura envolvendo fotoisomerização e fotociclização promovidas por irradiação ultravioleta.

Nesse cenário, inicialmente nos interessamos em explorar o potencial reativo de azometina iminas sob irradiação de luz visível e propomos que os facilmente gerados e reativos *α*-aminoalquil radicais seriam parceiros de acoplamento ideais para o desenvolvimento de uma nova estratégia de funcionalização fotorredox de íons azometina que levaria à síntese de *N*- (*β*-aminoalquil) pirazolidinonas sob condições de reação brandas.

Tendo demonstrado o potencial reativo dessas espécies mediante a catálise fotorredox, nós então as avaliamos em uma abordagem de um elétron para a instalação de ligação amida na presença de 4-carbamoil-1,4-dihidropiridinas como fontes de radicais carbamoíla prontamente disponíveis e estáveis. A principal relevância do protocolo desenvolvido se dá pela valiosa natureza dos compostos acessados, como bibliotecas de derivados de aminoácidos diversificados, incluindo substratos mais complexos e derivados de fármacos.

Nós demonstramos que a catálise fotorredox é uma excelente estratégia para a α-funcionalização de azometina iminas, levando facilmente ao acesso de compostos altamente funcionalizados através de um novo protocolo de α-amino funcionalização e pela instalação de ligação amida. O potencial dos métodos desenvolvidos foi demonstrado por meio de exemplos complexos envolvendo peptídeos, ingredientes farmacêuticos e amidas estericamente impedidas.

Table of Content

CHAPTER 1

1. Introduction

1.1 The Concepts of Photoredox Catalysis

Relevance

The exploration of visible light as energy source in the photocatalysis field has been carried out to access unique and unconventional reactivities by the rationalization of new reaction mechanisms. Given this relevant characteristic of non-traditional disconnections, it is a topic that has received considerable attention by the synthetic community over the past decade.

In terms of the organic synthetic tools, *i.e.,* the arsenal of methodologies available to forging different C-C and C-heteroatom bonds, many of them can be correlated, at a first moment, to classic polar mechanisms. The point in the discussion is that for many years the radical chemistry remained underexplored regarding the ionic chemistry, due to a misinterpreted idea that radical species are generated in an uncontrolled way and would be involved in poorly selective protocols.[1]

Clearly, the traditional methods of organic synthesis, such as the cross couplings and pericyclic reactions, are fundamental strategies for the construction of structurally diverse scaffolds. However, in combination with the important area of the radical chemistry, they offer a large possibility of transformations for the diversification of the structural skeletons of organic molecules.

The real scenario is that radical chemistry is extremely useful and there are several elegant methodologies employing radicals as reactive intermediates. It is noteworthy that these species present an outstanding translational potential and can be applied in different contexts in organic synthesis. This rich reactivity has attracted the synthetic organic chemists throughout history and currently such transformations have demonstrated unprecedented applications.

At the present, the field of organic synthesis is well developed, and the numerous available synthetic tools allow access to the most varied chemical structures, in a selective and efficient way. Cited as example are the synthesis of various functionally dense molecules and

[1] YAN, M.; LO, J. C.; EDWARDS, J. T. & BARAN, P. S. “Radicals: reactive intermediates with translational potential”. J. Am. Chem. Soc. **138**: 12692, 2016.

biologically important compounds.[2] In this aspect, it is clear how radical chemistry is equally important and useful in accessing many classes of compounds. This is a straightforward argument for how these two areas of organic synthesis, the polar and the radical, complement each other in an extraordinary way and benefit us from the results that can be obtained.

Recently, the photoredox catalysis field came up with the proposal to conceive a new aspect for the classical radical methodologies, operating under milder reaction conditions to generating reactive radical intermediates. The principle of this catalysis is given by the use of photocatalysts capable of participating in single-electron transfer (SET) processes with organic substrates after photoexcitation under visible light irradiation. The fundamental advantages associated with this catalytic approach are the non-need use of stoichiometric amounts of oxidants, reductants, high temperature and energetic ultraviolet irradiation – conditions commonly employed in the traditional methodologies based on radicals.

Many classical radical transformations are widely known, *e.g.*, the Meerwien arylation, Burchi reduction, Barton and Okada decarboxylation, Mukaiyama hydration, among others. These classical transformations, such as the methodologies for Minisci and Giese reactions, have had their protocols translated by the perspective of photocatalysis. Additionally, new protocols have been discovered over the last decade, through previously unplanned mechanisms via classical ionic or radical chemistry (**SCHEME 1.1**).

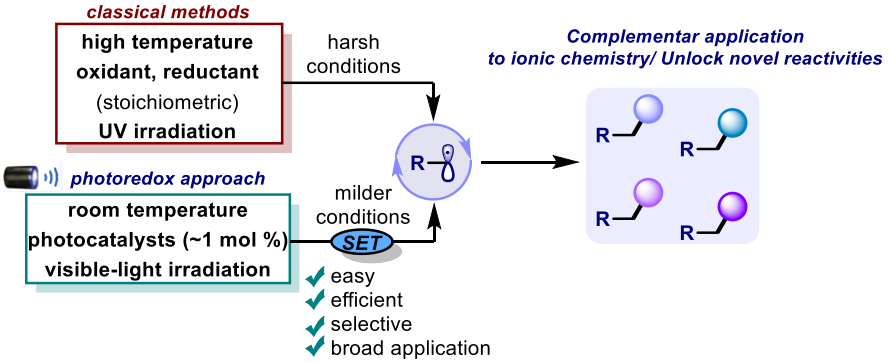

SCHEME 1.1 - Classical and modern approaches to radical chemistry complementing the ionic methodologies.

Photophysics

[2] (a) ROMERO, K. J.; GALLIHER, M. S.; PRATT, D. A. & STEPHENSON, C. R. J. "Radicals in natural product synthesis". Chem. Soc. Rev. **47**: 7851, 2018; (b) NICOLAOU, K. C.; VOURLOUMIS, D.; WINSSINGER, N. & BARAN, P. S. "The art and science of total synthesis at the dawn of the twenty-first century". Angew. Chem. Int. Ed. **39**: 44, 2000.

Photochemistry is associated with the chemistry of the excited electronic states, *i.e.,* the promotion of an electron in an orbital to a higher energy one. Regarding this field, the electromagnetic spectrum can be considered an extremely useful reference point for its understanding.[3]

It is known that the energy of monochromatic light E is proportional to its frequency (υ) and inversely proportional to its wavelength (λ) (**Eq. 1**). Considering that the energy required for a photochemical process to take place is in the range of ultraviolet and visible light irradiation, if carried out a correlation of these wavelengths with the energy associated with them, it will be noticed that this energy range corresponds to a value between 40 -140 kcal.mol^{-1}. By the association of such values with the bond dissociation energies (BDE) of common bonds found in organic compounds, it is possible to observe that the bond energies are easily covered by the UV-Vis spectra region - which has enough energy to break most organic bonds and lead to reactive intermediates that will be involved in further reaction pathways (**FIGURE 1.1**).

$$\boldsymbol{E = h\upsilon = h\frac{c}{\lambda}} \qquad \textbf{Eq. 1}$$

$$h = 6.626 \times 10^{-34}\ \mathrm{Js}^{-1}$$

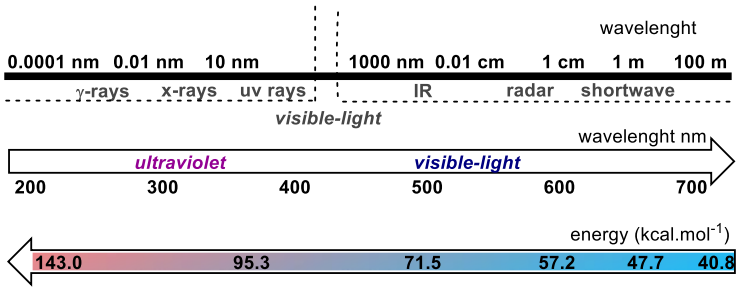

FIGURE 1.1 - Wavelength spectrum and correlated energies.

Before properly discussing the concepts of the photoredox catalysis, it is important to emphasize an important diagram, known as the Jablonski diagram. It summarizes photophysical processes, *i.e*., those that do not lead to changes in the chemical structure of the species. They are especially important given that these events precede the photochemical transformations (**FIGURE 1.2**).

[3] ANSLYN, E. V. & DOUGHERTY, D. A. Modern physical organic chemistry. Sausalito, CA: University Science, 2006. Print.

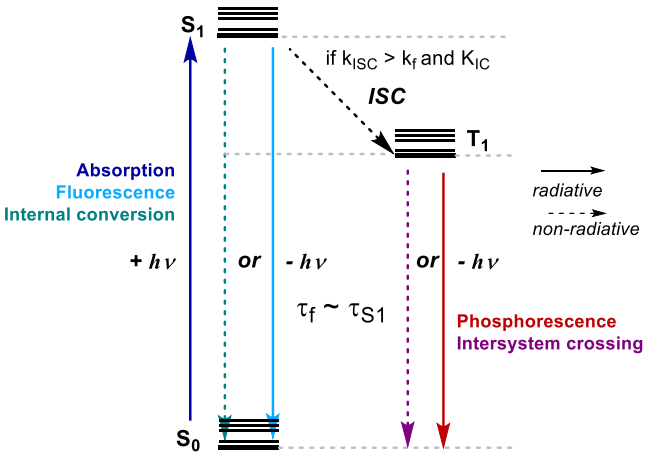

FIGURE 1.2 - Simplified Jablonski diagram.

The photochemistry is initiated in the excited states and is based on a competition between different processes that occur at different rates. It is important to have an idea of such values that governs the photophysical events to infer if a determined physical process could occur at the expense of others before the chemical event takes part.

Some general aspects should be considered before describing the photophysical events summarized by the Jablonski Diagram:

- The absorption of energy at a given wavelength only leads to a single electronic transition in the molecule (Stark-Einstein rule),
- The electronic transitions are spin-conservatives, what means that a fundamental singlet state S_0 goes to an excited singlet state S_1. There are other possible spin states - as the triplet state, which occurs with the change in spin orientation,
- According to the energy of the incident irradiation, other excited states can also be reached (S_1, S_2, S_n), however all the photochemical processes are initiated from the lower energy excited states (Kasha's Law) - the relaxation from the excited state of higher energy S_n to that of lower energy S_1 is very fast.

In the Jablonski diagram, energy surfaces (*i.e.*, vibrational modes and interconversions of chemical structures) are represented by the Morse potential placed along the X axis, while the Y axis in this diagram represents energy along the X coordinate of the reaction. According to the described diagram, there is a possible sequence of events:

Initially, the electrons occupy the ground state in the lowest energy molecular orbital (singlet state, S_0). Many other orbitals can exist in the same molecule as well (S_1, S_2, S_3, etc.). For those species with a closed shell (two paired electrons), the absorption of a photon leads to

the excitation of one electron from a bonding to an antibonding orbital (from HOMO, the highest occupied molecular orbital, to the LUMO, the lower occupied molecular orbital) when exposed to an irradiation source with appropriated energy – which corresponds to the energy difference between the ground and the excited state. The excited state energy after the absorption event is described as $E_{0,0}$ (since it involves the S_0 to S_1 transition) and its value can be extracted from the intersection point between the absorbance and emission spectrum using the **equation 1**. The same value can be estimated from the one-half Stokes shift given by the midpoint between absorption and emission maxima.

The absorption process takes place almost instantaneously since it involves an electronic movement which is much faster than a nuclear movement. In this way, there is no other photophysical event that competes with the described initial event.

The absorption efficiency is indicated by the molar absorptivity coefficient (ε) given by the Lambert-Beer law (**Eq. 2**). High values of molar absorptivity indicate an efficient absorption. The absorption spectrum of a specie can be acquired using a spectrophotometer and it is one of the initial measurements to be taken in photochemical studies. The absorption wavelength is essential for choosing the appropriate irradiation source to promote the necessary electronic excitation without promoting competitive parallel reactivities.

$$\log (I_o/I) = A = \varepsilon bc \qquad \textbf{Eq. 2}$$

A = absorption

I_0 = Intensity of incident light

I= Intensity of transmitted light

b = path length (cm)

c = concentration ($mol.L^{-1}$)

ε = molar absorptivity ($mol.L^{-1}.cm$)

In this scenario, it is noteworthy to note that light-emitting diodes (LEDs) have significantly contributed to the development of the photocatalysis field, since they have a narrow emission band, allowing chromophores to be selectively excited. Furthermore, these light sources are of high intensity.

The photophysical events from the reached excited state involve transitions to lower energy states via radiative (emitting light) and non-radioactive mechanisms (energy dissipated as heat). These subsequent events can be described as follow:

The decay to the ground state occurs via **internal conversion** (IC), a non-radiative mechanism, or via a radiative mechanism by photo emission, called **fluorescence**. Such events can be measured by obtaining an emission spectrum using a spectrophotometer, where the light emitted from the sample is detected at ninety degrees to avoid the detection of residual incident light. Non-radiative decay paths are considerably slower than radioactive ones and therefore we can consider the fluorescence lifetime to be approximate the lifetime of S_1 ($\tau_f \sim \tau_{S1}$).

A further possible event, called **intersystem crossing** (ISC), involves a spin orientation shift from the excited singlet state to the triplet state, which can be efficiently populated if k_{ISC} is fast enough to compete with k_f and k_{IC}. From the excited triplet state, the deactivation processes can occur via unusual non-radiative mechanisms and by **phosphorescence**, a radiative mechanism.

The lifetimes of triplet states (τ_{T1}) are generally order of magnitude longer than those of S_1 (micro/milli to nanoseconds). As previously mentioned, the processes are spin-conservative, and it is possible to establish a correlation between the lifetimes (τ) of the states according to the change in the spin orientation. The ISC (S_1 to T_1) and phosphorescence (T_1 to S_0) are spin prohibited events and therefore slower than fluorescence, for example. The longer the fluorescence lifetime, the greater the probability of the triplet state participating in a SET process before the deactivation to the ground state. It is also noteworthy that the decay by phosphorescence and non-radiative mechanisms are generally much slower than electron transfer events.

The singlet and triplet states are those that usually participate in bimolecular processes through electron or energy transfer events given that their lifetimes range from milli to nanoseconds – long-lived enough to them engage in subsequent transformations by quenching events (**FIGURE 1.3**). The triplet state has a longer lifetime, despite of the decay process to the ground state be prohibited by spin. Thus, when the molecule reaches the excited triplet state, it is prone to participate in such bimolecular events.

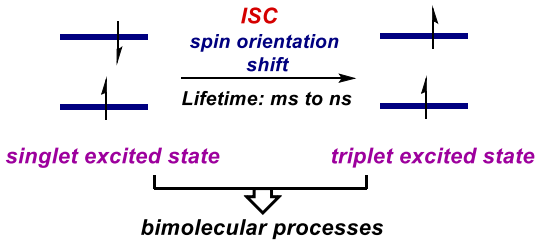

FIGURE 1.3 - Representative intersystem crossing event.

Two concepts are fundamental for the understanding of the involved photochemistry: those related with the bimolecular processes and quenching. For the collision of the excited state of a given specie with another reactive molecule takes place– the bimolecular process – it is necessary that the rate of this collision be competitive with the decay rate of the excited state. Quenching is a form of collision of the excited state with another substrate and is considered a relaxation process to the ground state.

In a definition, the term quenching can be used to refers to a decrease in the fluorescence intensity of a fluorophore.[4] Among the possible molecular interactions that lead to this deactivation process, collisional (or called dynamic quenching) is the most common to occur. Quenching measurement provides valuable information about the photophysical event initially involved prior to the photochemical transformation, as it can indicates which species are interacting with the fluorophore excited state. Many species can be used as collisional quenchers of fluorophores, such as amines, halogenated compounds, and oxygen itself, which is a powerful quencher of almost all fluorophores.

Molecular contact between the fluorophore (**F**) and the quencher (**Q**) is necessary for this photophysical event to occur, leading to the formation of an initial non-emissive complex. Note that the formation of this complex must occur before the decay of the excited state of the fluorophore (hence the importance of achieving long-lived excited states for the diffusion to the quencher).

The scheme below represents a general model of this process (**SCHEME 1.2**). The close contact between the species leads to the formation of a precursor complex. The quenching of the excited fluorophore gives rise to the successor complex, which escapes from the solvation sphere and leads to the reactive species involved in the further transformations.[5]

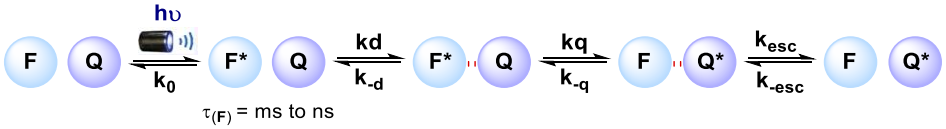

SCHEME 1.2 - General quenching process. Adapted from ref 5.

This event has a kinetic implication known as Stern-Volmer relationship. Basically, the lifetime of the excited state of the photocatalyst can be determined in the absence and presence of the quencher and depends on the concentration of this latter in the reaction medium. As the

[4] LAKOWICZ, J. R. Quenching of Fluorescence. In: Principles of Fluorescence Spectroscopy. Springer, Boston, MA, 1983. p. 277.

[5] ARIAS-ROTONDO, D. M. & MCCUSKER, J. K. "The photophysics of photoredox catalysis: a roadmap for catalyst design". Chem. Soc. Rev. **45**: 5803, 2016.

quencher concentration increases, it is possible to observe a decay of the excited state's emission intensity, *i.e.*, the extinction of this state by the bimolecular collision event. This is a useful tool to determine which of the species present is responsible quenching the fluorophore and, thus, to determine the initial reactional pathway of the reaction. In a quantitative way, the Stern-Volmer analysis indicates the quenching efficiency or the accessibility of the fluorophores to the quencher by the measurement of a constant called bimolecular quenching constant (kq).

Photoredox Catalysis

Concept

The traditional generation of reactive intermediates containing an unpaired electron makes use of radical initiators, such as AIBN and BEt_3, toxic reagents as Bu_3SnH, and most protocols employ high temperatures and UV irradiation. Other redox approaches as electrolysis, and photolysis also present considerable drawbacks. Considering the fundamentals of Green Chemistry,[6] which have been taken with important consideration in recent years, it is understandable why such classical approaches have fallen into disuse and therefore contributed to the rapid expansion of visible-light-driven photocatalysis.

A photochemical reaction, in general, is initiated by the direct excitation of a substrate or intermediate. When using catalytic species that absorb irradiation and convert it into potential energy for substrates, the approach is called photocatalysis. The key step is the absorption of a photon by the chromophore (*i.e.*, the photocatalyst) leading to a sequence of events based on electron and energy transfers, via the formation of electron donor-acceptor complexes (EDA) or hydrogen atom transfers (HAT) – such mechanisms depend on energies, lifetimes, and electrochemical properties of the substrates and photocatalysts in the ground and excited states (**FIGURE 1.4**).

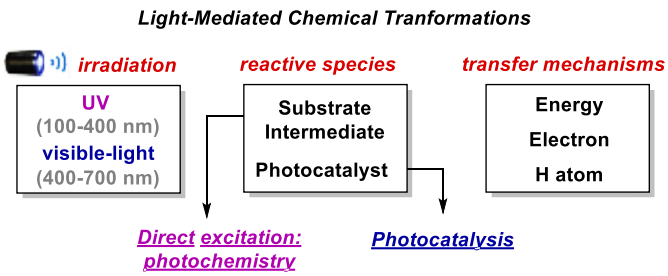

FIGURE 1.4 - Summary of catalytic methods promoted by UV-Vis irradiation.

[6] ANASTAS, P. & EGHBALI, N. "Green chemistry: principles and practice". Chem. Soc. Rev. **39**: 301, 2010.

The rapid development of photocatalysis is given by its advantages, highlighting the use of photocatalysts and visible light irradiation, leading to more selective and efficient transformations and allowing high functional group tolerance under mild conditions. Another interesting aspect is the possibility of modulation of the electrochemical properties of the metallic complexes and dyes usually used as photocatalysts through the modification of their ligands, which open up possibilities to unlock a wide range of reactivities under environmentally benign protocols.

The photocatalysts and mechanisms

The catalytic species employed in these processes usually are complexes capable of undergoing metal to ligand charge transfer (MLCT) under visible light irradiation, followed by an ISC event to populate the longer-lived excited triplet state ($rate_{diffusion} > rate_{relaxation}$). A subsequent SET event can lead to open-shell reactive species which are able to participate in various chemical transformations.

In this aspect, the use of octahedral polypyridyl complexes of iridium and ruthenium has become a fundamental factor for the development of the photoredox catalysis. Although they are the commonly employed complexes, important advances have been made in visible light mediated protocols using photoactive Cr^{III}, Fe^{II}, Cu^{I}, Zn^{II}, Zr^{IV}, Mo^{0} and U^{VI} complexes.[7] After the absorption of one photon with appropriate energy (ΔHOMO-LUMO), the excited states of these complexes present properties of strong oxidants and reductants, and this reactivity is responsible for the possible photoredox catalytic cycles.

The era of the photoredox catalysis has revived the use of the complex $[Ru(bpy)_3]^{2+}$ since the first report of its use as a photocatalyst in 1978[8] and nowadays it is the most employed and studied chromophore used as catalyst. Its versatile applications have established this complex as a useful model for understanding the photoredox concepts involved in this catalysis. Therefore, it is a great starting point to carry out this discussion considering its properties and mechanisms.[9]

The maximum absorption of the $[Ru(bpy)_3](PF_6)_2$ complex in acetonitrile is in the visible region, at λ = 452 nm, and occurs selectively since organic substrates generally do not directly

[7] LARSEN, C. B. & WENGER, O. S. “Photoredox catalysis with metal complexes made from earth-abundant elements”. Chem. Eur. J. **24**: 2039, 2018.
[8] HEDSTRAND, D. M.; KRUIZINGA, W. H. & KELLOGG, R. M. “Light induced and dye accelerated reductions of phenacyl onium salts by 1,4-dihydropyridines”. Tetrahedron Lett. **16**: 1255, 1978.
[9] KOIKE, T. & AKITA, M. “Visible-light radical reaction designed by Ru- and Ir-based photoredox catalysis”. Inorg. Chem. Front. **1**: 562, 2014.

absorb energy in this region of the electromagnetic spectrum. The ^{1}MLCT1 state reaches the long lived ^{3}MLCT1 state via intersystem crossing (k_{isc}). The high intensity MLCT electronic transition is from a metal-based orbital to a ligand orbital, and, in practice, this transfer simultaneously leads to the oxidation of the metal center and the reduction of one of the bipyridine ligands (**SCHEME 1.3**, **A**). The potential for this oxidation occurs is ~1 V, as measured by cyclic voltammetry of the complex in acetonitrile.[10] Two additional reduction events can also be observed, referring to reductions of the other two bipyridine ligands in the complex (**SCHEME 1.3**, **B**). The decay to the ground state occurs with maximum emission at λ = 620 nm and the energy difference between ^{3}MLCT – S_0 can be considered as the energy of the excited triplet state E_T (important value for evidence of energy transfer mechanisms).

The main mechanistic pathway in visible light-mediated photocatalysis is through SET events with other substrates leading to the generation of neutral, cationic, or anionic radicals that are able to engage in successive chemical transformations. This mechanism is describe as photoredox and will be illustrated in combination with the electrochemical properties of the model complex $[Ru(bpy)_3](PF_6)_2$.

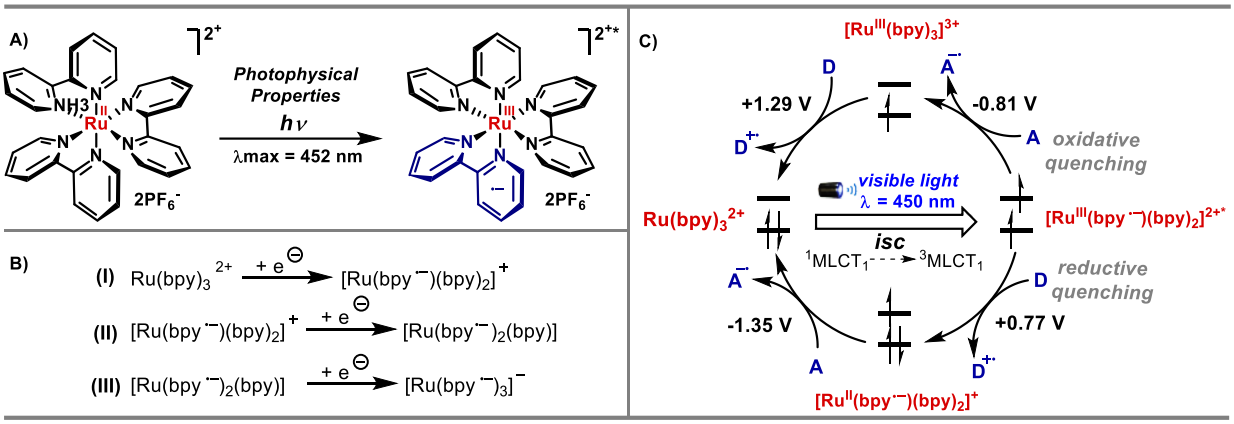

SCHEME 1.3 - A) Photophysical and B) electrochemical properties of $[Ru(bpy)_3](PF_6)_2$. C) The photoredox catalytic cycles.

The excited triplet state **$[Ru^{III}(bpy^{\bullet-})(bpy)_2]^{2+*}$** ($\tau$ = 1100 ns) can participate in bimolecular processes that are initiated by a reductive (reduction of $[Ru^{III}(bpy^{\bullet-})(bpy)_2]^{2+*}$) or oxidative (oxidation of $[Ru^{III}(bpy^{\bullet-})(bpy)_2]^{2+*}$) quenching. In the first case, the sequence of events involves an electron transfer from the donor specie **D** to the excited photocatalyst **$[Ru^{III}(bpy^{\bullet-})(bpy)_2]^{2+*}$**, leading to the reduced specie **$[Ru^{II}(bpy^{\bullet-})(bpy)_2]^{+}$** and the cation radical **$D^{+\bullet}$** , followed by

[10] (a) KALYANASUNDARAM, K. "Photophysics, photochemistry and solar energy conversion with tris(bipyridyl)ruthenium(II) and its analogues". Coordination Chemistry Reviews, **46**: 159, 1982; (b) TOKEL-TAKVORYAN, N. E.; HEMINGWAY, R. E. & BARD, A. J. "Electrogenerated chemiluminescence. XIII. Electrochemical and electrogenerated chemiluminescence studies of ruthenium chelates." J. Am. Chem. Soc. **95**: 6582, 1973.

regeneration of the complex to the ground state via SET with an electron acceptor specie **A**. In an oxidative quenching, the initial step involves the oxidation of the excited photocatalyst to **$[Ru^{III}(bpy)_3]^{3+}$** via SET with the acceptor specie **A**, and further decay to the ground state in the presence of the electron donor species **D**, which reduces the oxidized photocatalyst to regenerate it in the reaction cycle (**SCHEME 3**, **C**).

In the described general catalytic cycle, the intermediate reactive species can be generated in situ and are responsible for the regeneration of the photocatalyst in the reaction medium. Therefore, in this case, this process can be classified as redox-neutral. In other cases, contrary, there may be a need to employ additives with the role of sacrificial oxidants/reductants for the initial generation of the highly oxidizing/reducing species of the photocatalyst or its returning to the ground-state. Usually, amines and ascorbic acid are employed as sacrificial electron donors and oxygen and peroxodisulfate as electron acceptors in the photocatalytic reactions.

As observed by the reduction potentials in the **SCHEME 1.3**, the reductive quenching gives rise to a stronger reductant specie **$[Ru^{II}(bpy^{\bullet-})(bpy)_2]^{+}$** ($M/M^{-}$ = −1.35 V *vs* $M^{+}/*M$ = -0.81 V, *vs* SCE in ACN). In the same way, a highly oxidizing specie **$[Ru^{III}(bpy)_3]^{3+}$** is generated upon the oxidative quenching of the excited photocatalyst (M/M^{+} = 1.29 V *vs* $M^{-}/*M$ = 0.77 V, *vs* SCE in ACN).

The reduction potentials of photocatalysts and other involved species are key parameters for planning a photoredox transformation. For the photocatalysts, two pairs of potentials are described, one related to the species in their ground state and other to the excited state (**FIGURE 1.5**). These electrochemical values for the commonly used complexes are well reported in the literature[11] and are easily obtained by cyclic voltammetry (CV) experiments (for the ground state). For substrates and photocatalysts, the excited state potential values can be extracted from the Rehn-Weller relation – this is based on the ground state potential value obtained through CV and a correction of it considering the energy value $E_{0,0}$. This latter corresponds, in practice, to the phosphorescence emission in the Jablonski diagram. Additionally, there are other parameters that can influence the determination of these potentials in both states, such as temperature, solvent, concentration, electrodes. However, by employing the techniques described, useful results for the design of the experiment can be obtained. It is

[11] (a) TEEGARDIN, K.; DAY, J. I.; CHAN, J. & WEAVER, J. “Advances in photocatalysis: a microreview of visible light mediated ruthenium and iridium catalyzed organic transformations”. Org. Process Res. Dev. **20**: 1156, 2016; (b) ROTH, H. G.; ROMERO, N. A. & NICEWICZ, D. A. “Experimental and calculated electrochemical potentials of common organic molecules for applications to single-electron redox chemistry”. Synlett. **27**: 714, 2016.

worth to pointed out that the reduction potential always refers to the half-reduction reaction of the most oxidized species.

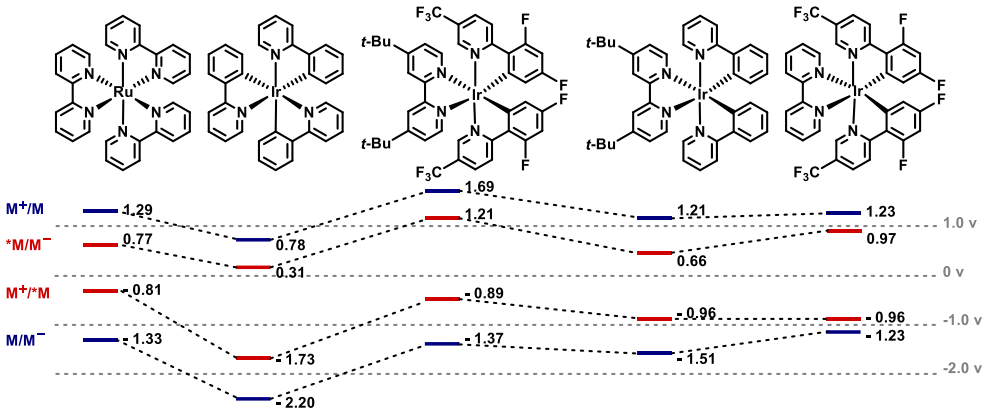

FIGURE 1.5 - Electrochemical properties of commonly used metal-based photocatalysts.

The general photoredox catalytic cycle described in the **SCHEME 1.3C** comprises variations, which may involve mechanisms via proton-coupled electron transfers (PCET) pathways. In these, both particles, the proton and the electron, are transferred from the donor to the sites of the acceptor in different arrangements.[12] Other useful photocatalytic routes to radicals have extended the application of the photoredox catalysts in combination with other catalytic activation modes, in the called synergistic or dual catalysis protocols.[13] The merger of the photoredox catalysts with organo[14] and acid catalysts,[15] and transition metal complexes[16] targeting at stereoselective, cross-coupling and multicomponent approaches has attracted the

[12] HOFFMANN, N. "Proton-coupled electron transfer in photoredox catalytic reactions". Eur. J. Org. Chem. **15**: 1982, **2017**.

[13] PRIER, C. K. & MACMILLAN, D. W. C. "Visible light photocatalysis in organic chemistry, (Eds.: Stephenson, C. R. J.; Yoon, T. P. & MacMillan, D. W. C.), Wiley-VCH, Weinheim, 2018, pp. 299.

[14] For selected reviews and book chapters, see: (a) MAVROSKOUFIS, A.; JAKOB, M. & HOPKINSON, M. N. "Light-promoted organocatalysis with *N*-heterocyclic carbenes". ChemPhotoChem. **4**: 5147, 2021; (b) ZEITLER, K. & NEUMANN, M. "Synergistic Visible Light Photoredox Catalysis. Chemical Photocatalysis", 2nd Edition, 2020, p. 245; (c) LIU, Y.-Y.; LIU., J.; LU, L.-Q. & XIAO, W-J. "Organocatalysis combined with photocatalysis". Topics in Current Chemistry. **377**: 1, 2019; (d) REY, Y. P.; HEPBURN, H. B. & MELCHIORRE, P. "Science of Synthesis, Photocatalysis in Organic Synthesis". 2019, p. 243-270.

[15] For selected examples, see: (a) SPECKMEIER, E.; FUCHSA, P. J. W. & ZEITLER, K. "A synergistic LUMO lowering strategy using Lewis acid catalysis in water to enable photoredox catalytic, functionalizing C–C cross-coupling of styrenes". Chem. Sci. **9**: 7096, 2018**;** (b) AMADOR, A. G.; SHERBROOK, E. M.; LU, Z. & YOON, T. P. "A general protocol for radical anion [3+2] cycloaddition enabled by tandem Lewis acid photoredox catalysis". Synthesis. **50** : 539, 2018; (c) LEE, K. N.; LEI, Z. & NGAI, M.-Y. "*β*-Selective reductive coupling of alkenylpyridines with aldehydes and imines via synergistic Lewis acid/photoredox catalysis". J. Am. Chem. Soc. **139** : 5003, 2017; (d) YOON, T. P. "Photochemical stereocontrol using tandem photoredox–chiral Lewis acid catalysis". Acc. Chem. Res. **49**: 2307, 2016.

[16] For selected reviews, see: (a) LIPP, A.; BADIR, S. O. & MOLANDER, G. A. "Stereoinduction in metallaphotoredox catalysis". Angew. Chem. Int. Ed. **60**: 1714, 2021; (b) PRIER, C. K.; RANKIC, D. A. & MACMILLAN, D. W. C. "Visible light photoredox catalysis with transition metal complexes: applications in organic synthesis". Chem. Rev. **113**: 5322, 2013.

interest of the synthetic community over the past years given the new disconnections accessed by them.

In addition to the photoredox mechanism, an alternative to the electron transfer event to access the excited triplet states of organic substrates is given by energy transfer mechanisms. The energy transfer (EnT) catalysis is defined as “the photophysical process in which an excited state of one molecular entity (the donor D) is deactivated to a lower-lying state by transferring energy to a second molecular entity (the acceptor A), which is thereby raised to a higher energy state”[17] **(SCHEME 1.4, A).**

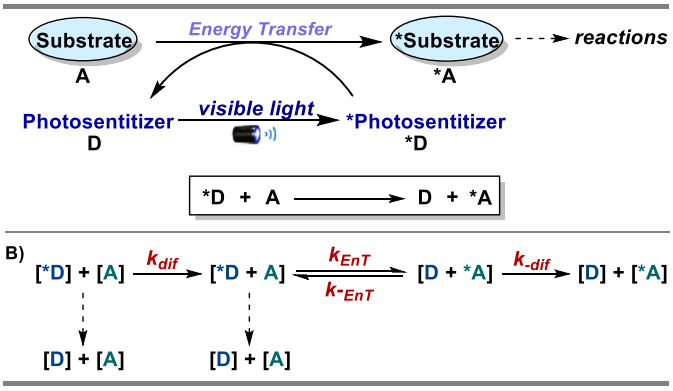

SCHEME 1.4 - A) Representative mechanism of photosensitization. B) Simplified molecular process of triplet–triplet energy transfer in solution.

This field, although less explored in relation to the photoredox catalysis, has been developed as a new trend in expansion with valuable synthetic applications. An important aspect to be considered is related to the experiments for the characterization of this mechanistic pathway, which are performed through transient absorption spectroscopy studies, Stern-Volmer analysis and the determination of triplet excited state energies through spectroscopic techniques.[18] Under this catalytic approach, the excited photocatalyst (D*) by visible-light absorption is able to transfer energy from its excited triplet state to a substrate (A) by exchange interactions (Dexter energy transfer) **(SCHEME 1.4, B)**.[19] The sensitized substrate is then prone to participate of subsequent radical-based pathways. By definition, the term photosensitizer is used for the excited photocatalyst engaging EnT events – although the photoredox catalysts (those participating in SET events) can also exhibit this property and *vice-versa*.

[17] VERHOEVEN, J. W. “Glossary of terms used in photochemistry”. Pure Appl. Chem. **68**: 2223, 1996.
[18] STRIETH-KALTHOFF, F.; JAMES, M. J.; TEDERS, M.; PITZER, L. & GLORIUS, F. “Energy transfer catalysis mediated by visible light: principles, applications, directions”. Chem. Soc. Rev. **47**: 7190, 2018.
[19] TURRO, N. J. “Modern Molecular Photochemistry”. University Science Books, Sausalito, 1991.

Another possible light-driven mechanism is by exploring the formation of electron donor-acceptor complexes EDA (or charge-transfer complexes, CT). As the name indicates, these complexes are formed by the ground state association between a donor electron rich specie (D) and an acceptor electron poor specie (A) in a diffusion event. In this case, the photoexcitation of the EDA complex in the visible light region is prone to occur and leads to an electron transfer event without the use of any external photocatalyst. Such sequence of events leverages a radical ion pair [$D^{\bullet+}/A^{\bullet-}$] under mild and catalyst-free conditions which can engages in a series of one-electron transformations **(SCHEME 1.5)**.[20]

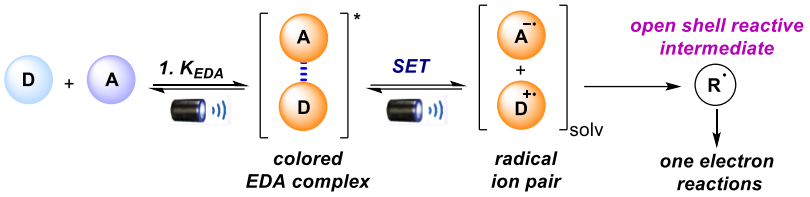

SCHEME 1.5 - General representation for an EDA-complex based mechanisms.

In these studies, a visual indicative of the EDA complex in solution is given after mixing the reaction components and exposition to irradiation, with a clear change in the color of the mixture being observed. In instrumental terms, absorbance measurements are able to reveal the formation of the EDA complex. The absorption measurements of the individual components are carried out and their absorption spectra recorded, and then the same analysis is carried out using an equimolar mixture of reagents. In cases where this complex is formed, a typical bathochromic shift (*i.e.*, longer wavelength) can be observed. The NMR technique can also be useful in indicating the formation of such redox active complexes.

Of fundamental importance for the design of new photocatalysts is the possibility of modulating the electrochemical properties of these complexes based on the structural characteristics of the ligands employed. When designing a transformation, it is equally important to determine the electrochemical characteristics of the substrates involved. From the potentials of these species, it is possible to predict whether there will be a match/mismatch with the photocatalyst specie so that the initial quenching occurs with the formation of reactive species that will engage the mechanistic cycle. The Nicewictz's group recently reported a useful study containing the values of ground state potentials for more than 180 substrates classified according to their functional groups.[11b]

[20] (a) ZHENG, L.; CAI, L.; TAO, K.; XIE, Z.; LAI, Y.-L. & GUO, W. "Progress in photoinduced radical reactions using electron donor-acceptor complexes". Asian J. Org. Chem. **10**: 711, 2021; (b) LIMA, C. G. S.; LIMA, T. M.; DUARTE, M.; JURBERG, I. D. & PAIXÃO, M. W. "Organic synthesis enabled by light-irradiation of EDA complexes: theoretical background and synthetic applications". ACS Catal. **6**: 1389, 2016.

In 2019, the Leonori's group reported an elegant protocol for the imino-functionalization of olefins via an oxidative generation of iminyl radicals followed by a cyclization–functionalization cascade with a broad range of SOMOphiles X–Y (**SCHEME 1.6**). In this study, the design of the α-hydroxy-acid substrate - the aminyl radical precursor - was accomplished by adding organyl groups at the methylenic position, lowering the $E_{1/2ox}$ and enabling an oxidative SET with the photocatalyst methyl acridinium perchlorate ($E^*_{1/2}$ = +2.06 V *vs* SCE).[21]

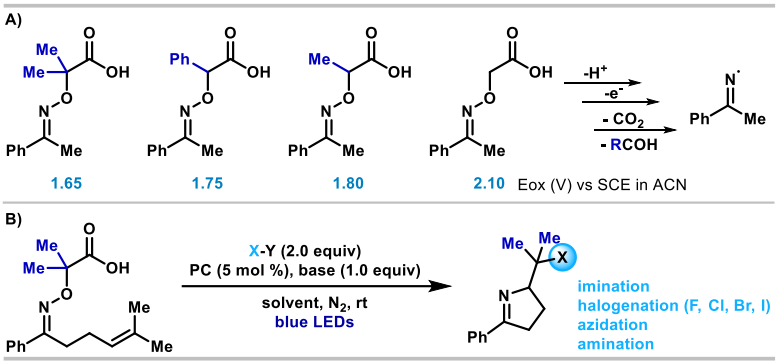

SCHEME 1.6 - Design of the iminyl radical precursor based on electrochemical properties.

As the **$[Ru(bpy)_3]^{2+}$** photocatalyst, considered a model for these transformations, iridium-based polypyridyl complexes have demonstrated broad versatility and useful applications in the field of the photoredox catalysis. Among the common key characteristics, these metal complexes absorb intensely in the visible light region (it makes the process selective in relation to organic groups present in the reaction medium); they also emit intensely, allowing important fluorescence studies be easily performed; their excited states are efficiently formed from the electronic absorption and have sufficiently long lifetimes to engage in bimolecular quenching processes; possess a reversible redox behavior (important for the regeneration of the catalytic cycle); are stable, commercially available and have well-known photophysical and electrochemical properties - useful for the design of new transformations.[5]

The organic dyes have also been extensively used as catalysts in such transformations, the called organophotocatalysts. They usually exhibit longer absorption wavelengths, such as Eosin Y (λ = 522 nm) and 4CzIPN (λ = 507 nm) and comparative redox potentials to those of metal-based photocatalysts. Therefore, by associating the corresponding energy values, the energy potentially applied in the transformations by this species is lower – although there is the advantage of being a metal-free catalyst. Thus, a balance of the redox and energetic properties of these species must be carried out during the design of the transformation.

[21] DAVIES, J.; SHEIKH, N. S. & LEONORI, D. “Photoredox imino functionalizations of olefins”. Angew. Chem. **129**: 13546, 2017.

Advances in photoredox catalysis

The renaissance of the use of $[Ru(bpy)_3]^{2+}$ as photocatalyst and the beginning of a new era of the radical-based transformations mediated by visible-light irradiation date back to 2008. Simultaneously, Yoon[22] and Nicewicz and MacMillan groups,[23] revealed innovative C-C bond forging protocols under photoredox catalysis (**SCHEME 1.7**). Yoon and co-workers demonstrated that $Ru(bpy)_3Cl_2$ could be used as an efficient photocatalyst for the formal [2+2] cycloaddition of (bis)enones by the generation of highly reducing specie $Ru(bpy)_3^{+}$ upon oxidative quenching with $^{i}Pr_2NEt$, which promotes the enone one electron reduction in the presence of the Lewis acid (**SCHEME 1.7, A**). Nicewicz and MacMillan elegantly disclosed an enantioselective intermolecular α-alkylation of aldehydes by merging photoredox catalysis with organocatalysis. The key step of the mechanism involves the addition of the SOMOphilic enamine formed upon condensation with the imidazolidinone catalyst to the electron-deficient alkyl radical generated via SET between the reduced photocatalyst and the alkyl halide (**SCHEME 1.7, B**).

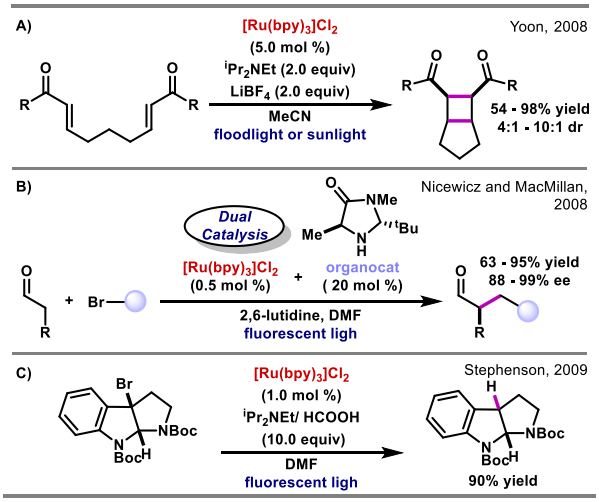

SCHEME 1.7 - Seminal protocols exploring the photoredox catalyst $Ru(bpy)_3Cl_2$.

Following these initial reports, the Stephenson's group developed a chemoselective tin-free reductive dehalogenation reaction mediated by visible-light.[24] The protocol proceeds via a SET event from the ammonium formate complex, generating the reduced reactive photocatalyst

[22] ISCHAY, M. A.; ANZOVINO, M. E.; DU, J. & YOON, T. P. "Efficient visible light photocatalysis of [2+2] enone cycloadditions". J. Am. Chem. Soc. **130**: 12886, 2008.

[23] NICEWICZ, D. A. & MACMILLAN, D. W. C. "Merging photoredox catalysis with organocatalysis: the direct asymmetric alkylation of aldehydes". Science, **322**: 77, 2008.

[24] NARAYANAM, J. M. R.; TUCKER, J. W. & STEPHENSON, C. R. J. "Electron-transfer photoredox catalysis: development of a tin-free reductive dehalogenation reaction". J. Am. Chem. Soc. **131**: 8756, 2009.

responsible for the carbon-halogen reduction in the substrate, followed by hydrogen abstraction to deliver the reduced compounds (**SCHEME 1.7, C**).

In the early years after the resurgence of this new approach for visible-light-mediated formation of radical intermediates, rapid advances were demonstrated and have established solid synthetic methodologies, which have been exceptionally expanded and applied in more recent methods. The Yoon's group, for example, has made a major contribution to the study of visible-light-driven cycloaddition by exploring the $1e^-$ reduction or $1e^-$ oxidation of alkenes for the promotion of (2 + 2)[15d, 22, 25], (3 + 2)[26] and (4 + 2)[27] cycloaddition reactions via ionic radicals, including stereoselective variants through dual catalysis protocols with chiral Lewis acids (**SCHEME 1.8, A**).

Tertiary amines have also been well explored as radical sources in combination with photoredox catalysis aiming at an easy access to *N*-containing heterocycles compounds.[28] Besides their use as sacrificial electron donors, their electron-rich nature is explored for the generation of amine radical cations, leading to functionalizations by exploring the *α*-aminoalkyl radicals as nucleophiles. Further oxidation gives rise to iminium ions, enabling the application in a series of reactions with nucleophiles. In 2012, Pandey and Reiser[29] demonstrated this concept in a visible-light mediated protocol catalyzed by Ir or Ru metal-complexes for the *α*-functionalization of *N*-aryltetrahydroisoquinolines. The *α*-aminoalkyl radical generated in the reductive quenching with the photocatalyst smoothly underwent the radical addition to electron-deficient olefins (**SCHEME 1.8, B**). Many other works have since explored the application of other cyclic/acyclic amines under this concept, leading to a series of functionalized *α*-amino compounds.

[25] (a) DU, J. & YOON, T. P. “Crossed intermolecular [2+2] cycloadditions of acyclic enones via visible light photocatalysis”. J. Am. Chem. Soc. **131**: 14604, 2009; (b) ISCHAY, M. A.; LU, Z. & YOON, T. P. “[2+2] Cycloadditions by oxidative visible light photocatalysis”. J. Am. Chem. Soc. **132**: 8572, 2010.

[26] LU, Z.; SHEN, M. & YOON, T. P. “[3+2] Cycloadditions of aryl cyclopropyl ketones by visible light photocatalysis”. J. Am. Chem. Soc. **133**: 1162, 2011.

[27] LIN, S.; ISCHAY, M. A.; FRY, C. G. & YOON, T. P. “Radical cation Diels–Alder cycloadditions by visible light photocatalysis”. J. Am. Chem. Soc. **133**: 19350, 2011.

[28] (a) NAKAJIMA, K.; MIYAKE, Y. & NISHIBAYASHI, Y. “Synthetic utilization of *α*-aminoalkyl radicals and related species in visible light photoredox catalysis”. Acc. Chem. Res. **49**: 1946, 2016; (b) MAITY, S. & ZHENG, N. “A photo touch on amines: new synthetic adventures of nitrogen radical cations”. Synlett. **23**: 1851, 2012.

[29] KOHLS, P.; JADHAV, D.; PANDEY, G. & REISER, O. “Visible light photoredox catalysis: generation and addition of *N*-aryltetrahydroisoquinoline-derived *α*-amino radicals to Michael acceptors”. Org. Lett. **14**: 672, 2012.

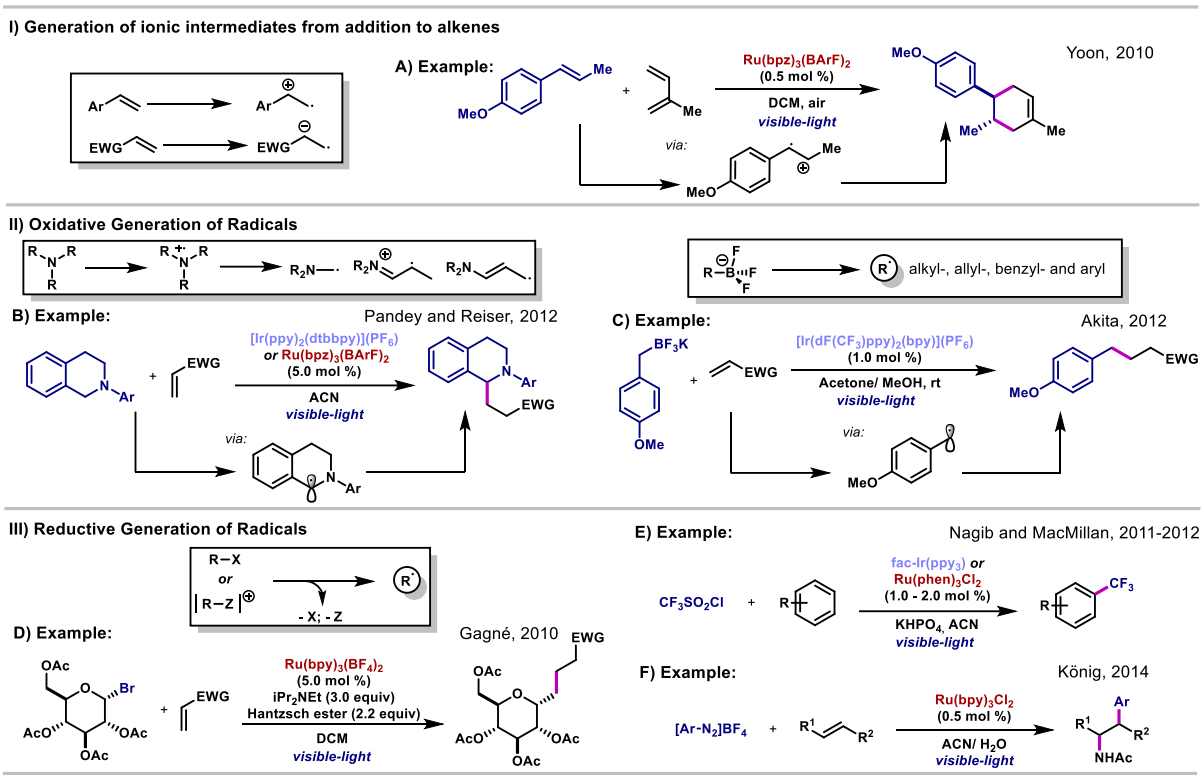

SCHEME 1.8 - Examples of seminal works disclosing new reactivities through photocatalytic one electron reactions.

Another interesting class of compounds that provide a facile and efficient access to radicals (and radical acceptors) upon SET oxidation in visible-light-driven photoredox catalysis is composed by organoborates derivatives, which have been explored as source of alkyl, allyl, benzyl and aryl radicals through a deboronation process.[30] In 2012, Akita and coworkers developed a new strategy for a photocatalytic oxidation of potassium organotrifluoroborates generating carbon-centered radicals in a redox-neutral Giese-type reaction with electron-deficient olefins (**SCHEME 1.8, C**).[30c] Molander and coworkers[31] and other researcher groups

[30] (a) KOIKE, T. & AKITA, M. "Combination of organotrifluoroborates with photoredox catalysis marking a new phase in organic radical chemistry". Org. Biomol. Chem. **14**: 6886, 2016; (b) MOLANDER, G. A. "Organotrifluoroborates: Another Branch of the Mighty Oak". J. Org. Chem. **80**: 7837, 2015; (c) YASU, Y.; KOIKE, T. & AKITA, M. "Visible light-induced selective generation of radicals from organoborates by photoredox catalysis". Adv. Synth. Catal. **354**: 3414, 2012.

[31] For recent examples, see: (a) YI, J.; BADIR, S. O.; ALAM, R. & MOLANDER, G. A. "Photoredox-catalyzed multicomponent Petasis reaction with alkyltrifluoroborates". Org. Lett. **21**: 4853, 2019 (b) CAMPBELL, M. W.; COMPTON, J. S.; KELLY, C. B. & MOLANDER, G. A. J. Am. Chem. Soc. **51**: 20069, 2019; (c) YUAN, M.; SONG, Z.; BADIR, S. O.; MOLANDER, G. A. & GUTIERREZ, O. "On the nature of C(sp^3)–C(sp^2) bond formation in nickel-catalyzed tertiary radical cross-couplings: a case study of Ni/photoredox catalytic cross-coupling of alkyl radicals and aryl halides". J. Am. Chem. Soc. **15**: 7225, 2020; (d) PRIMER, D. N. & MOLANDER, G. A. "Enabling the cross-coupling of tertiary organoboron nucleophiles through radical-mediated alkyl transfer". J. Am. Chem. Soc. **139**: 9847, 2017; (e) AMANI, J. & MOLANDER, G. A. "Direct conversion of carboxylic acids to alkyl ketones". Org. Lett. **13**: 3612, 2017; (f) MATSUI, J. K.; PRIMERA, D. A. & MOLANDER, G. A. "Metal-free C–H alkylation of heteroarenes with alkyltrifluoroborates: a general protocol for 1°, 2° and 3° alkylation". Chem. Sci. **8**: 3515, 2017; (g) MATSUI, J. K. &

today are still elegantly exploring this catalytic approach in more complex settings and dual catalytic protocols, demonstrating the versatility of such reactive species.

Moving into the direction of seminal photoredox reductive protocols, after the initial reports of Nicewicz and MacMillan in 2008 demonstrating the asymmetric intermolecular *α*-alkylation of aldehydes with activated alkyl bromides, and the Stephenson's work of tin-free reductive dehalogenation of alkyl halides, Gagné showed an intermolecular reductive visible-light-mediated conjugate addition of glycosyl halides to activated alkenes, enabling the rapid construction of *C*-glycosides with exclusive α-selectivity (**SCHEME 1.8, D**).[32] Later on, the remarkable work of Nagib and MacMillan introduced the direct trifluoromethylation of aryl and heteroaryl compounds via single-electron transfer reduction of triflyl chloride by means of oxidation of $^*Ru(phen)_3^{2+}$.[33] The generation of the electrophilic radical $\bullet CF_3$ is favorable and driven by the elimination of dimethyl sulfoxide and chloride and could be smoothly incorporated in a selective fashion to biologically active molecules (**SCHEME 1.8, E**). As a representative example of other excellent source of aryl radicals, the use of diaryldiazonium salts have been considered an alternative to the use of aryl halides for the generation of radical intermediates in photocatalytic protocols due to their relatively high reduction potentials.[34] The König's group has developed several photoredox approaches for arylation reactions with aryl diazonium salts.[35]

MOLANDER, G. A. "Organocatalyzed, photoredox heteroarylation of 2-trifluoroboratochromanones via C–H functionalization". Org. Lett. **19**: 950, 2017; (h) AMANI, J. & MOLANDER, G. A. "Synergistic photoredox/nickel coupling of acyl chlorides with secondary alkyltrifluoroborates: dialkyl ketone synthesis". J. Org. Chem. **82**: 1856, 2017; (i) HEITZ, D. R.; RIZWAN, K. & MOLANDER, G. A. "Visible-light-mediated alkenylation, allylation, and cyanation of potassium alkyltrifluoroborates with organic photoredox catalysts". **81**: 7308, 2016; (j) KARIMI-NAMI, R.; TELLIS, J. C. & MOLANDER, G. A. "Single-electron transmetalation: protecting-group-independent synthesis of secondary benzylic alcohol derivatives via photoredox/nickel dual catalysis". Org. Lett. **18**: 2572, 2016; (k) AMANI, J.; SODAGAR, E. & MOLANDER, G. A. "Visible light photoredox cross-coupling of acyl chlorides with potassium alkoxymethyltrifluoroborates: synthesis of *α*–alkoxyketones". Org. Lett. **18**: 732, 2016; (l) Ryu, D.; Primer, D. N.; Tellis, J. C. & Molander, G. A. Chem. Eur. J. **22**: 120, 2016; (m) KHATIB, M. E.; SERAFIM, R. A. M. & MOLANDER, G. A. "α-Arylation/heteroarylation of chiral α-aminomethyltrifluoroborates by synergistic iridium photoredox/nickel cross-coupling catalysis". Angew. Chem. Int. Ed. **55**: 254, 2016; (n) YAMASHITAA, Y.; TELLISA, J. C. & MOLANDER, G. A. "Protecting group-free, selective cross-coupling of alkyltrifluoroborates with borylated aryl bromides via photoredox/nickel dual catalysis". PNAS. **112**: 12026, 2015; (o) KARAKAYA, I.; PRIMER, D. N. & MOLANDER, G. A. "Photoredox cross-coupling: Ir/Ni dual catalysis for the synthesis of benzylic ethers". Org. Lett. **17**: 3294, 2015.

[32] ANDREWS, R. S.; BECKER, J. J. & GAGNÉ, M. R. "Intermolecular addition of glycosyl halides to alkenes mediated by visible light". Angew. Chem. Int. Ed. **49**: 7274, 2010.

[33] NAGIB, D. A. & MACMILLAN, D. W. C. "Trifluoromethylation of arenes and heteroarenes by means of photoredox catalysis". Nature. **480**: 224, 2011.

[34] BABU, S. S.; MUTHURAJA, P.; YADAV, P. & GOPINATH, P. "Aryldiazonium salts in photoredox catalysis – recent trends". Adv. Synt. Catal. **363**: 1782, 2021.

[35] (a) HARI, D. P.; SCHROLL, P. & KÖNIG, B. "Metal-free, visible-light-mediated direct C–H arylation of heteroarenes with aryl diazonium salts". J. Am. Chem. Soc. **134**: 2958, 2012; (b) HARI, D. P.; HERING, T. & KÖNIG, B. "Visible light photocatalytic synthesis of benzothiophenes". Org. Lett. **14**: 5334, 2012; (c) SCHROLL, P.; HARI, D. P. &

After the demonstration of the photocatalyzed direct C−H bond arylation of heteroarenes with aryl diazonium salts using eosin Y as a catalyst, his group showed the first example of a photocatalytic Meerwein addition reaction enabling C_{alky}-N bonds forging via an intermolecular amino-arylation of alkenes mediated by visible light (**SCHEME 1.8, F**).[36] The reaction operates through the generation of the aryl radical by a single-electron transfer from the excited state of the photocatalyst to the diazonium salt, followed by addition to the alkene to furnish the corresponding radical intermediate which after oxidation, nitrile addition and hydrolysis provides the amino arylated product.

After these initial innovative works, the field of photoredox catalysis has experienced rapid expansion over the last decade and is considered an important trend in the synthetic chemistry landscape. The variety of well-known photocatalysts capable of surpassing more than 60 kcal/mol of visible light energy to activate redox-labile substrates,[37] as well as the knowledge of their essential parameters for the development of new catalysts, have allowed new transformations to be exploited in an environmentally friendly, mild, and efficient way.

Given this intense focus on visible-light driven methodologies, there is a rich radical precursor toolbox available from feedstock chemicals, which have been shown impressive functional group compatibility and allowed multiple transformations with a wide range of reactional partners (**SCHEME 1.9**).[38] The **SCHEME 1.9** presents some well-known classes of radical precursors used in these protocols, as well as select examples of reaction components which these transformations engage with. The methodologies of reductive/oxidative decarboxylation (from *N*-hydroxyphytalimides and carboxylic acids, respectively), de-halogenation, deboronation from organoborates, oxidation of silicates and reduction of derivatives prepared from alcohols are part of the arsenal of useful and versatile reagents employed in this catalysis. As reactional partners, olefins and activated alkynes, alkynyls and allyl sulfones, within others have been successfully explored. It is important to emphasize the contribution of the protocols based on photoredox/Ni dual catalysis, employing electrophilic coupling partners such as (hetero)aryl bromides and several new classes of C(sp^2)-hybridized substrates, broadening the scope of this photocatalytic field.[37]

KÖNIG, B. “Photocatalytic arylation of alkenes, alkynes and enones with diazonium salts”. ChemistryOpen. **1**: 130, 2012; (d) T. HERING, D. P. HARI AND B. KÖNIG. J. Org. Chem. **77**: 10347, 2012.

[36] HARI, D. P.; HERING, T. & KÖNIG, B. “The photoredox-catalyzed Meerwein addition reaction: intermolecular amino-arylation of alkenes”. Angew. Chem. Int. Ed. **53**: 725, 2014.

[37] MATSUI, J. K.; LANG, S. B.; HEITZ, D. R. & MOLANDER, G. A. “Photoredox-mediated routes to radicals: the value of catalytic radical generation in synthetic methods development”. ACS Catal. **7**: 2563, 2017.

[38] ROSLIN, S. & ODELL, L. R. “Visible-light photocatalysis as an enabling tool for the functionalization of unactivated C(sp^3)-substrates”. Chem. Eur. J. **15**: 1993, 2017.

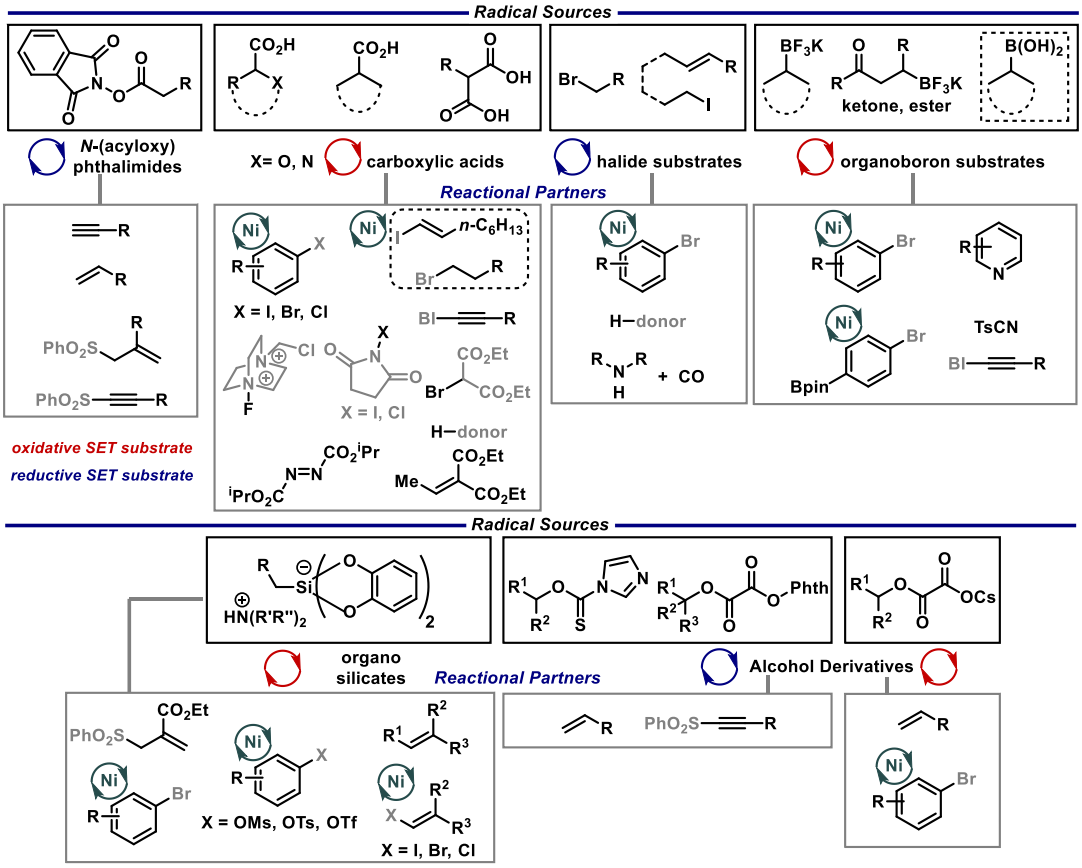

SCHEME 1.9 - Selected examples from the radical toolbox explored in the photocatalytic reactions.

1.2 Photogenerated α-Aminoalkyl Radicals: Synthetic Applications

Another class of useful radical precursors that will be discussed in more detail in this section is composed by amines, which are considered versatile building blocks in organic synthesis and represent a key scaffold given their well-known relevance, with high predisposition to exhibits biological activities. Most molecules structurally important to the agrochemical and pharmaceutical sectors contain amino groups and are commonly present in drug discovery programs (**FIGURE 1.6**). Given such relevance, the development of new synthetic protocols that are more efficient, broad, environmentally friendly, and accessible are highly desired and one of the main targets in chemistry research.

The functionalization of the C(sp^3)-H bonds α to the nitrogen atom has been adopted as a synthetic strategy that allows the direct preparation of derivatives containing the amino group and opens up possibilities for chemical space diversification by introducing structural complexity.

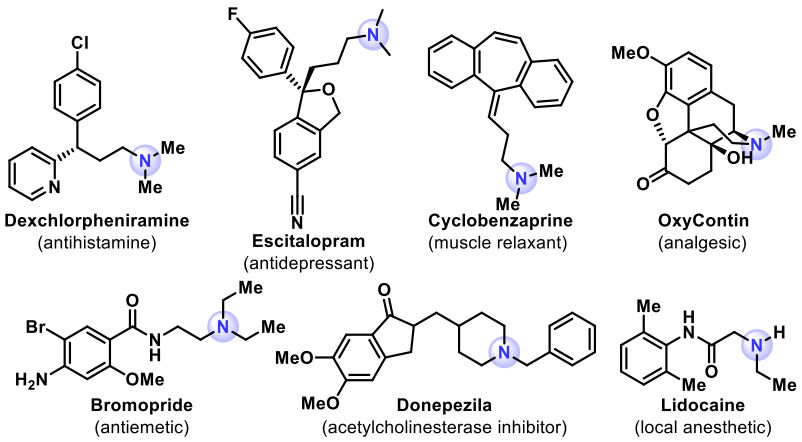

FIGURE 1.6 - Selected pharmaceuticals containing the amine group.

The methods usually employed for such transformations rely on the formation of reactive intermediates as α -amino cations, α -amino anions and α -amino radicals (**FIGURE 1.7**). The generation of the latter specie is well described, and traditional methodologies are based on energetic UV irradiation, use of stoichiometric photosensitizers and tin hydride based synthetic protocols.[39]

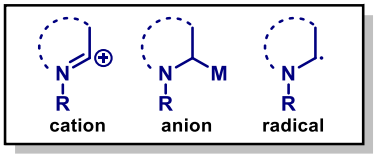

FIGURE 1.7 - Reactive intermediates for the functionalization of C(sp^3)-H bonds alpha to the nitrogen atom.

The growing advances in the visible light-driven methodologies have made the exploration of the transformations based on the generation of α-amino radicals receiving special attention over the last years, mainly by giving access to the preparation of such relevant structures under milder conditions, allowing high tolerance to functional groups and the use of more complex scaffolds.

The seminal works disclosed by Yoon,[22] MacMillan [23] and Stephenson[24] demonstrated the reactivity of amines as efficient quenchers of the photoexcited state of the *$Ru(pby)_3^{2+}$ photocatalyst, leading to its strongly reducing Ru^+ specie, key to subsequent reaction pathways (**SCHEME 1.10, A**). Initially, the use of these electron-rich species as additives in photocatalytic mechanisms was recognized, however, later on, amines began to be explored in relation to their

[39] (a) MITCHELL, E. A.; PESCHIULLI, A.; LEFEVRE, N.; MEERPOEL, L. & MAES, B. U. W. "Direct α-functionalization of saturated cyclic amines". Chem. Eur. J. **18**: 10092, 2012; (b) HOFFMANN, N. "Photochemical reactions as key steps in organic synthesis". Chem. Rev. **108**: 1052, 2008; (c) FAGNONI, M.; DONDI, D.; RAVELLI, D.; ALBINI, A. "Photocatalysis for the formation of the C-C bond". Chem. Rev. **107**: 2725, 2007.

synthetic potential as a source of reactive intermediate - thus representing a direct strategy for accessing nitrogen-containing compounds.

Given their electron-rich nature, amines are easily oxidized under photocatalytic conditions and allow the generation of α-amino nucleophiles (**SCHEME 1.10, B**). As known, the amines are efficient electron donors in SET processes and, due to their low oxidation potential, are easily oxidized to the corresponding *N*-centered radical cation **I**. The *α*-aminoalkyl radical **II** is then formed after proton removal and further oxidation (or loss of a hydrogen radical) can generates the iminium ion **III**.

From the single electron oxidation of neutral amines, the C-H bond adjacent to the nitrogen atom is weakened to approximately 42 kcal.mol^{-1} and deprotonation can easily take place leading to the generation of the corresponding *α*-amino radical and proton (**SCHEME 1.10, C**).[28a,40] Regarding this process, specific studies have demonstrated the mechanistic pathways by which the amines are susceptible to form the radical cations and provide C-H functionalized compounds.[41]

Other strategies for the generation of these nucleophilic radicals relies on the use of α-silylamines and α-amino acids, which through desilylation and decarboxylation, respectively, provide the radical cations very efficiently.

The control of the degree of oxidation of the amines is a determining factor in achieving the synthesis of the corresponding α-amino radicals, since these latter are even more prone to oxidation than the starting reagent [($E_{1/2\ (cation\ radical)}$ = −1.03 V *vs* SCE) *vs* ($E_{1/2\ (amine)}$ = +1.15 V *vs* SCE)] leading thus to the formation of the corresponding iminium ion - usually in the presence of excess of oxidant.[40] These species have also been explored in several classes of transformations with nucleophiles and represent another aspect of the use of α-amino radicals.

[40] WAYNER, D. D. M.; DANNENBERG, J. J. & GRILLER, D. “Oxidation potentials of *α*-amino radicals: bond dissociation energies for related radical cations”. Chem. Phys. Lett. **131**: 189, 1986.

[41] (a) ZHANG, X.; YEH, S.-R.; HONG, S.; FRECCERO, M.; ALBINI, A.; FALVEY, D. E. & MARIANO, P. S. “Dynamics of *α*-CH deprotonation and *α*-desilylation reactions of tertiary amine cation radicals”. J. Am. Chem. Soc. **116**: 4211, 1994; (b) ANNE, A.; HAPOIT, P.; MOIROUX, J.; NETA, P. & SAVEANT, J.-M. “Dynamics of proton transfer from cation radicals. kinetic and thermodynamic acidities of cation radicals of NADH analogues”. J. Am. Chem. Soc. **114**: 4694, 1992; (c) LEWIS, F. D.; HO, T.-I. & SIMPSON, J. T. “Photochemical addition of tertiary amines to stilbene. Stereoelectronic control of tertiary amine oxidation”. J. Org. Chem. **46**: 1077, 1981; (d) LEWIS, F. D. & HO, T.-I. “On the selectivity of tertiary amine oxidations”. J. Am. Chem. Soc. **102**: 1751; 1980.

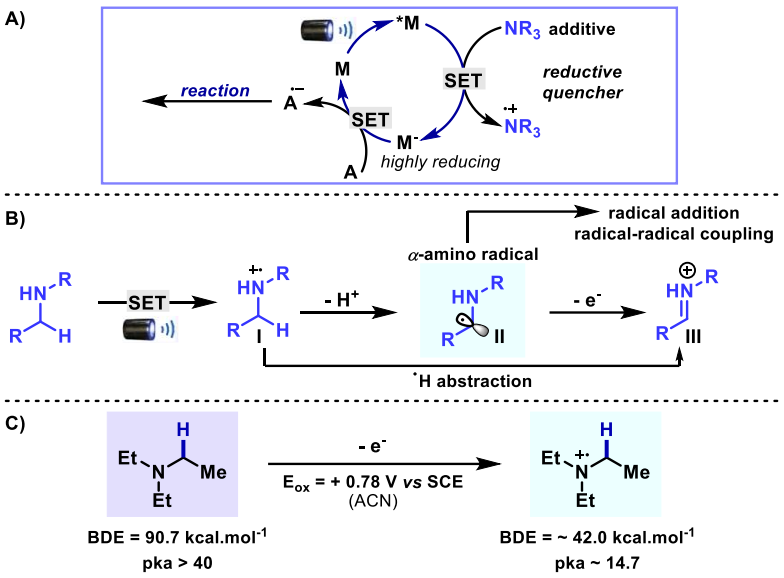

SCHEME 1.10 - A) Use of electron rich amines as additives in photoredox protocols. B) The generation of α-aminoalkyl radicals. C) Effects on the BDE and pka after the radical cation formation.

Although the formation of α-amino radicals via electrochemical oxidation of Et_3N in the presence of Ru(II) complexes had already been reported in 1977,[42] this strategy received more visibility with the development of the concepts of photoredox catalysis. Innovative methodologies involving the generation of reactive radical cationic intermediates from amines and subsequent couplings/additions to different reaction partners allowed the establishment of a direct and efficient C-H activation mode adjacent to nitrogen.

The advantage of using feedstock starting materials and milder reaction conditions led to a rapid expansion of this synthetic approach, mainly explored for the nucleophilic addition of *α*-amino radicals to olefins. As previously mentioned, one of the seminal works inaugurating the field of photoredox catalysis involved the addition of these reactive intermediates to α,β-unsaturated ketones,[29] which specifically reported the study of radicals generated from SET oxidation of *N*-aryl-1,2,3,4-tetrahydroisoquinoline derivatives. Nishibayashi, at the same time, reported a similar addition to activated olefins by using cyclic and acyclic amines, expanding the scope of this transformation.[43] In a subsequent work, important for the establishment of this synthetic approach, Melchiorre elegantly reported an asymmetric addition protocol via dual-catalysis to release cyclic enones making use of the organocatalysis principles for such

[42] HAYASHI, T. & HEGEDUS, L. S. "Photoinduced redox reactions of hydrophobic ruthenium (II) complexes". J. Am. Chem. Soc. **99**: 7094, 1977.

[43] MIYAKE, Y.; NAKAJIMA, K. & NISHIBAYASHI, Y. "Visible-light-mediated utilization of α-aminoalkyl radicals: addition to electron-deficient alkenes using photoredox catalysts". J. Am. Chem. Soc. **134**: 3338, 2012.

advancement.[44] Building in these inaugural works, MacMillan,[45] Doyle,[45e] Molander[46] and many other researches[47] have demonstrated the applicability of this concept in a range of transformations. It is worth noting the advances in this field in relation to the asymmetric synthesis of amines, involving photoredox protocols with chiral catalysts and auxiliaries.[48]

Addition of α-amino radicals to C=N bonds

Still considering the relevance of nitrogen-containing compounds, the functionalization of C=N bonds represents a powerful tool for the preparation of these key structures. Moving to the functionalization of imines and derivatives as acceptors under visible light photoredox catalysis as a contemporary approach, some remarkable achievements by means of the α-amino radical chemistry will be addressed.

The *α*-aminoalkyl radical intermediates can engage in reactions with imines and other C=N containing compounds by two different complementary mechanisms: 1) the first makes use of the innate electrophilicity of imines and derivatives and proceeds via addition of the nucleophilic α-amino radical, 2) the second possible reactional pathway involves the one electron reduction of imines followed by a radical-radical coupling with the α-amino radical generated upon SET oxidation. Both approaches have proven to be excellent strategies to achieve structural diversification through the insertion of amino functionalities in a single step.

Following their initial synthetic disconnection for the visible-light-mediated α-alkylation of amines with activated olefins,[49] Nishibayashi and coworkers then extended the protocol for the

[44] MURPHY, J. J.; BASTIDA, D.; PARIA, S.; FAGNONI, M. & MELCHIORRE, P. "Asymmetric catalytic formation of quaternary carbons by iminium ion trapping of radicals". Nature. **532**: 218, 2016.

[45] (a) NOBLE, A.; MCCARVER, S. J. & MACMILLAN, D. W. C. "Merging photoredox and nickel catalysis: decarboxylative cross-coupling of carboxylic acids with vinyl halides". J. Am. Chem. Soc. **137**: 624, 2015; (b) JEFFREY, J. L.; PETRONIJEVIĆ, F. R. & MACMILLAN, D. W. C. "Selective radical-radical cross-couplings: design of a formal *β*-Mannich reaction". J. Am. Chem. Soc. **137**: 8404, 2015; (c) NOBLE, A. & MACMILLAN, D. W. C. "Photoredox *α*-vinylation of *α*-amino acids and *N*-aryl amines". J. Am. Chem. Soc. **136**: 11602, 2014; (d) TERRETT, J. A.; CLIFT, M. D. & MACMILLAN, D. W. C. "Direct *β*-alkylation of aldehydes via photoredox organocatalysis". J. Am. Chem. Soc. **136**: 6858, 2014; (e) ZUO, Z.; AHNEMAN, D. T.; CHU, L.; TERRETT, J. A.; DOYLE, A. G. & MACMILLAN, D. W. C. "Merging photoredox with nickel catalysis: coupling of *α*-carboxyl sp^3-carbons with aryl halides". Science. **345**: 437, 2014; (f) PIRNOT, M. T.; RANKIC, D. A.; MARTIN, D. B. C. & MACMILLAN, D. W. C. "Photoredox activation for the direct *β*-arylation of ketones and aldehydes". Science **339**: 1593, 2013.

[46] (a) EL KHATIB, M.; SERAFIM, R. A. M. & MOLANDER, G. A. *α*-Arylation/heteroarylation of chiral *α*-aminomethyltrifluoroborates by synergistic iridium photoredox/nickel cross-coupling catalysis. Angew. Chem., Int. Ed. **55**: 254, 2016; (b) TELLIS, J. C.; PRIMER, D. N. & MOLANDER, G. A. "Single-electron transmetalation in organoboron cross-coupling by photoredox/nickel dual catalysis". Science. **345**: 433, 2014.

[47] AYCOCK, R. A.; PRATT, C. J. & JUI, N. T. "Aminoalkyl radicals as powerful intermediates for the synthesis of unnatural amino acids and peptides". ACS Catal. **8**: 9115, 2018.

[48] CULLEN, S. T. J. & FRIESTAD, G. K. "Synthesis of chiral amines by C–C bond formation with photoredox catalysis". Synthesis. **53**: 2319, 2021.

functionalization of azodicarboxylate esters in a radical-radical type mechanism with *N*-tetrahydroisoquinoline derivatives to give a C-N bond formation at its α-position (**SCHEME 1.11, A**).[49] Later, Li demonstrated the applicability of the method with isocyanates and isothiocyanates aiming at the synthesis of α-amino amide or α-amino thioamide from *N*,*N*-dimethylanilines (**SCHEME 1.11, B**).[50]

After the pioneering work showcasing the photoredox-catalyzed reductive dimerization of carbonyl compounds and imines,[51] Rueping's group reported a photocatalytic method for the synthesis of unsymmetric 1,2-diamines in a radical-radical aldimine–aniline coupling (**SCHEME 1.11, C**).[52] In this protocol, the reductive SET umpolung of the aldimine is the key step. A remarkable use of the persistent secondary α-amino radical anion was disclosed by Ooi and coworkers in an enantioselective transformation mediated by a chiral ionic Brønsted acid and photoredox catalysis. The highly enantioselective *α*-coupling of *N*-arylaminomethanes with *N*-sulfonyl imines using a *P*-spiro chiral arylaminophosphonium barfate and Ir-based photosensitizer under visible light irradiation was achieved and opened up new avenues for controlling the bond-forming processes of reactive radical intermediates (**SCHEME 1.11, D**).[53] The key control of the stereoselective pathway is given to the affinity of the *N*-sulfonyl imines anion radical to the hydrogen (H)-bond donor catalyst, leading to the enantioselective coupling with the aminomethyl radical through the chiral ionic pair showed in the **SCHEME 1.11, D**.

[49] MIYAKE, Y.; NAKAJIMA, K. & NISHIBAYASHI, Y. "Direct sp^3 C-H amination of nitrogen-containing benzoheterocycles mediated by visible-light-photoredox catalysts". Chem. - Eur. J. **18**: 16473, 2012.

[50] ZHOU, H.; LU, P.; GU, X. & LI, P. "Visible-light-mediated nucleophilic addition of an *α*-aminoalkyl radical to isocyanate or isothiocyanate". Org. Lett. **15**: 5646, 2013.

[51] NAKAJIMA, M.; FAVA, E.; LOESCHER, S.; JIANG, Z. & RUEPING, M. "Photoredox-catalyzed reductive coupling of aldehydes, ketones, and imines with visible light". Angew. Chem. Int. Ed. **54**: 8828, 2015.

[52] FAVA, E.; MILLET, A.; NAKAJIMA, M.; LOESCHER, S. & RUEPING, M. "Reductive umpolung of carbonyl derivatives with visible-light photoredox catalysis: direct access to vicinal diamines and amino alcohols via α-amino radicals and ketyl radicals". Angew. Chem. Int. Ed. **55**: 6776, 2016.

[53] URAGUCHI, D.; KINOSHITA, N.; KIZU, T. & OOI, T. "Synergistic catalysis of ionic Brønsted acid and photosensitizer for a redox neutral asymmetric *α*-coupling of *N*-arylaminomethanes with aldimines". J. Am. Chem. Soc. **137**: 13768, 2015.

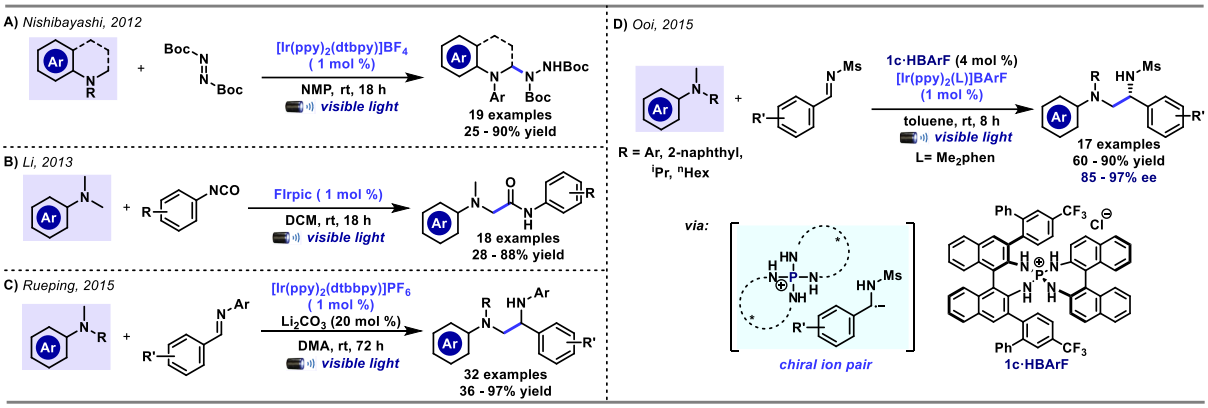

SCHEME 1.11 - Seminal works on photocatalytic functionalization of C=N bonds via addition of α-amino radicals.

After these pioneering works, this functionalization strategy from α-aminoalkyl radicals has undergone a rapid evolution and the current challenges lie in transformations from more complex substrates, multicomponent and stereoselective reactions and in the use of new acceptors to expand its applicability.

1.3 Exploration of 1,3-Dipoles of Azomethine Imines in Synthesis

Regarding to the exploration of versatile and structurally relevant substrates, azomethine imines are compounds derived from imines of recognized synthetic application due to their reactivity as 1,3-dipoles and given the presence of the heterocycle nucleus of pyrazolidinone in their structure.

Azomethine imines are allylic-type dipoles found under four main structural forms comprising 1) acyclic structures, 2) *N*,*N*'- and 3) *C*,*N*'-cyclic azomethine imines, and 4) those with all atoms included in the cyclic system (**FIGURE 1.8, A**).[54] Some of these compounds are unstable and difficult to isolate, mainly related to acyclic structures. Thus, the preparation of species containing a carbonyl substituent alpha to the terminal azomethine imine nitrogen allowed to bring stability to these structures, which can be easily manipulated and readily employed in synthetic methodologies. In this section, the use of structures of the type (*Z*)-*N*,*N*'-cyclic **I'**[61] will be emphasized and it will be represented in the mesomeric form **I**,[55] although it can be considered a resonance hybrid between the species of iminium ylide and diazonium ylide represented in the **FIGURE 1.8, B**.

[54] BELSKAYA, N. P.; BAKULEV, V. A. & FAN, Z. "Synthesis and (3+2) cycloaddition reactions of *N*,*N*'- and *C*,*N*'-cyclic azomethine imines". Chemistry of Heterocyclic Compounds. **52**: 627, 2016.

[55] (a) ESS, D. H. & HOUK, K. N. "Distortion/interaction energy control of 1,3-dipolar cycloaddition reactivity". J. Am. Chem. Soc. **129**: 10646, 2008; J. Am. Chem. Soc. "Theory of 1,3-dipolar cycloadditions: distortion/interaction and frontier molecular orbital models". **130**: 10187, 2008; (c) HOUK, K. N. & YAMAGUCHI, K. In 1,3-Dipolar Cycloaddition Chemistry; Padwa, A., Ed.; John Wiley & Sons, Inc.: New York, 1984, Vol. 2, p. 407.

Type **I'** dipoles are generally prepared through two reaction steps: the first involves the preparation of the pyrazolidinone ring through the addition of hydrazine monohydrate to methyl acrylate in refluxing EtOH, followed by a condensation reaction with the aldehyde species at room temperature in EtOH.[56] Thus, from readily available substrates, it is possible to access a large library of these versatile materials.

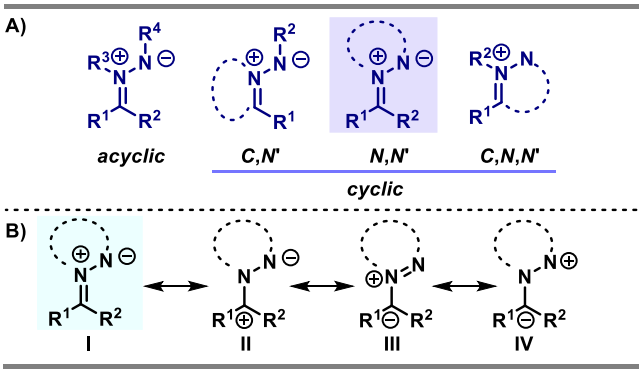

FIGURE 1.8 - A) The structural and B) mesomeric forms of azomethine imines.

The class of cycloaddition reactions is considered one of the most classical transformations in organic synthesis and since the establishment of the principles of 1,3-dipolar cycloaddition by Huisgen,[57] azomethine imines have already had their synthetic potential recognized in this chemistry as potent dipoles of rich structural nature.[58]

Although less explored than other 1,3-dipoles, such as azomethine ylides, nitrones, and nitrile oxides, the (*Z*)-*N*,*N*'-cyclic azomethine imines have been considered key starting materials in cycloaddition reactions. The (3+2) cycloadditions are considered extremely useful synthetic tools for the regioselective synthesis of (partially)saturated five membered heterocyclics in a direct way with a wide variety of dipolarophiles as olefins, alkynes, enones, isocyanides, and allenes.[59] Adding even more value to these compounds, several methodologies have been developed by employing metal catalysis, organocatalysis and dual-catalysis for the enantioselective construction of these heterocycles; extremely desirable in the transformations where multiple centers are formed at the same time.

---

[56] WINTERTON, S. E. & READY, J. M. "[3 + 2]-Cycloadditions of azomethine imines and ynolates". Org. Lett. **18**: 2608, 2016.

[57] HUISGEN, R.; FLEISCHMANN, R. & ECKELL, A. "Azomethin-imine, eine neue. Klasse zwitterionischer Verbindungen". Tetrahedron Lett. **12**: 1, 1960; (b) HUISGEN, R. "1.3-Dipolare cycloadditionen rückschau und ausblick". Angew. Chem. **75**: 604, 1963; (c) BREUGST, M. & REISSIG, H.-U. "The Huisgen reaction: milestones of the 1,3-dipolar cycloaddition". Angew. Chem. Int. Ed. **59**: 12293, 2020.

[58] DEEPTHI, A.; THOMAS, N. V. & SRUTHI, S. L. "An overview of the reactions involving azomethine imines over half a decade". New J. Chem. **45**: 8847, 2021.

[59] GROŠELJ, U.; SVETE, J.; AL MAMARI, H. H.; POŽGAN, F. & ŠTEFANE, B. "Metal-catalyzed [3+2] cycloadditions of azomethine imines". Chemistry of Heterocyclic Compounds". **54**: 214, 2018.

In addition to the classical (3+2) cycloadditions, azomethine imines have been widely used as reaction partners in other cycloadditions aiming to obtain poly and spirocyclic compounds in only one reaction step (**SCHEME 1.12, A**). These transformations include (3+3), (4+3), (5+3) and (3+1) cycloadditions, for example, and recent literature still continues to demonstrate how versatile these species can be even after so many years of exploration of this chemistry.

All these protocols have a strong biological appeal, since pyrazolidinone and pyrazolone heterocycles derivatives are obtained. They have demonstrated prominent importance in the pharmaceutical and agrochemical sectors and, specifically, the ring of *N*,*N*-bicyclic pyrazolidinone is often found in pesticides and herbicides, and in *β*-lactam antibiotics (**SCHEME 1.12, B**).[67]

In terms of synthetic applicability, azomethine imines have been associated with their use as 1,3-dipolar reagents in (3+2) cycloadditions and other cyclizations to obtain di-nitrogenated (poly)heterocyclic compounds. However, the innate electrophilicity of these species is likely to be explored through other parallel synthetic pathways to complement the strategies to directly obtain compounds derived from pyrazolones.

Their utilization as nucleophile acceptors in addition reactions has been less explored as useful synthons in synthesis. In 2009, the first nucleophilic addition to azomethine imines was reported for an enantioselective trifluoromethylation with Me_3SiCF_3 using a chiral phase transfer catalyst.[60] Other recent advances have demonstrated the enantioselective arylation of azomethine imines by using sodium tetraarylborates as nucleophiles[61] and a protocol for the asymmetric cyanation of azomethine imines by appling a developed chiral dipeptide-derived multifunctional organophosphine catalyst[62] (**SCHEME 1.13, A**).

[60] KAWAI, H.; KUSUDA, A.; NAKAMURA, S.; SHIRO, M. & SHIBATA, N. “Catalytic enantioselective trifluoromethylation of azomethine imines with trimethyl(trifluoromethyl)silane”. Angew. Chem. Int. Ed. **48**: 6324, 2009.
[61] SHINTANI, R.; SOH, Y. -T. & HAYASHI, T. “Rhodium-catalyzed asymmetric arylation of azomethine Imines”. Org. Lett. **12**: 4106, 2010
[62] WANG, H. Y.; ZHENG, C. W.; CHAI, Z.; ZHANG, J. X. & ZHAO, G. “Asymmetric cyanation of imines via dipeptide-derived organophosphine dual-reagent catalysis”. Nat. Commun. **7**: 12720, 2016.

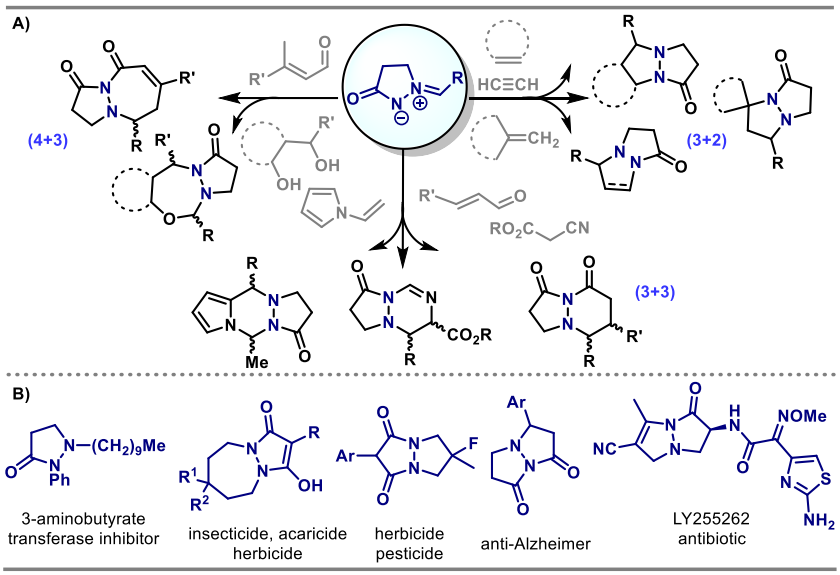

SCHEME 1.12 - A) The innate application of azomethine imines in cycloaddition reactions. B) Selected examples of biologically active compounds containing the pyrazolidinone di-nitrogenated ring.

Preliminary studies have already demonstrated the high photosensitivity of these species under UV light irradiation, as reported by Korobitsyna [63] and Tomaschewski[64] in 1983. In these works, a series of (aza)arylsubstituted pyrazolidinone-3-azomethine imines underwent photocyclization to the corresponding diaziridine upon irradiation (or heating). Next, Dorn[65] observed that phenyl and *p*-OMe-substituted phenyl pyrazolidinone-3-azomethine imines led to a small formation of centrosymmetric dimers photochemically via a [π4s + π4s] mechanism (**SCHEME 1.13, B**).

Although the reactivity of azomethine imines has been studied under photolytic conditions leading to the identification of their described cyclization/dimerization products, no study had been conducted until recently to further explore the potential of these reactive components in light-driven transformations. The establishment of photoredox catalysis led to an enormous expansion of this field, with a series of reactions described as already pointed out. However, there is still an ample opportunity to explore new protocols to forging C-C and C-X bonds.

Under these concepts, in 2019 Yang and coworkers challenged for the first time the use of *N*,*N*'-cyclic azomethine imines in a visible light-mediated photoredox protocol for their

[63] RODINA, L.; VERZHBA, O. A. & KOROBITSYNA, I. K. "Photochromism in a series of azomethinimines based on 4-phenyl-1,2,4-triazoline-3,5-dione ". Chem. Heterocycl. Com. **19**: 1345, 1983.
[64] GEISSLER, G.; FUST, W.; KRUGER, B. & TOMASCHEWSKI, G. "Azomethinimine. VII. Photochemisches und thermisches verhalten azarylsubstituierter pyrazolidon-(3)-azomethinimine". Adv. Synth. Catal. **325**: 205, 1983.
[65] DORN, T. & KREHER, H. "Addition-addition-elimination mechanism of 1,3-dipole "dimerization"". Tetrahedron Lett. **29**: 2939, 1988.

difluoroalkylation via a reductive radical–radical coupling process (**SCHEME 1.13, C**).[66] The difluorinated 3-pyrazolidinones were obtained in good to excellent yields under mild reaction conditions and showed good tolerance to a range of functional groups. The proposed mechanism for this transformation is given in the **SCHEME 1.14**.

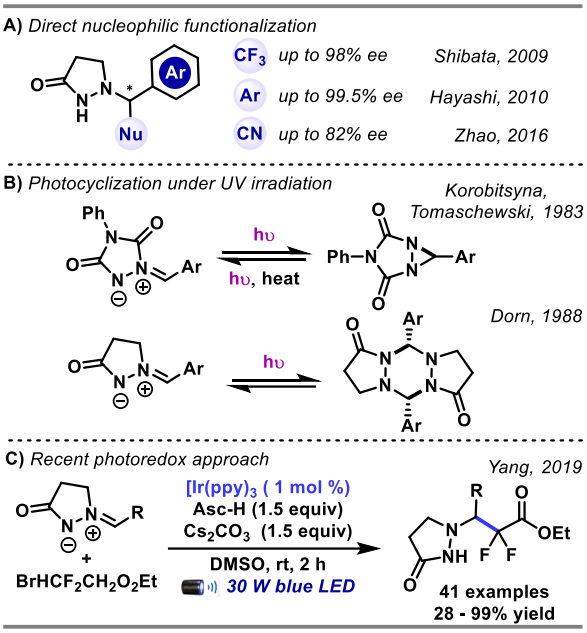

SCHEME 1.13 - A) Nucleophilic functionalization approaches and B) photosensitivity studies of azomethine imines. C) Recent photoredox approach achieving difluorinated 3-pyrazolidinones.

The highly reducing ***Ir(III)** specie (E_{red} = -1.82 V *vs*. Ag/AgCl in DMSO) generated upon visible light irradiation of the photocatalyst reduces the *N*,*N*'-cyclic azomethine imine **I** (E_{red} = -1.76 V *vs*. Ag/AgCl in DMSO) via SET leading to the radical anion **III** and **Ir(IV)**. Then, the ascorbic acid regenerates the Ir(III) photocatalyst by a SET event, and the ascorbyl radical generated from this process undergo a disproportionation reaction leveraging the dehydroascorbic acid **DAsc** and the anion ascorbate **Asc**$^-$. The latter is involved in the reduction of $BrCF_2CO_2Et$ to provide the reactive radical intermediate **IV**, which undergo a radical-radical cross-coupling with the initially generated radical **III** from the azomethine imine, giving rise, after deprotonation, to the difluorinated 3-pyrazolidinone product.

[66] XIA, P.-J.; YE, Z.-P.; SONG, D.; REN, J.-W.; WU, H. –W.; XIAO, J.-A.; XIANG, H. –Y.; CHEN, X. –Q. & YANG, H. "Photocatalytic reductive radical–radical coupling of *N*,*N*'-cyclicazomethine imines with difluorobromo derivatives". Chem. Commun. **55**: 2712, 2019.

This work represented how broad still could be the synthetic application of azomethine imines and enabled an unlock of other reactivity of these compounds.

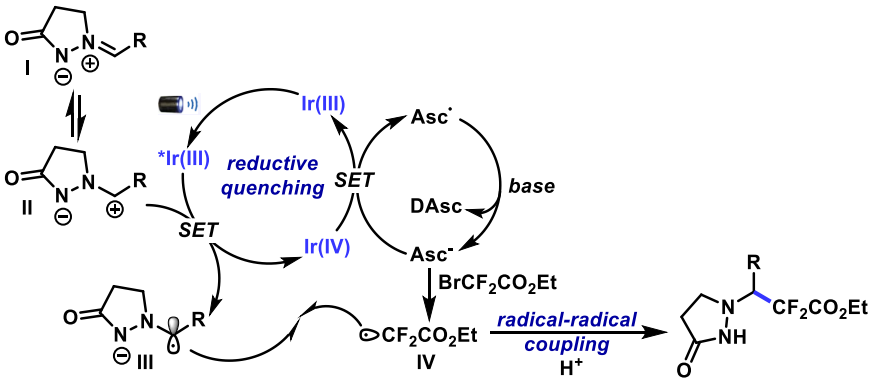

SCHEME 1.14 - Proposed mechanism for the radical–radical coupling reaction using *N*,*N*'-cyclic azomethine imines.

2. Visible-light Mediated α-Amino-Alkylation of Azomethine Imines – An Approach to *N*-(β-aminoalkyl)-pyrazolidinones

Published work: MATSUO, B. T.; CORREIA, J. T. M. & PAIXÃO, M. W. "Visible-light-mediated *α*-amino alkylation of azomethine imines: an approach to *N*-(*β*-aminoalkyl)pyrazolidinones". Org. Lett. **20**: 7891, 2020.

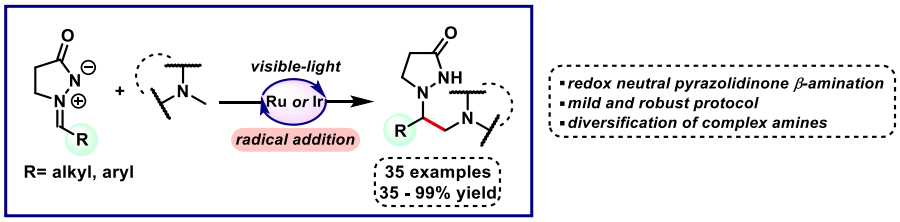

Herein, a mild and robust photocatalytic protocol for the combination of amino and pyrazolidinone functionalities through a radical *α*-amino-alkylation of azomethine iminium ions is demonstrated. This method presents a high functional group tolerance providing direct access to a large family of *N*-(*β-aminoalkyl*)-pyrazolidinones in good to excellent yields, including the *late-stage* incorporation of the pyrazolidinone moiety to pharmaceutical ingredients. We propose a plausible scenario for the C-C bond forming step which involves the radical addition followed by a spin-center-shift event.

RESULTS AND DISCUSSION

Inspired by previous reports and the scarce developments on visible-light mediated transformations of azomethine imines, we envisioned that *α*-aminoalkyl radicals would be suitable coupling partners for the development of a new photoredox azomethine imine functionalization strategy, in which they would behave as iminium-ions instead of as the well explored 1,3-dipoles. The *N*-centered radical generated after the radical addition is prone to undergo a spin-center-shift event (SCS),[67] leading to a more stabilized amidyl radical which supports the feasibility of this proposal. This approach could yield densely functionalized *N*-(*β*-aminoalkyl) pyrazolidinones under mild reaction conditions.

To evaluate the feasibility of this radical addition protocol, we started by studying the coupling of *N,N*-dimethylaniline **2a** (E_{ox}= 0.80 V *vs* SCE at 20 °C in MeCN)[68] with azomethine

[67] NACSA, E. D. & MACMILLAN, D. W. C. "Spin-center shift-enabled direct enantioselective *α*-benzylation of aldehydes with alcohols". J. Am. Chem. Soc. **140**: 3322, 2018.
[68] LUO, P.; FEINBERG, A. M.; GUIRADO, G.; FARID, S. & DINNOCENZO, J. P. "Accurate oxidation potentials of 40 benzene and biphenyl derivatives with heteroatom substituents". *J.* Org. Chem. **79**: 9297, 2014.

imine **1a**, using K_2CO_3 as base and in the presence of a series of photocatalysts **PC** (**SCHEME 1.15**).

SCHEME 1.15 – Model reaction for the reaction optimization.

The selected photocatalysts for this study are represented in **FIGURE 1.9** below, as well as their fundamental electrochemical characteristics for the viable planning of the transformation. Considering that tertiary amines are easily oxidized and based on previous reports in the literature, we assume that this reaction would be initiated by a reductive quenching of the photocatalyst leading to the generation of the corresponding *α*-amino radical in the presence of base. Thus, considering E_{ox} 2a = 0.80 V *vs* SCE, the photocatalysts present a reduction potential that matches this value for the SET event takes place.

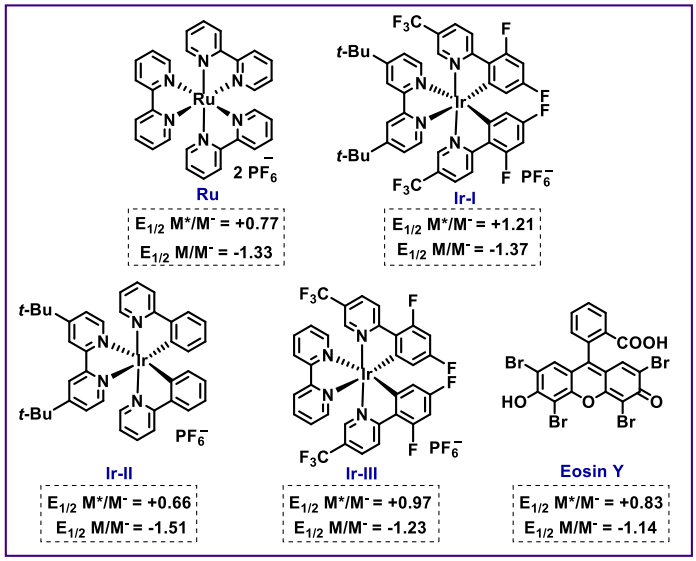

FIGURE 1.9 - Electrochemical characteristics of the screened photocatalysts.

To our delight, during the initial studies in acetonitrile**,** using 3 equivalents of K_2CO_3 as base and the ruthenium-based photocatalyst $[Ru(bpy)_3](PF_6)_2$ (**Ru**) ($E_{1/2}(M^{(II)*}/M^{(I)})$ = +0.77 V *vs* SCE in MeCN)[11] under blue LED irradiation (36 W Kessil H150 lamp λ= 456 nm) at room temperature the desired product **3a** was obtained in quantitative yield (**Table 1.1**, **entry 1**). Gratifyingly, little optimization was required for this transformation. Likewise, iridium-based photocatalysts (**Ir-I**, **II** and **III**) were also tested and successfully furnished **3a** in excellent yields

(**entries 2-4**). In this case, a slightly reduction in the yield was observed when the **Ir-II** photocatalyst was applied, probably due to the lower reduction potential of its excited state ***Ir-II**. When the reaction was conducted in the absence of base, only traces of **3a** were observed, showing that its presence is crucial for the generation of the desired initial radical intermediate (**entry 5**).

Organic dyes have been considered a greener alternative to transition metal complexes in photoredox catalysis and, particularly, **Eosin Y** has demonstrated outstanding reactivity in visible-light-mediated reactions.[69] Taking it into consideration, we evaluated the use of **Eosin Y** ($E_{1/2}(M^*/M^-)$ = +0.83 V *vs* SCE in MeCN) in our protocol since it exhibits similar electrochemical characteristics to Ru (II) photocatalyst.[70] This organic photocatalyst has maximum absorbance at $\lambda = 539$ nm and we evaluated its efficiency to promote the proposed transformation under green LED irradiation.
However, **Eosin Y** was not efficient in promoting the transformation (**entry 6**) and only traces of product were noticed.

Given the excellent results obtained with the metal complex catalysts, we chose to continue the development of our protocol by using the **Ru** catalyst due to its accessibility - considering 50 mg of photocatalyst in the Sigma's Aldrich Brazil website: **Ru** (BRL 54.55); **Ir-I** (BRL 375.00); **Ir-II** (BRL 420.00) and **Ir-III** (BRL 479.00).

Attempting in decrease catalyst amount, the photocatalyst loading to 0.5 mol% led to an erosion in the chemical yield of **3a** (**entry 7**). Moreover, the reaction time could be reduced to 7 h without affecting the yield (**entry 8**).

Ultimately, control experiments were carried out and demonstrated that the cooperative role between the photocatalyst, visible-light irradiation source and the degassed condition was essential for the effectiveness of the reaction outcome (**entries 9-11, respectively**).

Additional experiments were performed in an attempt to simplify the reaction conditions even further and the **SCHEME 1.16** reveals the details of this optimization. Regarding the reaction solvent, other polar solvents were evaluated and the transformation in DMSO or DMA were similarly highly efficient (**SCHEME 1.16, A**). Given the facility of working with the solvent of lower boiling point, we kept the use of MeCN in our protocol. Moreover, regarding the reaction

[69] HARI, D. P. & KÖNIG, B. "Synthetic applications of eosin Y in photoredox catalysis". Chem. Commun. **50**: 6688, 2014.
[70] FIDALY, K.; CEBALLOS, C.; FALGUIÈRES, A.; VEITIA, M. S.-I.; GUY, A. & FERROUD, C. "Visible light photoredox organocatalysis: a fully transition metal-free direct asymmetric *α*-alkylation of aldehydes". Green Chem. **14**: 1293, 2012.

time, further experiments revealed that this transformation occurs extremely efficiently in 3h, reducing the time found in the initial optimization. By reducing this reaction time by half, in 1.5h, on the contrary, demonstrated to have a great impact on the yield of the *N*-(*β*-aminoalkyl)pyrazolidinone of interest.

Table 1.1 - Optimization of reaction conditions[a]

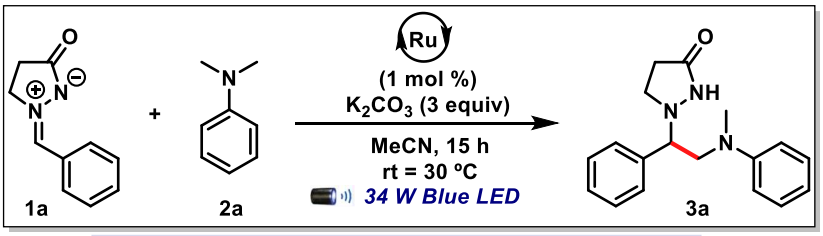

entry	deviation from standard conditions	3a (%)[b]
1	**none**	99
2	**Ir-I** instead of Ru	99
3	**Ir-II** instead of Ru	95
4	**Ir-III** instead of Ru	99
5	**Ir-I** and no base	traces
6[c]	**Eosin Y** instead of Ru	traces
7	**0.5 mol%** of Ru	84
8	reactional time of **7h**	98
9	no photocatalyst	nr
10	without LED	nr
11	without degassing	37

Reaction conditions: **1a** (0.15 mmol), **2a** (2 equiv, 0.30 mmol), catalyst (1 mol %) and K_2CO_3 (3 equiv, 0.45 mmol) in MeCN (1.0 mL). [b] Isolated yield. [c] Under green LED irradiation. Nr = no reaction.

Other parameters further evaluated involved the stoichiometry of the transformation in relation to the **2a** and **base** components (**SCHEME 1.16, B**). Decreasing to 2 equivalents of base was found to have a major effect on the reaction outcome, with yields dropping from 99% to 90%. More drastically, decreasing the equivalents of the amine component from 2.0 to 1.1 led to only 34% yield of the alkylated azomethine.

Finally, although a longer reaction time using 0.5 mol% of photocatalyst allowed obtaining the product **3a** in higher yields, it was not equally excellent as that obtained in the initial reaction condition using 1 mol% of **Ru** (**SCHEME 1.16, C**).

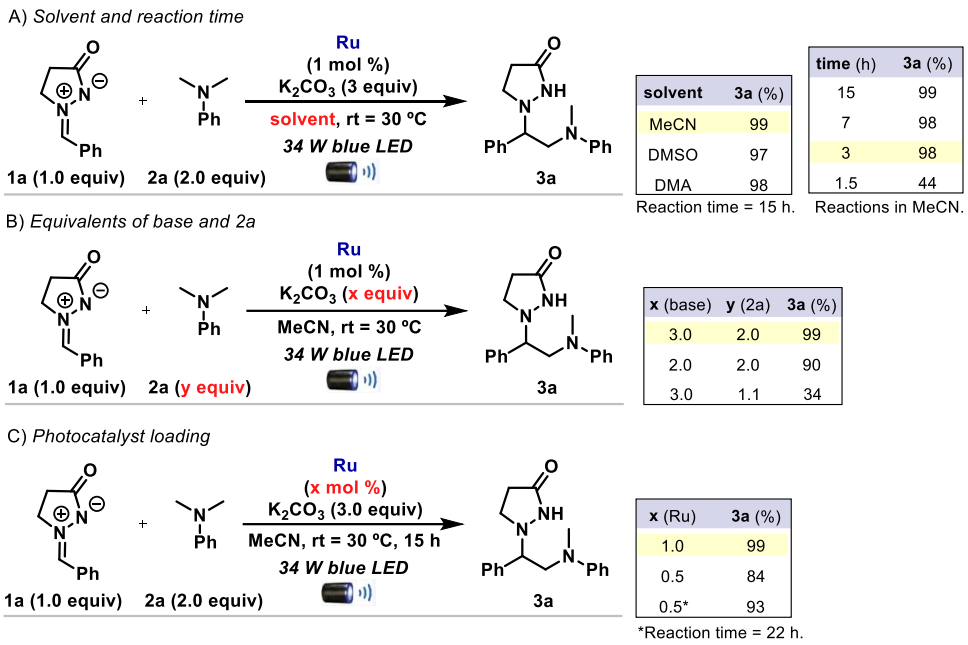

SCHEME 1.16 – Further reaction optimization.

With the optimized conditions in hands, the scope and limitations of this protocol were initially investigated in terms of a range of azomethine imines (**SCHEME 1.17**). The methodology showed outstanding functional group tolerance, with the outcome of the process being almost unaffected by variations in the aryl ring electron-density and substitution patterns. Fluorinated substrates underwent the α-amino-alkylation in moderate to excellent yields as observed for compounds **4** (99%) and **5** (61%). Bromine-substituted aryl substrates which are important synthons in transition metal mediated cross-coupling reactions also underwent the desired transformation smoothly, affording the corresponding products **6** and **7** in good yields (62% and 87%, respectively). The developed protocol also performed well when *ortho*-substituted azomethine imines were subjected to the optimized reaction conditions (**8** and **10**). Notably, substrates containing electron-donating groups displayed a similar chemical behavior, delivering the desired products in high chemical yields. Azomethine imines derived from thiophene-2-carbaldehyde afforded the corresponding product in low yield (**15**, 35%) while the azomethine imine derived from pyridine-2-carbaldehyde **16** gave the α-amino alkylated product in 98% yield. Interestingly, the cycle aliphatic azomethine imine, which exhibits a lower reduction potential, underwent the functionalization in satisfactory yield (**17**, 60%). We further evaluated the azomethine imine derived from racemic 3-methyl-pyrazolidinone, envisioning possible applications on asymmetric synthesis of dinitrogen-fused heterocycles. Under the optimized conditions, this reaction was highly efficient, yielding product **18** in 99% yield as a 1:1 mixture of

diastereoisomers. To further evaluate the scalability of the protocol, a 1 mmol scale experiment was performed, in which compound **3** was obtained in 63% yield.

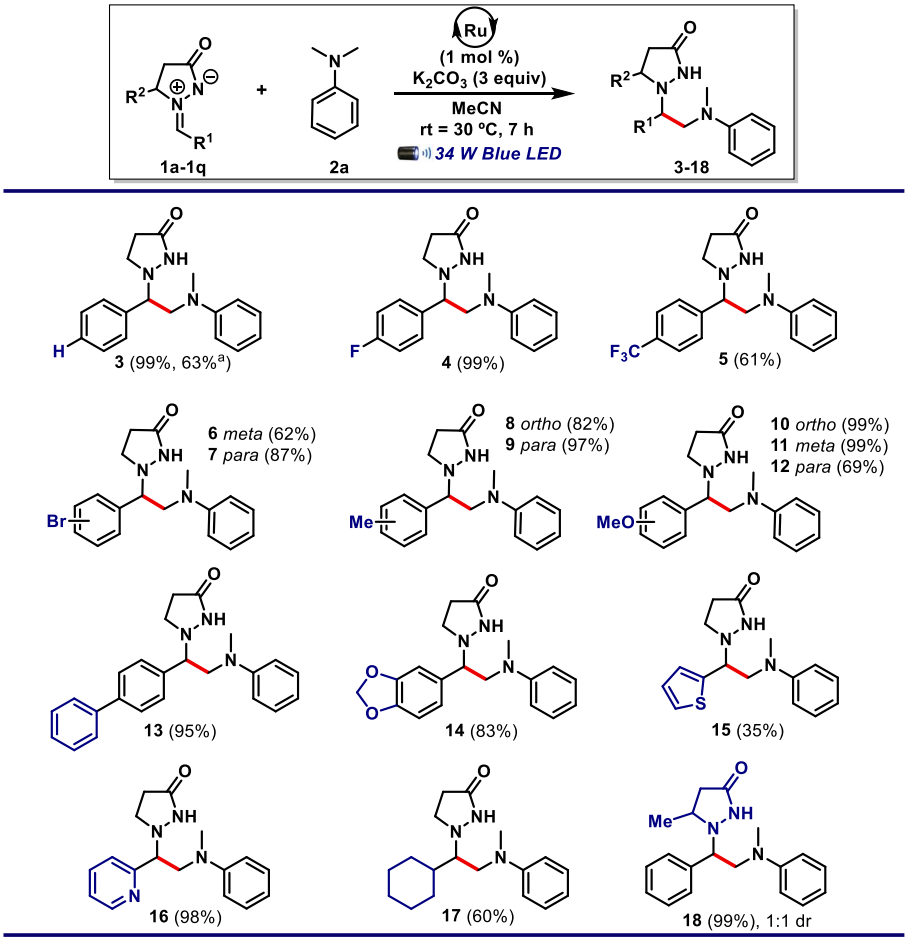

SCHEME 1.17 - Azomethine imine scope for the functionalization reaction with *N*,*N*-dimethylaniline **2a**. Reaction conditions: **1a** (0.15 mmol), **2a** (2 equiv, 0.30 mmol), **Ru** (1 mol %) and K_2CO_3 (3 equiv, 0.45 mmol) in MeCN (1.0 mL). Yields refer to isolated compounds after column chromatography. [a] Yield for the reaction on 1 mmol scale.

Next, we examined the scope and limitations with respect to the tertiary amine component. This study showed that the substituent nature on the aryl ring of the *N,N*-dimethylanilines displays a crucial influence on the reaction outcome. Following these observations and aiming to expand the applicability of the current transformation, the use of a more oxidizing photocatalyst showed to be necessary. Therefore, replacing $Ru(bpy)_3(PF_6)_2$ by $Ir[dF(CF_3)ppy]_2(dtbpy))PF_6$ (**Ir-I**) ($E_{1/2}(M^{(III)}*/M^{(II)})$ = +1.21 V *vs* SCE in MeCN) allowed the access to a range of *N*-(*β*-aminoalkyl)pyrazolonidinones (**SCHEME 1.18**). We selected this photocatalyst from the initial optimization studies, since it has a larger window in relation to electrochemical potentials and could cover more comprehensively the scope of tertiary amines.

Regarding the diversification on the aromatic ring of the *N*-alkyl-radical precursor, different substitution patterns and both electron-withdrawing and electron-donating groups

performed well, providing the corresponding products (**19**-**25**) in satisfactory to excellent yields. Notably, chlorinated and brominated *N,N*-dimethyl-anilines were suitable under the re-optimized condition (**20**-**23**) - opening up an orthogonal pathway for further derivatizations. Furthermore, electron-donating group at the *para* position on the aryl system proved to be a limitation of this reaction protocol (**28**).

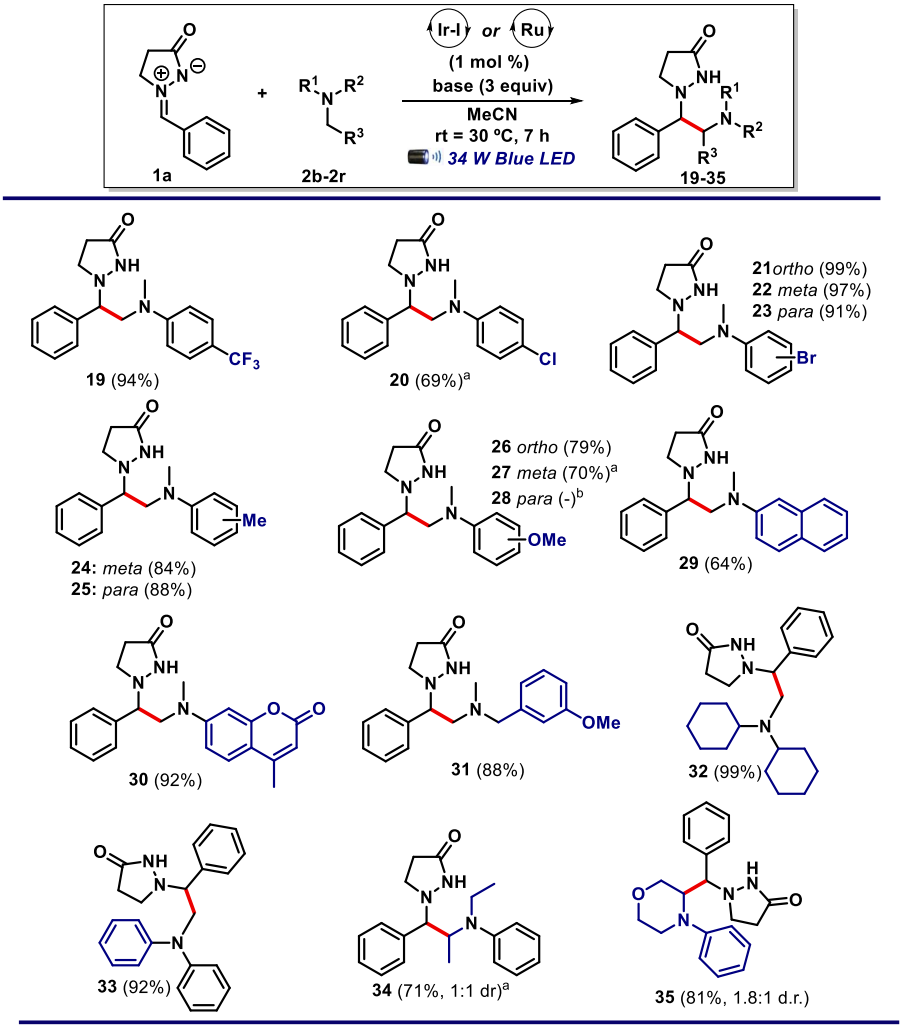

SCHEME 1.18 - Tertiary amine scope for the radical coupling with **1a**. Reaction conditions: **1a** (0.15 mmol), **2** (2 equiv, 0.30 mmol), **Ru** (1 mol %) and K_2CO_3 (3 equiv, 0.45 mmol) in MeCN (1.0 mL). Yields refer to isolated compounds after column chromatography. [a] Reactions conducted using Ru photocatalyst. [b] The starting material was recovered.

Remarkably, other structurally diverse tertiary amines, including trialkyl and benzylic amines, as well as the pharmacologically relevant 7-(dimethylamino)-4-methyl-coumarin, underwent this transformation with high selectivity and excellent yields (**29**-**34**). An *N*-aryl tertiary cyclic amine was also successfully challenged as *α*-amino radical source in this transformation, providing the corresponding pyrazolidinone decorated with the morpholine framework with good

yield (**35**). Unfortunately, benzyl tertiary amines as *N*-phenyl 1,2,3,4-tetrahydroisoquinoline were not reactive under the established protocol.

The design of simple and mild strategies for modifying complex structures is a fundamental goal in pharmaceutical industries.[71] Driven by this observation, we sought to demonstrate a direct application of the developed protocol for the *late-stage* C-H modification of pharmaceutical ingredients. We found that azomethine imine **1a** could be smoothly incorporated onto the chemical architectures of the muscle relaxant cyclobenzaprine (**36**), the antidepressant escitalopram (**37**) and dexchlorpheniramine (**38**) used as antihistamine in excellent yields (**SCHEME 1.19**).

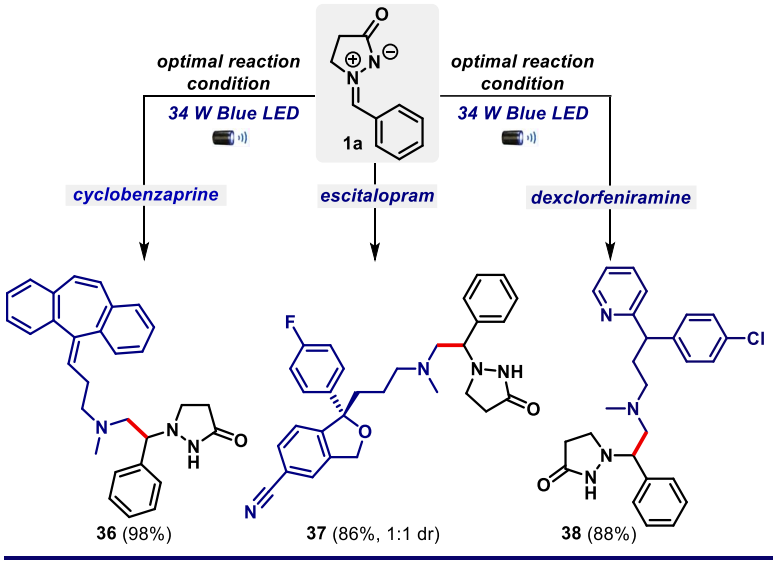

SCHEME 1.19 - Late-Stage modification of active pharmaceutical ingredients. Reaction conditions: **1a** (0.15 mmol), **pharmaceutical compound** (2 equiv, 0.30 mmol), **Ir-I** (1 mol %) and K_2CO_3 (3 equiv, 0.45 mmol) in MeCN (1.0 mL). Yields refer to isolated compounds after column chromatography.

The stable nitroxide free radical 2,2,6,6-tetramethylpiperidinyloxy (**TEMPO**) is a well-known carbon radical scavenger and has been broadly used for mechanistic investigation of radical-based reactions. Confirming the radical nature of our transformation, no product was observed when the reaction was carried out in the presence of excess of **TEMPO** (3 equiv) and 60% of the azomethine imine **1a** was recovered in this reaction.

To gain insight about the radical species generated in the reaction outcome, an aliquot was removed from the crude reaction medium and analyzed by mass spectrometry using an ACQUITY UPC^2-MS apparatus via direct infusion.

[71] CERNAK, T.; DYKSTRA, K. D.; TYAGARAJAN, S.; VACHAL, P. & KRSKA, S. W. “The medicinal chemist's toolbox for late-stage functionalization of drug-like molecules”. Chem. Soc. Rev. **45**: 546, 2016.

The MS Full scan experiments indicated the presence of the starting materials **1a** and **2a**, the radical scavenger TEMPO and no product formation could be detected (**FIGURE 1.10**). Additionally, the results indicated the trapping of the α-amino radical by TEMPO, giving the evidence to the reductive quenching that we believe the reaction proceeds through (**FIGURE 1.11**).

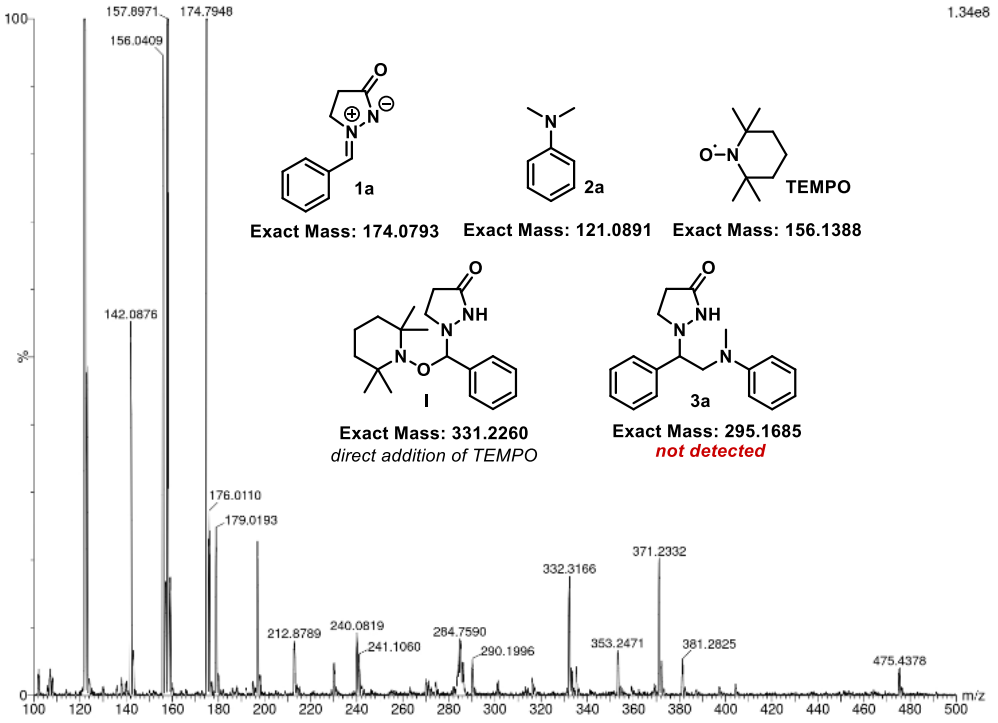

FIGURE 1.10 - MS full scan experiment via direct infusion of the reaction crude.

The mass chromatogram revealed a signal at *m/z* = 332.3166 that could be related to the TEMPO-azomethine imine adduct (**I**) with *m/z* =[M+H$^+$] = 332.2333. In order to investigate whether reduction of azomethine imine **1a** via SET in the presence of the photocatalysts would be feasible, we measured the reduction potential of this specie by cyclic voltammetry (**FIGURE 1.12**).

The cyclic voltammetry was acquired using a glassy carbon working electrode, a platinum counter electrode and Ag/$AgNO_3$ reference electrode. The analysis was performed under N_2 atmosphere and using a degasified solution of the compound in MeCN (1.0 mM) containing a 0.1 M solution of tetrabutylammonium perchlorate ($Bu_4N{\cdot}ClO_4$) in MeCN (10 mL).

The potentials were calibrated using ferrocene as standard. The potential range scanned was typically -2.0 V – 2.0 V at a 100 mV/s.

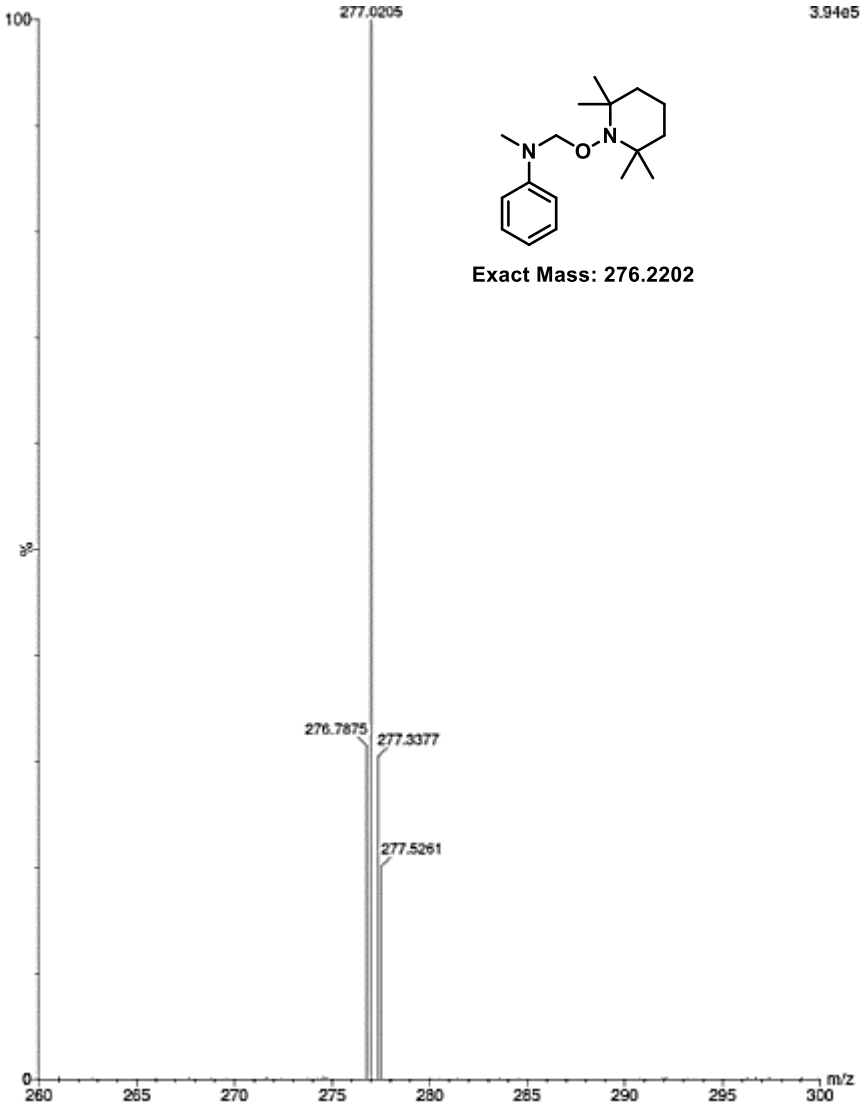

FIGURE 1.11 - Trapping of the α-amino radical by TEMPO.

As observed from the cyclic voltammetry experiment, azomethine imine **1a** presents a very negative reduction potential (E_{red}= -1.66 V *vs* SCE at 20 °C in MeCN). This negative value could not be covered by the potential ranges of the photocatalysts used in this study. Thus, the signal observed in the mass chromatogram must come from the direct addition of the radical scavenger TEMPO to the azomethine imine, since the mismatch of the redox potentials of the imine and the photocatalysts do not supports the formation of the reduced form of azomethine imine.

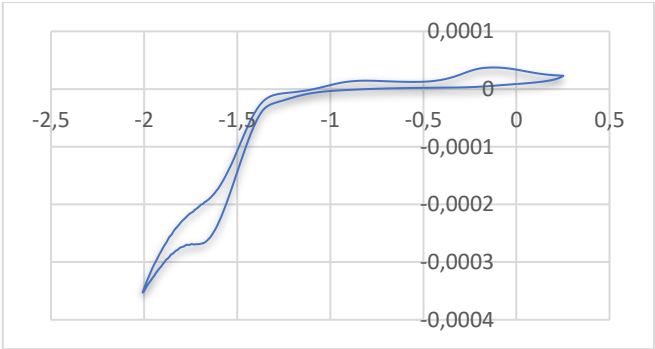

FIGURE 1.12 - CV study of **1a** in MECN, E_{red}= -1.66 V *vs* SCE. Cathodic scan from -2.0 to 0.25 V.

Given these considerations, two pathways could be considered for the reaction mechanism – they are strictly dependent of the relationship between the redox potential of the azomethine iminium ion and the photocatalysts employed. Both pathways begin with the quenching of the excited photocatalyst ($E_{1/2}$(M(II)*/M(I) = +0.77 V vs SCE in MeCN for Ru and $E_{1/2}$(M(III)*/M(II))= +1.21 V vs SCE in MeCN for Ir-I) by the amine **2a**. In the presence of base, the radical-cation **2a'** derived from this process is further converted to the respective transient *α*-amino alkyl radical intermediate **2a''** (**SCHEME 1.20**).

If the ground state of the reduced photocatalyst presents a suitable reduction potential, it would be able to reduce **1a** to the respective persistent *α*-amino alkyl radical **1a''**.[72] A radical-radical coupling between these intermediates followed by protonation would afford the product **3** (**SCHEME 1.20, A**).[73] However, as demonstrated, the azomethine iminium ions has a high reduction potential (E_{red}= -1.66 V *vs* SCE at 20 °C in MeCN) and cannot be reduced by ground-state Ru(I) or Ir(II) (E_{red}= -1.33 V vs SCE at 20 °C in MeCN and E_{red}= -1.37 V *vs* SCE at 20 °C in MeCN, respectively) employed in this study. Therefore, these facts rule out the possibility of a radical-radical coupling scenario.

On the other hand, taking into consideration the broad azomethine imine scope, we propose an alternative pathway, in which the nucleophilic radical **2a''** could directly attack **1a** to

[72] LEIFERTB, D.; STUDER, A. "The persistent radical effect in organic synthesis". Angew. Chem. Int. Ed. **59**: 47, 2020.

[73] (a) URAGUCHI, D.; KINOSHITA, N.; KIZU, T. & OOI, T. "Synergistic catalysis of ionic brønsted acid and photosensitizer for a redox neutral asymmetric *α*-coupling of *N*-arylaminomethanes with aldimines". J. Am. Chem. Soc. **137**: 13768, 2015; (b) FAVA, E.; MILLET, A.; NAKAJIMA, M.; LOESCHER, S. & RUEPING, M. "Reductive umpolung of carbonyl derivatives with visible-light photoredox catalysis: direct access to vicinal diamines and amino alcohols via *α*-amino radicals and ketyl radicals". Angew.Chem. Int. Ed. **55**: 6776, 2016; (c) ZHAO, Y.; CHEN, J.-R.; XIAO, W.-J. "Synthesis of hydrazide-containing chroman-2-ones and dihydroquinolin-2-ones via photocatalytic radical cascade reaction of aroylhydrozones". Org. Lett. **18**: 6304, 2016; (d) PATEL, N. R.; KELLY, C. B.; SIEGENFELD, A. P. & MOLANDER. G. A. "Mild, redox-neutral alkylation of imines enabled by an organic photocatalyst". ACS Catal. **7**: 1766, 2017; (e) JIA, J.; KANCHERLA, R.; RUEPING, M. & HUANG, L. "Allylic C(sp^3)–H alkylation via synergistic organo- and photoredox catalyzed radical addition to imines". Chem. Sci. **11**: 4954, 2020.

afford the *N*-centered cation radical intermediate **I (SCHEME 1.20, B)**. Once formed, this intermediate is prone to undergo a spin-center-shift event (SCS) with the spin density located on the amide nitrogen. This event leads to an stabilized amidyl radical intermediate **II**, which would be reduced by the ground-state Ru(I) or Ir(II) and protonated to provide the *N*-(*β*-aminoalkyl)pyrazolidinone **3**. This mechanistic scenario is more likely and is supported by previous reports in the literature.

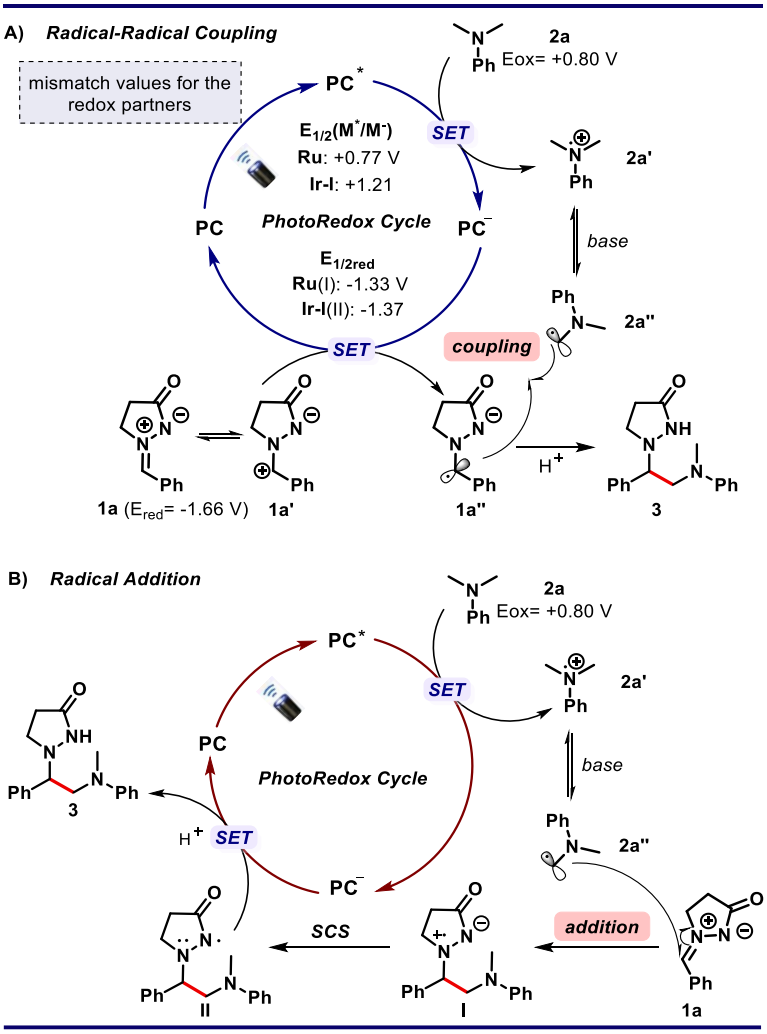

SCHEME 1.20 - Proposed mechanisms.

3. Conclusion

Under the optimized reaction conditions, a series of tertiary amines could be employed in the photoredox alkylation of azomethine imines. The developed protocol works under mild reaction conditions, using only 1 mol% of photocatalyst at room temperature providing a viable transformation to direct access pyrazolidinone-containing compounds with excellent yields. This method is an extension of the applicability of well-known α-amino radicals generated under visible-light irradiation and emerged as a useful possibility of formation of new C-C bonds using the underexploited iminium ion in this context.

In the reported protocol, substrates with different electronic and steric features were nicely engaged in good to excellent yields and with high functional group tolerance. From wide commercially available amines, an interesting library of *N*-(β-aminoalkyl)-pyrazolidinones was construct. Given the mild conditions, this approach provides a valuable contribution to successful access late-stage C-H modification of biologically relevant compounds.

One-electron C-C bond forming processes, notably, the coupling of alkyl-radicals to iminium-ions, have substantially been reported in the literature and are envisaged as a suitable alternative to the addition of alkyl-Grignard reagents. These radical-based reactions normally occur in the presence of stoichiometric amounts of SET reductants with the iminium ion preformed or *in-situ* generated from the respective amine, imine or imine-derivative. We disclosed a direct approach for the functionalization of azomethine imines via photoredox catalysis, by exploring complementary reactivity to those involving polar mechanisms and the traditional radical chemistry.

We believe that this contribution will serve as a stimulus to the community in expanding the application of the azomethine iminium ions as radical acceptors under photocatalytic conditions, which is currently underrepresented in literature.

4. Experimental Section

General Considerations

Unless otherwise stated, all reagents were purchased from commercial sources and used without additional purification. THF was freshly distilled under argon from the sodium anion of benzophenone. All other anhydrous solvents were purchased or obtained from in house solvent purification towers. HPLC grade solvents were used in the photocatalyzed reactions. All air or moisture-sensitive reactions were conducted in flame dried glassware under argon atmosphere. A 34 W Kessil H150 blue LED (emission: 380 – 525 nm) was used as the visible light source. All chemicals and photocatalysts were purchased and used as received from suppliers unless otherwise noted. Reactions were monitored by thin layer chromatography using Merck silica gel aluminum sheets 60 F254, using hexane/EtOAc or DCM/ MeOH as mobile phase and visualized by UV lamp, permanganate and vanillin stains. Flash column chromatography was accomplished using silica gel 60 (230-400 mesh) and hexane/EtOAc or DCM/ MeOH as eluent systems. ^{1}H and ^{13}C NMR spectra were recorded on Brucker NMR spectrometers (400 or 600 MHz for ^{1}H and 100 or 150 MHz for ^{13}C). Chemical shifts are given in ppm. Coupling constant values *J* are given in Hertz. The multiplicities are described as: brs = broad signal, s = singlet, d = doublet, t = triplet, q = quartet, dd = doublet of doublets, dt = doublet of triplets, dq = doublet of quartets, ddd = doublet of doublet of doublets, dddd = doublet of doublet of doublet of doublets and m = multiplet. Mass spectra data were recorded at Waters Technologies of Brazil using a Xevo G2-XS QTOF (ESI-QTOF) spectrometer.

Azomethine imine synthesis (1a – 1q) [74]

Pyrazolidin-3-one (S1):

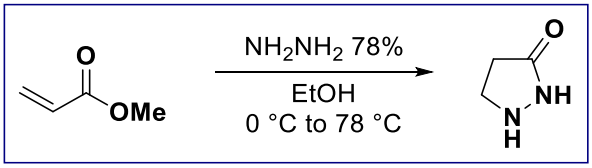

Pyrazolidin-3-one (S1) was prepared following the reported experimental procedure with slight modifications: in a flame-dried round bottom flask a solution of hydrazine monohydrate 78% (1.0 equiv) in absolute ethanol (4 M) was cooled to 0 °C using an ice bath. Methyl acrylate (1.0 equiv) was slowly added and the solution was stirred at 0 °C for 30 min and then was

[74] WINTERTON, S. E. & READY, J. M. "[3 + 2]-cycloadditions of azomethine imines and ynolates". Org. Lett. **18**: 2608, 2016.

heated to reflux using an oil bath until the reaction be completed judging by TLC analysis. The solution was concentrated under vacuum to yield the crude pyrazolidin-3-one as a clear or yellow oil. The pyrazolidin-3-one was used immediately in the next step without purification.

Synthesis of azomethine imines:

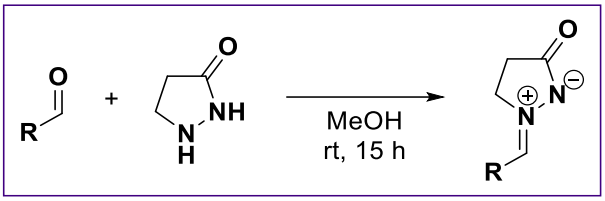

Azomethine imines were prepared following the reported experimental procedure with slight modifications: The crude pyrazolidinone **S1** (1.0 equiv) obtained in the previous step and the corresponding aldehydes (1.2 equiv) were dissolved in anhydrous MeOH (1 M). The mixture was stirred at room temperature overnight and then concentrated under vacuum to remove completely the solvent. Et_2O was added to precipitate the product (if the precipitation does not occur, it can be promoted by the addition of few drops of hexanes followed by cooling in the freezer). The resulting solid was collected by filtration, washed with Et_2O and dried to yield the final product. For substrates that could not precipitate, the reaction crudes were purified by column chromatography using DCM/ MeOH (10:1) as eluent.

N, N-Dimethylanilines (2a – 2r)

The following substituted *N, N*-dimethylanilines were used as starting materials for the scope evaluation. The compounds which were prepared according to literature experimental procedure[75,76] are indicated; otherwise, they were purchased from commercial sources.

[75] CHANDRASEKHARAM, M.; CHIRANJEEVI, B.; GUPTA, K. S. V. & SRIDHAR, B. 'Iron-catalyzed regioselective direct oxidative aryl–aryl cross-coupling". J. Org. Chem. **76**: 10229, 2011.

[76] JOHNSON, C. R.; ANSARI, M. I. & COOP, A. "Tetrabutylammonium bromide-promoted metal-free, efficient, rapid, and scalable synthesis of *N*-aryl amines". ACS Omega. **3**: 10886, 2018.

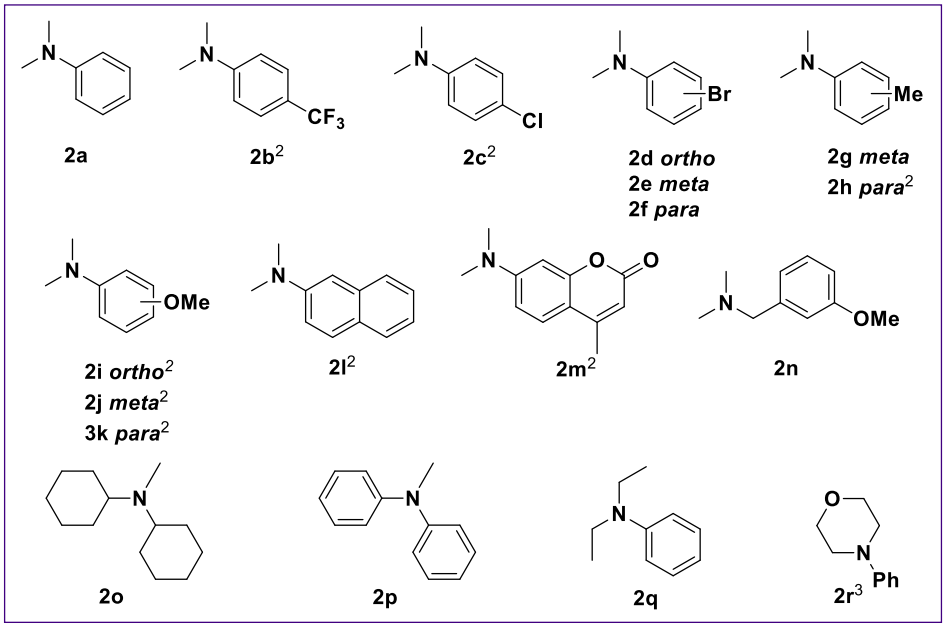

FIGURE S1 - *N*, *N*-dimethylanilines used as starting material during the scope study.

General Procedure (GP):

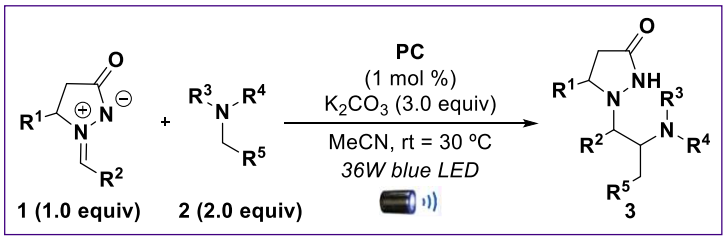

A dried Schlenk tube of borosilicate glass equipped with a stir bar was charged with the azomethine imine (0.15 mmol, 1.0 equiv), *N, N*-dimethylanilines (2.0 equiv), K_2CO_3 (3.0 equiv) and the photocatalyst (1 mol %). Acetonitrile (1 mL) was added and the Schlenk tube was sealed with PTFE/silicon septum and connected to a vacuum line. The solution was degassed 3 times *via* a freeze-pump-thaw procedure and stirred under irradiation by a 34 W Kessil H150 blue LED (emission: 380 – 525 nm) with the temperature controlled by a fan (the distance between the Schlenk tube and the lamp was ~ 3 cm and the achieved reaction temperature was 30 ºC). Upon completion, the solvent was removed under reduced pressure and the residue was purified by flash column chromatography using DCM and DCM/MeOH (20:1) as solvent mixture to afford the title compound.

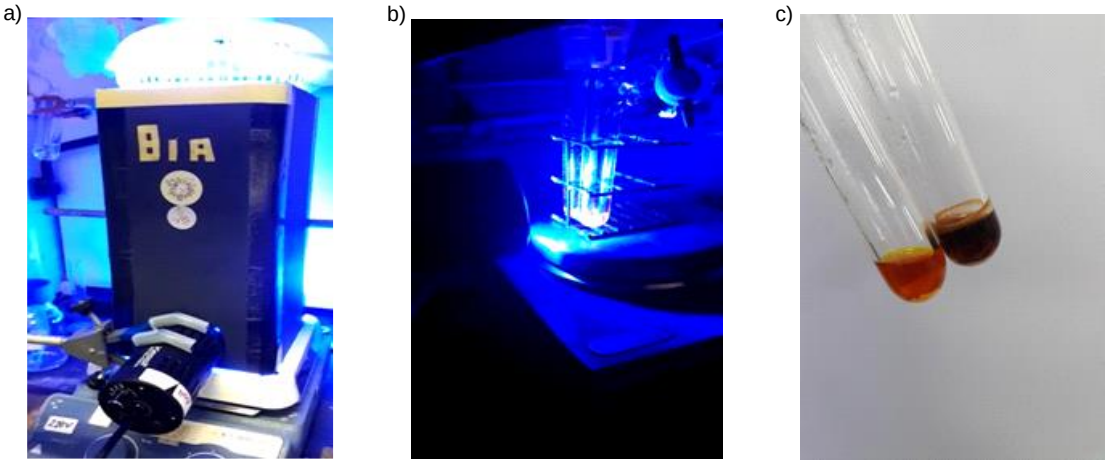

FIGURE S2 - General procedure. a) Reaction set-up. b) Schlenk's distance from the irradiation source. c) General aspect of the reaction mixture before (orange) and upon completion of reaction (dark brown) – using the Ru photocatalyst.

Reaction Performed at Larger-Scale for the Compound 3

The reaction was carried out following the **General Procedure.** A dried Schlenk tube of borosilicate glass equipped with a stir bar was charged with the azomethine imine **1a** (174 mg, 1.00 mmol), *N, N*-dimethylaniline **2a** (2.0 equiv), K_2C0_3 (3.0 equiv) and the photocatalyst (1 mol %). Acetonitrile (6.7 mL) was added and the Schlenk tube was sealed with PTFE/silicon septum and connected to a vacuum line. The solution was degassed 3 times *via* a freeze-pump-thaw procedure and stirred under irradiation during 24 h by a 34 W Kessil H150 blue LED (emission: 380 – 525 nm) with the temperature controlled by a fan (the distance between the Schlenk tube and the lamp was ~ 3 cm and the achieved reaction temperature was 30 ºC). Then, the solvent was removed under reduced pressure and the residue was purified by flash column chromatography using DCM and DCM/MeOH (20:1) as solvent mixture to afford the compound **3** as a colorless oil (185.8 mg, 63%).

Cyclic Voltammetry

Cyclic voltammetry was acquired using a glassy carbon working electrode, a platinum counter electrode and $Ag/AgNO_3$ reference electrode. The analysis were performed under N_2 atmosphere and using a degasified solution of the compound in MeCN (1.0 mM) containing a 0.1 M solution of tetrabutylammonium perchlorate ($Bu4N{\cdot}ClO_4$) in MeCN (10 mL). The potentials were calibrated using ferrocene as standard. The potential range scanned was typically -2.0 V – 2.0 V at a 100 mV/s.

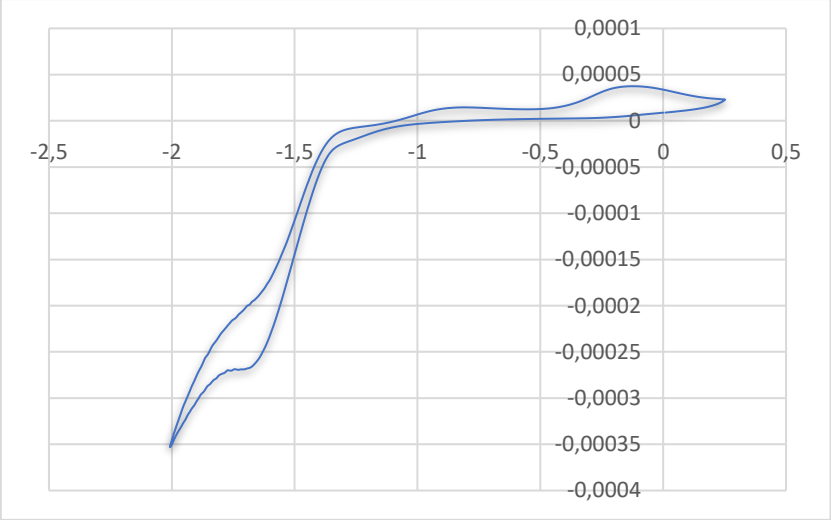

FIGURE S3 - CV STUDY OF 1A IN MECN, E_{RED}= -1.66 V VS. SCE. CATHODIC SCAN FROM -2.0 TO 0.25 V.

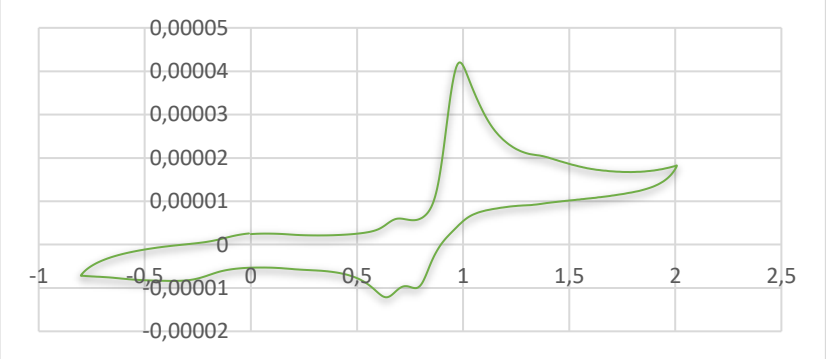

FIGURE S4 - CV study of 2a in MeCN, E_{ox}= 0.96 V vs. SCE. Anodic scan from 2.0 to -0.8 V.

Late-Stage Modification of Pharmaceutical Active Ingredients

The active ingredients were provided by the EMS pharmaceutical company in their respective hydrochloric salt forms. They were dissolved in EtOAc and washed with a saturated solution of K_2CO_3 or NaOH prior their use. The organic phases were dried over anhydrous Na_2SO_4, filtered and the solvent was removed under reduced pressure. The corresponding free amines were obtained as colorless oil and used directly in the photocatalyzed reaction according to the general procedure **GP** using the **Ir-I** complex as the photocatalyst under the optimized reaction condition.

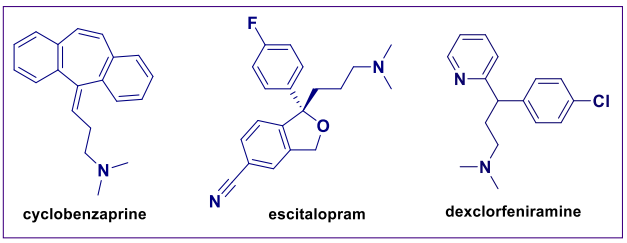

FIGURE S5 - The active ingredients modified in this study.

Trapping Experiment

The radical-trapping experiment was carried out using TEMPO as radical scavenger. The azomethine imine **1a** (0.15 mmol, 1.0 equiv), *N, N*-dimethylaniline **2a** (2.0 equiv), K_2C0_3 (3.0 equiv), TEMPO (3.0 equiv) and the **Ru** photocatalyst (1 mol %) were dissolved in acetonitrile (1 mL) in a dried Schlenk tube equipped with a stir bar. The Schlenk tube was sealed with PTFE/silicon septum and connected to a vacuum line and the solution was degassed 3 times *via* a freeze-pump-thaw procedure. The resulting solution was stirred under irradiation by 34 W Kessil H150 blue LED under a fan. After 1 h, an aliquot was removed from the crude reaction medium and analyzed by mass spectrometry using an ACQUITY UPC^2-MS apparatus via direct infusion.

Characterization Data of Compounds

<u>Cyclic Azomehtine Imine Scope</u>

1-(2-(methyl(phenyl)amino)-1-phenylethyl)pyrazolidin-3-one (3) was prepared according to **GP** and obtained as a colorless oil (43.8 mg, 99%) after purification by flash column chromatography (0 – 5% MeOH/ DCM). **^{1}H NMR** (400 MHz, $CDCl_3$): δ 8.04 (brs, 1H), 7.37 – 7.30 (m, 5H), 7.28 – 7.22 (m, 2H), 6.80 – 6.75 (m, 3H), 3.96 – 3.90 (m, 2H), 3.34 (q, *J* = 8.9 Hz, 1H), 3.30 – 3.23 (m, 1H), 3.19 (brs, 1H), 2.68 (s, 3H), 2.39 (dt, *J* = 15.8, 7.7 Hz, 1H), 2.27 (dt, *J* = 16.7, 8.4 Hz, 1H); **^{13}C NMR** (101 MHz, $CDCl_3$) δ 175.2, 149.1, 138.6, 129.4, 128.9, 128.5, 128.4, 117.3, 113.0, 113.2, 69.8, 58.9, 51.4, 39.6, 30.2; **HRMS** (ESI) m/z: $[M + H]^+$ Calcd for $C_{18}H_{22}N_3O$ 296.1757, Found: 296.1755.

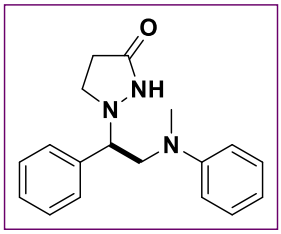

1-(1-(4-fluorophenyl)-2-(methyl(phenyl)amino)ethyl)pyrazolidin-3-one (4) was prepared according to **GP** and obtained as a colorless oil (46.9 mg, 99%) after purification by flash column chromatography (0 – 5% MeOH/ DCM). **^{1}H NMR** (400 MHz, $CDCl_3$): δ 8.25 (brs, 1H), 7.30 (dd, *J* = 8.4, 5.5 Hz, 2H), 7.27 – 7.23 (m, 2H), 7.05 (t, *J* = 8.5 Hz, 2H), 6.77 (t, *J* = 7.3 Hz, 1H), 6.73 (d, *J* = 8.2 Hz, 2H), 3.96 – 3.90 (m, 2H), 3.33 – 3.22 (m, 2H), 3.16 (brs, 1H), 2.65 (s, 3H), 2.39 (dt, *J* = 15.9, 7.8 Hz, 1H), 2.27 (dt, *J* = 16.7, 8.3 Hz, 1H); **^{13}C NMR** (101 MHz, $CDCl_3$) δ 175.0, 164.0, 161.5, 149.2, 134.5, 130.1, 1230.0, 129.5, 117.8, 116.1, 115.9, 113.3, 69.1, 59.4, 51.6, 39.7, 30.1; **HRMS** (ESI) m/z: $[M + H]^+$ Calcd for $C_{18}H_{21}FN_3O$ 314.1663, Found: 314.1672.

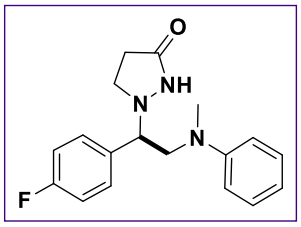

1-(2-(methyl(phenyl)amino)-1-(4-(trifluoromethyl)phenyl)ethyl)pyrazolidin-3-one (5) was prepared according to **GP** and obtained as a colorless oil (33.2 mg, 61%) after purification by flash column chromatography (0 – 5% MeOH/ DCM). **^{1}H NMR** (400 MHz, $CDCl_3$): δ 8.23 (brs, 1H), 7.62 (d, *J* = 8.0 Hz, 2H), 7.46 (d, *J* = 8.0 Hz, 2H), 7.27 – 7.23 (m, 2H), 6.79 (t, *J* = 7.3 Hz, 1H), 6.72 (d, *J* = 8.2 Hz, 2H), 4.04 – 3.94 (m, 2H), 3.36 – 3.26 (m, 2H), 3.13 (brs, 1H), 2.63 (s, 4H), 2.45 (dt, *J* = 16.0, 7.8 Hz, 1H), 2.30 (dt, *J* = 16.7, 8.3 Hz, 1H); **^{13}C NMR** (101 MHz, $CDCl_3$) δ 175.1, 149.0, 143.0, 129.5, 128.6, 126.0, 125.9, 118.0, 113.3, 69.5, 59.4, 51.7, 39.8, 30.0; **HRMS** (ESI) m/z: $[M + H]^+$ Calcd for $C_{19}H_{21}F_3N_3O$ 364.1631, Found: 364.1635.

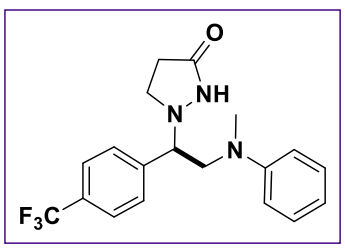

1-(1-(3-bromophenyl)-2-(methyl(phenyl)amino)ethyl)pyrazolidin-3-one (6) was prepared according to **GP** and obtained as a colorless oil (34.6 mg, 62%) after purification by flash column chromatography (0 – 5% MeOH/ DCM). **^{1}H NMR** (400 MHz, $CDCl_3$): δ 8.25 (brs, 1H), 7.30 (dd, *J* = 8.4, 5.5 Hz, 2H), 7.27 – 7.23 (m, 2H), 7.05 (t, *J* = 8.7 Hz, 2H), 6.77 (t, *J* = 7.3 Hz, 1H), 6.73 (d, *J* = 8.2 Hz, 2H), 3.96 – 3.90 (m, 2H), 3.33 – 3.22 (m, 2H), 3.16 (brs, 1H), 2.65 (s, 3H), 2.42 (dt, *J* = 15.9, 7.8 Hz, 1H), 2.27 (dt, *J* = 16.7, 8.3 Hz, 1H); **^{13}C NMR** (101 MHz, $CDCl_3$) δ 175.0, 164.0, 161.5, 149.1, 134.5, 130.1, 130.0, 129.5, 117.7, 116.1, 115.9, 113.2, 69.1, 59.4, 51.6, 39.6, 30.1; **HRMS** (ESI) m/z: $[M + H]^+$ Calcd for $C_{18}H_{21}BrN_3O$ 374.0862, Found: 374.0852.

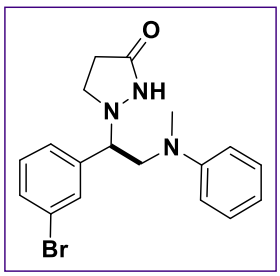

1-(1-(4-bromophenyl)-2-(methyl(phenyl)amino)ethyl)pyrazolidin-3-one (7) was prepared according to **GP** and obtained as a colorless oil (48.6 mg, 87%) after purification by flash column chromatography (0 – 5% MeOH/ DCM). **^{1}H NMR** (400 MHz, $CDCl_3$): δ 8.88 (brs, 1H), 7.49 (d, *J* = 8.0 Hz, 2H), 7.27 – 7.20 (m, 4H), 6.76 (t, *J* = 7.3 Hz, 1H), 6.70 (d, *J* = 8.2 Hz, 2H), 3.99 (dd, *J* = 14.4, 6.2 Hz, 1H), 3.92 (t, *J* = 6.6 Hz, 1H), 3.37 – 3.31 (m, 1H), 3.29 – 3.24 (m, 1H), 3.15 (brs, 1H), 2.63 (s, 3H), 2.42 (dt, *J* = 16.0, 7.8 Hz, 1H), 2.24 (dt, *J* = 16.7, 8.3 Hz, 1H); **^{13}C NMR** (101 MHz, $CDCl_3$) δ 175.5, 148.9, 137.8, 132.1, 130.2, 129.4, 122.4, 117.4, 112.8, 69.1, 58.6, 51.6, 39.7, 30.1; **HRMS** (ESI) m/z: $[M + H]^+$ Calcd for $C_{18}H_{21}BrN_3O$ 374.0862, Found: 374.0867.

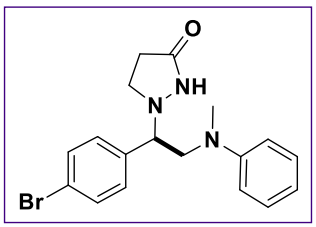

1-(2-(methyl(phenyl)amino)-1-(o-tolyl)ethyl)pyrazolidin-3-one (8) was prepared according to **GP** and obtained as a colorless oil (38.0 mg, 82%) after purification by flash column chromatography (0 – 5% MeOH/ DCM). **^{1}H NMR** (400 MHz, $CDCl_3$): δ 8.14 (brs, 1H), 7.51 (d, *J* = 7.6 Hz, 1H), 7.27 – 7.13 (m, 5H), 6.79 – 6.75 (m, 3H), 4.25 (t, *J* = 6.7 Hz, 1H), 3.96 (dd, *J* = 14.7, 6.7 Hz, 1H), 3.33 – 3.25 (m, 2H), 3.08 (brs, 1H), 2.63 (s, 1H), 2.48 (dt, *J* = 16.5, 8.1 Hz, 1H), 2.39 (dt, *J* = 16.5, 8.1 Hz, 1H), 2.21 (s, 3H); **^{13}C NMR** (101 MHz, $CDCl_3$) δ 174.5, 149.4, 137.3, 136.7, 130.9, 129.5, 127.9, 127.6, 126.8, 117.8, 113.2, 64.9, 59.7, 51.6, 39.3, 30.3, 19.9; **HRMS** (ASAP) **HRMS** (ESI) m/z: $[M + H]^+$ Calcd for $C_{19}H_{24}N_3O$ 310.1914, Found: 310.1911.

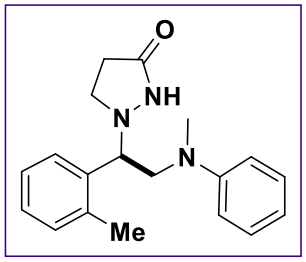

1-(2-(methyl(phenyl)amino)-1-(p-tolyl)ethyl)pyrazolidin-3-one (9) was prepared according to **GP** and obtained as a colorless oil (44.9 mg, 97%) after purification by flash column chromatography (0 – 5% MeOH/ DCM). **^{1}H NMR** (400 MHz, $CDCl_3$): δ 8.66 (brs, 1H), 7.28 – 7.16 (m, 6H), 6.79 – 6.74 (m, 3H), 3.98 (t, *J* = 7.1 Hz, 0H), 3.92 (dd, *J* = 14.0, 7.8 Hz, 1H), 3.38 (dd, *J* = 14.2, 6.1 Hz, 1H), 3.29 – 3.23 (m, 1H), 3.20 (brs, 1H), 2.68 (s, 3H), 2.37 (s, 3H), 2.37 (dt, *J* = 17.2, 10.0 Hz, 1H), 2.20 (dt, *J* = 16.8, 8.5 Hz, 1H); **^{13}C NMR** (101 MHz, $CDCl_3$) δ 175.2, 149.2, 138.2, 135.4, 129.6, 129.4, 128.4, 117.3, 113.1, 69.5, 59.0, 51.4, 39.6, 30.2, 21.3; **HRMS** (ESI) m/z: $[M + H]^+$ Calcd for $C_{19}H_{24}N_3O$ 310.1914, Found: 310.1918.

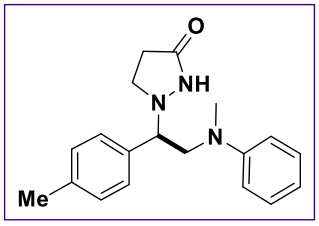

1-(1-(2-methoxyphenyl)-2-(methyl(phenyl)amino)ethyl)pyrazolidin-3-one (10) was prepared according to **GP** and obtained as a colorless oil (48.2 mg, 99%) after purification by flash column chromatography (0 – 5% MeOH/ DCM). **^{1}H NMR** (400 MHz, $CDCl_3$): δ 7.99 (s, 1H), 7.42 (d, *J* =

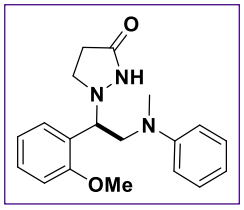

7.5 Hz, 1H), 7.30-7.23 (m, 3H), 6.99 (t, *J* = 7.5 Hz, 1H), 6.89 (d, *J* = 8.3 Hz, 1H), 6.83 (d, *J* = 8.3 Hz, 1H), 6.78 (t, *J* = 7.3 Hz, 1H), 4.60 (dd, *J* = 8.5, 4.6 Hz, 1H), 3.98 – 3.78 (m, 1H), 3.78 (s, 3H), 3.35 – 3.29 (m, 2H), 3.12 (d, *J* = 10.3 Hz, 1H), 2.84 (s, 3H), 2.38 – 2.24 (m, 2H); **^{13}C NMR** (101 MHz, $CDCl_3$) δ 174.2, 157.4, 149.8, 129.3, 129.2, 128.7, 121.1, 118.1, 114.0, 111.1, 61.6, 59.6, 55.7, 51.7, 39.3, 30.3; **HRMS** (ESI) m/z: $[M + H]^+$ Calcd for $C_{19}H_{24}N_3O_2$ 326.1863, Found: 326.1861.

1-(1-(3-methoxyphenyl)-2-(methyl(phenyl)amino)ethyl)pyrazolidin-3-one (11) was prepared according to **GP** and obtained as a colorless oil (48.3 mg, 99%) after purification by flash column chromatography (0 – 5% MeOH/ DCM). **^{1}H NMR** (400 MHz, $CDCl_3$): δ 8.42 (brs, 1H), 7.37 – 7.29 (m, 5H), 7.15 (t, *J* = 8.2 Hz, 1H), 6.33 (td, *J* = 9.0, 2.3 Hz, 2H), 6.25 – 6.24 (m, 1H), 3.99 – 3.91 (m, 2H), 3.78 (s, 3H), 3.35 (td, *J* = 10.8, 6.6 Hz, 1H), 3.30 – 3.23 (m, 1H), 3.20 (brs, 1H), 2.62 (s, 3H), 2.39 (dt, *J* = 16.1, 7.9 Hz, 1H), 2.22 (dt, *J* = 16.6, 8.3 Hz, 1H); **^{13}C NMR** (101 MHz, $CDCl_3$) δ 175.2, 160.9, 150.5, 149.8, 138.7, 130.1, 129.0, 128.5, 106.0, 102.15, 99.52, 69.88, 58.87, 55.22, 51.47, 39.63, 30.17; **HRMS** (ESI) m/z: $[M + H]^+$ Calcd for $C_{19}H_{24}N_3O_2$ 326.1863, Found: 326.1871.

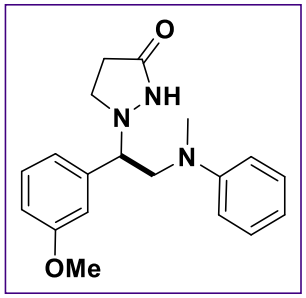

1-(1-(4-methoxyphenyl)-2-(methyl(phenyl)amino)ethyl)pyrazolidin-3-one (12) was prepared according to **GP** and obtained as a colorless oil (33.6 mg, 69%) after purification by flash column chromatography (0 – 5% MeOH/ DCM). **^{1}H NMR** (400 MHz, $CDCl_3$): δ 8.49 (brs, 1H), 7.27 – 7.23 (m, 4H), 6.88 (d, *J* = 8.4 Hz, 2H), 6.798– 6.73 (m, 3H), 3.97 – 3.87 (m, 2H), 3.81 (s, 3H), 3.34 (dd, *J* = 14.3, 6.2 Hz, 1H), 3.23 (dd, *J* = 9.2, 6.7 Hz, 1H), 3.18 (brs, 1H), 2.67 (s, 3H), 2.36 (dt, *J* = 15.8, 7.7 Hz, 1H), 2.21 (dt, *J* = 16.6, 8.3 Hz, 1H); **^{13}C NMR** (101 MHz, $CDCl_3$) δ 174.6, 159.8, 149.4, 130.4, 129.5, 129.5, 117.8, 114.4, 113.5, 69.3, 59.6, 55.4, 51.7, 39.6, 30.3; **HRMS** (ESI) m/z: $[M + H]^+$ Calcd for $C_{19}H_{24}N_3O_2$ 326.1863, Found: 326.1862.

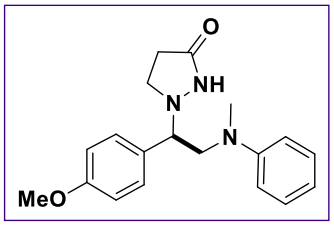

1-(1-([1,1'-biphenyl]-4-yl)-2-(methyl(phenyl)amino)ethyl)pyrazolidin-3-one (13) was prepared according to **GP** and obtained as a colorless oil (52.8 mg, 95%) after purification by flash column chromatography (0 – 5% MeOH/ DCM). **^{1}H NMR** (400 MHz, $CDCl_3$): δ 8.71 (s, 1H),

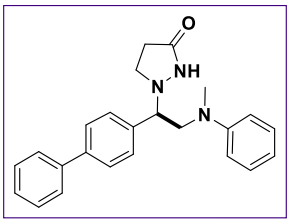

7.62 (dd, *J* = 7.9, 2.6 Hz, 4H), 7.50 – 7.38 (m, 5H), 7.31 – 7.28 (m, 2H), 6.82 – 6.78 (m, 3H), 4.08 – 4.01 (m, 2H), 3.49 – 3.42 (m, 1H), 3.38 – 3.31 (m, 1H), 3.26 (brs, 1H), 2.72 (s, 3H), 2.44 (dt, *J* = 15.9, 7.7 Hz, 1H), 2.29 (dt, *J* = 16.7, 8.4 Hz, 1H); **^{13}C NMR** (101 MHz, $CDCl_3$) δ 175.2, 149.2, 141.3, 140.5, 137.6, 129.4, 128.9, 127.6, 127.6, 127.1, 117.5, 113.1, 69.5, 59.1, 51.5, 39.7, 30.2; **HRMS** (ESI) m/z: $[M + H]^+$ Calcd for $C_{24}H_{26}N_3O$ 372.2070, Found: 372.2080.

1-(1-(benzo[d][1,3]dioxol-5-yl)-2-(methyl(phenyl)amino)ethyl)pyrazolidin-3-one (14) was prepared according to **GP** and obtained as a colorless oil (42.2 mg, 83%) after purification by flash column chromatography (0 – 5% MeOH/ DCM). **^{1}H NMR** (400 MHz, $CDCl_3$): δ 8.48 (s, 1H), 7.26 (t, *J* = 8.3 Hz, 2H), 6.88 (s, 1H), 6.80 – 6.73 (m, 5H), 5.99 (s, 2H), 3.94 (dd, *J* = 14.4, 6.6 Hz, 1H), 3.85 (t, *J* = 6.5 Hz, 1H), 3.34 (dd, *J* = 14.2, 6.3 Hz, 1H), 3.30 – 3.25 (m, 1H), 3.21 (brs, 1H), 2.71 (s, 3H), 2.43 (dt, *J* = 15.9, 7.8 Hz, 1H), 2.29 (dt, *J* = 16.7, 8.3 Hz, 1H); **^{13}C NMR** (101 MHz, $CDCl_3$) δ 175.1, 149.1, 148.2, 147.7, 132.4, 129.4, 122.2, 117.5, 113.1, 108.6, 108.3, 101.3, 69.5, 59.1, 51.4, 39.7, 30.2; **HRMS** (ESI) m/z: $[M + H]^+$ Calcd for $C_{19}H_{22}N_3O_3$ 340.1656, Found: 340.1668.

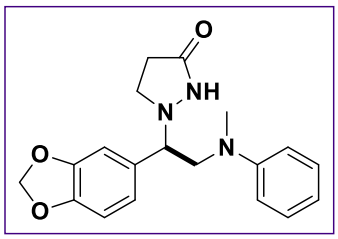

1-(2-(methyl(phenyl)amino)-1-(thiophen-2-yl)ethyl)pyrazolidin-3-one (15) was prepared according to **GP** and obtained as a colorless oil (15.9 mg, 35%) after purification by flash column chromatography (0 – 5% MeOH/ DCM). **^{1}H NMR** (400 MHz, $CDCl_3$): δ 8.37 (brs, 1H), 7.35 – 7.33 (m, 1H), 7.28 – 7.24 (m, 2H), 7.01 – 6.99 (m, 2H), 6.77 (d, *J* = 7.2 Hz, 1H), 6.73 (d, *J* = 8.5 Hz, 2H), 4.30 (t, *J* = 6.7 Hz, 1H), 3.93 (dd, *J* = 14.8, 6.9 Hz, 1H), 3.49 (dd, *J* = 14.9, 6.5 Hz, 1H), 3.40 – 3.28 (m, 2H), 2.80 (s, 3H), 2.26 (dt, *J* = 15.6, 7.5 Hz, 1H), 2.10 (dt, *J* = 17.0, 8.7 Hz, 1H); **^{13}C NMR** (101 MHz, $CDCl_3$) δ 176.0, 148.9, 139.9, 129.5, 127.4, 127.0, 126.4, 117.4, 112.9, 64.9, 58.9, 51.3, 39.6, 30.2; **HRMS** (ESI) m/z: $[M + H]^+$ Calcd for $C_{16}H_{20}N_3OS$ 302.1322, Found: 302.1321.

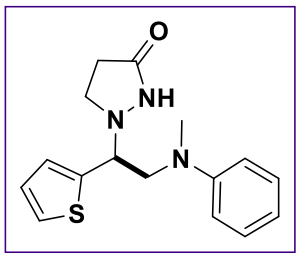

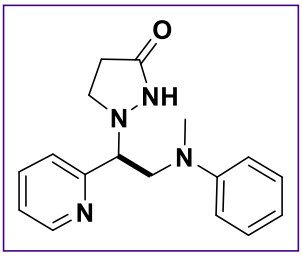

1-(2-(methyl(phenyl)amino)-1-(pyridin-2-yl)ethyl)pyrazolidin-3-one (16) was prepared according to **GP** and obtained as a colorless oil (43.7 mg, 98%) after purification by flash column chromatography (0 – 5% MeOH/ DCM). **^{1}H NMR** (400 MHz, $CDCl_3$): δ 8.67 (d, *J* = 4.8 Hz, 1H), 8.05 (brs, 1H), 7.65 (t, *J* = 7.7 Hz, 1H), 7.28 – 7.20 (m, 4H), 6.78 – 6.71 (m, 3H), 4.19 (t, *J* = 6.7 Hz, 1H), 3.98 (dd, *J* = 14.7, 6.4 Hz, 1H), 3.69 (dd, *J* = 14.7, 6.9 Hz, 1H), 3.46 (t, *J* = 8.1 Hz, 2H), 2.71 (s, 3H), 2.36 (t, *J* = 8.1 Hz, 2H); **^{13}C NMR** (101 MHz, $CDCl_3$) δ 174.8, 158.1, 150.0, 149.1, 136.8, 129.4, 124.4, 123.3, 117.4, 112.9, 69.9, 56.6, 50.6, 39.4, 30.3; **HRMS** (ESI) m/z: $[M + H]^+$ Calcd for $C_{17}H_{21}N_4O$ 297.1710, Found: 297.1713.

1-(1-cyclohexyl-2-(methyl(phenyl)amino)ethyl)pyrazolidin-3-one (17) was prepared according to **GP** and obtained as a colorless oil (27.2 mg, 60%) after purification by flash column chromatography (0 – 5% MeOH/ DCM). **^{1}H NMR** (400 MHz, $CDCl_3$): δ 8.55 (s, 1H), 7.19 (t, *J* = 7.8 Hz, 2H), 6.84 – 6.77 (m, 3H), 3.47 – 3.41 (m, 1H), 3.35 (dd, *J* = 14.4, 9.5 Hz, 1H), 3.19 (dd, *J* = 14.5, 2.5 Hz, 1H), 2.97 – 2.89 (m, 1H), 2.76 (s, 3H), 2.63 (dt, *J* = 9.7, 3.0 Hz, 1H), 2.43 (ddd, *J* = 16.4, 11.6, 8.8 Hz, 1H), 2.29 (ddd, *J* = 16.4, 8.6, 3.2 Hz, 1H), 1.75 – 1.56 (m, 5H), 1.28 – 0.98 (m, 6H); **^{13}C NMR** (101 MHz, $CDCl_3$) δ 172.7, 150.7, 129.4, 119.9, 116.2, 67.7, 56.5, 51.7, 40.0, 38.9, 31.0, 30.9, 27.3, 27.0, 26.7, 26.7; **HRMS** (ESI) m/z: $[M + H]^+$ Calcd for $C_{18}H_{28}N_3O$ 302.2227, Found: 302.2226.

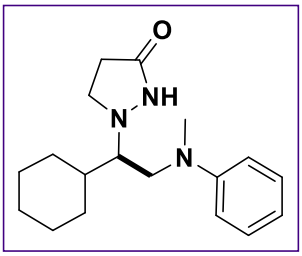

5-methyl-1-(2-(methyl(phenyl)amino)-1-phenylethyl)pyrazolidin-3-one (18) was prepared according to **GP** and obtained as a colorless oil (45.9 mg, 99%, 1:1 dr) after purification by flash column chromatography (0 – 5% MeOH/ DCM). **^{1}H NMR** (400 MHz, $CDCl_3$): δ 9.16 (brs, 1H), 8.87 (s, 1H), 7.28 – 7.20 (m, 10H), 7.17 – 7.11 (m, 4H), 7.65 – 7.53 (m, 6H), 4.07 – 3.95 (m, 3H), 3.84 (dd, *J* = 15.1, 7.0 Hz, 1H), 3.58 (dd, *J* = 15.1, 6.2 Hz, 2H), 3.43 – 3.35 (m, 1H), 3.24 (ddd, *J* = 19.5, 14.1, 7.9 Hz, 1H), 2.82 (dd, *J* = 16.8, 7.9 Hz, 1H), 2.76 (s, 3H), 2.32 (s, 3H), 1.90 (dd, *J* = 16.7, 8.2 Hz, 1H), 1.77 (d, *J* = 16.8 Hz, 1H), 1.60 (dd, *J* = 16.7, 2.6 Hz, 1H), 1.13 (d, *J* = 6.6 Hz, 1H), 1.01 (d, *J* = 6.7 Hz, 1H); **^{13}C NMR** (101 MHz, $CDCl_3$) δ 176.7, 176.0, 148.8, 148.7, 140.4, 137.3, 129.4, 129.1, 128.8, 128.4, 128.2, 128.2, 116.4, 116.3, 112.2, 112.0, 68.8, 67.9, 58.5, 57.0, 56.4, 56.1, 39.9, 39.4, 37.1, 35.2, 21.6, 21.4; **HRMS** (ESI) m/z: $[M + H]^+$ Calcd for $C_{19}H_{24}N_3O$ 310.1914, Found: 310.1916.

***N, N*- Dimethyl Anilines Scope**

1-(2-(methyl(4-(trifluoromethyl)phenyl)amino)-1-phenylethyl)pyrazolidin-3-one (19) was

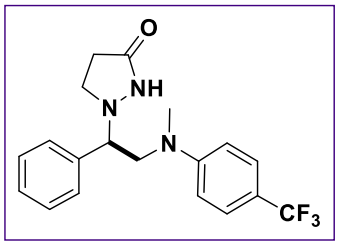

prepared according to **GP** and obtained as a colorless oil (51.2 mg, 94%) after purification by flash column chromatography (0 – 5% MeOH/ DCM). **^{1}H NMR** (400 MHz, $CDCl_3$): δ 9.02 (brs, 1H), 7.43 (d, *J* = 8.6 Hz, 2H), 7.36 – 7.32 (m, 3H), 7.30 – 7.28 (m, 2H), 6.64 (d, *J* = 8.6 Hz, 2H), 4.10 (dd, *J* = 14.8, 5.5 Hz, 1H), 3.93 (dd, *J* = 8.1, 5.5 Hz, 1H), 3.52 – 3.46 (m, 1H), 3.32 – 3.26 (m, 2H), 2.60 (s, 3H), 2.43 (dt, *J* = 16.5, 8.2 Hz, 1H), 2.18 (dt, *J* = 16.5, 8.1 Hz, 1H); **^{13}C NMR** (101 MHz, $CDCl_3$) δ 176.2, 150.8, 138.2, 129.1, 128.7, 128.6, 126.7 (q, *J* = 3.8 Hz), 125.2 (q, *J* = 270.2 Hz), 117.97 (q, *J* = 32.4 Hz), 111.2, 69.6, 57.3, 51.1, 39.7, 30.1; **HRMS** (ESI) m/z: $[M + H]^+$ Calcd for $C_{19}H_{21}F_3N_3O$ 364.1631, Found: 364.1637.

1-(2-((4-chlorophenyl)(methyl)amino)-1-phenylethyl)pyrazolidin-3-one (20) was prepared

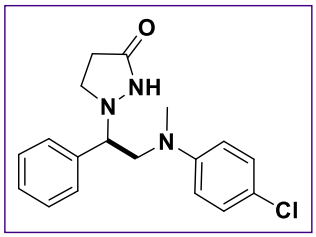

according to **GP** and obtained as a colorless oil (34.2 mg, 69%) after purification by flash column chromatography (0 – 5% MeOH/ DCM). **^{1}H NMR** (400 MHz, $CDCl_3$): δ 8.53 (brs, 1H), 7.37 – 7.28 (m, 5H), 7.16 (d, *J* = 8.8 Hz, 2H), 6.59 (d, *J* = 8.9 Hz, 2H), 3.97 – 3.87 (m, 2H), 3.37 (dd, *J* = 14.0, 6.4 Hz, 1H), 3.29 – 3.22 (m, 1H), 3.20 (brs, 1H), 2.59 (s, 3H), 2.40 (dt, *J* = 16.1, 7.8 Hz, 1H), 2.21 (dt, *J* = 16.6, 8.3 Hz, 1H); **^{13}C NMR** (101 MHz, $CDCl_3$) δ 175.4, 147.7, 138.4, 129.2, 129.0, 128.6, 128.5, 122.1, 114.0, 69.8, 58.7, 51.4, 39.7, 30.2; **HRMS** (ESI) m/z: $[M + H]^+$ Calcd for $C_{18}H_{21}ClN_3O$ 330.1368, Found: 330.13646.

1-(2-((2-bromophenyl)(methyl)amino)-1-phenylethyl)pyrazolidin-3-one (21) was prepared

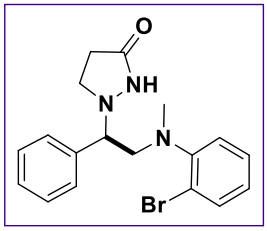

according to **GP** and obtained as a colorless oil (59.0 mg, 99%) after purification by flash column chromatography (0 – 5% MeOH/ DCM). **^{1}H NMR** (400 MHz, $CDCl_3$): δ 9.23 (s, 1H), 7.53 (d, J = 7.9 Hz, 1H), 7.31 – 7.23 (m, 5H), 7.19 (t, J = 7.6 Hz, 1H), 6.99 (d, J = 8.0 Hz, 1H), 6.92 (t, J = 7.6 Hz, 1H), 3.67 (d, J = 10.0 Hz, 1H), 3.40 (dd, J = 13.2, 10.1 Hz, 1H), 3.09 – 3.04 (m, 2H), 2.72 (s, 3H), 2.67– 2.59 (m, 1H), 2.32 – 2.19 (m, 1H); **^{13}C NMR** (101 MHz, $CDCl_3$) δ 172.8, 150.9, 138.3, 134.0, 129.0, 128.6, 128.5, 128.1, 126.0, 122.6, 121.5, 69.4, 63.7, 52.3, 43.4, 30.5; **HRMS** (ESI) m/z: $[M + H]^+$ Calcd for $C_{18}H_{21}BrN_3O$ 374.0862, Found: 374.0869.

1-(2-((3-bromophenyl)(methyl)amino)-1-phenylethyl)pyrazolidin-3-one (22) was prepared

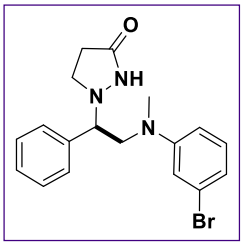

according to **GP** and obtained as a colorless oil (54.1 mg, 97%) after purification by flash column chromatography (0 – 5% MeOH/ DCM). **^{1}H NMR** (400 MHz, $CDCl_3$): δ 8.72 (s, 1H), 7.37 – 7.29 (m, 5H), 7.05 (t, *J* = 8.1 Hz, 1H), 6.82 (d, *J* = 7.8 Hz, 1H), 6.75 (s, 1H), 6.58 (d, *J* = 8.4 Hz, 1H), 3.98 (dd, *J* = 14.6, 5.9 Hz, 1H), 3.90 (t, *J* = 6.6 Hz, 1H), 3.41 (dd, *J* = 14.6, 7.4 Hz, 1H), 3.30 – 3.20 (m, 2H), 2.58 (s, 3H), 2.41 (dt, *J* = 16.3, 8.0 Hz, 1H), 2.20 (dt, *J* = 16.6, 8.2 Hz, 1H); **^{13}C NMR** (101 MHz, $CDCl_3$) δ 175.7, 150.1, 138.4, 130.5, 129.0, 128.6, 128.5, 123.7, 119.6, 115.3, 111.0, 69.7, 57.9, 51.3, 39.6, 30.2; **HRMS** (ESI) m/z: $[M + H]^+$ Calcd for $C_{18}H_{21}BrN_3O$ 374.0862, Found: 374.0866.

1-(2-((4-bromophenyl)(methyl)amino)-1-phenylethyl)pyrazolidin-3-one (23) was prepared

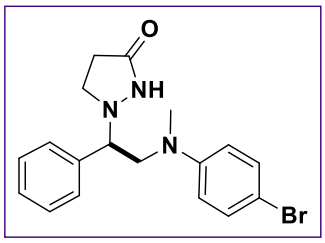

according to **GP** and obtained as a colorless oil (50.7 mg, 91%) after purification by flash column chromatography (0 – 5% MeOH/ DCM). **^{1}H NMR** (400 MHz, $CDCl_3$): δ 8.43 (s, 1H), 7.28 – 7.18 (m, 7H), 6.46 (d, *J* = 8.7 Hz, 2H), 3.90 – 3.80 (m, 2H), 3.30 (dd, *J* = 14.2, 6.7 Hz, 1H), 3.22 – 3.12 (m, 1H), 3.12 (brs, 1H), 2.51 (s, 3H), 2.32 (dt, *J* = 16.4, 8.1 Hz, 1H), 2.13 (dt, *J* = 16.5, 8.2 Hz, 1H); **^{13}C NMR** (101 MHz, $CDCl_3$) δ 175.6, 148.0, 138.4, 132.1, 129.0, 128.6, 128.5, 114.4, 109.1, 69.7, 58.4, 51.4, 39.7, 30.1; **HRMS** (ESI) m/z: $[M + H]^+$ Calcd for $C_{18}H_{21}BrN_3O$ 374.0862, Found: 374.0865.

1-(2-(methyl(3-methylphenyl)amino)-1-phenylethyl)pyrazolidin-3-one (24) was prepared

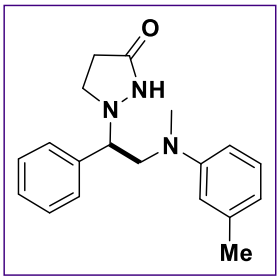

according to **GP** and obtained as a colorless oil (39.0 mg, 84%) after purification by flash column chromatography (0 – 5% MeOH/ DCM). **^{1}H NMR** (400 MHz, $CDCl_3$): δ 8.44 (brs, 1H), 3.38 – 3.31 (m, 5H), 7.14 (t, *J* = 7.8 Hz, 1H), 6.61 – 6.54 (m, 3H), 3.97 – 3.91 (m, 2H), 3.35 (q, *J* = 8.9 Hz, 1H), 3.30 – 3.23 (m, 1H), 3.18 (brs, 1H), 2.67 (s, 3H), 2.38 (dt, *J* = 15.8, 7.7 Hz, 1H), 2.32 (s, 3H), 2.24 (dt, *J* = 16.8, 8.4 Hz, 1H); **^{13}C NMR** (101 MHz, $CDCl_3$) δ 174.9, 149.4, 139.1, 138.7, 129.2, 129.0, 128.5, 118.6, 114.2, 110.5, 69.9, 59.4, 51.6, 39.6, 30.2, 22.0; **HRMS** (ESI) m/z: $[M + H]^+$ Calcd for $C_{19}H_{24}N_3O$ 310.1914, Found: 310.1912.

1-(2-(methyl(p-tolyl)amino)-1-phenylethyl)pyrazolidin-3-one (25) was prepared according to **GP** and obtained as a colorless oil (41.1 mg, 88%) after purification by flash column

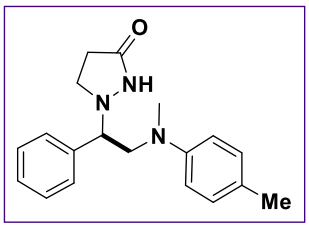

chromatography (0 – 5% MeOH/ DCM). **^{1}H NMR** (400 MHz, $CDCl_3$): δ 8.50 (brs, 1H), 7.38 – 7.28 (m, 5H), 7.06 (d, *J* = 8.3 Hz, 2H), 6.70 (d, *J* = 8.2 Hz, 2H), 3.91 – 3.85 (m, 2H), 3.33 – 3.21 (m, 2H), 3.11 (brs, 1H), 2.66 (s, 3H), 2.40 – 2.33 (m, 1H), 2.27 (s, 3H), 2.29 – 2.21 (m, 1H); **^{13}C NMR** (101 MHz, $CDCl_3$) δ 174.5, 147.4, 138.6, 129.9, 129.0, 128.46, 128.4, 127.4, 114.1, 69.9, 60.2, 51.7, 39.9, 30.2, 20.4; **HRMS** (ESI) m/z: $[M + H]^+$ Calcd for $C_{19}H_{24}N_3O$ 310.1914, Found: 310.1924.

1-(2-((2-methoxyphenyl)(methyl)amino)-1-phenylethyl)pyrazolidin-3-one (26) was prepared

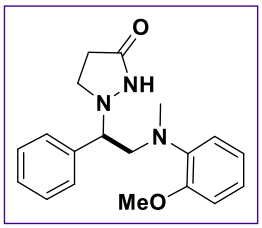

according to **GP** and obtained as a colorless oil (38.5 mg, 79%) after purification by flash column chromatography (0 – 5% MeOH/ DCM). **^{1}H NMR** (400 MHz, $CDCl_3$): δ 10.09 (brs, 1H), 7.36 – 7.28 (m, 5H), 7.09 (t, *J* = 7.8 Hz, 1H), 7.02 – 6.96 (m, 1H), 6.92 – 6.88 (m, 2H), 3.97 (s, 3H), 3.71 (d, *J* = 10.4 Hz, 1H), 3.46 (dd, *J* = 13.4, 10.5 Hz, 1H), 3.11 – 3.03 (m, 5H), 2.76 (s, 3H), 2.72 – 2.58 (m, 1H), 2.33 – 2.25 (m, 1H); **^{13}C NMR** (101 MHz, $CDCl_3$) δ 172.3, 153.8, 141.5, 138.2, 128.9, 128.4, 128.2, 125.0, 121.4, 121.0, 111.4, 69.4, 55.6, 52.5, 41.8, 30.5, 30.4; **HRMS** (ESI) m/z: $[M + H]^+$ Calcd for $C_{19}H_{24}N_3O_2$ 326.1863, Found: 326.1876.

1-(2-((3-methoxyphenyl)(methyl)amino)-1-phenylethyl)pyrazolidin-3-one (27) was

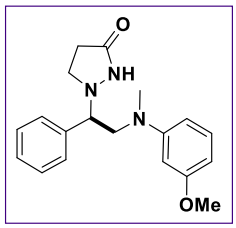

prepared according to **GP** and obtained as a colorless oil (34.0 mg, 70%) after purification by flash column chromatography (0 – 5% MeOH/ DCM). **^{1}H NMR** (400 MHz, $CDCl_3$): δ 8.42 (brs, 1H), 7.37 – 7.29 (m, 5H), 7.15 (t, *J* = 8.2 Hz, 1H), 6.34 (td, *J* = 9.0, 2.3 Hz, 2H), 6.24 (t, *J* = 2.5 Hz, 1H), 3.99 – 3.91 (m, 2H), 3.78 (s, 3H), 3.36 (td, *J* = 10.8, 6.6 Hz, 1H), 3.27 (dt, *J* = 10.3, 7.9 Hz, 1H), 3.21 (brs, 1H), 2.62 (s, 3H), 2.40 (dt, *J* = 16.1, 7.9 Hz, 1H), 2.23 (dt, *J* = 16.6, 8.3 Hz, 1H); **^{13}C NMR** (101 MHz, $CDCl_3$) δ 175.2, 160.9, 150.5, 138.7, 130.1, 129.0, 128.5, 106.0, 102.1, 99.5, 69.9, 58.9, 55.2, 51.5, 39.6, 30.2; **HRMS** (ESI) m/z: $[M + H]^+$ Calcd for $C_{19}H_{24}N_3O2$ 326.1863, Found: 326.1871.

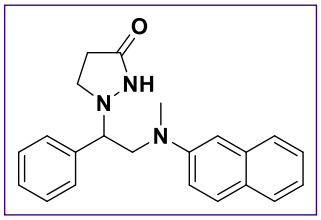

1-(2-(methyl(naphthalen-2-yl)amino)-1-phenylethyl)pyrazolidin-3-one (29) was prepared according to **GP** and obtained as a colorless oil (17.6 mg, 64%) after purification by flash column chromatography (0 – 5% MeOH/ DCM). **^{1}H NMR** (400 MHz, $CDCl_3$): δ 8.15 (d, *J* = 8.3 Hz, 1H), 7.78 (d, *J* = 8.1 Hz, 1H), 7.54 (d, *J* = 8.2 Hz, 1H), 7.50 (t, *J* = 7.7 Hz, 1H), 7.43 (t, *J* = 7.4 Hz, 1H), 7.33 (t, *J* = 8.0 Hz, 1H), 7.29 – 7.23 (m, 5H), 7.05 (d, *J* = 7.5 Hz, 1H), 3.79 (dd, *J* = 8.9, 3.1 Hz, 1H), 3.64 (dd, *J* = 13.4, 9.0 Hz, 1H), 3.20 – 3.15 (m, 2H), 2.86 (s, 3H), 2.25 (dd, *J* = 9.2, 4.7 Hz, 2H); **^{13}C NMR** (101 MHz, $CDCl_3$) δ 173.3, 148.7, 138.3, 135.0, 129.1, 128.7, 128.6, 128.2, 126.5, 126.3, 126.2, 125.6, 125.0, 123.2, 116.3, 69.7, 63.4, 52.2, 44.4, 30.4; **HRMS** (ESI) m/z: $[M + H]^+$ Calcd for $C_{22}H_{24}N_3O$ 346.1914, Found: 346.1924.

1-(2-(methyl(4-methyl-2-oxo-2H-chromen-7-yl)amino)-1-phenylethyl)pyrazolidin-3-one (30)

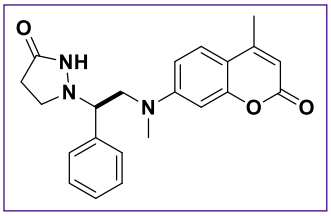

was prepared according to **GP** and obtained as a yellow solid (62.8 mg, 92%) after purification by flash column chromatography (0 – 5% MeOH/ DCM). **^{1}H NMR** (400 MHz, $CDCl_3$): δ 9.27 (brs, 1H), 7.31 – 7.32 (m, 6H), 6.50 (dd, *J* = 9.0, 2.5 Hz, 1H), 6.41 (d, *J* = 2.5 Hz, 1H), 5.90 (s, 1H), 4.12 (dd, *J* = 14.8, 5.4 Hz, 1H), 3.92 (dd, *J* = 8.4, 5.3 Hz, 1H), 3.48 (dd, *J* = 14.8, 8.4 Hz, 1H), 3.31 – 3.15 (m, 1H), 2.55 (s, 3H), 2.40 (dt, *J* = 16.6, 7.9 Hz, 1H), 2.26 (s, 3H), 2.13 (dt, *J* = 16.6, 8.1 Hz, 1H); **^{13}C NMR** (101 MHz, $CDCl_3$) δ 176.4, 162.1, 155.8, 152.9, 151.5, 138.0, 129.0, 128.7, 128.5, 125.5, 109.9, 109.4, 108.8, 98.4, 69.5, 57.0, 51.1, 39.9, 30.2, 18.5; **HRMS** (ESI) m/z: $[M + H]^+$ Calcd for $C_{22}H_{24}N_3O_3$ 378.1812, Found: 378.1804.

1-(2-((3-methoxybenzyl)(methyl)amino)-1-phenylethyl)pyrazolidin-3-one (31) was prepared

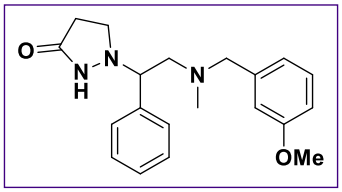

according to **GP** and obtained as a colorless oil (29.8 mg, 88%) after purification by flash column chromatography (0 – 5% MeOH/ DCM). **^{1}H NMR** (400 MHz, $CDCl_3$): δ 10.06 (brs, 1H), 7.32 – 7.26 (m, 3H), 7.25 – 7.20 (m, 3H), 6.84 – 6.79 (m, 3H), 3.79 (s, 3H), 3.66 (d, *J* = 12.8 Hz, 1H), 3.61 (dd, *J* = 10.6, 2.1 Hz, 1H), 3.37 (d, *J* = 12.8 Hz, 1H), 3.06 (td, *J* = 10.1, 3.9 Hz, 2H), 2.62 – 2.54 (m, 1H), 2.38 – 2.29 (m, 2H), 2.27 (s, 3H), 2.25 – 2.21 (m, 1H); **^{13}C NMR** (101 MHz, $CDCl_3$) δ 171.6, 160.0, 138.9, 138.1, 129.7, 128.9, 128.5, 128.0, 121.7, 114.2, 113.8, 69.2, 65.7, 63.1, 55.4, 52.7, 42.4, 30.6; **HRMS** (ESI) m/z: $[M + H]^+$ Calcd for $C_{20}H_{26}N_3O_2$ 340.2025, Found: 340.2032.

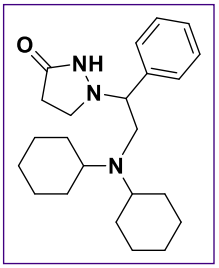

1-(2-(dicyclohexylamino)-1-phenylethyl)pyrazolidin-3-one (32) was prepared according to **GP** and obtained as a colorless oil (54.8 mg, 99%) after purification by flash column chromatography (0 – 5% MeOH/ DCM). **^{1}H NMR** (400 MHz, $CDCl_3$): δ 10.79 (s, 1H), 7.35 – 7.28 (m, 5H), 3.55 (d, *J* = 10.4 Hz, 1H), 3.08 (td, *J* = 9.2, 2.7 Hz, 1H), 2.94 (dd, *J* = 14.2, 10.6 Hz, 1H), 2.75 – 2.63 (m, 3H), 2.56 – 2.48 (m, 1H), 2.35 (ddd, *J* = 16.2, 12.1, 8.6 Hz, 1H), 2.22 (ddd, *J* = 16.2, 8.7, 2.7 Hz, 1H), 1.82 – 1.73 (m, 8H), 1.61 (d, *J* = 12.8 Hz, 2H), 1.47 (qd, *J* = 11.9, 3.5 Hz, 2H), 1.29 (dddd, *J* = 18.4, 14.7, 9.5, 5.2 Hz, 2H), 1.18 (dd, *J* = 11.5, 8.7 Hz, 4H), 1.07 (dddd, *J* = 16.0, 12.6, 8.1, 3.5 Hz, 2H); **^{13}C NMR** (101 MHz, $CDCl_3$) δ 170.6, 138.7, 128.8, 128.2, 128.0, 70.5, 58.4, 54.9, 53.2, 32.2, 30.4, 30.0, 26.5, 26.4, 26.1; **HRMS** (ESI) m/z: $[M + H]^+$ Calcd for $C_{23}H_{36}N_3O$ 370.2853, Found: 370.2864.

1-(2-(diphenylamino)-1-phenylethyl)pyrazolidin-3-one (33) was prepared according to **GP**

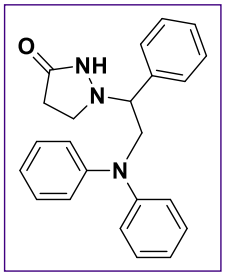

and obtained as a colorless oil (49.1 mg, 92%) after purification by flash column chromatography (0 – 5% MeOH/ DCM). **^{1}H NMR** (400 MHz, $CDCl_3$): δ 7.95 (brs, 1H), 7.23 – 7.18 (m, 5H), 7.14 – 7.10 (m, 4H), 6.85 (t, *J* = 7.3 Hz, 2H), 6.75 (d, *J* = 8.0 Hz, 4H), 4.18 (td, *J* = 9.9, 7.2 Hz, 1H), 3.92 – 3.85 (m, 2H), 3.18 (t, *J* = 8.0 Hz, 2H), 2.22 (dt, *J* = 16.1, 7.8 Hz, 1H), 2.05 (dt, *J* = 16.6, 8.2 Hz, 1H); **^{13}C NMR** (101 MHz, $CDCl_3$) δ 175.5, 148.1, 138.4, 129.4, 128.9, 128.6, 128.5, 121.9, 121.4, 69.7, 57.5, 51.4, 30.2; **HRMS** (ESI) m/z: $[M + H]^+$ Calcd for $C_{23}H_{24}N_3O$ 358.1914, Found: 358.1926.

1-(2-(ethyl(phenyl)amino)-1-phenylpropyl)pyrazolidin-3-one (34) was prepared according to

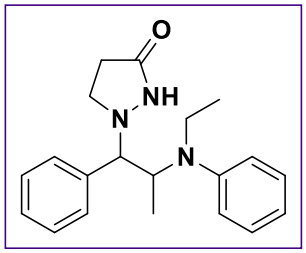

GP and obtained as a colorless oil (34.4 mg, 71%, 1:1 dr) after purification by flash column chromatography (0 – 5% MeOH/ DCM). **^{1}H NMR** (400 MHz, $CDCl_3$): δ 9.29 (brs, 1H), 8.59 (brs, 0.42H), 7.41 – 7.32 (m, 5H), 7.30 – 7.22 (m, 6H), 7.15 (t, *J* = 7.6 Hz, 2H), 7.06 (d, *J* = 8.1 Hz, 1H), 6.91 (t, *J* = 7.3 Hz, 0.67H), 6.75 (d, *J* = 8.5 Hz, 2H), 6.71 (d, *J* = 7.3 Hz, 0.72H), 4.30 (p, *J* = 6.6 Hz, 1H), 4.17 (h, *J* = 7.0, 0.72H), 3.82 (d, *J* = 9.4 Hz, 1H), 3.74 (d, *J* = 9.0 Hz, 0.65H), 3.54 (q, *J* = 10.3 Hz, 1H), 3.37 (ddd, *J* = 15.1, 8.6, 4.1 Hz, 1H), 3.26 – 2.92 (m, 4H), 2.32 – 2.13 (m, 1H), 1.83 (ddd, *J* = 16.5, 8.7, 4.1 Hz, 1H), 1.60 – 1.50 (m, 1H), 1.44 (d, *J* = 6.4 Hz, 4H), 1.19 (t, *J* = 6.9 Hz, 2H), 0.88 – 0.82 (m, 5H); **^{13}C NMR** (101 MHz, $CDCl_3$) δ 176.6, 174.1, 148.45, 148.2, 137.91, 135.9, 129.5, 129.5, 129.1, 129.0, 128.5, 128.3, 128.1, 119.8, 117.9, 117.6, 115.9, 75.6, 74.3, 55.9, 52.2, 50.9, 39.1, 37.9,

30.4, 30.3, 16.1, 14.0, 13.2; **HRMS** (ESI) m/z: $[M + H]^+$ Calcd for $C_{20}H_{26}N_3O$ 324.2070, Found: 324.2080.

1-(phenyl(4-phenylmorpholin-3-yl)methyl)pyrazolidin-3-one (35) was prepared according to **GP** and obtained as a colorless oil (41.2 mg, 81% as a mixture of diastereoisomers, 1.8:1 dr) after purification by flash column chromatography (0 – 5% MeOH/ DCM). **^{1}H NMR** (400 MHz, $CDCl_3$): δ 7.38 – 7.39 (m, 5H), 7.33 (t, *J* = 7.8 Hz, 2H), 6.99 (d, *J* = 8.2 Hz, 2H), 6.87 (td, *J* = 7.3, 1.1 Hz, 1H), 4.44 (d, *J* = 10.1 Hz, 1H), 3.98 (dd, *J* = 9.7, 2.6 Hz, 1H), 3.94 – 3.90 (m, 1H), 3.77 – 3.64 (m, 2H), 3.54 (dd, *J* = 11.6, 3.1 Hz, 1H), 3.37 (d, *J* = 12.5 Hz, 1H), 3.31 (d, *J* = 11.6 Hz, 1H), 3.23 – 3.18 (m, 1H), 3.13 (td, *J* = 11.1, 10.1, 3.4 Hz, 1H), 1.96 – 1.89 (m, 1H), 1.72 – 1.65 (m, 1H); ***^{13}C NMR** (101 MHz, $CDCl_3$) δ 175.8, 150.5, 136.7, 129.9, 129.2, 129.1, 128.8, 119.8, 116.5, 68.9, 66.9, 66.0, 61.1, 52.4, 42.7, 30.4; **HRMS** (ESI) m/z: $[M + H]^+$ Calcd for $C_{20}H_{24}N_3O_2$ 338.1863, Found: 338.1858. (*Datas for the isolated diastereoisomer).

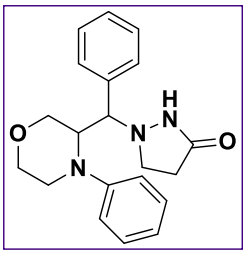

1-(2-((3-(5H-dibenzo[a,d][7]annulen-5-ylidene)propyl)(methyl)amino)-1-phenylethyl)pyrazolidin-3-one (36) was prepared according to **GP** and obtained as a colorless oil (66.4 mg, 98%) after purification by flash column chromatography (0 – 5% MeOH/ DCM). **^{1}H NMR** (400 MHz, $CDCl_3$): δ 9.98 (brs, 1H), 7.39 – 7.28 (m, 10H), 7.27 – 7.22 (m, 3H), 6.89 – 6.81 (m, 2H), 5.53 (td, *J* = 6.9, 6.4, 4.5 Hz, 1H), 3.53 (t, *J* = 9.7 Hz, 1H), 3.07 (qd, *J* = 9.0, 3.0 Hz, 1H), 2.92 (ddd, *J* = 13.0, 10.6, 4.8 Hz, 1H), 2.67 – 2.26 (m, 8H), 2.24 (s, 3H); **^{13}C NMR** (101 MHz, $CDCl_3$) δ 171.5, 143.3, 142.5, 138.1, 137.2, 134.8, 134.8, 134.0, 131.4, 131.4, 131.1, 130.9, 128.9, 128.8, 128.7, 128.6, 128.4, 128.3, 128.0, 128.0, 127.7, 127.1, 126.9, 69.1, 65.6, 58.0, 57.9, 52.7, 42.1, 42.1, 30.5, 26.0, 25.8; **HRMS** (ESI) m/z: $[M + H]^+$ Calcd for $C_{30}H_{32}N_3O$ 450.2540, Found: 450.2549.

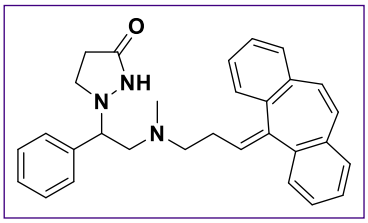

(S)-1-(4-fluorophenyl)-1-(3-(methyl((R)-2-(3-oxopyrazolidin-1-yl)-2-phenylethyl)amino)propyl)-1,3-dihydroisobenzofuran-5-carbonitrile (37) was prepared according to **GP** and obtained as a colorless oil (64.3 mg, 86%, 1:1 dr) after purification by flash column chromatography (0 – 5% MeOH/ DCM). **^{1}H NMR** (400 MHz, $CDCl_3$): δ 10.15 (brs, 1H), 7.56 (dd, *J* = 8.1, 3.0 Hz, 1H), 7.51 – 7.46 (m, 1H), 7.44 – 7.39 (m, 3H), 7.29 – 7.21 (m, 2H), 7.19 – 7.16 (m, 3H), 6.96 (t, *J* = 8.6 Hz, 2H), 5.15 (dd, *J* = 13.0, 3.4 Hz, 1H), 5.09 (dd, *J* = 13.1, 5.6 Hz, 1H), 3.49 (dt, *J* = 11.1, 2.4 Hz, 1H), 3.03 (td, *J* = 9.6, 2.7 Hz, 1H), 2.86 (t, *J* = 12.0 Hz, 1H), 2.53 (dd, *J* = 20.7, 9.5 Hz, 1H), 2.43 (dt, *J* = 13.4, 7.1 Hz, 1H), 2.34 – 2.17 (m, 5H), 2.12 (d, *J* = 4.3 Hz, 3H), 2.09 – 2.03 (m, 1H), 1.42 (dqt, *J* = 31.5, 12.8, 6.5 Hz, 2H); **^{13}C NMR** (101 MHz, $CDCl_3$) δ 171.6, 162.2 (d, *J* = 246.2 Hz), 149.6, 140.2, 139.5, 139.4, 137.9, 132.2, 129.0, 128.5, 128.0, 126.9, 126.8, 125.3 (d, *J* = 3.8 Hz), 123.1, 123.0, 118.8, 115.5 (d, *J* = 21.4 Hz), 111.9, 91.1, 91.1, 71.5, 71.4, 69.0, 66.4, 58.0, 58.0, 52.8, 41.8, 41.6, 39.2, 30.6, 21.3, 21.2; **HRMS** (ESI) m/z: $[M + H]^+$ Calcd for $C_{30}H_{32}FN_4O_2$ 499.2504, Found: 499.2505.

1-(2-((3-(4-chlorophenyl)-3-(pyridin-2-yl)propyl)(methyl)amino)-1-phenylethyl)pyrazolidin-3-one (38)

was prepared according to **GP** and obtained as a colorless oil (59.4 mg, 88%) after purification by flash column chromatography (0 – 5% MeOH/ DCM). **^{1}H NMR** (400 MHz, $CDCl_3$): δ 10.24 (brs, 1H), 8.60 (t, *J* = 5.5 Hz, 1H), 7.60 (t, *J* = 7.7 Hz, 1H), 7.37 – 7.32 (m, 5H), 7.29 – 7.26 (m, 5H), 7.18 (dd, *J* = 7.9, 3.3 Hz, 1H), 7.14 (t, *J* = 6.3, 1H), 4.09 (dt, *J* = 14.2, 7.5 Hz, 1H), 3.55 (t, *J* = 11.5 Hz, 1H), 3.13 – 3.08 (m, 1H), 3.01 (brs, 1H), 2.67 – 2.45 (m, 3H), 2.34 – 2.19 (m, 8H); **^{13}C NMR** (101 MHz, $CDCl_3$) δ 171.4, 162.7, 162.5, 149.5, 141.8, 141.8, 138.0, 136.9, 136.8, 132.5, 129.5, 128.9, 128.8, 128.5, 128.1, 128.0, 123.2, 123.0, 121.8, 69.1, 65.9, 56.4, 52.8, 52.7, 50.9, 50.7, 42.3, 42.0, 31.8, 30.6; **HRMS** (ESI) m/z: $[M + H]^+$ Calcd for $C_{26}H_{30}ClN_4O$ 449.2103, Found: 449.2101.

NMR Spectra

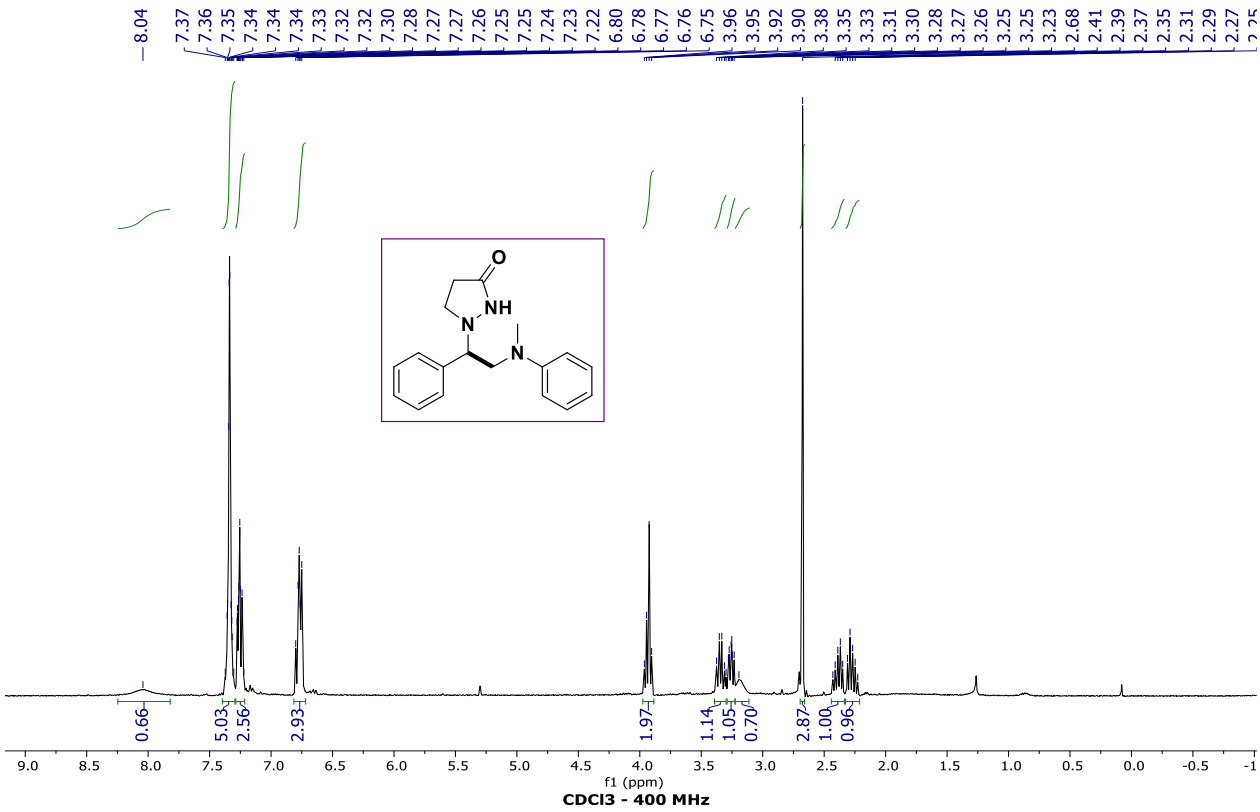
8.04
7.37
7.36
7.35
7.34
7.34
7.34
7.33
7.32
7.32
7.30
7.28
7.27
7.27
7.26
7.25
7.25
7.24
7.23
7.22
6.80
6.78
6.77
6.76
6.75
3.96
3.95
3.92
3.90
3.38
3.35
3.33
3.31
3.30
3.28
3.27
3.26
3.25
3.25
3.23
2.68
2.41
2.39
2.37
2.35
2.31
2.29
2.27
0.66
5.03
2.56
2.93
1.97
1.14
1.05
0.70
2.87
1.00
0.96
O
NH
N
N
f1 (ppm)
CDCl3 - 400 MHz

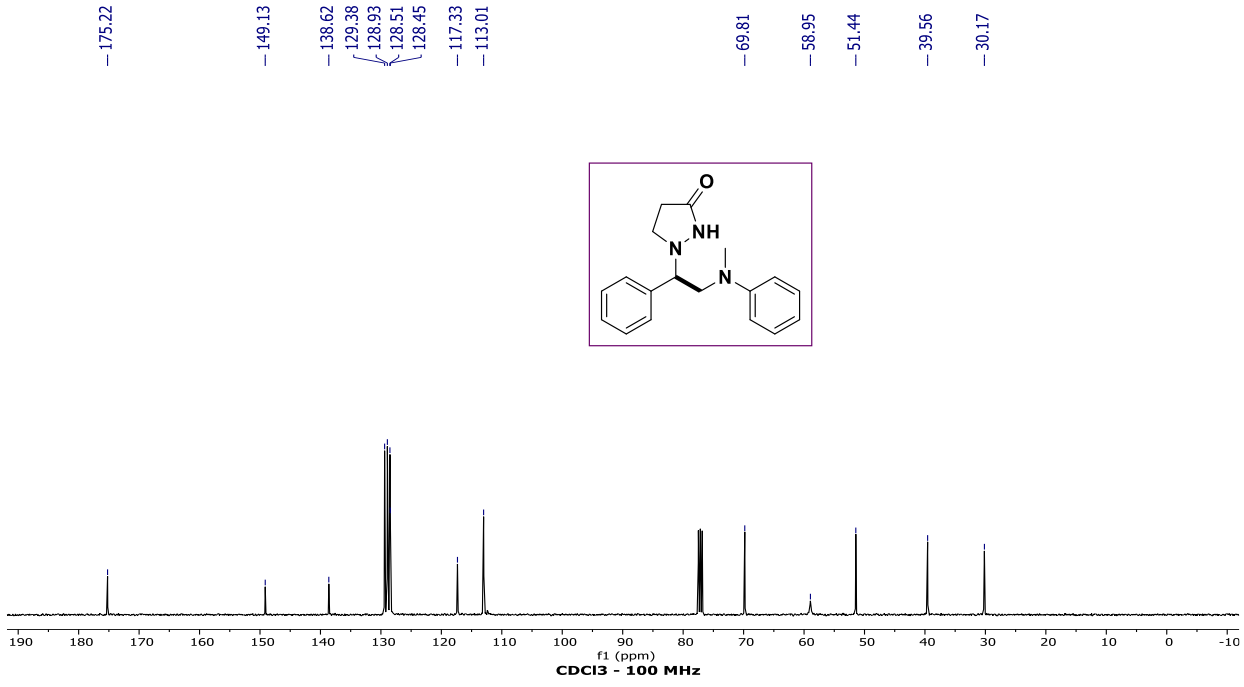
175.22
149.13
138.62
129.38
128.93
128.51
128.45
117.33
113.01
69.81
58.95
51.44
39.56
30.17
O
NH
N
N
f1 (ppm)
CDCl3 - 100 MHz

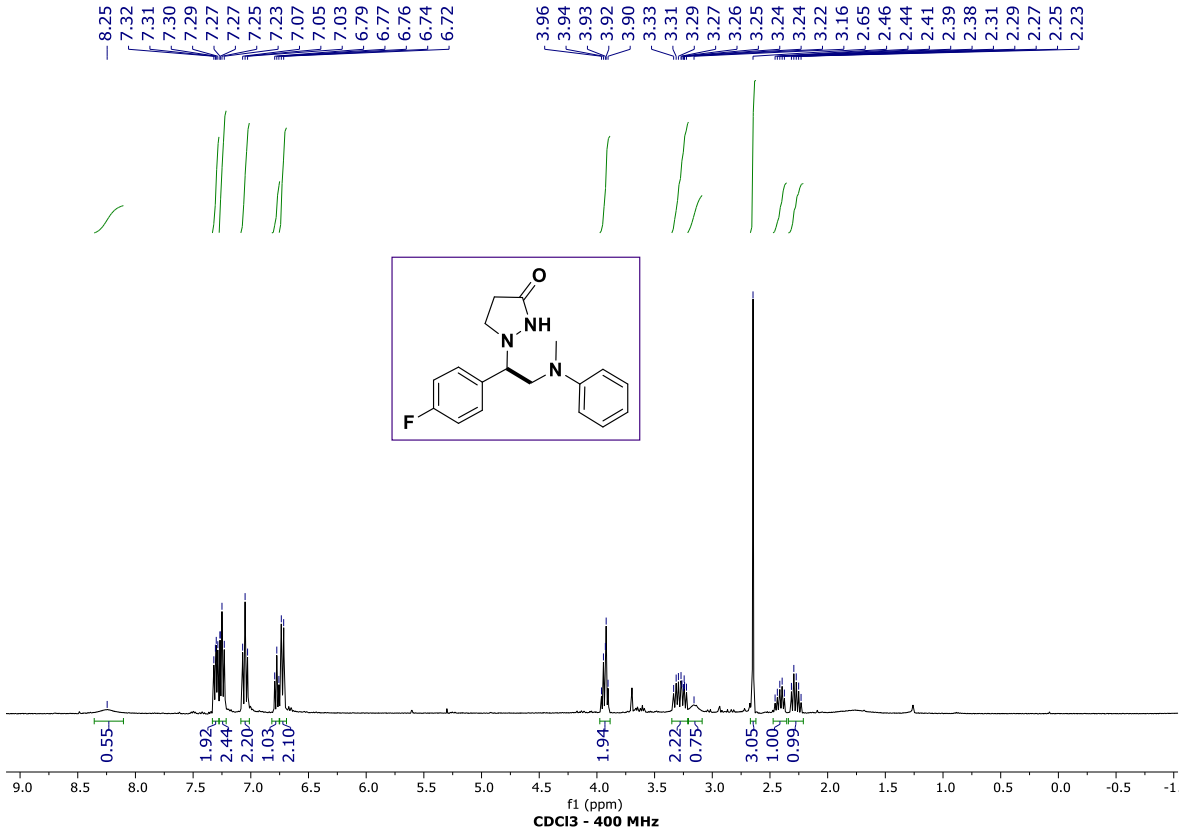
8.25
7.32
7.31
7.30
7.29
7.27
7.27
7.25
7.23
7.07
7.05
7.03
6.79
6.77
6.76
6.74
6.72
3.96
3.94
3.93
3.92
3.90
3.33
3.31
3.29
3.27
3.26
3.25
3.24
3.24
3.22
3.16
2.65
2.46
2.44
2.41
2.39
2.38
2.31
2.29
2.27
2.25
2.23
O
NH
N
N
F
0.55
1.92
2.44
2.20
1.03
2.10
1.94
2.22
0.75
3.05
1.00
0.99
f1 (ppm)
CDCl3 - 400 MHz

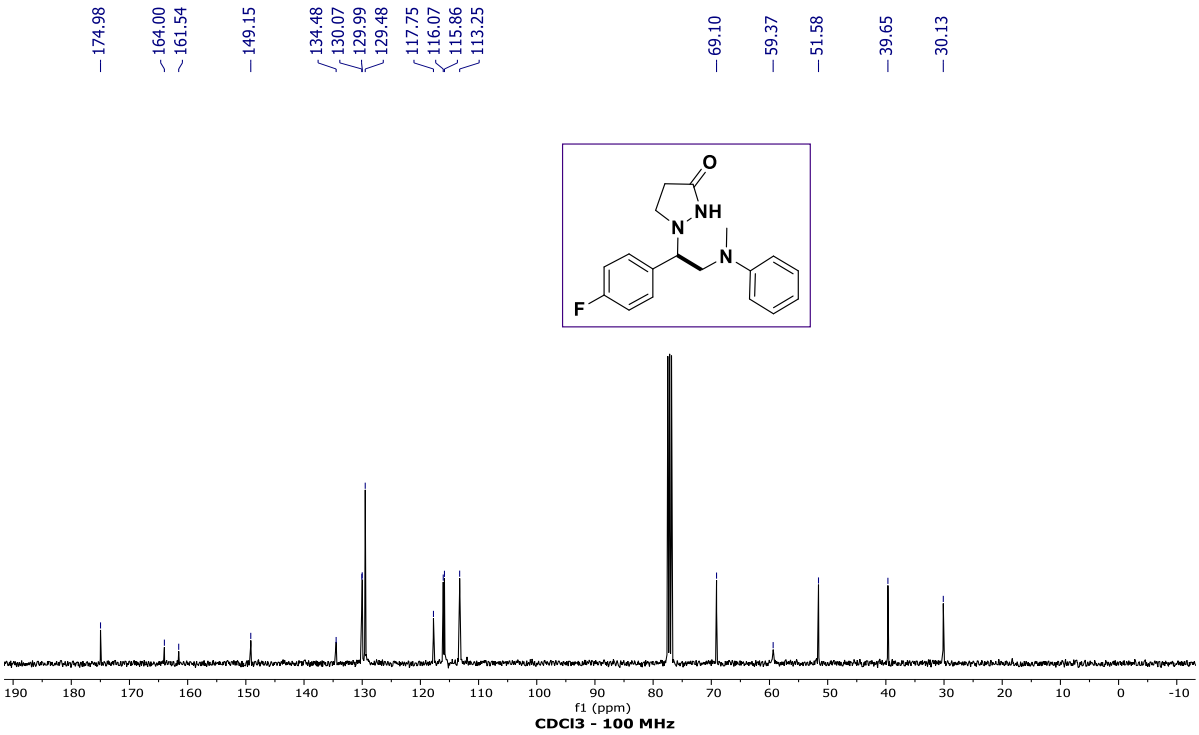
174.98
164.00
161.54
149.15
134.48
130.07
129.99
129.48
117.75
116.07
115.86
113.25
69.10
59.37
51.58
39.65
30.13
O
NH
N
N
F
f1 (ppm)
CDCl3 - 100 MHz

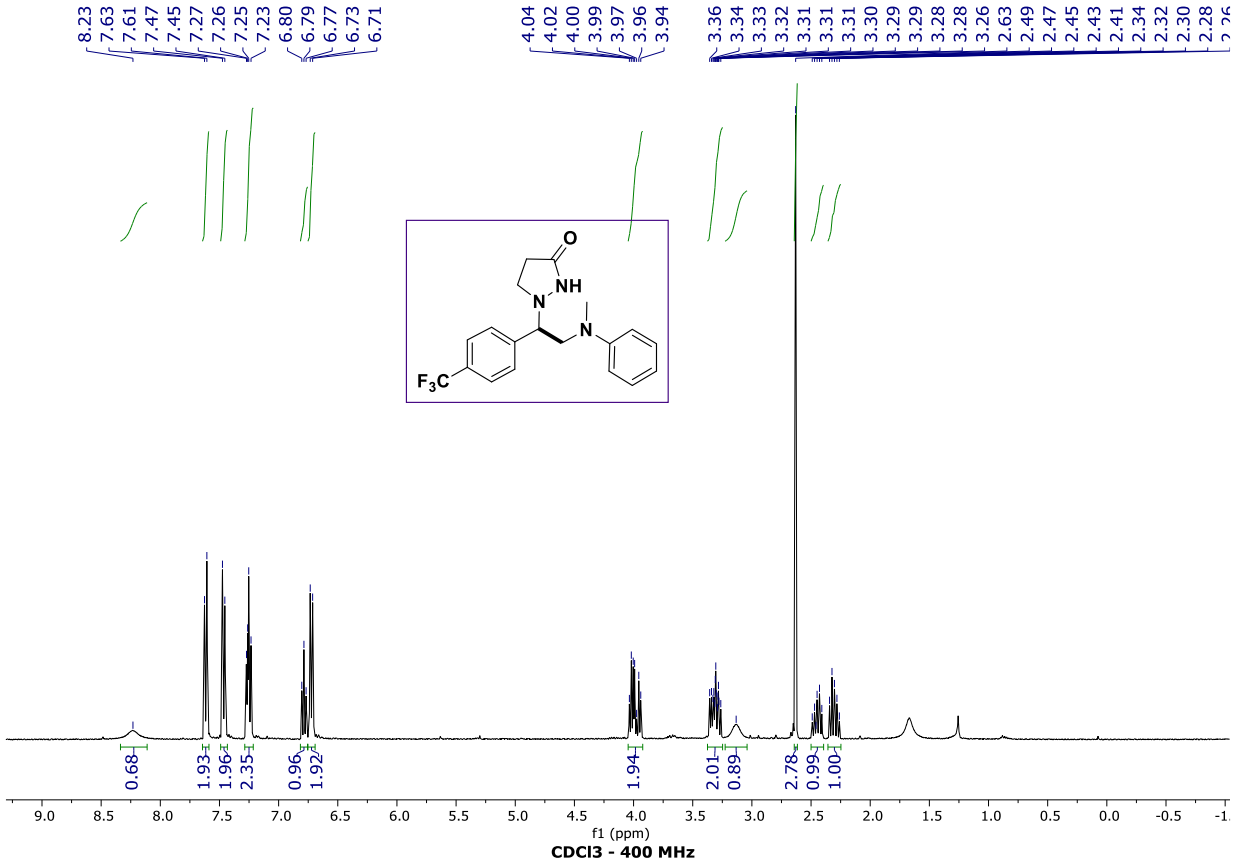
8.23
7.63
7.61
7.47
7.45
7.27
7.26
7.25
7.23
6.80
6.79
6.77
6.73
6.71
4.04
4.02
4.00
3.99
3.97
3.96
3.94
3.36
3.34
3.33
3.32
3.31
3.31
3.31
3.30
3.29
3.29
3.28
3.28
3.26
2.63
2.49
2.47
2.45
2.43
2.41
2.34
2.32
2.30
2.28
O
NH
N
N
F3C
0.68
1.93
1.96
2.35
0.96
1.92
1.94
2.01
0.89
2.78
0.99
1.00
f1 (ppm)
CDCl3 - 400 MHz

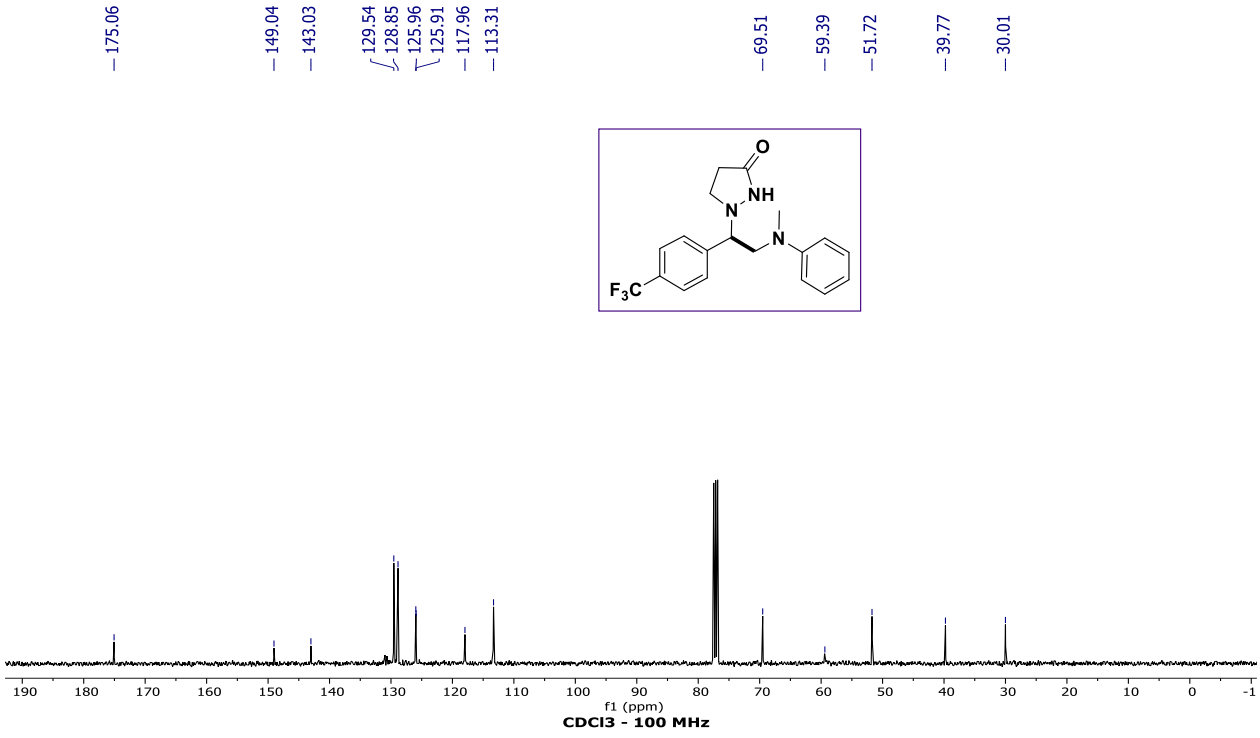
175.06
149.04
143.03
129.54
128.85
125.96
125.91
117.96
113.31
69.51
59.39
51.72
39.77
30.01
O
NH
N
N
F3C
f1 (ppm)
CDCl3 - 100 MHz

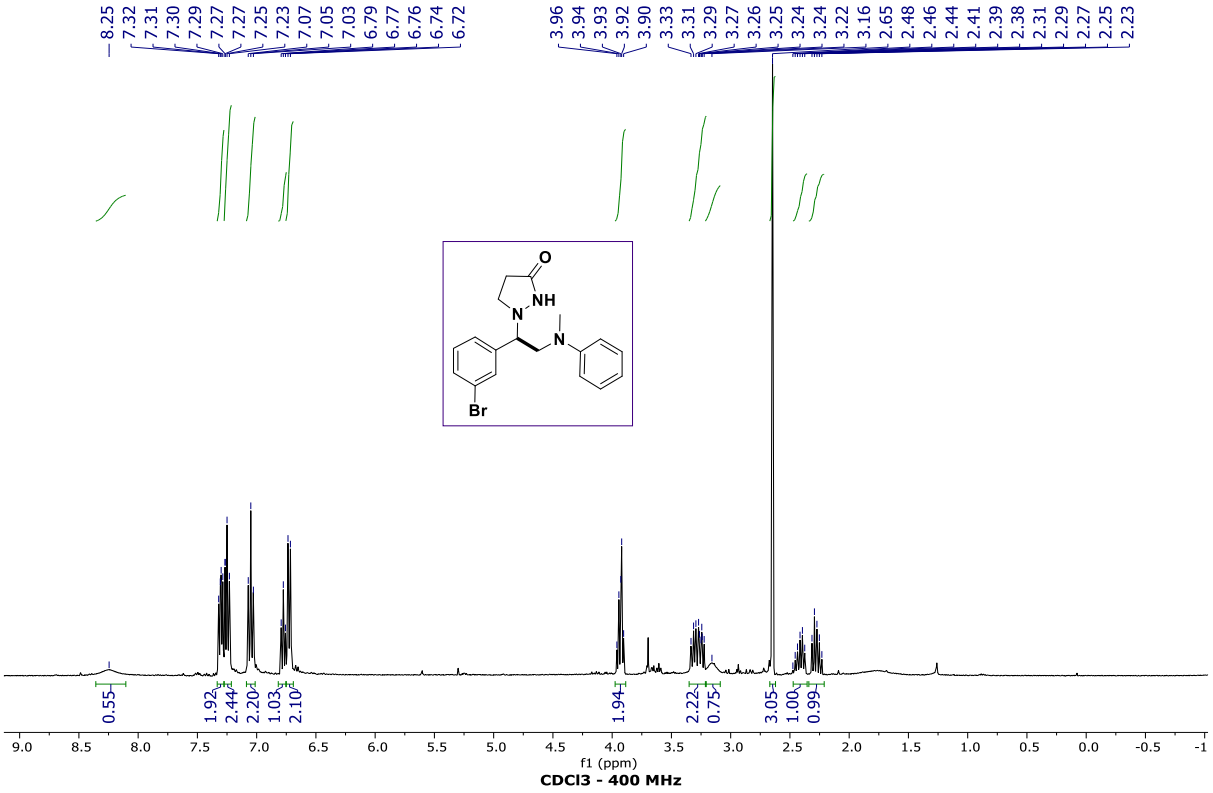
8.25
7.32
7.31
7.30
7.29
7.27
7.27
7.25
7.23
7.07
7.05
7.03
6.79
6.77
6.76
6.74
6.72
3.96
3.94
3.93
3.92
3.90
3.33
3.31
3.29
3.27
3.26
3.25
3.24
3.24
3.22
3.16
2.65
2.48
2.46
2.44
2.41
2.39
2.38
2.31
2.29
2.27
2.25
2.23
O
NH
N
N
Br
0.55
1.92
2.44
2.20
1.03
2.10
1.94
2.22
0.75
3.05
1.00
0.99
f1 (ppm)
CDCl3 - 400 MHz

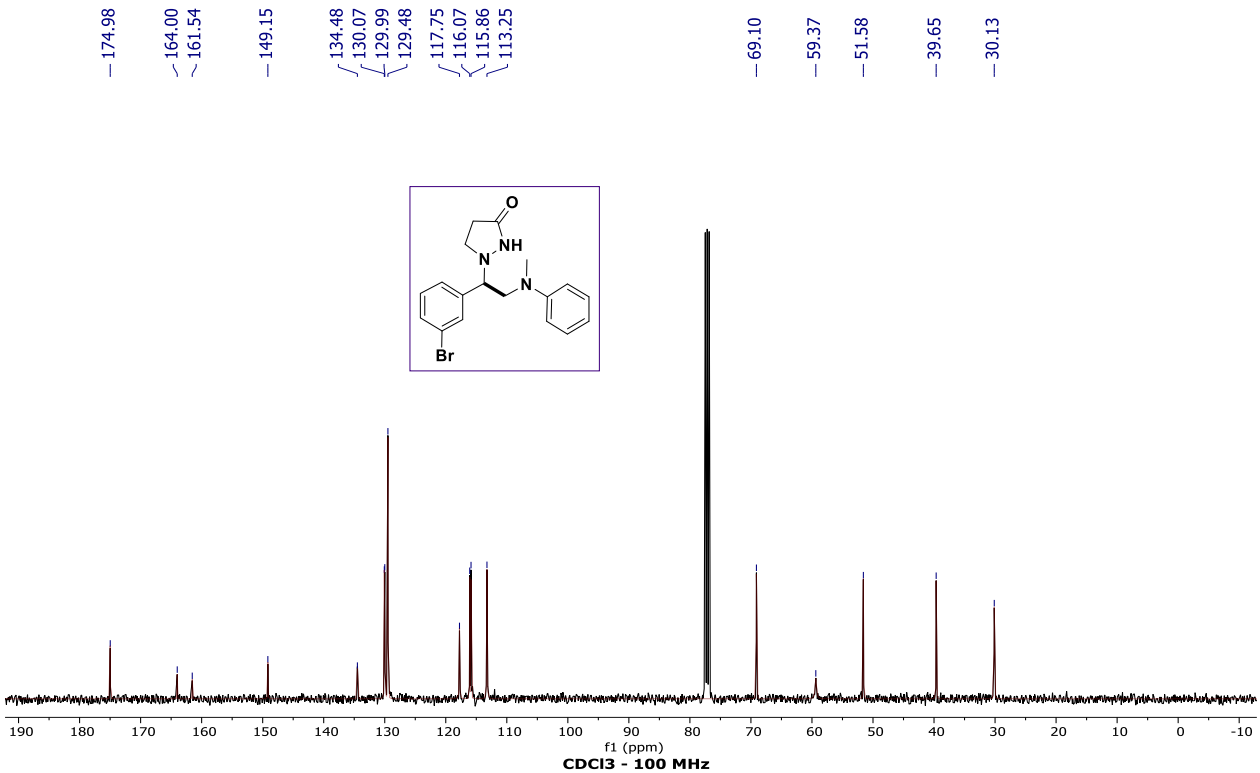
174.98
164.00
161.54
149.15
134.48
130.07
129.99
129.48
117.75
116.07
115.86
113.25
69.10
59.37
51.58
39.65
30.13
O
NH
N
N
Br
f1 (ppm)
CDCl3 - 100 MHz

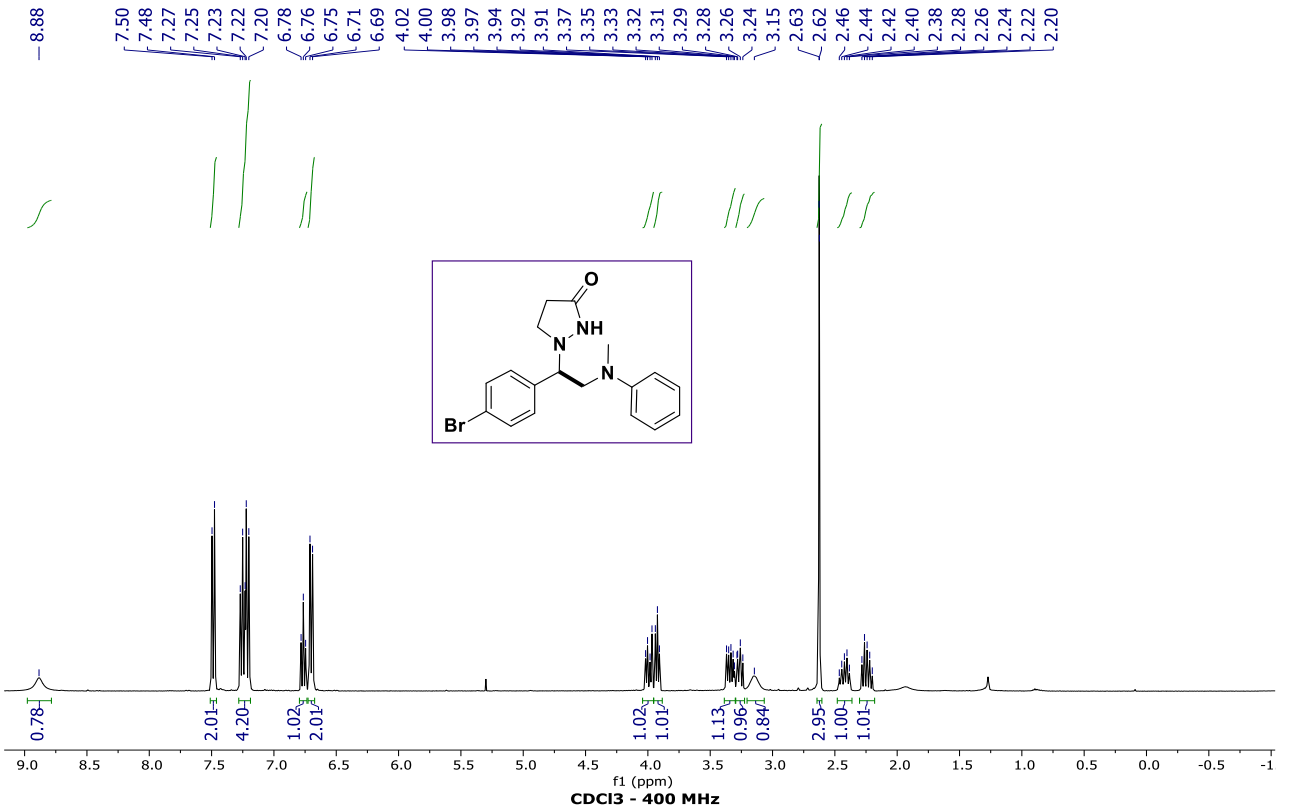
8.88
7.50
7.48
7.27
7.25
7.23
7.22
7.20
6.78
6.76
6.75
6.71
6.69
4.02
4.00
3.98
3.97
3.94
3.92
3.91
3.37
3.35
3.33
3.32
3.31
3.29
3.28
3.26
3.24
3.15
2.63
2.62
2.46
2.44
2.42
2.40
2.38
2.28
2.26
2.24
2.22
2.20
O
NH
N
N
Br
0.78
2.01
4.20
1.02
2.01
1.02
1.01
1.13
0.96
0.84
2.95
1.00
1.01
f1 (ppm)
CDCl3 - 400 MHz

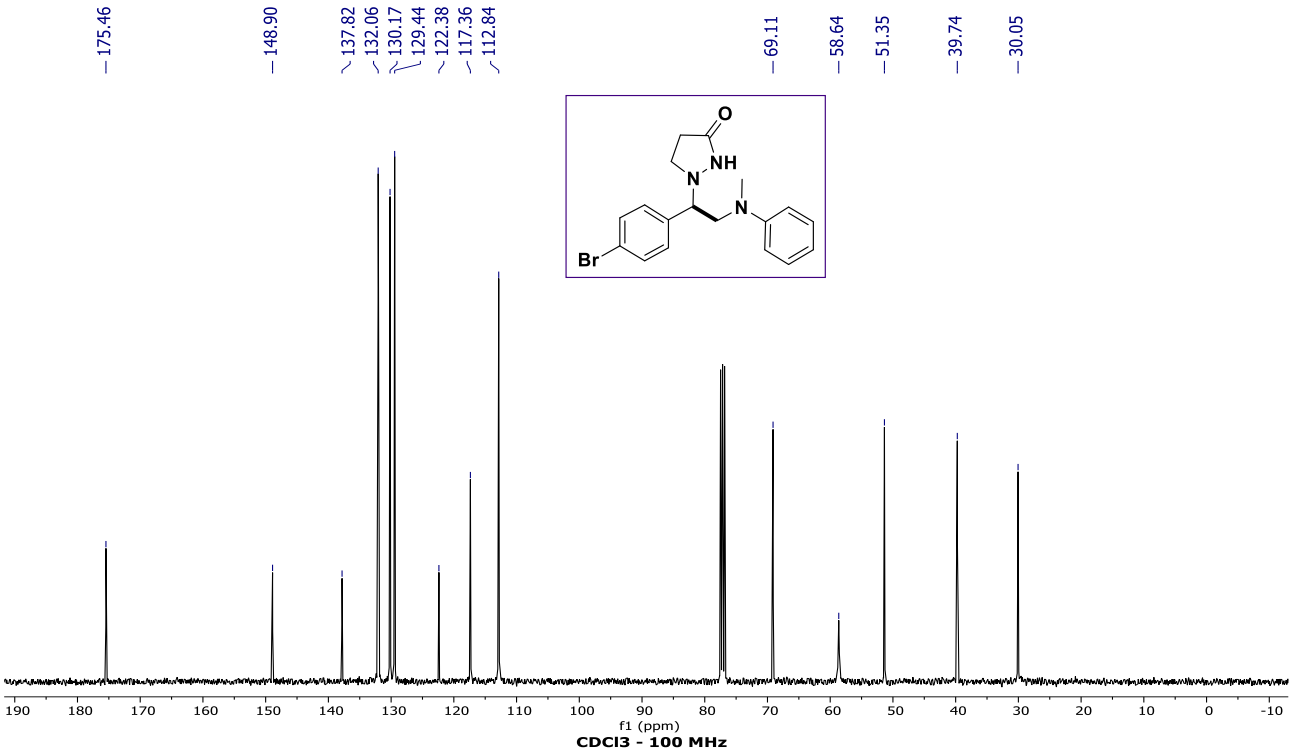
175.46
148.90
137.82
132.06
130.17
129.44
122.38
117.36
112.84
69.11
58.64
51.35
39.74
30.05
O
NH
N
N
Br
f1 (ppm)
CDCl3 - 100 MHz

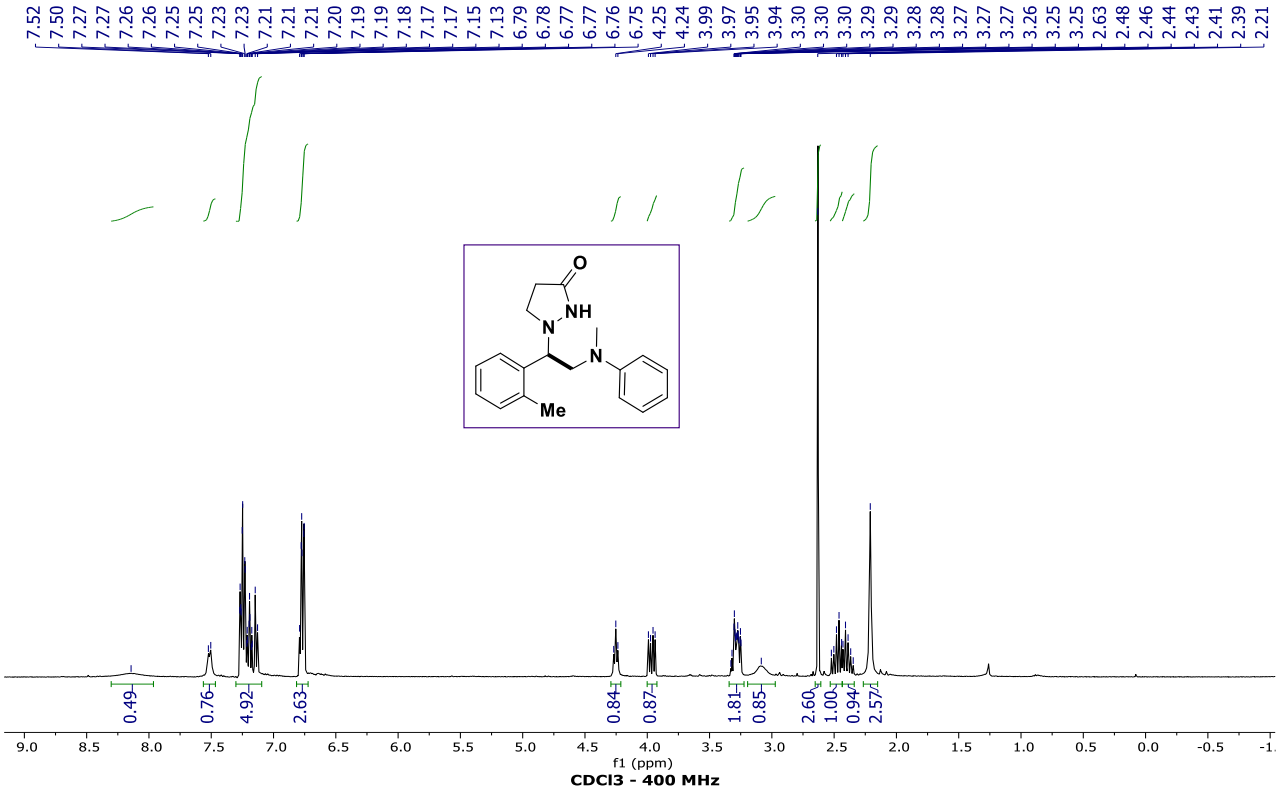
7.52 7.50 7.27 7.27 7.26 7.26 7.25 7.25 7.23 7.23 7.21 7.21 7.21 7.20 7.19 7.19 7.18 7.17 7.17 7.15 7.13 6.79 6.78 6.77 6.77 6.76 6.75 4.25 4.24 3.99 3.97 3.95 3.94 3.30 3.30 3.29 3.29 3.28 3.28 3.27 3.27 3.27 3.26 3.25 3.25 2.63 2.48 2.46 2.44 2.43 2.41 2.39 2.21
O
NH
N
N
Me
0.49 0.76 4.92 2.63 0.84 0.87 1.81 0.85 2.60 1.00 0.94 2.57
f1 (ppm)
CDCl3 - 400 MHz

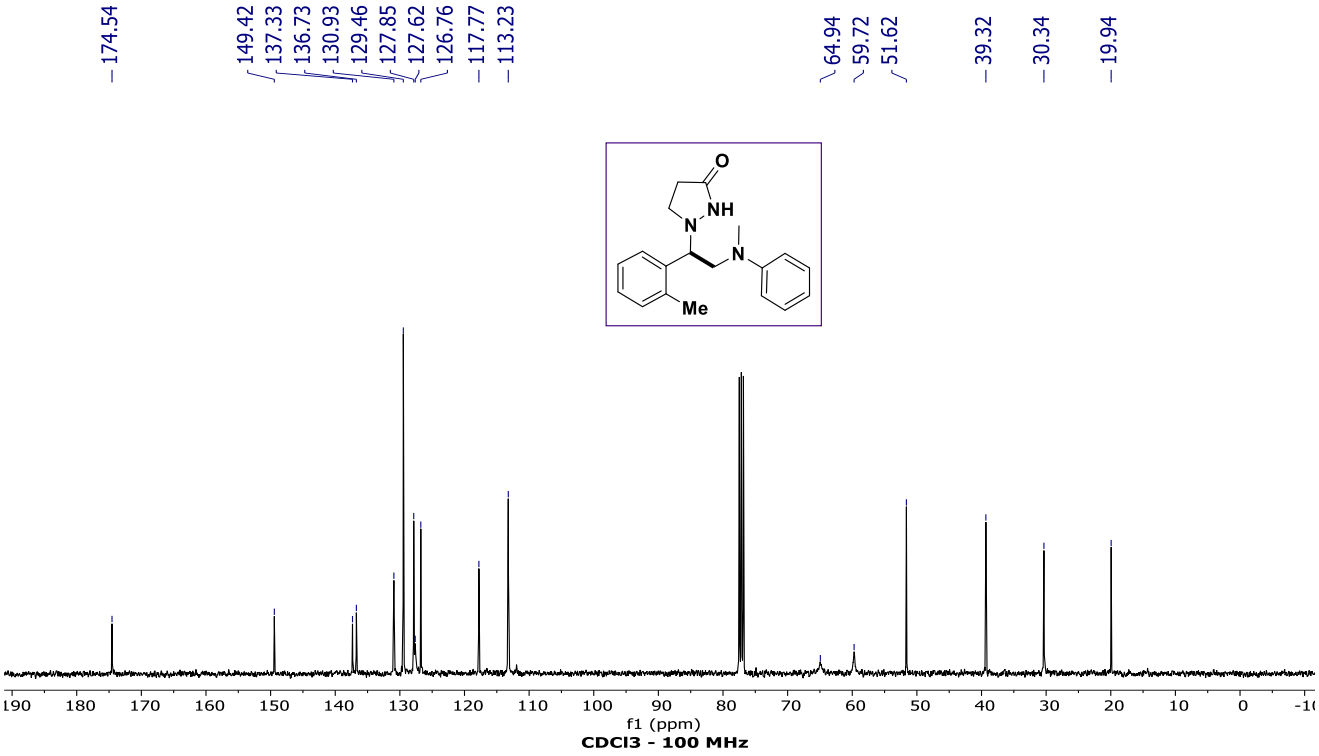
174.54
149.42 137.33 136.73 130.93 129.46 127.85 127.62 126.76
117.77 113.23
64.94 59.72 51.62
39.32 30.34 19.94
O
NH
N
N
Me
f1 (ppm)
CDCl3 - 100 MHz

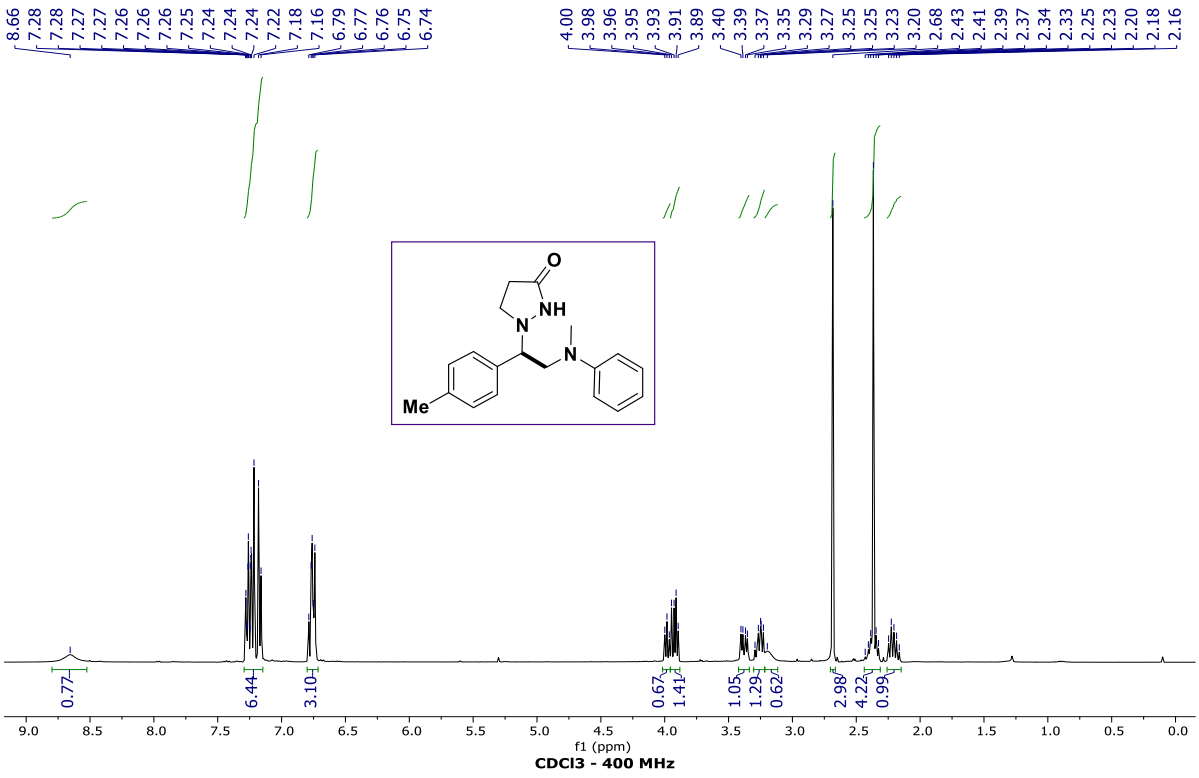
8.66 7.28 7.28 7.27 7.27 7.27 7.26 7.26 7.26 7.25 7.24 7.24 7.24 7.22 7.18 7.16 6.79 6.77 6.76 6.75 6.74
4.00 3.98 3.96 3.95 3.93 3.91 3.89 3.40 3.39 3.37 3.35 3.29 3.27 3.25 3.25 3.23 3.20 2.68 2.43 2.41 2.39 2.37 2.34 2.33 2.25 2.23 2.20 2.18 2.16
O
NH
N
N
Me
0.77 6.44 3.10 0.67 1.41 1.05 1.29 0.62 2.98 4.22 0.99
f1 (ppm)
CDCl3 - 400 MHz

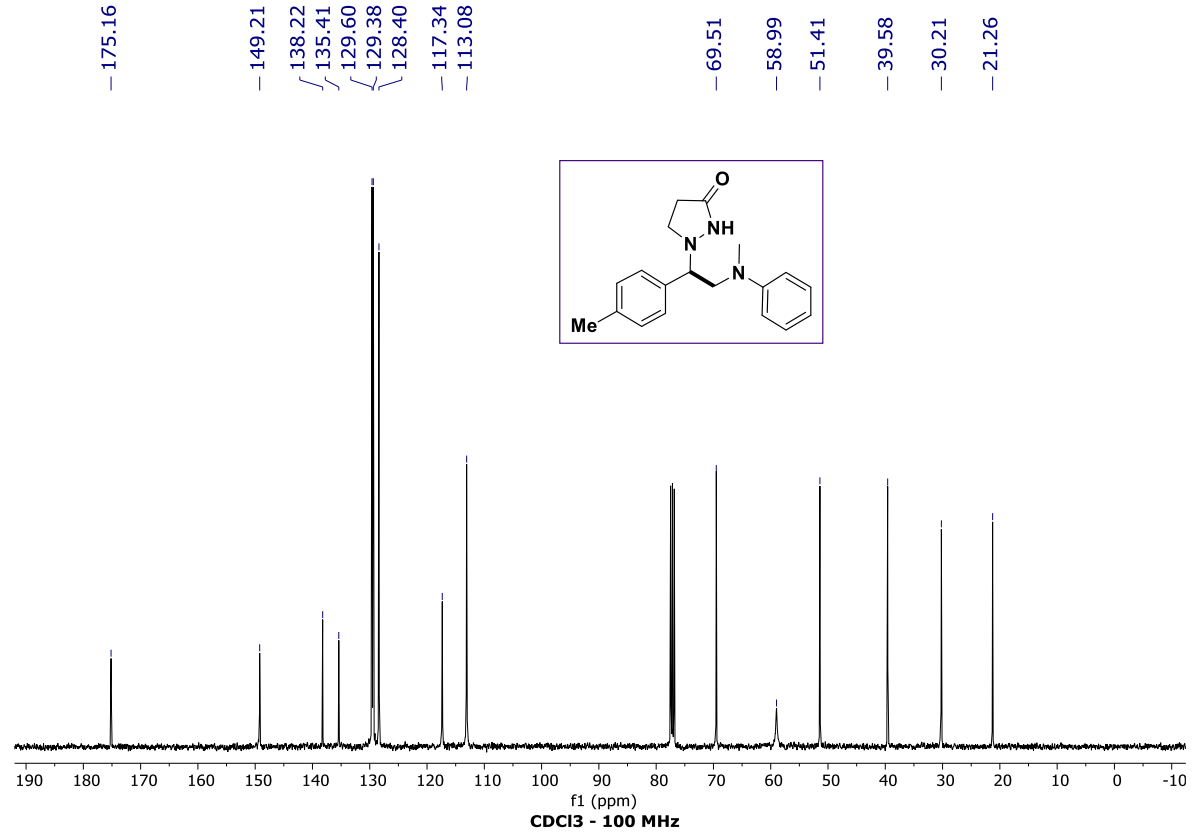
175.16 149.21 138.22 135.41 129.60 129.38 128.40 117.34 113.08 69.51 58.99 51.41 39.58 30.21 21.26
O
NH
N
N
Me
f1 (ppm)
CDCl3 - 100 MHz

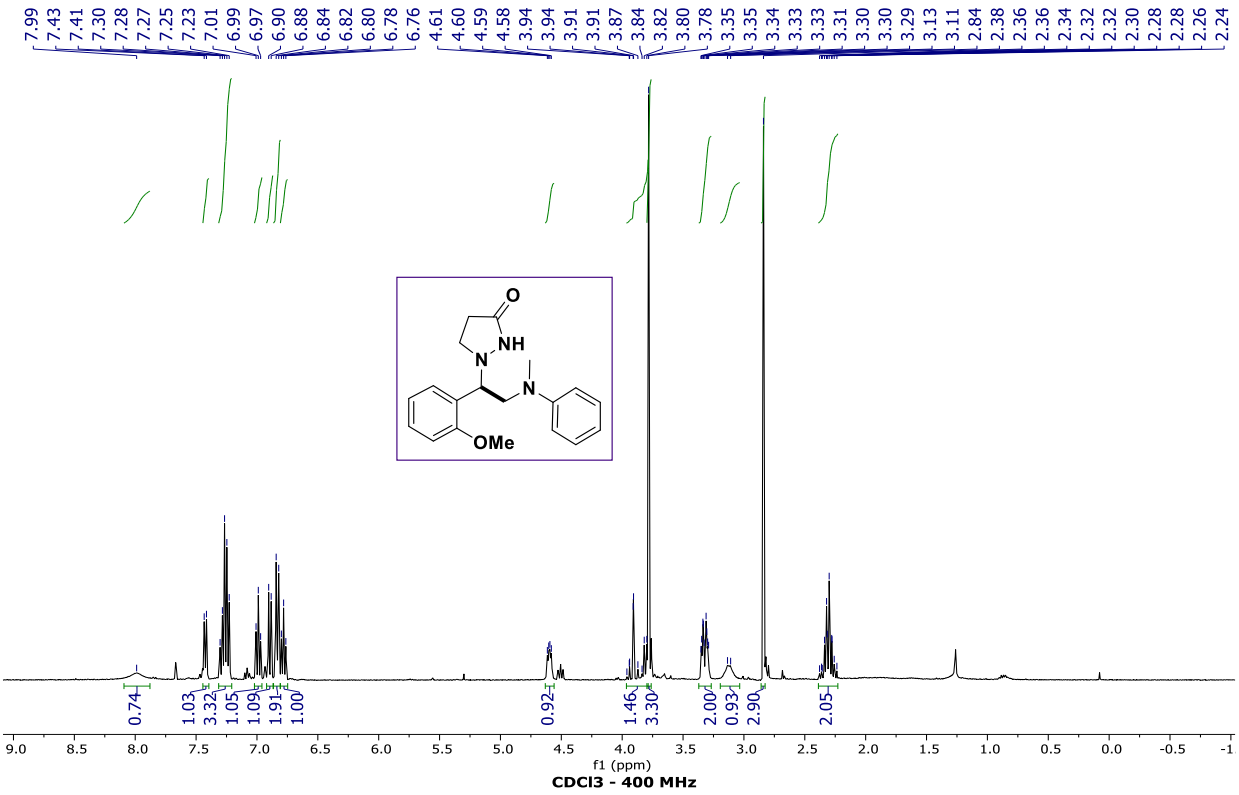
7.99 7.43 7.41 7.30 7.28 7.27 7.25 7.23 7.01 6.99 6.97 6.90 6.88 6.84 6.82 6.80 6.78 6.76 4.61 4.60 4.59 4.58 3.94 3.94 3.91 3.91 3.87 3.84 3.82 3.80 3.78 3.35 3.35 3.34 3.33 3.33 3.31 3.30 3.30 3.29 3.13 3.11 2.84 2.38 2.36 2.36 2.34 2.32 2.32 2.30 2.28 2.28 2.26 2.24
O
NH
N
N
OMe
0.74 1.03 3.32 1.05 1.09 1.91 1.00 0.92 1.46 3.30 2.00 0.93 2.90 2.05
f1 (ppm)
CDCl3 - 400 MHz

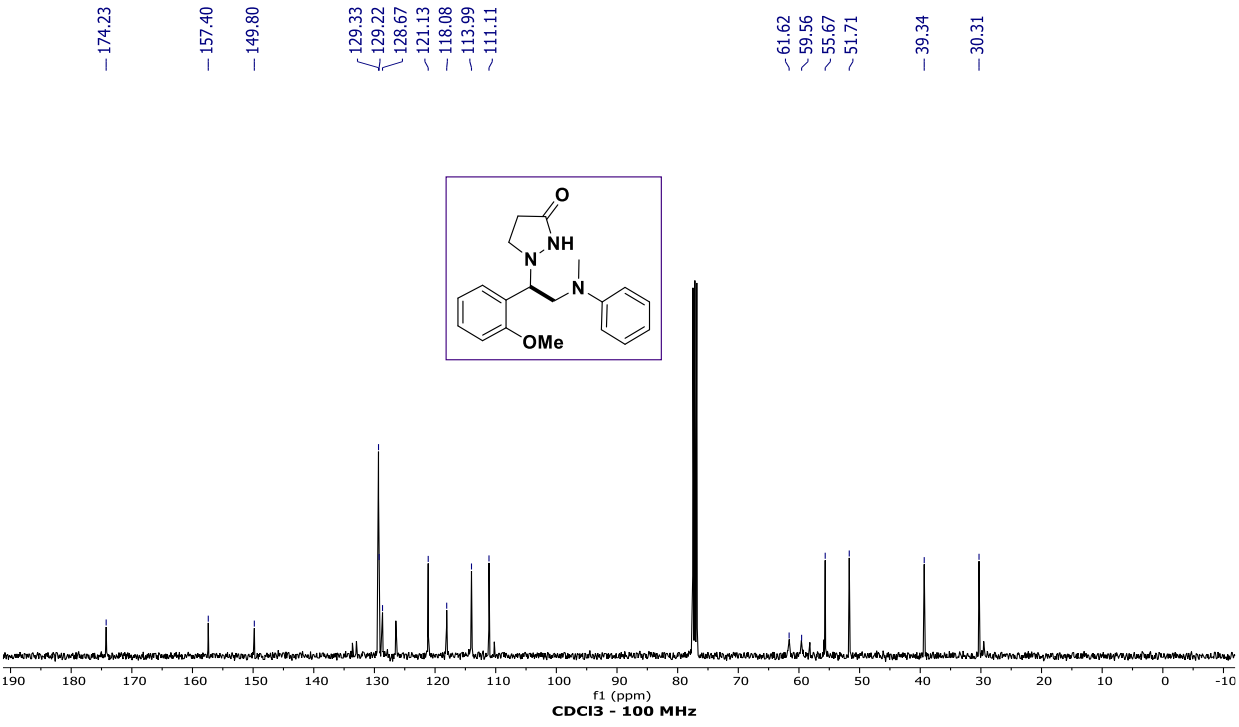
174.23 157.40 149.80 129.33 129.22 128.67 121.13 118.08 113.99 111.11 61.62 59.56 55.67 51.71 39.34 30.31
O
NH
N
N
OMe
f1 (ppm)
CDCl3 - 100 MHz

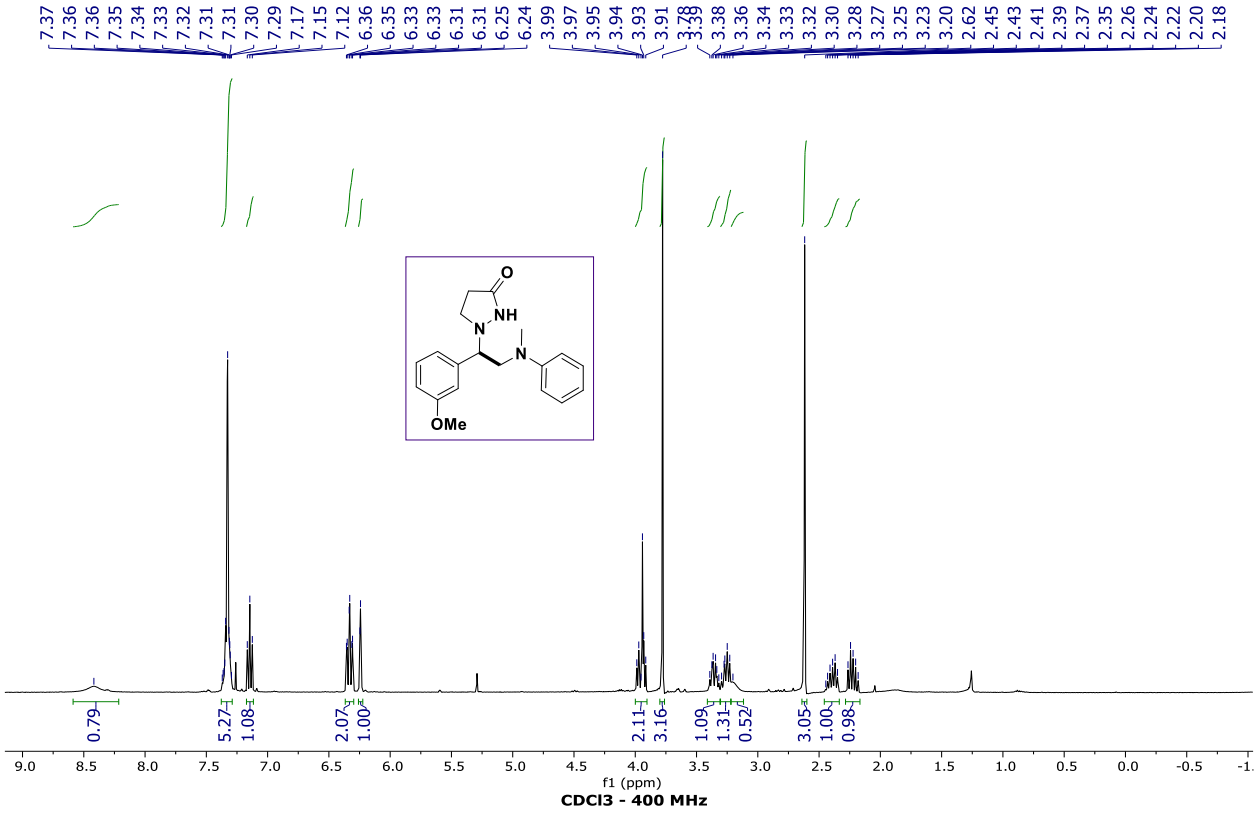

CDCl3 - 400 MHz

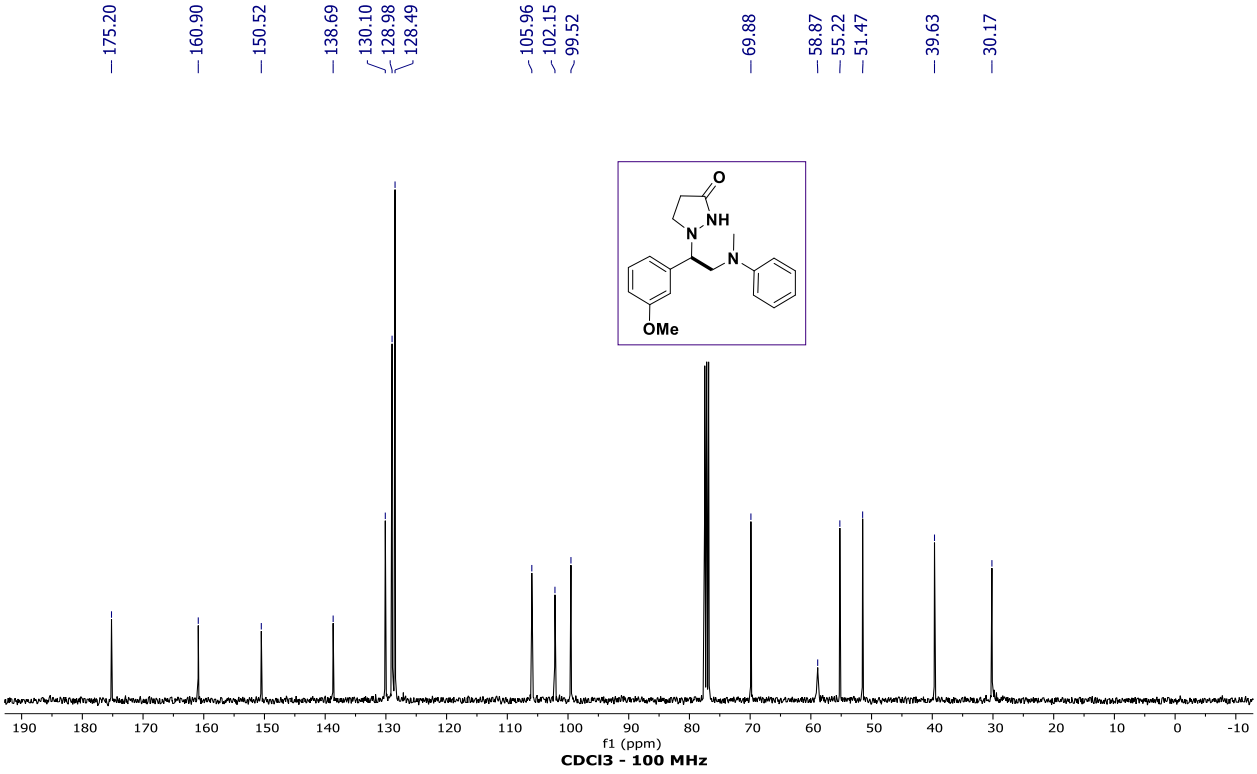

CDCl3 - 100 MHz

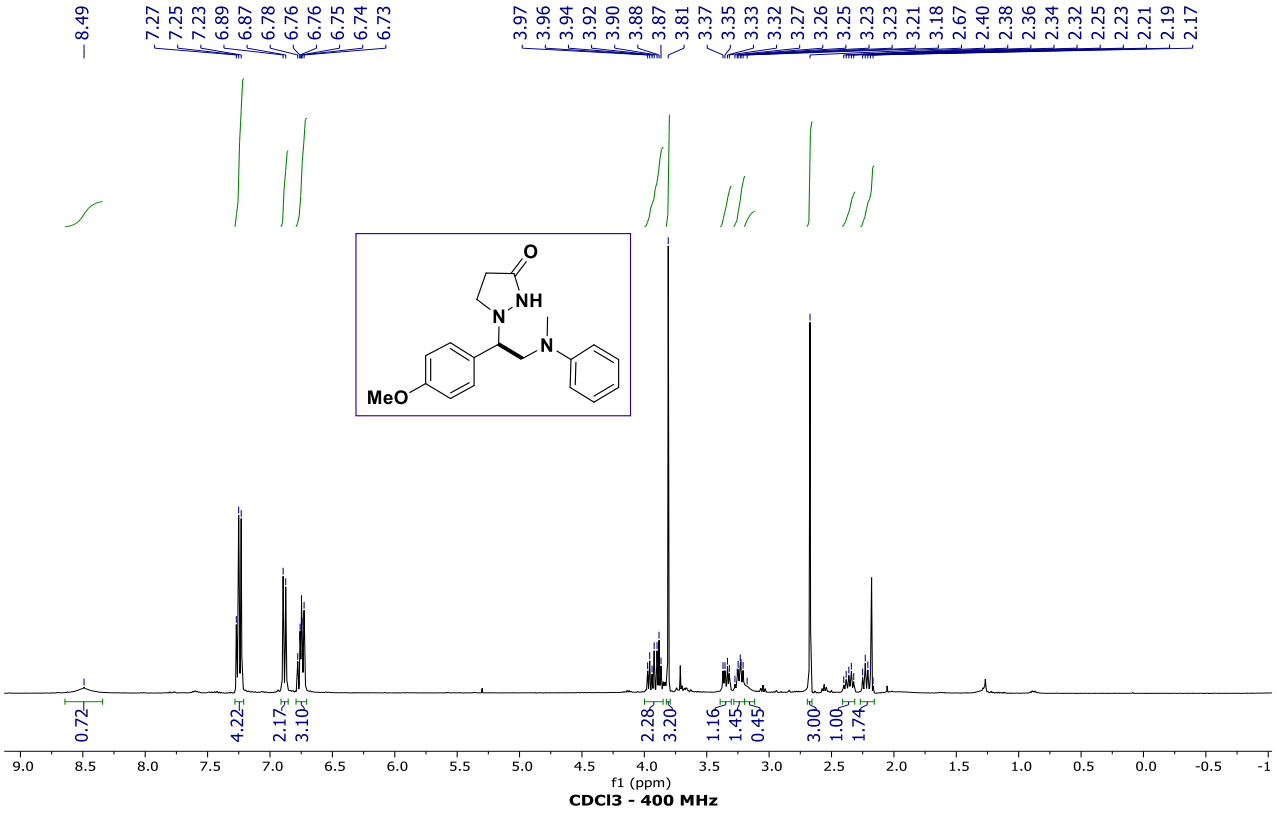
8.49
7.27
7.25
7.23
6.89
6.87
6.78
6.76
6.76
6.75
6.74
6.73
3.97
3.96
3.94
3.92
3.90
3.88
3.87
3.81
3.37
3.35
3.33
3.32
3.27
3.26
3.25
3.23
3.23
3.21
3.18
2.67
2.40
2.38
2.36
2.34
2.32
2.25
2.23
2.21
2.19
2.17
O
NH
N
N
MeO
0.72
4.22
2.17
3.10
2.28
3.20
1.16
1.45
0.45
3.00
1.00
1.74
f1 (ppm)
CDCl3 - 400 MHz

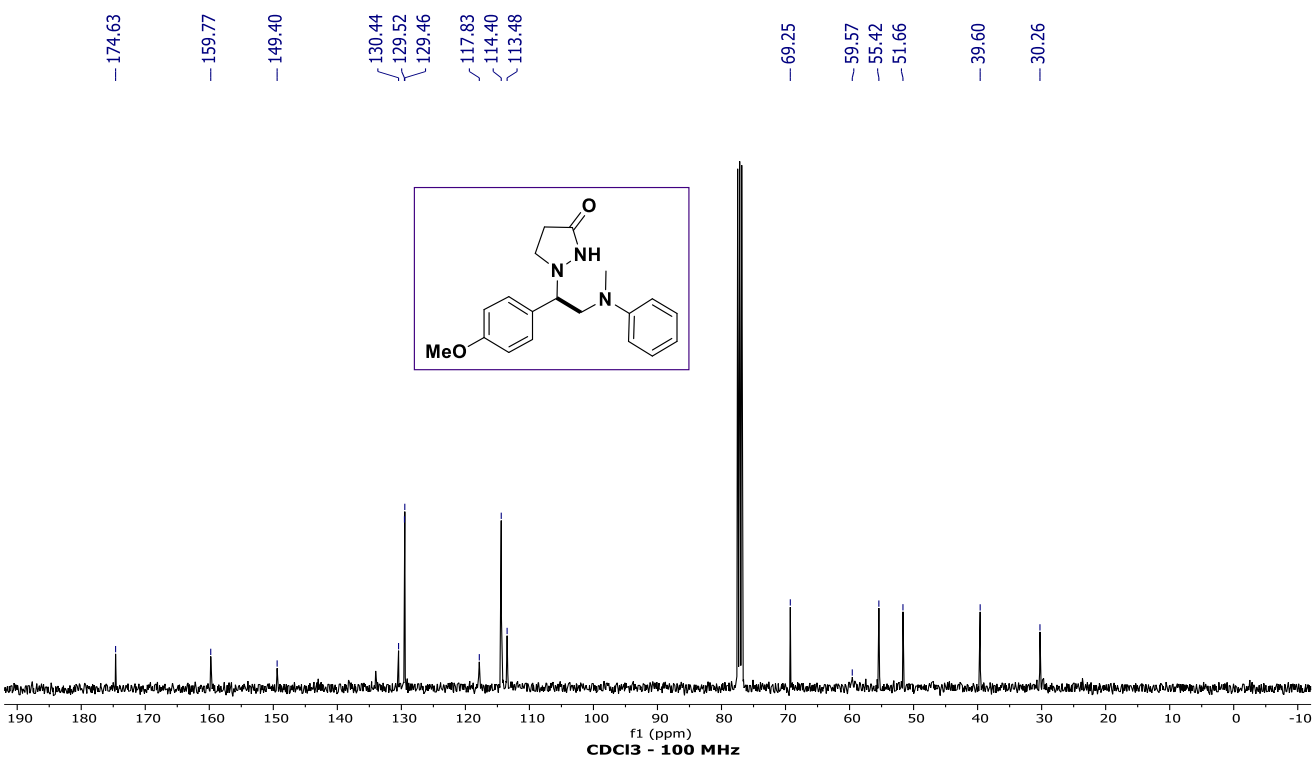
174.63
159.77
149.40
130.44
129.52
129.46
117.83
114.40
113.48
69.25
59.57
55.42
51.66
39.60
30.26
O
NH
N
N
MeO
f1 (ppm)
CDCl3 - 100 MHz

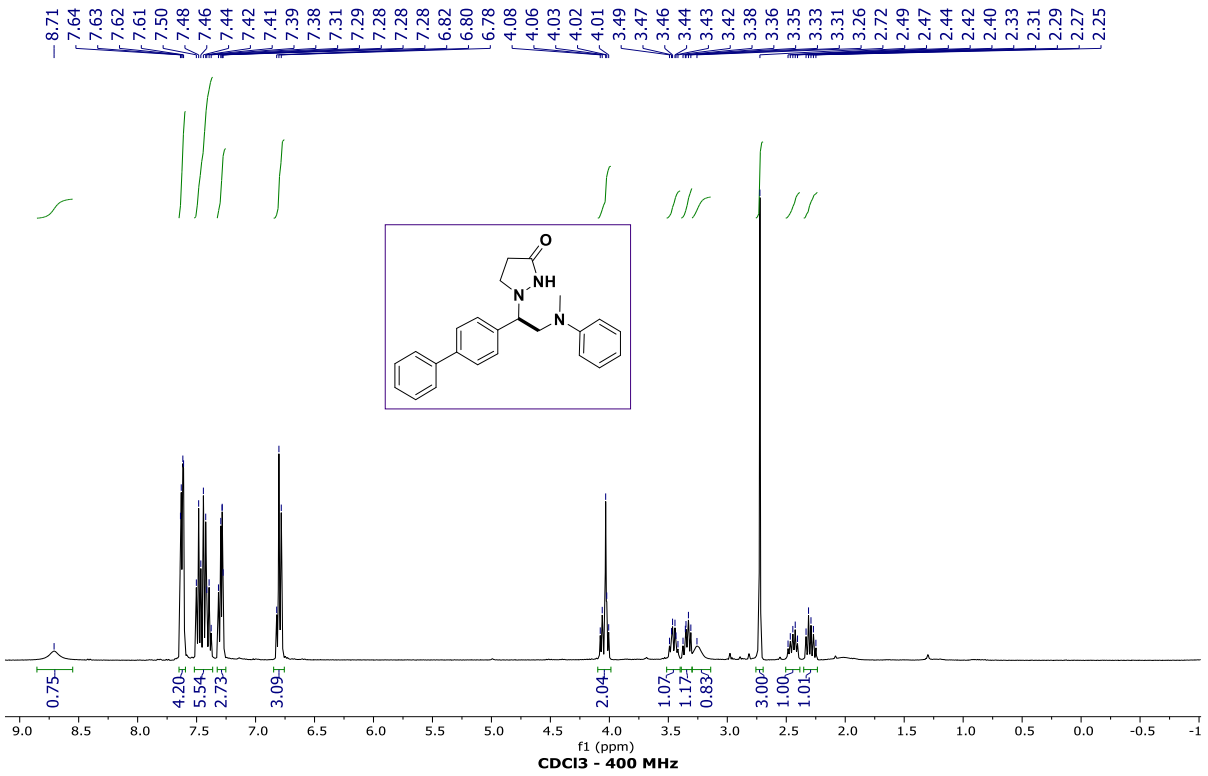
8.71
7.64
7.63
7.62
7.61
7.50
7.48
7.46
7.44
7.42
7.41
7.39
7.38
7.31
7.29
7.28
7.28
7.28
6.82
6.80
6.78
4.08
4.06
4.03
4.02
4.01
3.49
3.47
3.46
3.44
3.43
3.42
3.38
3.36
3.35
3.33
3.31
3.26
2.72
2.49
2.47
2.44
2.42
2.40
2.33
2.31
2.29
2.27
2.25
O
NH
N
N
0.75
4.20
5.54
2.73
3.09
2.04
1.07
1.17
0.83
3.00
1.00
1.01
f1 (ppm)
CDCl3 - 400 MHz

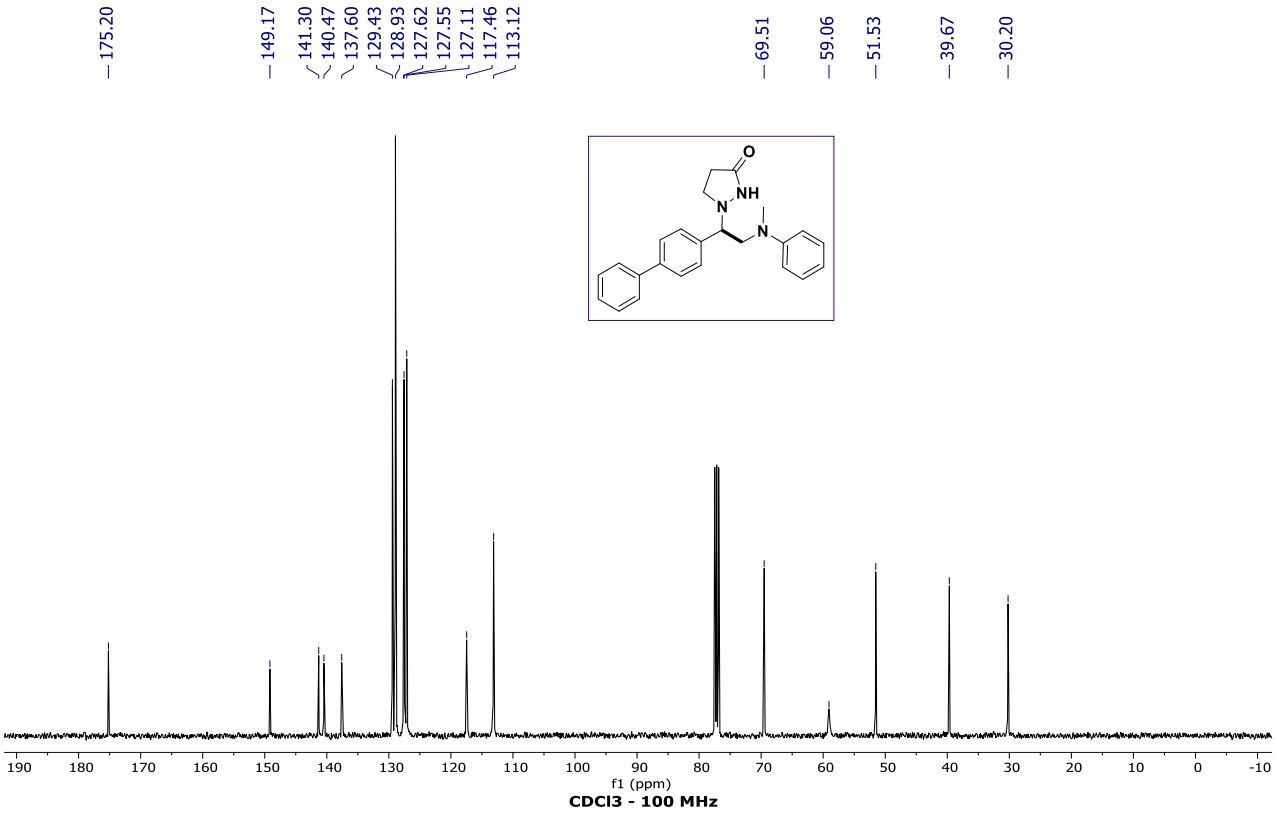
175.20
149.17
141.30
140.47
137.60
129.43
128.93
127.62
127.55
127.11
117.46
113.12
69.51
59.06
51.53
39.67
30.20
O
NH
N
N
f1 (ppm)
CDCl3 - 100 MHz

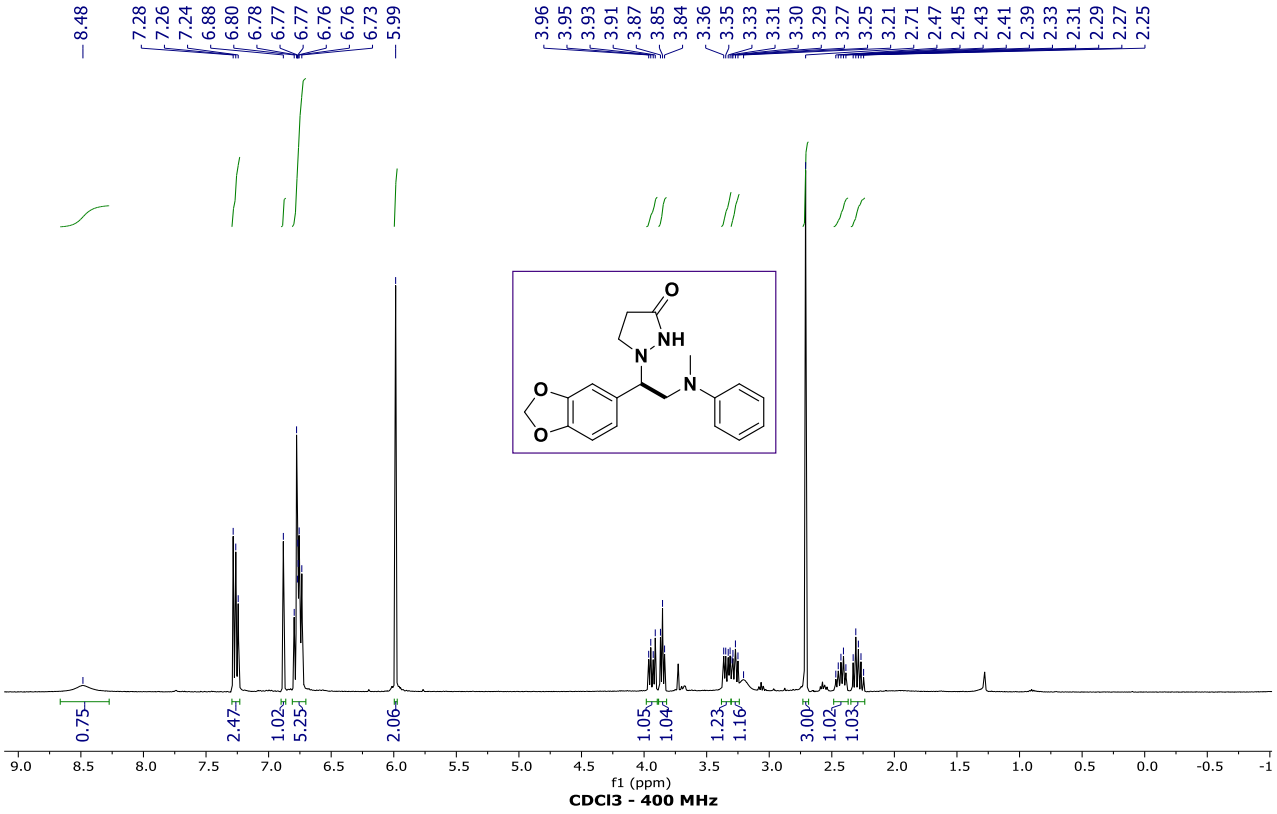
8.48
7.28
7.26
7.24
6.88
6.80
6.78
6.77
6.77
6.76
6.76
6.73
5.99
3.96
3.95
3.93
3.91
3.87
3.85
3.84
3.36
3.35
3.33
3.31
3.30
3.29
3.27
3.25
3.21
2.71
2.47
2.45
2.43
2.41
2.39
2.33
2.31
2.29
2.27
2.25
0.75
2.47
1.02
5.25
2.06
1.05
1.04
1.23
1.16
3.00
1.02
1.03
f1 (ppm)
CDCl3 - 400 MHz

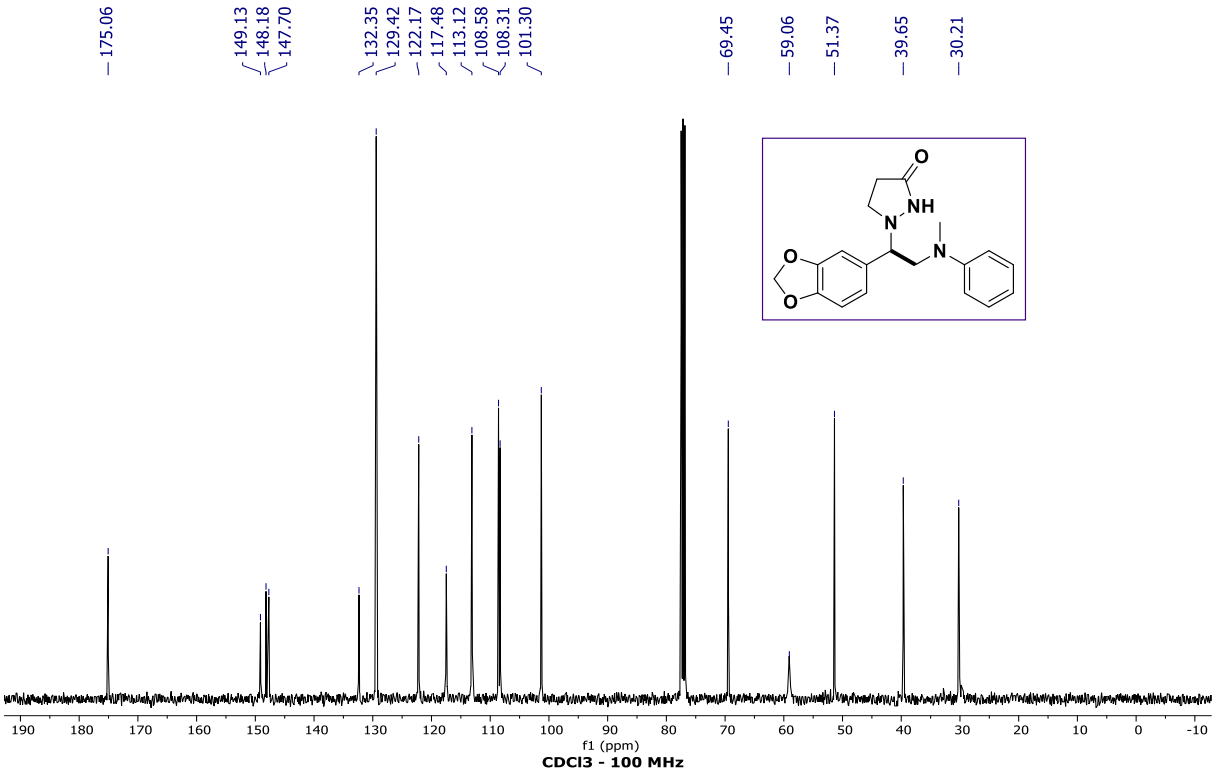
175.06
149.13
148.18
147.70
132.35
129.42
122.17
117.48
113.12
108.58
108.31
101.30
69.45
59.06
51.37
39.65
30.21
f1 (ppm)
CDCl3 - 100 MHz

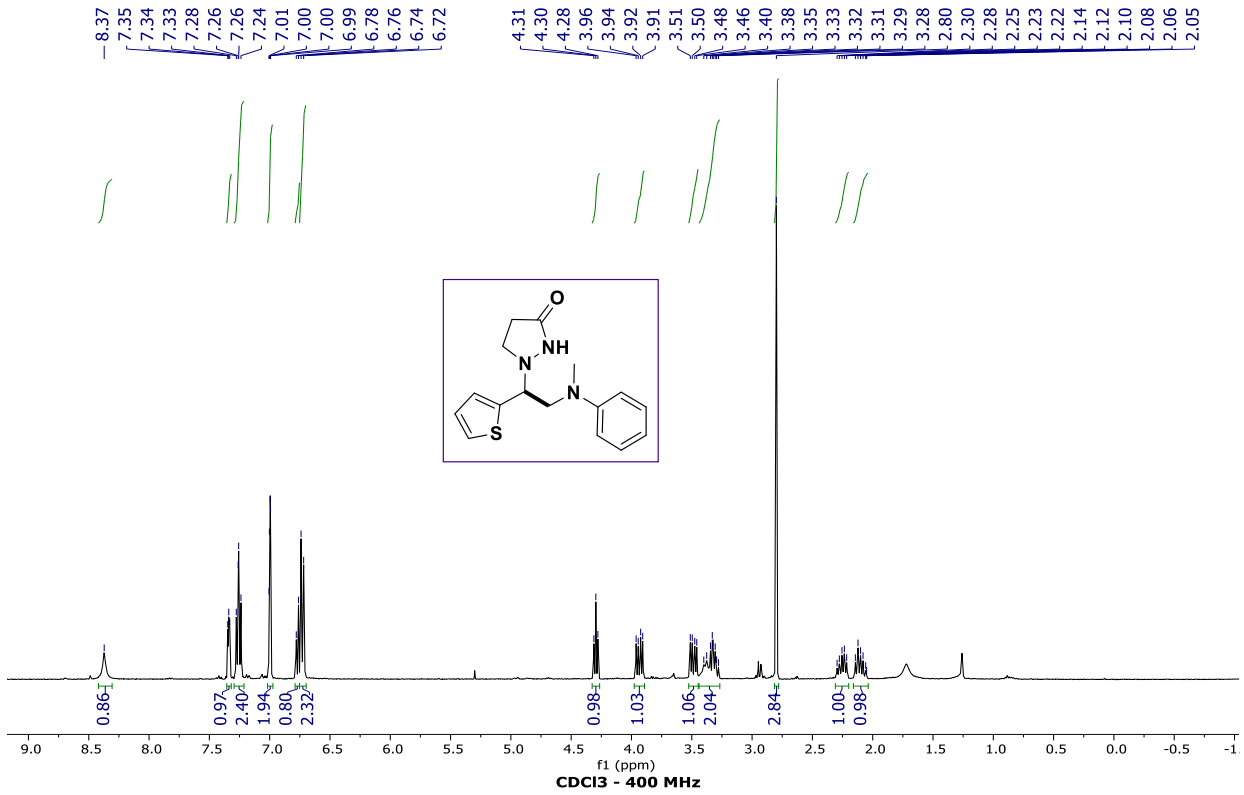
8.37
7.35
7.34
7.33
7.28
7.26
7.26
7.24
7.01
7.00
7.00
6.99
6.78
6.76
6.74
6.72
4.31
4.30
4.28
3.96
3.94
3.92
3.91
3.51
3.50
3.48
3.46
3.40
3.38
3.35
3.33
3.32
3.31
3.29
3.28
2.80
2.30
2.28
2.25
2.23
2.22
2.14
2.12
2.10
2.08
2.06
2.05
O
NH
N
N
S
0.86
0.97
2.40
1.94
0.80
2.32
0.98
1.03
1.06
2.04
2.84
1.00
0.98
f1 (ppm)
CDCl3 - 400 MHz

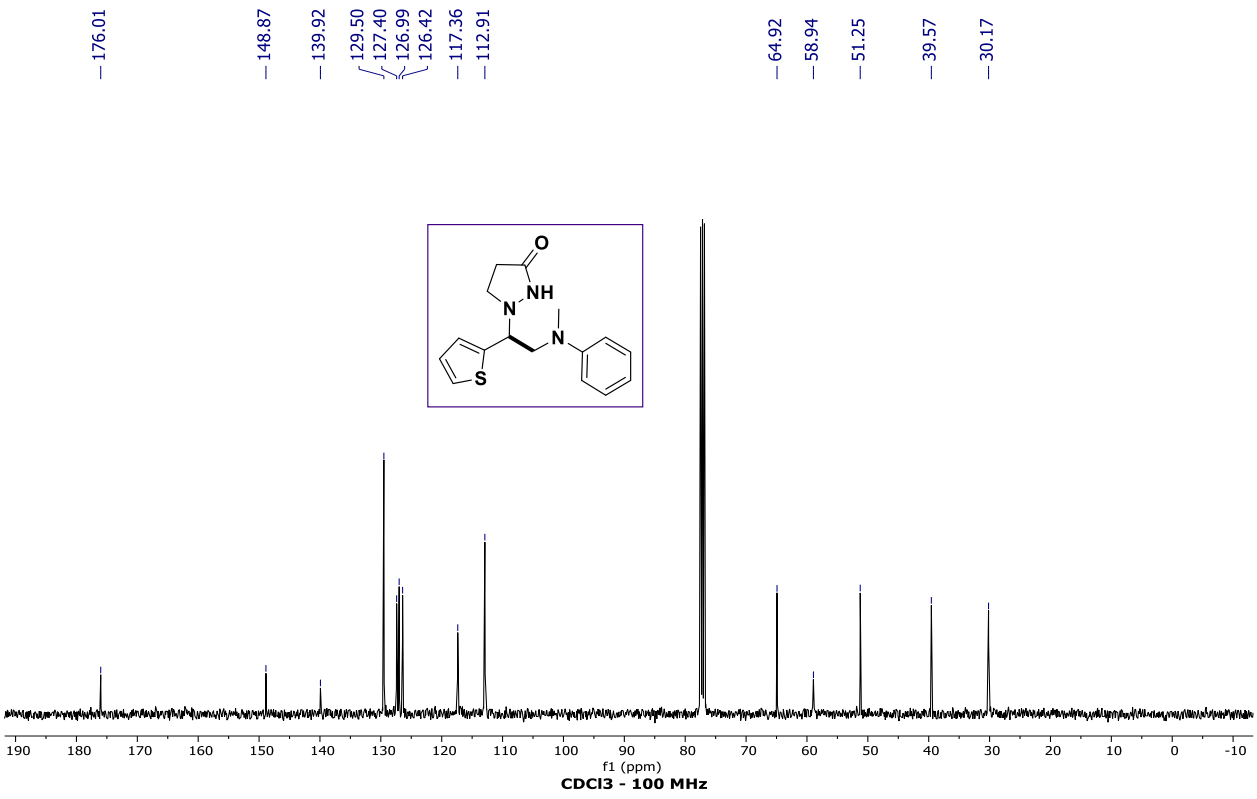
176.01
148.87
139.92
129.50
127.40
126.99
126.42
117.36
112.91
64.92
58.94
51.25
39.57
30.17
O
NH
N
N
S
f1 (ppm)
CDCl3 - 100 MHz

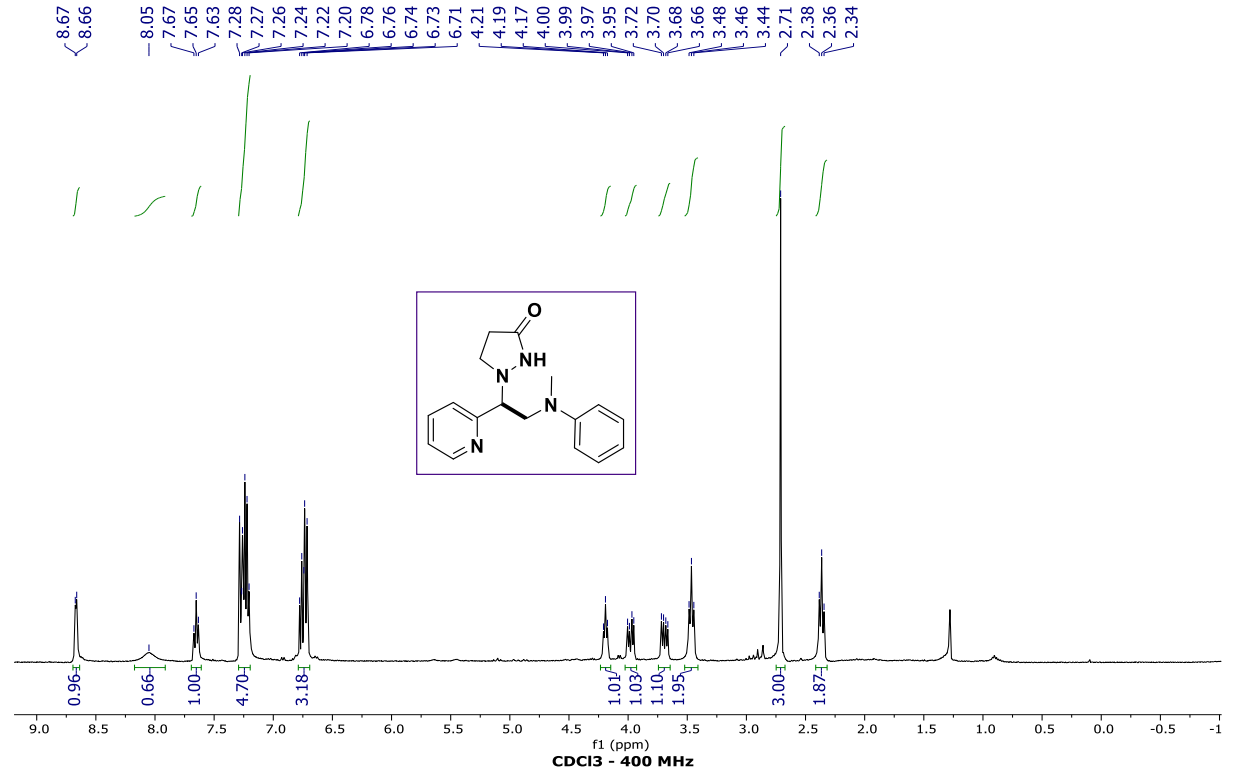
8.67
8.66
8.05
7.67
7.65
7.63
7.28
7.27
7.26
7.24
7.22
7.20
6.78
6.76
6.74
6.73
6.71
4.21
4.19
4.17
4.00
3.99
3.97
3.95
3.72
3.70
3.68
3.66
3.48
3.46
3.44
2.71
2.38
2.36
2.34
O
NH
N
N
N
0.96
0.66
1.00
4.70
3.18
1.01
1.03
1.10
1.95
3.00
1.87
f1 (ppm)
CDCl3 - 400 MHz

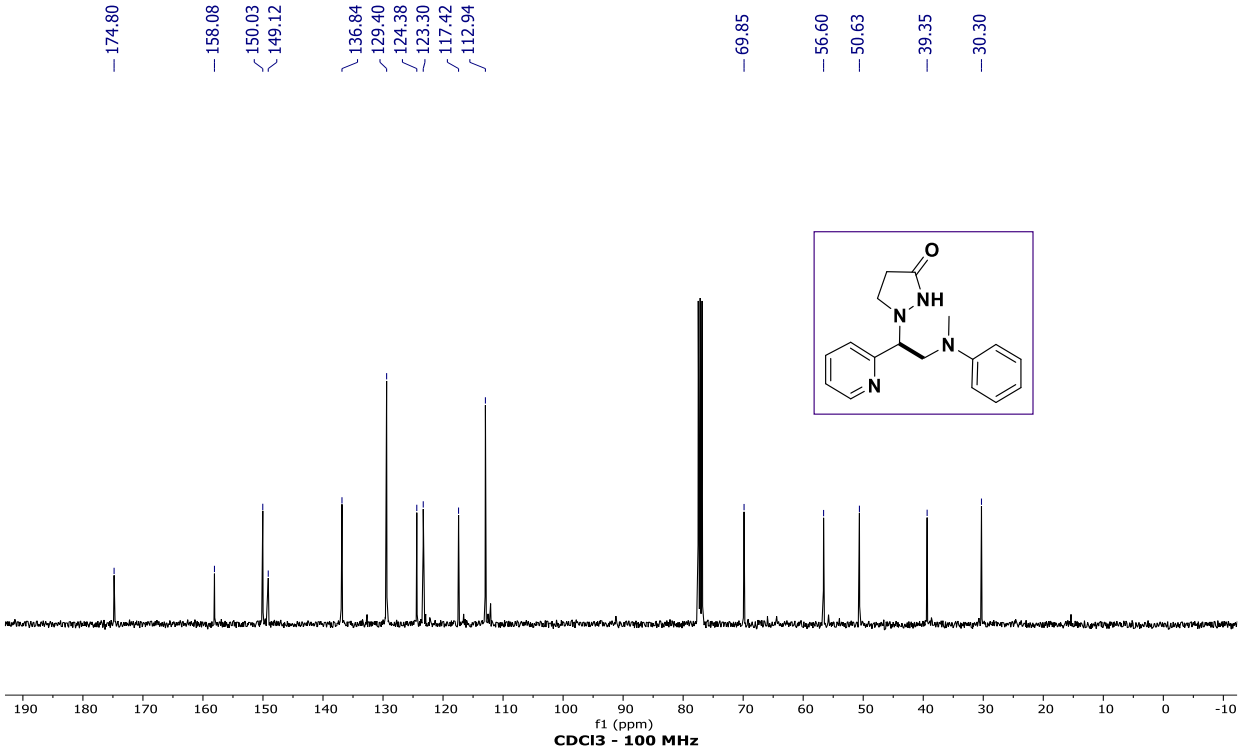
174.80
158.08
150.03
149.12
136.84
129.40
124.38
123.30
117.42
112.94
69.85
56.60
50.63
39.35
30.30
O
NH
N
N
N
f1 (ppm)
CDCl3 - 100 MHz

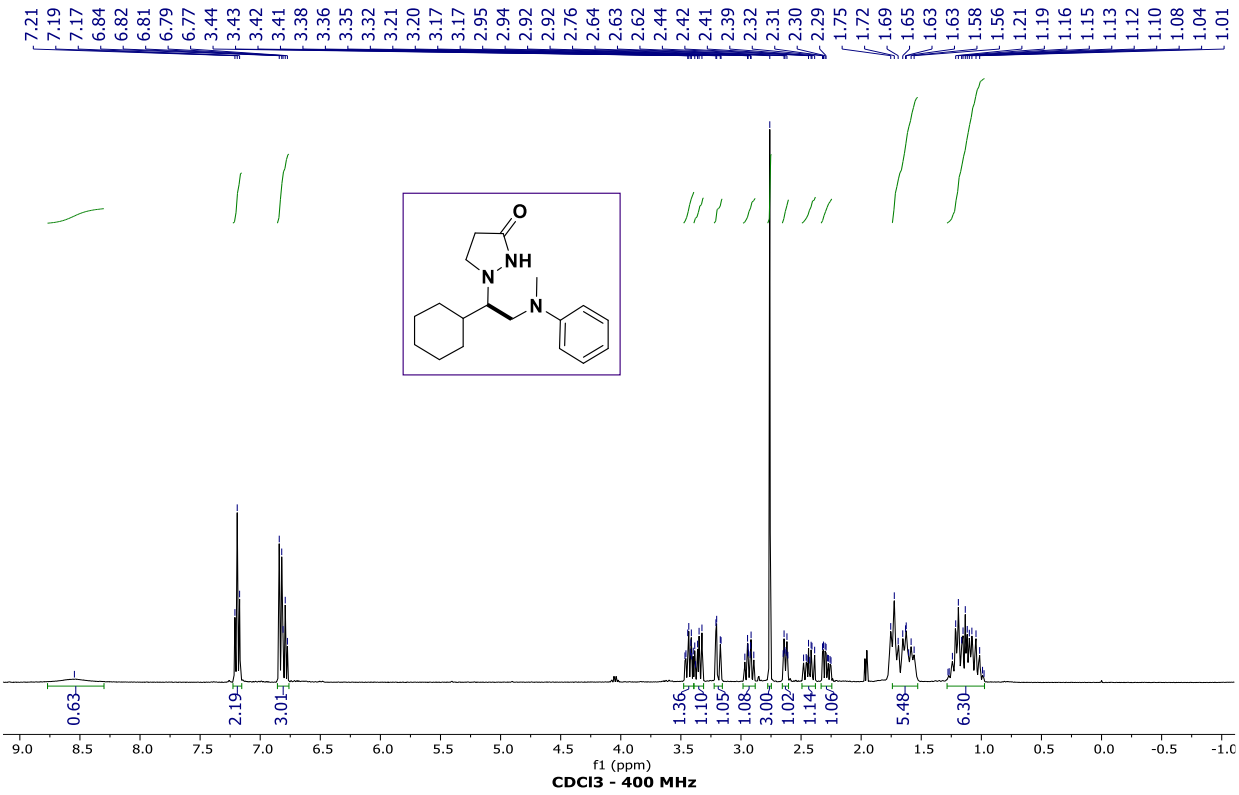
7.21 7.19 7.17 6.84 6.82 6.81 6.79 6.77 3.44 3.43 3.42 3.41 3.38 3.36 3.35 3.32 3.21 3.20 3.17 3.17 2.95 2.94 2.92 2.92 2.76 2.64 2.63 2.62 2.44 2.42 2.41 2.39 2.32 2.31 2.30 2.29 1.75 1.72 1.69 1.65 1.63 1.63 1.58 1.56 1.21 1.19 1.16 1.15 1.13 1.12 1.10 1.08 1.04 1.01
O
NH
N
N
0.63 2.19 3.01 1.36 1.10 1.05 1.08 3.00 1.02 1.14 1.06 5.48 6.30
f1 (ppm)
CDCl3 - 400 MHz

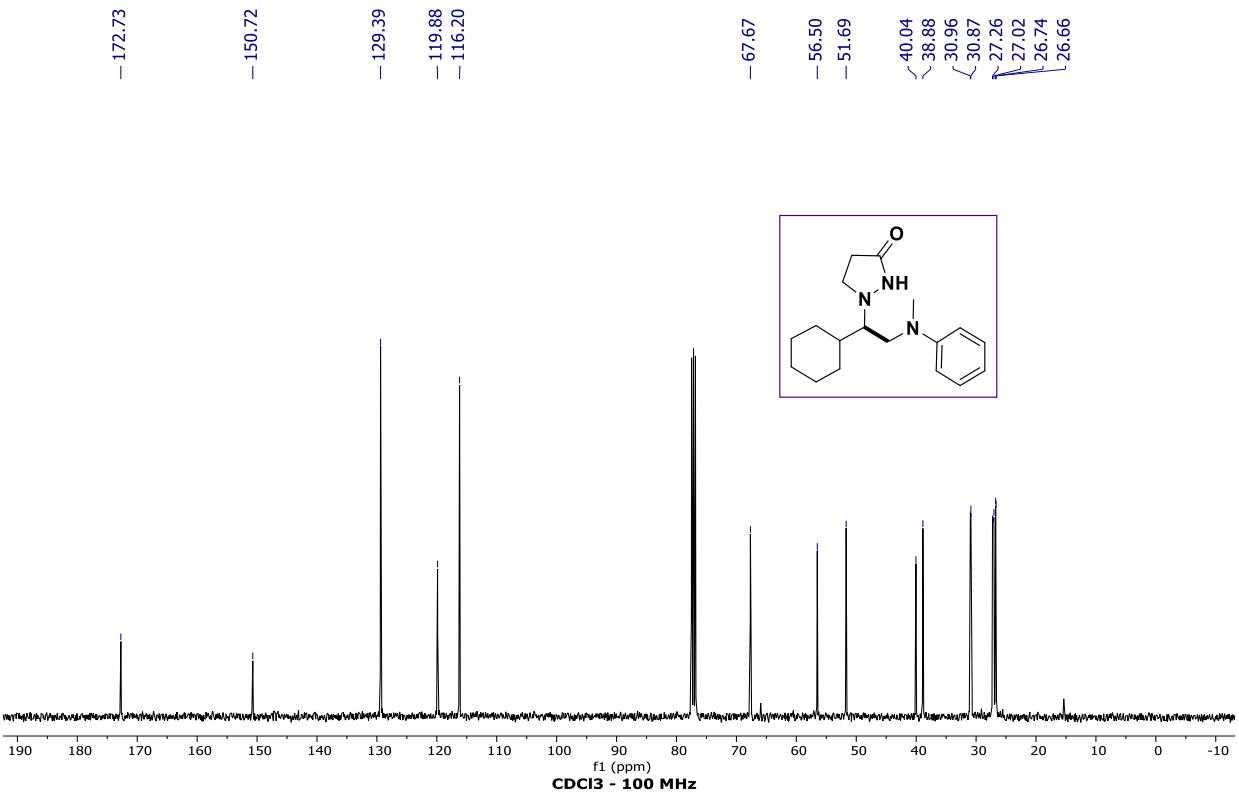
172.73 150.72 129.39 119.88 116.20 67.67 56.50 51.69 40.04 38.88 30.96 30.87 27.26 27.02 26.74 26.66
O
NH
N
N
f1 (ppm)
CDCl3 - 100 MHz

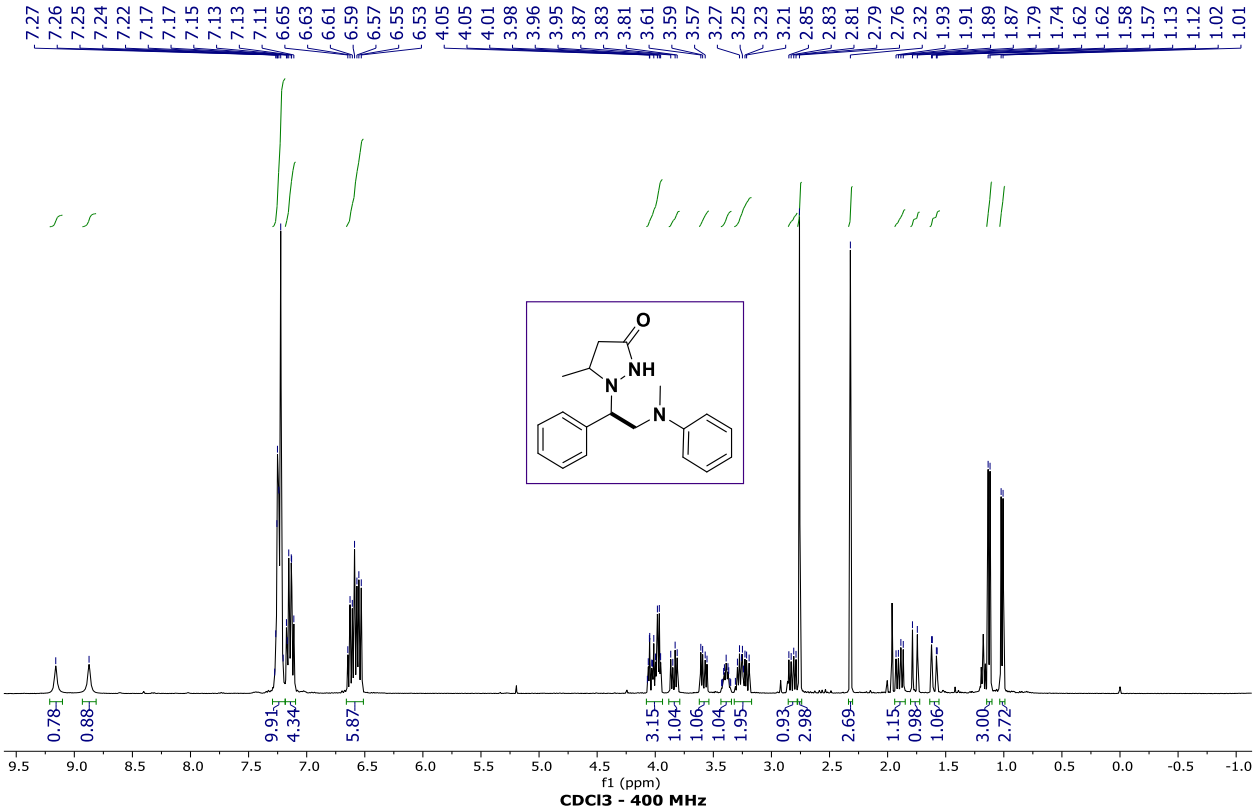

CDCl3 - 400 MHz

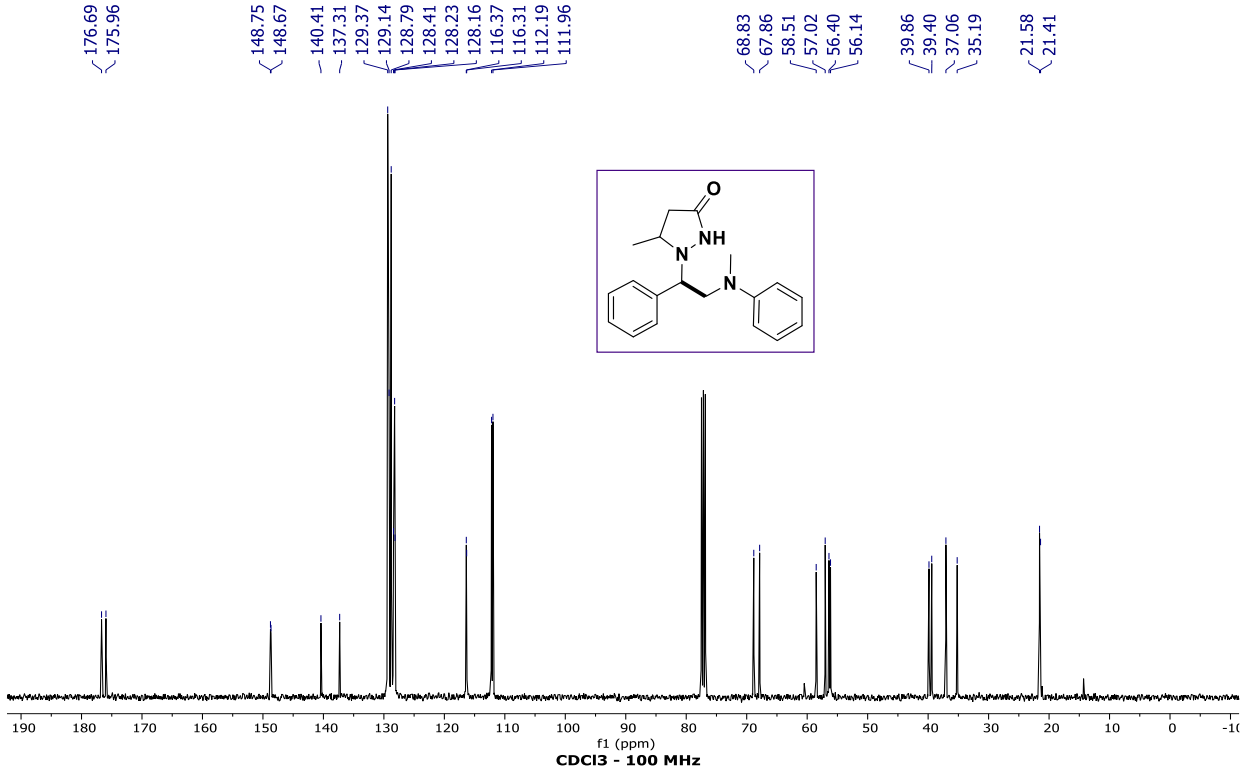

CDCl3 - 100 MHz

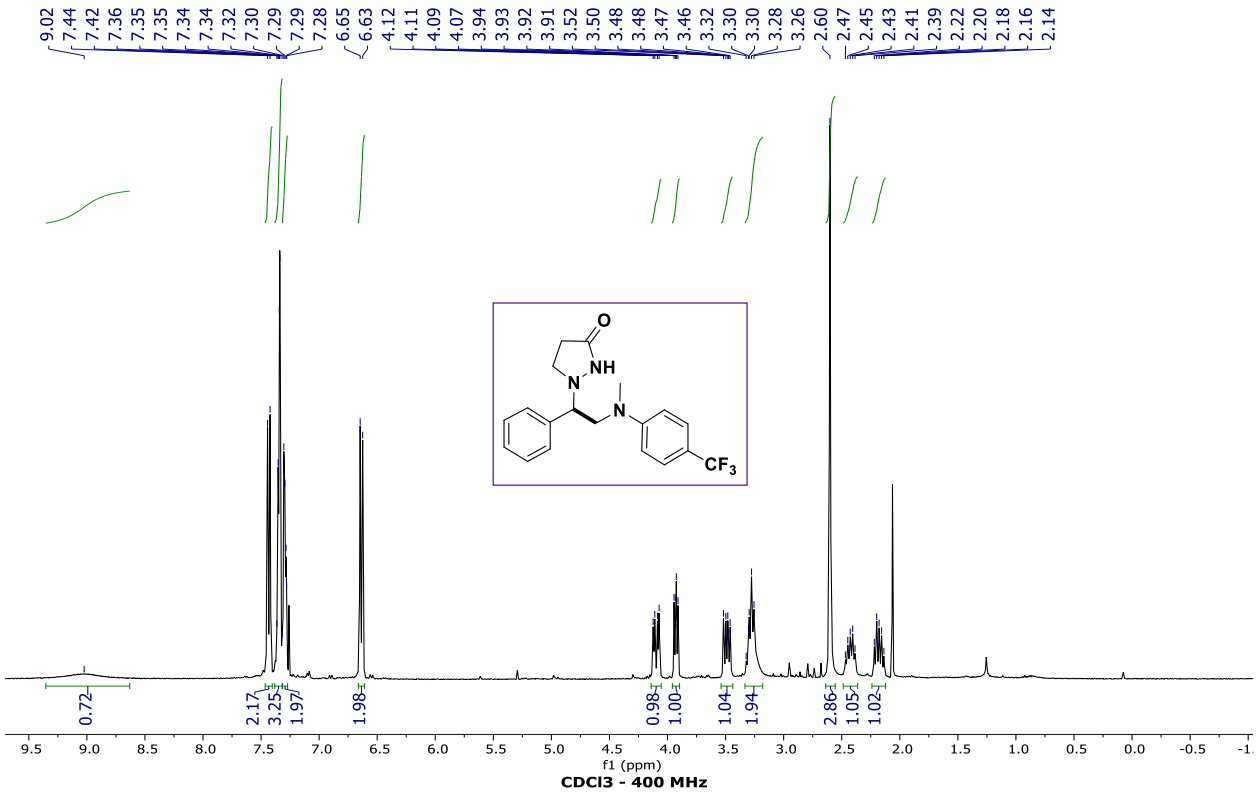
9.02 7.44 7.42 7.36 7.35 7.35 7.34 7.34 7.32 7.30 7.29 7.29 7.28 6.65 6.63 4.12 4.11 4.09 4.07 3.94 3.93 3.92 3.91 3.52 3.50 3.48 3.48 3.47 3.46 3.32 3.30 3.30 3.28 3.26 2.60 2.47 2.45 2.43 2.41 2.39 2.22 2.20 2.18 2.16 2.14
O
NH
N
N
CF3
0.72 2.17 3.25 1.97 1.98 0.98 1.00 1.04 1.94 2.86 1.05 1.02
f1 (ppm)
CDCl3 - 400 MHz

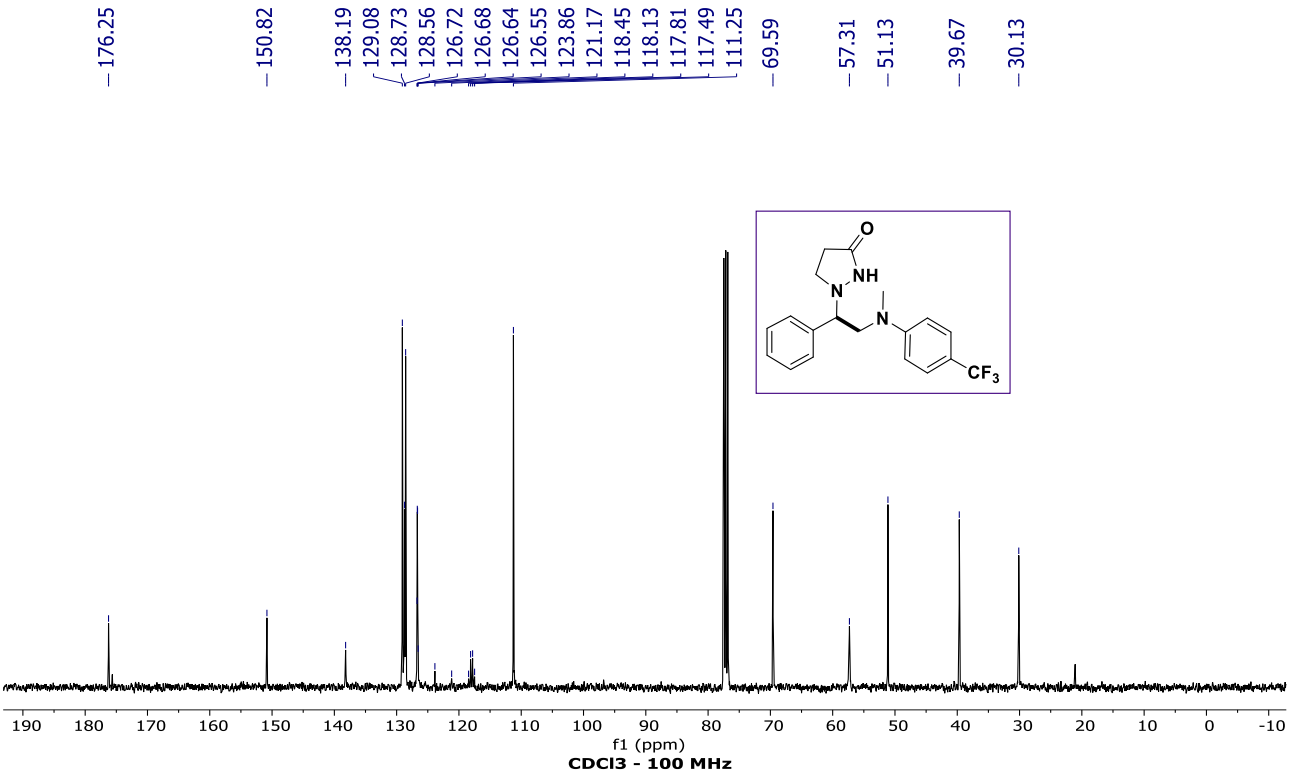
176.25 150.82 138.19 129.08 128.73 128.56 126.72 126.68 126.64 126.55 123.86 121.17 118.45 118.13 117.81 117.49 111.25 69.59 57.31 51.13 39.67 30.13
O
NH
N
N
CF3
f1 (ppm)
CDCl3 - 100 MHz

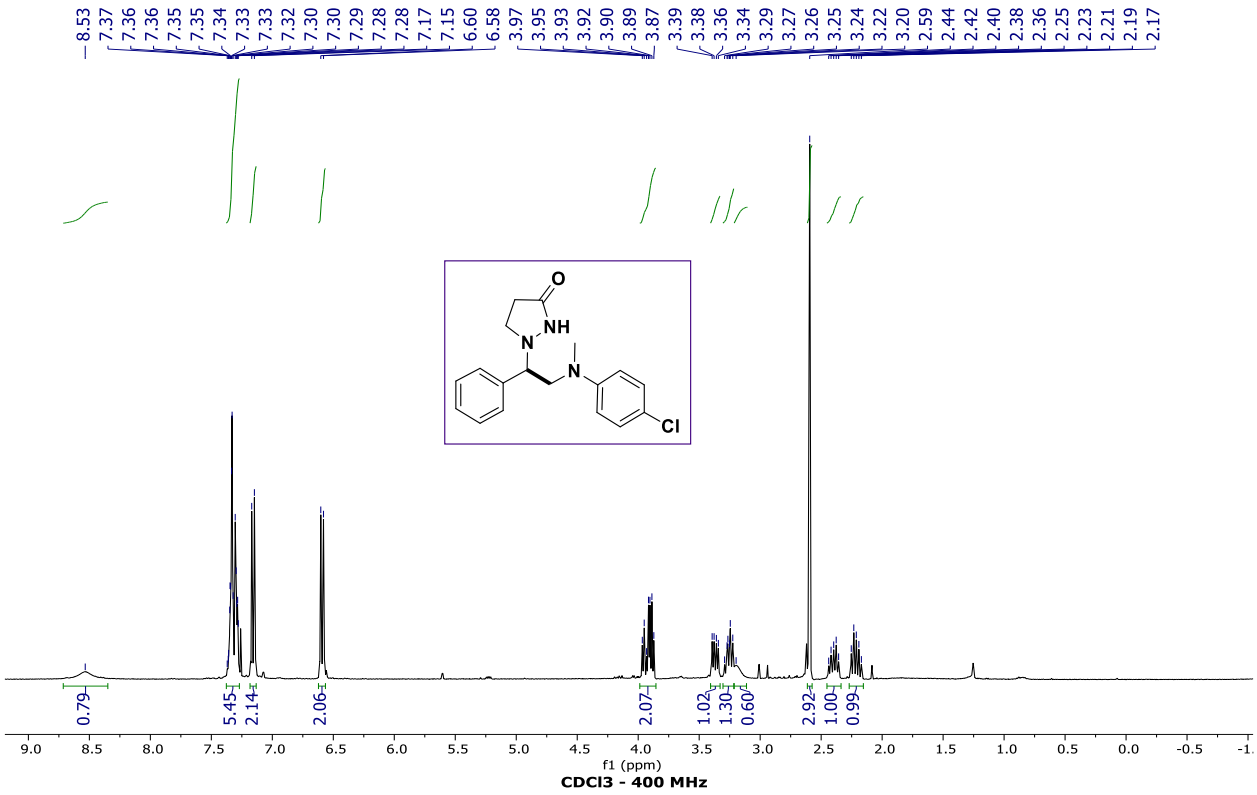
8.53
7.37
7.36
7.36
7.35
7.35
7.34
7.33
7.33
7.32
7.30
7.30
7.29
7.28
7.28
7.17
7.15
6.60
6.58
3.97
3.95
3.93
3.92
3.90
3.89
3.87
3.39
3.38
3.36
3.34
3.29
3.27
3.26
3.25
3.24
3.22
3.20
2.59
2.44
2.42
2.40
2.38
2.36
2.25
2.23
2.21
2.19
2.17
O
NH
N
N
Cl
0.79
5.45
2.14
2.06
2.07
1.02
1.30
0.60
2.92
1.00
0.99
f1 (ppm)
CDCl3 - 400 MHz

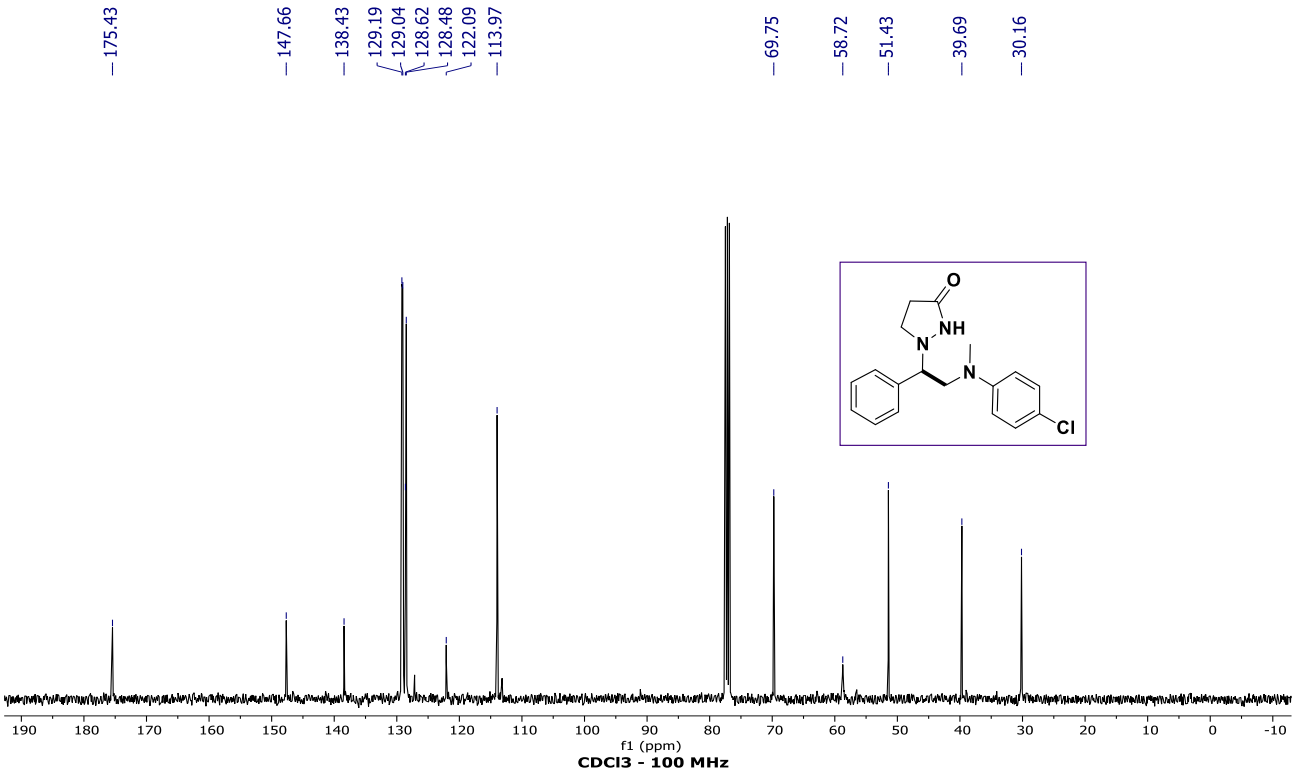
175.43
147.66
138.43
129.19
129.04
128.62
128.48
122.09
113.97
69.75
58.72
51.43
39.69
30.16
O
NH
N
N
Cl
f1 (ppm)
CDCl3 - 100 MHz

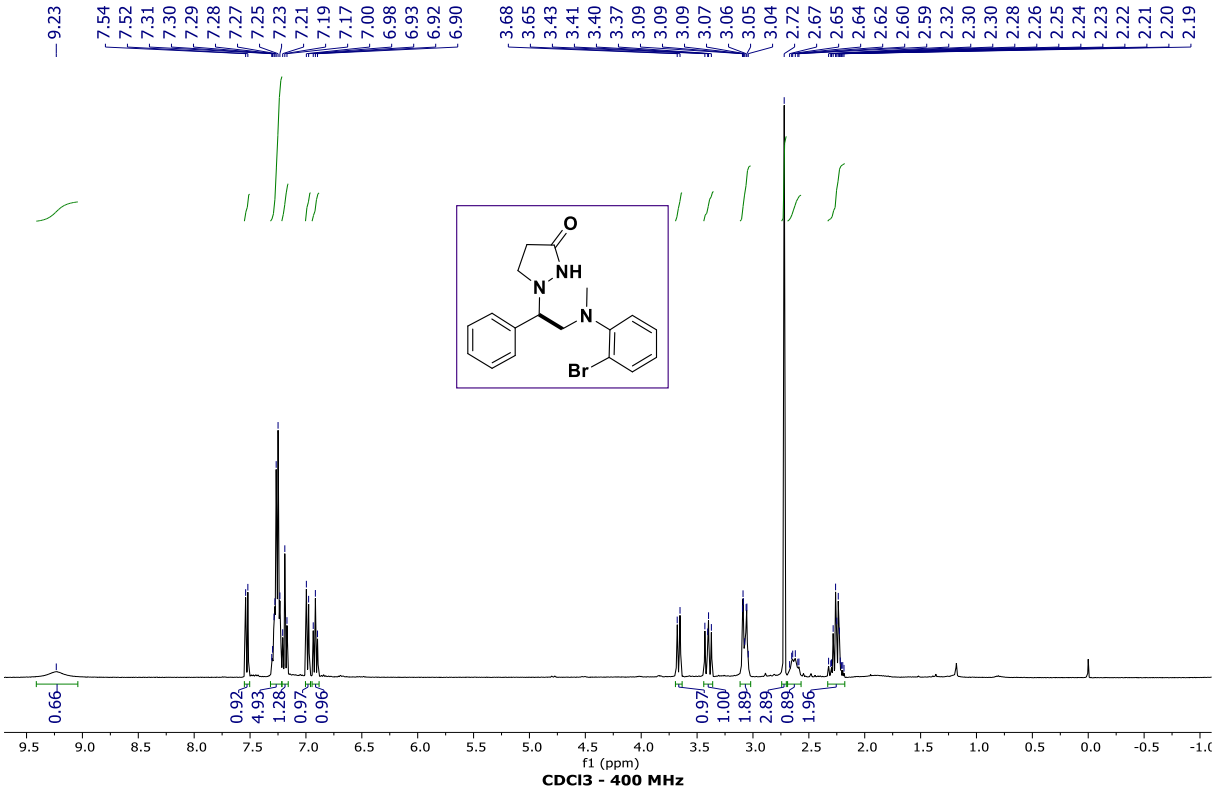
9.23
7.54
7.52
7.31
7.30
7.29
7.28
7.27
7.25
7.23
7.21
7.19
7.17
7.00
6.98
6.93
6.92
6.90
3.68
3.65
3.43
3.41
3.40
3.37
3.09
3.09
3.09
3.07
3.06
3.05
3.04
2.72
2.67
2.65
2.64
2.62
2.60
2.59
2.32
2.30
2.30
2.28
2.26
2.25
2.24
2.23
2.22
2.21
2.20
2.19
O
NH
N
N
Br
0.66
0.92
4.93
1.28
0.97
0.96
0.97
1.00
1.89
2.89
0.89
1.96
f1 (ppm)
CDCl3 - 400 MHz

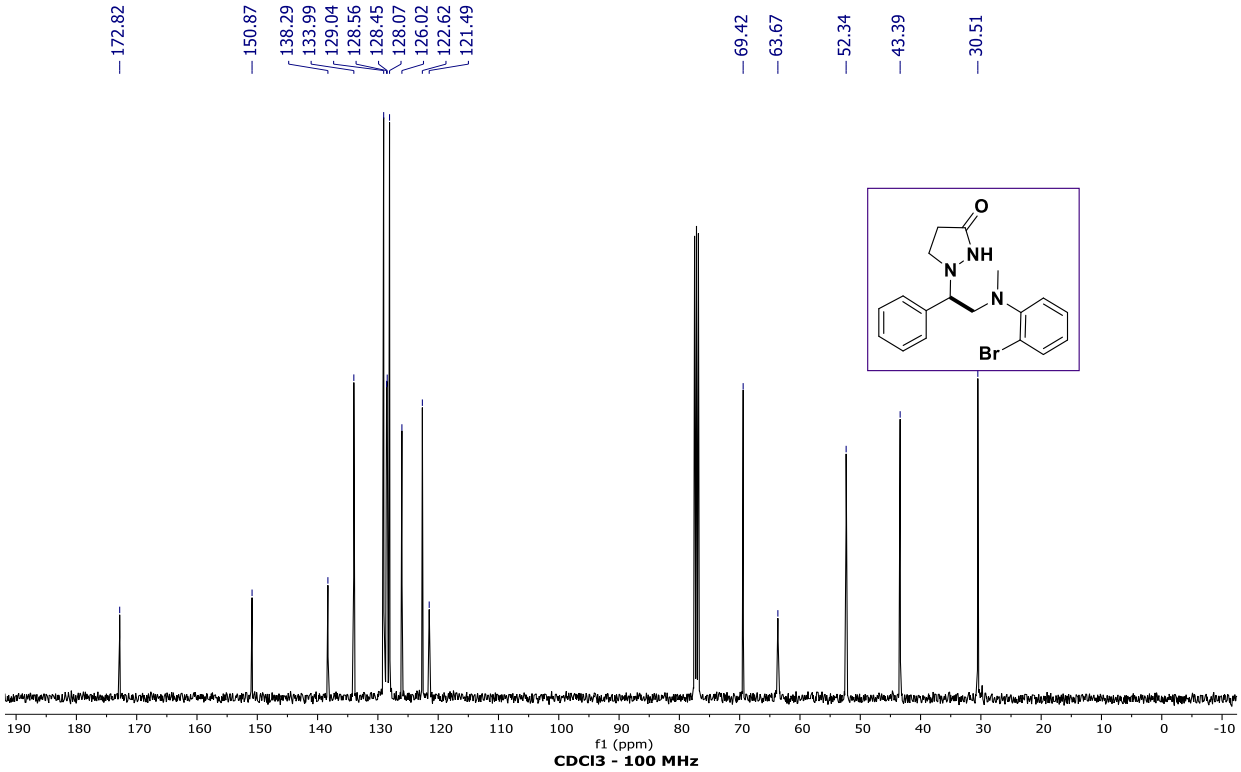
172.82
150.87
138.29
133.99
129.04
128.56
128.45
128.07
126.02
122.62
121.49
69.42
63.67
52.34
43.39
30.51
O
NH
N
N
Br
f1 (ppm)
CDCl3 - 100 MHz

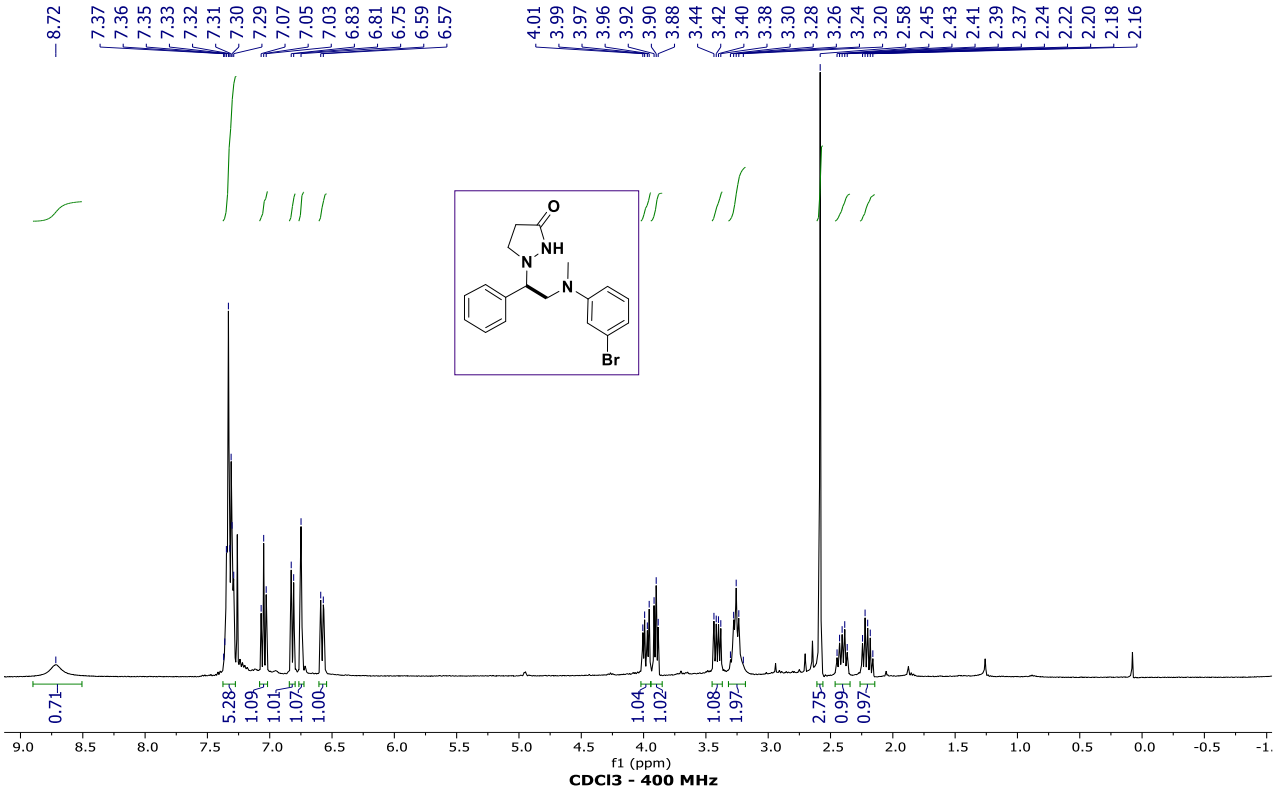
8.72
7.37
7.36
7.35
7.33
7.32
7.31
7.30
7.29
7.07
7.05
7.03
6.83
6.81
6.75
6.59
6.57
4.01
3.99
3.97
3.96
3.92
3.90
3.88
3.44
3.42
3.40
3.38
3.30
3.28
3.26
3.24
3.20
2.58
2.45
2.43
2.41
2.39
2.37
2.24
2.22
2.20
2.18
2.16
O
NH
N
N
Br
0.71
5.28
1.09
1.01
1.07
1.00
1.04
1.02
1.08
1.97
2.75
0.99
0.97
f1 (ppm)
CDCl3 - 400 MHz

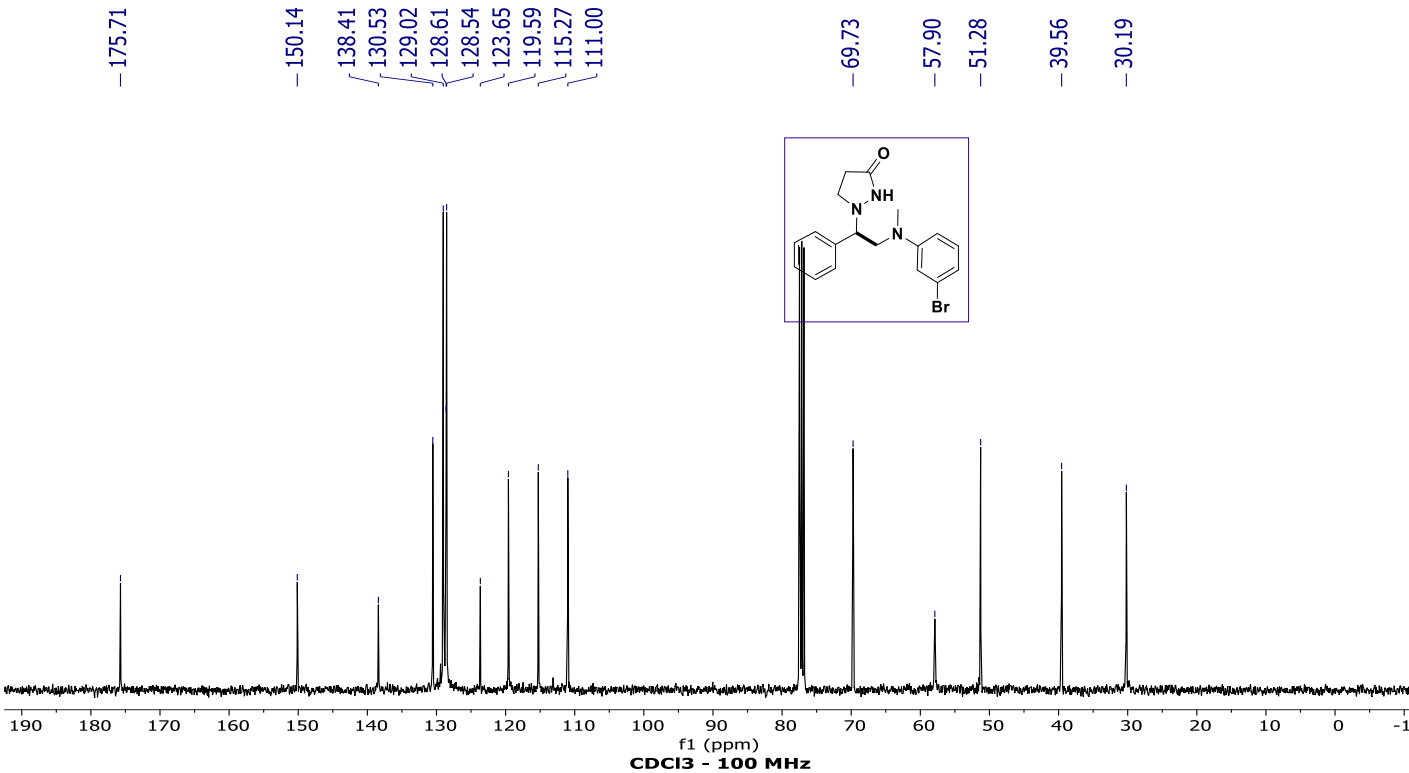
175.71
150.14
138.41
130.53
129.02
128.61
128.54
123.65
119.59
115.27
111.00
69.73
57.90
51.28
39.56
30.19
O
NH
N
N
Br
f1 (ppm)
CDCl3 - 100 MHz

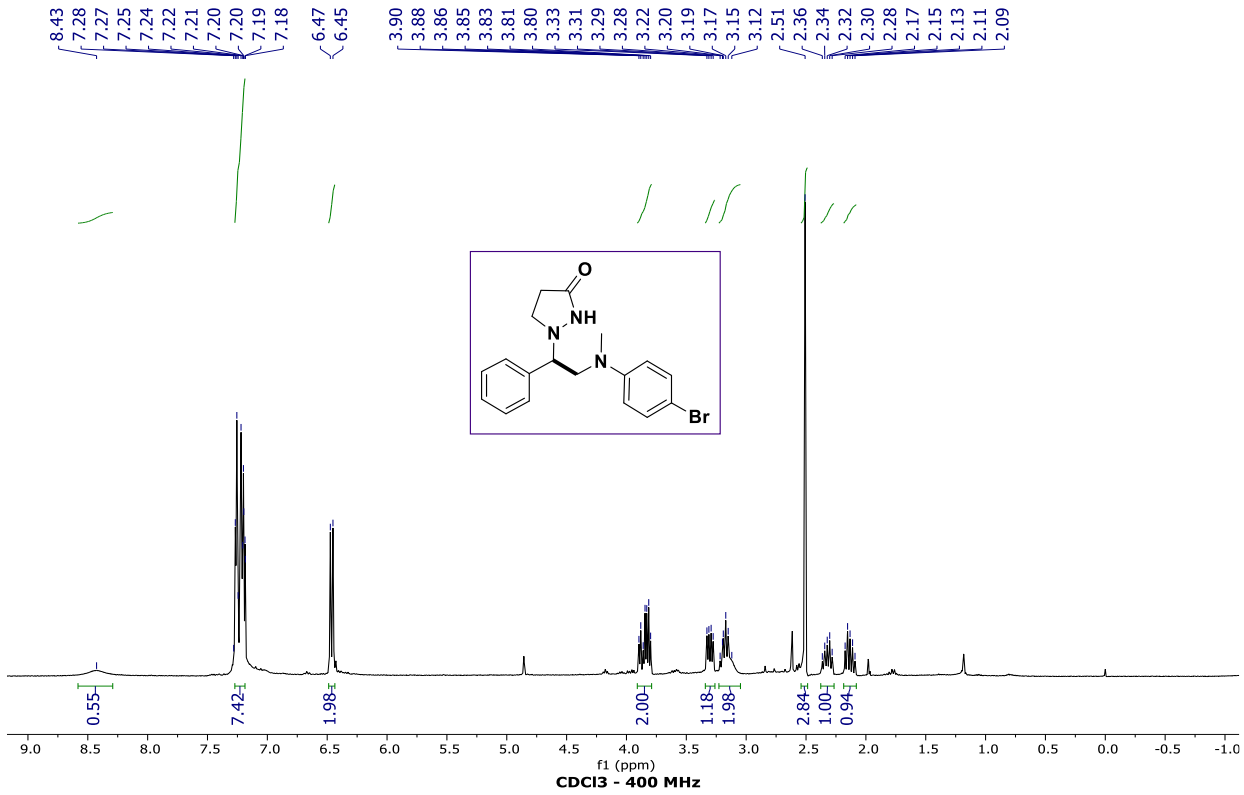
8.43
7.28
7.27
7.25
7.24
7.22
7.21
7.20
7.20
7.19
7.18
6.47
6.45
3.90
3.88
3.86
3.85
3.83
3.81
3.80
3.33
3.31
3.29
3.28
3.22
3.20
3.19
3.17
3.15
3.12
2.51
2.36
2.34
2.32
2.30
2.28
2.17
2.15
2.13
2.11
2.09
O
NH
N
N
Br
0.55
7.42
1.98
2.00
1.18
1.98
2.84
1.00
0.94
f1 (ppm)
CDCl3 - 400 MHz

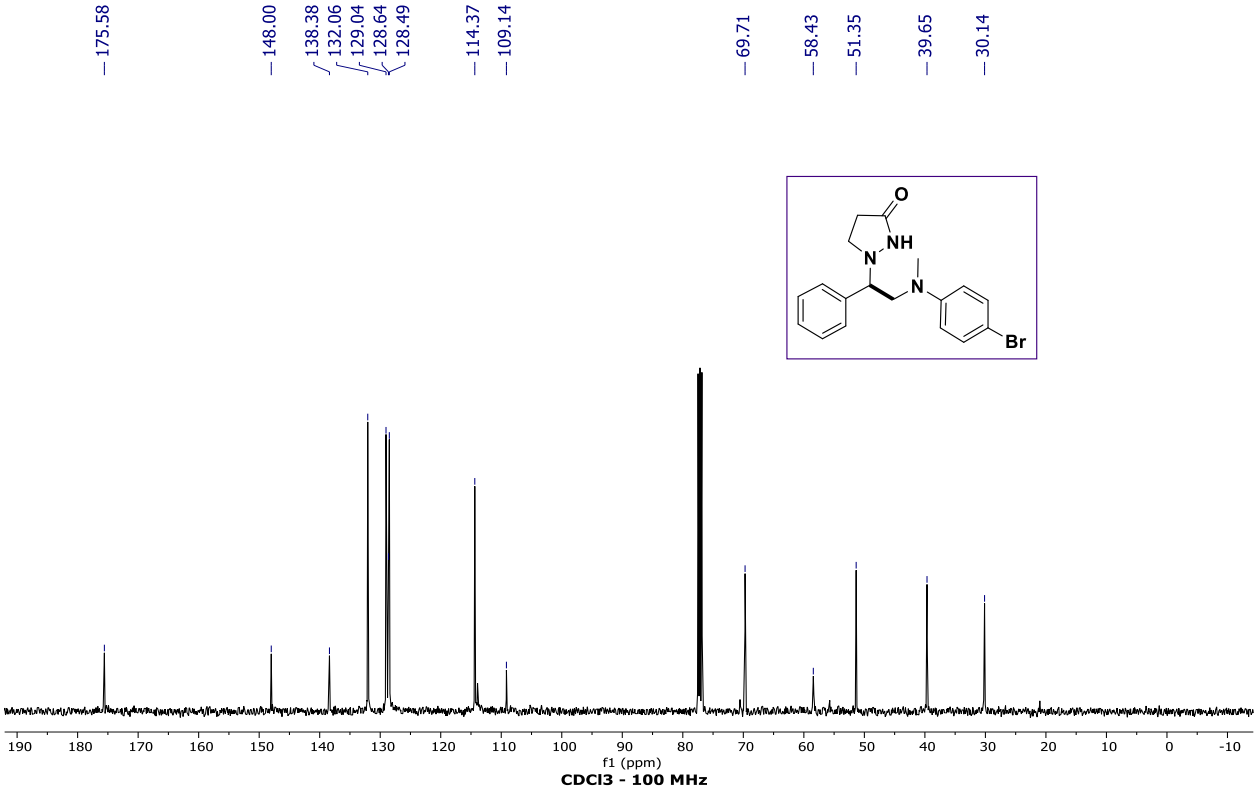
175.58
148.00
138.38
132.06
129.04
128.64
128.49
114.37
109.14
69.71
58.43
51.35
39.65
30.14
O
NH
N
N
Br
f1 (ppm)
CDCl3 - 100 MHz

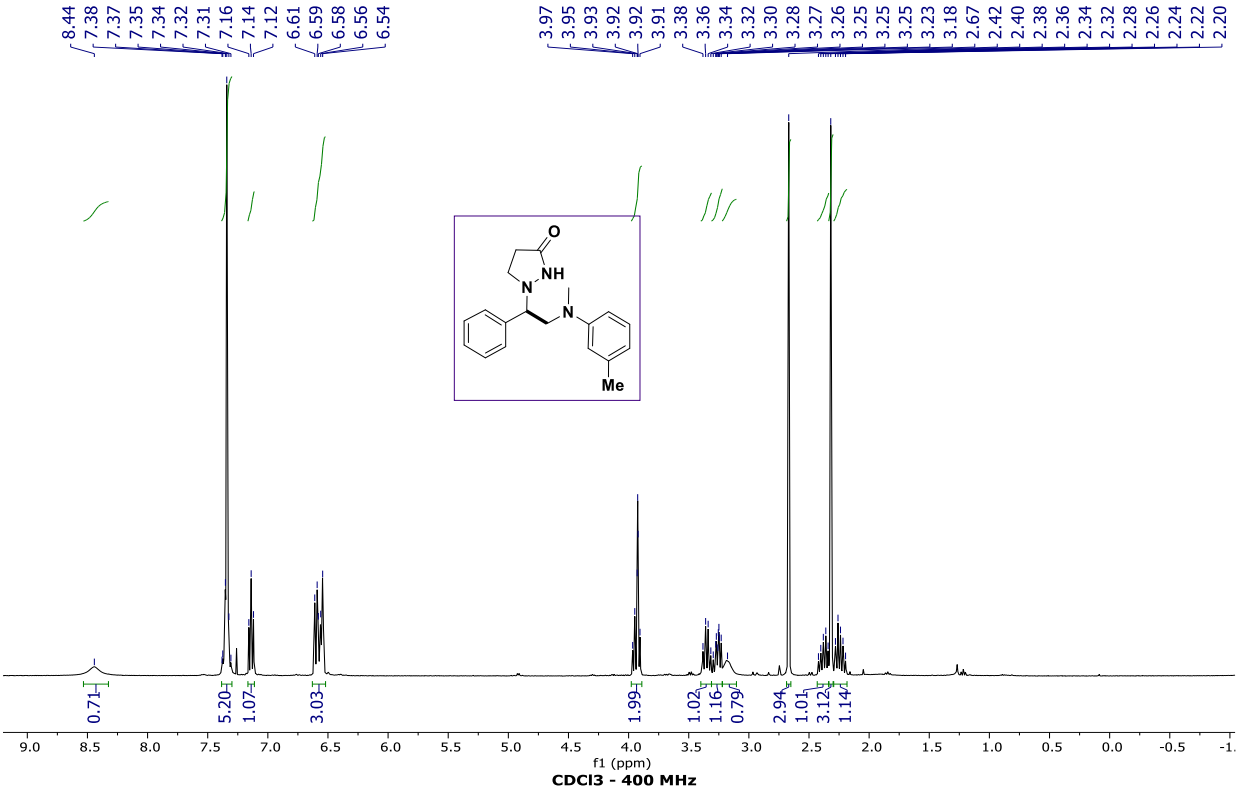

CDCl3 - 400 MHz

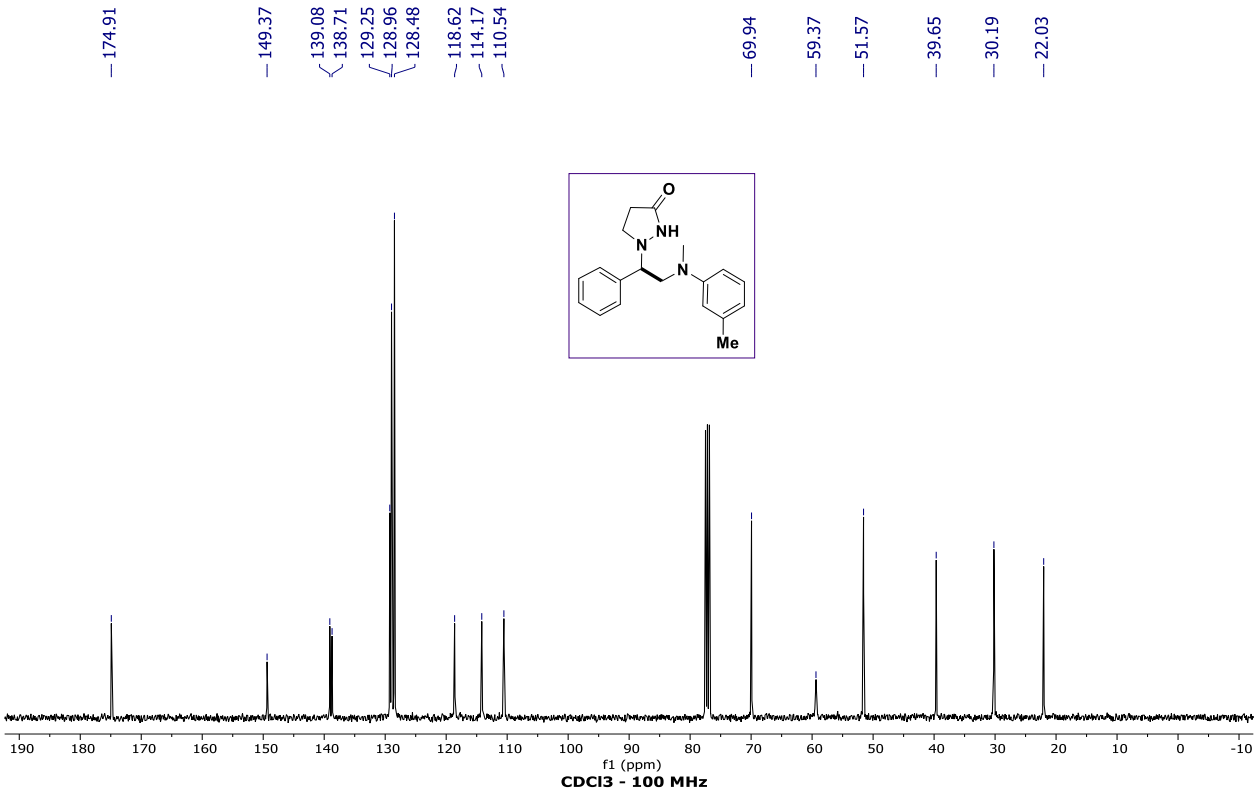

CDCl3 - 100 MHz

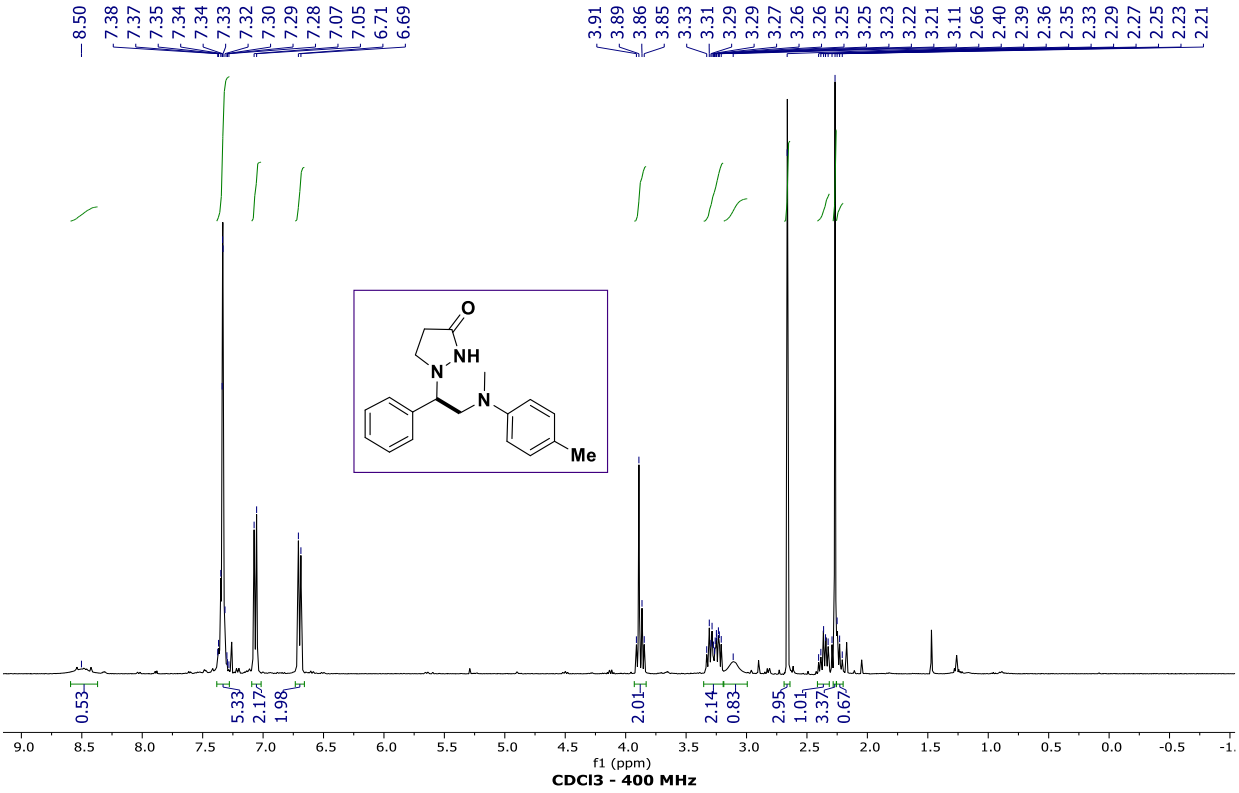
8.50
7.38
7.37
7.35
7.34
7.34
7.33
7.32
7.30
7.29
7.28
7.07
7.05
6.71
6.69
3.91
3.89
3.86
3.85
3.33
3.31
3.29
3.29
3.27
3.26
3.26
3.25
3.25
3.23
3.22
3.21
3.11
2.66
2.40
2.39
2.36
2.35
2.33
2.29
2.27
2.25
2.23
2.21
O
NH
N
N
Me
0.53
5.33
2.17
1.98
2.01
2.14
0.83
2.95
1.01
3.37
0.67
f1 (ppm)
CDCl3 - 400 MHz

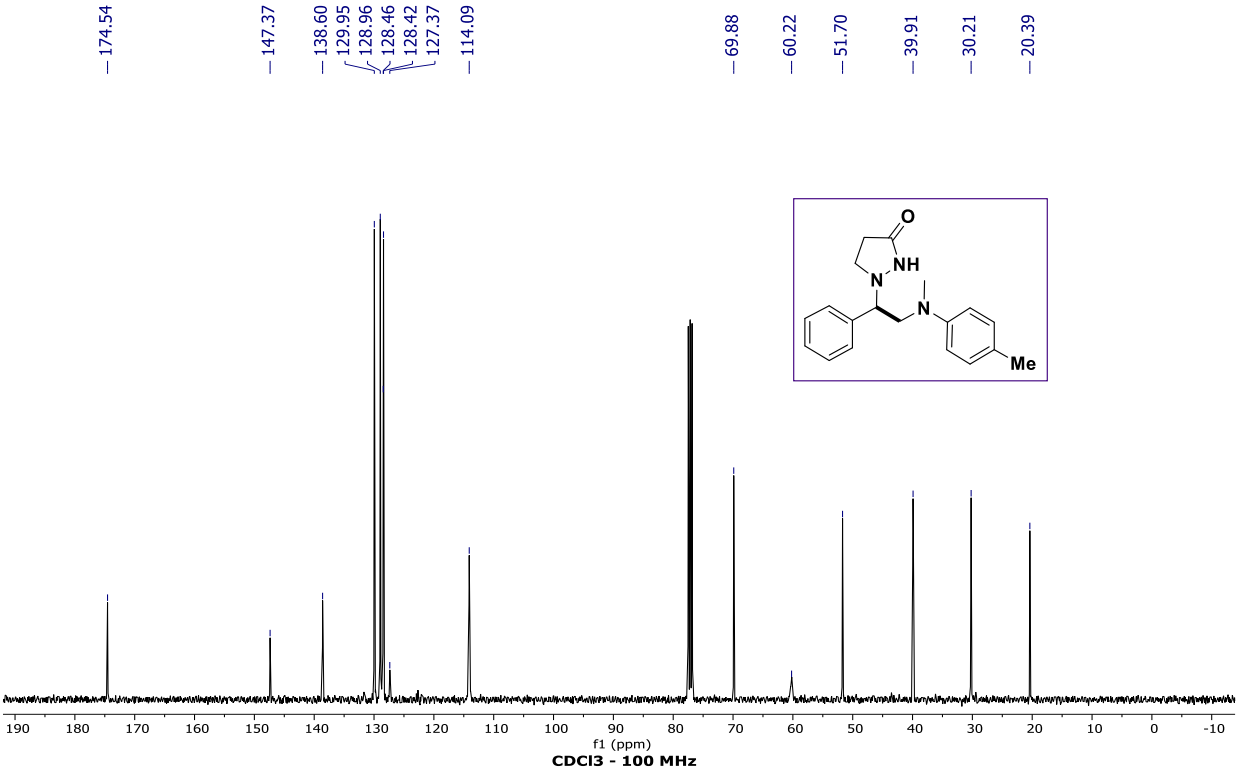
174.54
147.37
138.60
129.95
128.96
128.46
128.42
127.37
114.09
69.88
60.22
51.70
39.91
30.21
20.39
O
NH
N
N
Me
f1 (ppm)
CDCl3 - 100 MHz

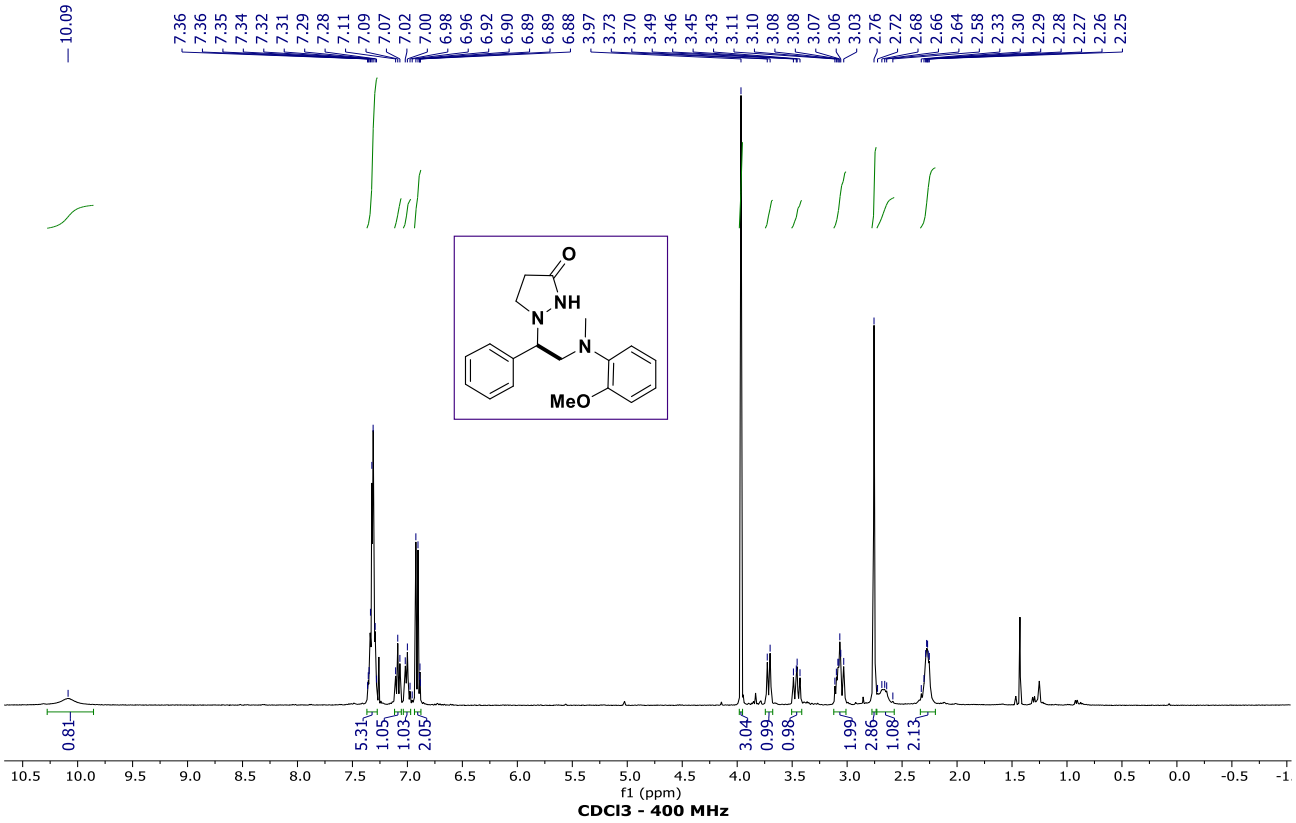
10.09
7.36
7.36
7.35
7.34
7.32
7.31
7.29
7.28
7.11
7.09
7.07
7.02
7.00
6.98
6.96
6.92
6.90
6.89
6.89
6.88
3.97
3.73
3.70
3.49
3.46
3.45
3.43
3.11
3.10
3.08
3.08
3.07
3.06
3.03
2.76
2.72
2.68
2.66
2.64
2.58
2.33
2.30
2.29
2.28
2.27
2.26
2.25
O
NH
N
N
MeO
0.81
5.31
1.05
1.03
2.05
3.04
0.99
0.98
1.99
2.86
1.08
2.13
f1 (ppm)
CDCl3 - 400 MHz

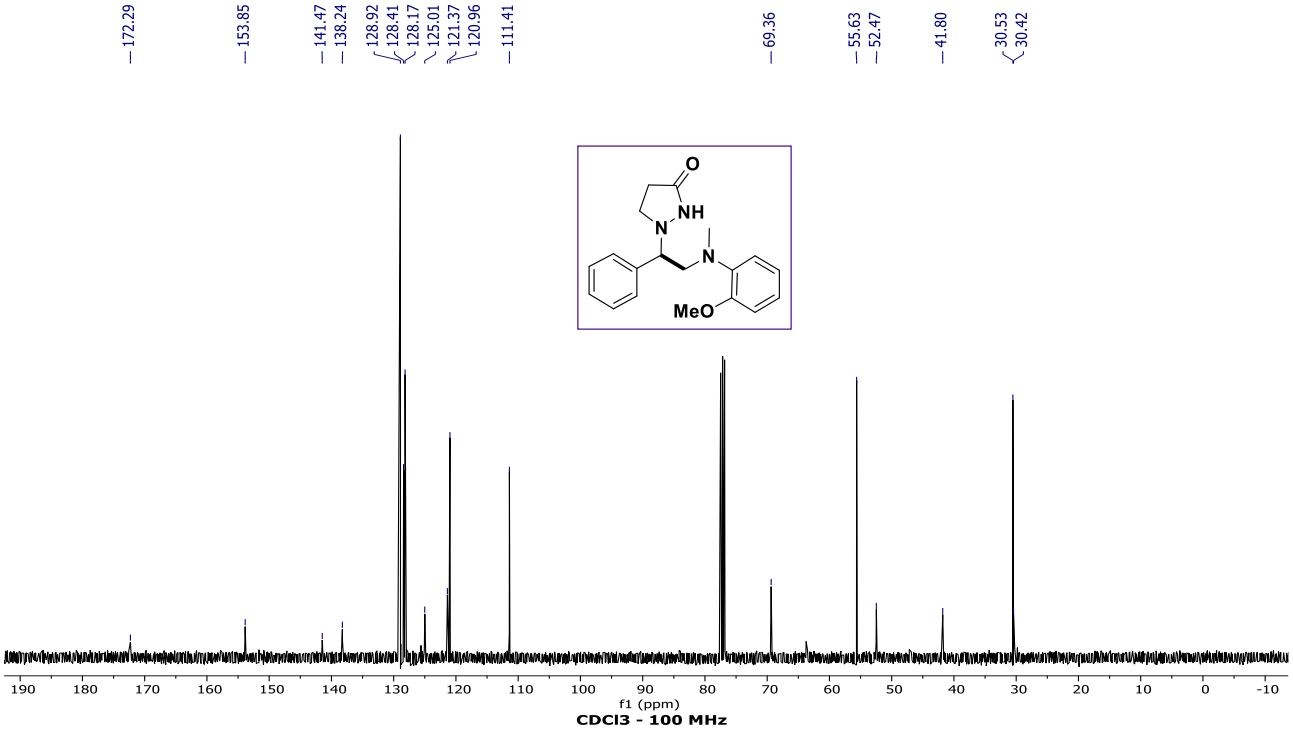
172.29
153.85
141.47
138.24
128.92
128.41
128.17
125.01
121.37
120.96
111.41
69.36
55.63
52.47
41.80
30.53
30.42
O
NH
N
N
MeO
f1 (ppm)
CDCl3 - 100 MHz

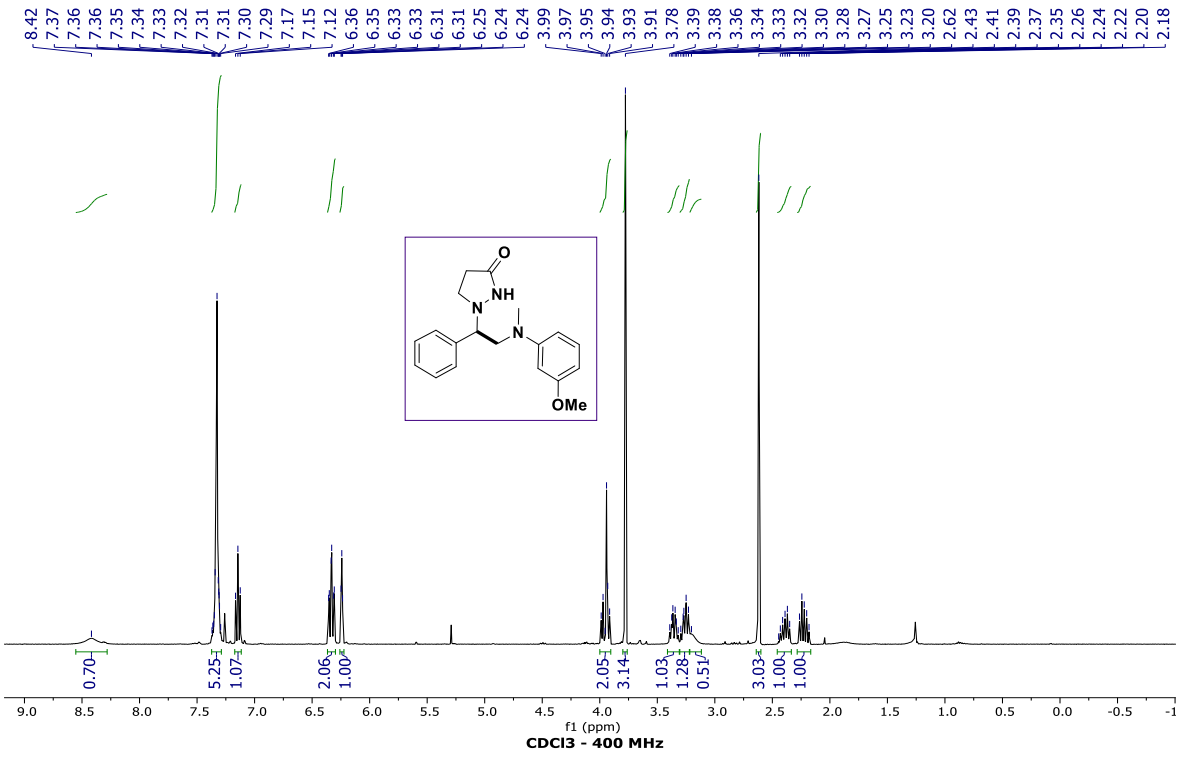
8.42 7.37 7.36 7.36 7.35 7.34 7.33 7.32 7.31 7.31 7.30 7.29 7.17 7.15 7.12 6.36 6.35 6.33 6.33 6.31 6.31 6.25 6.24 6.24 3.99 3.97 3.95 3.94 3.93 3.91 3.78 3.39 3.38 3.36 3.34 3.33 3.32 3.30 3.28 3.27 3.25 3.23 3.20 2.62 2.43 2.41 2.39 2.37 2.35 2.26 2.24 2.22 2.20 2.18
O
NH
N
N
OMe
0.70 5.25 1.07 2.06 1.00 2.05 3.14 1.03 1.28 0.51 3.03 1.00 1.00
f1 (ppm)
CDCl3 - 400 MHz

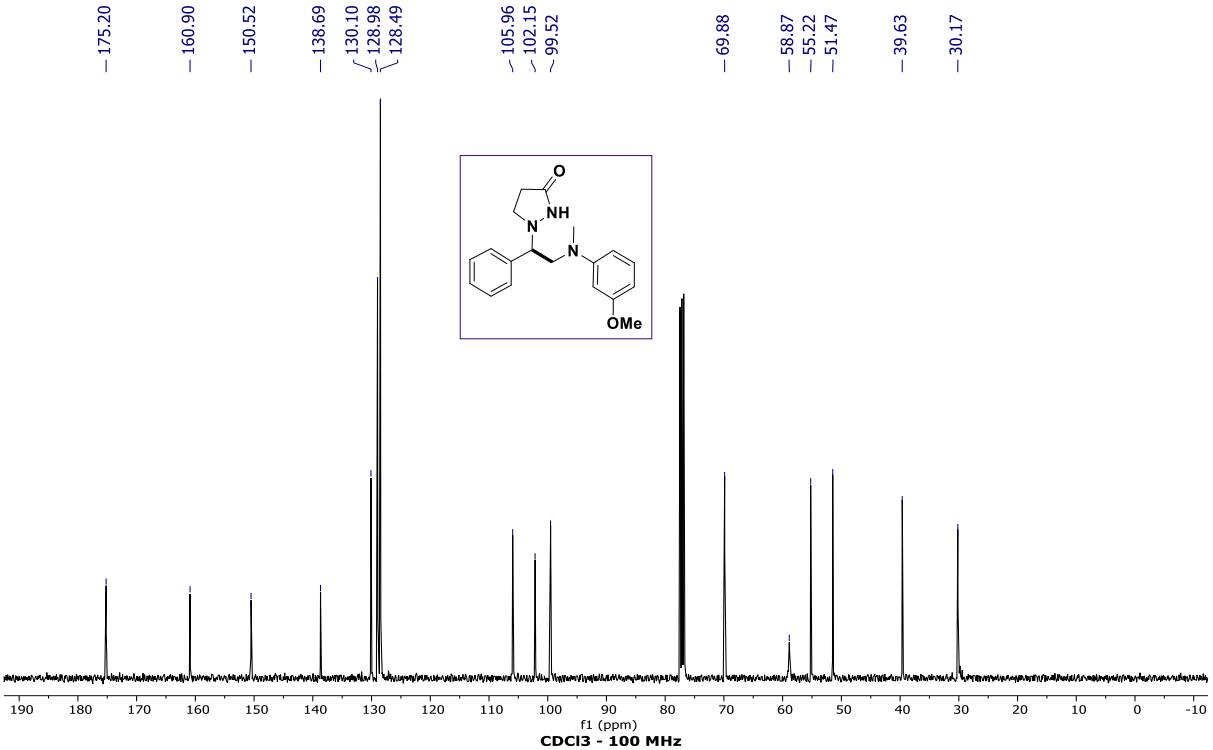
175.20 160.90 150.52 138.69 130.10 128.98 128.49 105.96 102.15 99.52 69.88 58.87 55.22 51.47 39.63 30.17
O
NH
N
N
OMe
f1 (ppm)
CDCl3 - 100 MHz

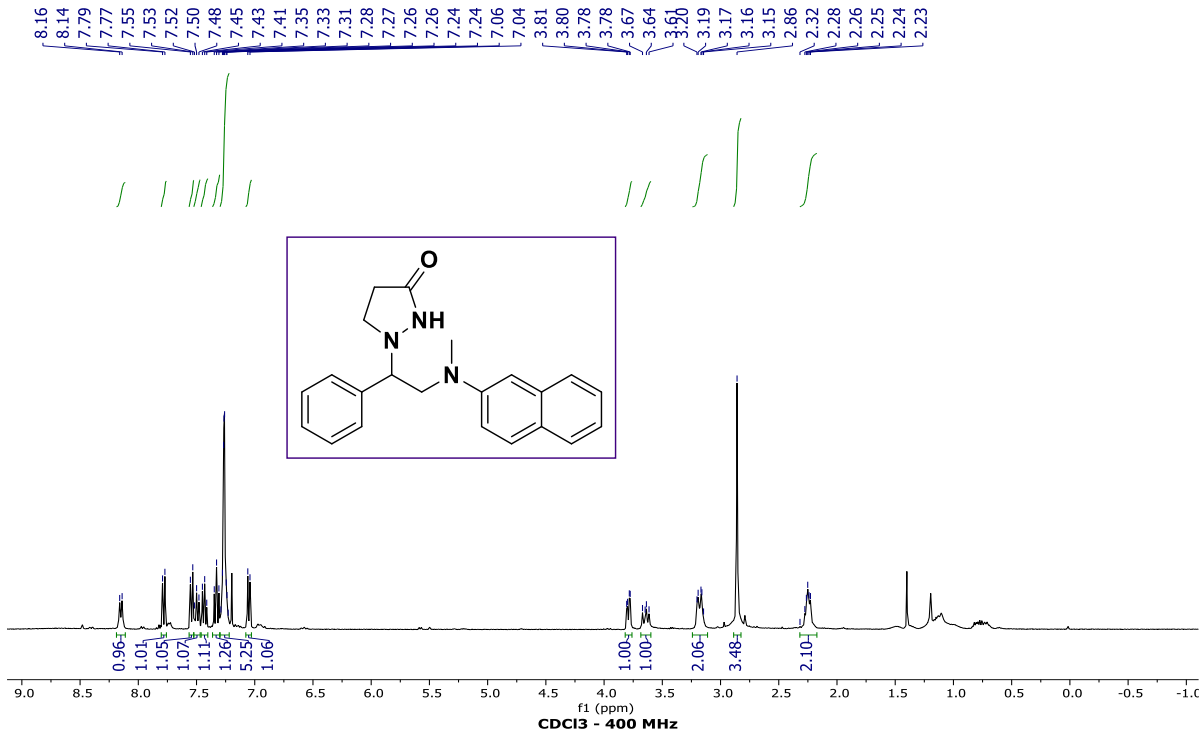
8.16 8.14 7.79 7.77 7.55 7.53 7.52 7.50 7.48 7.45 7.43 7.41 7.35 7.33 7.31 7.28 7.27 7.26 7.26 7.24 7.24 7.06 7.04 3.81 3.80 3.78 3.78 3.67 3.64 3.61 3.20 3.19 3.17 3.16 3.15 2.86 2.32 2.28 2.26 2.25 2.24 2.23
O
NH
N
N
0.96 1.01 1.05 1.07 1.11 1.26 5.25 1.06 1.00 1.00 2.06 3.48 2.10
f1 (ppm)
CDCl3 - 400 MHz

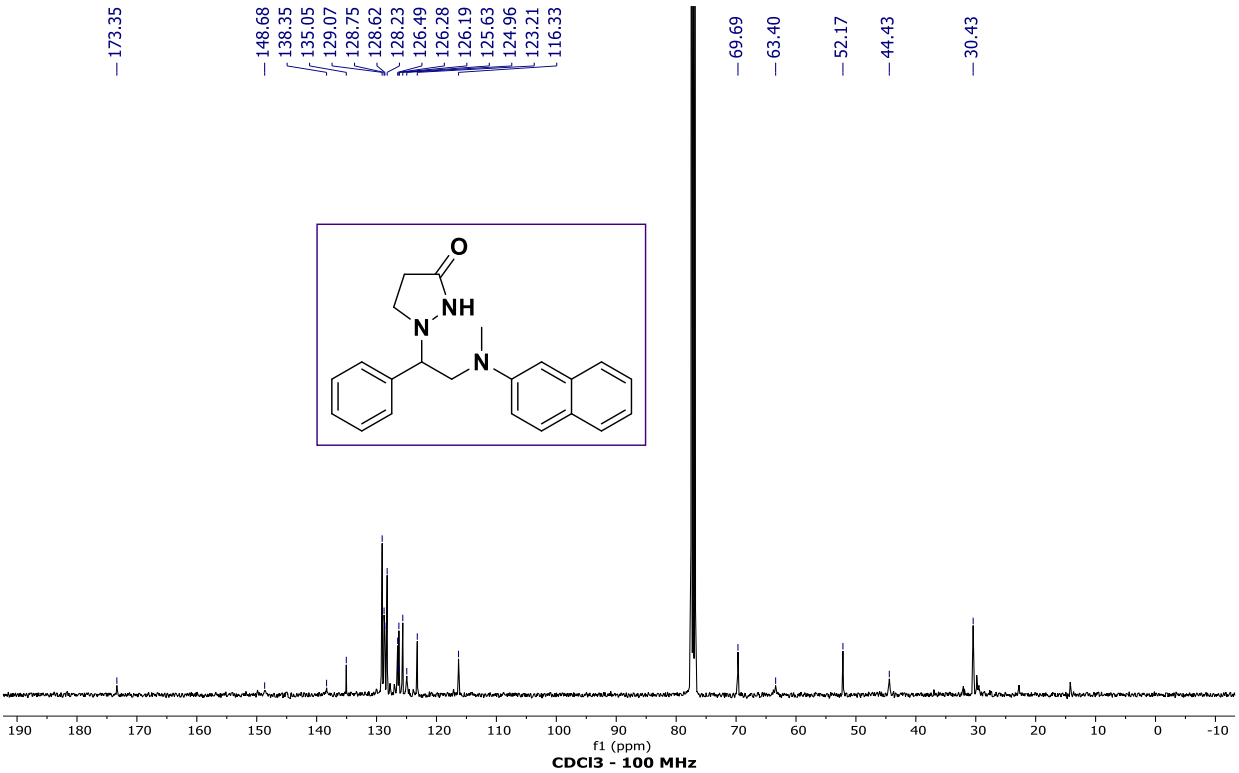
173.35 148.68 138.35 135.05 129.07 128.75 128.62 128.23 126.49 126.28 126.19 125.63 124.96 123.21 116.33 69.69 63.40 52.17 44.43 30.43
O
NH
N
N
f1 (ppm)
CDCl3 - 100 MHz

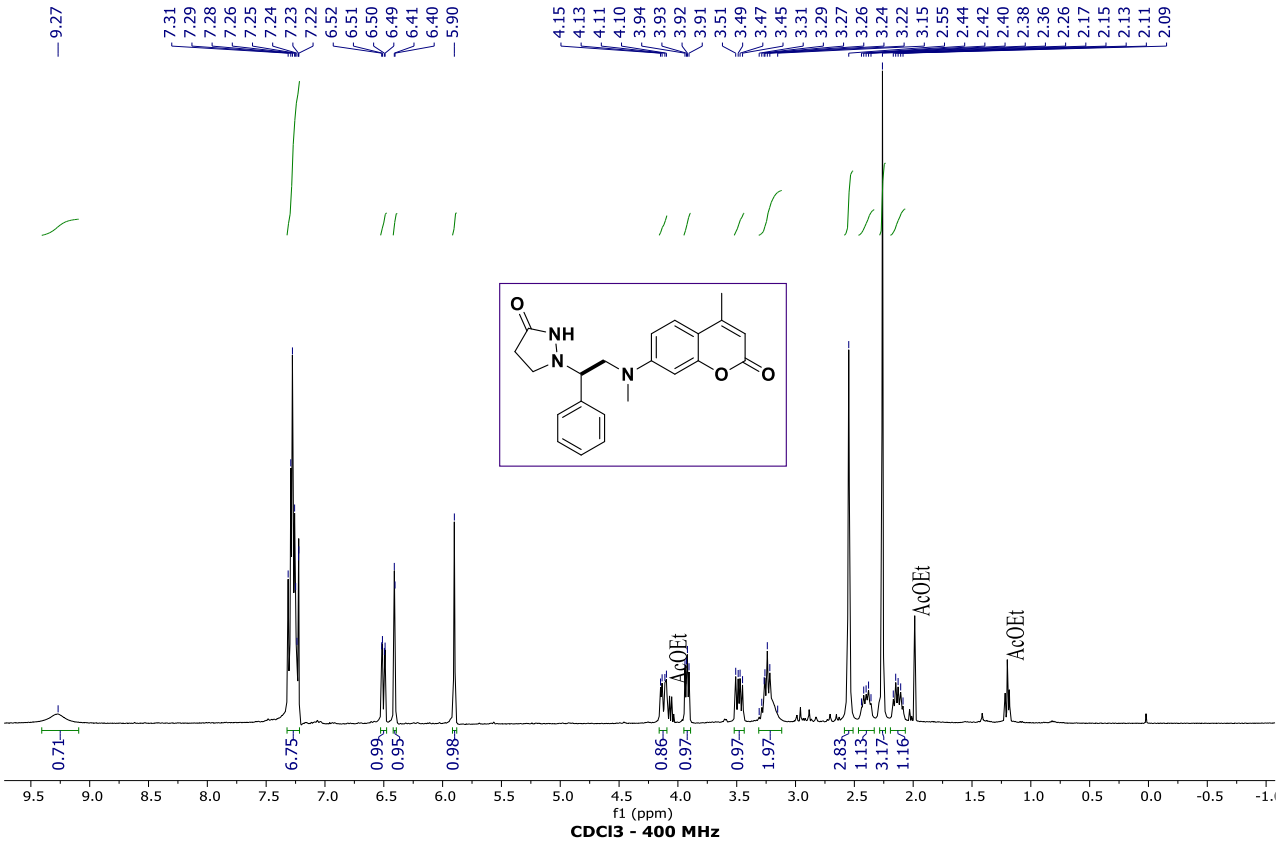
9.27
7.31
7.29
7.28
7.26
7.25
7.24
7.23
7.22
6.52
6.51
6.50
6.49
6.41
6.40
5.90
4.15
4.13
4.11
4.10
3.94
3.93
3.92
3.91
3.51
3.49
3.47
3.45
3.31
3.29
3.27
3.26
3.24
3.22
3.15
2.55
2.44
2.42
2.40
2.38
2.36
2.26
2.17
2.15
2.13
2.11
2.09
AcOEt
AcOEt
0.71
6.75
0.99
0.95
0.98
0.86
0.97
0.97
1.97
2.83
1.13
3.17
1.16
f1 (ppm)
CDCl3 - 400 MHz

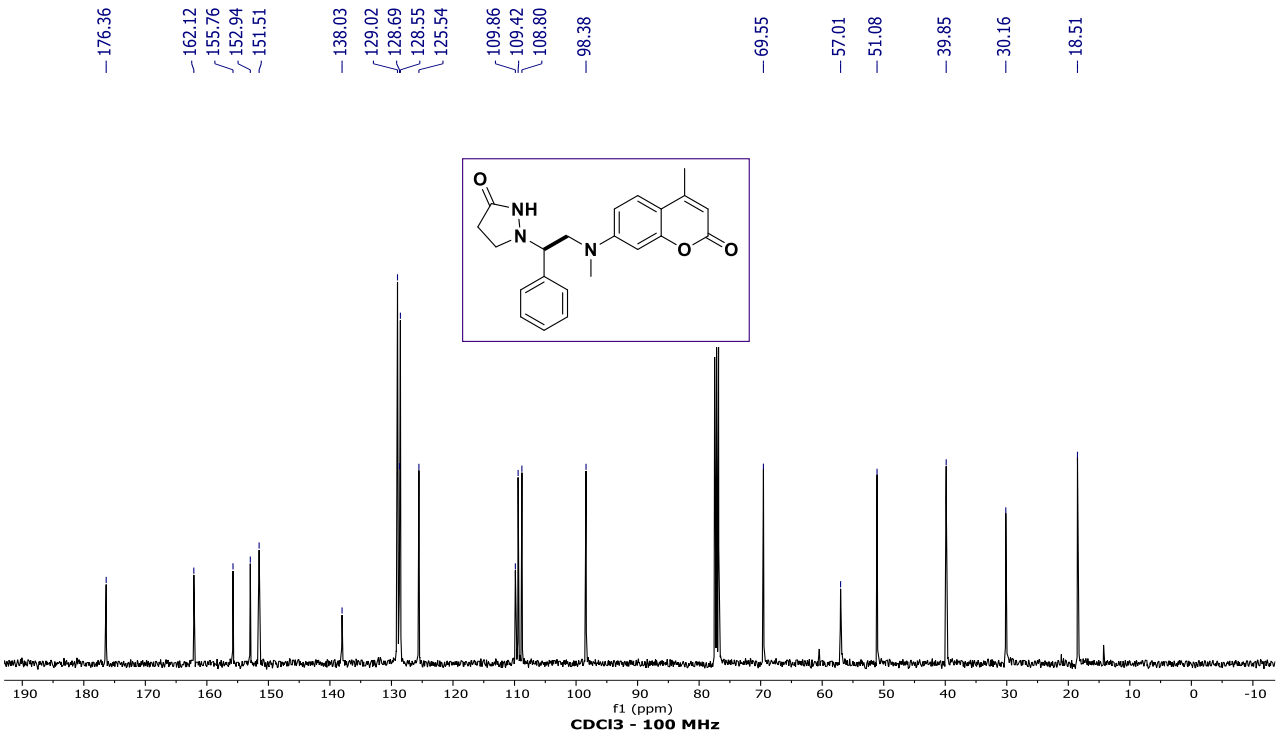
176.36
162.12
155.76
152.94
151.51
138.03
129.02
128.69
128.55
125.54
109.86
109.42
108.80
98.38
69.55
57.01
51.08
39.85
30.16
18.51
f1 (ppm)
CDCl3 - 100 MHz

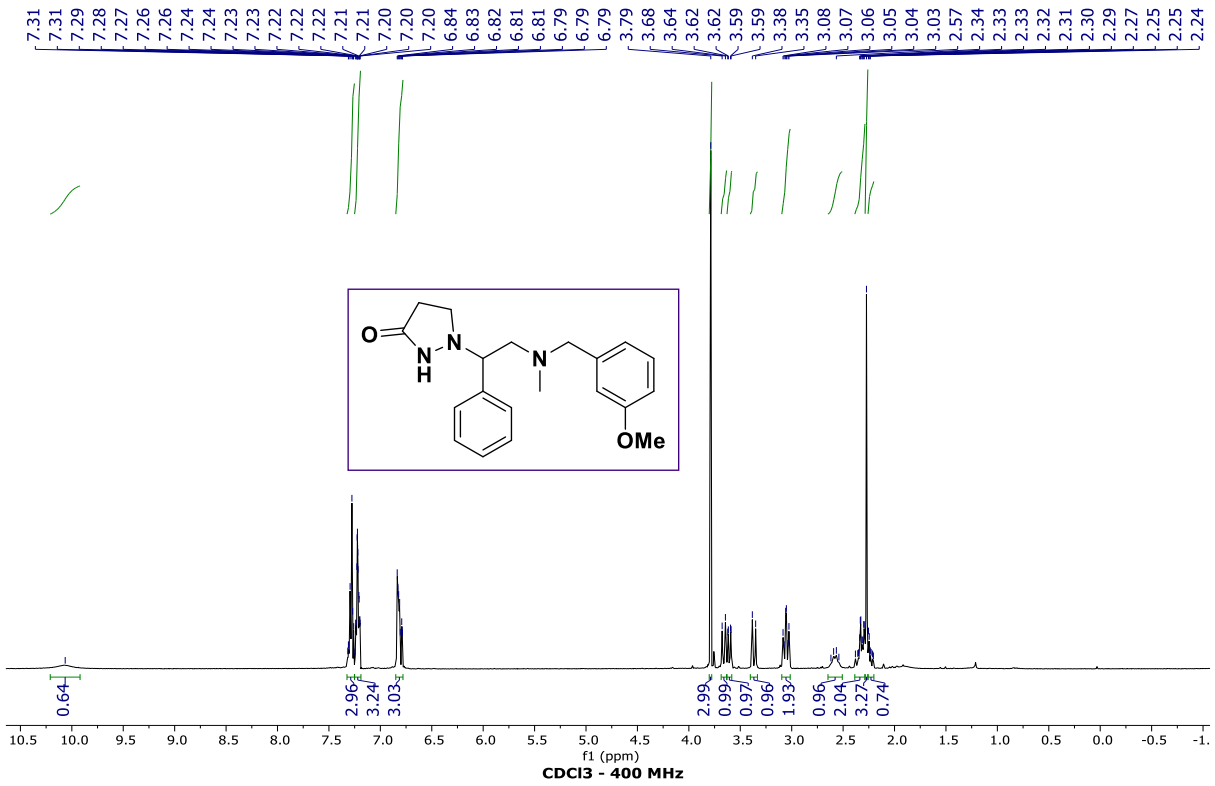
7.31 7.31 7.29 7.28 7.27 7.26 7.26 7.24 7.24 7.23 7.23 7.22 7.22 7.22 7.21 7.21 7.20 7.20 7.20 6.84 6.83 6.82 6.81 6.81 6.79 6.79 6.79
3.79 3.68 3.64 3.62 3.62 3.59 3.59 3.38 3.35 3.08 3.07 3.06 3.05 3.04 3.03 2.57 2.34 2.33 2.33 2.32 2.31 2.30 2.29 2.27 2.25 2.25 2.24
O
N
N
H
N
OMe
0.64
2.96
3.24
3.03
2.99
0.99
0.97
0.96
1.93
0.96
2.04
3.27
0.74
10.5 10.0 9.5 9.0 8.5 8.0 7.5 7.0 6.5 6.0 5.5 5.0 4.5 4.0 3.5 3.0 2.5 2.0 1.5 1.0 0.5 0.0 -0.5
f1 (ppm)
CDCl3 - 400 MHz

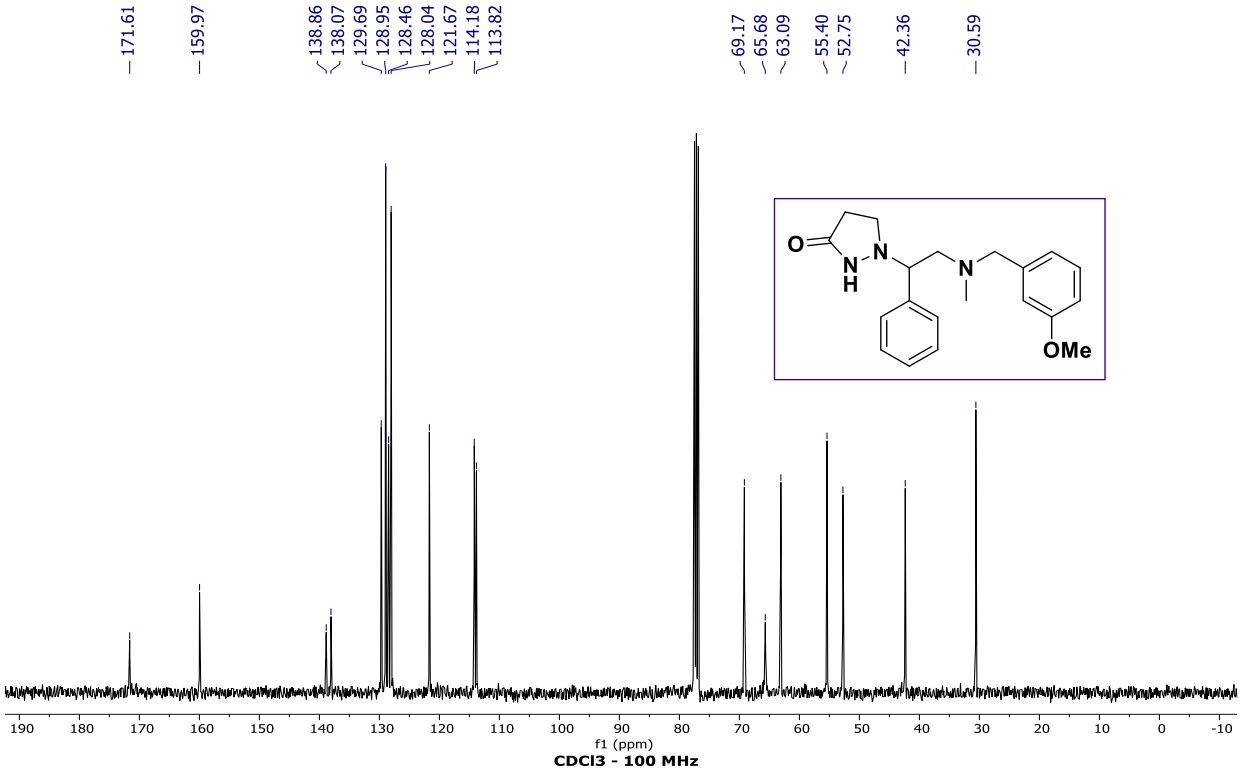
171.61
159.97
138.86
138.07
129.69
128.95
128.46
128.04
121.67
114.18
113.82
69.17
65.68
63.09
55.40
52.75
42.36
30.59
O
N
N
H
N
OMe
190 180 170 160 150 140 130 120 110 100 90 80 70 60 50 40 30 20 10 0 -10
f1 (ppm)
CDCl3 - 100 MHz

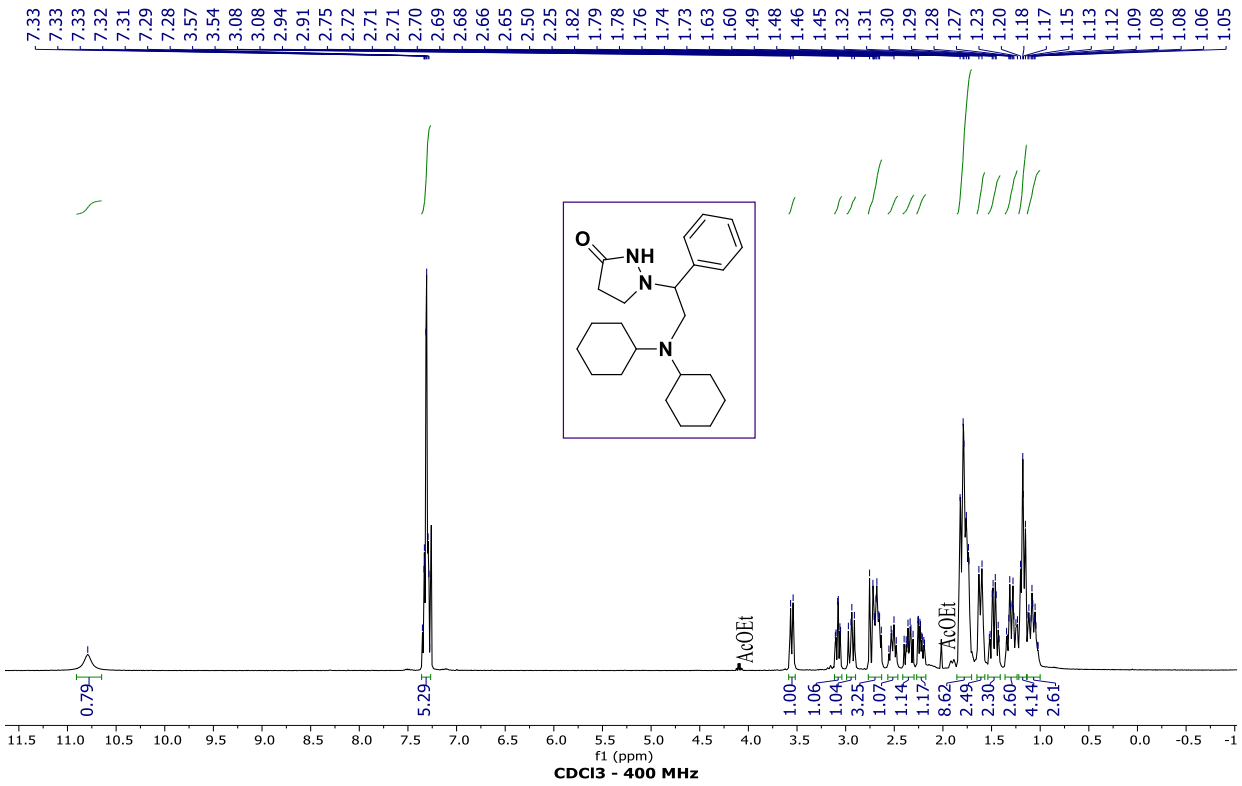
7.33 7.33 7.33 7.32 7.31 7.29 7.28 3.57 3.54 3.08 3.08 2.94 2.91 2.75 2.72 2.71 2.71 2.70 2.69 2.68 2.66 2.65 2.50 2.25 1.82 1.79 1.78 1.76 1.74 1.73 1.63 1.60 1.49 1.48 1.46 1.45 1.32 1.31 1.30 1.29 1.28 1.27 1.23 1.20 1.18 1.17 1.15 1.13 1.12 1.09 1.08 1.08 1.06 1.05
O
NH
N
N
AcOEt
AcOEt
0.79
5.29
1.00
1.06
1.04
3.25
1.07
1.14
1.17
8.62
2.49
2.30
2.60
4.14
2.61
f1 (ppm)
CDCl3 - 400 MHz

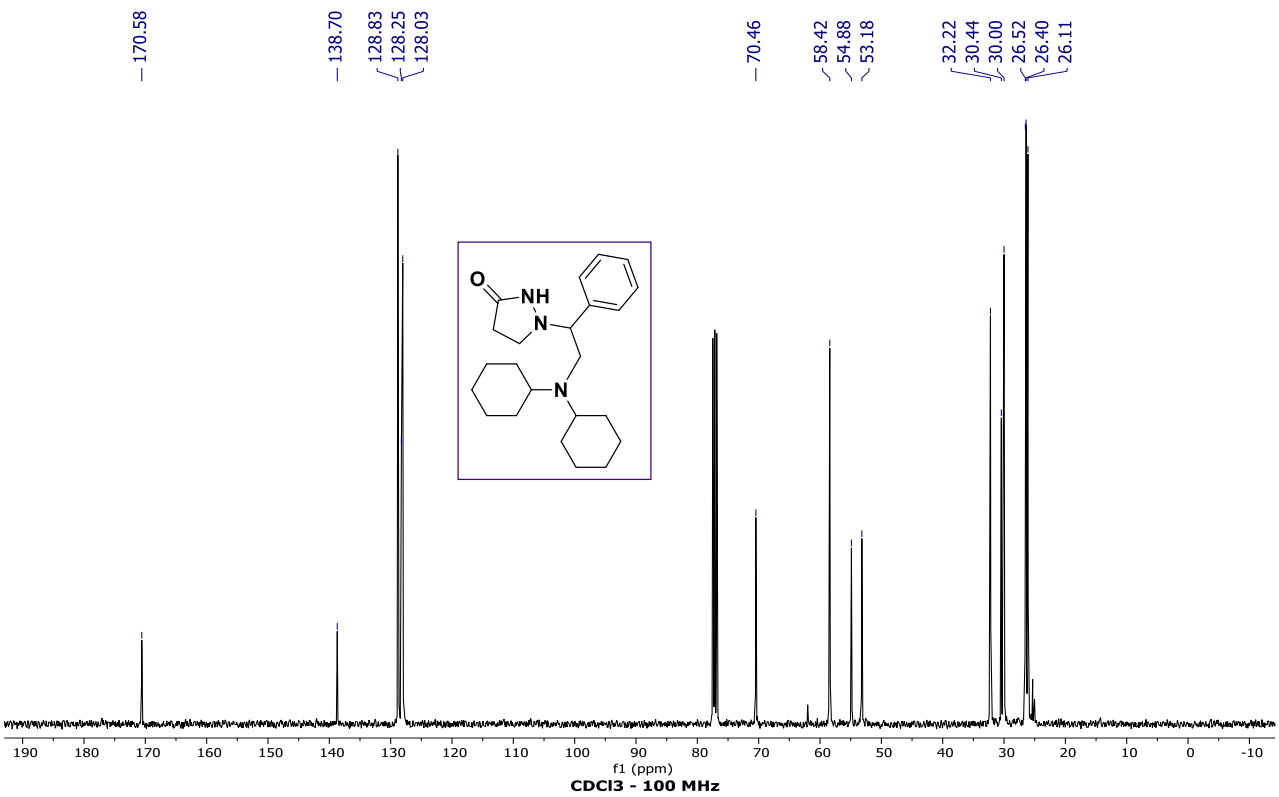
170.58
138.70
128.83
128.25
128.03
70.46
58.42
54.88
53.18
32.22
30.44
30.00
26.52
26.40
26.11
O
NH
N
N
f1 (ppm)
CDCl3 - 100 MHz

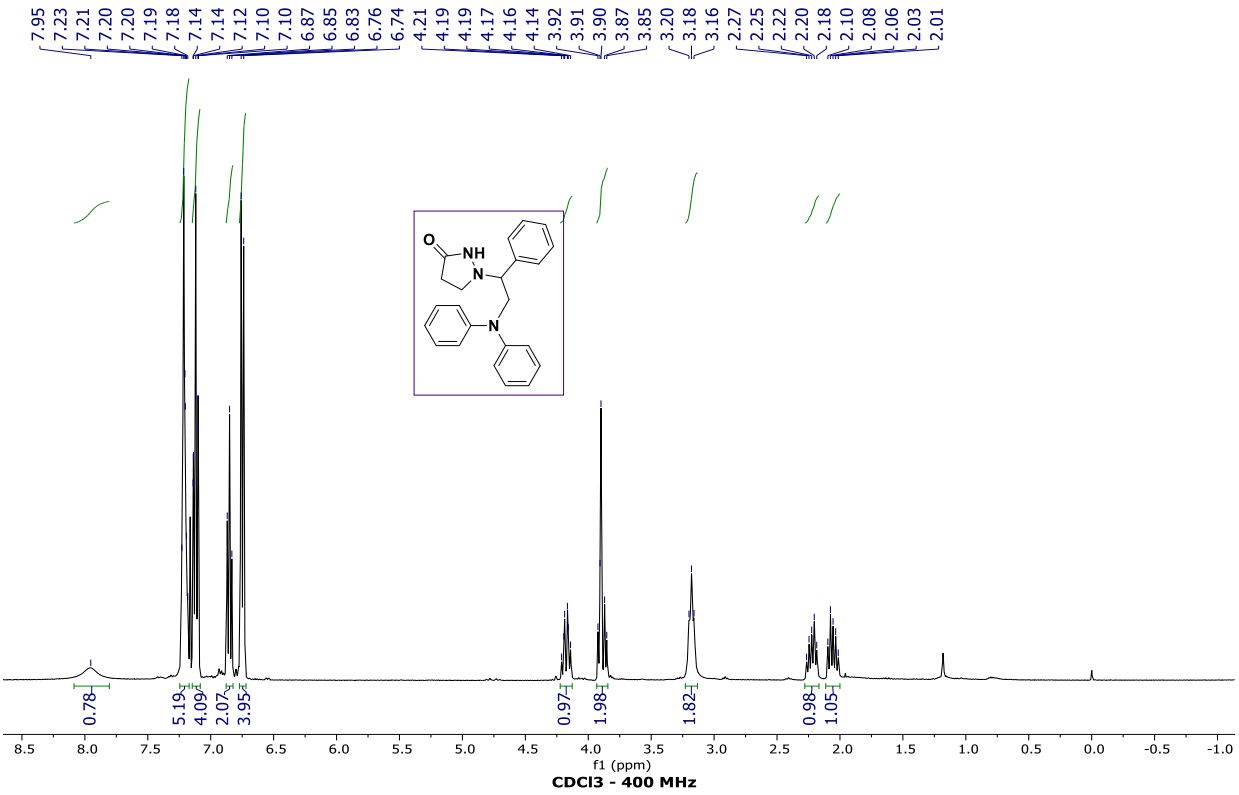
7.95
7.23
7.21
7.20
7.20
7.19
7.18
7.14
7.14
7.12
7.10
7.10
6.87
6.85
6.83
6.76
6.74
4.21
4.19
4.19
4.17
4.16
4.14
3.92
3.91
3.90
3.87
3.85
3.20
3.18
3.16
2.27
2.25
2.22
2.20
2.18
2.10
2.08
2.06
2.03
2.01
O
NH
N
N
0.78
5.19
4.09
2.07
3.95
0.97
1.98
1.82
0.98
1.05
f1 (ppm)
CDCl3 - 400 MHz

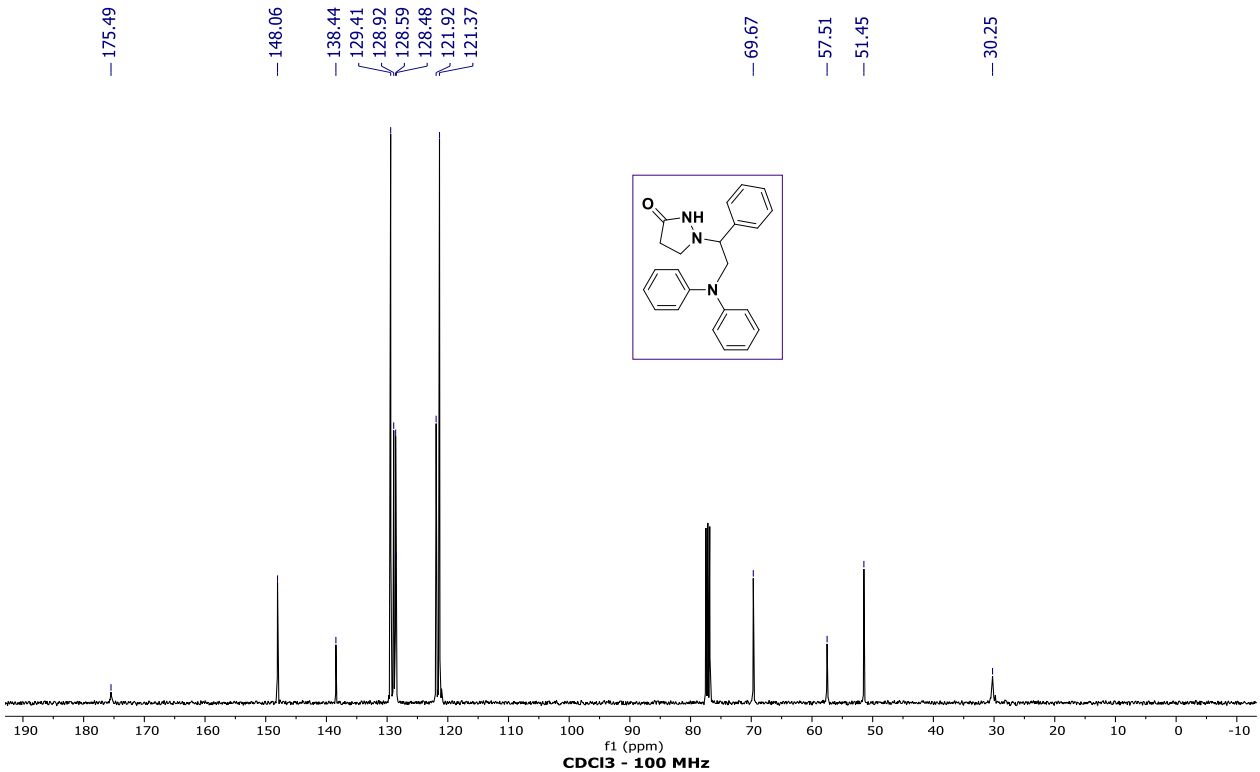
175.49
148.06
138.44
129.41
128.92
128.59
128.48
121.92
121.37
69.67
57.51
51.45
30.25
O
NH
N
N
f1 (ppm)
CDCl3 - 100 MHz

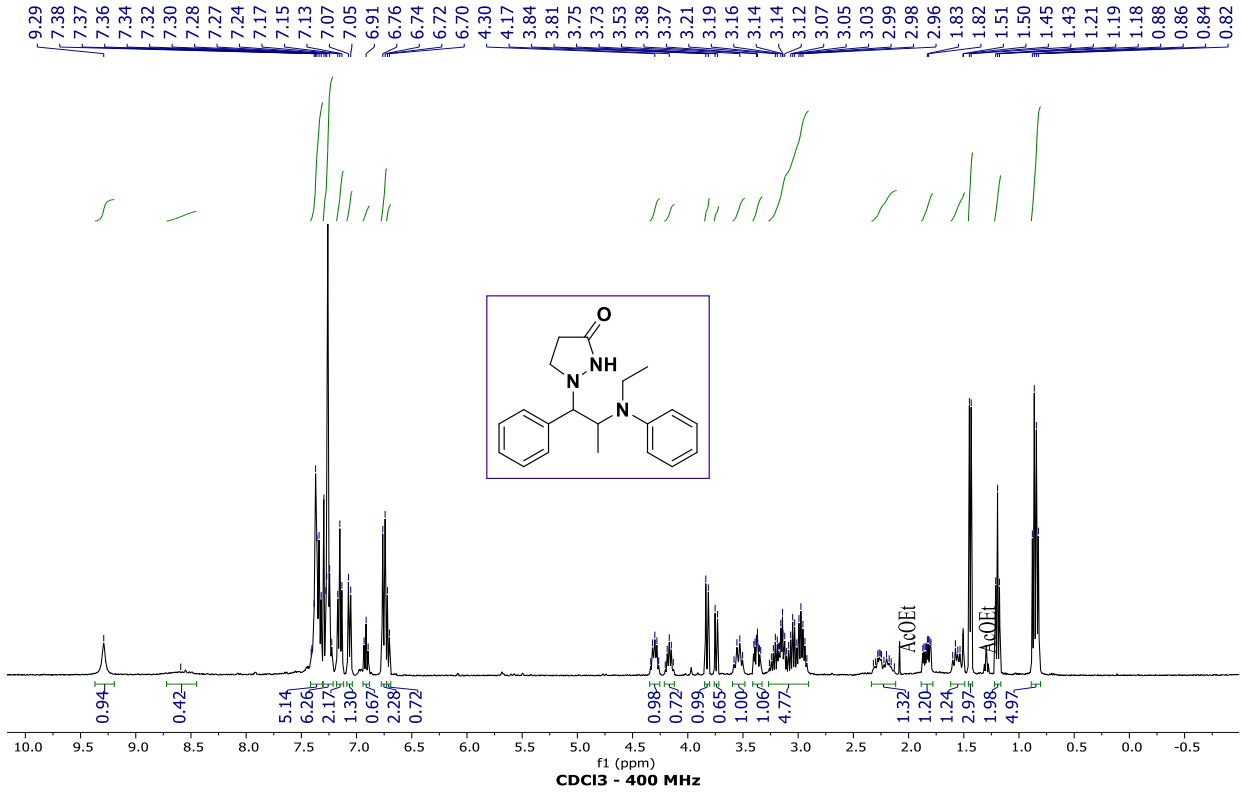
9.29 7.38 7.37 7.36 7.34 7.32 7.30 7.28 7.27 7.24 7.17 7.15 7.13 7.07 7.05 6.91 6.76 6.74 6.72 6.70 4.30 4.17 3.84 3.81 3.75 3.73 3.53 3.38 3.37 3.21 3.19 3.16 3.14 3.14 3.12 3.07 3.05 3.03 2.99 2.98 2.96 1.83 1.82 1.51 1.50 1.45 1.43 1.21 1.19 1.18 0.88 0.86 0.84 0.82
O
NH
N
N
AcOEt
AcOEt
0.94 0.42 5.14 6.26 2.17 1.30 0.67 2.28 0.72 0.98 0.72 0.99 0.65 1.00 1.06 4.77 1.32 1.20 1.24 2.97 1.98 4.97
10.0 9.5 9.0 8.5 8.0 7.5 7.0 6.5 6.0 5.5 5.0 4.5 4.0 3.5 3.0 2.5 2.0 1.5 1.0 0.5 0.0 -0.5
f1 (ppm)
CDCl3 - 400 MHz

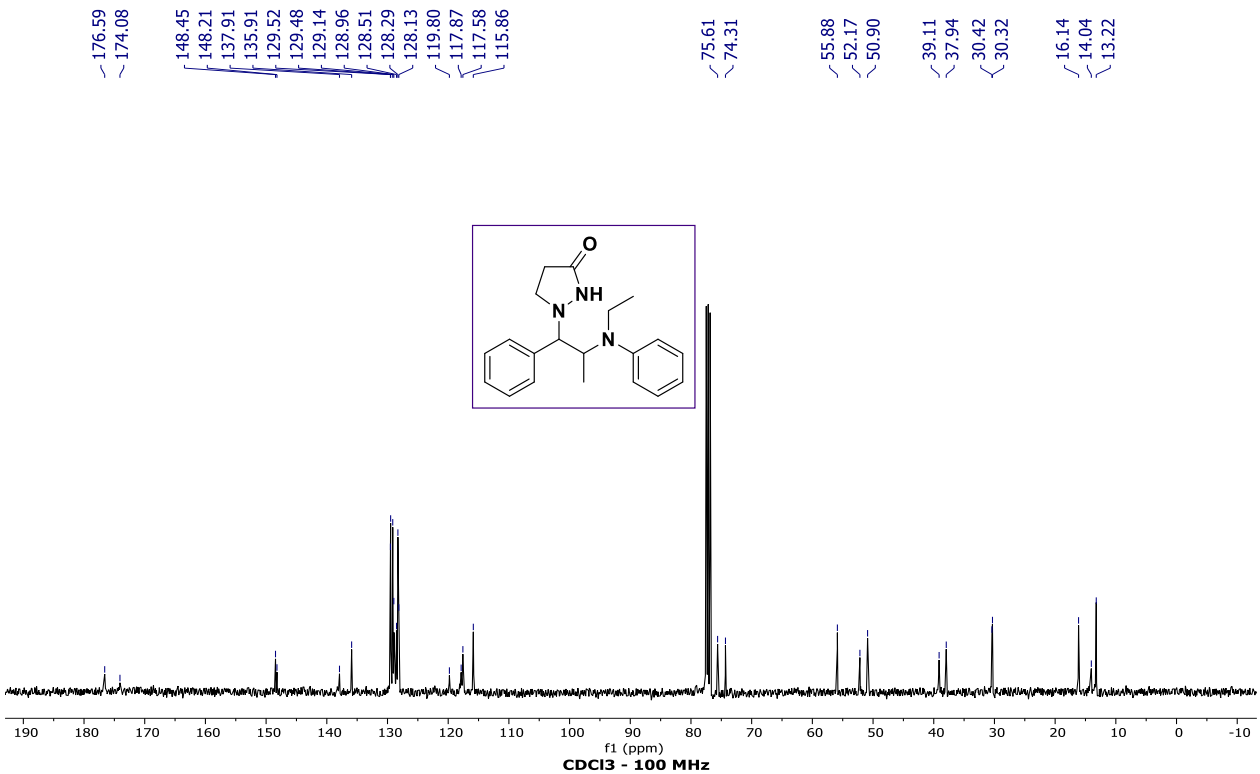
176.59 174.08 148.45 148.21 137.91 135.91 129.52 129.48 129.14 128.96 128.51 128.29 128.13 119.80 117.87 117.58 115.86 75.61 74.31 55.88 52.17 50.90 39.11 37.94 30.42 30.32 16.14 14.04 13.22
O
NH
N
N
190 180 170 160 150 140 130 120 110 100 90 80 70 60 50 40 30 20 10 0 -10
f1 (ppm)
CDCl3 - 100 MHz

isolated diastereoisomer

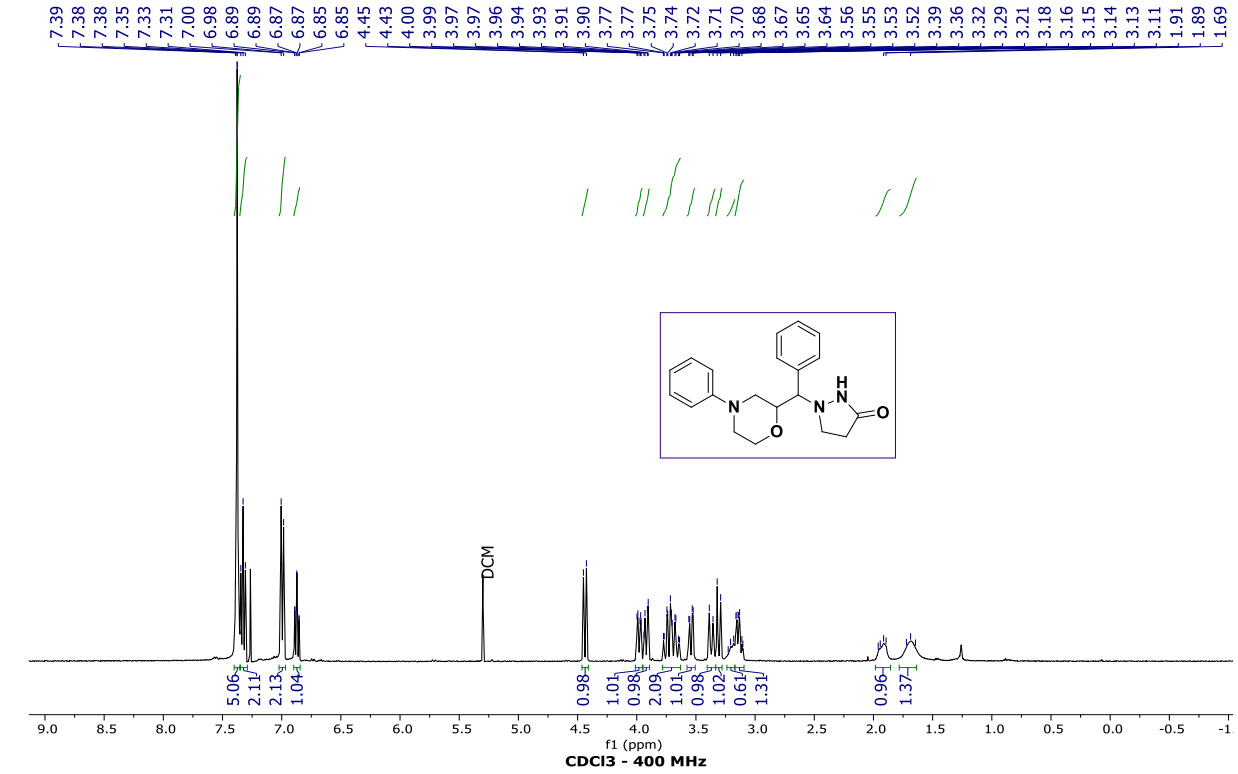

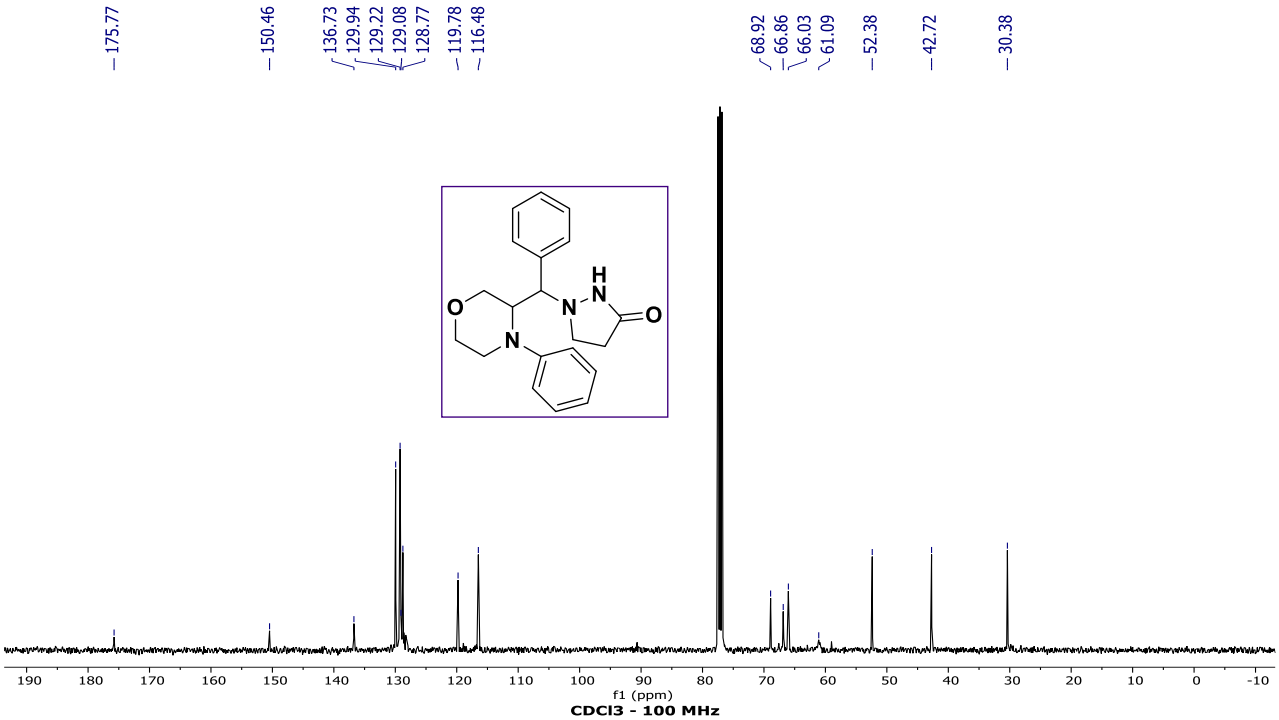

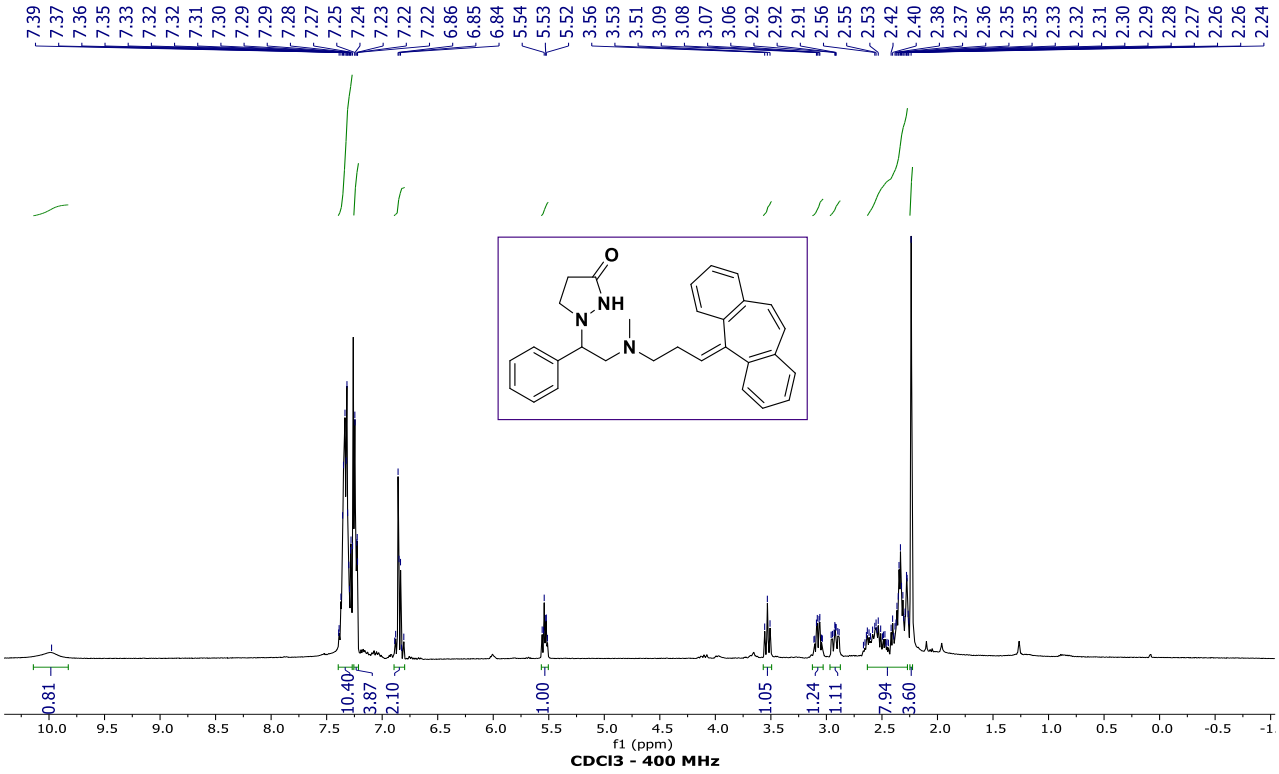
7.39 7.37 7.36 7.35 7.33 7.32 7.32 7.31 7.30 7.29 7.29 7.28 7.27 7.25 7.24 7.23 7.22 7.22 6.86 6.85 6.84 5.54 5.53 5.52 3.56 3.53 3.51 3.09 3.08 3.07 3.06 2.92 2.92 2.91 2.56 2.55 2.53 2.42 2.40 2.38 2.37 2.36 2.35 2.35 2.33 2.32 2.31 2.30 2.29 2.28 2.27 2.26 2.24
O
NH
N
N
0.81 10.40 3.87 2.10 1.00 1.05 1.24 1.11 7.94 3.60
f1 (ppm)
CDCl3 - 400 MHz

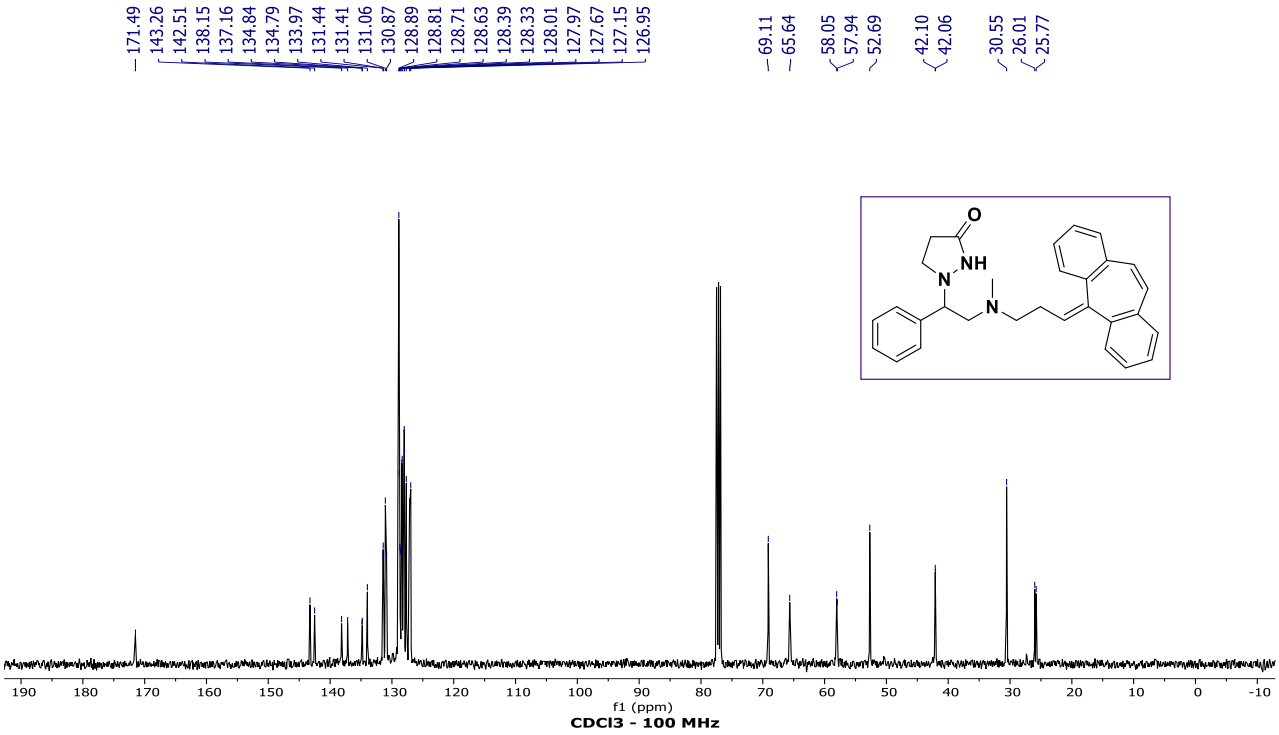
171.49 143.26 142.51 138.15 137.16 134.84 134.79 133.97 131.44 131.41 131.06 130.87 128.89 128.81 128.71 128.63 128.39 128.33 128.01 127.97 127.67 127.15 126.95
69.11 65.64 58.05 57.94 52.69 42.10 42.06 30.55 26.01 25.77
O
NH
N
N
f1 (ppm)
CDCl3 - 100 MHz

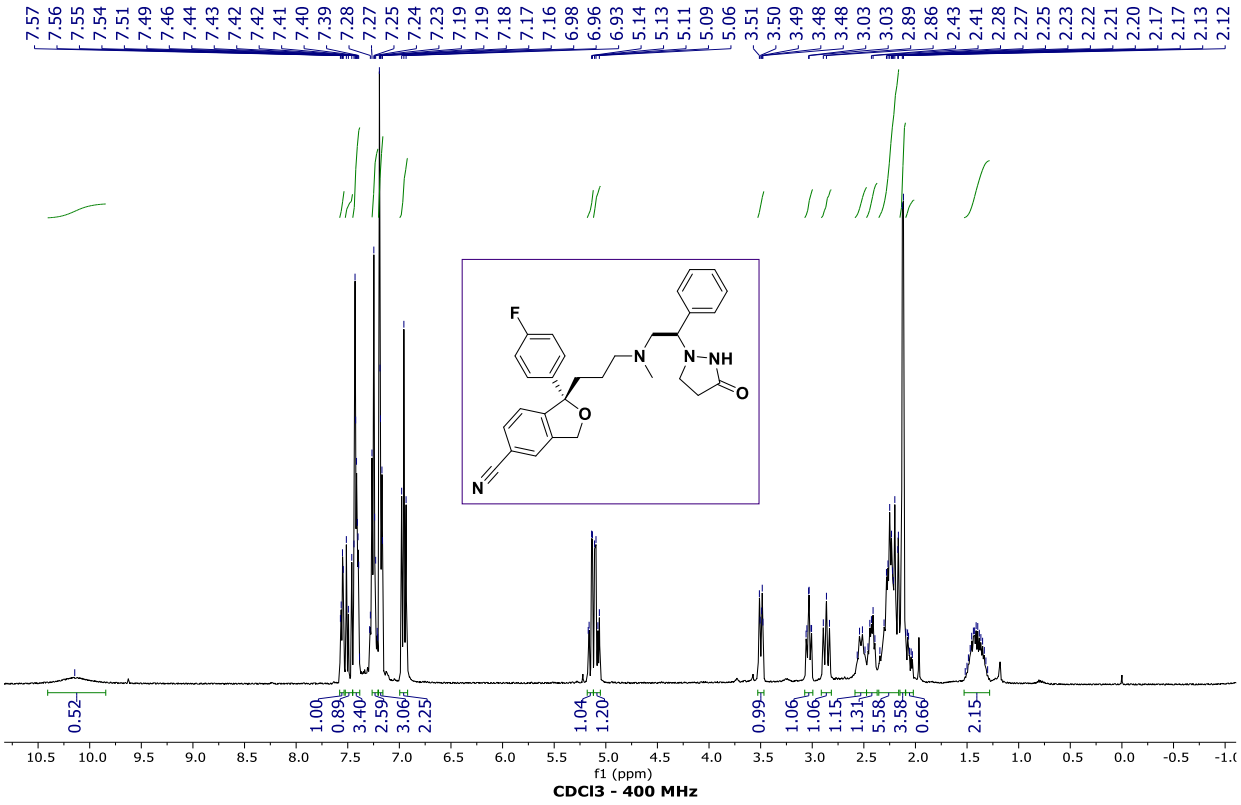
7.57 7.56 7.55 7.54 7.51 7.49 7.46 7.44 7.43 7.42 7.42 7.41 7.40 7.39 7.28 7.27 7.25 7.24 7.23 7.19 7.19 7.18 7.17 7.16 6.98 6.96 6.93 5.14 5.13 5.11 5.09 5.06 3.51 3.50 3.49 3.48 3.48 3.03 3.03 2.89 2.86 2.43 2.41 2.28 2.27 2.25 2.23 2.22 2.21 2.20 2.17 2.17 2.13 2.12
0.52 1.00 0.89 3.40 2.59 3.06 2.25 1.04 1.20 0.99 1.06 1.06 1.15 1.31 5.58 3.58 0.66 2.15
f1 (ppm)
CDCl3 - 400 MHz

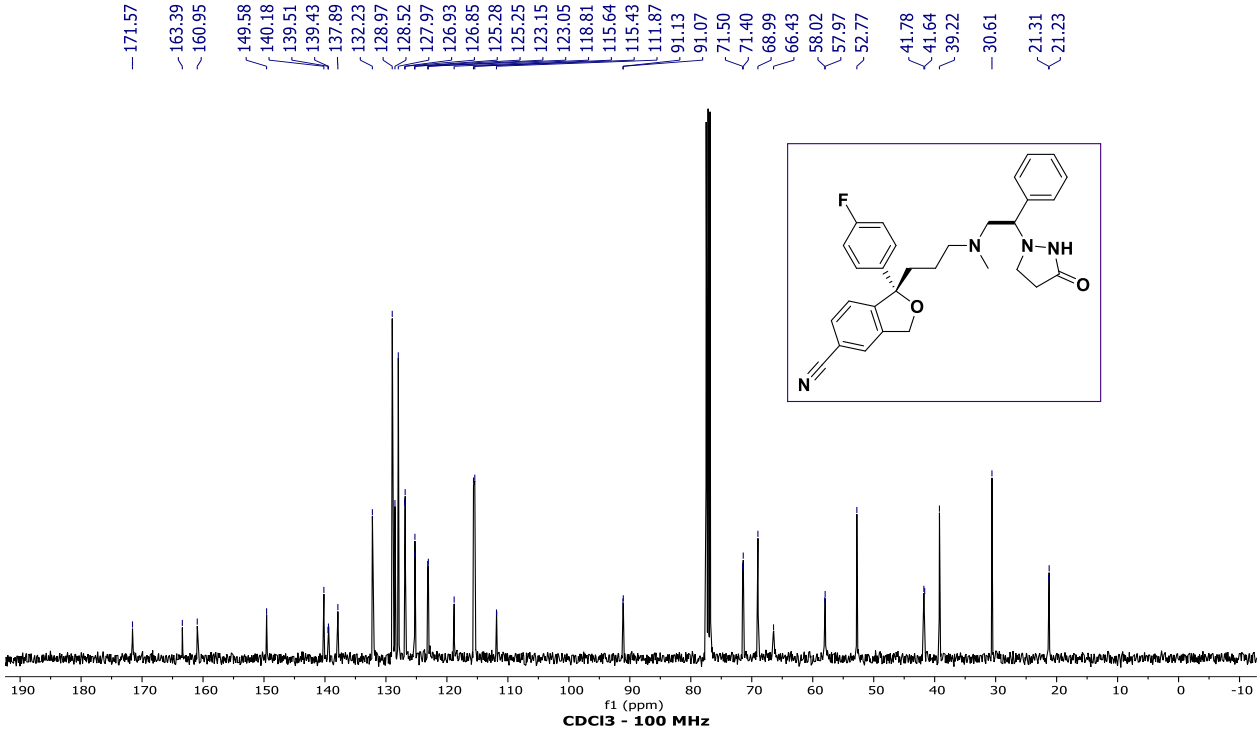
171.57 163.39 160.95 149.58 140.18 139.51 139.43 137.89 132.23 128.97 128.52 127.97 126.93 126.85 125.28 125.25 123.15 123.05 118.81 115.64 115.43 111.87 91.13 91.07 71.50 71.40 68.99 66.43 58.02 57.97 52.77 41.78 41.64 39.22 30.61 21.31 21.23
f1 (ppm)
CDCl3 - 100 MHz

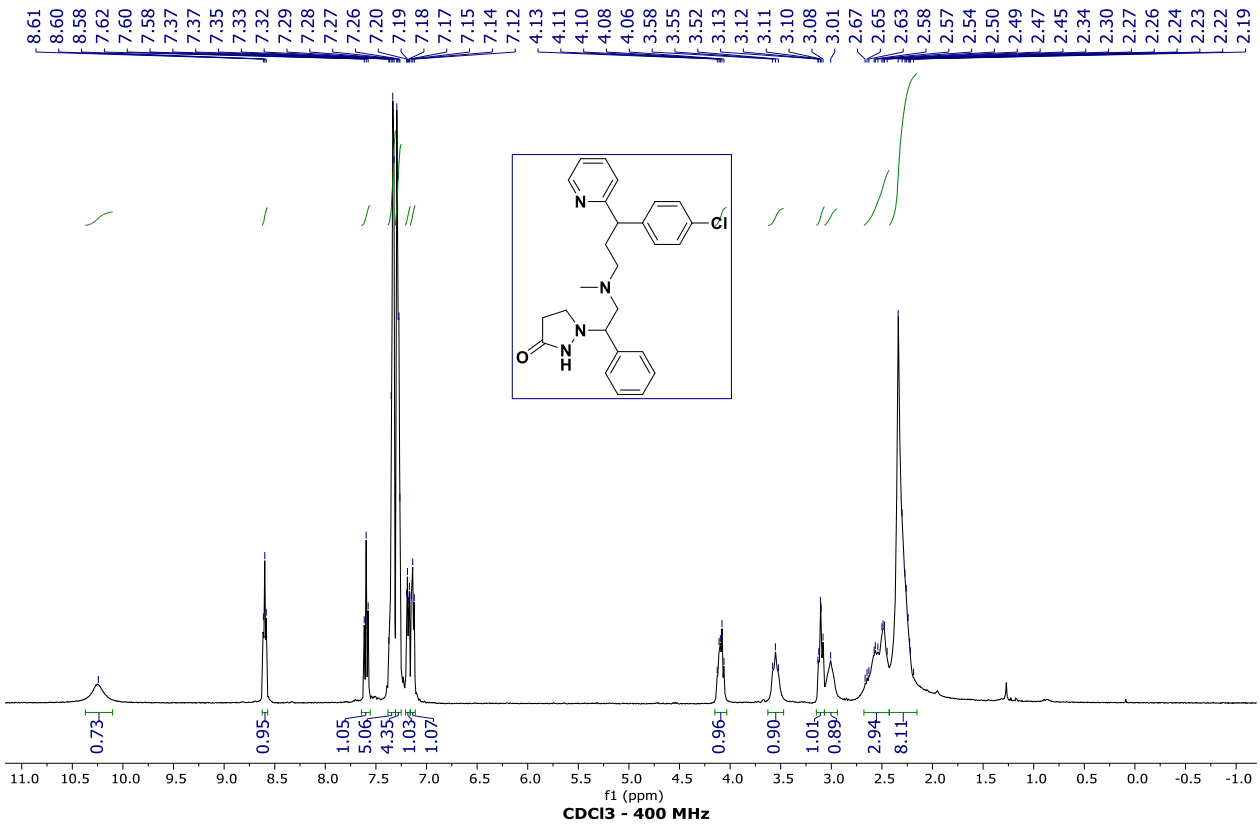
8.61 8.60 8.58 7.62 7.60 7.58 7.37 7.37 7.35 7.33 7.32 7.29 7.28 7.27 7.26 7.20 7.19 7.18 7.17 7.15 7.14 7.12
4.13 4.11 4.10 4.08 4.06 3.58 3.55 3.52 3.13 3.12 3.11 3.10 3.08 3.01
2.67 2.65 2.63 2.58 2.57 2.54 2.50 2.49 2.47 2.45 2.34 2.30 2.27 2.26 2.24 2.23 2.22 2.19
0.73 0.95 1.05 5.06 4.35 1.03 1.07 0.96 0.90 1.01 0.89 2.94 8.11
f1 (ppm)
CDCl3 - 400 MHz

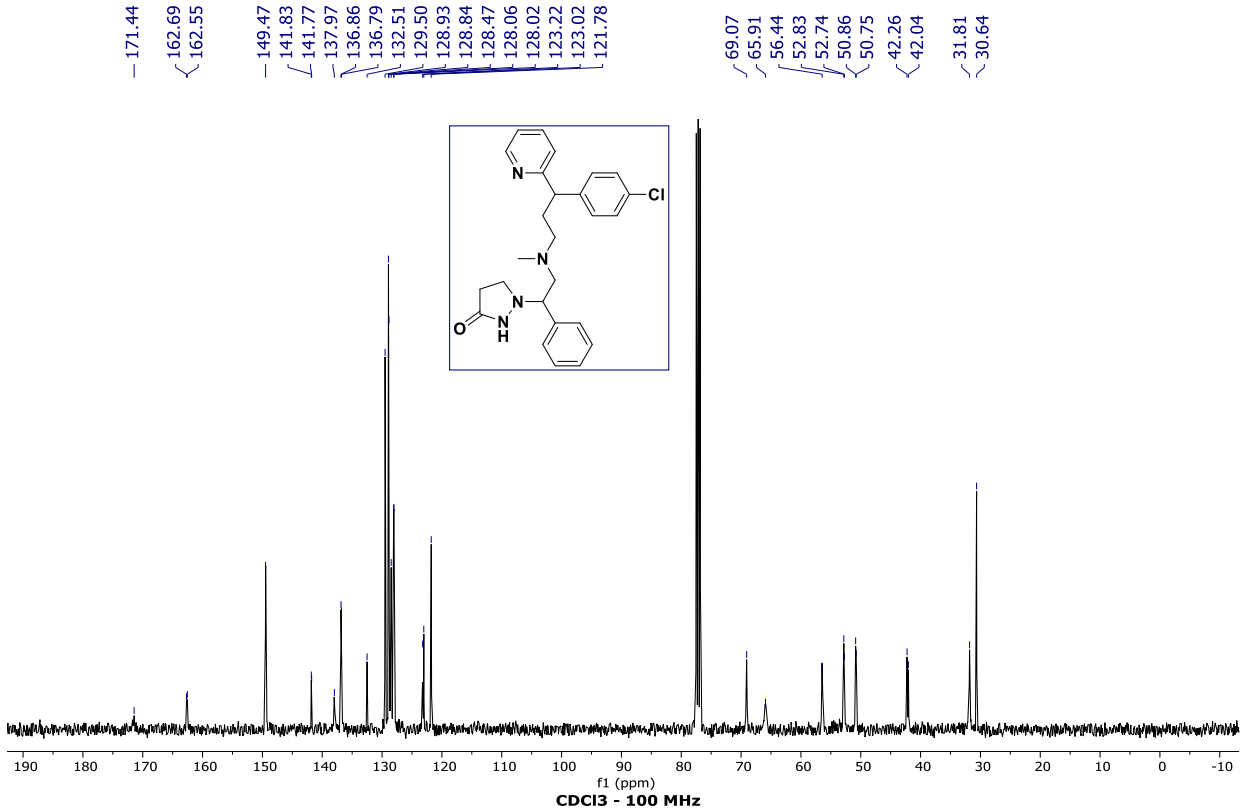
171.44 162.69 162.55 149.47 141.83 141.77 137.97 136.86 136.79 132.51 129.50 128.93 128.84 128.47 128.06 128.02 123.22 123.02 121.78
69.07 65.91 56.44 52.83 52.74 50.86 50.75 42.26 42.04 31.81 30.64
f1 (ppm)
CDCl3 - 100 MHz

5. References

1 YAN, M.; LO, J. C.; EDWARDS, J. T. & BARAN, P. S. “Radicals: reactive intermediates with translational potential”. J. Am. Chem. Soc. **138**: 12692, 2016.

2 (a) ROMERO, K. J.; GALLIHER, M. S.; PRATT, D. A. & STEPHENSON, C. R. J. “Radicals in natural product synthesis”. Chem. Soc. Rev. **47**: 7851, 2018; (b) NICOLAOU, K. C.; VOURLOUMIS, D.; WINSSINGER, N. & BARAN, P. S. “The art and science of total synthesis at the dawn of the twenty-first century”. Angew. Chem. Int. Ed. **39**: 44, 2000.

3 ANSLYN, E. V. & DOUGHERTY, D. A. Modern physical organic chemistry. Sausalito, CA : University Science, 2006. Print.

4 LAKOWICZ, J. R. Quenching of Fluorescence. In: Principles of Fluorescence Spectroscopy. Springer, Boston, MA, 1983. p. 277.

5 ARIAS-ROTONDO, D. M. & MCCUSKER, J. K. “The photophysics of photoredox catalysis: a roadmap for catalyst design”. Chem. Soc. Rev. **45**: 5803, 2016.

6 ANASTAS, P. & EGHBALI, N. “Green chemistry: principles and practice”. Chem. Soc. Rev. **39**: 301, 2010.

7 LARSEN, C. B. & WENGER, O. S. “Photoredox catalysis with metal complexes made from earth-abundant elements”. Chem. Eur. J. **24**: 2039, 2018.

8 HEDSTRAND, D. M.; KRUIZINGA, W. H. & KELLOGG, R. M. “Light induced and dye accelerated reductions of phenacyl onium salts by 1,4-dihydropyridines”. Tetrahedron Lett. **16** : 1255, 1978.

9 KOIKE, T. & AKITA, M. “Visible-light radical reaction designed by Ru- and Ir-based photoredox catalysis”. Inorg. Chem. Front. **1**: 562, 2014.

10 (a) KALYANASUNDARAM, K. “Photophysics, photochemistry and solar energy conversion with tris(bipyridyl)ruthenium(II) and its analogues”. Coordination Chemistry Reviews, **46**: 159, 1982; (b) TOKEL-TAKVORYAN, N. E.; HEMINGWAY, R. E. & BARD, A. J. “Electrogenerated chemiluminescence. XIII. Electrochemical and electrogenerated chemiluminescence studies of ruthenium chelates.” J. Am. Chem. Soc. **95**: 6582, 1973.

11 (a) TEEGARDIN, K.; DAY, J. I.; CHAN, J. & WEAVER, J. “Advances in photocatalysis: a microreview of visible light mediated ruthenium and iridium catalyzed organic transformations”. Org. Process Res. Dev. **20**: 1156, 2016; (b) ROTH, H. G.; ROMERO, N. A. & NICEWICZ, D. A.

“Experimental and calculated electrochemical potentials of common organic molecules for applications to single-electron redox chemistry”. Synlett. **27**: 714, 2016.

12 HOFFMANN, N. “Proton-coupled electron transfer in photoredox catalytic reactions”. Eur. J. Org. Chem. **15**: 1982, 2017.

13 PRIER, C. K. & MACMILLAN, D. W. C. “Visible light photocatalysis in organic chemistry, (Eds.: Stephenson, C. R. J.; Yoon, T. P. & MacMillan, D. W. C.), Wiley-VCH, Weinheim, 2018, pp. 299.

14 For selected reviews and book chapters, see: (a) MAVROSKOUFIS, A.; JAKOB, M. & HOPKINSON, M. N. “Light-promoted organocatalysis with *N*-heterocyclic carbenes”. ChemPhotoChem. **4**: 5147, 2021; (b) ZEITLER, K. & NEUMANN, M. “Synergistic Visible Light Photoredox Catalysis. Chemical Photocatalysis”, 2nd Edition, 2020, p. 245; (c) LIU, Y.-Y.; LIU., J.; LU, L.-Q. & XIAO, W-J. “Organocatalysis combined with photocatalysis”. Topics in Current Chemistry. **377**: 1, 2019; (d) REY, Y. P.; HEPBURN, H. B. & MELCHIORRE, P. “Science of Synthesis, Photocatalysis in Organic Synthesis”. 2019, p. 243-270.

15 For selected examples, see: (a) SPECKMEIER, E.; FUCHSA, P. J. W. & ZEITLER, K. “A synergistic LUMO lowering strategy using Lewis acid catalysis in water to enable photoredox catalytic, functionalizing C–C cross-coupling of styrenes”. Chem. Sci. **9**: 7096, 2018**;** (b) AMADOR, A. G.; SHERBROOK, E. M.; LU, Z. & YOON, T. P. “A general protocol for radical anion [3+2] cycloaddition enabled by tandem Lewis acid photoredox catalysis”. Synthesis. **50**: 539, 2018; (c) LEE, K. N.; LEI, Z. & NGAI, M.-Y. “*β*-Selective reductive coupling of alkenylpyridines with aldehydes and imines via synergistic Lewis acid/photoredox catalysis”. J. Am. Chem. Soc. **139**: 5003, 2017; (d) YOON, T. P. “Photochemical stereocontrol using tandem photoredox–chiral Lewis acid catalysis”. Acc. Chem. Res. **49**: 2307, 2016.

16 For selected reviews, see: (a) LIPP, A.; BADIR, S. O. & MOLANDER, G. A. “Stereoinduction in metallaphotoredox catalysis”. Angew. Chem. Int. Ed. **60**: 1714, 2021; (b) PRIER, C. K.; RANKIC, D. A. & MACMILLAN, D. W. C. “Visible light photoredox catalysis with transition metal complexes: applications in organic synthesis”. Chem. Rev. **113** : 5322, 2013.

17 VERHOEVEN, J. W. “Glossary of terms used in photochemistry”. Pure Appl. Chem. **68**: 2223, 1996.

18 STRIETH-KALTHOFF, F.; JAMES, M. J.; TEDERS, M.; PITZER, L. & GLORIUS, F. “Energy transfer catalysis mediated by visible light: principles, applications, directions”. Chem. Soc. Rev. **47**: 7190, 2018.

19 TURRO, N. J. “Modern Molecular Photochemistry”. University Science Books, Sausalito, 1991.

20 (a) ZHENG, L.; CAI, L.; TAO, K.; XIE, Z.; LAI, Y.-L. & GUO, W. “Progress in photoinduced radical reactions using electron donor-acceptor complexes”. Asian J. Org. Chem. **10** : 711, 2021; (b) LIMA, C. G. S.; LIMA, T. M.; DUARTE, M.; JURBERG, I. D. & PAIXÃO, M. W. “Organic synthesis enabled by light-irradiation of EDA complexes: theoretical background and synthetic applications”. ACS Catal. **6**: 1389, 2016.

21 DAVIES, J.; SHEIKH, N. S. & LEONORI, D. “Photoredox imino functionalizations of olefins”. Angew. Chem. **129**: 13546, 2017.

22 ISCHAY, M. A.; ANZOVINO, M. E.; DU, J. & YOON, T. P. “Efficient visible light photocatalysis of [2+2] enone cycloadditions”. J. Am. Chem. Soc. **130**: 12886, 2008.

23 NICEWICZ, D. A. & MACMILLAN, D. W. C. “Merging photoredox catalysis with organocatalysis: the direct asymmetric alkylation of aldehydes”. Science, **322**: 77, 2008.

24 NARAYANAM, J. M. R.; TUCKER, J. W. & STEPHENSON, C. R. J. “Electron-transfer photoredox catalysis: development of a tin-free reductive dehalogenation reaction”. J. Am. Chem. Soc. **131**: 8756, 2009.

25 (a) DU, J. & YOON, T. P. “Crossed intermolecular [2+2] cycloadditions of acyclic enones via visible light photocatalysis”. J. Am. Chem. Soc. **131**: 14604, 2009; (b) ISCHAY, M. A.; LU, Z. & YOON, T. P. “[2+2] Cycloadditions by oxidative visible light photocatalysis”. J. Am. Chem. Soc. **132**: 8572, 2010.

26 LU, Z.; SHEN, M. & YOON, T. P. “[3+2] Cycloadditions of aryl cyclopropyl ketones by visible light photocatalysis”. J. Am. Chem. Soc. **133**: 1162, 2011.

27 LIN, S.; ISCHAY, M. A.; FRY, C. G. & YOON, T. P. “Radical cation Diels–Alder cycloadditions by visible light photocatalysis”. J. Am. Chem. Soc. **133**: 19350, 2011.

28 (a) NAKAJIMA, K.; MIYAKE, Y. & NISHIBAYASHI, Y. “Synthetic utilization of *α*-aminoalkyl radicals and related species in visible light photoredox catalysis”. Acc. Chem. Res. **49**: 1946, 2016; (b) MAITY, S. & ZHENG, N. “A photo touch on amines: new synthetic adventures of nitrogen radical cations”. Synlett. **23**: 1851, 2012.

29 KOHLS, P.; JADHAV, D.; PANDEY, G. & REISER, O. “Visible light photoredox catalysis: generation and addition of *N*-aryltetrahydroisoquinoline-derived *α*-amino radicals to Michael acceptors”. Org. Lett. **14**: 672, 2012.

30 (a) KOIKE, T. & AKITA, M. “Combination of organotrifluoroborates with photoredox catalysis marking a new phase in organic radical chemistry”. Org. Biomol. Chem. **14**: 6886, 2016; (b) MOLANDER, G. A. “Organotrifluoroborates: Another Branch of the Mighty Oak”. J. Org. Chem. **80**: 7837, 2015; (c) YASU, Y.; KOIKE, T. & AKITA, M. “Visible light-induced selective generation of radicals from organoborates by photoredox catalysis”. Adv. Synth. Catal. **354**: 3414, 2012.

31 For recent examples, see: (a) YI, J.; BADIR, S. O.; ALAM, R. & MOLANDER, G. A. “Photoredox-catalyzed multicomponent Petasis reaction with alkyltrifluoroborates”. Org. Lett. **21**: 4853, 2019 (b) CAMPBELL, M. W.; COMPTON, J. S.; KELLY, C. B. & MOLANDER, G. A. J. Am. Chem. Soc. **51**: 20069, 2019; (c) YUAN, M.; SONG, Z.; BADIR, S. O.; MOLANDER, G. A. & GUTIERREZ, O. “On the nature of C(sp^3)–C(sp^2) bond formation in nickel-catalyzed tertiary radical cross-couplings: a case study of Ni/photoredox catalytic cross-coupling of alkyl radicals and aryl halides”. J. Am. Chem. Soc. **15**: 7225, 2020; (d) PRIMER, D. N. & MOLANDER, G. A. “Enabling the cross-coupling of tertiary organoboron nucleophiles through radical-mediated alkyl transfer”. J. Am. Chem. Soc. **139**: 9847, 2017; (e) AMANI, J. & MOLANDER, G. A. “Direct conversion of carboxylic acids to alkyl ketones”. Org. Lett. **13**: 3612, 2017; (f) MATSUI, J. K.; PRIMERA, D. A. & MOLANDER, G. A. “Metal-free C–H alkylation of heteroarenes with alkyltrifluoroborates: a general protocol for 1°, 2° and 3° alkylation”. Chem. Sci. **8**: 3515, 2017; (g) MATSUI, J. K. & MOLANDER, G. A. “Organocatalyzed, photoredox heteroarylation of 2-trifluoroboratochromanones via C–H functionalization”. Org. Lett. **19**: 950, 2017; (h) AMANI, J. & MOLANDER, G. A. “Synergistic photoredox/nickel coupling of acyl chlorides with secondary alkyltrifluoroborates: dialkyl ketone synthesis”. J. Org. Chem. **82**: 1856, 2017; (i) HEITZ, D. R.; RIZWAN, K. & MOLANDER, G. A. “Visible-light-mediated alkenylation, allylation, and cyanation of potassium alkyltrifluoroborates with organic photoredox catalysts”. **81**: 7308, 2016; (j) KARIMI-NAMI, R.; TELLIS, J. C. & MOLANDER, G. A. “Single-electron transmetalation: protecting-group-independent synthesis of secondary benzylic alcohol derivatives via photoredox/nickel dual catalysis”. Org. Lett. **18**: 2572, 2016; (k) AMANI, J.; SODAGAR, E. & MOLANDER, G. A. “Visible light photoredox cross-coupling of acyl chlorides with potassium alkoxymethyltrifluoroborates: synthesis of *α*-alkoxyketones”. Org. Lett. **18**: 732, 2016; (l) Ryu, D.; Primer, D. N.; Tellis, J. C. & Molander, G. A. Chem. Eur. J. **22** : 120, 2016; (m) KHATIB, M. E.; SERAFIM, R. A. M. & MOLANDER, G. A. “α-Arylation/heteroarylation of chiral α-aminomethyltrifluoroborates by synergistic iridium photoredox/nickel cross-coupling catalysis”. Angew. Chem. Int. Ed. **55**: 254, 2016; (n) YAMASHITAA, Y.; TELLISA, J. C. & MOLANDER, G. A. “Protecting group-free, selective cross-coupling of alkyltrifluoroborates with borylated aryl bromides via photoredox/nickel dual catalysis”. PNAS. **112**: 12026, 2015; (o) KARAKAYA, I.;

PRIMER, D. N. & MOLANDER, G. A. “Photoredox cross-coupling: Ir/Ni dual catalysis for the synthesis of benzylic ethers”. Org. Lett. **17**: 3294, 2015.

32 ANDREWS, R. S.; BECKER, J. J. & GAGNÉ, M. R. “Intermolecular addition of glycosyl halides to alkenes mediated by visible light”. Angew. Chem. Int. Ed. **49**: 7274, 2010.

33 NAGIB, D. A. & MACMILLAN, D. W. C. “Trifluoromethylation of arenes and heteroarenes by means of photoredox catalysis”. Nature. **480**: 224, 2011.

34 BABU, S. S.; MUTHURAJA, P.; YADAV, P. & GOPINATH, P. “Aryldiazonium salts in photoredox catalysis – recent trends”. Adv. Synt. Catal. **363**: 1782, 2021.

35 (a) HARI, D. P.; SCHROLL, P. & KÖNIG, B. “Metal-free, visible-light-mediated direct C–H arylation of heteroarenes with aryl diazonium salts”. J. Am. Chem. Soc. **134**: 2958, 2012; (b) HARI, D. P.; HERING, T. & KÖNIG, B. “Visible light photocatalytic synthesis of benzothiophenes”. Org. Lett. **14**: 5334, 2012; (c) SCHROLL, P.; HARI, D. P. & KÖNIG, B. “Photocatalytic arylation of alkenes, alkynes and enones with diazonium salts”. ChemistryOpen. **1**: 130, 2012; (d) T. HERING, D. P. HARI AND B. KÖNIG. J. Org. Chem. **77**: 10347, 2012.

36 HARI, D. P.; HERING, T. & KÖNIG, B. “The photoredox-catalyzed Meerwein addition reaction: intermolecular amino-arylation of alkenes”. Angew. Chem. Int. Ed. **53**: 725, 2014.

37 MATSUI, J. K.; LANG, S. B.; HEITZ, D. R. & MOLANDER, G. A. “Photoredox-mediated routes to radicals: the value of catalytic radical generation in synthetic methods development”. ACS Catal. **7**: 2563, 2017.

38 ROSLIN, S. & ODELL, L. R. “Visible-light photocatalysis as an enabling tool for the functionalization of unactivated C(sp^3)-substrates”. Chem. Eur. J. **15**: 1993, 2017.

39 (a) MITCHELL, E. A.; PESCHIULLI, A.; LEFEVRE, N.; MEERPOEL, L. & MAES, B. U. W. “Direct α-functionalization of saturated cyclic amines”. Chem. Eur. J. **18**: 10092, 2012; (b) HOFFMANN, N. “Photochemical reactions as key steps in organic synthesis”. Chem. Rev. **108**: 1052, 2008; (c) FAGNONI, M.; DONDI, D.; RAVELLI, D.; ALBINI, A. “Photocatalysis for the formation of the C-C bond”. Chem. Rev. **107**: 2725, 2007.

40 WAYNER, D. D. M.; DANNENBERG, J. J. & GRILLER, D. “Oxidation potentials of α-amino radicals: bond dissociation energies for related radical cations”. Chem. Phys. Lett. **131**: 189, 1986.

41 (a) ZHANG, X.; YEH, S.-R.; HONG, S.; FRECCERO, M.; ALBINI, A.; FALVEY, D. E. & MARIANO, P. S. “Dynamics of α-CH deprotonation and α-desilylation reactions of tertiary amine

cation radicals". J. Am. Chem. Soc. **116**: 4211, 1994; (b) ANNE, A.; HAPOIT, P.; MOIROUX, J.; NETA, P. & SAVEANT, J.-M. "Dynamics of proton transfer from cation radicals. kinetic and thermodynamic acidities of cation radicals of NADH analogues". J. Am. Chem. Soc. **114**: 4694, 1992; (c) LEWIS, F. D.; HO, T.-I. & SIMPSON, J. T. "Photochemical addition of tertiary amines to stilbene. Stereoelectronic control of tertiary amine oxidation". J. Org. Chem. **46**: 1077, 1981; (d) LEWIS, F. D. & HO, T.-I. "On the selectivity of tertiary amine oxidations". J. Am. Chem. Soc. **102**: 1751; 1980.

42 HAYASHI, T. & HEGEDUS, L. S. "Photoinduced redox reactions of hydrophobic ruthenium (II) complexes". J. Am. Chem. Soc. **99**: 7094, 1977.

43 MIYAKE, Y.; NAKAJIMA, K. & NISHIBAYASHI, Y. "Visible-light-mediated utilization of *α*-aminoalkyl radicals: addition to electron-deficient alkenes using photoredox catalysts". J. Am. Chem. Soc. **134**: 3338, 2012.

44 MURPHY, J. J.; BASTIDA, D.; PARIA, S.; FAGNONI, M. & MELCHIORRE, P. "Asymmetric catalytic formation of quaternary carbons by iminium ion trapping of radicals". Nature. **532**: 218, 2016.

45 (a) NOBLE, A.; MCCARVER, S. J. & MACMILLAN, D. W. C. "Merging photoredox and nickel catalysis: decarboxylative cross-coupling of carboxylic acids with vinyl halides". J. Am. Chem. Soc. **137**: 624, 2015; (b) JEFFREY, J. L.; PETRONIJEVIĆ, F. R. & MACMILLAN, D. W. C. "Selective radical-radical cross-couplings: design of a formal *β*-Mannich reaction". J. Am. Chem. Soc. **137** : 8404, 2015; (c) NOBLE, A. & MACMILLAN, D. W. C. "Photoredox *α*-vinylation of *α*-amino acids and *N*-aryl amines". J. Am. Chem. Soc. **136**: 11602, 2014; (d) TERRETT, J. A.; CLIFT, M. D. & MACMILLAN, D. W. C. "Direct *β*-alkylation of aldehydes via photoredox organocatalysis". J. Am. Chem. Soc. **136**: 6858, 2014; (e) ZUO, Z.; AHNEMAN, D. T.; CHU, L.; TERRETT, J. A.; DOYLE, A. G. & MACMILLAN, D. W. C. "Merging photoredox with nickel catalysis: coupling of *α*-carboxyl sp^3-carbons with aryl halides". Science. **345**: 437, 2014; (f) PIRNOT, M. T.; RANKIC, D. A.; MARTIN, D. B. C. & MACMILLAN, D. W. C. "Photoredox activation for the direct *β*-arylation of ketones and aldehydes". Science. **339**: 1593, 2013.

46 (a) EL KHATIB, M.; SERAFIM, R. A. M. & MOLANDER, G. A. *α*-Arylation/heteroarylation of chiral *α*-aminomethyltrifluoroborates by synergistic iridium photoredox/nickel cross-coupling catalysis. Angew. Chem., Int. Ed. **55**: 254, 2016; (b) TELLIS, J. C.; PRIMER, D. N. & MOLANDER, G. A. "Single-electron transmetalation in organoboron cross-coupling by photoredox/nickel dual catalysis". Science. **345**: 433, 2014.

47 AYCOCK, R. A.; PRATT, C. J. & JUI, N. T. “Aminoalkyl radicals as powerful intermediates for the synthesis of unnatural amino acids and peptides”. ACS Catal. **8**: 9115, 2018.

48 CULLEN, S. T. J. & FRIESTAD, G. K. “Synthesis of chiral amines by C–C bond formation with photoredox catalysis”. Synthesis. **53**: 2319, 2021.

49 MIYAKE, Y.; NAKAJIMA, K. & NISHIBAYASHI, Y. “Direct sp^3 C-H amination of nitrogen-containing benzoheterocycles mediated by visible-light-photoredox catalysts”. Chem. - Eur. J. **18**: 16473, 2012.

50 ZHOU, H.; LU, P.; GU, X. & LI, P. “Visible-light-mediated nucleophilic addition of an *α*-aminoalkyl radical to isocyanate or isothiocyanate”. Org. Lett. **15**: 5646, 2013.

51 NAKAJIMA, M.; FAVA, E.; LOESCHER, S.; JIANG, Z. & RUEPING, M. “Photoredox-catalyzed reductive coupling of aldehydes, ketones, and imines with visible light”. Angew. Chem. Int. Ed. **54**: 8828, 2015.

52 FAVA, E.; MILLET, A.; NAKAJIMA, M.; LOESCHER, S. & RUEPING, M. “Reductive umpolung of carbonyl derivatives with visible-light photoredox catalysis: direct access to vicinal diamines and amino alcohols via α-amino radicals and ketyl radicals”. Angew. Chem. Int. Ed. **55**: 6776, 2016.

53 URAGUCHI, D.; KINOSHITA, N.; KIZU, T. & OOI, T. “Synergistic catalysis of ionic Brønsted acid and photosensitizer for a redox neutral asymmetric *α*-coupling of *N*-arylaminomethanes with aldimines”. J. Am. Chem. Soc. **137**: 13768, 2015.

54 BELSKAYA, N. P.; BAKULEV, V. A. & FAN, Z. “Synthesis and (3+2) cycloaddition reactions of *N*,*N*'- and *C*,*N’*-cyclic azomethine imines”. Chemistry of Heterocyclic Compounds. **52**: 627, 2016.

55 (a) ESS, D. H. & HOUK, K. N. “Distortion/interaction energy control of 1,3-dipolar cycloaddition reactivity”. J. Am. Chem. Soc. **129**: 10646, 2008; J. Am. Chem. Soc. “Theory of 1,3-dipolar cycloadditions: distortion/interaction and frontier molecular orbital models”. **130**: 10187, 2008; (c) HOUK, K. N. & YAMAGUCHI, K. In 1,3-Dipolar Cycloaddition Chemistry; Padwa, A., Ed.; John Wiley & Sons, Inc.: New York, 1984, Vol. 2, p. 407.

56 WINTERTON, S. E. & READY, J. M. “[3 + 2]-Cycloadditions of azomethine imines and ynolates”. Org. Lett. **18**: 2608, 2016.

57 HUISGEN, R.; FLEISCHMANN, R. & ECKELL, A. “Azomethin-imine, eine neue. Klasse zwitterionischer Verbindungen”. Tetrahedron Lett. **12**: 1, 1960; (b) HUISGEN, R. “1.3-Dipolare

cycloadditionen rückschau und ausblick". Angew. Chem. **75**: 604, 1963; (c) BREUGST, M. & REISSIG, H.-U. "The Huisgen reaction: milestones of the 1,3-dipolar cycloaddition". Angew. Chem. Int. Ed. **59**: 12293, 2020.

58 DEEPTHI, A.; THOMAS, N. V. & SRUTHI, S. L. "An overview of the reactions involving azomethine imines over half a decade". New J. Chem. **45**: 8847, 2021.

59 GROŠELJ, U.; SVETE, J.; AL MAMARI, H. H.; POŽGAN, F. & ŠTEFANE, B. "Metal-catalyzed [3+2] cycloadditions of azomethine imines". Chemistry of Heterocyclic Compounds". **54**: 214, 2018.

60 KAWAI, H.; KUSUDA, A.; NAKAMURA, S.; SHIRO, M. & SHIBATA, N. "Catalytic enantioselective trifluoromethylation of azomethine imines with trimethyl(trifluoromethyl)silane". Angew. Chem. Int. Ed. **48**: 6324, 2009.

61 SHINTANI, R.; SOH, Y. -T. & HAYASHI, T. "Rhodium-catalyzed asymmetric arylation of azomethine Imines". Org. Lett. **12**: 4106, 2010

62 WANG, H. Y.; ZHENG, C. W.; CHAI, Z.; ZHANG, J. X. & ZHAO, G. "Asymmetric cyanation of imines via dipeptide-derived organophosphine dual-reagent catalysis". Nat. Commun. **7**: 12720, 2016.

63 RODINA, L.; VERZHBA, O. A. & KOROBITSYNA, I. K. "Photochromism in a series of azomethinimines based on 4-phenyl-1,2,4-triazoline-3,5-dione ". Chem. Heterocycl. Com. **19**: 1345, 1983.

64 GEISSLER, G.; FUST, W.; KRUGER, B. & TOMASCHEWSKI, G. "Azomethinimine. VII. Photochemisches und thermisches verhalten azarylsubstituierter pyrazolidon-(3)-azomethinimine". Adv. Synth. Catal. **325**: 205, 1983.

65 DORN, T. & KREHER, H. "Addition-addition-elimination mechanism of 1,3-dipole "dimerization"". Tetrahedron Lett. **29**: 2939, 1988.

66 XIA, P.-J.; YE, Z.-P.; SONG, D.; REN, J.-W.; WU, H. –W.; XIAO, J.-A.; XIANG, H. –Y.; CHEN, X. –Q. & YANG, H. "Photocatalytic reductive radical–radical coupling of *N*,*N*'-cyclicazomethine imines with difluorobromo derivatives". Chem. Commun. **55**: 2712, 2019.

67 NACSA, E. D. & MACMILLAN, D. W. C. "Spin-center shift-enabled direct enantioselective *α*-benzylation of aldehydes with alcohols". J. Am. Chem. Soc. **140**: 3322, 2018.

68 LUO, P.; FEINBERG, A. M.; GUIRADO, G.; FARID, S. & DINNOCENZO, J. P. “Accurate oxidation potentials of 40 benzene and biphenyl derivatives with heteroatom substituents”. *J.* Org. Chem. **79**: 9297, 2014.

69 TEEGARDIN, K.; DAY, J. I.; CHAN, J.; WEAVER, J. “Advances in photocatalysis: a microreview of visible light mediated ruthenium and iridium catalyzed organic transformations”. Org. Process Res. Dev. **20**: 1156, 2016.

69 HARI, D. P. & KÖNIG, B. “Synthetic applications of eosin Y in photoredox catalysis”. Chem. Commun. **50**: 6688, 2014.

70 FIDALY, K.; CEBALLOS, C.; FALGUIÈRES, A.; VEITIA, M. S.-I.; GUY, A. & FERROUD, C. “Visible light photoredox organocatalysis: a fully transition metal-free direct asymmetric *α*-alkylation of aldehydes”. Green Chem. **14**: 1293, 2012.

71 CERNAK, T.; DYKSTRA, K. D.; TYAGARAJAN, S.; VACHAL, P. & KRSKA, S. W. “The medicinal chemist's toolbox for late-stage functionalization of drug-like molecules”. Chem. Soc. Rev. **45**: 546, 2016.

72 LEIFERTB, D.; STUDER, A. “The persistent radical effect in organic synthesis”. Angew. Chem. Int. Ed. **59**: 47, 2020.

73 (a) URAGUCHI, D.; KINOSHITA, N.; KIZU, T. & OOI, T. “Synergistic catalysis of ionic brønsted acid and photosensitizer for a redox neutral asymmetric *α*-coupling of *N*-arylaminomethanes with aldimines”. J. Am. Chem. Soc. **137**: 13768, 2015; (b) FAVA, E.; MILLET, A.; NAKAJIMA, M.; LOESCHER, S. & RUEPING, M. “Reductive umpolung of carbonyl derivatives with visible-light photoredox catalysis: direct access to vicinal diamines and amino alcohols via *α*-amino radicals and ketyl radicals”. Angew.Chem. Int. Ed. **55**: 6776, 2016; (c) ZHAO, Y.; CHEN, J.-R.; XIAO, W.-J. “Synthesis of hydrazide-containing chroman-2-ones and dihydroquinolin-2-ones via photocatalytic radical cascade reaction of aroylhydrozones”. Org. Lett. **18**: 6304, 2016; (d) PATEL, N. R.; KELLY, C. B.; SIEGENFELD, A. P. & MOLANDER. G. A. “Mild, redox-neutral alkylation of imines enabled by an organic photocatalyst”. ACS Catal. **7**: 1766, 2017; (e) JIA, J.; KANCHERLA, R.; RUEPING, M. & HUANG, L. “Allylic C(sp^3)–H alkylation via synergistic organo- and photoredox catalyzed radical addition to imines”. Chem. Sci. **11**: 4954, 2020.

74 WINTERTON, S. E. & READY, J. M. “[3 + 2]-cycloadditions of azomethine imines and ynolates”. Org. Lett. **18**: 2608, 2016.

75 CHANDRASEKHARAM, M.; CHIRANJEEVI, B.; GUPTA, K. S. V. & SRIDHAR, B. 'Iron-catalyzed regioselective direct oxidative aryl–aryl cross-coupling". J. Org. Chem. **76**: 10229, 2011.

76 JOHNSON, C. R.; ANSARI, M. I. & COOP, A. "Tetrabutylammonium bromide-promoted metal-free, efficient, rapid, and scalable synthesis of *N*-aryl amines". ACS Omega. **3**: 10886, 2018.

CHAPTER 2

1. Introduction

1.1 The Amide Linkage

Relevance and Methods

Amide-containing architectures present an enormous relevance as part of pharmaceuticals, natural products, and biologically active compounds (**FIGURE 2.1**). Approximately 30% of the transformations in the field of medicinal chemistry, for example, are directed to the construction of amide bonds.[1]

Given such prevalence as a key functional group in these aforementioned compounds, there is a continuing interest in developing efficient synthetic routes capable to install this functionality under mild reaction conditions. This feature is especially important considering the biological structures of peptides and proteins based on the amide linkage.

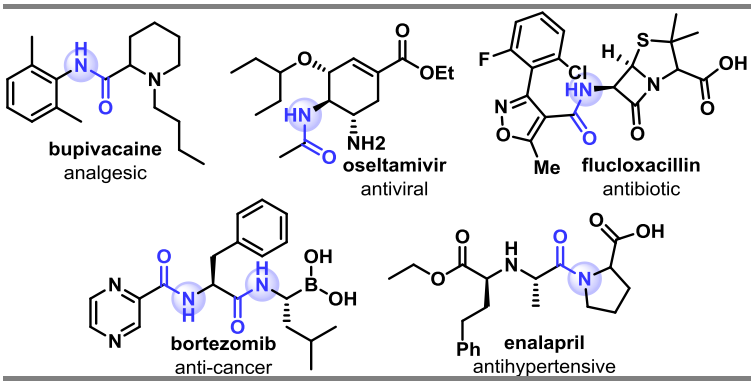

FIGURE 2.1 - Selected examples of amide-containing pharmaceuticals.

Traditionally, classical methodologies involve amidation strategies based on the construction of C-N bonds. Among these, the amine acylation protocols in the presence of activated esters are the most widely explored and, not coincidentally, this reaction represents about 16% of the transformations used in the synthesis of pharmaceuticals.[2]

The well-known methods of condensation by the coupling of carboxylic acids with amines and expulsion of a molecule of water are those commonly applied in the routine of

[1] BROWN, D. G. & BOSTRÖM, J. "Analysis of past and present synthetic methodologies on medicinal chemistry: where have all the new reactions gone?". J. Med. Chem. **59**: 4443, 2016.
[2] ROUGHLEY, S. D. & JORDAN, A. M. "The medicinal chemist's toolbox: an analysis of reactions used in the pursuit of drug candidates". J. Med. Chem. **54**: 3451, 2011.

synthetic laboratories. However, harsh reaction conditions are usually employed to avoid the formation of carboxylate-ammonium salts and coupling agents are need to mediate the amide synthesis, for example, *N*,*N*′-dicyclohexylcarbodiimide (DCC), 1-ethyl-3-(3′-dimethylaminopropyl)-carbodiimide hydrochloride (EDC), *N*-[(dimethylamino)-1*H*-1,2,3-triazolo[4,5-*b*]pyridin-1-ylmethylene]-*N*-methylmethanaminium hexafluorophosphate *N*-oxide (HATU), among others (**SCHEME 2.1, A**). Although efficient and robust, these methods are not compatible with sterically congested amines, decrease the atom economy of the transformation since the coupling reagents are stoichiometric and lead to waste products (ureas and phosphonamides) that need be separated from the final products.[3]

In addition to the use of well-known coupling reagents, other methodologies[4] make use of 1) catalytic acylation with boronic acids, 2) generation of activated carboxylates from the reaction of aldehydes (α,β-unsaturated, formylcyclopropanes, α-haloaldehydes, epoxyaldehydes) with *N*-heterocyclic carbene (NHC) as catalysts, 3) oxidative amidation of amines from alcohols and aldehydes using palladium, copper/silver and ruthenium (**SCHEME 2.1, B)**, 4) chemoselective bonding methods, as the Staudinger bonding and the α-ketoacid–hydroxylamine decarboxylative bonding (**SCHEME 2.1, C**).

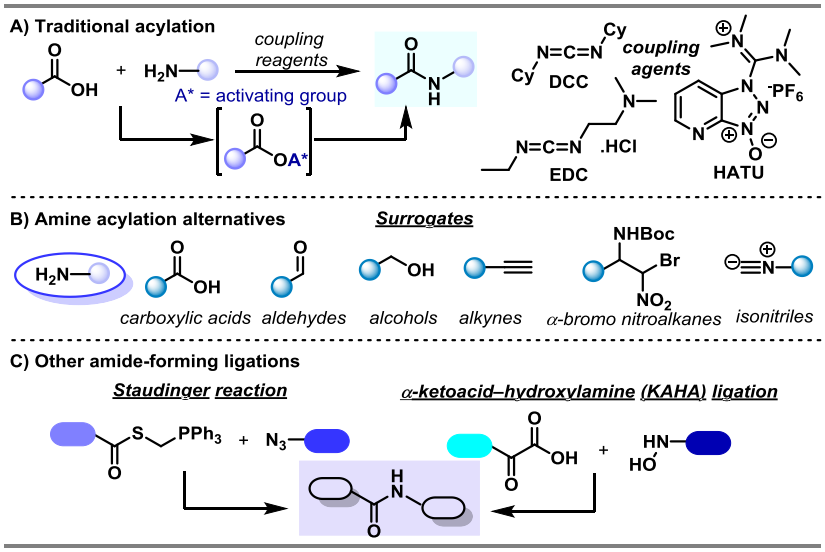

SCHEME 2.1 - Amidation strategies based on the construction of C-N bonds.

Given the drawbacks of the traditional amine acylation protocols, a broad class of metal-catalyzed methods to form amide bonds has emerged as an alternative. Regarding the

[3] SEAVILL, P. W. & WILDEN, J. D. “The preparation and applications of amides using electrosynthesis”. Green Chem. **22**: 7737, 2020.
[4] PATTABIRAMAN, V. R. & BODE, J. W. “Rethinking amide bond synthesis”. Nature. **480**: 471, 2011.

arsenal of synthetic tools available to access compounds containing the amide group, other methodologies are based on C-C bond formation, complementing the more traditional methods based on C-N bonds. Isocyanates, for example, have been found to be useful amide synthons in metal-catalyzed protocols.[5] The high electrophilicity of isocyanates make them excellent reaction partners in the presence of different nucleophiles and these protocols represent a direct and efficient way to obtain amide compounds. As coupling partners are reported the use of organometallic reagents, unsaturated C–C bonds, reductive couplings with aryl halides, aryl esters and tosylates, for example (**SCHEME 2.2, A**). In 2012, Bode disclosed a seminal work addressing the challenge of preparing hindered and electron-deficient amides from the direct coupling of isocyanates with Grignard reagents (**SCHEME 2.2, B**).[6] In other remarkable protocol, Martin and coworkers demonstrated the preparation of primary, secondary, and tertiary amides in the first Ni-catalyzed reductive amidation of unactivated alkyl halides with isocyanates (**SCHEME 2.2, B**).[7]

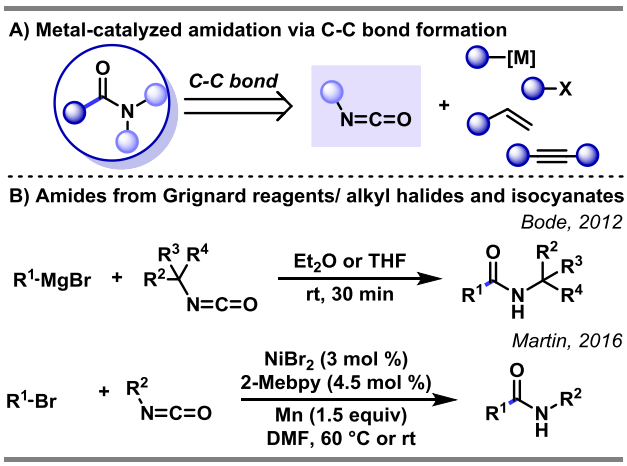

SCHEME 2.2 - A) Amide linkage by C-C bond ligation B) and from Grignard reagents and alkyl halides.

New disconnection approaches also relies on the exploration of CO_2 as amide surrogates via catalytic carboxylation with a series of coupling partners followed by the classical C–N bond formation.

Given the immense relevance of this class of compounds, it is of extreme interest the availability of a great diversity of methodologies that allow synthetic designs through different

[5] SERRANO, E. & MARTIN, R. “Forging amides through metal-catalyzed C–C coupling with isocyanates”. Eur. J. Org. Chem. **24**: 3051, 2018.
[6] SCHÄFER, G.; MATTHEY, C.; BODE, J. W. “Facile synthesis of sterically hindered and electron-deficient secondary amides from isocyanates”. Angew. Chem. Int. Ed. **51**: 9173, 2012.
[7] SERRANO, E.; MARTIN, R. “Nickel-catalyzed reductive amidation of unactivated alkyl bromides” Angew. Chem. Int. Ed. **55**: 11207, 2016.

starting substrates and reaction conditions. Similarly occurred to another classes of transformations, photoredox catalysis has emerged as an important trend in the context of amide preparation.

The Photoredox Approach

The reductive cross-coupling protocols generating nucleophiles in situ from halides require stoichiometric amounts of reductants, which is one of the major disadvantages of these reactions. Molander and coworkers envisioned that these transformations could be compared with visible-light driven photoredox cross-couplings, since a radical is generated in the photoredox cycle and then engages in the nickel catalytic cycle via an oxidative capture by the metal center, leading to the key Ni(III) specie (**SCHEME 2.3, A**).

In this remarkable work, a nickel-catalyzed photoredox amidation of alkylsilicates and aryl/alkyl isocyanates was elegantly disclosed under mild conditions, in an overall redox-neutral protocol and with a wide range of tolerated functional groups (**SCHEME 2.3, B**).[8] The mechanistic scenario involves a nickel-isocyanate adduct (**II**) upon radical addition to the Ni(II) carbonyl-amido intermediate (**I**). The resulting Ni(III) complex undergoes reductive elimination to leverages the C−C bond formation, followed by protonation. The resulting Ni(I) complex prevenient from this step can be regenerated in the photoredox cycle by the highly reducing specie of $Ru(bpy)^{3+}$ and, consequently, making the general process redox-neutral.

[8] ZHENG, S.; PRIMER, D. N. & MOLANDER, G. A. “Nickel/photoredox-catalyzed amidation via alkylsilicates and isocyanates”. ACS Catal. **7**: 7957, 2017.

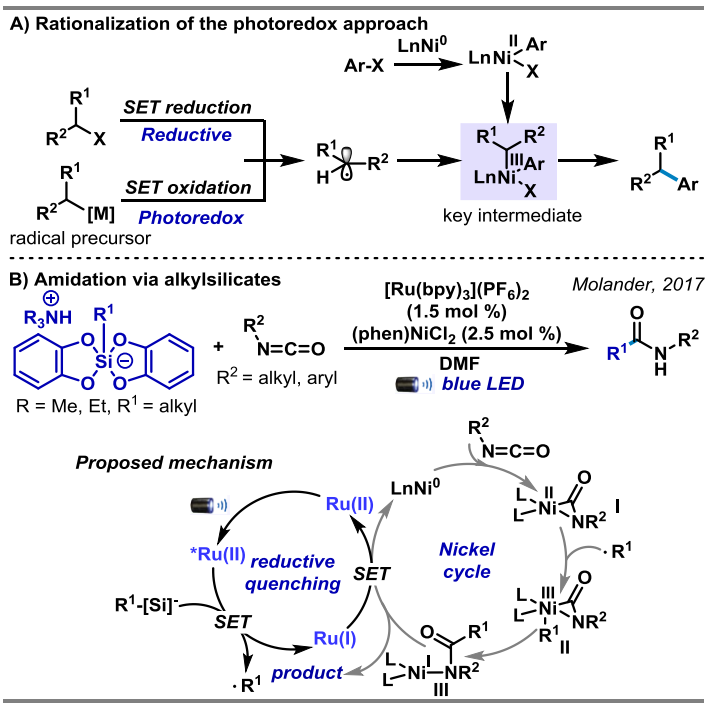

SCHEME 2.3 - Nickel/photoredox-catalyzed amidation between alkyl silicates and isocyanates.

Given the prevalence of amides in pharmaceutical compounds, there is a continuous demand for the design of new efficient and simple methods, avoiding the generation of waste, as well as the use of stoichiometric reagents. In this scenario, the photoredox catalysis once again has appeared as an excellent alternative in parallel with traditional methods.

Still focusing on forging amides through mechanisms via C-C bonds, Polyzos recently reported a light-induced alternative that avoids the use of harsh conditions of the traditional transition metal catalyzed carbonylative amidations. The first protocol for the photoredox catalyzed carbonylative amidation of aryl, heteroaryl and alkyl halides compatible with primary, secondary, and tertiary amines was reported. The process is proposed to occur via a unique tandem photocatalytic cycle of $[Ir(ppy)_2(dtb\text{-}bpy)]^+$, which engages aryl and unactivated alkyl halides to furnish amides using carbon monoxide as *C1* building block under continuous flow operation (**SCHEME 2.4**).[9]

[9] FORNI, J. A.; MICIC, N.; CONNELL, T. U.; WERAGODA, G. & POLYZOS, A. "Tandem photoredox catalysis: enabling carbonylative amidation of aryl and alkylhalides". Angew. Chem. **59**: 18646, 2020.

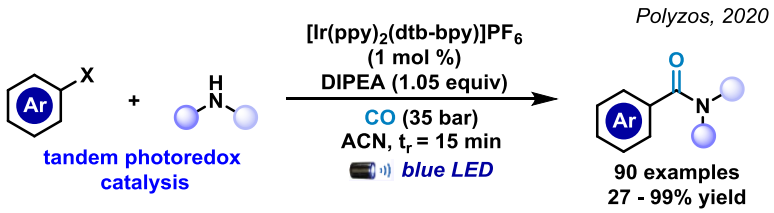

SCHEME 2.4 - Carbonylative amidation of aryl and alkylhalides via tandem photoredox catalysis.

The robustness and versatility of such protocols reinforce the importance of developing metal-, base-, and additive-free photoredox-catalyzed amide formation strategies as a green one-pot approach. In this way, many other groups have directed their efforts towards the elaboration of new transformations and diversification of the available tools to reach the preparation of this class of compounds.

Traditional protocols via formation of C-N bonds have also made considerable advances in this field. This year, Chen and coworkers reported the direct transformation of carboxylic acids to amides by photoredox catalysis in a strategy where suitable amine sources capture the acyl radicals produced via SET in the redox cycle.[10] This photoredox deoxygenation amidation template between carboxylic acids and amineboranes was well tolerated to a series of (hetero)aromatic acids and aliphatic acids containing different functional groups. Other recent reports in the literature have established methods driven by visible light photoredox catalysis from the classic combination of carboxylic acids with amines,[11] thioacetic acids and amines[12] or employing diverse components such as for the amidation of benzylic alcohols,[13] esterification with perfluoroalkyl iodide,[14] among others.

Despite significant progress on amide forging photocatalytic strategies, there is still a gap for the design of new protocols. These new reactions, ideally, should complement the existing ones and allow the functionalization/preparation of complex substrates and natural products/drugs analogues by installing amide bonds, which are considered key to many biological processes.

1.2 Photogenerated Carbamoyl Radicals: Synthetic Applications

[10] MIAO, Y.-Q.; KANG, J.-X.; MA, Y.-N. & CHEN, X. “Visible light-mediated synthesis of amides from carboxylic acids and amine-boranes”. Green Chem. **23**: 3595, 2021.
[11] SRIVASTAVA, V.; SINGH. P. K. & SINGH, P. P. “Visible light photoredox catalysed amidation of carboxylic acids with amines”. Tetrahedron Lett. **60**: 40, 2019.
[12] SONG, W.; DONG, K. & LI, M. “Visible light-induced amide bond formation”. Org. Lett. **22**: 371, 2020.
[13] GASPA, S.; FARINA, A.; TILOCCA, M.; PORCHEDDU, A.; PISANO, L.; CARRARO, M.; AZZENA, U. & DE Luca, L. “Visible-light photoredox-catalyzed amidation of benzylic alcohols”. J. Org. Chem. **85**: 11679, 2020.
[14] XIAO, Y.; CHUN, Y.-K.; CHENG, S.-C.; NG, C.-O.; TSE, M.-K.; LEI, N.-Y.; LIU, R. & KO, C.-C. “Photocatalytic amidation and esterification with perfluoroalkyl iodide”. Catal. Sci. Technol. **11**: 556, 2021.

Differing from the extensive applications of acyl radicals, the reactive intermediates of carbamoyl radicals have been less explored. These species are usually accessed through light-mediated protocols, redox systems or thermally. Regarding the photochemical approaches, the carbamoyl radicals have recently received important attention in visible light-induced transformations. This amide synthon contains the structural unit of interest ready to be directly installed in the reaction acceptors. Given the versatility of these nucleophilic radicals, they are considered key intermediates in the synthesis of structurally relevant scaffolds, such as natural products and heterocycles.

The Fenton-type processes have been well explored to access carbamoyl radicals in a redox system composed by $FeSO_4$, H_2O_2, and H_2SO_4 in formamide or *N*-methylformamide. Under these conditions, a hydroxyl radical can be generated after the reaction of hydrogen peroxide with Fe(II) under heating in acidic medium, leveraging Fe(III) and water. The key hydroxyl radical formed presents a high oxidation potential, capable of abstracting a hydrogen from the formamide to provide the carbamoyl radical. This nucleophilic intermediate is then capable to undergoes an addition reaction to unsaturated systems, giving rise to a second radical intermediate that can be oxidized by Fe(III) to produce the corresponding products and the catalytic Fe(II). The carbamoyl radicals accessed under these conditions can be applied directly in the preparation of primary amides, which are also prone to participate in cascade reactions to furnish high functionalized heterocycles.

Andrade *et al.* have elegantly explored such reactivity and demonstrated a straightforward access to amide-containing compounds (**SCHEME 2.5**); key intermediates to access a series of structural relevant heterocycles via tandem radical addition/ cyclization/ rearomatization reactions.[15] In their studies, the adaptation to the photo-Fenton under UV irradiation and flow conditions represented an improvement for the carbamoyl radical generation from formamide and the efficient construction of oxindoles.[16] The applicability of the developed protocol was later demonstrated in the preparation of (±)-coixspirolactam scaffolds[17] and biobased spiroimides.[18] An ultimately advancement was made by developing

[15] CORREIA, V. G.; ABREU, J. C.; BARATA, C. A. E. & ANDRADE, L. H. “Iron-catalyzed synthesis of oxindoles: application to the preparation of pyrroloindolines”. Org. Lett. **19**: 1060, 2017.
[16] SANABRIA, M. N.; HORNINK, M. M.; CORREIA, V. G.; & ANDRADE, L. H. “Nontraditional application of the photo-fenton process: a novel strategy for molecular construction using formamide and flow chemistry”. Org. Process Res. Dev. **24**: 2288, 2020.
[17] NASCIMENTO, V. R.; SUENAGA, M. L. S. & ANDRADE, L. H. “An efficient approach for the synthesis of new (±)-coixspirolactams”. Org. Biomol. Chem. **18**: 5458, 2020.
[18] HORNINK, M. M.; LOPES, A. U. & ANDRADE, L. H. “Biobased spiroimides from itaconic acid and formamides: molecular targets for a novel synthetic application of renewable chemicals”. Synthesis. **53**: 296, 2021.

an ultrafast (10 s) diastereoselective synthesis of 2-quinolinone-fused *γ*-lactones from Fenton's reagents in formamide with 1,7-enynes in a cascade reaction assisted by microwave irradiation.[19]

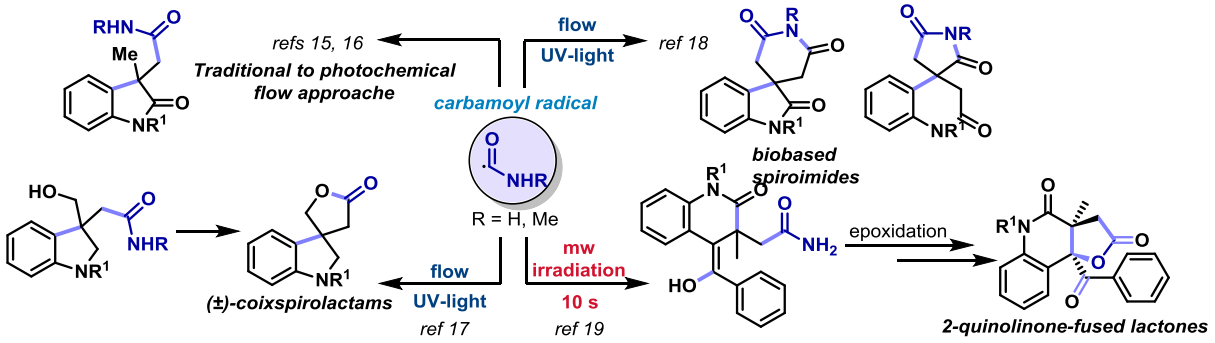

SCHEME 2.5 – Andrade's approaches for carbamoyl radical installation from Fenton's reagents and formamide/ *N*-methylformamide.

The installation of these radicals is an interesting strategy for the direct preparation of amide-containing compounds and some transformations have been reported regarding the generation of these carbon atom-centered radical species. The common approaches involving their generation relies on the photocatalyzed hydrogen atom transfer from formamides[13] or by photoredox catalysis by using substituted oxamic acids or *N*-hydroxyphthalimido oxamides.

The first reductive generation of carbamoyl radical by means of visible-light driven photocatalysis was disclosed by Donald and coworkers in 2017. In their work, a redox-neutral protocol was developed for the synthesis of fused cyclic and spirocyclic 3,4-dihydroquinolin-2-ones from *N*-hydroxyphthalimido esters (**SCHEME 2.6, A**).[20] Later on, an alternative strategy for the synthesis of 3,4-dihydroquinolin-2(1*H*)-ones was reported via a photoredox decarboxylation of oxamic acids in aqueous media.[21] The oxidative generation of carbamoyl radicals is followed by the addition to activated olefins in a sequence of events involving cyclization and aromatization (**SCHEME 2.6, B, left**). At the same time, Landais independently had showed the reactivity of oxamic acids under oxidative conditions leading to

[19] SACCHELLI, B. A. L.; ROCHA, B. C. & ANDRADE, L. H. "Cascade reactions assisted by microwave irradiation: ultrafast construction of 2-quinolinone-fused γ-lactones from *N*-(o-ethynylaryl)acrylamides and formamide". Org. Lett. **23**: 5071, 2021.
[20] PETERSEN, W. F.; TAYLOR, R. J. K. & DONALD, J. R. "Photoredox-catalyzed procedure for carbamoyl radical generation: 3,4-dihydroquinolin-2-one and quinolin-2-one synthesis". Org. Biomol. Chem. **15**: 5831, 2017.
[21] BAI, Q.; JIN, C.; HE, J. & FENG, G. "Carbamoyl radicals via photoredox decarboxylation of oxamic acids in aqueous media: access to 3,4-dihydroquinolin-2(1*H*)-ones". Org. Lett. **20**: 2172, 2018.

an *in-situ* generation of isocyanates using the organophotocatalyst 4CZIPN.[22] The reaction proceeds through the oxidation of the carbamoyl radical intermediate by the photocatalyst radical cation $PC^{\bullet+}$, giving rise to the protonated isocyanate, followed by the reaction with alcohols or amines to give urethanes and ureas, respectively (**SCHEME 2.6, B, right**). The same concept of metal free photocatalyzed decarboxylation of oxamic acids was explored later for the carbamoyl radical installation on heteroaromatic bases, including access to heteroaryl amides derived from aminoacids without racemization (**SCHEME 2.6, B, bottom**).[23]

In 2019, Hong and coworkers developed a protocol to expand the application of Minisci-type reactions, which usually involve the functionalization with alkyl groups. Their strategy allowed site-divergent carbamoylation (and phosphinoylation) of pyridine derivatives driven by visible light in the presence of 3-phosphonated quinolinones (PC*, E^*_{red} = −1.29 V *vs* SCE) as photocatalyst.[14] The photoexcited organocatalyst PC* is capable of participating in a SET event with a sacrificial amount of *N*-ethoxypyridinium, leveraging the ethoxy radical that engages in an intermolecular HAT with the formamide. The radical addition, followed by deprotonation, and N−O cleavage gives rise to the carbamoylated compound (**SCHEME 2.6, C**). The application of the protocol was further demonstrated for the late-stage functionalization of bisacodyl, vismodegib, and pyriproxyfen.

[22] PAWAR, G. G.; ROBERT, F.; GRAU, E.; CRAMAIL, H. & LANDAIS, Y. “Visible-light photocatalyzed oxidative decarboxyla-tion of oxamic acids: a green route to urethanes and ureas”. Chem. Commun. **54**: 9337, 2018.
[23] JATOI, A. H.; PAWAR, G. G.; ROBERT, F. & LANDAIS, Y. “Visible-light mediated carbamoyl radical addition to heteroarenes”. Chem. Commun. **55**: 466, 2019.

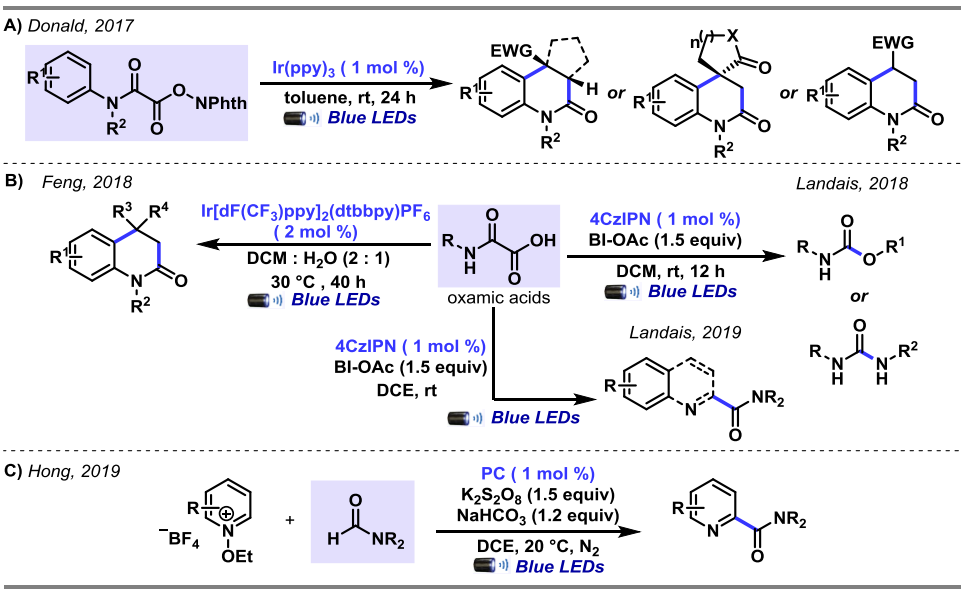

SCHEME 2.6 - Recent photoredox approaches for carbamoyl radical generation.

4-substituted-1,4-dihydropyridines (DHPs), also known as Hantzsch esters (HE), are bench-stable solids, easily synthesized from commercially available starting materials in one step, and offer high structural diversification. Their preparation involves a classical condensation reaction between aldehydes, *β*-ketoesters, and ammonium acetate, making them a very accessible radical feedstock (**SCHEME 2.7**). These species are susceptible to become fully aromatic pyridines due to their facile oxidation (E_{ox} ~ +1.05 V *vs* SCE)[24] and are prone to provide the corresponding radical after fragmentation via single-electron oxidation by visible-light irradiation in the presence of a suitable photocatalyst. Besides the exploration of DHPs as alkyl, acyl, and proton sources,[25] they are also useful precursors for the generation of the less explored carbamoyl radicals under photocatalytic conditions.

[24] (a) WEI, X.; WANG, L.; JIA, W.; DU, S.; WU, L. & LIU, Q. "Metal-free-mediated oxidation aromatization of 1,4-dihydropyridines to pyridines using visible light and air". Chin. J. Chem. **32**: 1245, 2014; (b) CHENG, J. P.; LU, Y.; ZHU, X. Q.; SUN, Y.; BI, F. & HE, J. "Heterolytic and homolytic N−H bond dissociation energies of 4-substituted hantzsch 2,6-dimethyl-1,4-dihydropyridines and the effect of one-electron transfer on the N−H bond activation". J. Org. Chem. **65**: 3853, 2000.

[25] (a) MILLIGAN, J. A.; PHELAN, J. P.; BADIR, S. O. & Molander, G. A. "Alkyl carbon–carbon bond formation by nickel/photoredox cross-coupling". Angew. Chem. Int. Ed. **58**: 6152, 2019; (b) WANG, P.-Z.; CHEN, J.-R. & XIAO, W.-J. "Hantzsch esters: an emerging versatile class of reagents in photoredox catalyzed organic synthesis". Org. Biomol. Chem. **17**: 6936, 2019; (c) HUANGA, W. & CHENG, X. "Hantzsch esters as multifunctional reagents in visible-light photoredox catalysis". Synlett. **27**: A, 2016; (d) ZHENG, C. & YOU, S. -L. "Transfer hydrogenation with Hantzsch esters and related organic hydride donors". Chem. Soc. Rev. **41**: 2498, 2012.

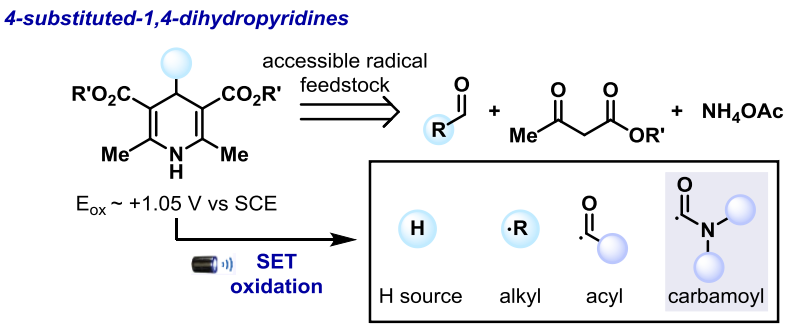

SCHEME 2.7 – Synthesis and application of DHP species as radical/ proton source.

The utilization of DHPs as carbamoyl radical source in photoredox catalysis is a recent alternative. Last year, Melchiorre demonstrated a mild strategy for a catalytic amide synthesis that enables the direct carbamoylation of (hetero)aryl bromides promoted by a dual catalytic system between a Ni complex and the 4CzIPN photocatalyst (**SCHEME 2.8, A**).[26] In this work, the (*L*)-alanine-derived dihydropyridine was designed based on the precedents of using DHPs as sources of alkyl and acyl radicals and the authors realized that carbamoyl radicals would be efficiently generated from such oxidative cleavage as well.

Interestingly, the scope of this transformation comprised some examples from DHPs prepared from amino acids (8 examples) and one example was demonstrated from a dipeptide. The protocol was showed to be complementary to the conventional carbonylation chemistry and allowed the coupling of important biological structures to furnish (hetero)aryl amides.

Then, Wangelin presented a protocol for carbamoylation of alkenes using the organic dye 3DPAFIPN as photocatalyst and by the exploration of EDA complexes with DHPs.[27] The Giese-type reaction extended the functionalization chemistry with *C*1-building blocks, although only activated olefins were well tolerated and the scope of DHPs did not include more complex scaffolds (**SCHEME 2.8, B, left**). Also recently, Hong and coworkers disclosed a catalyst-free pyridine functionalization enabled by the EDA complex between *N*-amidopyridinium salts and 1,4-DHPs under visible-light irradiation.[28] The protocol's scope included various types of alkyl, acyl, and carbamoyl radicals leading to few examples of C*4*-

[26] ALANDINI, N.; BUZZETTI, L.; FAVI, G.; SCHULTE, T.; CANDISH, L.; COLLINS, K. D. & MELCHIORRE, P. "Amide synthesis by nickel/photoredox-catalyzed direct carbamoylation of (hetero)aryl bromides". Angew. Chem. Int. Ed. **59**: 5248, 2020.
[27] CARDINALE, L.; KONEV, M. O. & VON WANGELIN, A. "Photoredox-catalyzed addition of carbamoyl radicals to olefins: a 1,4-dihydropyridine approach". J. Chem. Eur. J. **26**: 8239, 2020.
[28] KIM, I.; PARK, S. & HONG, S. "Functionalization of pyridinium derivatives with 1,4-dihydropyridines enabled by photoinduced charge transfer". Org. Lett. **22**: 8730, 2020.

selective pyridine carbamoylations including the late-stage modification of a variety of biologically relevant compounds (**SCHEME 2.8, B, right**).

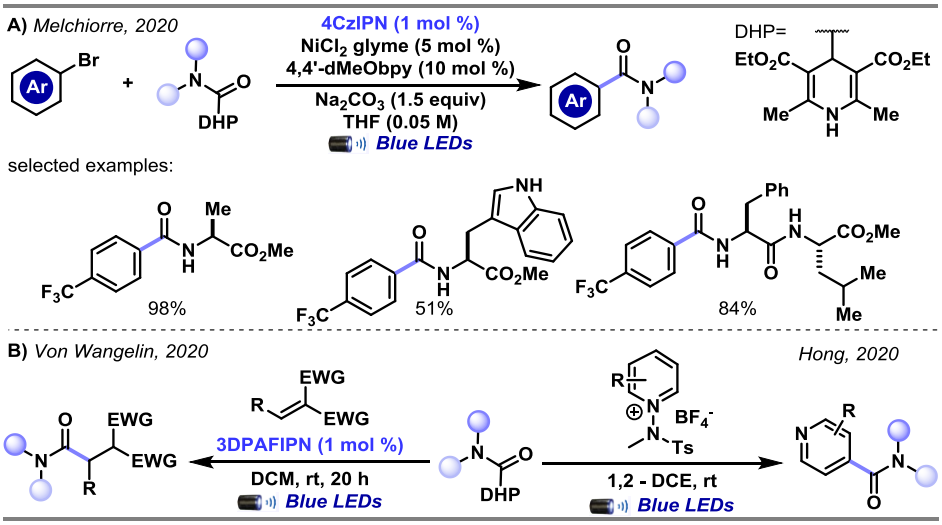

SCHEME 2.8 – Recent carbamoyl radical generation from DHPs and applications in photocatalysis.

Given the advantages provided by photoredox catalysis (room temperature, use of visible light and high functional-group tolerance), it has been considered a valuable strategy for the development of biocompatible protocols and interesting chemoselective biomolecule modifications. Supporting such relevance, peptides have displayed a crucial role in current drug discovery programs providing an array of potent and preferential biological activities, making them an attractive target to modify and encouraging the development of novel bioconjugation protocols.[29]

In this scenario, the development of methodologies, such as those demonstrated by the Melchiorre group, enabling easy access to biological structural entities and their derivatives such as unnatural amino acids and peptides is an important trend. And given the mild conditions found in photocatalysis, this combination has proven to be powerful and is certainly one of the key synthetic tools in the modern organic synthesis scene.

[29] (a) BOTTECCHIA, C. & NOËL, T. "Photocatalytic modification of amino acids, peptides, and proteins". Chem. - A Eur. J. **25**: 26, 2019; (b) LIU, J.-Q., SHATSKIY, A., MATSUURA, B. S. & KÄRKÄS, M. D. "Recent advances in photoredox catalysis enabled functionalization of *α*-amino acids and peptides: concepts, strategies and mechanisms". Synthesis. **51**: 2759, 2019.

2. Carbamoylation of Azomethine Imines via Visible-Light Photoredox Catalysis

Published work: MATSUO, B. T.; OLIVEIRA, P. H. R.; CORREIA, J. T. M. & PAIXÃO, M. W. "Carbamoylation of Azomethine Imines via Visible-Light Photoredox Catalysis". Org. Lett. **23**: 6775, 2021.

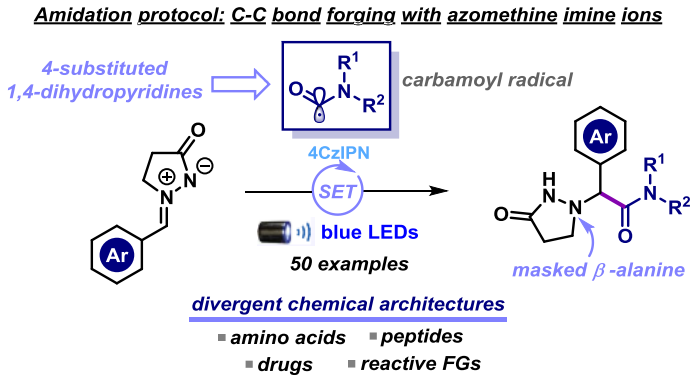

A versatile and robust photocatalytic methodology to forge amide functional groups from azomethine imine ions is described. This protocol is distinguished by its broad scope, and mild reaction conditions which are well suited for the preparation of structurally complex compounds in the form of amino acids, peptides, and small drug-like molecules. Moreover, the pyrazolidinone core generated could be easily converted into β-alanine analogues.

RESULTS AND DISCUSSION

Inspired by the initial findings in the generation of carbamoyl radicals, we envisioned engaging DHPs in an unprecedent photocatalytic carbamoylation of imine derivatives. This transformation would represent a mild and easy strategy to construct biologically relevant scaffolds, and complement those protocols involving aryl halides,[26] activated olefins[27] and aza-heterocycles functionalizations.[28]

The selected coupling partners, azomethine imine ions, are known as important building blocks, which can easily be transformed into biologically relevant nitrogen-containing heterocycles.[30] The reactivity of this class of molecules has been exhaustively explored as 1,3-dipoles, however, only recently their reactivity towards radical addition has been investigated.

[30] NÁJERA, C.; SANSANO, J. M. & YUS, M. "1,3-Dipolar cycloadditions of azomethine imines". Org. Biomol. Chem. **13**: 8596, 2015.

In this work, we described the construction of valuable amide compounds in a C-C bond forging strategy between DHPs derivatives and azomethine iminium ions in a mild and robust protocol. Considering the advantages of the metal-free organic photocatalysts, we envisioned 4CzIPN to be a suitable catalyst system to promote the proposed carbamoylation reaction ($E_{1/2}(PC^*/PC^-)$ = + 1.35 V *vs* SCE).[31]

For the optimization of the reaction conditions, we selected the cyclohexylamine-derived dihydropyridine **2a** as the model substrate in combination with the azomethine imine **1a** under 456 nm blue led irradiation (**SCHEME 2.9**). Based on our previous work,[32] we assumed that this transformation would take place via a reductive quenching since azomethine **1a** shows a very negative reduction potential to be directly reduced by the chosen photocatalyst (E_{red} 1a = - 1.6 V *vs* SCE and $E_{1/2}(PC^+/PC^*)$ = - 1.04 V *vs* SCE). Initially, in order to assure that the quenching of photocatalyst in the SET oxidation of **2a** would be suitable, we obtained experimentally the reduction potential for the selected DHP.

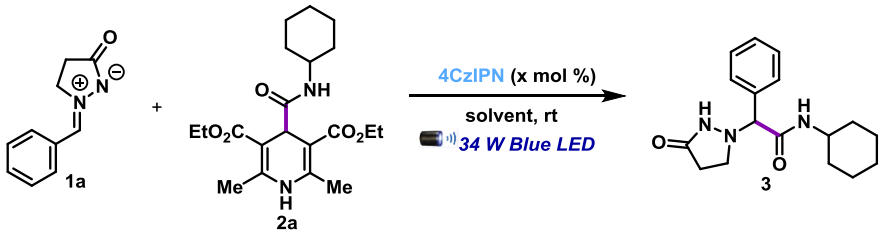

SCHEME 2.9 – Model substrates for the study of the carbamoylation reaction.

The cyclic voltammetry study was performed using a glassy carbon working electrode, a Pt wire auxiliary electrode, and an Ag/AgCl (satd. KCl) reference electrode. The ferrocene was considered as the external standard and the analysis was performed under N_2 atmosphere using a degasified solution of the **2a** in MeCN (0.5 mM) containing a 0.1 M $TBAPF_6$ solution in MeCN. The potential range scanned was - 2.5 V – + 2.5 V at a 100 $mV.s^{-1}$. From this measurement, we obtained such a value as being E_{red} 2a = + 1.21 V *vs* SCE, which agrees with the average value obtained for these species (**FIGURE 2.2**).

The literature standard potential value for the 4CZIPN photocatalyst is given by $E_{1/2}(PC^*/PC^-)$ = + 1.35 V *vs* SCE, leading us to the conclusion that the reductive quenching

[31] SHANG, T.-Y.; LU, L.-H.; CAO, Z.; LIU, Y.; HE, W.-M. & YU, B. "Recent advances of 1,2,3,5-tetrakis(carbazol-9-yl)-4,6-dicyanobenzene (4CzIPN) in photocatalytic transformations". Chem. Commun. **55**: 5408, 2019.

[32] MATSUO, B. T.; CORREIA, J. T. M. & PAIXÃO, M. W. "Visible-light-mediated *α*-amino alkylation of azomethine imines: an approach to *N*-(*β*-aminoalkyl)pyrazolidinones". Org. Lett. **20**: 7891, 2020.

process of this specie via SET with **2a** would be likely to occur. After this basic conclusion, we started to evaluate the reactional parameters for the optimization of the proposed transformation.

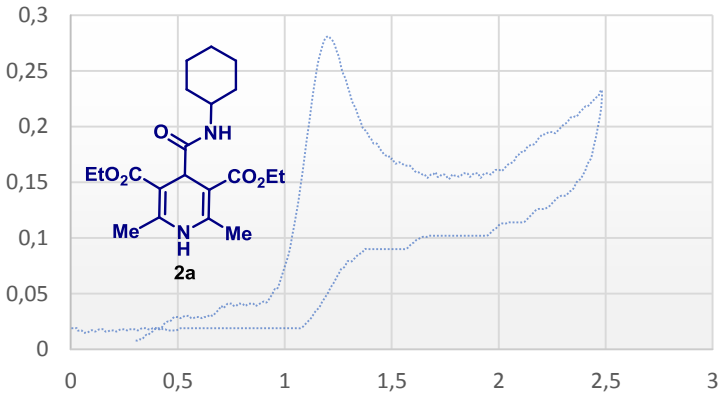

FIGURE 2.2 - CV of **2a** [0.5 mM] in [0.1 M] $TBAPF_6$ in MeCN. Scan rate: 100 $mV.s^{-1}$.

We identified that using only 1 mol% of the photocatalyst we were able to obtain the corresponding product *N*-cyclohexyl-2-(3-oxopyrazolidin-1-yl)-2-phenylacetamide **3** in 70% yield in acetonitrile under 456 nm blue light emitting diode irradiation (**Table 2.1, entry 1**). Further optimization found that acetonitrile is the most suitable solvent (**entries 2-4**) and that a more concentrated condition leads to a slight decrease in the yield (**entry 5**). Lower or higher catalyst loading showed to be detrimental to the reaction outcome (**entries 6-7**). Stoichiometry (**entry 8**), and additives (**entries 9-12**) were further screened, and the initial condition from entry 1 was established as the optimal condition to access the carbamoylated compound **3**.

TABLE 2.1 - Evaluation of reaction parameters [a]

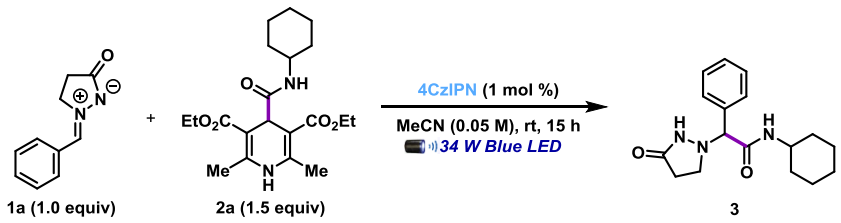

entry	deviation from standard conditions	3 (%)[b]
1	**none**	**70**
2	**THF** instead of MeCN	68
3	**EtOAc** instead of MeCN	43
4	**DCM** instead of MeCN	54
5	**[ ] = 0.1 M**	63
6	**2.5 mol%** of 4-CzIPN	54
7	**5 mol%** of 4-CzIPN	15
8	**reverse stoichiometry**	52
9	**K_2CO_3** (2 equiv)	64
10	**KH_2PO_4** (10 mol %)	40
11	**$PhCO_2H$** (10 mol %)	65
12	**CSA** (10 mol %)	61

4CzIPN

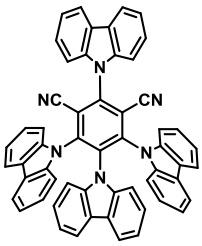

$E_{1/2}(PC^*/PC^-) = +1.35$ V
$E_{1/2}(PC+/PC^*) = -1.04$ V

[a] Reaction conditions: **1a** (0.15 mmol), **2a** (1.5 equiv, 0.225 mmol), **4CzIPN** (1 mol %) in MeCN (3.0 mL). [b] Isolated yields after column chromatography.

Having found the optimal reaction condition, we began to evaluate the scope of this transformation for a range of aryl azomethine imine ions (**SCHEME 2.10**). As seen in Scheme 2.10, aryl azomethine imines bearing either electron-withdrawing substituents (*p*-CF_3 **4** or *p*-F **5**) and electron-donating groups (*p*-Me **8** or *p*-OMe **9**) underwent the carbamoylation with **2a** in moderate to good yields. Importantly, substrates containing aryl bromides could be successfully tolerated, allowing for further functionalization by transition metal mediated cross-coupling reactions (compounds **6** and **10**). Other substitution pattern did not show substantial influence in the reaction outcome and, notably, ortho and meta substitution were well tolerated (**11**, **10** and **12**, respectively). Likewise, pyridine (**13**) and furan (**14**), privileged pharmacophores, were also competent towards the carbamoyl radical installation. The azomethine imine bearing a phenyl substituent on the pyrazolidinone ring also showed to be compatible to the reaction conditions furnishing the product **15**.

To demonstrate the applicability of this method to late-stage functionalization of dense molecules, we aimed at extending our methodology to the substrate-containing etodolac, an anti-inflammatory and analgesic drug. Its structure possesses benzylic C-H and acidic N-H bonds which are known to interfere with radical pathways. Gratifyingly, subjecting the

etodolac derivative to our reaction conditions, we were able to access the desired product **16** in excellent yield.

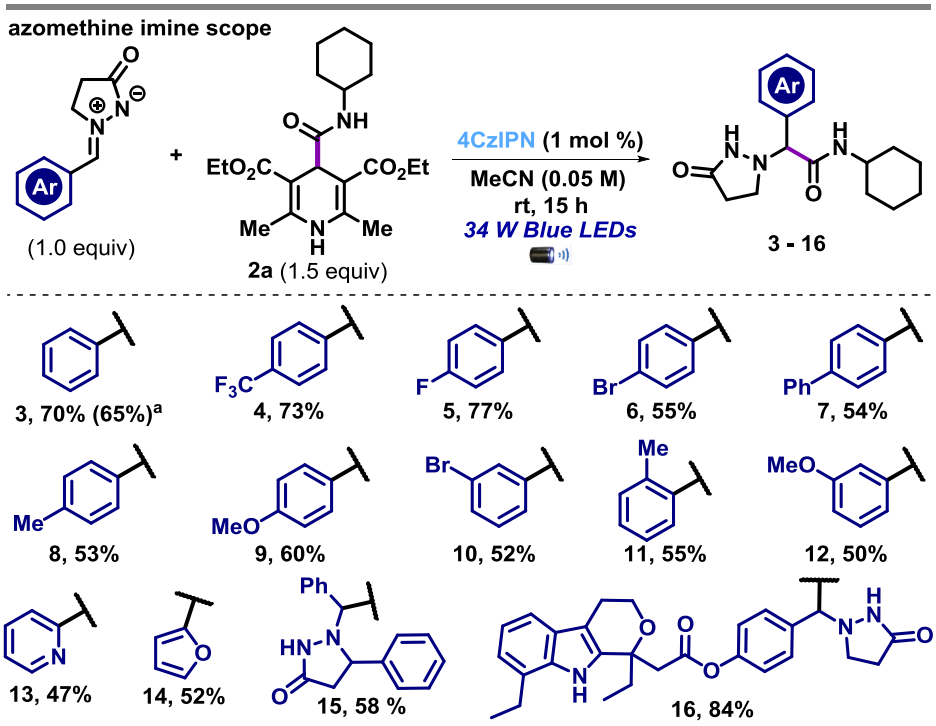

SCHEME 2.10 - Scope for the carbamoylation of azomethine imines. Reactions performed at room temperature for 15 h under blue LED irradiation and using **azomethine imine** (0.15 mmol), **carbamoyl radical precursor** (1.5 equiv, 0.225 mmol), **4CzIPN** (1 mol %) in MeCN (3.0 mL). The yields refer to isolated compounds after purification. [a] 1.0 mmol scale.

Recently, the reactivity of nitrones within the context of photoredox catalysis has also been reported to undergo (3 + 2) cycloadditions[33] and react in radical addition reactions with aromatic aldehydes,[34] tertiary amines,[35] fluorinated groups,[36] imidazo[1,2-*a*]pyridines[37] and *α*-

[33] (a) HAUN, G.; PANEQUE, A. N.; ALMOND, D. W.; AUSTIN, B. E. & MOURA-LETTS, G. Synthesis of chromenoisoxazolidines from substituted salicylic nitrones via visible-light photocatalysis". Org. Lett. **21**: 1388, 2019; (b) JANG, G. S.; LEE, J.; SEO, J. & WOO, S. K. "Synthesis of 4-isoxazolines via visible-light photoredox-catalyzed [3 + 2] cycloaddition of oxaziridines with alkynes". Org. Lett. **19**: 6448, 2017; (c) ZHENG, L.; GAO, F.; YANG, C.; GAO, G.-L.; ZHAO, Y.; GAO, Y. & XIA, W. "Visible-light-mediated anti-regioselective nitrone 1,3-dipolar cycloaddition reaction and synthesis of bisindolylmethanes". Org. Lett. **19**: 5086, 2017.

[34] YE, C.-X.; MELCAMU, Y. Y; LI, H.-H.; CHENG, J.-T.; ZHANG, T.-T.; RUAN, Y.-P.; ZHENG, X.; LU, X. & HUANG, P.-Q. "Dual catalysis for enantioselective convergent synthesis of enantiopure vicinal amino alcohols". Nat. Commun. **9**: 1, 2018.

[35] LIU, Y.-C.; ZHENG, X. & HUANG, P.-Q. "Photoredox catalysis for the coupling reaction of nitrones with aromatic tertiary amines". Acta Chim. Sinica. **77**: 850, 2019.

[36] SUPRANOVICH, V. I.; LEVIN, V. V.; STRUCHKOVA, M. I. & DILMAN, A. D. "Photocatalytic reductive fluoroalkylation of nitrones". Org. Lett. **20**: 840, 2018.

[37] TANG, F.; GUAN, Z. & HE, Y.-H. "Free regioselective carbonylation of imidazo[1,2-*a*]pyridines via photoredox catalysis using nitrones". Asian J. Org. Chem. **8**: 867, 2019.

amino acids.[38] Considering the importance of this system to easily access nitrogen containing compounds and the presence of *N*-hydroxylamines in pharmaceuticals,[39] we were curious if nitrone derivatives could be amenable to our optimized reaction conditions. To our delight, the carbamoylation proceeded well for all cases, affording the respective phenylglycine amide-derivatives **17**-**19** in good yields (**SCHEME 2.11**).

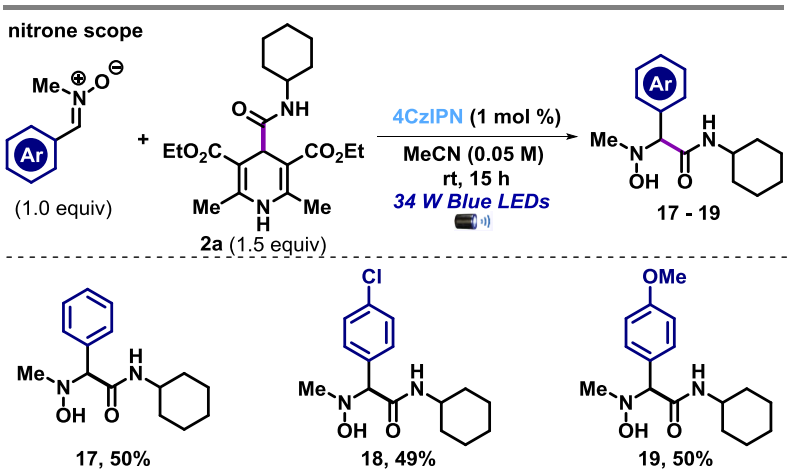

SCHEME 2.11 - Scope for the carbamoylation of nitrones. Reactions performed at room temperature for 15 h under blue LED irradiation and using **nitrone** (0.15 mmol), **carbamoyl radical precursor** (1.5 equiv, 0.225 mmol), **4CzIPN** (1 mol %) in MeCN (3.0 mL). The yields refer to isolated compounds after purification.

The growing application of modified peptides as drug candidates, lead us to evaluate the feasibility of the developed visible-light mediate protocol for the direct installation of proteinogenic amino acids across the azomethine imine scaffold – such combination allows in a single event, the synthesis of non-natural amino acids and the assembly of modified peptides (**SCHEME 2.12, top, left**).

Gratifyingly, the reaction tolerated a broad scope of amino acid derivatives, including those containing nonpolar side chain (*L*-Val, *L*-Ala, *L*-Pro, *L*-Met and *L*-Ile), polar uncharged (*L*-Ser) and aromatic systems (*L*-Tyr, *L*-Trp and *L*-Phe) which could smoothly be transformed with good chemical yields (compounds **20**-**30**). Non-proteinogenic amino acids from the *L*−(+)-*α*-phenylglycine and 2-methylalanine were nicely incorporated to the azomethine imine providing the compounds **31** and **32**, respectively.

[38] LI, H.-H.; LI, J.-Q.; ZHENG, X. & HUANG, P.-Q. 'Photoredox-catalyzed decarboxylative cross-coupling of *α*-amino acids with nitrones". Org. Lett. **23**: 876, 2021.

[39] (a) DEROSA, T. F. Significant Pharmaceuticals Reported in US Patents, Vol. 1; Elsevier Science, 2007; (b) MIRET-CASALS, L.; BAELO, A.; JULIÁN, E.; ASTOLA, J.; LOBO-RUIZ, A.; ALBERICIO, F. & TORRENTS, E. "Hydroxylamine derivatives as a new paradigm in the search of antibacterial agents". ACS Omega. **12**: 17057, 2018.

To further demonstrate the versatility of our method, we next turned our attention to explore the reactivity of dipeptides with the azomethine imine **1a** (**SCHEME 2.12, top, right**). Pleasantly, the protocol allowed the synthesis of tripeptides containing the modified phenylglycine residue in good to high yields (compounds **33**-**39**), showcasing possible opportunities for exploration of bioconjugation strategies. The dipeptides scope included sequences having *L*-Val, *L*-Met, *L*-Phe, *L*-Leu, *L*-Pro, *L*-Ser, *L*-Ile and *L*-Phg residues and which are useful handle groups for further modification of the peptide side chain. Notably, oxidation labile methionine residues were well tolerated under our protocol.

As a further demonstration of the utility of this new radical addition protocol, we examined its capacity to generate hybrid-architecture containing natural products and medicinal agents (**SCHEME 2.12, bottom, left**). As shown, the pendant steroid lithocholic acid exhibited good reactivity with **1a**, giving rise to the highly functionalized adduct **40** in moderated chemical yield. Moreover, drug-like small molecules from the antiepileptic pregabalin and memantine, which is used in the treatment of the Alzheimer's disease, were successfully installed onto **1a** in good to excellent yield (compounds **41** and **42**, respectively).

Our method is also amenable to other secondary and tertiary amides with unmasked functional handles groups (**SCHEME 2.12, bottom, right**). Likewise, aromatic, and aliphatic carbamoyl radicals were successfully installed, as the electron poor 3,5-CF_3-aromatic carbamoyl radical (**47**). Unprotected functional groups including alkyne (**45**), alkene (**46**), triethyl silicate (**48**), and phenol (**49**) did not dramatically affect the reaction outcome affording the respective carmoylated products in moderate to good yields. Finally, we demonstrate obtaining the tertiary amides derived from pyrrolidine (**51**) and piperidine (**52**) in good yields as well.

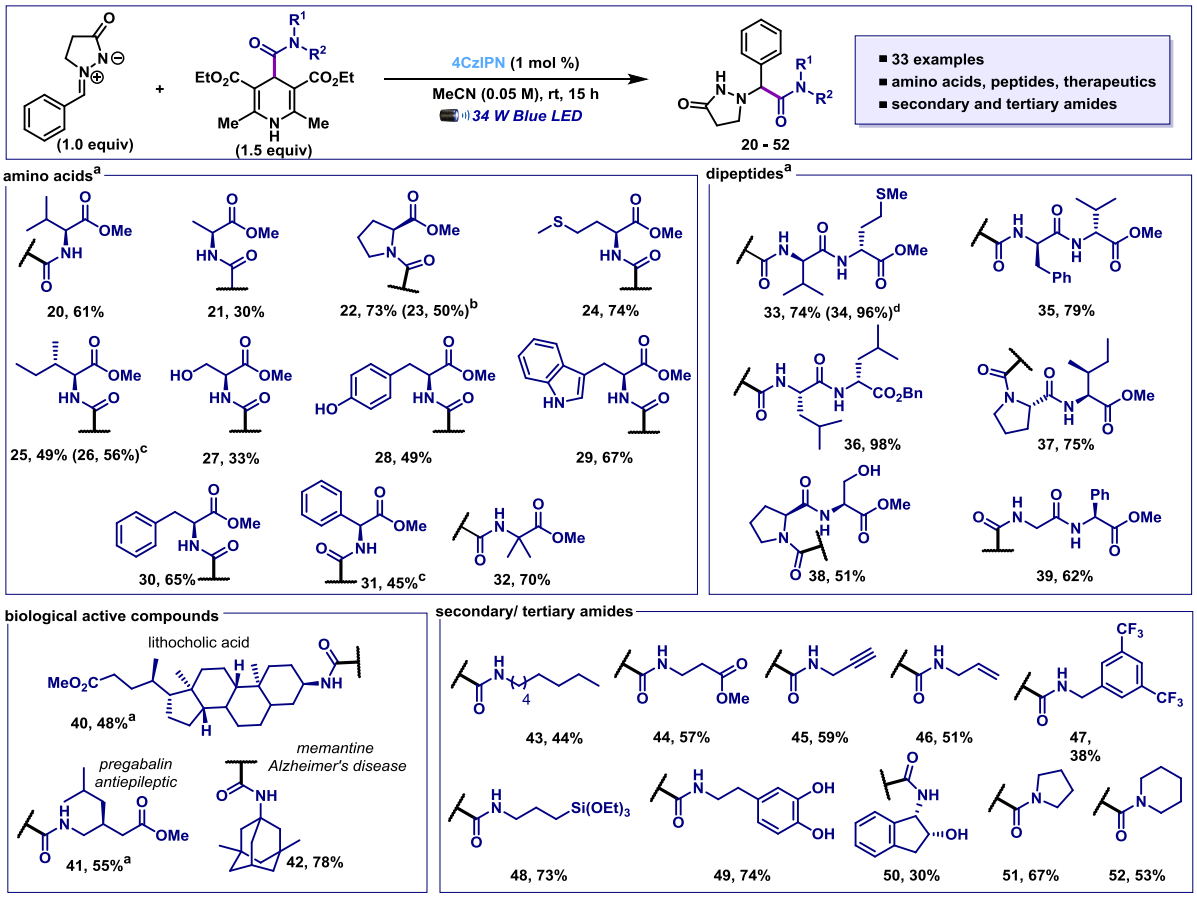

SCHEME 2.12 - Scope for the carbamoylation of azomethine imines. Reactions performed at ambient temperature for 15 h under blue LED irradiation and using **azomethine imine** (0.15 mmol), **carbamoyl radical precursor** (1.5 equiv, 0.225 mmol), **4CzIPN** (1 mol %) in MeCN (3.0 mL). The yields refer to isolated compounds after purification. [a] Compounds obtained as a mixture of 1:1 dr. [b] Using the 3-phenyl substituted pyrazolidinone azomethine imine. [c] Using the *p*-$CF_3C_6H_4$ azomethine imine. [d] Using the *p*-BrC_6H_4 azomethine imine.

To showcase the utility and importance of our carbamoylated products, we next subjected examples of obtained analogues to late-stage structural modification (**SCHEME 2.13**). The pyrazolidinone moiety of the obtained structures can be considered a masked form for the nonproteinogenic amino acid β-alanine. Notably, the primary amide group is a key structural motif as useful building blocks and presented in many pharmaceuticals and therefore routinely used in medicinal chemistry programs. The carbamoylated product **3** could be selectively reduced, using pre-treated Raney Ni under H_2 atmosphere at room temperature, delivering the amino propanamide **53** (**SCHEME 2.13a**). The product containing the *L*-Ala residue **21** was sequentially submitted to the same reductive condition affording the primary amide **54** (**SCHEME 2.13b**).

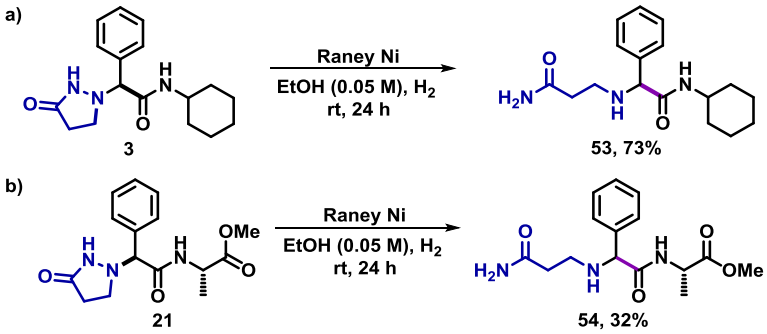

SCHEME 2.13 - Reductive cleavage of the pyrazolidinone moiety. Reactions performed on 0.2 mmol scale using 700 mg of **Raney Ni** 2800 previously washed with EtOH and under H_2 atmosphere using a gas filled balloom.

Lastly, a series of control experiments were conducted to better rationalize the sequence of events presented in the reaction mechanism.

UV-Vis Absorption Spectroscopy

In relation to the ground state characterization of substrate **2a**, we measured the absorption value through UV-Visible (UV-vis) absorption spectroscopy. From a qualitative point of view, the UV-vis spectroscopy provides us with the information about which chromophores are capable to be excited under the employed portion of light ($\lambda = 456$ nm), preventing side reactions from occurring. Melchiorre have reported that 4-alkyl-1,4-dihydropyridines (alkyl-DHP) can directly reach the electronically excited state (alkyl-DHP*) upon light absorption ($\lambda = 405$ nm) leading to the generation of C(sp^3)-centered radicals without the need for an external photocatalyst.[40]

The UV-Vis spectra of the cyclohexylamine-derived dihydropyridine **2a** showed an absorption maximum at λ = 352 nm (**FIGURE 2.3**) This value ruled out the possibility of occurring a direct excitation under the blue LED irradiation source employed in this study (λ = 456 nm). At its wavelength, the only active specie is the photocatalyst 4CZIPN, which exhibits absorption at 507 nm.[41]

[40] BUZZETTI, L.; PRIETO, A.; ROY, S. R. & MELCHIORRE, P. “Radical-based C-C bond-forming processes enabled by the photoexcitation of 4-alkyl-1,4-dihydropyridines”. Angew. Chem. Int. Ed. **56**: 15039, 2017.
[41] UOYAMA, H.; GOUSHI, K.; SHIZU, K.; NOMURA, H. & ADACHI, C. “Highly efficient organic light-emitting diodes from delayed fluorescence”. Nature. **492**: 234, 2012.

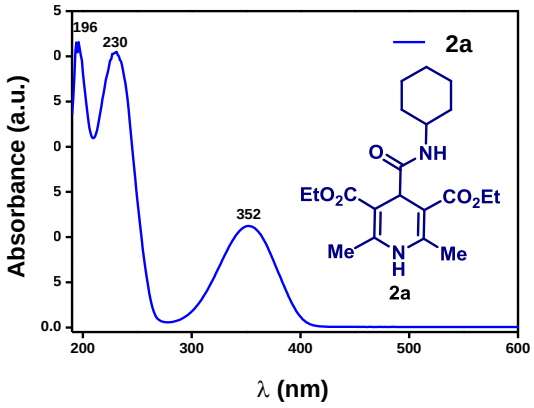

FIGURE 2.3 - Absorption spectra of a solution of **2a** (MeCN, 0.9 uM).

Wangelin and coworkers demonstrated in their work that the addition of the carbamoyl radical from 1,4-dihydropyridines to activated olefins is likely to occur via an EDA complex between the reactants.[27] An evident bathochromic shift was observed when combining both reagents with considerable absorbance at λ = 455 nm. To exclude this possibility, the UV-Vis spectra of **1a**, **2a**, and of their equimolar combination were acquired. The result ruled out a possible formation of an EDA complex since no bathochromic shift could be noticed when the spectra of the equimolar mixture was recorded. It was observed, in this case, a sum of the isolated measurements (**FIGURE 2.4**).

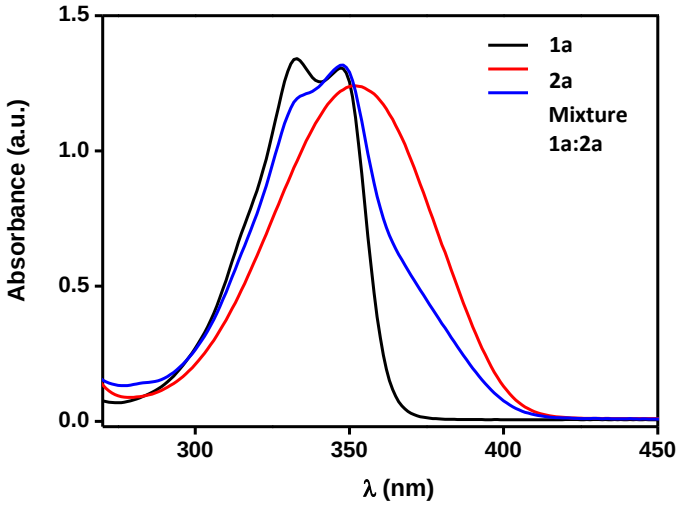

FIGURE 2.4 - UV-Vis spectra of azomethine **1a** (black line, 0.05 M in MeCN), 4-carbamoyl-1,4-dihydropyridine **2a** (red line, 0.05 M in MeCN), and the equimolar mixture of **1a** and **2a** (blue line, 0.05 M in MeCN).

Fluorescence Quenching Experiment

Then, another useful analysis as an indicative of the reaction mechanism was performed based on the emission profile of the photocatalyst fluorophore. As highlighted in the introductory chapter, the deactivation of excited states leads to the luminescence event and the luminescence quenching refers to any process that decreases the fluorescence/ phosphorescence intensity of a sample.

Luminescence can be characterized as fluorescence (from $^*S_1$ states) or phosphorescence (from $^*T_1$ states) and the rates of these events range from milli/micro to nanoseconds. The phosphorescence event, as it involves a spin prohibited transition ($^*T_1$ to S_0), decays more slowly to the ground state, causing the excited triplet state to have a longer lifetime, enough to it engage in a bimolecular process.

Collisional quenching with another reactive specie, called quencher, is the most common deactivation event and implies in a kinetic competition, which is governed by the Stern-Volmer equation. This analysis correlates the emission intensity of the fluorophore as the concentration of quencher in the sample varies. Therefore, it is an experiment that provides useful information about the species that interact with each other in the excited state deactivation process – giving us an indicative if the event is more likely to proceed via an oxidative or reductive quenching.

The collisional quenching of fluorescence is given by the Stern–Volmer relationship:

$$\frac{\mathbf{I0}}{\mathbf{I}} = \mathbf{1} + \mathbf{K}\boldsymbol{D}\ \mathbf{x}\ [\mathbf{Q}]$$

$$\mathbf{K}\boldsymbol{D} = \mathbf{k_q}\ \mathbf{x}\ \mathbf{t_0} \quad [\text{Eq. 1}]$$

Considering:

I_0 = intensity, or rate of catalyst fluorescence, without the quencher

I = = intensity, or rate of catalyst fluorescence, with the quencher

K_D = Stern-Volmer quenching constant

[Q] = concentration of the quencher

k_q= bimolecular quenching constant

t_0= lifetime of the emissive excited state of the catalyst without the quencher

The excited state lifetime or emission intensity of the fluorophore can be determined in the absence (I_0) and presence (I) of quencher, leading to the determination of the Stern-

Volmer quenching constant K_D. The quenching analysis is represented as the plot of I_0/I as a function of [Q] with a slope equal to K_D. The bimolecular quenching constant (kq) derived from such measurement is considered an indicative about the efficiency of the quenching process.

The Stern-Volmer relationship considers the fluorescence intensities observed in the absence and presence of quencher. Since the fluorescence intensity observed for a fluorophore is proportional to its concentration in the excited state, under continuous illumination a constant population of excited fluorophores is established. However, in the presence of a quencher, the fluorescence intensity is expected to decrease proportionally to the increase of the quencher concentration. This decrease occurred since the quenching depopulates the excited state without fluorescence emission.[42]

In this experiment, the fluorescence measurements were acquired at room temperature using a RF-5301 PC Fluorescence Spectrophotometer with excitation slits open at 1.5 nm and emission slit open at 3 nm. The emission quenching was performed using quartz cuvettes with argon-purged solvent (MeCN). All the prepared solutions were degassed and successively added to the cuvette using a gas tight syringe through a rubber septum fitted with an argon balloon.

The emission profile of continuously irradiated solution of 4CZIPN was recorded initially in absence of quencher, with maximum emission at λ = 546 nm. Then, a solution of the quencher **2a** in acetonitrile was successively added, leading to the concentrations indicated in **FIGURE 2.5**, and the corresponding emissions were recorded. As observed from the ratio of $\mathbf{I_0/I}$ vs λ **(nm)** an obvious radiative deactivation of the excited states occurred as the quencher concentration was increased.

[42] LAKOWICZ, J. R. Quenching of Fluorescence. In: Principles of Fluorescence Spectroscopy. Springer, Boston, MA, 1983. p. 277.

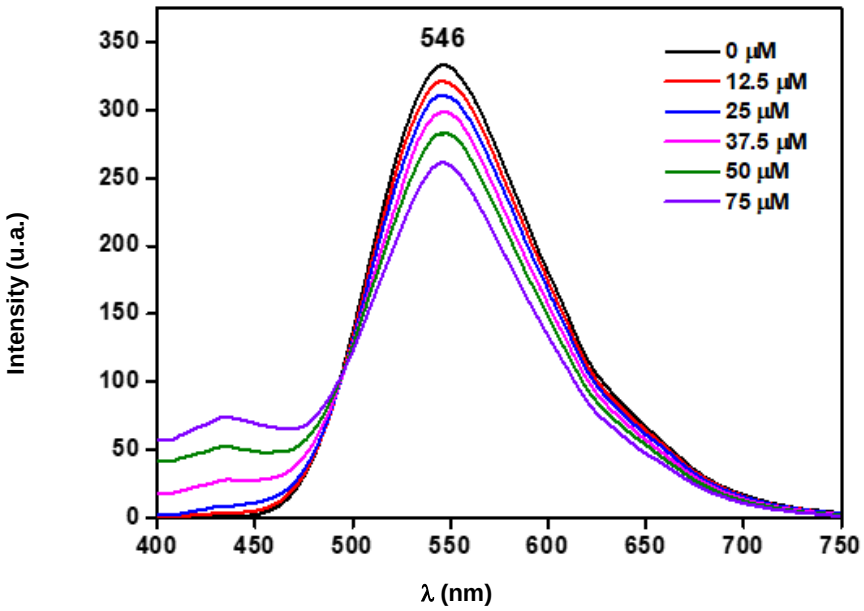

FIGURE 2.5 - Emission of the 4CZIPN solution (black line, MeCN) recorded in presence of increasing amounts of DHP **2a** as quencher.

The plot I_0/I as a function of [Q] following the Stern-Volmer equation gives a linear relationship as showed in the **FIGURE 2.6**:

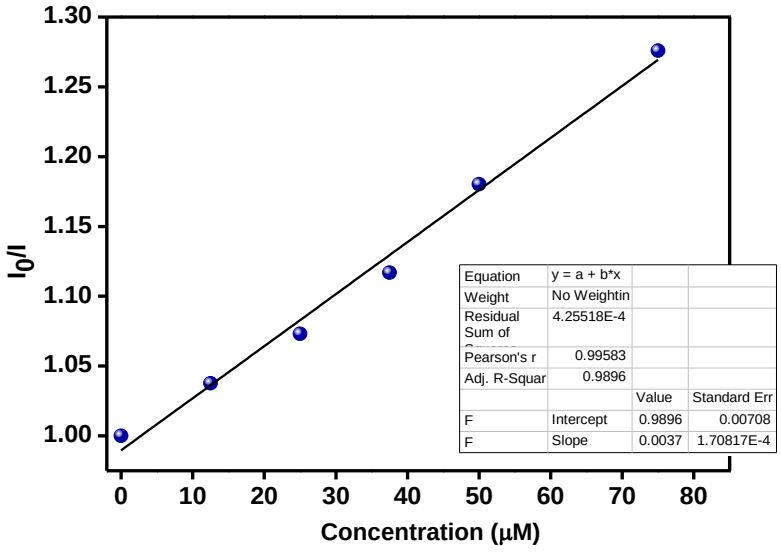

FIGURE 2.6 - Stern-Volmer plot analysis derived from the data extracted from FIGURE 2.5.

The Stern–Volmer Relationship

The data obtained from the Stern-Volmer analysis allowed the determination of the kinetic of the photophysical intermolecular deactivation process, following the Stern–Volmer relationship:

The quencher rate coefficient was determined from the Stern-Volmer equation (1) and using a lifetime of t_0 = 5.1 μs for 4CZIPN.

$$\mathbf{K_q} = 7.2 \times 10^8 \text{ L. mol}^{-1}\text{. s}^{-1}$$

The resulting bimolecular quenching constant (k_q) indicates the efficiency of quenching or the accessibility of the fluorophore to the quencher. The value matches the typical diffusion-controlled quenching values ($k_q \sim 10^{10}$ M^{-1}. s^{-1}) and indicates a high efficiency of quenching of **2a**. Values of k_q smaller than the diffusion-controlled value can be resulted of steric shielding of the fluorophore or a low quenching efficiency.[42]

Trapping Experiment

The fleeting nature of radical intermediates makes their isolation and characterization difficult to be achieved. Due to the paramagnetic nature of this species, they are susceptible to be detected by electron paramagnetic resonance (EPR) spectroscopy. Another indicative of radical species generated in situ can be observed by trapping them with radical scavengers, as the widely employed TEMPO (2,2,6,6-Tetramethyl-1-piperidinyloxy).

In order to elucidate the radical species being formed in our carbamoylation protocol and gain insight into the reaction mechanism, the radical-trapping experiment was carried out using TEMPO as radical scavenger. The starting material **1a** (0.15 mmol, 1.0 equiv), **2a** (0.22 mmol, 1.5 equiv), the photocatalyst 4CzIPN (1 mol %) and TEMPO (3.0 equiv) were dissolved in 3.0 mL of MeCN in a dried Schlenk tube equipped with a stir bar. The Schlenk tube was sealed with PTFE/silicon septum and connected to a vacuum line and the solution was degassed 3 times via a freeze-pump-thaw procedure. The resulting solution was stirred for 15 h at ~5 cm from the irradiation source (a 34 W Kessil H150 blue LED lamp) (**SCHEME 2.14**).

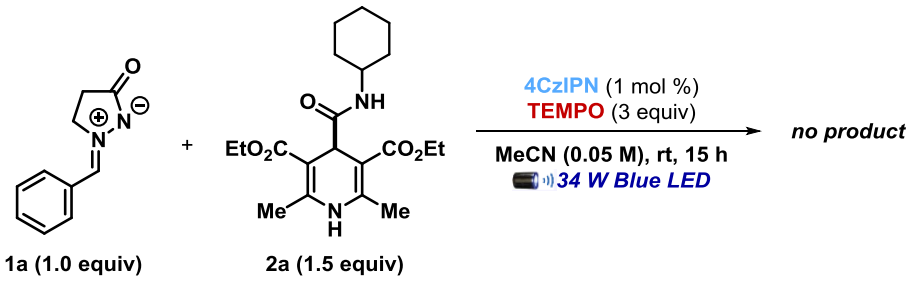

SCHEME 2.14 - Radical-trapping experiment in the presence of TEMPO.

After the reaction time, the product **3** could not be noticed on TLC plate. An aliquot was removed from the crude reaction and a sample was prepared in 1 % HCOOH/ MeOH and analyzed by mass spectrometry using an ACQUITY UPC^2-MS apparatus through direct infusion.

The MS full scan experiment indicated the presence of the radical scavenger and the starting material **1a** as showed in **FIGURE 2.7**. Additionally, the peak at *m/z* 283.1702 could be evidence of the trapping of the carbamoyl radical by **TEMPO** (**I**). The peak at *m/z* 332.1838 is associated with the direct addition of the radical scavenger to the azomethine imine (**II**), since the mismatch of the redox potentials of the iminium ion and the photocatalyst do not supports the formation of the reduced azomethine imine, as discussed in the mechanism proposal. Besides these peaks, other intermediates were evidenced as showed in the **FIGURE 2.7**.

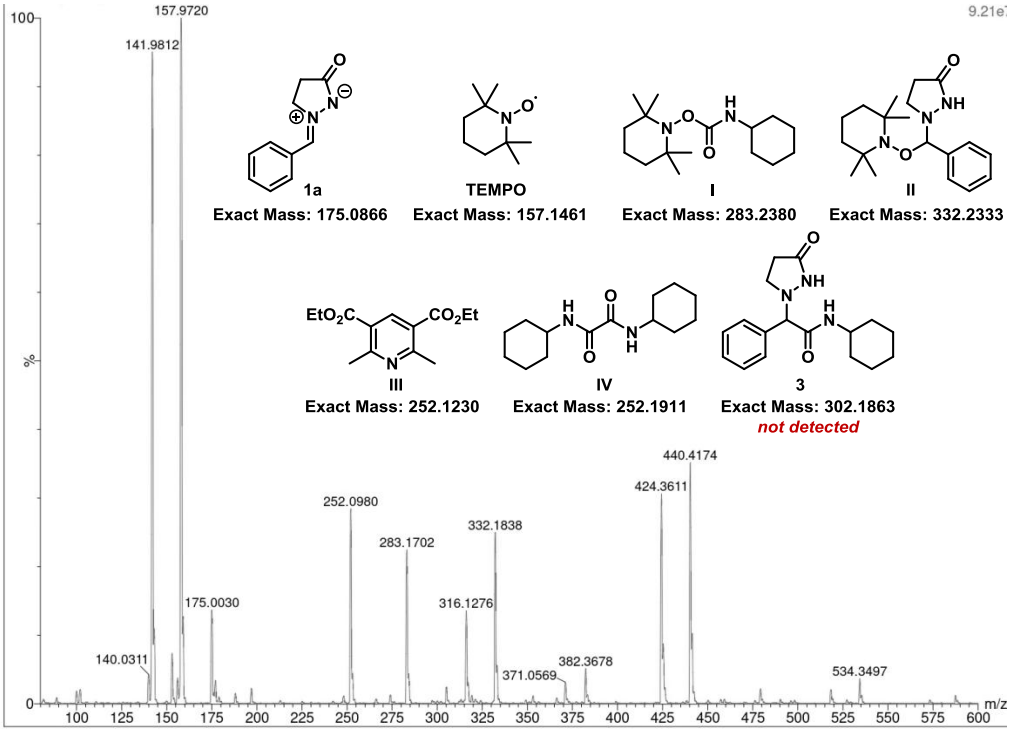

FIGURE 2.7 - MS full scan experiment via direct infusion of the reaction crude. The exact mass of compounds are reported as the $[M+H]^+$ adduct.

Control Reactions

Control experiments were carried out in order to investigate the reactivity of the reaction components under photolytic conditions. Thus, the reactions were conducted under the optimized condition in **a)** the absence of the carbamoyl radical source and in **b)** the absence of azomethine imine as the trapper of the generated radical. The reaction crudes were analyzed by HRMS (ESI-QTOF) (**FIGURE 2.8**).

As seen in **FIGURE 2.8a**, the reaction in the absence of the radical precursor **2a** and under the optimized reaction condition only led to the recovery of starting material **1a**. The azomethine imine could be observed on TLC plate after the reaction time and was characterized by ^{1}H NMR confirming its structure. Although there are reports of dimerization of this specie, it is only known to occur under more energetic UV irradiation. Thus, we expected starting material **1a** to be recovered without side transformations.

DHPs are easily oxidized given their average oxidation potential value (~1.0 V vs SCE). In the presence of the photocatalyst PC and under visible light irradiation, the triplet excited state *PC of the photocatalyst is strongly oxidizing and leads to the oxidation of **2a**.

Further fragmentation of the system gives rise to the corresponding pyridine and the carbamoyl radical.

In the absence of the trapping reaction component **1a**, the dimerization product of this specie was observed (**FIGURE 2.8b**). Furthermore, we detected via HRMS the presence of starting material **2a** and pyridine. It is worth noting that during the evaluation of the reaction scope we observed (via ^{1}H NMR – **FIGURE 2.9**) the formation of dimers from the carbamoyl radical-radical coupling. This is one factor that we believe contributes to the transformation yield not being excellent in all cases.

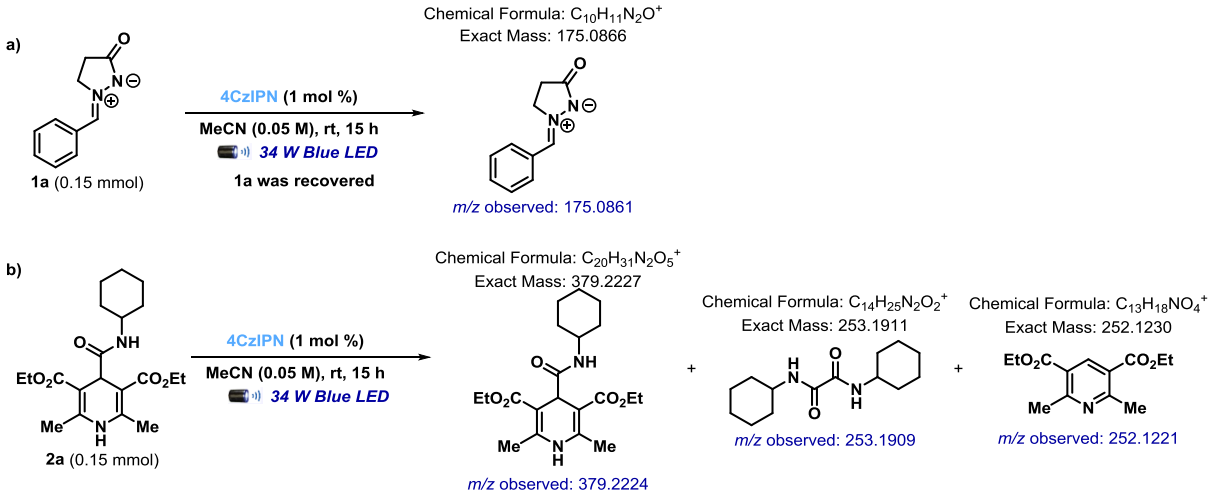

FIGURE 2.8 - Control experiments to evaluate the reactivity of the isolated components under the optimized reaction condition.

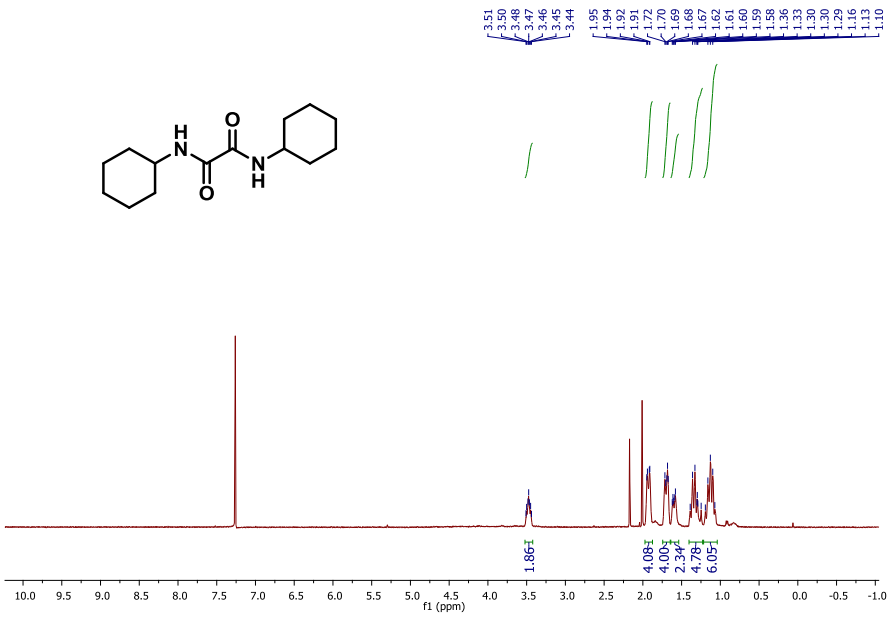

FIGURE 2.9 – ^{1}H NMR ($CDCl_3$, 400 MHz) spectra of the carbamoyl dimer. ^{1}H NMR (400 MHz, $CDCl_3$) δ 3.47 (ddd, J = 14.5, 10.5, 3.9 Hz, 2H), 1.95 – 1.91 (m, 4H), 1.72 – 1.67 (m, 4H), 1.62 – 1.58 (m, 2H), 1.39 – 1.25 (m, 4H), 1.19 – 1.07 (m, 6H).

After all these considerations provided by the experiments described above, a plausible mechanism is outlined in **SCHEME 2.15**. Under 456 nm blue LED irradiation, the photocatalyst **4CzIPN** ($\lambda = 507$ nm) is efficiently converted to its long-lived triplet excited state **4CzIPN*** (μ = 5.1 ns). The **4CzIPN*** ($E_{1/2}(PC^*/PC^-)$ = + 1.35 V *vs* SCE) is oxidizing enough to promote the SET oxidation of **2a** (E_{ox} 2a = + 1.21 V *vs* SCE), which after fragmentation, generates the corresponding carbamoyl radical **A**. The addition of **A** to the azomethine iminium **1a** gives rise to the amidyl intermediate **B** after a spin-center shift event. Further, this reactive intermediate undergoes SET reduction with the reduced photocatalyst to provide, after protonation, the desired product **3**. It is important to emphasize that the SET reduction of **1a** should not be feasible given its highly negative reduction potential (E_{red} 1a = - 1.6 V *vs* SCE and $E_{1/2}(PC^+/PC^*)$ = - 1.04 V *vs* SCE). Moreover, the fluorescence quenching study within the redox potentials corroborates to identify the reductive quenching of the photocatalyst as the initial mechanistic step.

Additionally, the reaction in the presence of the radical scavenger TEMPO (3 equiv) did not lead to the formation of the product and the TEMPO adduct **I** was detected. Control experiments also disclosed the role of the irradiation source and the photocatalyst for the carbamoylation reaction outcome.

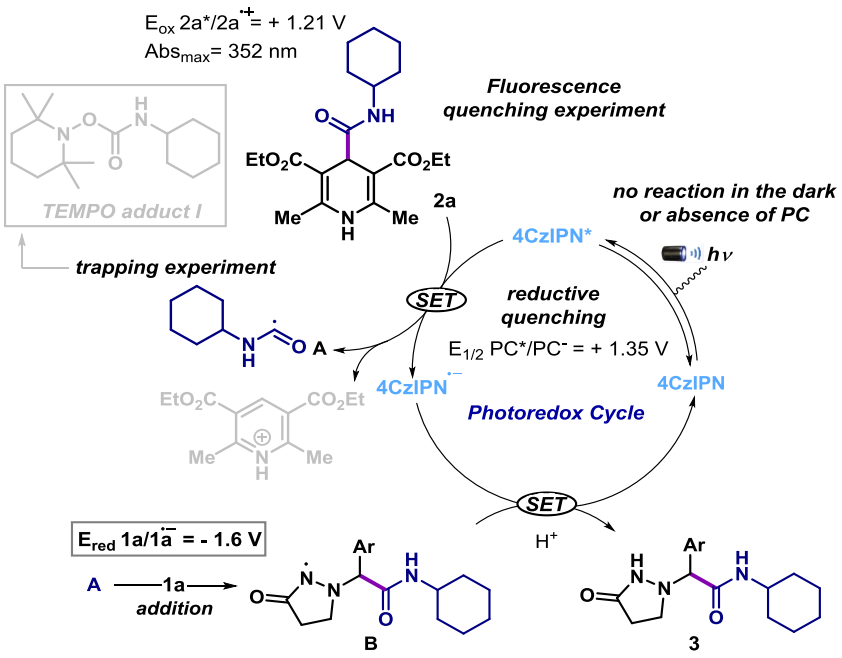

SCHEME 2.15 - Proposed mechanism for the carbamoylation of azomethine imine ions under the photocatalytic protocol.

3. Conclusion

In this work we have demonstrated the application of azomethine imine as powerful electrophilic partners in photoredox-mediated transformations. The approach disclosed herein complements the protocols available in the literature regarding the exploration of these reactive species under photocatalytic conditions and has showed that there is still a gap to be filled that goes beyond classic cycloaddition reactions.

The chosen carbamoyl radical precursor, DHPs, proven to be an efficient source of amide synthons which can then be engaged in photoredox protocols. The DHPs have the advantage of being derived from commercially available aldehydes and amines and are prepared in a two-step sequence. The developed photocatalytic protocol for the synthesis of amide-containing compounds complements those already described in the literature and, importantly, is an alternative to traditional methods that make use of harsh conditions, using stoichiometry amounts of reactants and leading to byproducts difficult to be eliminated. Thus, our method can be considered an enhanced strategy for amide bond installation since the amide synthon is ready to be installed and generated under mild reaction conditions. The disclosed approach also complements the few reports in the literature using DHPs as

carbamoyl radical source, contrary to the well-explored applications as proton, alkyl, and acyl radical sources.

The milder conditions are amenable to transformations aiming at late-stage functionalization, modification of biomolecules, natural products, and drugs. As described in our study, all these classes of versatile and important structures were tolerated in the carbamoylation reaction.

In summary, we demonstrated a robust photocatalytic strategy for amidation of azomethine imines ions via a C-C bond coupling by applying the generation of carbamoyl radicals from readily available DHPs. This technology allowed the straightforward access to a wide range of carbamoylated compounds through a simple and versatile protocol, using only 1 mol% of photocatalyst and a small excess of the radical precursor. Crucially, the radical addition platform displayed high functional tolerance and amenability towards biologically-like relevant scaffolds, as amino acids, proteins, and drugs, and compounds containing fragile functionalities as tertiary bonds and reactive groups.

Therefore, the protocol represents a new strategy for the structural diversification of the chemical space of these important classes of compounds. Additionally, the direct application for obtaining primary amides from the simple reductive cleavage of the pyrazolidinone nucleus was demonstrated, leading to β–alanine derivatives containing multiple reactive sites liable to orthogonal derivatizations.

4. Experimental Section

General Considerations

Unless otherwise stated, all reagents were purchased from commercial sources and used without additional purification. THF was freshly distilled under argon from the sodium anion of benzophenone. All other anhydrous solvents were purchased or obtained from in house solvent purification towers. HPLC grade solvents were used in the photocatalyzed reactions.

All air or moisture-sensitive reactions were conducted in flame dried glassware under nitrogen atmosphere.

All reactions were monitored by thin layer chromatography using Merck silica gel aluminum sheets 60 F254, using hexane/acetone, hexane/EtOAc or DCM/MeOH as mobile phase and visualized by UV lamp, permanganate and vanillin stains.

Flash column chromatography was accomplished using silica gel 60 (230-400 mesh) and hexane/acetone, hexane/EtOAc or DCM/MeOH as eluent systems.

^{1}H and ^{13}C spectra were recorded on Brucker NMR spectrometers at 298 K. ^{1}H (400 MHz) and ^{13}C (126 MHz) NMR chemical shifts are reported relative to internal TMS (δ = 0.00 ppm; $CDCl_3$: 7.26 ppm for ^{1}H nuclei and 77.16 for ^{13}C nuclei); (δ = 0.00 ppm; DMSO-*d6*: 2.50 ppm for ^{1}H nuclei and 40.00 for ^{13}C nuclei); (δ = 0.00 ppm; CD_3OD: 3.31 ppm for ^{1}H nuclei and 49.0 for ^{13}C nuclei). Chemical shifts are given in ppm. Coupling constant values *J* are given in Hertz. The multiplicities are described as: brs = broad signal, s = singlet, d = doublet, t = triplet, q = quartet, dd = doublet of doublets, dt = doublet of triplets, dq = doublet of quartets, ddd = doublet of doublet of doublets, dddd = doublet of doublet of doublet of doublets and m = multiplet.

Mass spectra data were recorded at Waters Technologies of Brazil. The samples were solubilized in acetonitrile/water 90:10 and analyzed by ASAP probe in the Xevo G2-XS QTOF spectrometer. Spectra were acquired in MS mode.

The diastereoisomeric ratios were determined by NMR analysis of crude reactions.

Photoreactions

A 34 W Kessil H150 blue LED (emission: 456 nm) was used as the visible light source. All chemicals and photocatalysts were purchased and used as received from suppliers unless otherwise noted. The photocatalyst 2,4,5,6-Tetra(carbazol-9-yl)isophthalonitrile 4CzIPN was prepared following the reported experimental procedure.[43] HPLC grade solvents were used in the photocatalyzed reactions.

Experimental Set-Up

Photoredox reactions were kept under blue LED irradiation using Schlenk tubes as reaction vessels (up to 3 Schlenk tubes per reactor). They were placed at approximately 7 cm from the irradiation source and the temperature (~30 °C) was controlled using a desk fan placed above the photoreactor.

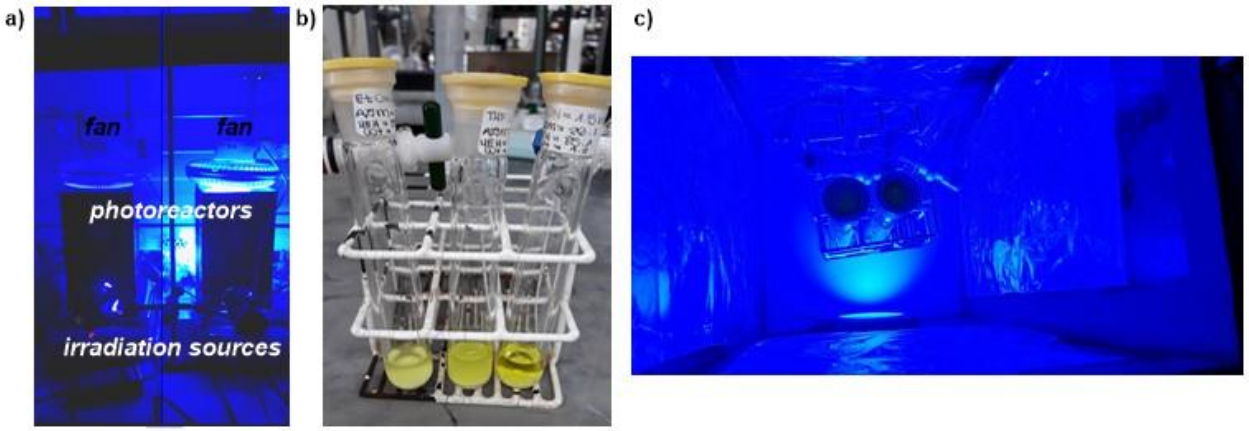

FIGURE S1 - Experimental set-up for the photocatalyzed reactions. a) Photoreactors with the irradiation source and the external fan. b) The Schlenk tubes filled with the reaction mixture. c) Schlenk's distance from the irradiation source inside the photoreactor.

Starting Materials Preparation

Azomethine Imine Synthesis (3' – 16')

Pyrazolidin-3-one (S1):

[43] LUO, J. & ZHANG, J. "Donor–acceptor fluorophores for visible-light-promoted organic synthesis: photoredox/Ni dual catalytic C(sp^3)–C(sp^2) cross-coupling". ACS Catal. **6**: 873, 2016.

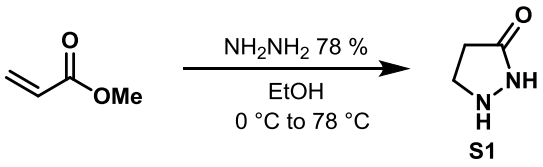

SCHEME S1- Preparation of pyrazolidin-3-one S1.

Pyrazolidin-3-one **S1** was prepared following the reported experimental procedure:[44] in a flame-dried round bottom flask a solution of hydrazine monohydrate 78 % (1.0 equiv) in absolute ethanol (4 M) was cooled to 0 °C using an ice bath. Methyl acrylate (1.0 equiv) was slowly added, and the solution was stirred at 0 °C for 30 min and then was heated to reflux using an oil bath and stirred until the reaction be completed judging by TLC analysis. The solution was concentrated under vacuum to yield the crude pyrazolidin-3-one as a clear or yellow oil. The pyrazolidin-3-one was used immediately in the next step without purification.

Azomethine Imines:

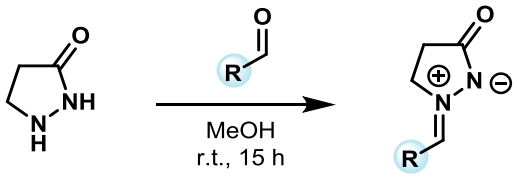

SCHEME S2 - Preparation of azomethine imines.

Azomethine imines were prepared following the reported experimental procedure:[2] The crude pyrazolidinone **S1** (1.0 equiv) obtained in the previous step and the corresponding aldehydes (1.2 equiv) were dissolved in anhydrous MeOH (1 M). The mixture was stirred at room temperature overnight and then concentrated under vacuum to remove the solvent. Et_2O was added to precipitate the product (if the precipitation does not occur, it can be promoted by the addition of few drops of hexanes followed by cooling in the freezer). The resulting solid was collected by filtration, washed with Et_2O and dried to yield the final product. For substrates that do not precipitate, the reaction crudes were purified by column chromatography using DCM/ MeOH (20:1) as eluent.

The following **azomethine imines** were used as starting materials for the scope evaluation. The reported compounds were prepared and characterized according to

[44] WINTERTON, S. E. & READY, J. M. "[3 + 2]-Cycloadditions of azomethine imines and ynolates". Org. Lett. **18**: 2608, 2016.

literature[2-6]. The compound **16**' was prepared using the same experimental procedure[2] and its spectroscopic data is reported in the appropriated session in the SI.

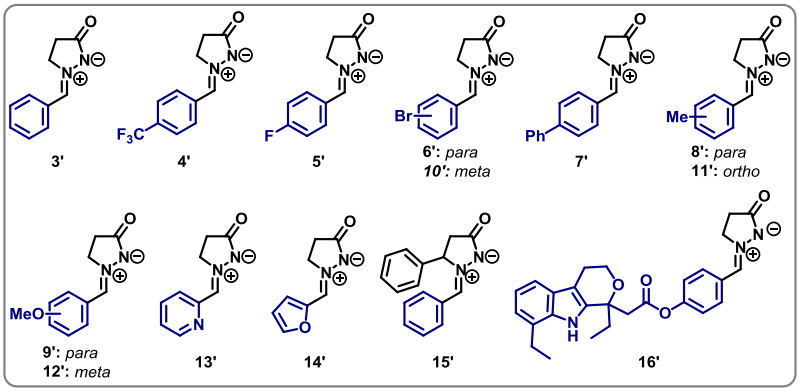

SCHEME S3 - Azomethine imines used as starting material during the scope study.

Spectroscopic data of *C*,*N*-Cyclic Azomethine Imines:

3', 4', 6', 9', 13', 15'[2]; 5', 8', 12', 14' [45]; 7' [46]; 10' [47] and 11' [48].

N-Methyl-Nitrone Synthesis (17' – 19')

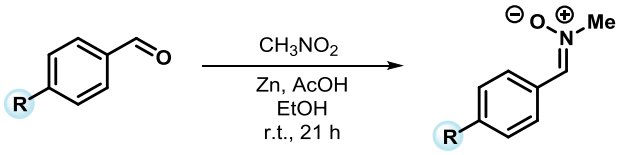

SCHEME S4 - Preparation of *N*-Methyl-Nitrones.

N-methyl-nitrones were prepared following the reported experimental procedure:[49,50] To a solution of aromatic aldehyde (1.0 equiv), nitromethane (4.0 equiv) and zinc powder (6

[45] DU, Q.; NEUDÖRFL, J.-M. & SCHMALZ, H.-G. "Chiral phosphine–phosphite ligands in asymmetric gold catalysis: highly enantioselective synthesis of furo[3,4-*d*]-tetrahydropyridazine derivatives through [3+3]-cycloaddition". Chem. Eur. J. **24**: 2379, 2018.

[46] LI, C.; WANG, C. -S.; LI, T.-Z.; MEI, G.-J. & SHI, F. "Brønsted acid-catalyzed (4 + 3) cyclization of *N*,*N*′-cyclic azomethine imines with isatoic anhydrides". Org. Lett. **21**: 598, 2019.

[47] SHINTANI, R. & FU, G. C. "A New copper-catalyzed [3 + 2] cycloaddition: enantioselective coupling of terminal alkynes with azomethine imines to generate five-membered nitrogen heterocycles". J. Am. Chem. Soc. **125**: 10778, 2003.

[48] SHINTANI, R. & HAYASHI, T. "Palladium-catalyzed [3 + 3] cycloaddition of trimethylenemethane with azomethine imines". J. Am. Chem. Soc. **128**: 6330, 2006.

[49] PAGOTI, S.; DUTTA, D. & DASH, J. "A magnetoclick imidazolidinone nanocatalyst for asymmetric 1,3-dipolar cycloadditions". Adv. Synth. Catal. **355**: 3532, 2013.

[50] ANDRADE, M. M.; BARROS, M. T. & PINTO, R. C. "Exploiting microwave-assisted neat procedures: synthesis of *N*-aryl and *N*-alkylnitrones and their cycloaddition en route for isoxazolidines". Tetrahedron. **64**: 10521, 2008.

equiv) in 95% ethanol (0.19 M) at 0 °C was added glacial acetic acid (7 equiv) dropwise over a period of 1 h. Next, the mixture was allowed to stir for 20 h at room temperature. The suspension was filtered; the filtrate concentrated under vacuum, and the crude mixture was purified by flash column chromatography using AcOEt/ MeOH (50:1) as eluent to give the corresponding nitrone.

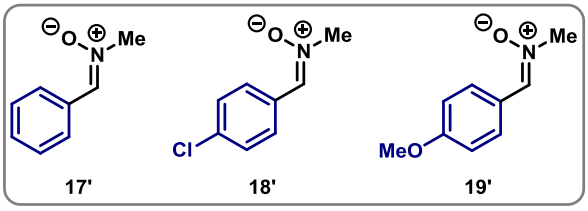

SCHEME S5 - *N*-Methyl-nitrones used as starting material during the scope study.

Spectroscopic data of *N*-Methyl Nitrones:

17', 18' [7] and 19'[8].

Carbamoyl-1,4-Dihydropyridines Synthesis (20' – 52')

Synthesis of 3,5-diethoxycarbonyl-2,6-dimethyl-1,4-dihydropyridine-4-carboxylic acid (S2)

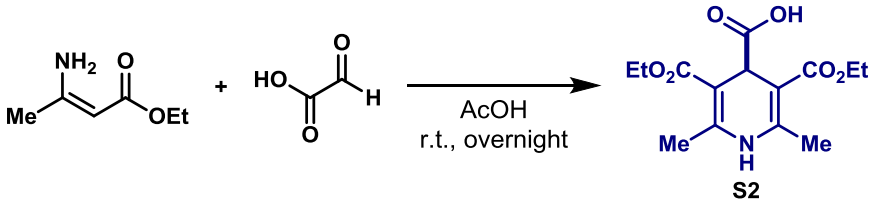

SCHEME S6 - Preparation of 1,4-dihydropyridine-4-carboxylic acid.

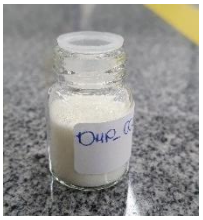

The 1,4-dihydropyridine-4-carboxylic acid was prepared following the reported experimental procedure:[51] A solution of glyoxylic acid 50 % wt in H_2O (1 equiv) was slowly added to a solution of ethyl-3-aminocrotonate (2.0 equiv) in glacial acetic acid (2.7 M) at 0 °C. A yellow precipitate is formed (**Figure S2**), and the resulting mixture was left stirring overnight at room temperature. The solid was filtered, washed with acetic acid and water, and dried under

[51] DUBUR, G. Y. & ULDRIKIS, Y. R. "Preparation of 3,5-diethoxycarbonyl-2,6-dimethyl-1,4-dihydro-isonicotinic acid and 3,5-diacetyl-2,6-dimethyl-1,4-dihydroisoni-cotinic acid and their salts". Chem. Heterocycl. Compd. **5**: 762, 1972.

reduced pressure to give the 1,4-dihydropyridine-4-carboxylic acid as a white solid (image on the left) (yield = 35 %)

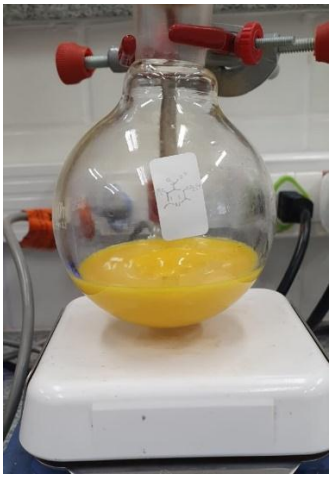

FIGURE S2 - General aspect of the reaction mixture after the glyoxylic acid addition.

4-Carbamoyl-1,4-Dihydropyridines 20' - 52'

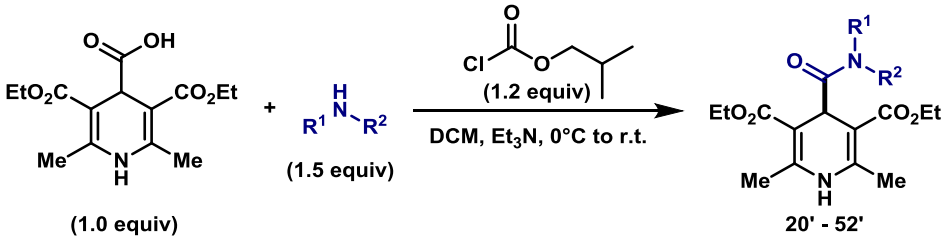

SCHEME S7 - Preparation of 4-carbamoyl-1,4-dihydropyridines 20' – 52'.

The 1,4-DHPs were prepared following the reported experimental procedure:[26] In a 50 mL round bottom flask under N_2 atmosphere, 1,4-dihydropyridine-4-carboxylic acid **S2** (1.5 mmol) was suspended in DCM (0.2 M), followed by addition of Et_3N (1.1 equiv or 2.2 equiv when using the amine hydrochloride salt). Then isobutyl chloroformate (1.2 equiv) was added dropwise at 0 °C. The resulting mixture was left to stir at 0 °C for 10 min and additional 20 min at room temperature. Next, the amine (1.5 equiv) was added, and the reaction was stirred at room temperature until completion, judging by TLC analysis. The solution was diluted with DCM, washed with saturated $NaHCO_3$ and water. The combined organic layers were dried with Na_2SO_4, concentrated, and precipitated with hexanes and filtered or purified by flash chromatography (30% Acetone in Hexanes or 2% MeOH in DCM) to afford the corresponding 4-carbamoyl-1,4-dihydropyridine.

The following **4-carbamoyl-1,4-dihydropyridines** were used as starting materials for the scope evaluation. The reported compounds were prepared and characterized according to literature.[10] The new compounds were prepared using the same experimental procedure and their spectroscopic data are reported in the appropriated session in the SI (compounds 22', 25', 31', 32', 33', 35', 36', 37', 38', 39', 40', 41', 43', 44', 45', 47', 48', 49' and 50').

Spectroscopic data of 4-carbamoyl-1,4-dihydropyridines:

20', 21', 24', 27', 28', 29', 30', 42', 46', 51', 52' [10]

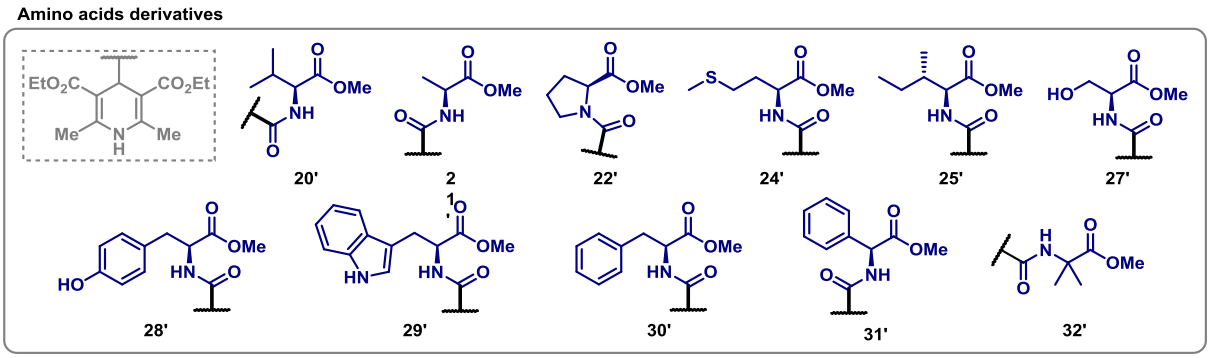

SCHEME S8 - 4-carbamoyl-1,4-dihydropyridines derived from amino acids.

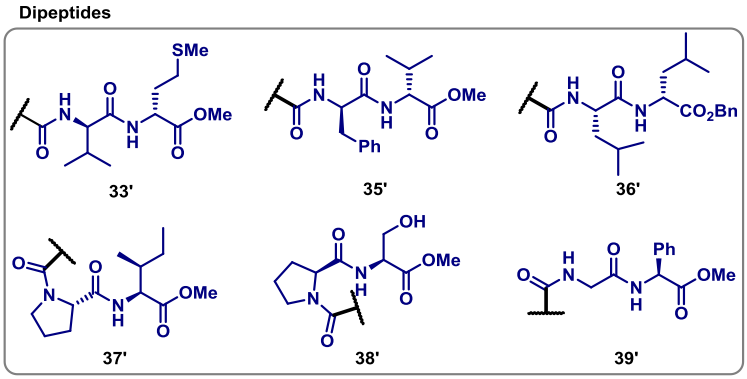

SCHEME S9 - 4-carbamoyl-1,4-dihydropyridines derived from dipeptides.

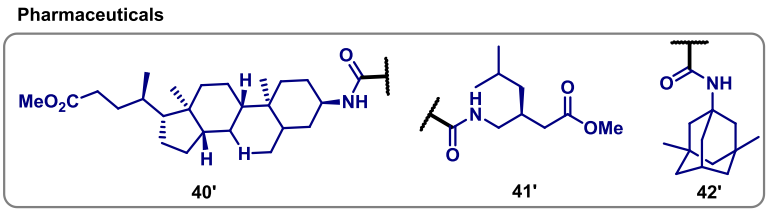

SCHEME S10 - 4-carbamoyl-1,4-dihydropyridines derived from pharmaceutical compounds.

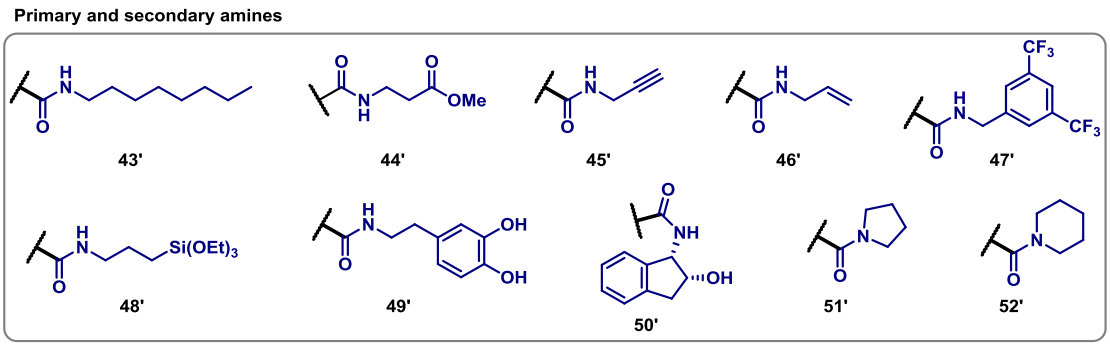

SCHEME S11 - 4-carbamoyl-1,4-dihydropyridines derived from primary and secondary amines.

General Procedure for Carbamoylation of Azomethine Imines (GP1)

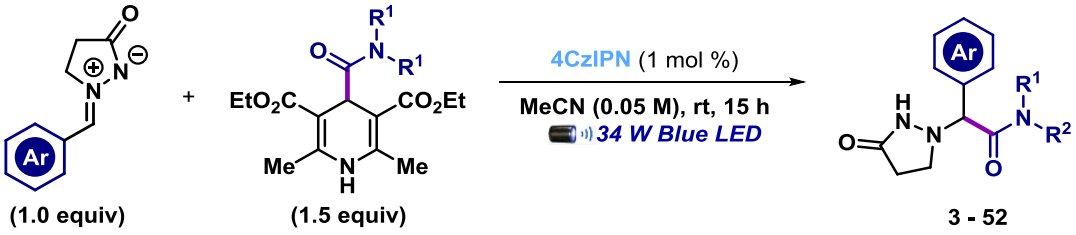

A dried Schlenk tube of borosilicate glass equipped with a stir bar was charged with the azomethine imine (0.15 mmol, 1.0 equiv), the 4-carbamoyl-1,4-dihydropyridine (1.5 equiv) and the photocatalyst 4CzIPN (1 mol %). Acetonitrile (3 mL) was added and the Schlenk tube was sealed with PTFE/silicon septum and connected to a vacuum line. The solution was degassed 3 times *via* a freeze-pump-thaw procedure and stirred under irradiation by a 34 W Kessil H150 blue LED (emission: 456 nm) with the temperature controlled by a fan (~ 30 °C). Upon completion, the solvent was removed under reduced pressure and the residue was purified by flash column chromatography using DCM and DCM/ MeOH (20:1) as solvent mixture to afford the title compound.

Gram-Scale Reaction

A dried Schlenk tube of borosilicate glass equipped with a stir bar was charged with the azomethine imine (1.0 mmol, 1.0 equiv), the carbamoyl-1,4-dihydropyridine (1.5 equiv) and the photocatalyst 4CzIPN (1 mol %). Acetonitrile (20 mL) was added and the Schlenk tube was sealed with PTFE/silicon septum and connected to a vacuum line. The solution was degassed 3 times *via* a freeze-pump-thaw procedure and stirred under irradiation by 2 x 34 W

Kessil H150 blue LED (emission: 456 nm) with the temperature controlled by a fan (~ 30 °C). Upon completion, the solvent was removed under reduced pressure and the residue was purified by flash column chromatography using DCM and DCM/ MeOH (20:1) as solvent mixture to afford the title compound.

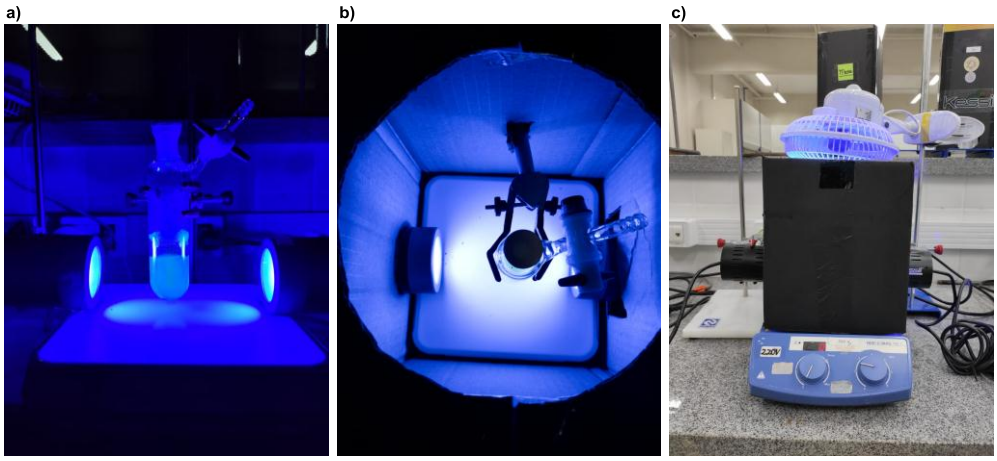

FIGURE S3 - Experimental set-up for the gram-scale experiment. a) Reaction vessel irradiated by two external 34 W Kessil H150 blue LED lamps. b) Schlenk tube disposal inside the photoreactor. c) Photoreactor equipped with two irradiation sources and the external fan.

General Procedure for Carbamoylation of Nitrones (GP2)

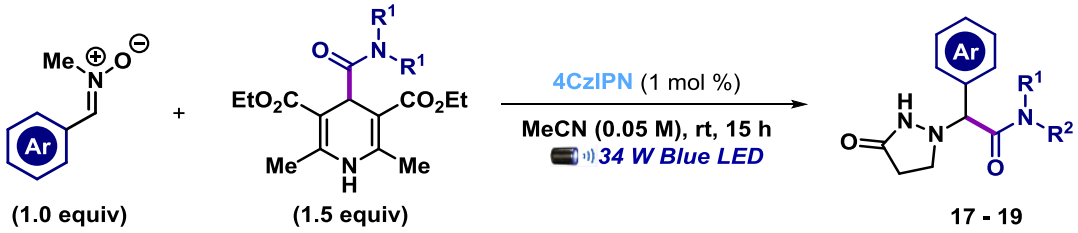

A dried Schlenk tube of borosilicate glass equipped with a stir bar was charged with the nitrone (0.15 mmol, 1.0 equiv), the 4-carbamoyl-1,4-dihydropyridine (1.5 equiv) and the photocatalyst 4CzIPN (1 mol %). Acetonitrile (3 mL) was added and the Schlenk tube was sealed with PTFE/silicon septum and connected to a vacuum line. The solution was degassed 3 times *via* a freeze-pump-thaw procedure and stirred under irradiation by a 34 W Kessil H150 blue LED (emission: 456 nm) with the temperature controlled by a fan (~ 30 °C). Upon completion, the solvent was removed under reduced pressure and the residue was purified by flash column chromatography using DCM and DCM/ MeOH (20:1) as solvent mixture to afford the title compound.

General Procedure for the Pyrazolidinone Reductive Cleavage (GP3)

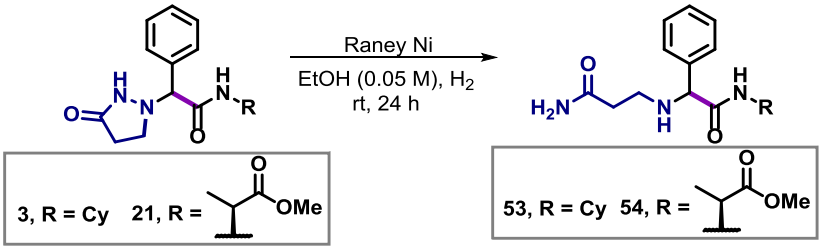

700 mg of Raney®-Nickel 2800 (slurry in H_2O) was added to a small vial and the catalyst was washed 3 times with EtOH. Then, a solution of **3** or **21** (0.2 mmol) in EtOH (4 mL) was added to the vial containing the activated catalyst, which was sealed with a septum. The reaction mixture was placed under H_2 atmosphere using balloons containing H_2 and kept under vigorous agitation for 24 h at room temperature. The reaction crude was filtered through celite, concentrated under reduced pressure, and purified by column chromatography (DCM/ MeOH 9:1) to furnish the corresponding primary amides **53** or **54**.

Compound Characterization

Starting Materials

2-(4-(2-(1,8-diethyl-1,3,4,9-tetrahydropyrano[3,4-*b*]indol-1-yl)acetoxy)benzylidene)-5-oxopyrazolidin-2-ium-1-ide (16')

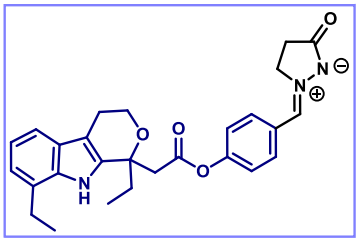

The compound **16'** was obtained as a yellow solid (394.9 mg, 43 %) following the general procedure for the synthesis of azomethine imines (2.0 mmol scale). The crude material was purified by flash column chromatography (DCM/ MeOH 20:1). **^{1}H NMR (DMSO-d_6, 400 MHz):** δ 10.64 (s, 1H), 8.32 – 8.28 (m, 2H), 7.64 (s, 1H), 7.26 (d, *J* = 7.3 Hz, 1H), 7.12 (d, *J* = 8.7 Hz, 2H), 6.95 – 6.89 (m, 2H), 4.54 (t, *J* = 8.0 Hz, 2H), 4.05 – 3.99 (m, 2H), 3.32 (d, *J* = 13.4 Hz, 1H), 3.09 (d, *J* = 13.3 Hz, 1H), 2.85 (q, *J* = 7.4 Hz, 2H), 2.74 – 2.66 (m, 2H), 2.58 – 2.53 (m, 2H), 2.16 (dt, *J* = 14.6, 7.2 Hz, 1H), 2.11 – 2.04 (m, 1H), 1.25 (t, *J* = 7.5 Hz, 3H), 0.72 (t, *J* = 7.2 Hz, 3H). **^{13}C NMR (DMSO-d_6, 101 MHz):** δ 184.4, 168.1, 151.9, 135.6, 134.6, 132.3, 131.0, 127.6, 126.6, 126.0, 122.1, 119.8, 118.8, 115.5, 107.5, 79.2, 75.7, 60.2, 57.3, 42.8, 30.9, 29.2, 23.8, 21.9, 14.5, 7.9. **HRMS (ESI):** m/z calc. for $C_{27}H_{29}N_3O_4$ $[M+H]^+$ 460.2231, found 460.2228.

(*S*)-diethyl-4-(2-(methoxycarbonyl)pyrrolidine-1-carbonyl)-2,6-dimethyl-1,4-dihydropyridine-3,5-dicarboxylate (22')

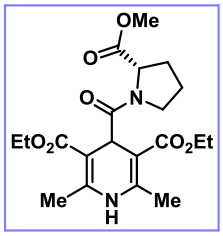

The compound **22'** was obtained as a yellow solid (312.2 mg, 51 %) following the general procedure for the synthesis of 4-carbamoyl-1,4-dihydropyridines (1.5 mmol scale). The crude material was purified by flash column chromatography (*n*-hexane/acetone 7:3). **^{1}H NMR ($CDCl_3$, 400 MHz):** δ 8.58 (s, 1H), 4.85 (s, 1H), 4.40 (dd, *J* = 8.6, 4.8 Hz, 1H), 4.26 – 4.20 (m, 1H), 4.17 – 4.12 (m, 4H), 3.58 (s, 3H), 2.23 (dt, *J* = 13.0, 7.3 Hz, 2H), 2.16 (s, 3H), 2.10 (s, 3H), 2.06 – 2.01 (m, 1H),), 1.96 – 1.89 (m, 2H), 1.30 (t, *J* = 7.2 Hz, 3H), 1.26 (t, *J* = 7.0 Hz, 3H). **^{13}C NMR ($CDCl_3$, 101 MHz):** δ 174.5, 172.9, 167.9, 167.6, 148.5, 147.8, 98.5, 97.8, 59.9, 59.5, 51.9, 47.5, 39.5, 29.4, 25.4, 19.4, 18.8, 14.7. **HRMS (ESI):** m/z calc. for $C_{20}H_{28}N_2O_7$ $[M+H]^+$ 409.1969, found 409.1968.

Diethyl-4-(((2*S*,3*S*)-1-methoxy-3-methyl-1-oxopentan-2-yl)carbamoyl)-2,6-dimethyl-1,4-dihydropyridine-3,5-dicarboxylate (25')

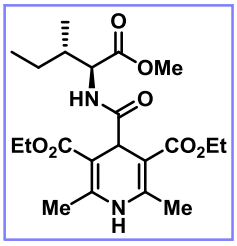

The compound **25'** was obtained as a yellow solid (381.8 mg, 60%) following the general procedure for the synthesis of 4-carbamoyl-1,4-dihydropyridines (1.5 mmol scale). The crude material was purified by flash column chromatography (*n*-hexane/acetone 7:3)**^{1}H NMR ($CDCl_3$, 400 MHz):** δ 7.63 (brs, 1H), 7.12 (d, *J* = 9.0 Hz, zH), 4.66 (s, 1H), 4.25 – 4.11 (m, 4H), 3.68 (s, 3H), 2.21 (s, 3H), 2.16 (s, 3H), 1.90 – 1.83 (m, 1H), 1.47 – 1.37 (m, 1H), 1.29 (td, *J* = 7.0, 3.1 Hz, 6H), 1.25 – 1.10 (m, 1H), 0.92 – 0.87 (m, 6H).**^{13}C NMR ($CDCl_3$, 101 MHz):** δ 174.5, 172.3, 167.8, 147.6, 97.8, 60.4, 60.2, 56.7, 52.01, 41.6, 37.9, 25.1, 19.1, 19.1, 15.6, 14.5, 14.4, 11.7. **HRMS (ESI):** m/z calc. for $C_{21}H_{33}N_2O_7$ $[M+H]^+$ 425.2282, found 425.2298.

Diethyl-(*S*)-4-((2-methoxy-2-oxo-1-phenylethyl)carbamoyl)-2,6-dimethyl-1,4-dihydropyridine-3,5-dicarboxylate (31')

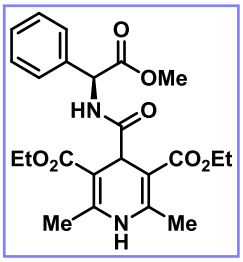

The compound **31'** was obtained as a white solid (313.1 mg, 47 %) following the general procedure for the synthesis of 4-carbamoyl-1,4-dihydropyridines (1.5 mmol scale). The crude material was purified by flash column chromatography (*n*-hexane/acetone 7:3). **^{1}H NMR ($CDCl_3$, 400 MHz):** δ 7.70 (d, *J* = 7.5 Hz, 1H), 7.32 – 7.30 (m, 5H), 5.46 (d, *J* = 7.4 Hz, 1H), 4.68 (s, 1H), 4.25 – 4.20 (m, 2H), 4.15 – 4.10 (m, 2H), 3.68 (s, 3H), 2.19 (s, 3H), 1.83 (s, 3H), 1.30 (t, *J* = 7.1 Hz, 3H), 1.21 (t, *J* = 7.1 Hz, 3H). **^{13}C NMR**

($CDCl_3$, 101 MHz): δ 174.0, 171.1, 167.9, 167.7, 147.9, 147.6, 137.0, 129.0, 128.9, 128.4, 127.3, 127.2, 97.8, 97.3, 60.4, 60.2, 56.7, 52.8, 41.6, 19.1, 18.6, 14.5, 14.4. **HRMS (ESI):** m/z calc. for $C_{23}H_{28}N_2O_7$ $[M+H]^+$ 445.1969, found 445.1995.

Diethyl 4-((1-methoxy-2-methyl-1-oxopropan-2-yl)carbamoyl)-2,6-dimethyl-1,4-dihydropyridine-3,5-dicarboxylate (32')

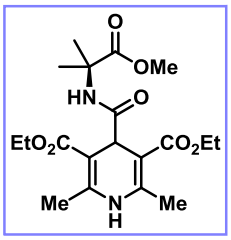

The compound **32'** was obtained as a white solid (445.7 mg, 75 %) following the general procedure for the synthesis of 4-carbamoyl-1,4-dihydropyridines (1.5 mmol scale). The crude material was purified by flash column chromatography (*n*-hexane/acetone 7:3). **^{1}H NMR ($CDCl_3$, 400 MHz):** δ 7.63 (brs, 1H), 6.97 (brs, 1H), 4.53 (s, 1H), 4.18 (q, *J* = 6.8 Hz, 4H), 3.64 (s, 3H), 2.19 (s, 6H), 1.49 (s, 6H), 1.29 (t, *J* = 7.0 Hz, 6H). **^{13}C NMR ($CDCl_3$, 101 MHz):** δ 175.0, 173.8, 167.8, 147.4, 98.0, 60.2, 56.2, 52.5, 42.3, 25.1, 19.1, 14.6. **HRMS (ESI):** m/z calc. for $C_{19}H_{29}N_2O_7$ $[M+H]^+$ 397.1969, found 397.1956.

Diethyl-4-(((*R*)-1-(((*R*)-1-methoxy-4-(methylthio)-1-oxobutan-2-yl)amino)-3-methyl-1-oxobutan-2-yl)carbamoyl)-2,6-dimethyl-1,4-dihydropyridine-3,5-dicarboxylate (33')

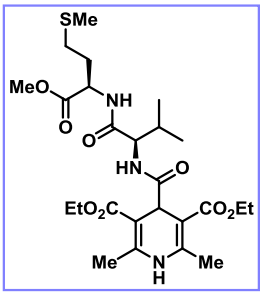

The compound **33'** was obtained as a yellow solid (405.9 mg, 50 %) following the general procedure for the synthesis of 4-carbamoyl-1,4-dihydropyridines (1.5 mmol scale). The crude material was purified by flash column chromatography (*n*-hexane/acetone 7:3). **^{1}H NMR ($CDCl_3$, 400 MHz):** δ 8.18 (brs, 1H), 7.10 (d, *J* = 7.9 Hz, 1H), 6.94 (d, *J* = 8.9 Hz, 1H), 4.58 (q, *J* = 6.5, 6.0 Hz, 1H), 4.52 (s, 1H), 4.30 – 4.27 (m, 1H), 4.23 – 4.06 (m, 4H), 3.66 (s, 3H), 2.35 (ddd, *J* = 17.1, 8.3, 4.8 Hz, 2H), 2.12 (s, 3H), 2.10 (s, 3H), 2.04 (s, 3H), 2.02 – 1.97 (m, 1H), 1.24 (t, *J* = 7.1 Hz, 6H), 0.88 (d, *J* = 6.6 Hz, 6H). **^{13}C NMR ($CDCl_3$, 101 MHz):** δ 175.2, 172.2, 171.4, 168.8, 167.9, 147.5, 98.2, 97.9, 60.6, 60.4, 58.5, 52.4, 51.6, 42.8, 31.4, 30.1, 29.8, 19.4, 19.2, 19.1, 17.1, 15.5, 14.6, 14.5. **HRMS (ESI):** m/z calc. for $C_{25}H_{40}N_3O_8S^+$ $[M+H]^+$ 542.2531, found 542.2567.

Diethyl-4-(((*R*)-1-(((*R*)-1-methoxy-3-methyl-1-oxobutan-2-yl)amino)-1-oxo-3-phenylpropan-2-yl)carbamoyl)-2,6-dimethyl-1,4-dihydropyridine-3,5-dicarboxylate (35')

The compound **35'** was obtained as a yellow solid (367.8 mg, 44 %) following the general procedure for the synthesis of 4-carbamoyl-1,4-dihydropyridines (1.5 mmol scale). The crude material was purified by flash column chromatography (*n*-hexane/acetone 7:3). **^{1}H NMR**

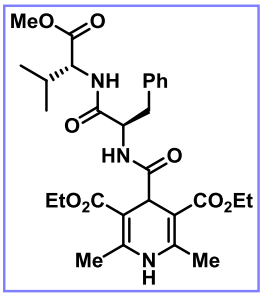

(CDCl$_3$, 400 MHz): δ 7.74 (s, 1H), 7.30 – 7.21 (m, 5H), 7.08 (d, *J* = 8.2 Hz, 1H), 6.73 (d, *J* = 8.5 Hz, 1H), 4.67 (q, *J* = 7.7 Hz, 1H), 4.54 (s, 1H), 4.44 (dd, *J* = 8.4, 5.5 Hz, 1H), 4.11 (dddd, *J* = 24.7, 13.7, 11.1, 7.0 Hz, 4H), 3.69 (s, 3H), 3.18 (dd, *J* = 14.3, 5.6 Hz, 1H), 3.08 (dd, *J* = 14.3, 7.6 Hz, 1H), 2.18 (s, 3H), 2.10 (s, 3H), 2.14 – 2.06 (m, 1H), 1.24 (t, *J* = 7.1 Hz, 6H), 0.87 – 0.84 (m, 6H). **^{13}C NMR (CDCl$_3$, 101 MHz):** δ 175.0, 171.9, 171.0, 168.2, 167.7, 147.5, 136.9, 129.3, 128.6, 126.9, 97.9, 97.7, 60.3, 60.2, 57.5, 54.6, 52.0, 42.1, 37.6, 31.2, 19.1, 19.0, 18.9, 18.1, 14.5, 14.4. **HRMS (ESI):** m/z calc. for $C_{29}H_{40}N_3O_8^+$ $[M+H]^+$ 558.2810, found 558.2823.

Diethyl-4-(((*S*)-1-(((*R*)-1-(benzyloxy)-4-methyl-1-oxopentan-2-yl)amino)-4-methyl-1-oxopentan-2-yl)carbamoyl)-2,6-dimethyl-1,4-dihydropyridine-3,5-dicarboxylate (36')

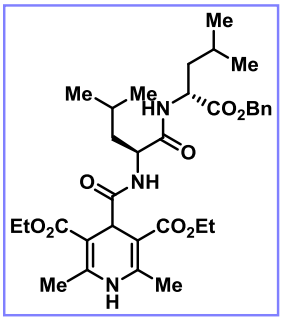

The compound **36'** was obtained as a yellow solid (570.4 mg, 62 %) following the general procedure for the synthesis of 4-carbamoyl-1,4-dihydropyridines (1.5 mmol scale). The crude material was purified by flash column chromatography (*n*-hexane/acetone 7:3).**^{1}H NMR (CDCl$_3$, 400 MHz):** δ 8.34 (s, 1H), 7.35 – 7.29 (m, 5H), 7.03 (d, *J* = 8.5 Hz, 1H), 6.69 (d, *J* = 7.9 Hz, 1H), 5.14 (q, *J* = 12.3 Hz, 2H), 4.65 (td, *J* = 8.8, 5.2 Hz, 1H), 4.50 (s, 1H), 4.38 (ddd, *J* = 11.4, 7.9, 3.8 Hz, 1H), 4.26 – 4.05 (m, 4H), 2.14 (s, 3H), 2.08 (s, 3H), 1.80 (ddd, *J* = 13.9, 9.9, 3.8 Hz, 1H), 1.66 – 1.58 (m, 2H), 1.57 – 1.48 (m, 3H), 1.25 (dtd, *J* = 14.2, 7.2, 1.7 Hz, 6H), 0.93 – 0.81 (m, 12H). **^{13}C NMR (CDCl$_3$, 101 MHz):** δ 175.6, 172.7, 172.2, 168.5, 167.9, 147.7, 147.1, 135.7, 128.6, 128.4, 128.2, 98.5, 97.4, 66.9, 60.3, 52.2, 50.7, 43.3, 40.9, 40.4, 24.6, 23.4, 22.9, 21.8, 20.9, 18.9, 14.6, 14.5. **HRMS (ESI):** m/z calc. for $C_{33}H_{48}N_3O_8^+$ $[M+H]^+$ 614.3436, found 614.3447.

Diethyl-4-((*S*)-2-(((2*S*,3*R*)-1-methoxy-3-methyl-1-oxopentan-2-yl)carbamoyl)pyrrolidine-1-carbonyl)-2,6-dimethyl-1,4-dihydropyridine-3,5-dicarboxylate (37')

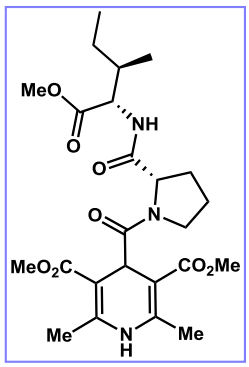

The compound **37'** was obtained as a yellow solid (148.5 mg, 19 %) following the general procedure for the synthesis of 4-carbamoyl-1,4-dihydropyridines (1.5 mmol scale). The crude material was purified by flash column chromatography (*n*-hexane/acetone 7:3). **^{1}H NMR (CDCl$_3$, 400 MHz):** δ 8.44 (s, 1H), 6.83 (d, *J* = 8.5 Hz, 1H), 4.69 (s, 1H), 4.56 (d,

J = 7.6 Hz, 1H), 4.50 (dd, *J* = 8.6, 4.8 Hz, 1H), 4.27 – 4.20 (m, 2H), 4.15 (q, *J* = 7.1 Hz, 4H), 3.68 (s, 3H), 2.14 (s, 1H), 2.13 (s, 3H), 2.07 (s, 3H), 2.03 – 1.94 (m, 3H), 1.25 (td, *J* = 7.1, 3.3 Hz, 7H), 0.89 (dd, *J* = 7.1, 3.3 Hz, 2H), 0.81 (t, *J* = 8.0 Hz, 6H). **^{13}C NMR ($CDCl_3$, 101 MHz):** δ 175.5, 172.1, 172.0, 168.4, 167.7, 147.9, 147.4, 98.6, 61.0, 60.1, 59.9, 56.5, 51.8, 47.4, 40.0, 37.4, 29.6, 24.9, 24.3, 19.3, 19.3, 15.2, 14.5, 14.3, 11.4. **HRMS (ESI):** m/z calc. for $C_{26}H_{39}N_3O_8$ $[M+H]^+$ 522.2810, found 522.2811.

Dimethyl 4-((*S*)-2-(((*S*)-3-hydroxy-1-methoxy-1-oxopropan-2-yl)carbamoyl)pyrrolidine-1-carbonyl)-2,6-dimethyl-1,4-dihydropyridine-3,5-dicarboxylate (38')

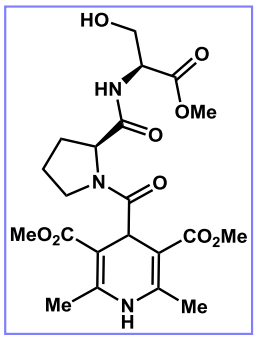

The compound **38'** was obtained as a yellow oil (147.2 mg, 21%) following the general procedure for the synthesis of 4-carbamoyl-1,4-dihydropyridines (1.5 mmol scale). The crude material was purified by flash column chromatography (*n*-hexane/acetone 7:3). **^{1}H NMR ($CDCl_3$, 400 MHz):** δ 7.57 (s, 1H), 6.90 (d, *J* = 8.4 Hz, 1H), 4.65 (s, 1H), 4.66 – 4.62 (m, 1H), 4.43 (dd, *J* = 8.1, 4.1 Hz, 1H), 4.28 (td, *J* = 11.7, 5.8 Hz, 1H), 4.23 – 4.10 (m, 4H), 3.85 (dd, *J* = 11.6, 2.9 Hz, 1H), 3.73 (s, 3H), 3.67 (dd, *J* = 11.6, 4.1 Hz, 1H), 2.26 – 2.19 (m, 1H), 2.17 (s, 3H), 2.11 (s, 3H), 2.14 – 2.07 (m, 1H), 1.97 (dd, *J* = 13.1, 7.4 Hz, 1H), 1.31 – 1.24 (m, 6H). **^{13}C NMR ($CDCl_3$, 126 MHz):** δ 174.0, 171.1, 167.9, 167.7, 147.9, 147.6, 137.0, 129.0, 128.9, 128.5, 127.3, 127.2, 97.8, 97.3, 60.4, 60.2, 56.8, 52.8, 41.6, 19.0, 18.6, 14.5, 14.43. **HRMS (ESI)** m/z calc. for $C_{23}H_{34}N_3O_9$ $[M+H]^+$ 496.2290, found 496.2295.

Diethyl (*S*)-4-((2-((2-methoxy-2-oxo-1-phenylethyl)amino)-2-oxoethyl)carbamoyl)-2,6-dimethyl-1,4-dihydropyridine-3,5-dicarboxylate (39')

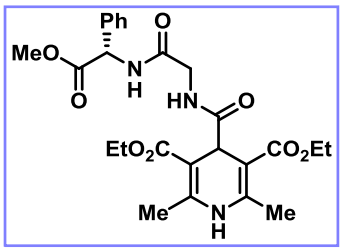

The compound **39'** was obtained as a yellow oil (293.2 mg, 39%) following the general procedure for the synthesis of 4-carbamoyl-1,4-dihydropyridines (1.5 mmol scale). The crude material was purified by flash column chromatography (*n*-hexane/acetone 7:3). **^{1}H NMR ($CDCl_3$, 400 MHz):** δ 7.42 – 7.30 (m, 5H), 7.10 (t, *J* = 5.7 Hz, 1H), 5.59 (d, *J* = 7.5 Hz, 1H), 4.54 (s, 1H), 4.13 (q, *J* = 7.2 Hz, 2H), 4.09 – 3.99 (m, 2H), 3.97 (d, *J* = 5.9 Hz, 2H), 3.70 (s, 3H), 2.19 (d, *J* = 3.4 Hz, 6H), 1.27 – 1.22 (m, 6H). **^{13}C NMR ($CDCl_3$, 126 MHz):** δ 175.5, 171.1, 168.9, 168.2, 168.0, 147.5, 147.2, 136.3, 129.0, 128.6, 127.5, 98.3, 98.0, 60.5, 60.4, 56.3, 52.8, 43.5, 42.6, 19.4, 19.3, 14.5. **HRMS (ESI):** m/z calc. for $C_{25}H_{32}N_3O_8^+$ $[M+H]^+$ 502.2184, found 502.2214.

Diethyl-4-(((3*R*,8*R*,9*S*,10*S*,13*R*,14*S*,17*R*)-17-((*R*)-5-methoxy-5-oxopentan-2-yl)-10,13 dimethylhexadecahydro-1H-cyclopenta[a]phenanthren-3-yl)carbamoyl)-2,6-dimethyl-1,4-dihydropyridine-3,5-dicarboxylate (40')

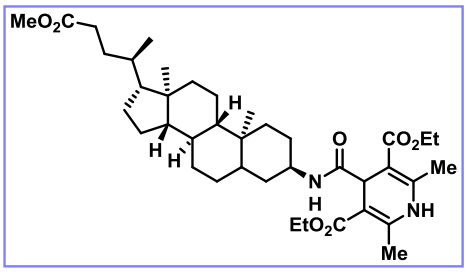

The compound **40'** was obtained as a white solid (651.7 mg, 65%) following the general procedure for the synthesis of 4-carbamoyl-1,4-dihydropyridines (1.5 mmol scale). The crude material was purified by flash column chromatography (*n*-hexane/acetone 7:3). **^{1}H NMR ($CDCl_3$, 400 MHz):** δ 8.14 (s, 1H), 7.17 (d, *J* = 7.6 Hz, 1H), 4.60 (s, 1H), 4.24 – 4.12 (m, 4H), 4.06 – 4.04 (m, 1H), 3.65 (s, 3H), 2.34 (ddd, *J* = 15.3, 10.1, 5.1 Hz, 1H), 2.24 – 2.20 (m, 1H), 2.19 (s, 3H), 2.18 (s, 3H), 1.98 – 1.93 (m, 2H), 1.88 – 1.76 (m, 3H), 1.55 (t, *J* = 11.4 Hz, 3H), 1.49 – 1.29 (m, 9H), 1.28 – 1.24 (m, 8H), 1.17 – 1.03 (m, 6H), 0.90 (d, *J* = 6.4 Hz, 3H), 0.64 (s, 3H). **^{13}C NMR ($CDCl_3$, 126 MHz):** δ 174.9, 173.9, 168.35, 168.3, 147.5, 98.0, 76.8, 60.2, 60.2, 56.6, 56.1, 51.6, 45.4, 42.9, 41.8, 40.3, 39.9, 37.8, 35.8, 35.5, 35.2, 31.2, 31.1, 30.9, 28.3, 26.9, 26.3, 25.1, 24.3, 24.1, 21.1, 19.1, 19.1, 18.4, 14.6, 14.6, 12.2. **HRMS (ESI):** m/z calc. for $C_{39}H_{61}N_2O_7^+$ $[M+H]^+$ 669.4473, found 669.4481.

Diethyl (*S*)-4-((2-(2-methoxy-2-oxoethyl)-4-methylpentyl)carbamoyl)-2,6-dimethyl-1,4-dihydropyridine-3,5-dicarboxylate (41')

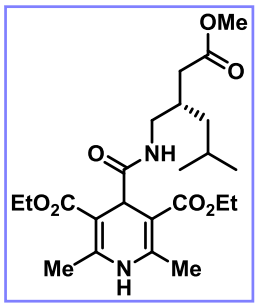

The compound **41'** was obtained as a white solid (447.7 mg, 66%) following the general procedure for the synthesis of 4-carbamoyl-1,4-dihydropyridines (1.5 mmol scale). The crude material was purified by flash column chromatography (*n*-hexane/acetone 7:3). **^{1}H NMR ($CDCl_3$, 400 MHz):** δ 7.70 (s, 1H), 6.78 (t, *J* = 6.1 Hz, 1H), 4.56 (s, 1H), 4.18 (dt, *J* = 7.0, 5.5 Hz, 4H), 3.66 (s, 3H), 3.28 – 3.22 (m, 2H, 3.15 – 3.09 (m, 1H), 2.21 (s, 6H), 2.07 (dd, *J* = 12.7, 6.5 Hz, 1H), 1.64 – 1.56 (m, 1H), 1.45 (t, *J* = 7.1 Hz, 1H), 1.28 (td, *J* = 7.1, 0.9 Hz, 6H), 1.19 – 1.05 (m, 2H), 0.86 (dd, *J* = 9.6, 6.6 Hz, 6H). **^{13}C NMR ($CDCl_3$, 126 MHz):** δ 174.9, 173.4, 168.1, 147.4, 98.2, 60.3, 51.6, 42.6, 41.8, 41.4, 37.1, 33.5, 25.3, 22.8, 19.3, 14.5. δ. **HRMS (ESI):** m/z calc. for $C_{23}H_{37}N_2O_7^+$ $[M+H]^+$ 453.2595, found 453.2593.

Diethyl 2,6-dimethyl-4-(octylcarbamoyl)-1,4-dihydropyridine-3,5-dicarboxylate (43')

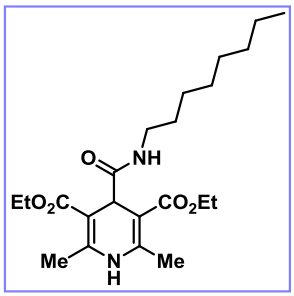

The product **43'** was obtained as a yellow solid (355.2 mg, 58%) following the general procedure for the synthesis of 4-carbamoyl-1,4-dihydropyridines (1.5 mmol scale). The crude material was purified by flash column chromatography (*n*-hexane/acetone 7:3). **^{1}H NMR ($CDCl_3$, 400 MHz):** δ 8.34 (s, 1H), 6.72 (t, *J* = 5.6 Hz, 1H), 4.55 (s, 1H), 4.17 (q, *J* = 7.1 Hz, 4H), 3.17 (q, *J* = 6.7 Hz, 2H), 2.18 (s, 6H), 1.46 – 1.43 (m, 2H), 1.29 – 1.25 (m, 16H), 0.87 (t, *J* = 6.7 Hz, 3H). **^{13}C NMR ($CDCl_3$, 101 MHz):** δ 174.9, 168.2, 147.7, 97.8, 60.1, 41.8, 39.6, 31.9, 29.7, 29.4, 29.4, 26.9, 22.8, 18.9, 14.5, 14.2. **HRMS (ESI):** m/z calc. for $C_{22}H_{36}N_2O_5$ $[M+H]^+$ 409.2697, found 409.2695.

Diethyl 4-((3-methoxy-3-oxopropyl)carbamoyl)-2,6-dimethyl-1,4-dihydropyridine-3,5-dicarboxylate (44')

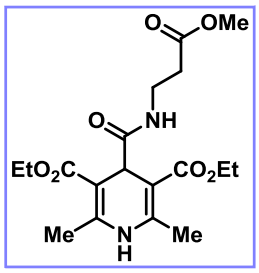

The product **44'** was obtained as a yellow solid (412.7 mg, 72%) following the general procedure for the synthesis of 4-carbamoyl-1,4-dihydropyridines (1.5 mmol scale). The crude material was purified by flash column chromatography (*n*-hexane/acetone 7:3). **^{1}H NMR ($CDCl_3$, 400 MHz):** δ 7.99 (s, 1H), 7.01 (t, *J* = 6.0 Hz, 1H), 4.53 (s, 1H), 4.17 (q, *J* = 7.1 Hz, 4H), 3.68 (s, 3H), 3.47 (q, *J* = 6.3 Hz, 2H), 2.48 (t, *J* = 6.3 Hz, 2H), 2.19 (s, 6H), 1.27 (t, *J* = 7.1 Hz, 6H). **^{13}C NMR ($CDCl_3$, 101 MHz):** δ 175.0, 172.5, 167.9, 147.6, 97.9, 60.2, 51.8, 41.8, 35.1, 34.2, 19.0, 14.5. **HRMS (ESI):** m/z calc. for $C_{18}H_{27}N_2O_7$ $[M+Na]^+$ 405.1632, found 405.1632.

Diethyl 2,6-dimethyl-4-(prop-2-yn-1-ylcarbamoyl)-1,4-dihydropyridine-3,5-dicarboxylate (45')

The product **45'** was obtained as a yellow solid (350.8 mg, 70%) following the general procedure for the synthesis of 4-carbamoyl-1,4-dihydropyridines (1.5 mmol scale). The crude material was purified by flash column chromatography (*n*-hexane/acetone 7:3). **^{1}H NMR ($CDCl_3$, 400 MHz):** δ 7.64 (brs, 1H), 6.98 (t, *J* = 5.1 Hz, 1H), 4.58 (s, 1H), 4.19 (q, *J* = 6.9 Hz, 5H), 3.98 (dd, *J* = 4.9, 2.0 Hz, 2H), 2.21 (s, 6H), 2.16 (s, 1H), 1.29 (t, *J* = 6.8 Hz, 6H).**^{13}C NMR ($CDCl_3$, 101 MHz):** δ 174.5, 167.9, 147.5, 97.6, 79.7, 71.2, 60.2, 41.5, 29.2, 19.1, 14.4. **HRMS (ESI):** m/z calc. for $C_{17}H_{22}N_2O_5$ $[M+H]^+$ 335.1601, found 335.1606.

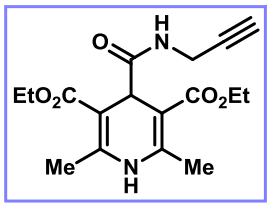

Diethyl-4-((3,5-bis(trifluoromethyl)benzyl)carbamoyl)-2,6-dimethyl-1,4-dihydropyridine-3,5-dicarboxylate (47')

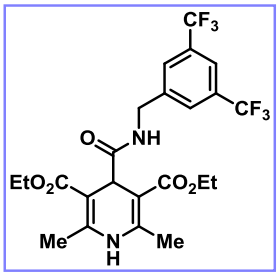

The product **47'** was obtained as a yellow solid (650 mg, 83%) following the general procedure for the synthesis of 4-carbamoyl-1,4-dihydropyridines (1.5 mmol scale). The crude material was purified by flash column chromatography (*n*-hexane/acetone 7:3). **^{1}H NMR ($CDCl_3$, 400 MHz):** δ 7.67 (s, 1H), 7.57 (s, 2H), 7.33 (t, *J* = 6.3 Hz, 1H), 7.19 (s, 1H), 4.56 (s, 1H), 4.46 (d, *J* = 6.2 Hz, 2H), 4.11 (q, *J* = 7.1 Hz, 4H), 2.07 (s, 6H), 1.19 (t, *J* = 7.1 Hz, 6H). **^{13}C NMR ($CDCl_3$, 101 MHz):** δ 175.1, 168.2, 147.4, 142.0, 131.8 (q, *J* = 33.4 Hz), 127.1, 123.4 (q, *J* = 272.8 Hz), 121.2 – 121.1 (m), 98.0, 60.5, 42.5, 42.0, 19.2, 14.4. **HRMS (ESI):** m/z calc. for $C_{23}H_{24}F_6N_2O_5$ $[M+Na]^+$ 545.1482, found 545.1494.

Diethyl-2,6-dimethyl-4-((3-(triethoxysilyl)propyl)carbamoyl)-1,4-dihydropyridine-3,5-dicarboxylate (48')

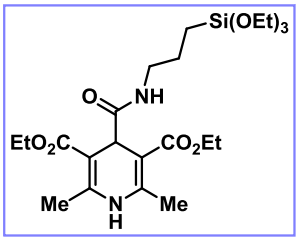

The product **48'** was obtained as a yellow solid (502.7 mg, 67%) following the general procedure for the synthesis of 4-carbamoyl-1,4-dihydropyridines (1.5 mmol scale). The crude material was purified by flash column chromatography (*n*-hexane/acetone 7:3). **^{1}H NMR ($CDCl_3$, 400 MHz):** δ 7.95 (s, 1H), 6.72 (t, *J* = 5.9 Hz, 1H), 4.54 (s, 1H), 4.17 (q, *J* = 7.1 Hz, 4H), 3.80 (q, *J* = 7.0 Hz, 6H), 3.18 (q, *J* = 6.7 Hz, 2H), 2.19 (s, 6H), 1.60 – 1.53 (m, 2H), 1.27 (t, *J* = 7.4 Hz, 6H), 1.23 – 1.19 (m, 9H), 0.61 – 0.57 (m, 2H). **^{13}C NMR ($CDCl_3$, 101 MHz):** δ 174.7, 168.1, 147.5, 98.1, 60.2, 58.5, 42.2, 41.8, 23.3, 19.1, 18.4, 14.6, 7.8. **HRMS (ESI):** m/z calc. for $C_{23}H_{41}N_2O_8Si$ $[M+H]^+$ 501.2627, found 501.2631.

Diethyl 4-((3,4-dihydroxyphenethyl)carbamoyl)-2,6-dimethyl-1,4-dihydropyridine-3,5-dicarboxylate (49')

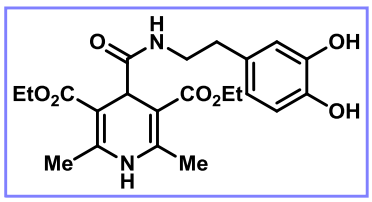

The compound **49'** was obtained as a white solid (181.5 mg, 28%) following the general procedure for the synthesis of 4-carbamoyl-1,4-dihydropyridines (1.5 mmol scale). The crude material was purified by flash column chromatography (*n*-hexane/acetone 7:3). **^{1}H NMR (Metanol-*d*4, 400 MHz):** δ 6.69

(d, *J* = 7.9 Hz, 1H), 6.62 (d, *J* = 1.2 Hz, 1H), 6.49 (dd, *J* = 8.0, 2.1 Hz, 1H), 4.50 (s, 1H), 4.14 (q, *J* = 7.1 Hz, 4H), 3.38 – 3.33 (m, 2H), 2.62 (t, *J* = 7.0 Hz, 2H), 2.30 (s, 6H), 1.26 (t, *J* = 7.1 Hz, 6H). **^{13}C NMR (Metanol-*d*4, 126 MHz):** δ 176.4, 169.4, 149.3, 146.3, 144.8, 131.8, 120.9, 116.7, 116.3, 98.8, 61.2, 42.5, 41.8, 35.7, 18.9, 14.7. **HRMS (ESI):** m/z calc. for $C_{22}H_{28}N_2O_7$ $[M+H]^+$ 433.1969, found 433.1988.

Diethyl 4-(((1*S*,2*R*)-2-hydroxy-2,3-dihydro-1H-inden-1-yl)carbamoyl)-2,6-dimethyl-1,4-dihydropyridine-3,5-dicarboxylate (50')

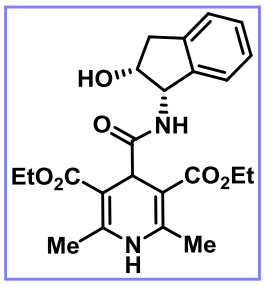

The product **50'** was obtained as a yellow solid (327.6 mg, 51%) following the general procedure for the synthesis of 4-carbamoyl-1,4-dihydropyridines (1.5 mmol scale). The crude material was purified by flash column chromatography (*n*-hexane/acetone 7:3). **^{1}H NMR ($CDCl_3$, 400 MHz):** δ 8.00 (s, 1H), 7.33 – 7.19 (m, 4H), 6.96 (d, *J* = 8.4 Hz, 1H), 5.33 (dd, *J* = 8.4, 4.8 Hz, 1H), 4.64 – 4.61 (m, 2H), 4.28 – 4.12 (m, 4H), 3.14 (dd, *J* = 16.5, 5.1 Hz, 1H), 3.00 (brs, 1H), 2.28 (s, 3H), 2.24 (s, 3H), 1.26 (q, *J* = 7.0 Hz, 6H). **^{13}C NMR ($CDCl_3$, 101 MHz):** δ 175.6, 168.5, 167.7, 147.5, 140.5, 128.3, 127.1, 125.5, 124.2, 98.6, 98.2, 73.4, 60.6, 60.3, 58.4, 43.1, 39.6, 19.3, 19.2, 14.6, 14.5. **HRMS (ESI):** m/z calc. for $C_{23}H_{29}N_2O_6$ $[M+H]^+$ 429.2020, found 429.2016.

Scope for the carbamoylation of azomethine imines

***N*-cyclohexyl-2-(3-oxopyrazolidin-1-yl)acetamide (3)**

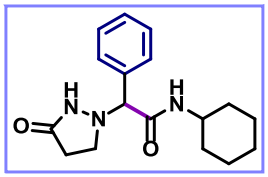

The product **3** was obtained as a colorless oil (31.6 mg, 70%) following the general procedure GP1. The crude material was purified by flash column chromatography (DCM/MeOH 20:1). **^{1}H NMR ($CDCl_3$, 400 MHz):** δ 7.39-7.34 (m, 5H), 6.20 (brs, 1H), 4.23 (s, 1H), 3.72 (qt, *J* = 8.5, 4.0 Hz, 1H), 3.24 (dt, *J* = 10.7, 7.5 Hz, 2H), 2.38 (t, *J* = 7.4 Hz, 2H), 1.82 (td, *J* = 12.4, 4.1 Hz, 2H), 1.68-1.55 (m, 3H), 1.37 – 1.26 (m, 2H), 1.10 (pd, *J* = 11.8, 3.4 Hz, 3H). **^{13}C NMR ($CDCl_3$, 126 MHz):** δ 174.4, 168.6, 135.1, 129.2, 129.2, 128.5, 76.1, 50.1, 48.4, 32.9, 32.8, 29.6, 25.5, 24.8. **HRMS (ESI):** m/z calc. for $C_{17}H_{24}N_3O_2$ $[M+H]^+$ 302.1863, found 302.1861.

***N*-cyclohexyl-2-(3-oxopyrazolidin-1-yl)-2-(4-(trifluoromethyl)phenyl)acetamide (4)**

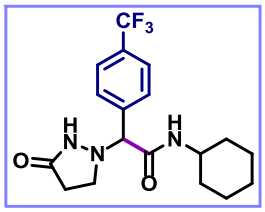

The product **4** was obtained as a colorless oil (40.4 mg, 73%) following the general procedure GP1. The crude material was purified by flash column chromatography (DCM/MeOH 20:1). **^{1}H NMR ($CDCl_3$, 400 MHz):** δ 7.64 (d, *J* = 8.0 Hz, 2H), 7.54 (d, *J* = 8.0 Hz, 2H), 6.30 (brs, 1H), 4.35 (s, 1H), 3.76 – 3.68 (m, 1H), 3.31 (q, *J* = 8.9 Hz, 2H), 2.44 (dq, *J* = 16.8, 9.0 Hz, 2H), 1.84 (t, *J* = 16.6 Hz, 2H), 1.69 – 1.57 (m, 3H), 1.38 – 1.27 (m, 2H), 1.19 – 1.07 (m, 3H). **^{13}C NMR ($CDCl_3$, 126 MHz):** δ 174.7, 167.7, 139.1, 131.6 (q, *J* = 32.2 Hz), 128.9, 126.2 (q, *J* = 3.9 Hz), 123.9(q, *J* = 271.9 Hz), 75.7, 50.7, 48.5, 32.9, 32.9, 29.5, 25.5, 24.8. **HRMS (ESI):** m/z calc. for $C_{18}H_{23}F_3N_3O_2$ $[M+H]^+$ 370.1737, found 370.1733.

N-cyclohexyl-2-(4-fluorophenyl)-2-(3-oxopyrazolidin-1-yl)acetamide (5)

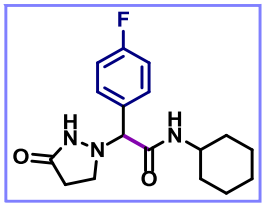

The product **5** was obtained as a colorless oil (36.8 mg, 77%) following the general procedure GP1. The crude material was purified by flash column chromatography (DCM/MeOH 20:1). **^{1}H NMR ($CDCl_3$, 400 MHz):** δ 7.42 (dd, *J* = 8.4, 5.3 Hz, 2H), 7.08 (t, *J* = 8.3 Hz, 2H), 6.27 (brs, 1H), 4.38 (s, 1H), 3.75 (dtt, *J* = 11.1, 8.0, 3.8 Hz, 1H), 3.34 (q, *J* = 8.2 Hz, 2H), 2.51 – 2.37 (m, 2H), 1.84 (dd, *J* = 12.2, 4.1 Hz, 2H), 1.69 – 1.65 (m, 2H), 1.60 (dt, *J* = 12.2, 3.8 Hz, 1H), 1.34 (qt, *J* = 12.3, 3.7 Hz, 2H), 1.13 (dddd, *J* = 15.7, 11.8, 7.9, 3.8 Hz, 3H). **^{13}C NMR ($CDCl_3$, 126 MHz):** δ 174.7, 168.5, 163.1 (d, *J* = 248.7 Hz), 131.1, 130.3 (d, *J* = 8.3 Hz), 116.2 (d, *J* = 21.7 Hz), 75.3, 50.6, 48.3, 32.9, 29.6, 25.5, 24.8. **HRMS (ESI):** m/z calc. for $C_{17}H_{23}FN_3O_2$ $[M+H]^+$ 320.1769, found 320.1765.

2-(4-bromophenyl)-*N*-cyclohexyl-2-(3-oxopyrazolidin-1-yl)acetamide (6)

The product **6** was obtained as a colorless oil (31.3 mg, 55%) following the general procedure GP1. The crude material was purified by flash column chromatography (DCM/MeOH 20:1). **^{1}H NMR ($CDCl_3$, 400 MHz):** δ 7.44 (d, *J* = 8.0 Hz, 2H), 7.21 (d, *J* = 8.4 Hz, 2H), 6.16 (brs, 1H), 4.16 (s, 1H), 3.65 (dtt, *J* = 10.9, 8.8, 3.9 Hz, 1H), 3.21 (q, *J* = 9.0, 8.5 Hz, 2H), 2.40 – 2.30 (m, 2H), 1.81 – 1.73 (m, 2H), 1.63 – 1.58 (m, 2H), 1.56 – 1.51 (m, 1H), 1.33 – 1.19 (m, 2H), 1.13 – 0.99 (m, 3H). **^{13}C NMR ($CDCl_3$, 126 MHz):** δ 174.6, 168.1, 134.2, 132.4, 130.1, 123.4, 75.4, 50.6, 48.4, 32.9, 29.5, 25.5, 24.8. **HRMS (ESI):** m/z calc. for $C_{17}H_{23}BrN_3O_2$ $[M+H]^+$ 380.0968, found 380.0975.

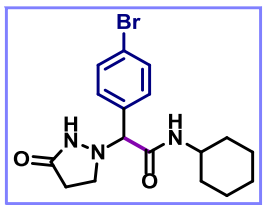

2-([1,1'-biphenyl]-4-yl)-*N*-cyclohexyl-2-(3-oxopyrazolidin-1-yl)acetamide (7)

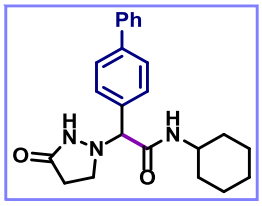

The product **7** was obtained as a colorless oil (30.5 mg, 54%) following the general procedure GP1. The crude material was purified by flash column chromatography (DCM/MeOH 20:1). **^{1}H NMR ($CDCl_3$, 400 MHz):** δ 7.54 – 7.49 (m, 4H), 7.40 – 7.36 (m, 4H), 7.32 – 7.28 (m, 1H), 6.10 (brs, 1H), 4.19 (s, 1H), 3.74 – 3.63 (m, 1H), 3.25 – 3.19 (m, 2H), 2.37 (t, *J* = 8.9 Hz, 2H), 1.82 – 1.76 (m, 2H), 1.60 (dt, *J* = 13.5, 3.8 Hz, 2H), 1.55 – 1.50 (m, 1H), 1.33 – 1.21 (m, 2H), 1.12 – 1.02 (m, 3H). **^{13}C NMR ($CDCl_3$, 126 MHz):** δ 174.4, 168.7, 142.2, 140.2, 134.1, 129.0, 128.9, 128.0, 127.8, 127.2, 75.9, 50.7, 48.3, 33.0, 32.9, 29.6, 25.5, 24.8. **HRMS (ESI):** m/z calc. for $C_{23}H_{28}N_3O_2$ $[M+H]^+$ 378.2176, found 378.2170.

***N*-cyclohexyl-2-(3-oxopyrazolidin-1-yl)-2-(p-tolyl)acetamide (8)**

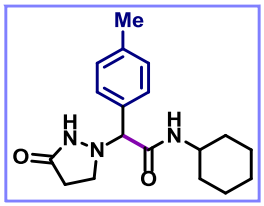

The product **8** was obtained as a colorless oil (25.1 mg, 53%) following the general procedure GP1. The crude material was purified by flash column chromatography (DCM/MeOH 20:1). **^{1}H NMR ($CDCl_3$, 400 MHz):** δ 7.19 (d, *J* = 7.8 Hz, 2H), 7.11 (d, *J* = 7.8 Hz, 2H), 6.01 (brs, 1H), 4.11 (s, 1H), 3.71 – 3.62 (m, 1H), 3.17 (dt, *J* = 10.8, 7.4 Hz, 2H), 2.33 (t, *J* = 8.2 Hz, 2H), 2.28 (s, 3H), 1.75 (t, *J* = 12.0 Hz, 2H), 1.59 (dt, *J* = 14.5, 4.6 Hz, 2H), 1.52 (dt, *J* = 7.7, 4.0 Hz, 1H), 1.32 – 1.18 (m, 2H), 1.11 – 0.98 (m, 3H). **^{13}C NMR ($CDCl_3$, 126 MHz):** δ 174.3, 168.9, 139.2, 132.0, 130.0, 128.4, 75.8, 50.6, 48.2, 33.0, 32.9, 29.7, 25.5, 24.8, 21.3. **HRMS (ESI):** m/z calc. for $C_{18}H_{26}N_3O_2$ $[M+H]^+$ 316.2020, found 316.2015.

***N*-cyclohexyl-2-(4-methoxyphenyl)-2-(3-oxopyrazolidin-1-yl)acetamide (9)**

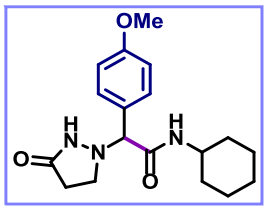

The product **9** was obtained as a colorless oil (29.8 mg, 60%) following the general procedure GP1. The crude material was purified by flash column chromatography (DCM/MeOH 20:1). **^{1}H NMR ($CDCl_3$, 400 MHz):** δ 7.29 (d, *J* = 8.3 Hz, 2H), 6.89 (d, *J* = 8.3 Hz, 2H), 6.14 (brs, 1H), 4.15 (s, 1H), 3.81 (s, 3H), 3.78 – 3.70 (m, 1H), 3.22 (dt, *J* = 10.9, 7.4 Hz, 2H), 2.38 (t, *J* = 8.2 Hz, 1H), 1.87 – 1.81 (m, 2H), 1.69 – 1.57 (m, 3H), 1.38 – 1.24 (m, 2H), 1.18 – 1.06 (m, 3H). **^{13}C NMR ($CDCl_3$, 126 MHz):** δ 174.5, 169.1, 160.2, 129.8, 127.1, 114.6, 75.4, 55.4, 50.5, 48.2, 32.9, 29.7, 25.5, 24.8. **HRMS (ESI):** m/z calc. for $C_{18}H_{26}N_3O_3$ $[M+H]^+$ 332.1969, found 332.1973.

2-(3-bromophenyl)-*N*-cyclohexyl-2-(3-oxopyrazolidin-1-yl)acetamide (10)

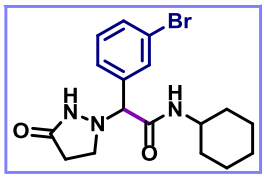

The product **10** was obtained as a colorless oil (29.6 mg, 52%) following the general procedure GP1. The crude material was purified by flash column chromatography (DCM/MeOH 20:1). **^{1}H NMR ($CDCl_3$, 400 MHz):** δ 7.51 (s, 1H), 7.44 (d, *J* = 7.9 Hz, 1H), 7.30 (d, *J* = 7.6 Hz, 1H), 7.21 – 7.17 (m, 1H), 6.25 (brs, 1H), 4.22 (s, 1H), 3.67 (q, *J* = 11.5, 10.6 Hz, 1H), 3.26 (dd, *J* = 17.6, 8.6 Hz, 2H), 2.47 – 2.35 (m, 2H), 1.78 (t, *J* = 10.2 Hz, 2H), 1.61 (dt, *J* = 13.2, 3.9 Hz, 2H), 1.56 – 1.51 (m, 1H), 1.32 – 1.22 (m, 2H), 1.08 (tt, *J* = 12.9, 6.1 Hz, 3H). **^{13}C NMR ($CDCl_3$, 126 MHz):** δ 174.5, 167.8, 137.1, 132.5, 131.5, 130.8, 127.2, 123.3, 75.3, 50.6, 48.4, 32.9, 32.9, 29.5, 25.5, 24.8. **HRMS (ESI):** m/z calc. for $C_{17}H_{23}BrN_3O_2$ $[M+H]^+$ 380.0968, found 380.0961.

***N*-cyclohexyl-2-(3-oxopyrazolidin-1-yl)-2-(o-tolyl)acetamide (11)**

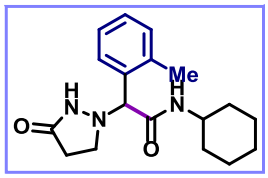

The product **11** was obtained as a colorless oil (26.0 mg, 55%) following the general procedure GP1. The crude material was purified by flash column chromatography (DCM/MeOH 20:1). **^{1}H NMR ($CDCl_3$, 400 MHz):** δ 7.33 (d, *J* = 7.3 Hz, 1H), 7.21 – 7.10 (m, 3H), 5.98 (brs, 1H), 4.53 (s, 1H), 3.69 – 3.62 (m, 1H), 3.22 – 3.13 (m, 1H), 2.42 – 2.29 (m, 2H), 2.41 (s, 3H), 1.81 – 1.69 (m, 2H), 1.55 (t, *J* = 18.6 Hz, 3H), 1.29 – 1.18 (m, 2H), 1.10 – 0.95 (m, 3H). **^{13}C NMR ($CDCl_3$, 126 MHz):** δ 174.0, 168.8, 138.0, 137.9, 131.7, 131.0, 129.1, 126.9, 77.5, 50.7, 48.3, 32.9, 32.8, 29.8, 25.5, 24.8, 20.3. **HRMS (ESI):** m/z calc. for $C_{18}H_{26}N_3O_2$ $[M+H]^+$ 316.2020, found 316.2016.

***N*-cyclohexyl-2-(3-methoxyphenyl)-2-(3-oxopyrazolidin-1-yl)acetamide (12)**

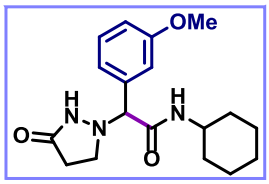

The product **12** was obtained as a colorless oil (24.8 mg, 50%) following the general procedure GP1. The crude material was purified by flash column chromatography (DCM/MeOH 20:1). **^{1}H NMR ($CDCl_3$, 400 MHz):** δ 7.21 (t, *J* = 7.9 Hz, 1H), 6.89 (d, *J* = 7.7 Hz, 1H), 6.86 (s, 1H), 6.82 (dd, *J* = 8.4, 2.1 Hz, 1H), 6.08 (brs, 1H), 4.11 (s, 1H), 3.74 (s, 3H), 3.71 – 3.62 (m, 1H), 3.18 (dt, *J* = 10.6, 7.9 Hz, 1H), 2.36 (t, *J* = 8.1 Hz, 2H), 1.96 (brs, 1H), 1.77 (td, *J* = 11.5, 10.8, 3.2 Hz, 2H), 1.62 – 1.57 (m, 2H), 1.55 – 1.50 (m, 1H), 1.32 – 1.16 (m, 2H), 1.11 – 0.99 (m, 3H). **^{13}C NMR ($CDCl_3$, 126 MHz):** δ 174.4, 168.6, 160.1, 136.7, 130.3, 120.6, 114.8,

113.8, 76.1, 55.4, 50.6, 48.2, 32.9, 32.9, 29.6, 25.5, 24.8. **HRMS (ESI):** m/z calc. for $C_{18}H_{26}N_3O_3$ $[M+H]^+$ 332.1969, found 332.1982.

_N_-cyclohexyl-2-(3-oxopyrazolidin-1-yl)-2-(pyridin-2-yl)acetamide (13)

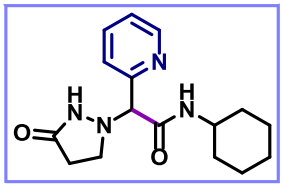

The product **13** was obtained as a colorless oil (21.3 mg, 47%) following the general procedure GP1. The crude material was purified by flash column chromatography (DCM/MeOH 20:1). **^{1}H NMR ($CDCl_3$, 400 MHz):** δ 8.56 (d, *J* = 4.5 Hz, 1H), 7.73 (tt, *J* = 7.7, 1.5 Hz, 1H), 7.50 (d, *J* = 7.8 Hz, 1H), 7.31 – 7.27 (m, 1H), 6.69 (d, *J* = 8.4 Hz, 1H), 4.50 (s, 1H), 3.68 (tq, *J* = 10.9, 3.9 Hz, 1H), 3.45 (brs, 1H), 3.41 – 3.34 (m, 1H), 2.49 (tt, *J* = 13.5, 6.8 Hz, 2H), 1.77 (dd, *J* = 22.6, 12.8 Hz, 2H), 1.64 (dt, *J* = 12.4, 3.8 Hz, 2H), 1.58 – 1.54 (m, 1H), 1.30 (dddd, *J* = 21.5, 12.6, 9.1, 4.5 Hz, 2H), 1.11 (tdd, *J* = 15.3, 11.8, 7.3 Hz, 3H). **^{13}C NMR ($CDCl_3$, 126 MHz):** δ 174.5, 167.4, 155.2, 149.6, 137.6, 123.9, 123.8, 77.3, 50.7, 48.4, 32.8, 32.7, 29.6, 25.5, 24.8. **HRMS (ESI):** m/z calc. for $C_{16}H_{23}N_4O_2$ $[M+H]^+$ 303.1816, found 303.1809.

_N_-cyclohexyl-2-(furan-2-yl)-2-(3-oxopyrazolidin-1-yl)acetamide (14)

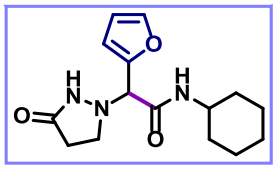

The product **14** was obtained as a colorless oil (22.7 mg, 52%) following the general procedure GP1. The crude material was purified by flash column chromatography (DCM/MeOH 20:1). **^{1}H NMR ($CDCl_3$, 400 MHz):** δ 7.44 (s, 1H), 6.45 (d, *J* = 3.5 Hz, 1H), 6.42 (brs, 1H), 6.39 (dt, *J* = 3.1, 1.3 Hz, 1H), 4.47 (s, 1H), 3.78 (dtt, *J* = 10.6, 7.1, 4.0 Hz, 1H), 3.46 (brs, 1H), 3.34 (dt, *J* = 11.5, 7.5 Hz, 1H), 2.25 (td, *J* = 8.4, 2.3 Hz, 2H), 1.88 (dt, *J* = 12.3, 4.1 Hz, 2H), 1.69 (dt, *J* = 13.2, 3.9 Hz, 2H), 1.60 (dt, *J* = 12.7, 4.0 Hz, 1H), 1.35 (td, *J* = 14.6, 14.2, 7.6 Hz, 2H), 1.21 – 1.10 (m, 3H). **^{13}C NMR ($CDCl_3$, 126 MHz):** δ 174.9, 166.3, 147.6, 143.7, 111.9, 111.3, 68.6, 50.4, 48.5, 32.9, 29.4, 25.5, 24.8. **HRMS (ESI):** m/z calc. for $C_{15}H_{22}N_3O_3$ $[M+H]^+$ 292.1656, found 292.1652.

(2S)-_N_-cyclohexyl-2-(3-oxo-5-phenylpyrazolidin-1-yl)-2-phenylacetamide (15)

The product **15** was obtained as a colorless oil (33.0 mg, 58 %) following the general procedure **GP1**. The crude material was purified by flash column chromatography

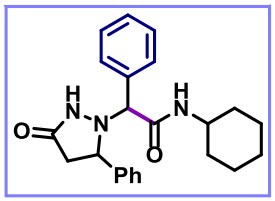

(DCM/MeOH 20:1). Reported spectra of one diastereoisomer. **^{1}H NMR ($CDCl_3$, 400 MHz):** δ 7.34 – 7.32 (m, 2H), 7.25 – 7.17 (m, 6H), 7.13 – 7.11 (m, 2H), 5.94 (s, 1H), 4.50 (s, 1H), 4.38 (d, *J* = 6.5 Hz, 1H), 3.70 – 3.63 (m, 1H), 2.87 (dd, *J* = 16.5, 8.1 Hz, 1H), 2.30 (d, *J* = 16.8 Hz, 1H), 1.72 (dd, *J* = 12.4, 9.5 Hz, 2H), 1.52 (t, *J* = 16.2 Hz, 2H), 1.28 – 1.18 (m, 3H), 1.07 – 0.92 (m, 3H). **^{13}C NMR ($CDCl_3$, 126 MHz):** δ 173.5, 168.3, 129.5, 129.2, 128.8, 128.0, 126.7, 76.2, 63.2, 48.5, 36.8, 32.9, 32.8, 25.5, 24.8. **HRMS (ESI)** m/z calc. for $C_{23}H_{28}N_3O_2$ $[M+H]^+$ 378.2176 found 378.2182.

4-(2-(cyclohexylamino)-2-oxo-1-(3-oxopyrazolidin-1-yl)ethyl)phenyl 2-(1,8-diethyl-1,3,4,9-tetrahydropyrano[3,4-b]indol-1-yl)acetate (16)

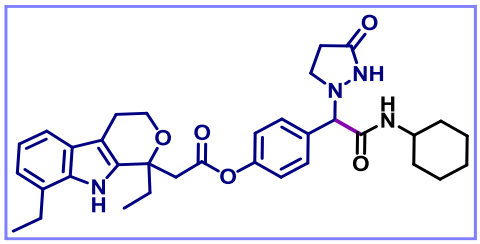

The product **16** was obtained as a white solid (73.8 mg, 84%) following the general procedure GP1. The crude material was purified by flash column chromatography (DCM/MeOH 20:1). **^{1}H NMR ($CDCl_3$, 400 MHz):** δ 8.72 (s, 1H), 7.41 (d, *J* = 8.4 Hz, 2H), 7.37 (d, *J* = 7.9 Hz, 1H), 7.09 – 7.00 (m, 4H), 6.14 (brs, 1H), 4.22 (s, 1H), 4.09 (dt, *J* = 10.1, 4.8 Hz, 1H), 4.01 (ddd, *J* = 11.5, 7.5, 4.4 Hz, 1H), 3.78 – 370 (m, 1H), 3.29 – 3.23 (m, 2H), 3.17 (d, *J* = 16.3 Hz, 1H), 2.90 – 2.45 (m, 5H), 2.53 – 2.36 (m, 2H), 2.14 (ddt, *J* = 34.1, 14.5, 7.3 Hz, 2H), 1.94 – 1.59 (m, 10H), 1.31 (td, *J* = 7.5, 3.2 Hz, 3H), 0.90 (t, *J* = 7.3 Hz, 3H). **^{13}C NMR ($CDCl_3$, 126 MHz):** δ 174.4, 171.1, 168.3, 150.9, 135.4, 134.7, 133.2, 129.6, 126.7, 126.3, 122.4, 120.7, 119.9, 116.1, 109.0, 75.6, 74.9, 60.9, 50.8, 48.3, 43.4, 33.0, 32.9, 31.0, 29.5, 25.5, 24.8, 24.2, 22.5, 13.9, 7.8. **HRMS (ESI):** m/z calc. for $C_{34}H_{43}N_4O_5$ $[M+H]^+$ 587.3228, found 587.3235.

Scope for the carbamoylation of nitrones

_N_-cyclohexyl-2-(hydroxy(methyl)amino)-2-phenylacetamide (17)

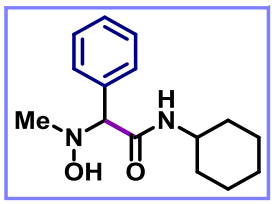

The product **17** was obtained as a yellow oil (19.5 mg, 50%) following the general procedure GP2. The crude material was purified by flash column chromatography (DCM/MeOH 20:1). **^{1}H NMR ($CDCl_3$, 400 MHz):** δ 7.39 – 7.32 (m, 5H), 6.30 (d, *J* = 8.1 Hz, 1H), 4.08 (s, 1H), 3.81-7.72 (m, 1H), 2.53 (s, 3H), 1.86 (d, *J* = 11.1 Hz, 2H), 1.62 (m,

3H), 1.38-1.28 (m, 2H), 1.17 – 1.10 (m, 3H). **^{13}C NMR ($CDCl_3$, 126 MHz):** δ 170.0, 160.4, 136.0, 128.9, 128.7, 78.9, 48.1, 45.7, 33.0, 25.6, 24.9. **HRMS (ESI):** m/z calc. for $C_{15}H_{23}N_2O_2$ $[M+H]^+$ 263.1754, found 263.1763.

2-(4-chlorophenyl)-*N*-cyclohexyl-2-(hydroxy(methyl)amino)acetamide (18)

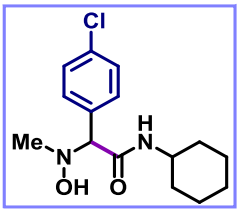

The product **18** was obtained as a colorless oil (21.8 mg, 49%) following the general procedure **GP2**. The crude material was purified by flash column chromatography (DCM/MeOH 20:1). **^{1}H NMR ($CDCl_3$, 400 MHz):** δ 7.42 (d, *J* = 8.4 Hz, 2H), 7.34 (d, *J* = 8.4 Hz, 2H), 6.63 (d, *J* = 6.9 Hz, 1H), 4.44 (s, 1H), 3.79 – 3.69 (m, 1H), 2.65 (s, 3H), 1.90 – 1.82 (m, 2H), 1.68 (ddd, *J* = 16.2, 7.9, 3.9 Hz, 2H), 1.62 – 1.57 (m, 1H), 1.32 (td, *J* = 13.2, 1.7 Hz, 2H), 1.25 (s, 1H), 1.22 – 1.08 (m, 3H). **^{13}C NMR ($CDCl_3$, 126 MHz):** δ 169.5, 134.6, 134.4, 130.1, 129.8, 129.1, 128.2, 78.1, 48.2, 45.8, 33.0, 33.0, 25.6, 24.9. **HRMS (ESI)** m/z calc. for $C_{15}H_{22}ClN_2O_2$ $[M+H]^+$ 297.1364, found 297.1378.

***N*-cyclohexyl-2-(hydroxy(methyl)amino)-2-(4-methoxyphenyl)acetamide (19)**

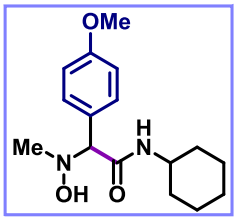

The product **19** was obtained as a white solid (22 mg, 50 %) following the general procedure GP2. The crude material was purified by flash column chromatography (DCM/MeOH 20:1). **^{1}H NMR ($CDCl_3$, 400 MHz):** δ 7.29 (d, *J* = 7.9 Hz, 2H), 6.87 (d, *J* = 8.0 Hz, 2H), 6.13 (d, *J* = 7.7 Hz, 1H), 4.01 (s, 1H), 3.80 (s, 3H), 3.78 – 3.74 (m, 1H), 2.51 (s, 3H), 1.87 (d, *J* = 11.6 Hz, 2H), 1.68 – 1.58 (m, 3H), 1.39 – 1.29 (m, 2H), 1.13 (ddd, *J* = 14.7, 11.6, 2.5 Hz, 3H). **^{13}C NMR ($CDCl_3$, 126 MHz):** δ 170.3, 159.9, 129.9, 114.3, 78.1, 55.4, 48.1, 45.5, 33.1, 25.6, 24.9. **HRMS (ESI):** m/z calc. for $C_{16}H_{25}N_2O_3$ $[M+H]^+$ 293.1860, found 293.1866.

Scope for the 4-carbamoyl-1,4-dihydropyridines

Methyl-(2-(3-oxopyrazolidin-1-yl)-2-phenylacetyl)-*L*-valinate (20)

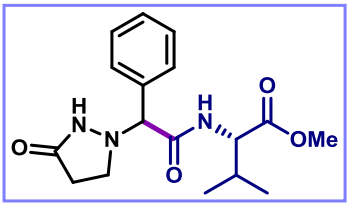

The product **20** was obtained as a yellow oil (30.5 mg, 61%, 1:1 dr) following the general procedure GP1. The crude material was purified by flash column chromatography (DCM/MeOH 20:1). **^{1}H NMR ($CDCl_3$, 400 MHz):** δ 7.47 – 7.45 (m, 2H), 7.42 – 7.35 (m, 3H), 7.03 (d, *J* = 9.6 Hz, 1H), 4.55 (dd, *J* = 9.6, 4.3 Hz, 1H), 4.41 (brs, 1H), 3.77 (s, 3H), 7.48 – 7.40 (m, 1H), 3.22 (brs, 1H), 2.64 – 2.53 (m, 1H),

2.44 (dd, *J* = 25.2, 14.8 Hz, 1H), 2.26 (tt, *J* = 14.0, 6.9 Hz, 1H), 0.90 (d, *J* = 6.9 Hz, 3H), 0.85 (d, *J* = 6.8 Hz, 3H). **^{13}C NMR ($CDCl_3$, 101 MHz):** δ 174.8, 174.5, 173.0, 169.9, 135.1, 129.3, 129.3, 129.2, 129.1, 128.8, 128.0, 75.6, 56.8, 56.6, 52.9, 52.6, 50.3, 31.3, 30.6, 29.8, 29.6, 19.3, 19.1, 17.7, 17.6. **HRMS (ESI):** m/z calc. for $C_{17}H_{24}N_3O_4$ $[M+H]^+$ 334.1761, found 334.1752.

Methyl-(2-(3-oxopyrazolidin-1-yl)-2-phenylacetyl)-*L*-alaninate (21)

The product **21** was obtained as a yellow oil (13.7 mg, 30%, 1:1 dr) following the general procedure GP1. The crude material was purified by flash column chromatography (DCM/MeOH 20:1). **^{1}H NMR ($CDCl_3$, 400 MHz):** δ 7.45 – 7.37 (m, 10H), 7.12 (d, *J* = 7.8 Hz, 1H), 6.91 (d, *J* = 7.7 Hz, 1H), 4.65 – 4.54 (m, 2H), 4.30 (s, 1H), 4.27 (s, 1H), 3.77 (s, 3H), 3.74 (s, 3H), 3.54 – 3.52 (m, 1H), 3.47 (t, *J* = 6.6 Hz, 1H), 3.39 – 3.25 (m, 2H), 2.60 – 2.50 (m, 1H), 2.44 – 2.38 (m, 2H), 2.36 – 2.29 (m, 1H), 1.41 (d, *J* = 7.4 Hz, 3H), 1.38 (d, *J* = 7.1 Hz, 3H).**^{13}C NMR ($CDCl_3$, 101 MHz):** δ 174.7, 174.5, 174.4, 173.7, 169.9, 169.4, 129.3, 129.2, 128.9, 128.1, 77.4, 75.8, 53.1, 52.8, 48.0, 47.7, 29.8, 29.8, 18.22, 17.7. **HRMS (ESI):** m/z calc. for $C_{15}H_{20}N_3O_4$ $[M+H]^+$ 306.1448, found 306.1458.

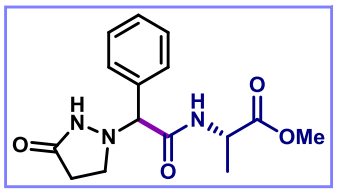

Methyl-2-(3-oxopyrazolidin-1-yl)-2-phenylacetyl)-*L*-prolinate (22)

The product **22** was obtained as a white solid (36.4 mg, 73%, 1:1 dr) following the general procedure GP1. The crude material was purified by flash column chromatography (DCM/MeOH 20:1). **^{1}H NMR ($CDCl_3$, 400 MHz):** δ 7.87 (brs, 1H), 7.68 (brs, 1H), 7.42 – 7.37 (m, 10H), 4.51 (dd, *J* = 8.2, 4.1 Hz, 1H), 4.45 (s, 1H), 4.44 – 4.41 (m, 1H), 4.23 – 4.11 (m, 1H), 3.75 (s, 3H), 3.71 (dd, *J* = 7.2, 4.3 Hz, 1H), 3.67 (s, 3H), 3.46 – 3.41 (m, 1H), 3.25 – 3.18 (m, 2H), 3.16 – 3.11 (m, 1H), 3.05 – 2.99 (m, 1H), 2.36 – 2.25 (m, 2H), 2.17 – 2.09 (m, 3H), 2.07 – 1.99 (m, 2H), 1.96 – 1.88 (m, 2H), 1.86 – 1.77 (m, 4H).**^{13}C NMR ($CDCl_3$, 126 MHz):** δ 187.9, 174.7, 174.5, 172.5, 172.1, 169.2, 168.8, 168.7, 130.1, 129.7, 129.4, 129.2, 129.0, 106.7, 73.5, 73.5, 59.5, 59.4, 52.6, 52.3, 49.8, 49.4, 46.9, 46.7, 30.2, 30.0, 28.7, 28.6, 25.1, 24.8. **HRMS (ESI):** m/z calc. for $C_{17}H_{22}N_3O_4$ $[M+H]^+$ 332.1605, found 332.1601.

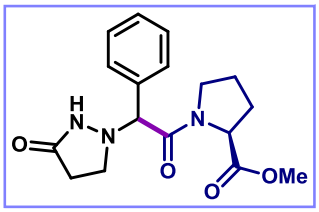

Methyl (2-(3-oxo-5-phenylpyrazolidin-1-yl)-2-phenylacetyl)-*L*-prolinate (23)

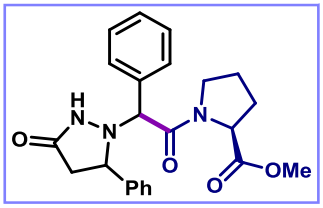

The product **23** was obtained as a colorless oil (30 mg, 50 %, 1:1 dr) following the general procedure GP1. **^{1}H** The crude material was purified by flash column chromatography (DCM/MeOH 20:1). **NMR ($CDCl_3$, 400 MHz):** δ 7.85 (s, 1H), 7.79 (s, 1H), 7.41 (dd, *J* = 7.1, 4.2 Hz, 4H), 7.30 (d, *J* = 5.2 Hz, 3H), 7.23 (d, *J* = 4.8 Hz, 3H), 7.19 – 7.12 (m, 10H), 4.70 (s, 1H), 4.64 (s, 1H), 4.53 – 4.47 (m, 1H), 4.46 – 4.41 (m, 2H), 4.34 (dd, *J* = 8.9, 3.8 Hz, 1H), 3.76 (s, 3H), 3.63 (s, 3H), 3.53 – 3.45 (m, 2H), 3.30 (dd, *J* = 16.1, 7.0 Hz, 1H), 3.21 – 3.13 (m, 2H), 3.05 (dd, *J* = 16.9, 8.9 Hz, 1H), 2.47 – 2.43 (m, 1H), 2.39 (dd, *J* = 17.6, 3.5 Hz, 1H), 2.08 – 1.92 (m, 5H), 1.88 – 1.82 (m, 3H). **^{13}C NMR ($CDCl_3$, 126 MHz):** δ 173.3, 172.8, 172.5, 172.23, 168.4, 168.1, 141.4, 141.3, 133.5, 132.9, 129.8, 129.5, 129.2, 128.8, 128.4, 128.3, 127.3, 127.3, 126.6, 126.5, 73.9, 73.5, 62.6, 61.7, 59.7, 59.6, 52.6, 52.3, 47.0, 46.6, 37.6, 37.0, 28.7, 28.5, 25.1, 24.9. **HRMS (ESI):** m/z calc. for $C_{23}H_{26}N_3O_4$ $[M+H]^+$ 408.1918, found 408.1916.

Methyl-(3-oxopyrazolidin-1-yl)(phenyl)methyl)-*L*-methioninate (24)

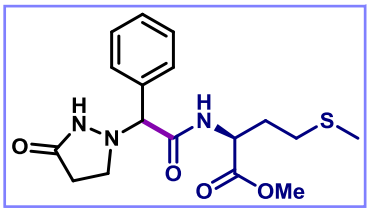

The product **24** was obtained as a yellow oil (40.5 mg, 74%, 1:1 dr) following the general procedure GP1. The crude material was purified by flash column chromatography (DCM/MeOH 20:1). **^{1}H NMR ($CDCl_3$, 400 MHz):** δ 7.41 – 7.36 (m, 4H), 7.34 – 7.29 (m, 6H), 4.65 (dtd, *J* = 16.1, 8.4, 4.7 Hz, 2H), 4.27 (s, 1H), 4.24 (s, 1H), 3.71 (s, 3H), 3.68 (s, 3H), 3.28 (dq, *J* = 26.1, 8.8 Hz, 2H), 2.41 – 2.22 (m, 6H), 2.06 (dtd, *J* = 16.3, 13.0, 11.9, 6.7 Hz, 2H), 1.95 (s, 3H), 1.92 (s, 3H). **^{13}C NMR ($CDCl_3$, 101 MHz):** δ 174.8, 174.5, 172.7, 169.9, 134.9, 129.3, 129.2, 128.8, 128.0, 75.8, 53.1, 52.9, 51.5, 51.2, 50.3, 31.2, 30.8, 30.3, 30.1, 29.8, 29.7, 15.6, 15.6. **HRMS (ESI):** m/z calc. for $C_{17}H_{24}N_3O_4S$ $[M+H]^+$ 366.1482, found 366.1474.

Methyl-(2-(3-oxopyrazolidin-1-yl)-2-phenylacetyl)-*L*-isoleucinate (25)

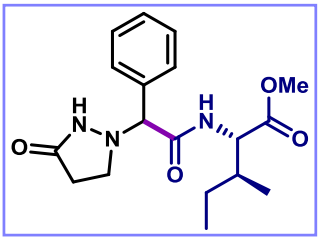

The product **25** was obtained as a colorless oil (25.5 mg, 49%, 1:1 dr) following the general procedure GP1. The crude material was purified by flash column chromatography (DCM/MeOH 20:1). **^{1}H NMR ($CDCl_3$, 400 MHz):** δ 7.47 – 7.29 (m, 10H), 7.13 (d, *J* = 8.9

Hz, 1H), 7.01 (d, *J* = 9.4 Hz, 1H), 4.58 (dd, *J* = 9.4, 4.4 Hz, 2H), 4.35 (s, 1H), 4.29 (s, 1H), 3.76 (s, 3H), 3.72 (s, 3H), 3.34 (dq, *J* = 18.7, 8.6, 8.1 Hz, 2H), 2.60 – 2.30 (m, 4H), 1.99 – 1.93 (m, 1H), 1.89 – 1.80 (m, 1H), 1.40 – 1.21 (m, 4H), 0.93 – 0.87 (m, 6H), 0.85 – 0.77 (m, 6H). **^{13}C NMR ($CDCl_3$, 126 MHz):** δ 174.8, 174.6, 173.1, 172.8, 170.1, 169.7, 135.0, 129.3, 129.2, 129.1, 128.9, 128.1, 128.0, 75.7, 56.3, 52.8, 52.5, 37.8, 37.2, 29.8, 29.7, 25.1, 15.9, 15.6, 11.8, 11.6. **HRMS (ESI):** m/z calc. for $C_{18}H_{26}N_3O_4$ $[M+H]^+$ 348.1918, found 348.1938.

Methyl (2-(3-oxopyrazolidin-1-yl)-2-(4-(trifluoromethyl)phenyl)acetyl)-*L*-isoleucinate (26)

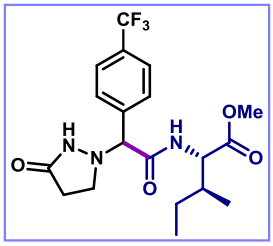

The product **26** was obtained as a colorless oil (34.9 mg, 56%, 1:1 dr) following the general procedure GP1. The crude material was purified by flash column chromatography (DCM/MeOH 20:1). **^{1}H NMR ($CDCl_3$, 400 MHz):** δ 7.70 – 7.56 (m, 8H), 7.08 (d, *J* = 9.6 Hz, 1H), 4.60 – 4.55 (m, 2H), 4.54 (s, 1H), 4.38 (s, 1H), 3.76 (s, 3H), 3.75 (s, 3H), 3.41 (dtt, *J* = 11.7, 8.5, 3.5 Hz, 2H), 2.64 – 2.50 (m, 2H), 2.39 (dt, *J* = 16.4, 8.0 Hz, 2H), 2.00 – 1.90 (m, 1H), 1.79 (brs, 1H), 1.39 – 1.23 (m, 2H), 1.20 – 1.00 (m, 2H), 0.88 (t, *J* = 7.3 Hz, 3H), 0.80 (d, *J* = 6.9 Hz, 6H), 0.78 – 0.72 (m, 3H). **^{13}C NMR ($CDCl_3$, 126 MHz):** δ 175.2, 174.6, 173.5, 169.2, 169.1, 139.4, 139.1, 131.23 (q, *J* = 29.9 Hz), 129.1, 128.4, 126.2 (d, *J* = 3.4 Hz), 125.9 (d, *J* = 3.3 Hz), 123.9 (dd, *J* = 272.4, 15.8 Hz), 76.5, 75.0, 56.3, 56.1, 52.9, 52.7, 50.3, 50.1, 37.9, 37.2, 29.8, 29.5, 25.1, 25.0, 15.9, 15.6, 11.7, 11.6. **HRMS (ESI):** m/z calc. for $C_{19}H_{25}F_3N_3O_4$ $[M+H]^+$ 416.1800, found 416.1804.

Methyl-(2-(3-oxopyrazolidin-1-yl)-2-phenylacetyl)-*L*-serinate (27)

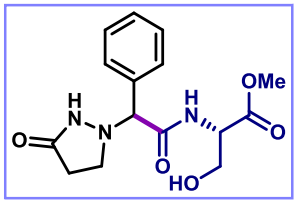

The product **27** was obtained as a colorless oil (15.8 mg, 33%, 1:1 dr) following the general procedure GP1. The crude material was purified by flash column chromatography (DCM/MeOH 20:1). **^{1}H NMR ($CDCl_3$, 400 MHz):** δ 7.71 (d, *J* = 7.2 Hz, 2H), 7.47 – 7.44 (m, 2H), 7.38 – 7.34 (m, 8H), 4.63 (d, *J* = 7.5 Hz, 1H), 4.55 (dd, *J* = 6.6, 3.5 Hz, 1H), 4.39 (s, 1H), 4.33 (s, 1H), 4.03 – 3.93 (m, 4H), 3.78 (s, 6H), 3.36 (dt, *J* = 12.0, 8.3 Hz, 3H), 3.06 – 3.01 (m, 1H), 2.66 (dt, *J* = 17.4, 9.0 Hz, 1H), 2.53 (t, *J* = 7.1 Hz, 1H), 2.33 (ddt, *J* = 17.3, 13.9, 6.9 Hz, 2H). **^{13}C NMR ($CDCl_3$, 126 MHz):** δ 176.7, 171.0, 169.6, 135.2, 129.3, 129.2, 128.2, 62.8, 62.6, 55.5, 54.8, 53.2, 52.9, 50.4, 49.7, 30.0, 29.9. **HRMS (ESI):** m/z calc. for $C_{15}H_{20}N_3O_5$ $[M+H]^+$ 322.1397, found 322.1410.

Methyl ((3-oxopyrazolidin-1-yl)(phenyl)methyl)-*L*-tyrosinate (28)

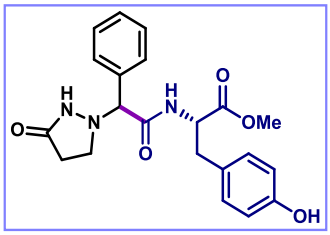

The product **28** was obtained as a colorless oil (29.5 mg, 49%, 1:1 dr) following the general procedure GP1. Reported spectra of the major diastereoisomer. The crude material was purified by flash column chromatography (DCM/MeOH 20:1). **^{1}H NMR (Methanol-*d*4, 400 MHz):** δ 7.90 (s, 1H), 7.41 – 7.32 (m, 5H), 6.76 (d, *J* = 8.1 Hz, 2H), 6.54 (d, *J* = 8.3 Hz, 2H), 4.63 (dd, *J* = 8.5, 5.2 Hz, 1H), 4.42 (s, 1H), 3.69 (s, 3H), 3.22 – 3.19 (m, 2H), 3.01 (dd, *J* = 13.9, 5.1 Hz, 1H), 2.86 (dd, *J* = 14.0, 8.7 Hz, 1H), 2.41 – 2.34 (m, 2H). **^{13}C NMR (Methanol-*d*4, 126 MHz):** δ 177.4, 173.3, 172.0, 157.3, 136.5, 131.3, 131.1, 130.1, 129.9, 129.8, 128.3, 116.2, 75.8, 55.0, 52.7, 37.1, 30.3. **HRMS (ESI):** m/z calc. for $C_{21}H_{23}N_3O_5$ $[M]^+$ 397.1638, found 398.1656.

Methyl-(3-oxopyrazolidin-1-yl)(phenyl)methyl)-*L*-tryptophanate (29)

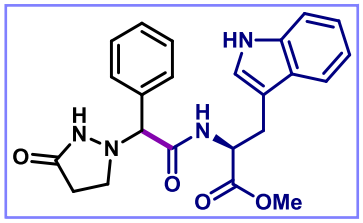

The product **29** was obtained as a yellow oil (42.2 mg, 67%,1:1 dr) following the general procedure GP1. Reported spectra of the major diastereoisomer. The crude material was purified by flash column chromatography (DCM/MeOH 20:1). **^{1}H NMR ($CDCl_3$, 400 MHz):** δ 8.43 (brs, 1H), 7.50 (d, *J* = 7.8 Hz, 1H), 7.39 – 7.29 (m, 6H), 7.25 – 7.13 (m, 3H), 6.91 (brs, 1H), 4.95 – 4.90 (m, 1H), 4.36 (s, 1H), 3.75 (s, 3H), 3.30 (d, *J* = 5.6 Hz, 2H), 2.43 – 2.32 (m, 2H), 2.30 – 2.17 (m, 2H). **^{13}C NMR ($CDCl_3$, 101 MHz):** δ 174.4, 173.3, 136.2, 134.4, 129.1, 128.2, 127.5, 123.0, 122.5, 119.9, 118.5, 111.6, 109.4, 76.5, 53.0, 52.6, 49.9, 29.6, 26.9. **HRMS (ESI):** m/z calc. for $C_{23}H_{25}N_4O_4$ $[M+H]^+$ 421.1870, found 421.1863.

Methyl (2-(3-oxopyrazolidin-1-yl)-2-phenylacetyl)-*L*-phenylalaninate (30)

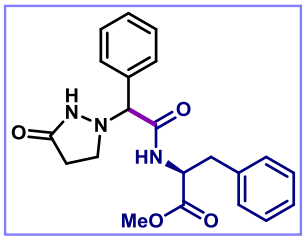

The product **30** was obtained as a yellow oil (37.2 mg, 65%,1:1 dr) following the general procedure GP1. The crude material was purified by flash column chromatography (DCM/MeOH 20:1). **^{1}H NMR (Methanol-*d*4, 400 MHz):** δ 8.02 (d, *J* = 8.2 Hz, 1H), 7.36 – 7.32 (m, 8H), 7.24 – 7.18 (m, 5H), 7.14 – 7.12 (m, 5H), 6.98 – 6.95 (m, 2H), 4.72 (ddd, *J* = 11.5, 9.2, 5.1 Hz, 2H), 4.42 (s, 1H), 4.35 (s, 1H), 3.70 (s, 6H), 3.23 (dd, *J* = 13.9, 5.0 Hz, 2H), 3.19 – 3.15 (m, 2H), 3.13 (dd, *J* = 13.9, 5.1 Hz, 2H), 2.99 (ddd, *J* =

22.2, 13.9, 9.3 Hz, 2H), 2.42 – 2.33 (m, 4H). **^{13}C NMR (Methanol-*d*4, 101 MHz):** δ 177.5, 173.4, 173.2, 172.1, 172.0, 138.1, 137.8, 136.6, 136.4, 133.9, 130.7, 130.3, 130.1, 130.1, 129.9, 129.85, 129.8, 129.6, 129.5, 127.9, 127.8, 76.6, 75.9, 54.9, 54.8, 52.9, 52.8, 51.3, 51.1, 37.8, 37.7, 30.3. **HRMS (ESI):** m/z calc. for $C_{21}H_{24}N_3O_4$ $[M+H]^+$ 382.1761, found 382.1757.

Methyl (2*R*)-2-(2-(3-oxopyrazolidin-1-yl)-2-(4-(trifluoromethyl)phenyl)acetamido)-2-phenylacetate (31)

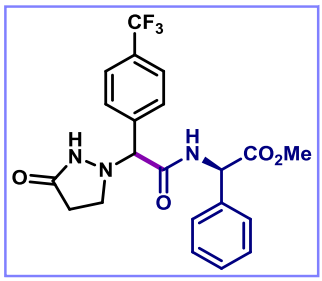

The product **31** was obtained as a white solid (78 mg, 45 %, 1:1 d.r) following the general procedure GP1. The crude material was purified by flash column chromatography (DCM/MeOH 20:1). **^{1}H NMR (Methanol-*d*4, 400 MHz):** δ 7.71– 7.61 (m, 8H), 7.32 – 7.25 (m, 10H), 5.46 (s, 1H), 5.40 (s, 1H), 4.67 (s, 1H), 4.63 (s, 1H), 3.69 (s, 3H), 3.59 (s, 3H), 3.40 – 3.28 (m, 4H), 2.43 (brs, 4H). **^{13}C NMR (Methanol-*d*4, 101 MHz):** δ 177.7, 172.4, 172.3, 171.1, 170.9, 141.1, 136.9, 136.7, 132.0, 131.7, 130.7, 130.6, 129.9, 129.9, 129.7, 128.8, 128.7, 126.6, 126.5, 126.5, 75.3, 74.9, 58.3, 58.1, 53.1, 53.1, 51.5, 51.3, 30.3. **HRMS (ESI):** m/z calc. for $C_{21}H_{21}F_3N_3O_4$ $[M+H]^+$ 436.1479, found 436.1507.

Methyl 2-methyl-2-(2-(3-oxopyrazolidin-1-yl)-2-phenylacetamido)propanoate (32)

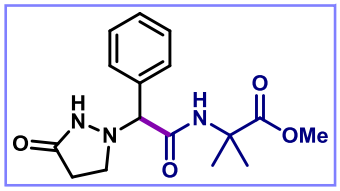

The product **32** was obtained as a yellow oil (33.5 mg, 70%) following the general procedure GP1. **^{1}H NMR** The crude material was purified by flash column chromatography (DCM/MeOH 20:1). **($CDCl_3$, 400 MHz):** δ 7.39 – 7.35 (m, 5H), 6.89 (brs, 1H), 4.20 (s, 1H), 3.71 (s, 3H), 3.30 (dt, *J* = 10.8, 7.6 Hz, 1H), 2.41 (tt, *J* = 16.6, 9.2 Hz, 2H), 1.52 (s, 3H), 1.49 (s, 3H). **^{13}C NMR ($CDCl_3$, 101 MHz):** δ 175.4, 174.5, 169.6, 134.7, 129.3, 128.6, 76.6, 56.9, 53.1, 50.5, 29.8, 25.5, 24.5. **HRMS (ESI):** m/z calc. for $C_{16}H_{22}N_3O_4$ $[M+H]^+$ 320.1605, found 320.1607.

Methyl (2-(3-oxopyrazolidin-1-yl)-2-phenylacetyl)-*L*-valyl-*L*-methioninate (33)

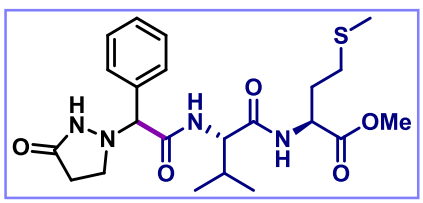

The product **33** was obtained as a yellow oil (51.5 mg, 74%, 1:1 dr) following the general procedure GP1. The

crude material was purified by flash column chromatography (DCM/MeOH 20:1). **^{1}H NMR ($CDCl_3$, 400 MHz):** δ 7.34 – 7.08 (m, 20H), 7.01 (d, *J* = 7.9 Hz, 1H), 6.77 (d, *J* = 8.7 Hz, 2H), 4.86 – 4.71 (m, 2H), 4.48 – 4.36 (m, 2H), 4.22 (s, 1H), 4.21 (s, 1H), 3.72 (s, 3H), 3.69 (s, 3H), 3.13 – 2.95 (m, 4H), 2.53 – 2.46 (m, 1H), 2.42 – 2.25 (m, 3H), 2.20 – 1.95 (m, 4H), 1.40 (dt, *J* = 11.0, 6.8 Hz, 2H), 0.89 – 0.80 (m, 8H), 0.68 (t, *J* = 7.2 Hz, 4H). **^{13}C NMR ($CDCl_3$, 101 MHz):** δ 174.9, 174.6, 172.2, 172.2, 171.9, 171.0, 170.7, 170.1, 135.2, 134.9, 129.4, 129.3, 128.9, 128.0, 75.6, 58.4, 58.1, 52.7, 52.7, 52.0, 51.7, 31.4, 31.2, 31.1, 30.9, 30.0, 29.8, 29.7, 19.5, 19.2, 18.1, 17.9, 15.6, 15.5. **HRMS (ESI):** m/z calc. for $C_{22}H_{33}N_4O_5S$ $[M+H]^+$ 465.2166, found 465.2163.

Methyl (2-(4-bromophenyl)-2-(3-oxopyrazolidin-1-yl)acetyl)-*L*-valyl-*L*-methioninate (34)

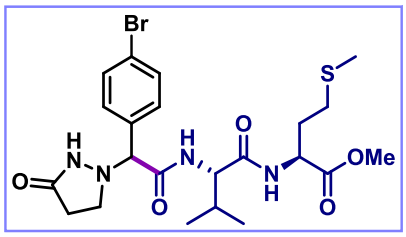

The product **34** was obtained as a yellow oil (78.1 mg, 96%, 1:1 dr) following the general procedure GP1. Reported spectra of the major diastereoisomer. The crude material was purified by flash column chromatography (DCM/MeOH 20:1). **^{1}H NMR ($CDCl_3$, 400 MHz):** δ 7.51 (d, *J* = 7.9 Hz, 1H), 7.32 (d, *J* = 7.8 Hz, 1H), 7.13 (d, *J* = 8.9 Hz, 1H), 6.89 (d, *J* = 7.6 Hz, 1H), 4.70 (q, *J* = 7.3 Hz, 1H), 4.35 – 4.27 (m, 1H), 4.26 (s, 1H), 3.75 (s, 3H), 3.33 (dq, *J* = 18.9, 9.3 Hz, 2H), 2.50 (t, *J* = 7.2 Hz, 2H), 2.46 – 2.31 (m, 2H), 2.20 – 2.12 (m, 1H), 2.09 (s, 3H), 2.00 (tt, *J* = 13.9, 7.0 Hz, 2H), 0.90 (t, *J* = 7.6 Hz, 3H).**^{13}C NMR ($CDCl_3$, 101 MHz):** δ 174.7, 172.2, 171.8, 170.2, 134.2, 132.4, 129.6, 123.3, 76.3, 58.1, 52.7, 52.0, 50.0, 31.1, 30.9, 30.0, 29.6, 19.5, 18.0, 15.6. **HRMS (ESI):** m/z calc. for $C_{22}H_{32}BrN_4O_5S$ $[M+H]^+$ 543.1271, found 543.1294.

Methyl (2-(3-oxopyrazolidin-1-yl)-2-phenylacetyl)-*L*-phenylalanyl-*L*-valinate (35)

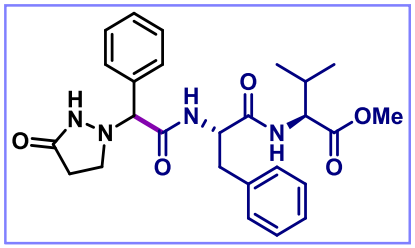

The product **35** was obtained as a yellow oil (56.9 mg, 79%, 1:1 dr) following the general procedure GP1. The crude material was purified by flash column chromatography (DCM/MeOH 20:1). **^{1}H NMR ($CDCl_3$, 400 MHz):** δ 7.36 – 7.06 (m, 6H), 7.01 (d, *J* = 7.9 Hz, 0H), 6.77 (d, *J* = 8.7 Hz, 1H), 4.87 – 4.68 (m, 1H), 4.50 – 4.34 (m, 1H), 4.22 (s, 1H), 4.21 (s, 1H), 3.72 (s, 1H), 3.69 (s, 1H), 3.16 – 2.93 (m, 1H), 2.55 – 2.39 (m, 0H), 2.31 (dp, *J* = 15.9, 7.8 Hz, 1H), 2.04 (ddq, *J* = 26.4, 12.8, 6.6 Hz, 1H), 1.40 (dt, *J* = 11.0,

6.8 Hz, 1H), 0.91 – 0.78 (m, 2H), 0.68 (t, *J* = 7.2 Hz, 1H). **^{13}C NMR ($CDCl_3$, 101 MHz):** δ 174.6, 172.0, 171.9, 170.7, 170.3, 170.0, 136.3, 136.1, 134.7, 129.4, 129.2, 129.2, 129.1, 129.1, 128.9, 128.8, 128.7, 128.5, 128.2, 127.3, 127.2, 76.6, 76.0, 57.7, 57.5, 54.0, 53.9, 52.2, 52.2, 50.4, 50.1, 37.9, 37.3, 31.0, 30.9, 29.7, 29.5, 18.9, 18.8, 17.8, 17.6. **HRMS (ESI):** m/z calc. for $C_{26}H_{33}N_4O_5$ $[M+H]^+$ 481.2445, found 481.2446.

Benzyl (2-(3-oxopyrazolidin-1-yl)-2-phenylacetyl)-*L*-leucyl-*L*-leucinate (36)

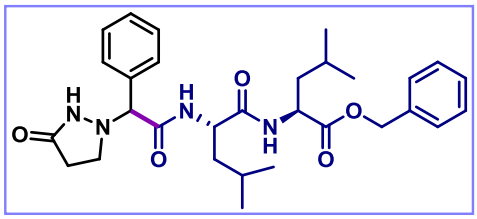

The product **36** was obtained as a yellow oil (78.8 mg, 98%, 1:1 dr) following the general procedure GP1. The crude material was purified by flash column chromatography (DCM/MeOH 20:1). **^{1}H NMR ($CDCl_3$, 400 MHz):** δ 7.41 – 7.32 (m, 17H), 7.03 (d, *J* = 7.7 Hz, 1H), 6.99 (d, *J* = 8.7 Hz, 1H), 6.63 (d, *J* = 7.4 Hz, 1H), 5.24 – 5.12 (m, 4H), 4.58 (td, *J* = 8.9, 4.1 Hz, 1H), 4.48 (p, *J* = 7.8 Hz, 2H), 4.33 (s, 1H), 4.31 (s, 1H), 3.36 – 3.29 (m, 2H), 2.63 – 2.46 (m, 2H), 2.37 – 2.21 (m, 2H), 1.66 – 1.47 (m, 12H), 0.90 – 0.85 (m, 16H), 0.79 – 0.75 (m, 8H). **^{13}C NMR ($CDCl_3$, 101 MHz):** δ 174.7, 174.4, 173.6, 173.1, 172.4, 171.9, 170.5, 169.9, 135.3, 135.0, 129.2, 129.0, 128.6, 128.6, 128.4, 128.4, 127.9, 75.3, 67.5, 67.4, 51.1, 50.9, 50.8, 50.7, 41.2, 40.9, 40.7, 40.0, 29.7, 29.6, 24.9, 24.9, 24.8, 24.7, 22.9, 22.9, 21.9, 21.7. **HRMS (ESI):** m/z calc. for $C_{30}H_{41}N_4O_5$ $[M+H]^+$ 537.3071, found 537.3077.

Methyl (-2-(3-oxopyrazolidin-1-yl)-2-phenylacetyl)-*L*-prolyl-*L*-isoleucinate (37)

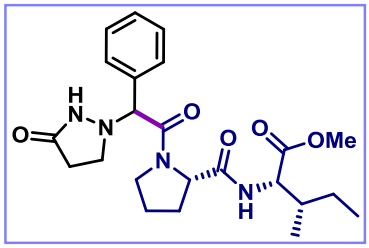

The product **37** was obtained as a yellow oil (49.9 mg, 75%, 1:1 dr) following the general procedure GP1. The crude material was purified by flash column chromatography (DCM/MeOH 20:1). **^{1}H NMR ($CDCl_3$, 400 MHz):** δ 8.33 (s, 1H), 8.17 (d, *J* = 9.0 Hz, 1H), 7.48 (ddd, *J* = 7.1, 3.9, 2.0 Hz, 3H), 7.45 – 7.42 (m, 1H), 7.41 – 7.37 (m, 5H), 4.57 (ddd, *J* = 9.6, 5.9, 2.8 Hz, 2H), 4.49 (dd, *J* = 8.5, 4.7 Hz, 1H), 4.44 (dd, *J* = 8.6, 5.0 Hz, 1H), 4.40 (s, 1H), 3.79 (s, 3H), 3.69 (s, 3H), 3.71 – 3.66 (m, 2H), 3.61 – 3.55 (m, 2H), 3.27 – 3.13 (m, 2H), 3.10 – 3.01 (m, 2H), 2.48 – 2.23 (m, 4H), 2.10 – 1.80 (m, 10H), 1.50 – 1.33 (m, 4H), 0.93 – 0.87 (m, 12H). **^{13}C NMR ($CDCl_3$, 101 MHz):** δ 174.9, 173.4, 172.3, 170.5, 170.4, 170.3, 170.1, 132.8, 129.9, 129.6, 129.5, 129.4, 129.3, 74.6, 60.0, 57.8, 57.0, 56.7, 52.8, 52.1, 49.5, 49.4, 47.2, 47.0, 38.1, 37.6, 30.1, 27.2,

26.2, 25.1, 25.1, 25.0, 24.2, 15.8, 15.7, 11.7, 11.7. **HRMS (ESI):** m/z calc. for $C_{23}H_{33}N_4O_5$ $[M+H]^+$ 445.2445, found 445.2475.

Methyl (2-(3-oxopyrazolidin-1-yl)-2-phenylacetyl)-*L*-prolyl-*L*-serinate (38)

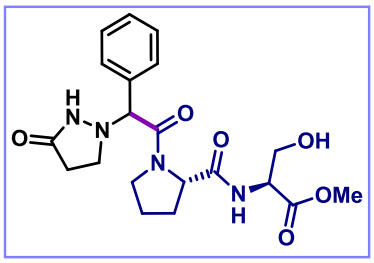

The product **38** was obtained as a yellow oil (31 mg, 51 %, 1:1 dr) following the general procedure GP1. The crude material was purified by flash column chromatography (DCM/MeOH 20:1). **^{1}H NMR ($CDCl_3$, 400 MHz):** δ 8.37 (brs, 1H), 7.81 (d, *J* = 7.8 Hz, 1H), 7.46 – 7.40 (m, 5H), 4.62 (dd, *J* = 16.4, 7.3 Hz, 2H), 4.51 (s, 1H), 4.05 (dd, *J* = 11.1, 2.5 Hz, 1H), 3.90 (d, *J* = 10.6 Hz, 1H), 3.78 (s, 3H), 3.71 – 3.64 (dd, m, 1H), 3.29 – 3.22 (m, 1H), 3.16 – 3.05 (m, 2H), 2.55 – 2.49 (m, 1H), 2.29 – 2.24 (m, 2H), 2.12 – 2.08 (m, 1H), 1.85 – 1.75 (m, 2H). **^{13}C NMR ($CDCl_3$, 101 MHz):** δ 175.3, 171.3, 169.8, 132.6, 129.6, 129.3, 74.03, 62.5, 60.6, 54.7, 52.9, 49.1, 47.0, 30.0, 27.4, 24.8. **HRMS (ESI):** m/z calc. for $C_{20}H_{27}N_4O_6$ $[M+H]^+$ 419.1925, found 419.1924.

Methyl (2*S*)-2-(2-(2-(3-oxopyrazolidin-1-yl)-2-phenylacetamido)acetamido)-2-phenylacetate (39)

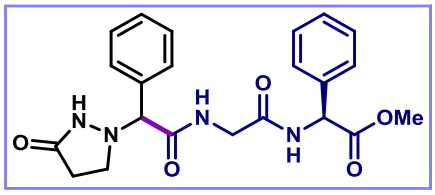

The product **39** was obtained as a yellow oil (39.4 mg, 62%, 1:1 dr) following the general procedure GP1. The crude material was purified by flash column chromatography (DCM/MeOH 20:1). **^{1}H NMR ($CDCl_3$, 400 MHz):** δ 7.37 – 7.29 (m, 10H), 7.15 (d, *J* = 6.6 Hz, 1H), 7.01 (d, *J* = 7.4 Hz, 1H), 5.57 (d, *J* = 7.1 Hz, 1H), 4.29 (dd, *J* = 6.5 Hz, 1H), 4.24 (d, *J* = 16.5, 7.3 Hz, 1H), 4.09 (dd, *J* = 17.9, 7.4 Hz, 1H), 3.72 (s, 3H), 3.32 (p, *J* = 8.9 Hz, 1H), 3.13 (brs, 1H), 2.52 (brs, 1H), 2.31 (dt, *J* = 16.1, 7.9 Hz, 1H). **^{13}C NMR ($CDCl_3$, 101 MHz):** δ 174.8, 174.8, 171.5, 171.3, 170.9, 170.8, 169.0, 168.9, 136.0, 135.7, 134.8, 129.2, 129.2, 128.9, 128.8, 128.4, 128.3, 127.5, 127.4, 76.4, 56.7, 56.7, 53.2, 53.1, 50.1, 50.1, 42.4, 42.3, 29.8, 29.8. **HRMS (ESI):** m/z calc. for $C_{22}H_{25}N_4O_5$ $[M+H]^+$ 425.1819, found 425.1844.

Methyl-(4*R*)-4-((3*R*,8*R*,9*S*,10*S*,13*R*,14*S*,17*R*)-10,13-dimethyl-3-(2-(3-oxopyrazolidin-1-yl)-2-phenylacetamido)hexadecahydro-1*H*-cyclopenta[a]phenanthren-17-yl)pentanoate (40)

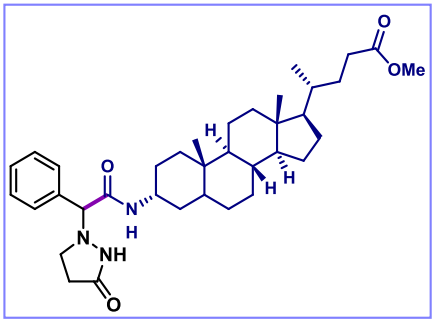

The product **40** was obtained as a yellow oil (42.6 mg, 48%) following the general procedure GP1. The crude material was purified by flash column chromatography (DCM/MeOH 20:1). **^{1}H NMR ($CDCl_3$, 400 MHz):** δ 7.37 – 7.24 (m, 5H), 6.46 (brs, 1H), 4.24 (s, 1H), 4.08 – 4.03 (m, 1H), 3.59 (s, 1H), 3.25 (dd, *J* = 17.0, 8.5 Hz, 1H), 2.45 – 2.20 (m, 3H), 2.14 (ddd, *J* = 15.6, 9.7, 6.4 Hz, 1H), 1.95 – 1.85 (m, 2H), 1.82 – 1.67 (m, 3H), 1.51 – 1.42 (m, 3H), 1.34 – 0.90 (m, 17H), 0.83 (d, *J* = 5.9 Hz, 6H), 0.76 – 0.68 (m, 2H), 0.56 (s, 3H). **^{13}C NMR ($CDCl_3$, 101 MHz):** δ 174.9, 174.3, 168.7, 135.1, 129.4, 128.5, 128.5, 76.0, 56.5, 56.0, 51.6, 50.7, 45.5, 42.8, 40.2, 39.8, 38.2, 35.7, 35.4, 35.1, 31.4, 31.4, 31.1, 31.1, 30.5, 30.3, 29.6, 28.3, 26.8, 26.8, 26.2, 24.7, 24.5, 24.3, 21.1, 18.3, 12.1. **HRMS (ESI):** m/z calc. for $C_{36}H_{54}N_3O_4$ $[M+H]^+$ 592.4109, found 592.4105.

Methyl 4-methyl-3-((2-(3-oxopyrazolidin-1-yl)-2-phenylacetamido)methyl)hexanoate (41)

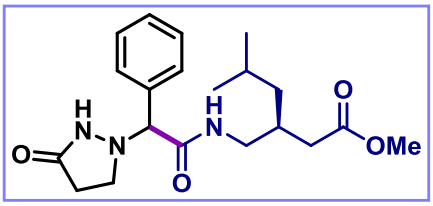

The product **41** was obtained as a yellow oil (30.9 mg, 55%) following the general procedure GP1. The crude material was purified by flash column chromatography (DCM/MeOH 20:1). **^{1}H NMR ($CDCl_3$, 400 MHz):** δ 7.74 (brs, 1H), 7.42 – 7.34 (m, 5H), 6.61 – 6.54 (m, 1H), 4.22 (s, 1H), 3.65 (d, *J* = 5.7 Hz, 3H), 3.30 – 3.21 (m, 3H), 3.14 (ddt, *J* = 13.7, 10.2, 6.8 Hz, 1H), 2.41 – 2.32 (m, 2H), 2.27 – 2.20 (m, 1H), 2.14 (dt, *J* = 15.2, 7.7 Hz, 1H), 2.09 – 2.02 (m, 1H), 1.55 (dp, *J* = 13.2, 6.6 Hz, 1H), 1.03 (td, *J* = 7.1, 3.9 Hz, 2H), 0.83 (dd, *J* = 6.6, 1.4 Hz, 3H), 0.79 (dd, *J* = 12.9, 6.5 Hz, 3H). **^{13}C NMR ($CDCl_3$, 101 MHz):** δ 174.5, 174.5, 174.1, 174.0, 170.0, 135.4, 135.3, 129.4, 129.3, 128.4, 128.4, 76.4, 76.4, 52.0, 52.0, 50.7, 50.6, 43.4, 43.3, 41.8, 37.5, 37.4, 33.2, 29.7, 25.2, 22.8, 22.8, 22.6, 22.5. **HRMS (ESI):** m/z calc. for $C_{20}H_{30}N_3O_4$ $[M+H]^+$ 376.2231, found 376.2225.

***N*-((1*r*,3*R*,5*S*,7*r*)-3,5-dimethyladamantan-1-yl)-2-(3-oxopyrazolidin-1-yl)-2-phenylacetamide (42)**

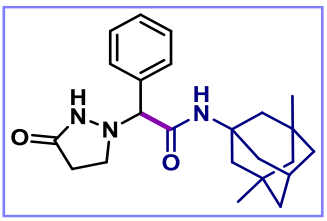

The product **42** was obtained as a yellow oil (44.6 mg, 78%) following the general procedure **GP1**. The crude material was purified by flash column chromatography (DCM/MeOH 20:1). **^{1}H NMR ($CDCl_3$, 400 MHz):** δ 7.41 – 7.36 (m, 5H), 6.00 (s, 1H), 4.21 (s, 1H), 3.29 (dd, *J* = 16.2, 8.3 Hz, 2H), 2.43 - 2.38 (m, 2H), 2.13 – 2.11 (m, 1H), 1.77 (s, 2H), 1.57 (dd, *J* = 26.2, 11.7 Hz, 4H), 1.30 – 1.25 (m, 4H), 1.12 (s, 2H), 0.82 (s, 6H). **^{13}C NMR ($CDCl_3$, 101 MHz):** δ 174.1, 168.3, 134.9, 129.4, 128.5, 76.4, 53.9, 50.6, 47.5, 42.6, 40.0, 32.5, 30.1, 29.6. **HRMS (ESI)** m/z calc. for $C_{23}H_{32}N_3O_2$ $[M+H]^+$ 382.2489, found 382.2483.

***N*-octyl-2-(3-oxopyrazolidin-1-yl)-2-phenylacetamide (43)**

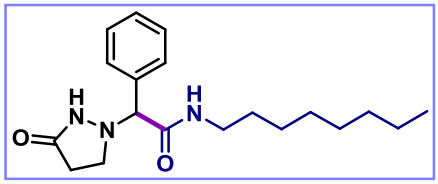

The product **43** was obtained as a yellow oil (22.0 mg, 44%) following the general procedure GP1. The crude material was purified by flash column chromatography (DCM/MeOH 20:1). **^{1}H NMR ($CDCl_3$, 400 MHz):** δ 7.38 – 7.34 (m, 5H), 6.32 (brs, 1H), 4.22 (s, 1H), 3.21 (tq, *J* = 13.7, 7.0 Hz, 2H), 2.39 (t, *J* = 8.0 Hz, 2H), 1.46 – 1.38 (m, 12H), 1.30 – 1.21 (m, 12H), 0.86 (t, *J* = 6.8 Hz, 3H). **^{13}C NMR ($CDCl_3$, 101 MHz):** δ 174.7, 169.7, 135.2, 129.2, 129.2, 128.5, 76.2, 50.6, 39.5, 31.8, 29.6, 29.5, 29.2, 26.9, 22.7, 14.2. **HRMS (ESI):** m/z calc. for $C_{19}H_{30}N_3O_2$ $[M+H]^+$ 332.2333, found 332.2358.

Methyl 3-(2-(3-oxopyrazolidin-1-yl)-2-phenylacetamido)propanoate (44)

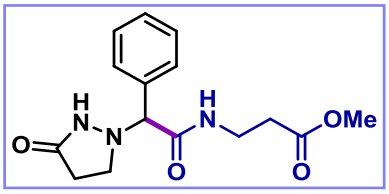

The product **44** was obtained as a white solid (26.3 mg, 57%) following the general procedure GP1. The crude material was purified by flash column chromatography (DCM/MeOH 20:1). **^{1}H NMR ($CDCl_3$, 400 MHz):** δ 7.38 – 7.33 (m, 5H), 4.24 (s, 1H), 3.65 (s, 3H), 3.55 – 3.39 (m, 2H), 3.29 – 3.23 (m, 2H), 2.58 – 2.43 (m, 3H), 2.34 (dd, *J* = 16.6, 8.3 Hz, 1H). **^{13}C NMR ($CDCl_3$, 101 MHz):** δ 174.8, 173.3, 169.8, 135.2, 129.2, 129.1, 128.4, 76.2, 52.1, 50.4, 35.0, 33.4, 29.6. **HRMS (ESI):** m/z calc. for $C_{15}H_{20}N_3O_4$ $[M+H]^+$ 306.1448, found 306.1444.

2-(3-oxopyrazolidin-1-yl)-2-phenyl-*N*-(prop-2-yn-1-yl)acetamide (45)

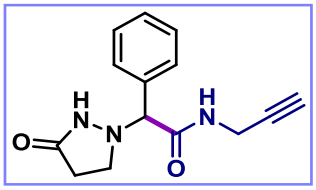

The product **45** was obtained as a white solid (22.7 mg, 59%) following the general procedure GP1. The crude material was purified by flash column chromatography (DCM/MeOH 20:1). **^{1}H NMR ($CDCl_3$, 400 MHz):** δ 7.40 – 7.36 (m, 5H), 6.71 (brs, 1H), 4.29 (s, 1H), 4.02 (d, *J* = 3.1 Hz, 2H), 3.26 (dd, *J* = 16.3, 8.1 Hz, 2H), 2.47 – 2.31 (m, 2H), 2.22 (t, *J* = 2.5 Hz, 1H).**^{13}C NMR ($CDCl_3$, 101 MHz):** δ 174.7, 169.5, 134.7, 131.7, 129.3, 128.6, 79.2, 75.9, 72.1, 50.5, 29.6, 29.3.**HRMS (ESI):** m/z calc. for $C_{14}H_{16}N_3O_2$ $[M+H]^+$ 258.1237, found 258.1235.

***N*-allyl-2-(3-oxopyrazolidin-1-yl)-2-phenylacetamide (46)**

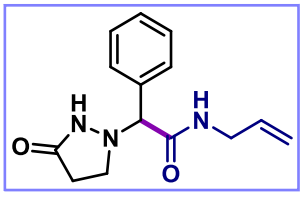

The product **46** was obtained as a white solid (19.8 mg, 51%) following the general procedure GP1. The crude material was purified by flash column chromatography (DCM/MeOH 20:1). **^{1}H NMR ($CDCl_3$, 400 MHz):** δ 7.42 – 7.35 (m, 5H), 6.41 (brs, 1H), 5.76 (ddt, *J* = 17.1, 10.4, 5.6 Hz, 1H), 5.09 – 5.02 (m, 2H), 4.27 (s, 1H), 3.91 – 3.79 (m, 2H), 3.26 (dt, *J* = 10.8, 4.1 Hz, 2H), 2.42 – 2.37 (m, 2H). **^{13}C NMR ($CDCl_3$, 101 MHz):** δ 174.7, 169.7, 135.2, 133.7, 129.3, 129.3, 128.5, 116.8, 76.2, 50.6, 41.8, 29.7. **HRMS (ESI):** m/z calc. for $C_{14}H_{18}N_3O_2$ $[M+H]^+$ 260.1394, found 260.1382.

***N*-(3,5-bis(trifluoromethyl)benzyl)-2-(3-oxopyrazolidin-1-yl)-2-phenylacetamide (47)**

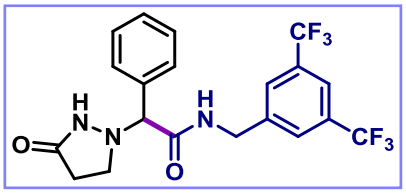

The product **47** was obtained as a colorless oil (25.4 mg, 38%) following the general procedure GP1. The crude material was purified by flash column chromatography (DCM/MeOH 20:1). **^{1}H NMR ($CDCl_3$, 400 MHz):** δ 7.73 (s, 1H), 7.52 (s, 1H), 7.42 – 7.38 (m, 5H), 7.01 (brs, 1H), 4.61 (dd, *J* = 15.7, 6.4 Hz, 1H), 4.49 (dd, *J* = 15.9, 5.6 Hz, 1H), 4.44 (s, 1H), 3.33 (q, *J* = 8.4 Hz, 1H), 3.24 (brs, 1H), 2.49 – 2.34 (m, 2H).**^{13}C NMR ($CDCl_3$, 126 MHz):** δ 175.0, 170.1, 140.8, 134.5, 132.0 (q, *J* = 33.5 Hz), 129.7, 129.6, 128.3, 127.5, 123.22 (d, *J* = 272.8 Hz), 121.5 (hept, *J* = 3.8 Hz), 76.0, 50.5, 42.4, 29.6. **HRMS (ESI):** m/z calc. for $C_{20}H_{18}F_6N_3O_2$ $[M+H]^+$ 446.1298, found 446.1292.

2-(3-oxopyrazolidin-1-yl)-2-phenyl-*N*-(3-(triethoxysilyl)propyl)acetamide (48)

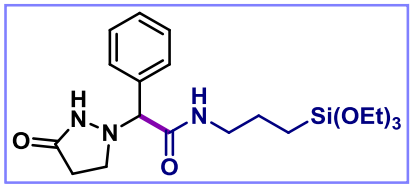

The product **48** was obtained as a white solid (46.3 mg, 73%) following the general procedure GP1. The crude material was purified by flash column chromatography (DCM/MeOH 20:1). **^{1}H NMR ($CDCl_3$, 400 MHz):** δ 7.31 – 7.25 (m, 3H), 6.40 (t, *J* = 5.5 Hz, 1H), 4.13 (s, 1H), 3.69 (q, *J* = 7.0 Hz, 6H), 3.14 (h, *J* = 7.6 Hz, 4H), 2.37 – 2.22 (m, 2H), 1.49 (p, *J* = 7.1 Hz, 2H), 1.11 (t, *J* = 7.0 Hz, 9H), 0.46 – 0.42 (m, 2H). **^{13}C NMR ($CDCl_3$, 126 MHz):** δ 174.6, 169.8, 135.4, 129.3, 129.2, 128.5, 76.3, 58.6, 50.6, 41.7, 29.7, 22.8, 18.4, 7.7. **HRMS (ESI):** m/z calc. for $C_{20}H_{34}N_3O_5Si$ $[M+H]^+$ 424.2262, found 424.2259.

***N*-(3,4-dihydroxyphenethyl)-2-(3-oxopyrazolidin-1-yl)-2-phenylacetamide (49)**

The product **49** was obtained as a white solid (39.7 mg, 74%) following the general procedure GP1. The crude material was purified by flash column chromatography (DCM/MeOH 20:1). **^{1}H NMR (Methanol-*d*4, 400 MHz):** δ 7.42 – 7.35 (m, 5H), 6.65 (s, 1H), 6.63 – 6.62 (m, 1H), 6.42 (dd, *J* = 8.0, 1.7 Hz, 1H), 4.33 (s, 1H), 3.38 (dt, *J* = 6.8, 5.1 Hz, 1H), 3.21 (t, *J* = 7.8 Hz, 1H), 2.68 – 2.60 (m, 1H), 2.38 (t, *J* = 7.6 Hz, 1H).

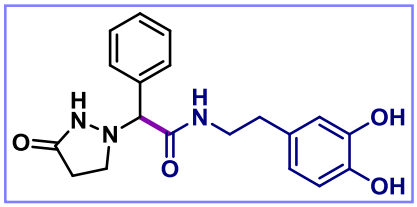

^{13}C NMR (Methanol-*d*4, 101 MHz): δ 177.6, 172.1, 163.7, 146.3, 144.8, 136.9, 131.8, 129.9, 129.8, 129.8, 121.2, 116.9, 116.4, 76.6, 51.2, 41.9, 35.5, 30.3. **HRMS (ESI):** m/z calc. for $C_{19}H_{22}N_3O_4$ $[M+H]^+$ 356.1605, found 356.1600

***N*-((1*R*,2*S*)-2-hydroxy-2,3-dihydro-1*H*-inden-1-yl)-2-(3-oxopyrazolidin-1-yl)-2-phenylacetamide (50)**

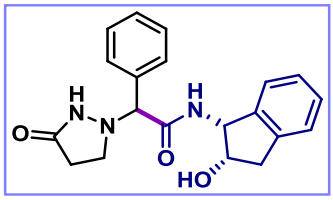

The product **50** was obtained as a white solid (15.8 mg, 30%) following the general procedure GP1. The crude material was purified by flash column chromatography (DCM/MeOH 20:1). **^{1}H NMR ($CDCl_3$, 400 MHz):** δ 9.47 (brs, 1H), 7.50 (dd, *J* = 7.2, 2.1 Hz, 2H), 7.43 – 7.39 (m, 3H), 7.28 – 7.21 (m, 5H), 6.98 (d, *J* = 7.5 Hz, 1H), 5.37 (dd, *J* = 9.4, 5.2 Hz, 1H), 4.72 – 4.70 (m, 1H), 4.40 (s, 1H), 3.34 (dt, *J* = 11.8, 8.9 Hz, 1H), 3.14 (d, *J* = 5.7 Hz, 1H), 2.96 (dd, *J* = 17.0, 8.2 Hz, 1H), 2.63 (dt, *J* = 17.3, 8.8 Hz, 1H), 2.30 (ddd, *J* = 17.0, 9.0, 5.8 Hz, 1H). **^{13}C NMR ($CDCl_3$, 126 MHz):** δ 175.8, 170.6,

140.7, 140.4, 135.6, 129.3, 129.2, 128.4, 128.1, 127.2, 125.4, 124.3, 77.2, 73.0, 57.3, 49.7, 40.1, 29.9. **HRMS (ESI):** m/z calc. for $C_{20}H_{22}N_3O_4$ $[M+H]^+$ 352.1656, found 352.1649.

1-(2-oxo-1-phenyl-2-(pyrrolidin-1-yl)ethyl)pyrazolidin-3-one (51)

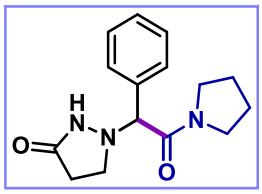

The product **51** was obtained as a colorless oil (27.4 mg, 67%) following the general procedure GP1. The crude material was purified by flash column chromatography (DCM/MeOH 20:1). **^{1}H NMR ($CDCl_3$, 400 MHz):** δ 7.48 (dd, *J* = 6.7, 2.9 Hz, 2H), 7.41 – 7.35 (m, 3H), 4.71 (s, 1H), 3.62 (dt, *J* = 10.0, 6.2 Hz, 1H), 3.49 (dt, *J* = 12.8, 6.8 Hz, 1H), 3.35 – 3.21 (m, 4H), 3.04 (dt, *J* = 10.1, 6.7 Hz, 1H), 2.33 (dt, *J* = 16.0, 8.0 Hz, 1H), 1.84 – 1.67 (m, 4H). **^{13}C NMR ($CDCl_3$, 126 MHz):** δ 177.3, 170.1, 134.9, 130.8, 130.2, 130.0, 73.6, 47.5, 30.6, 26.9, 24.8. **HRMS (ESI):** m/z calc. for $C_{15}H_{20}N_3O_2$ $[M+H]^+$ 274.1550, found 274.1571.

1-(2-oxo-1-phenyl-2-(piperidin-1-yl)ethyl)pyrazolidin-3-one (52)

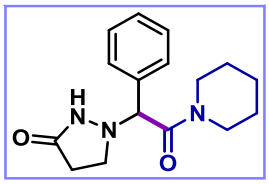

The product **52** was obtained as a colorless oil (22.8 mg, 53%) following the general procedure GP1. The crude material was purified by flash column chromatography (DCM/MeOH 20:1). **^{1}H NMR ($CDCl_3$, 400 MHz):** δ 7.39 – 3.35 (m, 5H), 4.70 (s, 1H), 3.72 (dd, *J* = 13.2, 6.4 Hz, 1H), 3.39 – 3.29 (m, 3H), 3.21 (t, *J* = 5.4 Hz, 2H), 3.31 – 3.21 (m, 1H), 2.08 (brs, 1H), 1.58 – 1.46 (m, 4H), 1.40 – 1.27 (m, 2H). **^{13}C NMR ($CDCl_3$, 126 MHz):** δ 174.4, 167.7, 132.7, 129.7, 129.4, 129.3, 72.2, 49.4, 46.6, 43.4, 30.0, 25.5, 25.4, 24.3. **HRMS (ESI):** m/z calc. for $C_{16}H_{22}N_3O_2$ $[M+H]^+$ 288.1707, found 288.1703.

Derivatization

3-((2-(cyclohexylamino)-2-oxo-1-phenylethyl)amino)propanamide (53)

The product **53** was obtained as a white solid (44.0 mg, 73%) following the general procedure

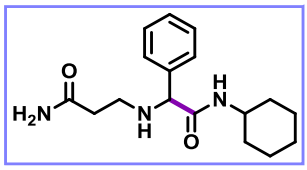

GP3. The crude material was purified by flash column chromatography (DCM/MeOH 9:1). **^{1}H NMR ($CDCl_3$, 400 MHz):** δ 7.37 – 7.29 (m, 5H), 6.87 (d, *J* = 8.4 Hz, 1H), 6.45 (brs, 1H), 5.58 (brs, 1H), 4.22 (s, 1H), 3.72 (ddt, *J* = 14.5, 10.9, 5.5 Hz, 1H), 2.95 – 2.84 (m, 2H), 2.43 (qt, *J* = 9.7, 5.3 Hz, 2H), 1.87 – 1.82 (m, 2H), 1.67 (d, *J* = 13.7 Hz, 2H), 1.61 – 1.57 (m, 1H), 1.37 – 1.27 (m, 2H), 1.25 – 1.09 (m, 3H). **^{13}C NMR ($CDCl_3$, 126 MHz):** δ

174.6, 171.0, 139.3, 128.9, 128.3, 127.5, 67.3, 48.1, 44.0, 35.3, 32.9, 25.5, 24.9. **HRMS (ESI):** m/z calc. for $C_{17}H_{26}N_3O_2$ $[M+H]^+$ 304.2020, found 304.2040.

2S)-methyl 2-(2-((3-amino-3-oxopropyl)amino)-2-phenylacetamido)propanoate (54)

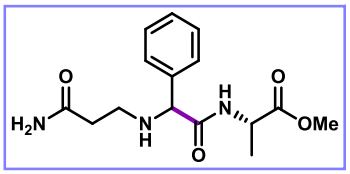

The product **54** was obtained as a yellow oil (13.5 mg, 32%) following the general procedure GP3. Reported signals of the major diastereoisomer (3:1) (* for overlapped signals). The crude material was purified by flash column chromatography (DCM/MeOH 9:1). **^{1}H NMR ($CDCl_3$, 400 MHz):** δ 7.41 – 7.31 (m, 7H)*, 6.34 (s, 1H), 5.53 (s, 1H), 4.61 – 4.54 (m, 2H)*, 4.21 (d, *J* = 8.3 Hz, 1H), 3.73 (s, 3H), 3.00 – 2.90 (m, 2H), 2.55 – 2.29 (m, 3H)*, 1.40 (dd, *J* = 11.7, 5.0 Hz, 4H)*. **^{13}C NMR ($CDCl_3$, 126 MHz):** δ 174.5, 174.3, 173.9, 173.4, 171.9, 169.3, 138.7, 129.3, 129.2, 128.9, 128.4, 127.6, 127.2, 67.6, 67.1, 52.7, 52.5, 47.9, 47.7, 44.3, 43.8, 29.7, 18.1. **HRMS (ESI):** m/z calc. for $C_{15}H_{21}N_3O_4$ $[M+H]^+$ 308.1605, found 308.1612.

Unsuccessful Substrates

4-carbamoyl-1,4-dihydropyridines:

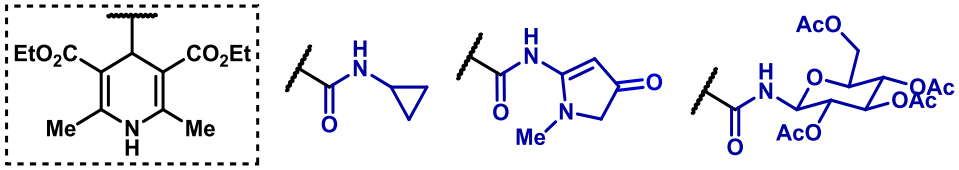

1.3-Dipoles:

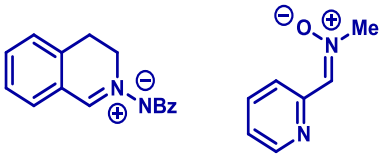

NMR Spectra

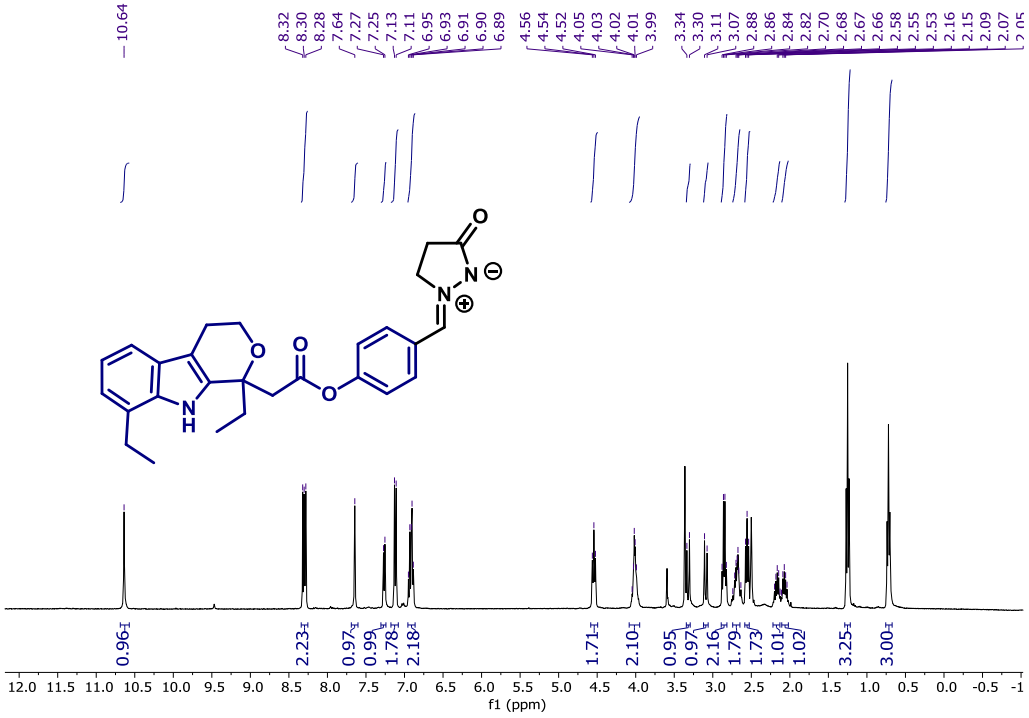

[1]H NMR (DMSO-d6, 400 MHz) of 16'.

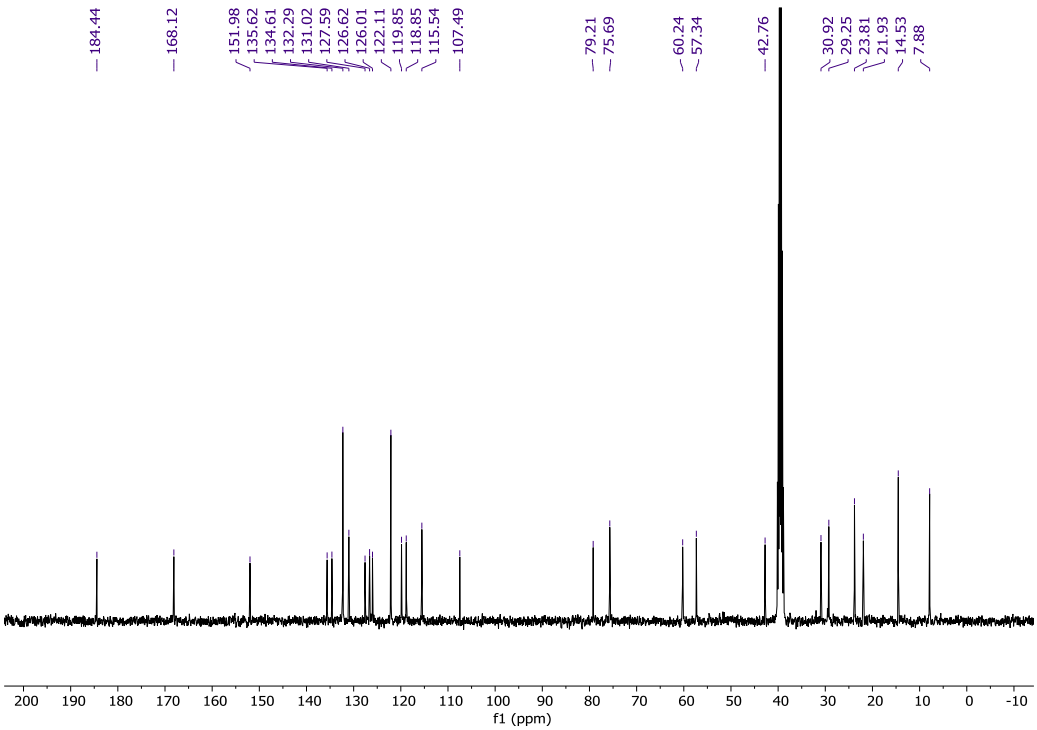

[13]C NMR (DMSO-d6, 126 MHz) of 16'.

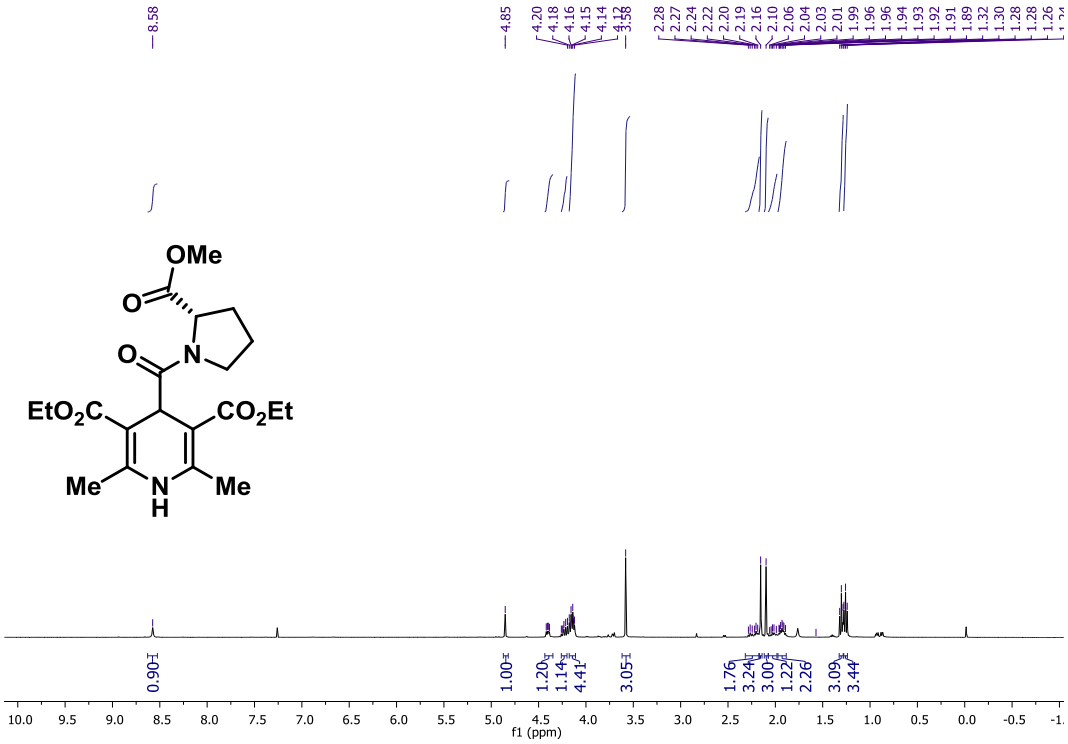

^{1}H NMR ($CDCl_3$, 400 MHz) of 22'.

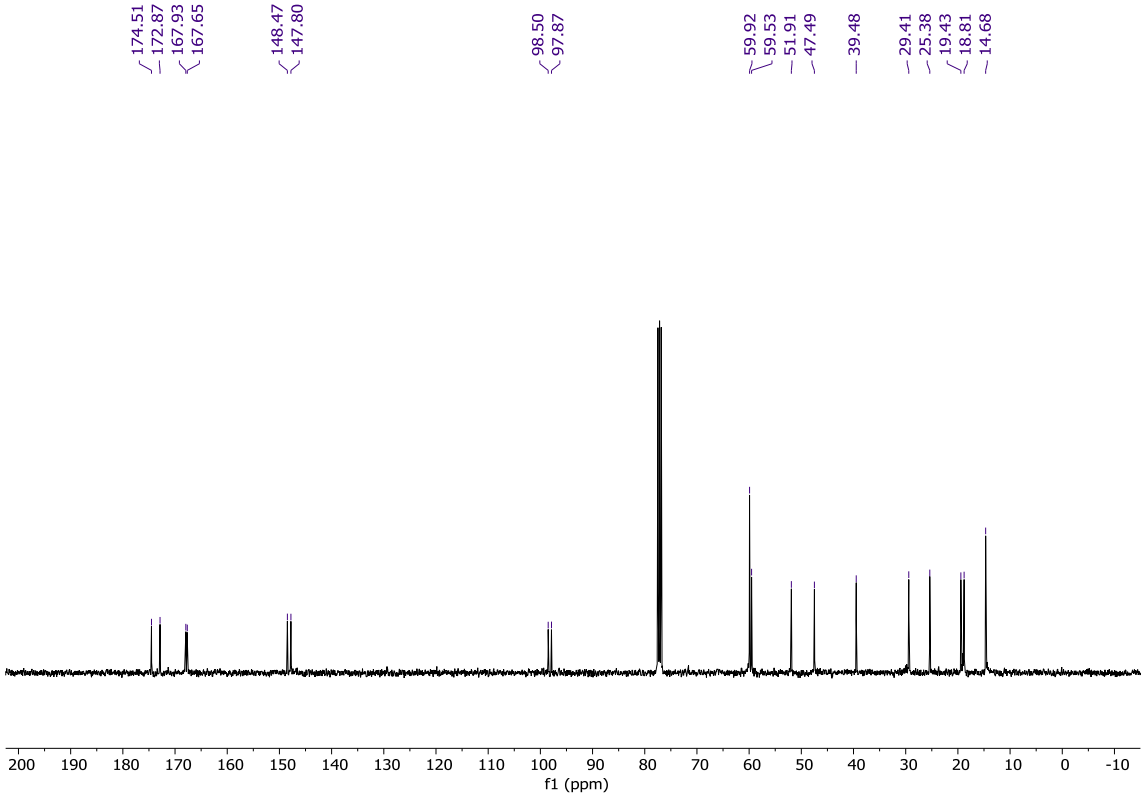

^{13}C NMR ($CDCl_3$, 126 MHz) of 22'.

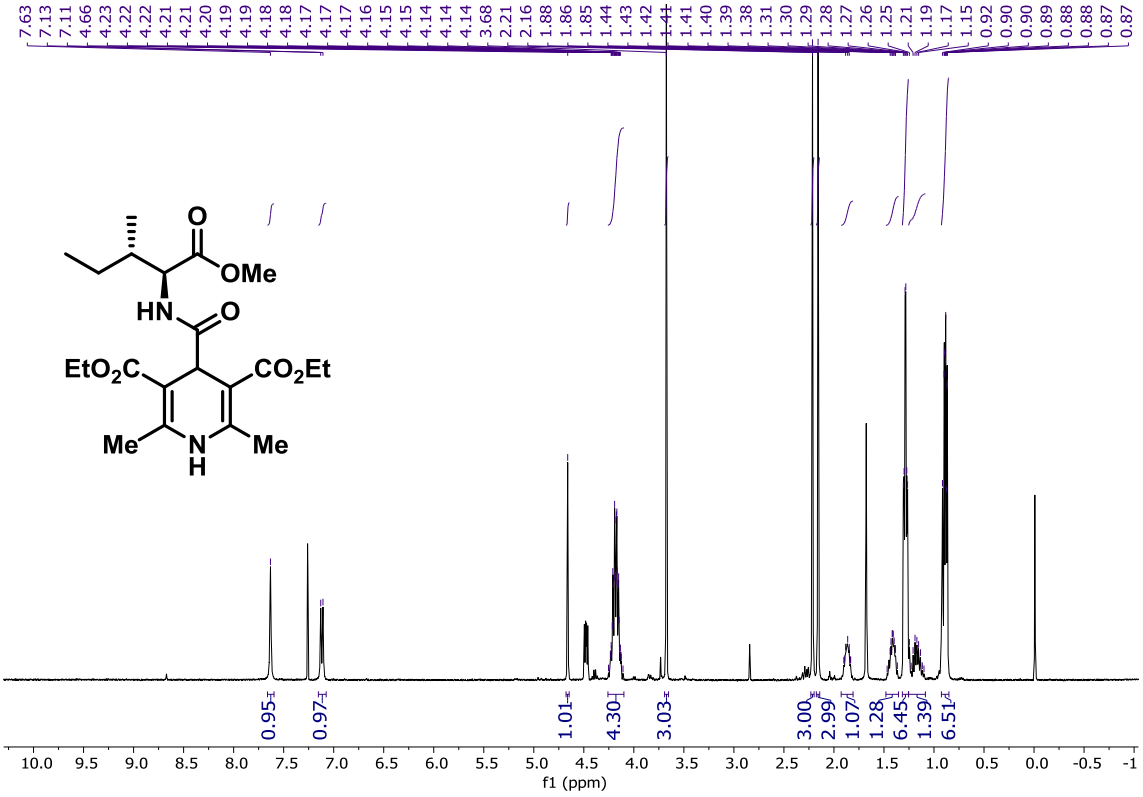

[1]H NMR (CDCl3, 400 MHz) of 25'.

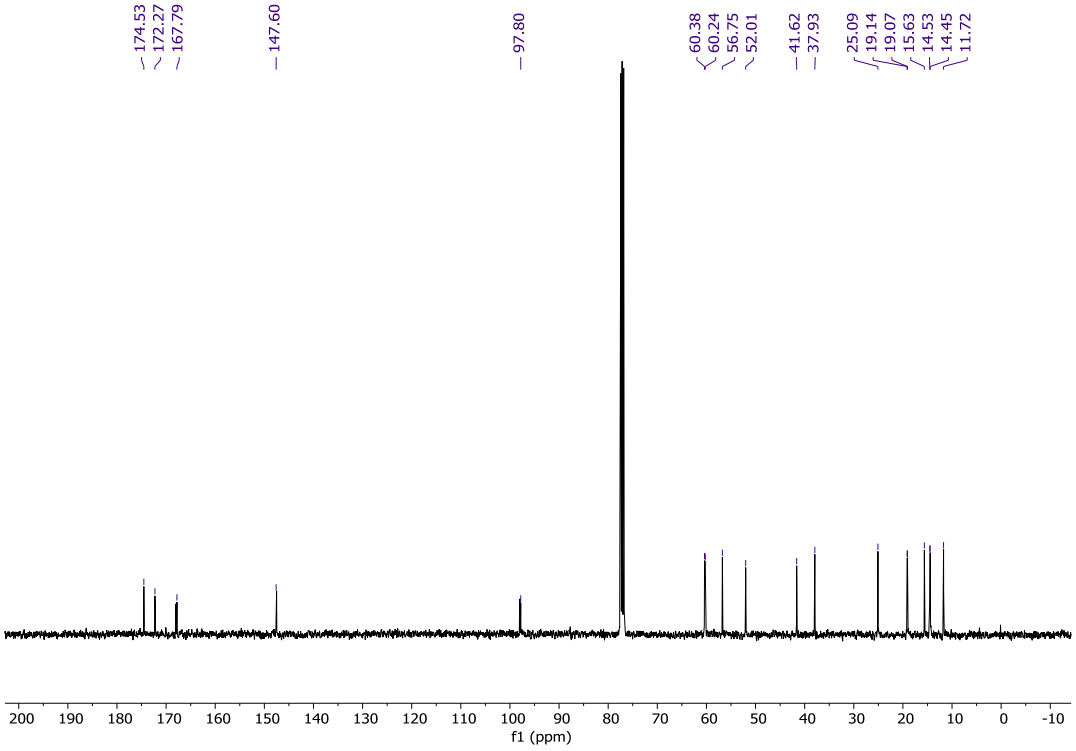

[13]C NMR (CDCl3, 126 MHz) of 25'.

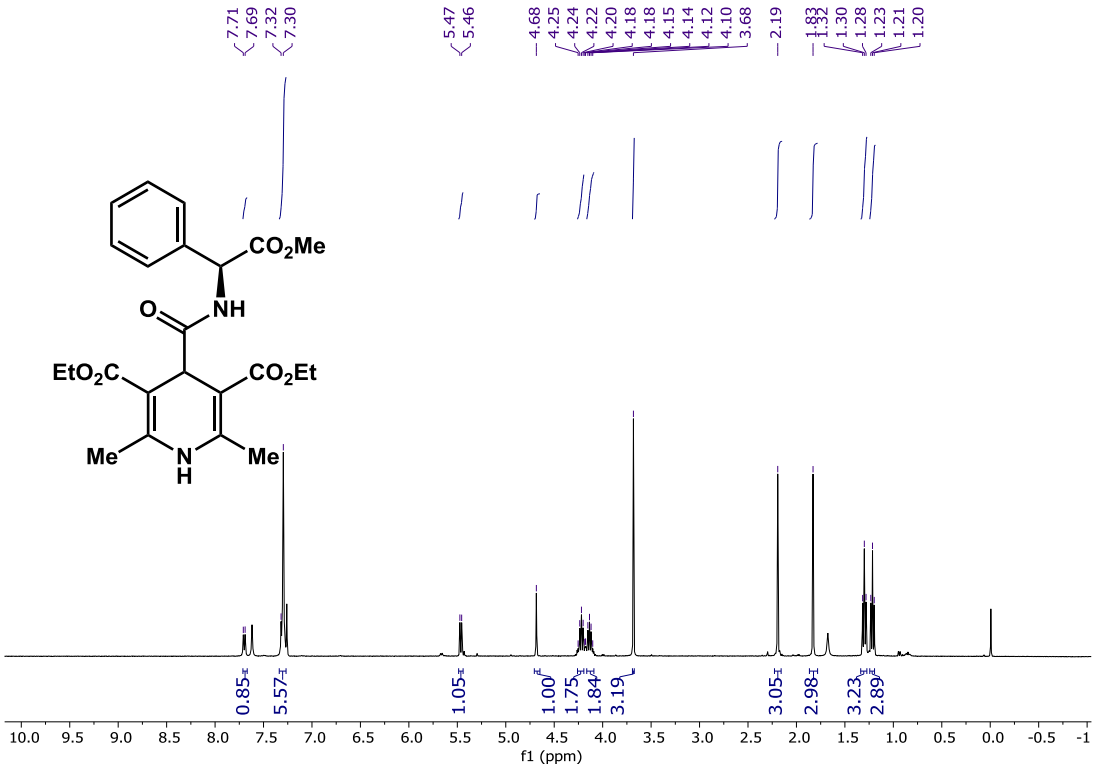

[1]H NMR (CDCl3, 400 MHz) of 31'.

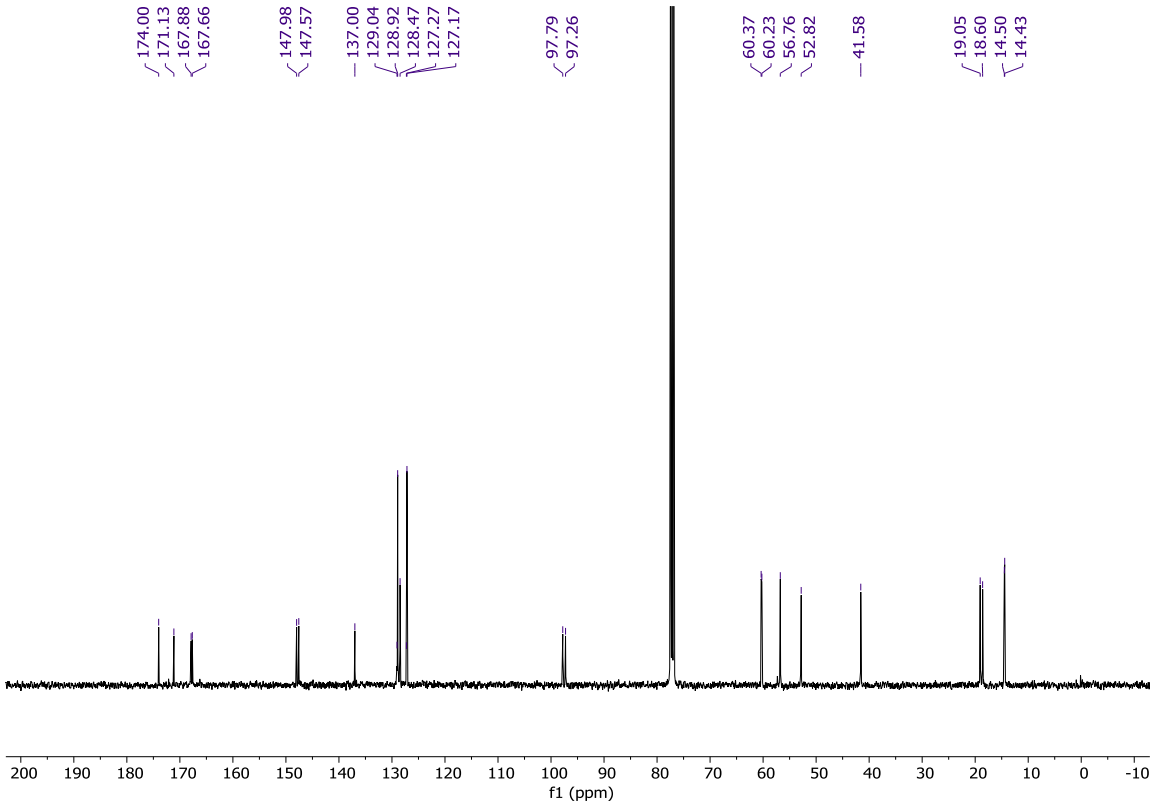

[13]C NMR (CDCl3, 126 MHz) of 31'.

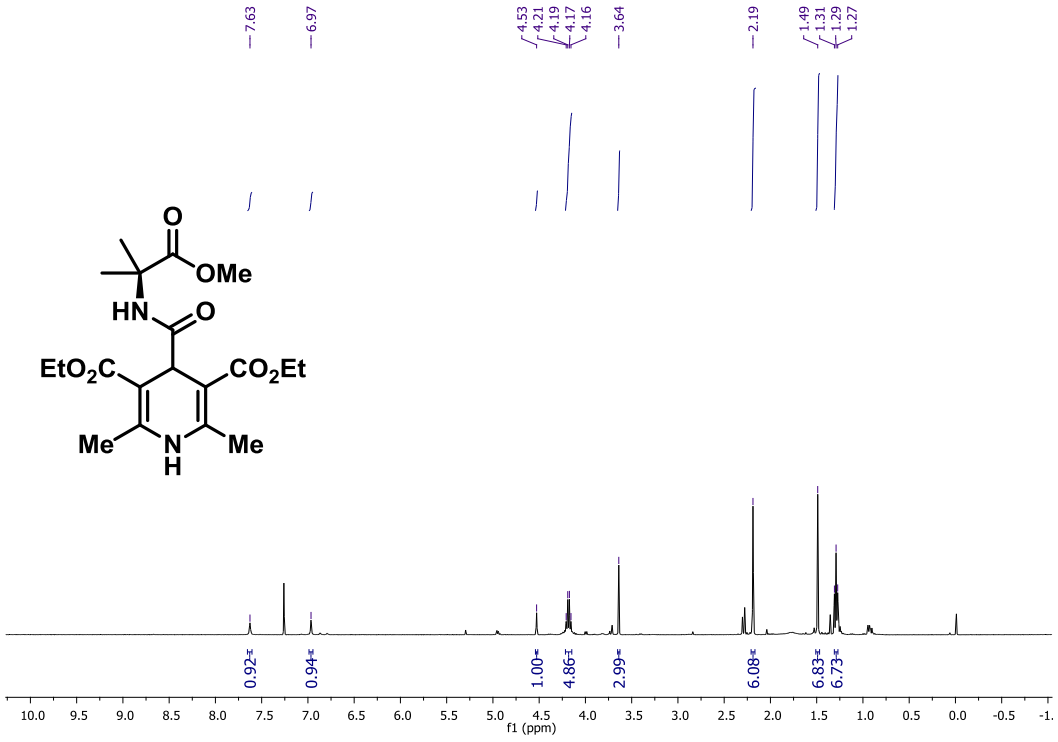

^{1}H NMR (CDCl3, 400 MHz) of 32'.

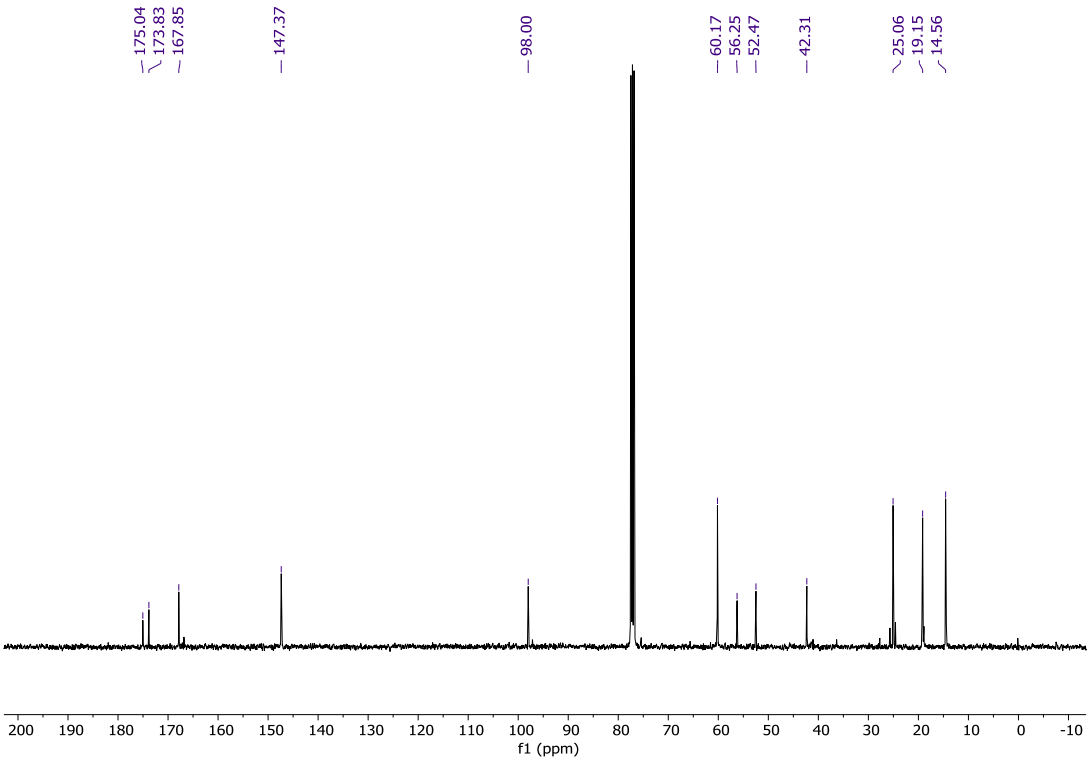

^{13}C NMR (CDCl3, 126 MHz) of 32'.

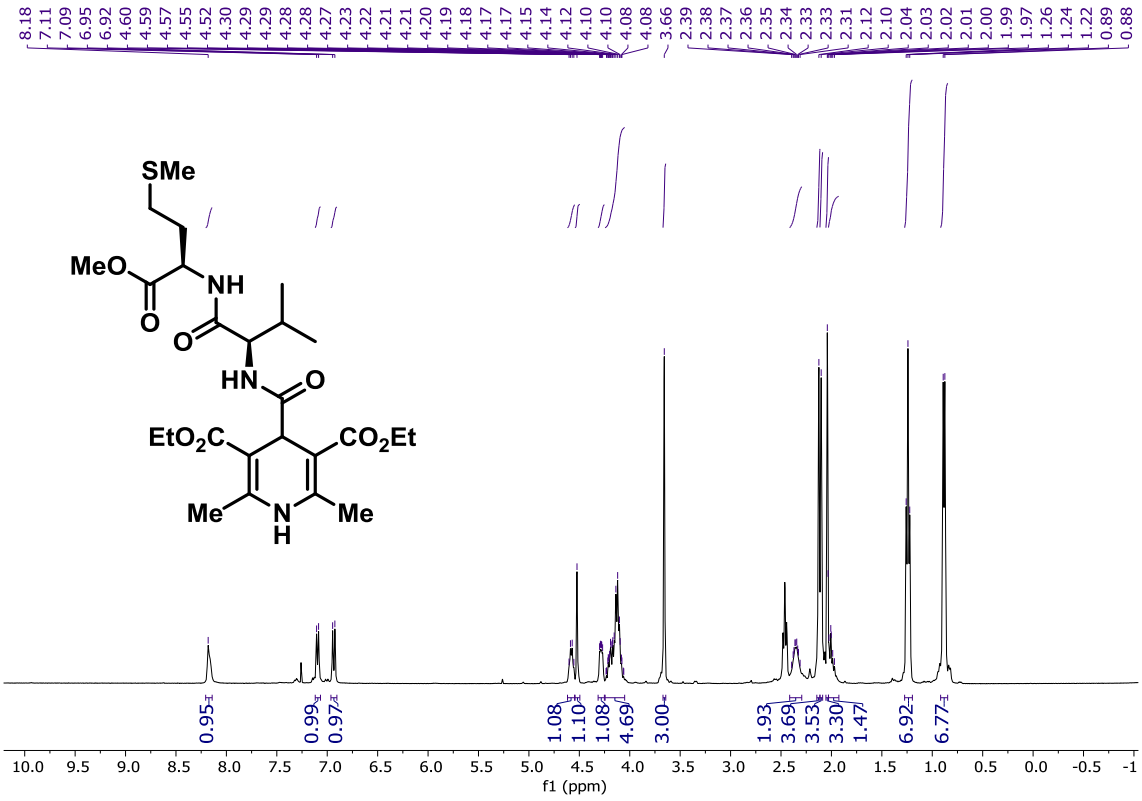

^{1}H NMR (CDCl3, 400 MHz) of 33'.

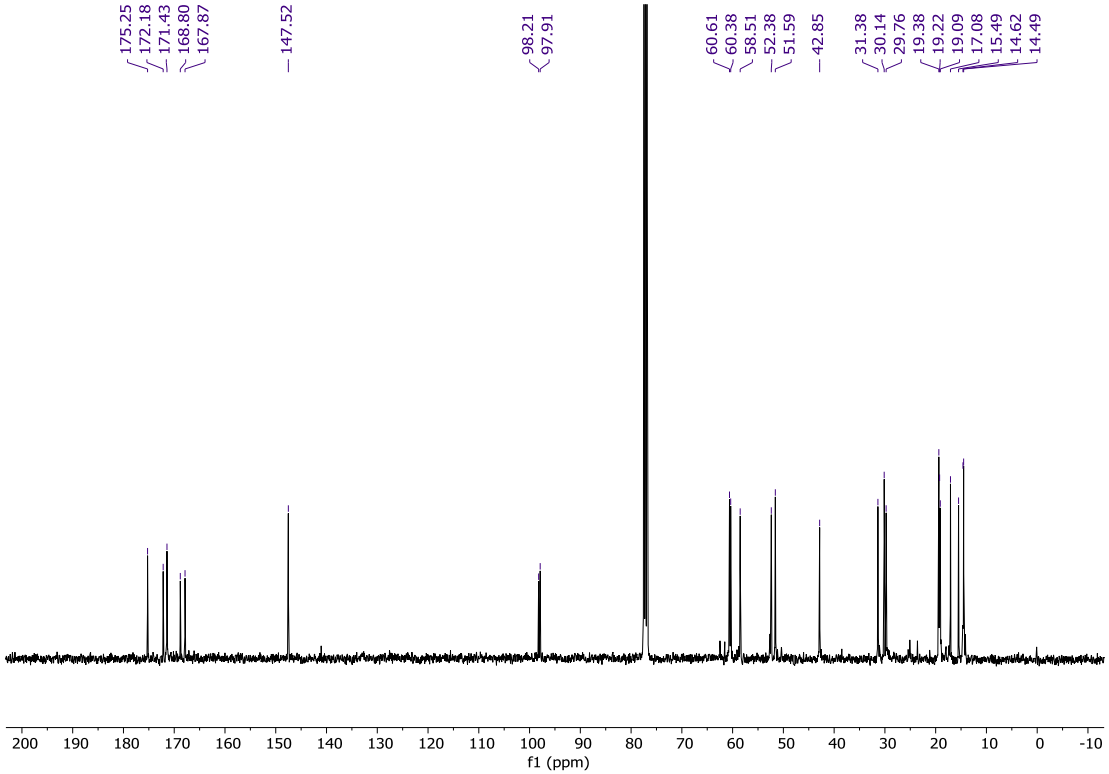

^{13}C NMR (CDCl3, 126 MHz) of 33'.

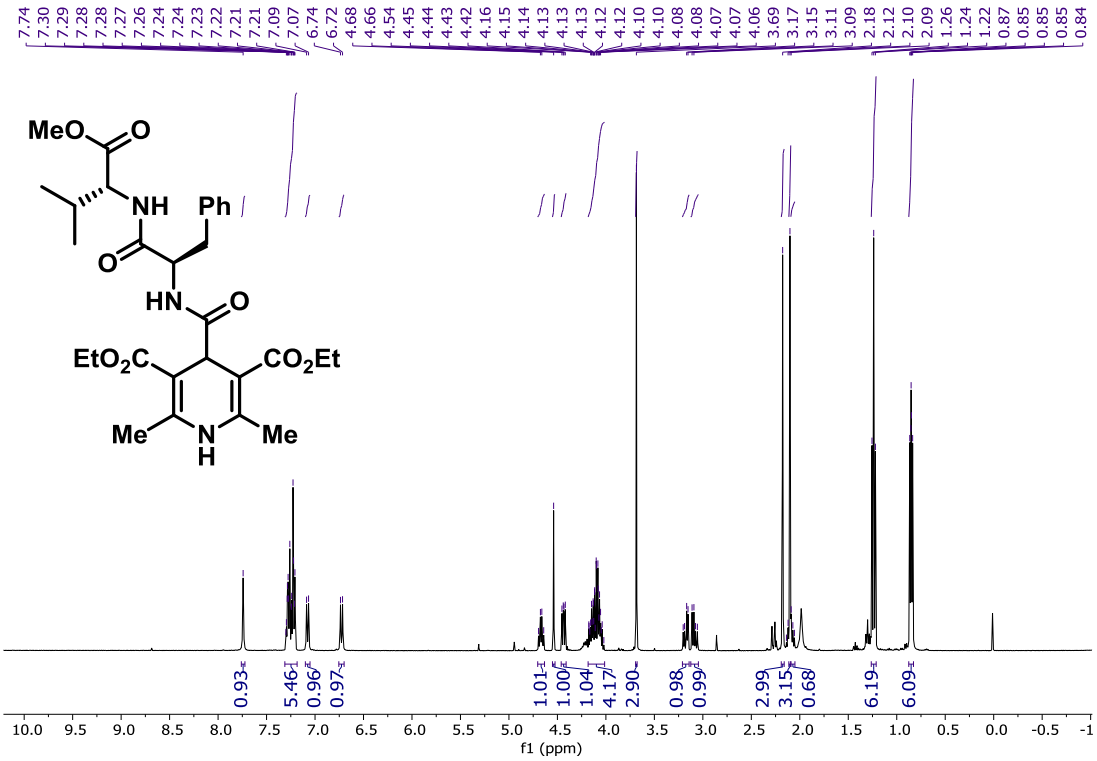

^{1}H NMR (CDCl3, 400 MHz) of 35'.

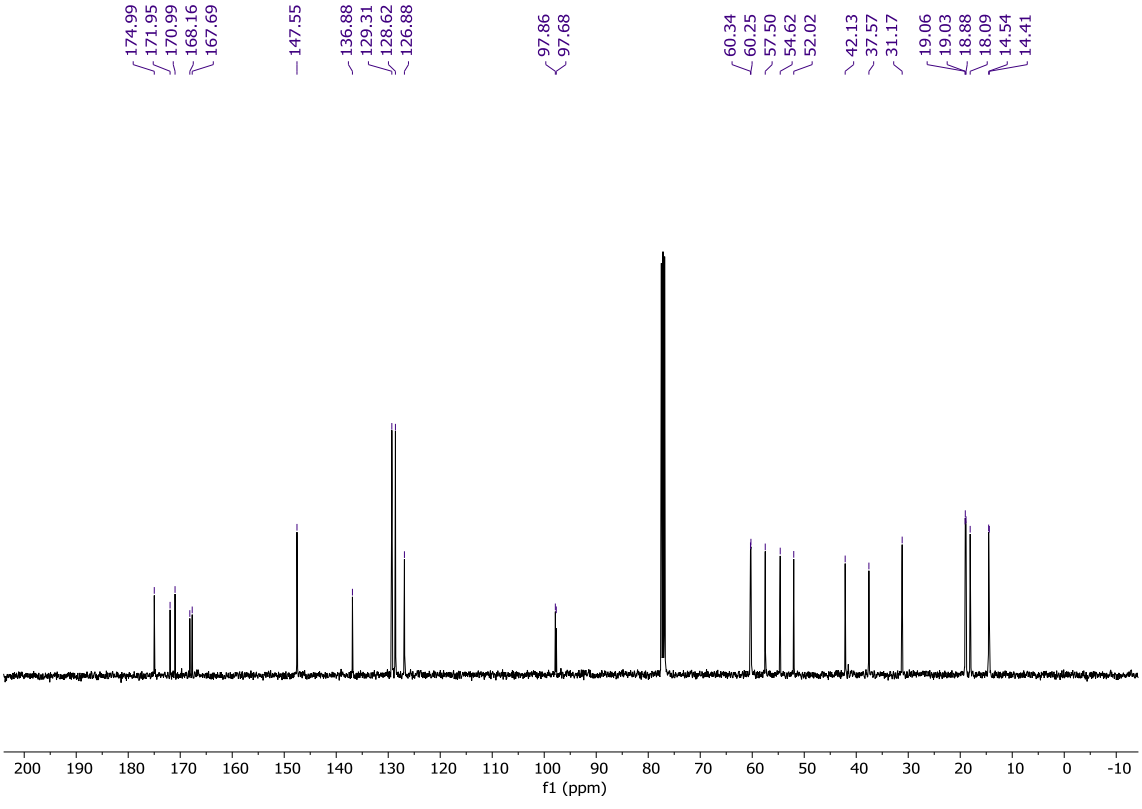

^{13}C NMR (CDCl3, 126 MHz) of 35'.

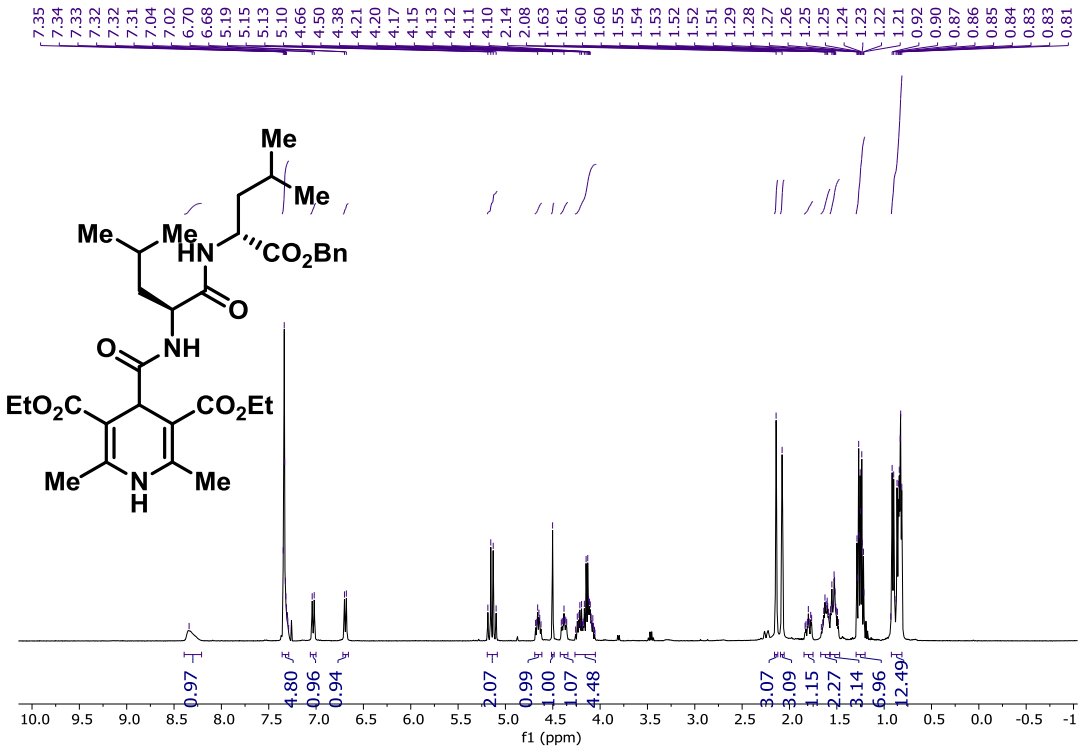

[1]H NMR (CDCl3, 400 MHz) of 36'.

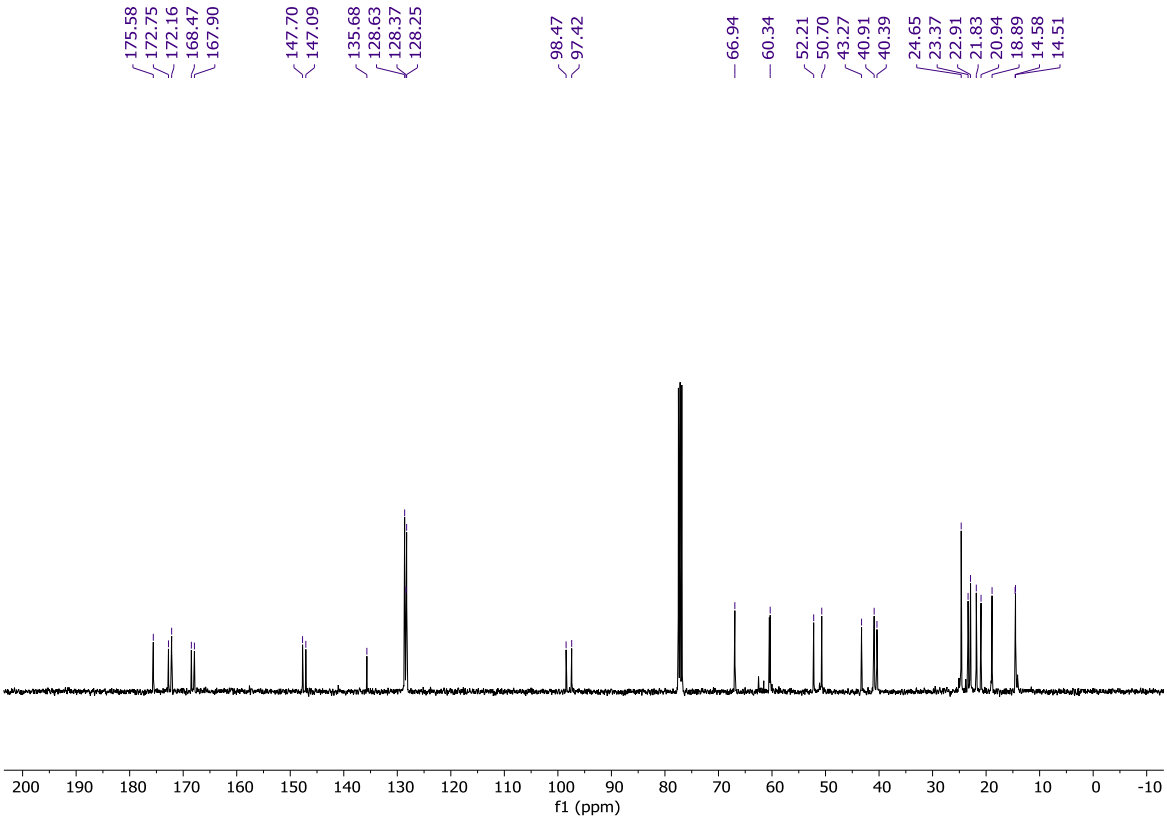

[13]C NMR (CDCl3, 126 MHz) of 36'.

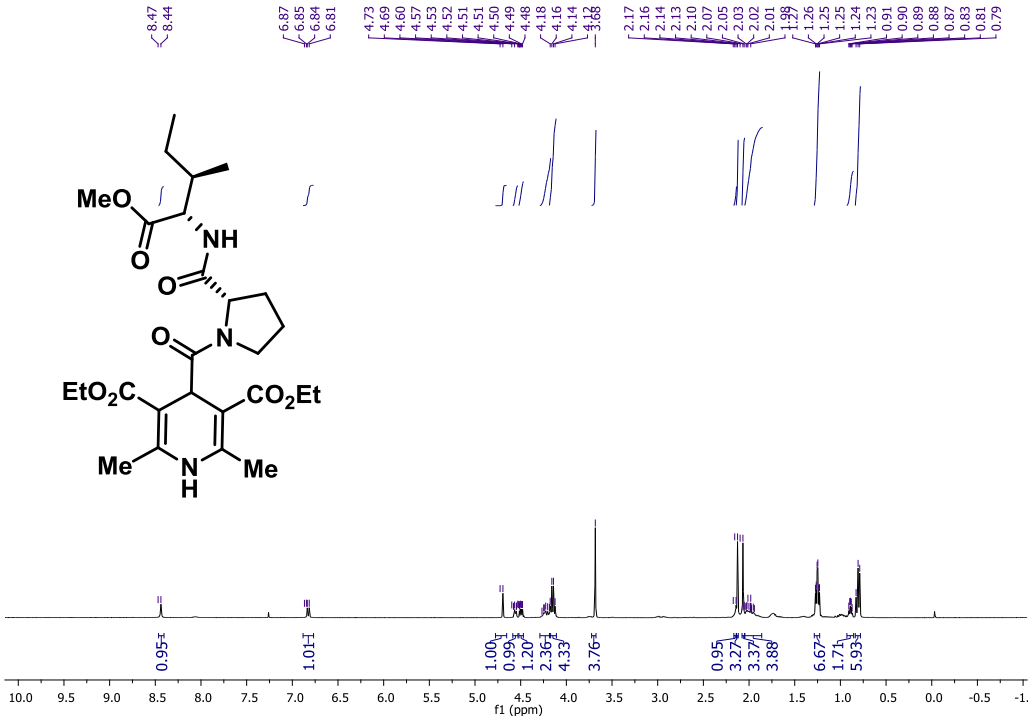

[1]H NMR (CDCl3, 400 MHz) of 37'.

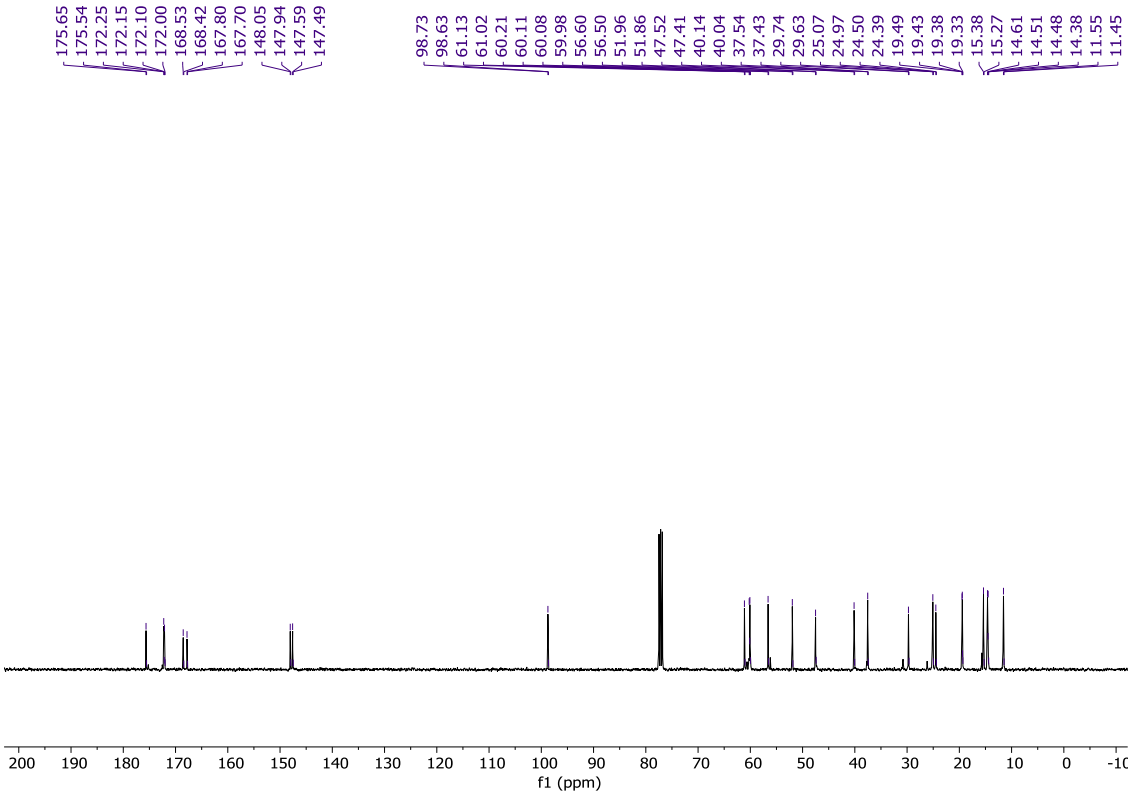

[13]C NMR (CDCl3, 126 MHz) of 37'.

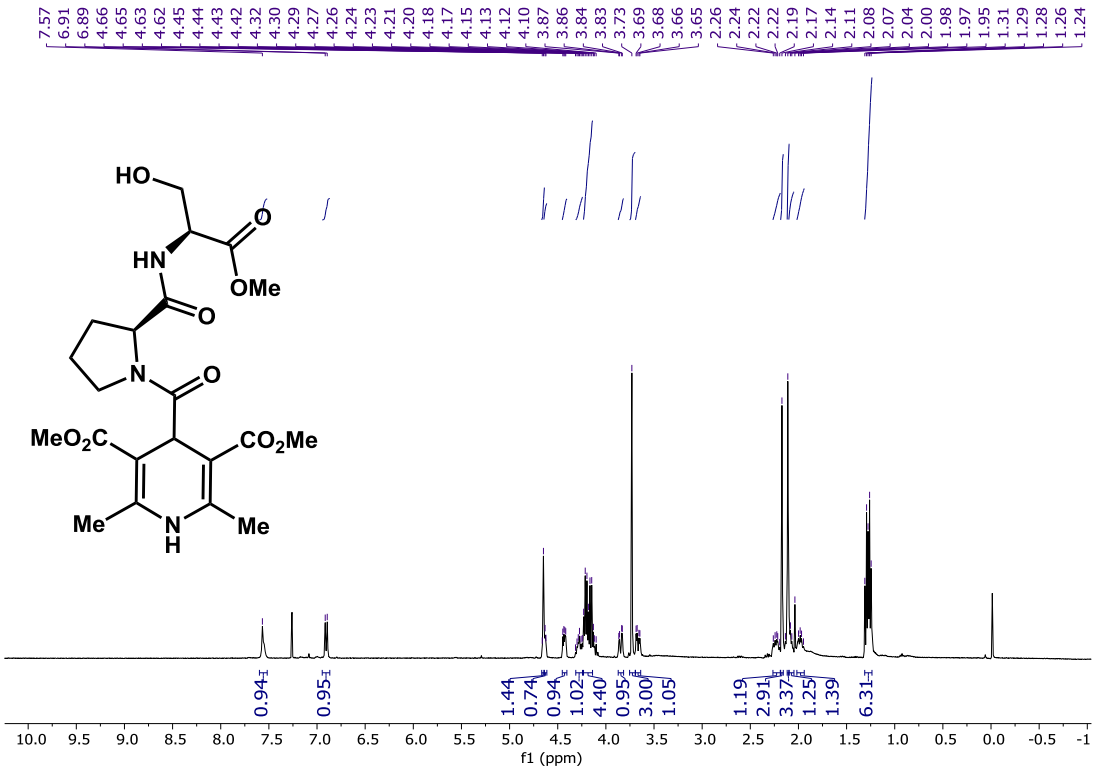

[1]H NMR (CDCl3, 400 MHz) of 38'.

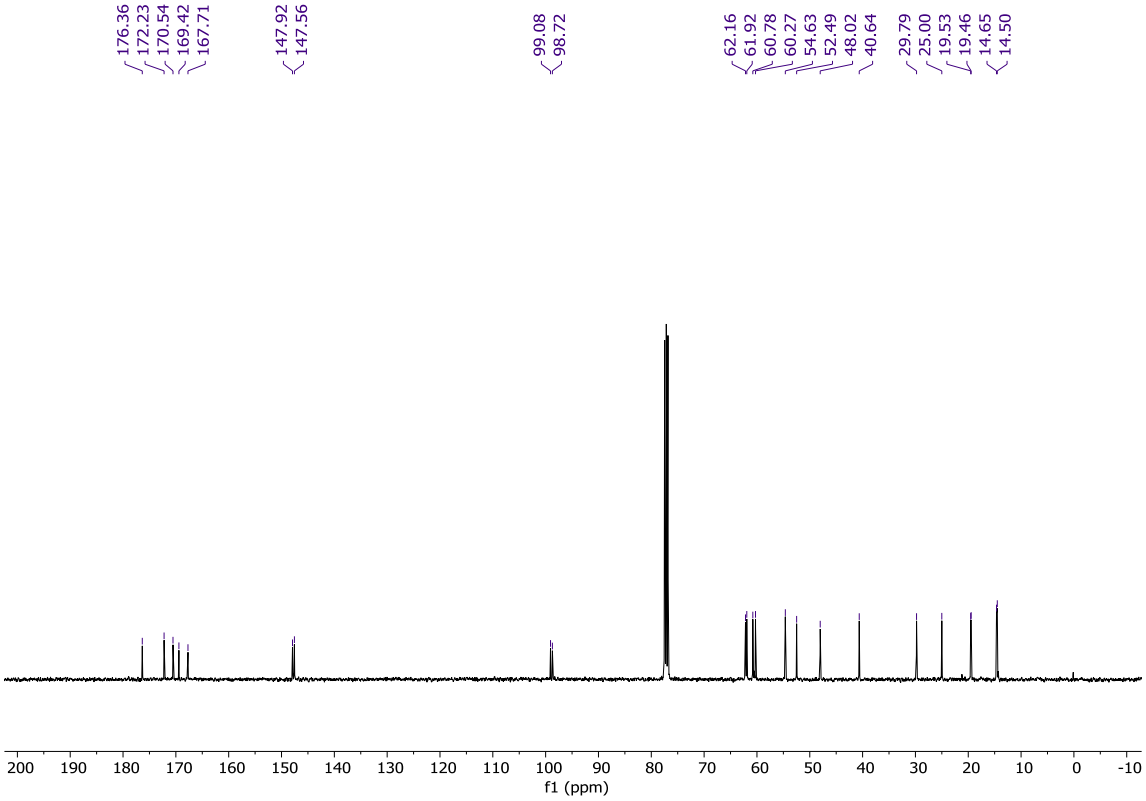

[13]C NMR (CDCl3, 126 MHz) of 38'.

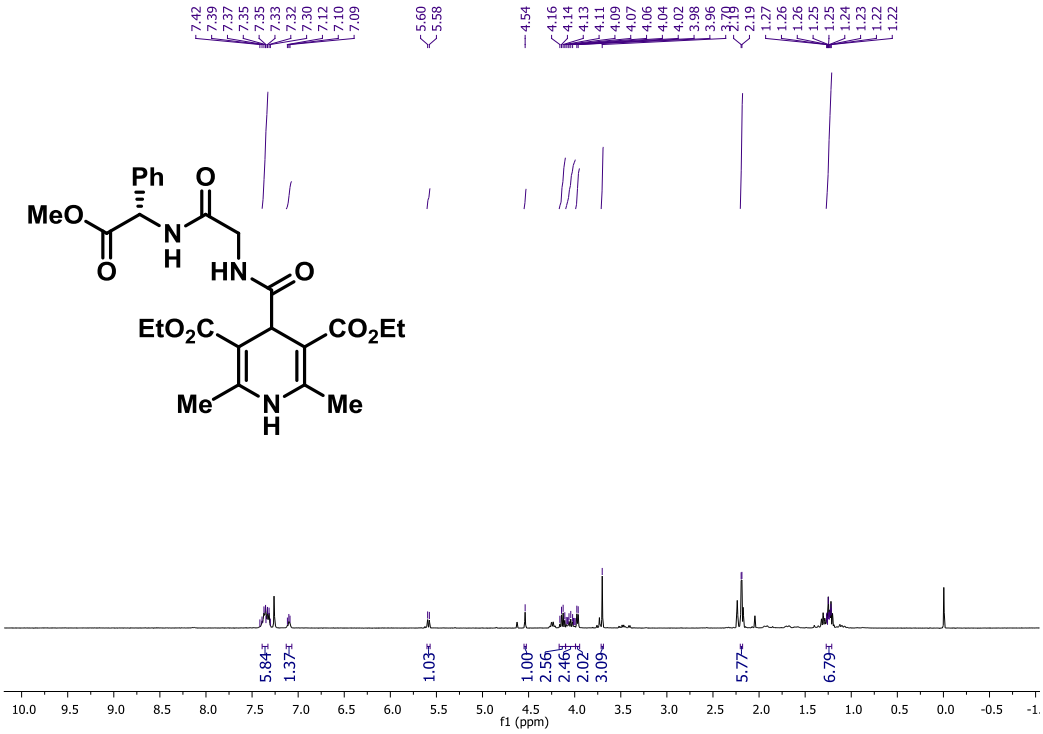

[1]H NMR (CDCl3, 400 MHz) of 39'.

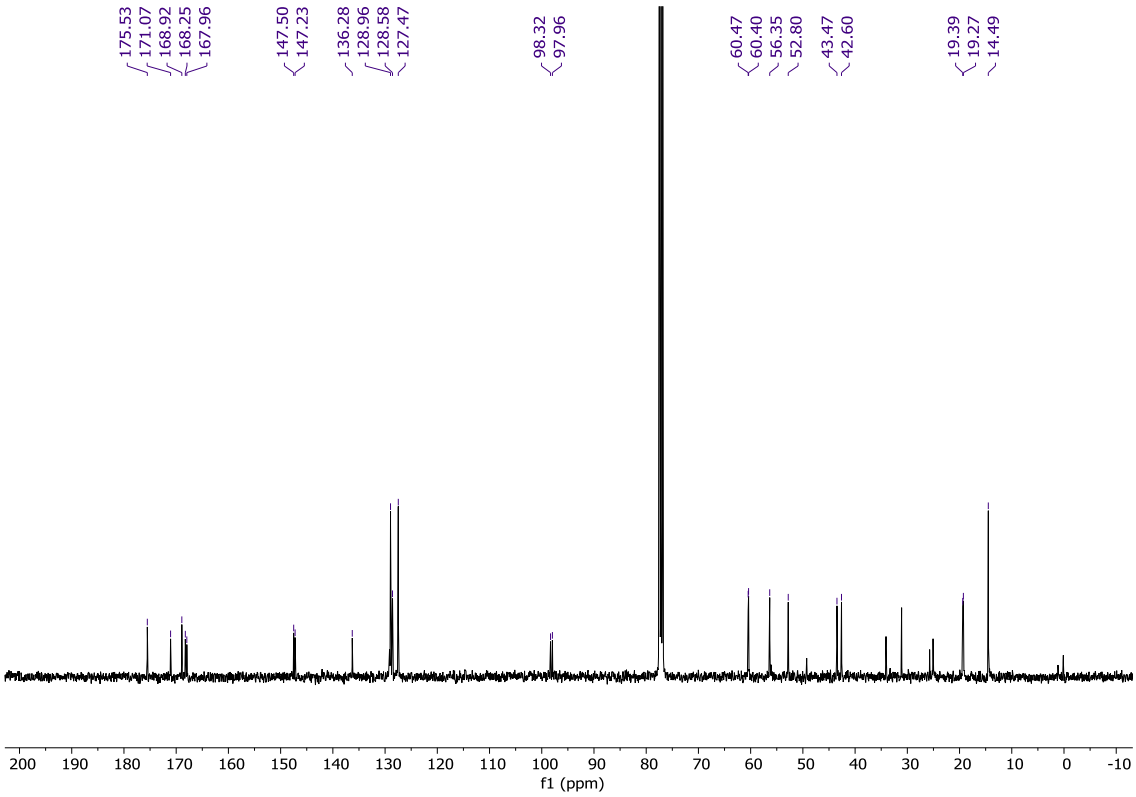

[13]C NMR (CDCl3, 126 MHz) of 39'.

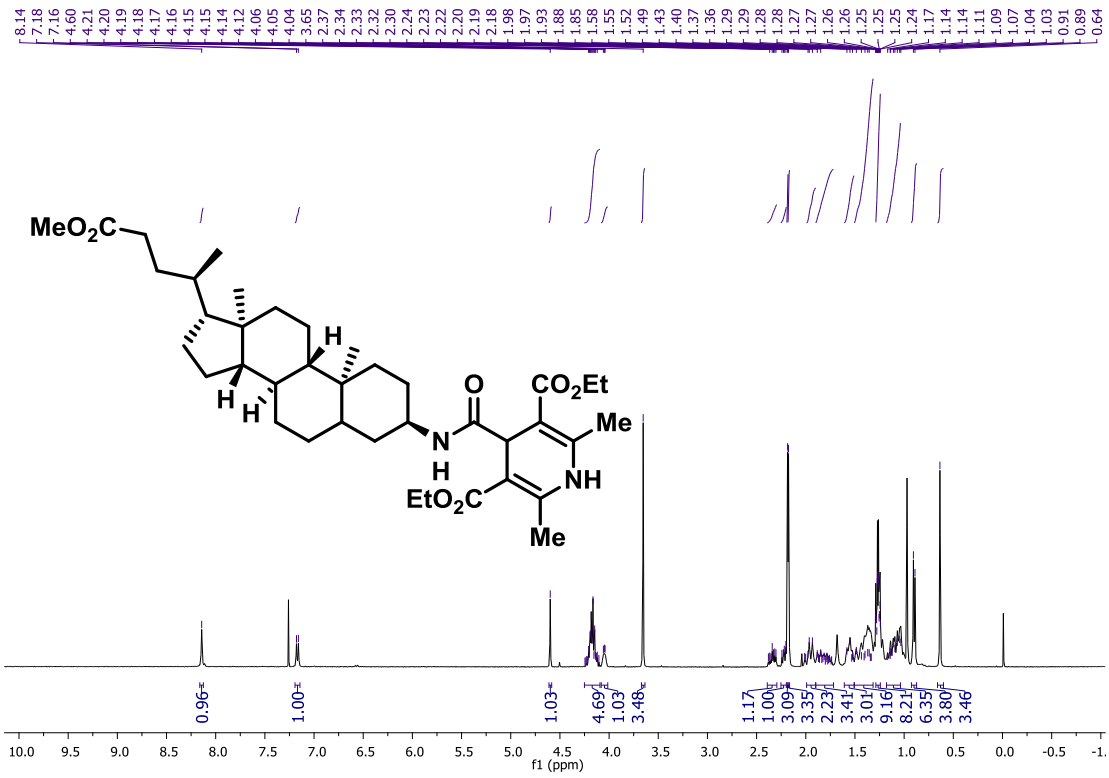

[1]H NMR (CDCl3, 400 MHz) of 40'.

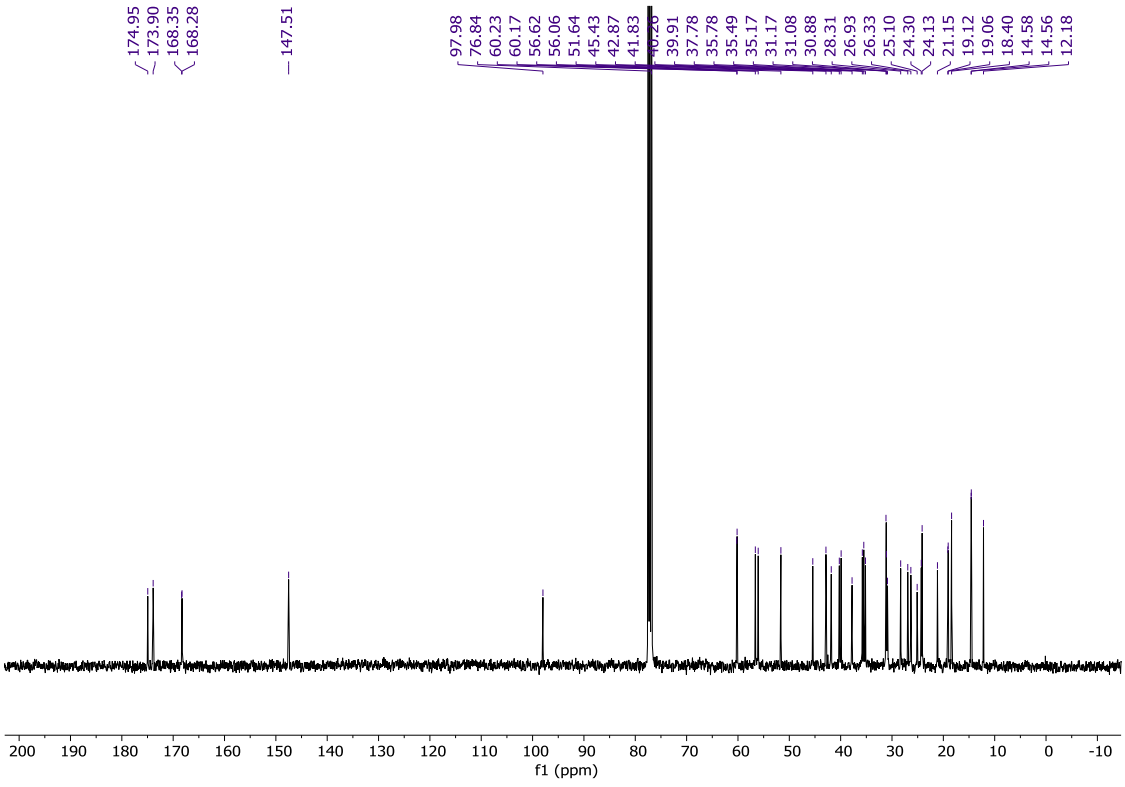

[13]C NMR (CDCl3, 126 MHz) of 40'.

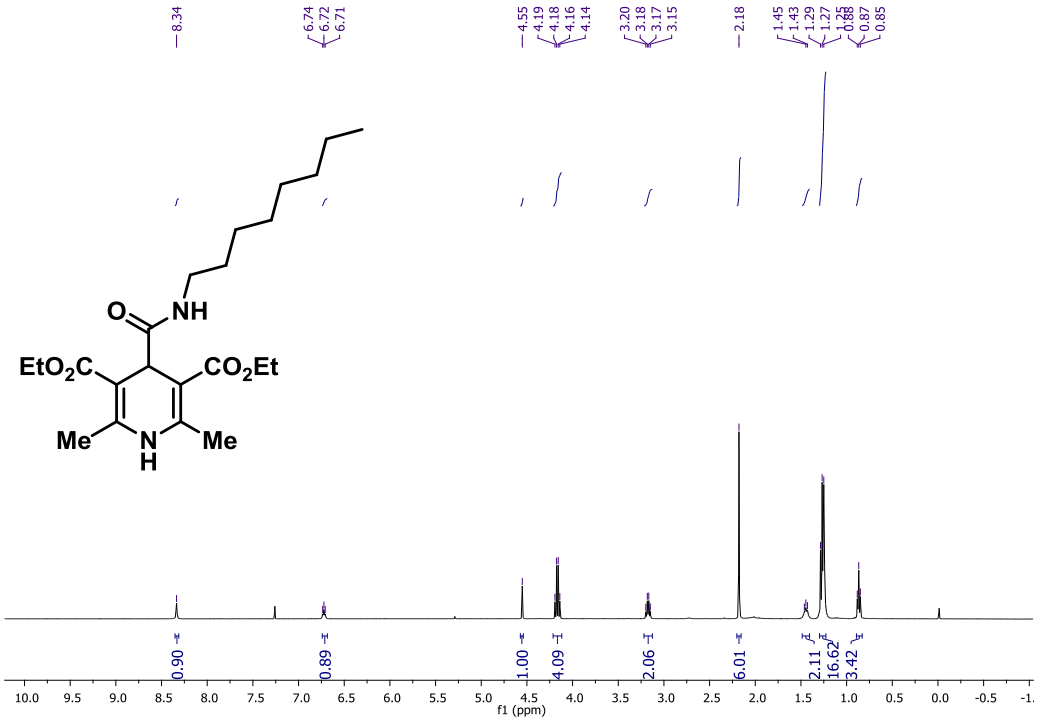

^{1}H NMR (CDCl3, 400 MHz) of 43'.

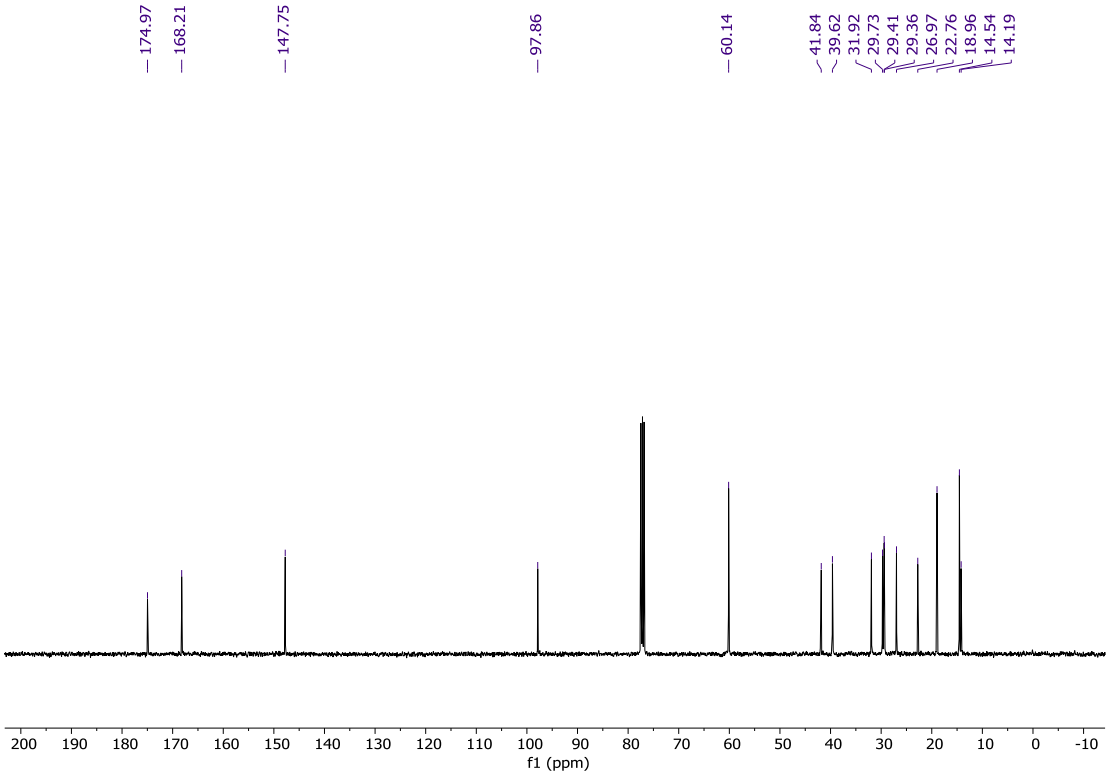

^{13}C NMR (CDCl3, 126 MHz) of 43'.

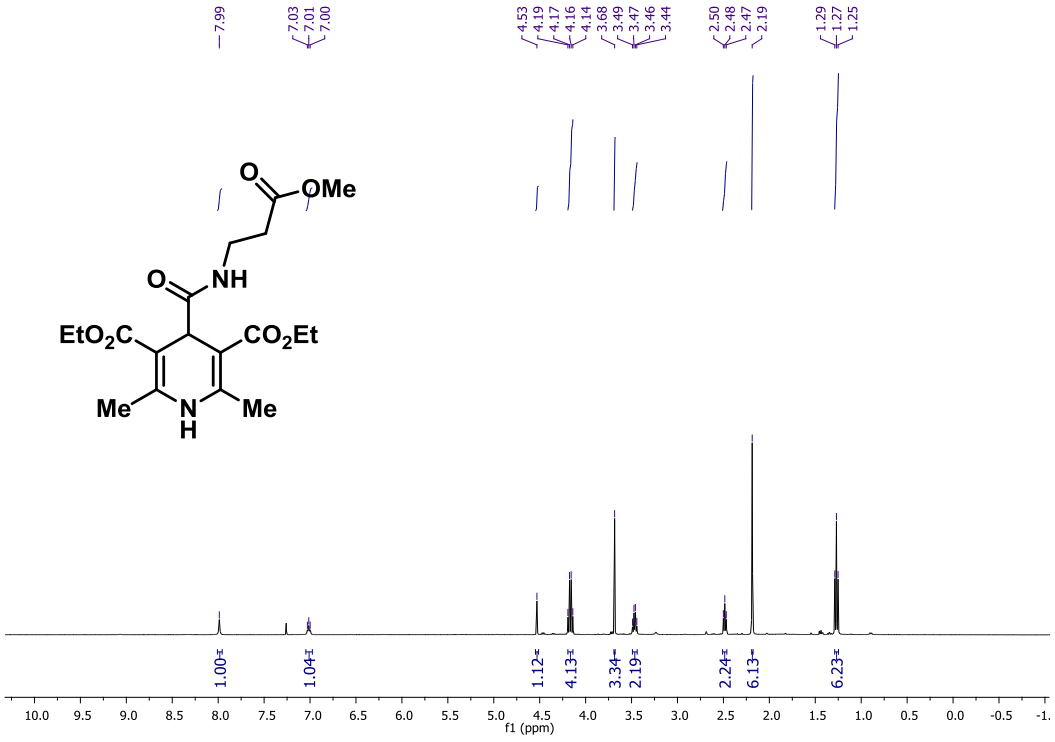

^{1}H NMR (CDCl3, 400 MHz) of 44'.

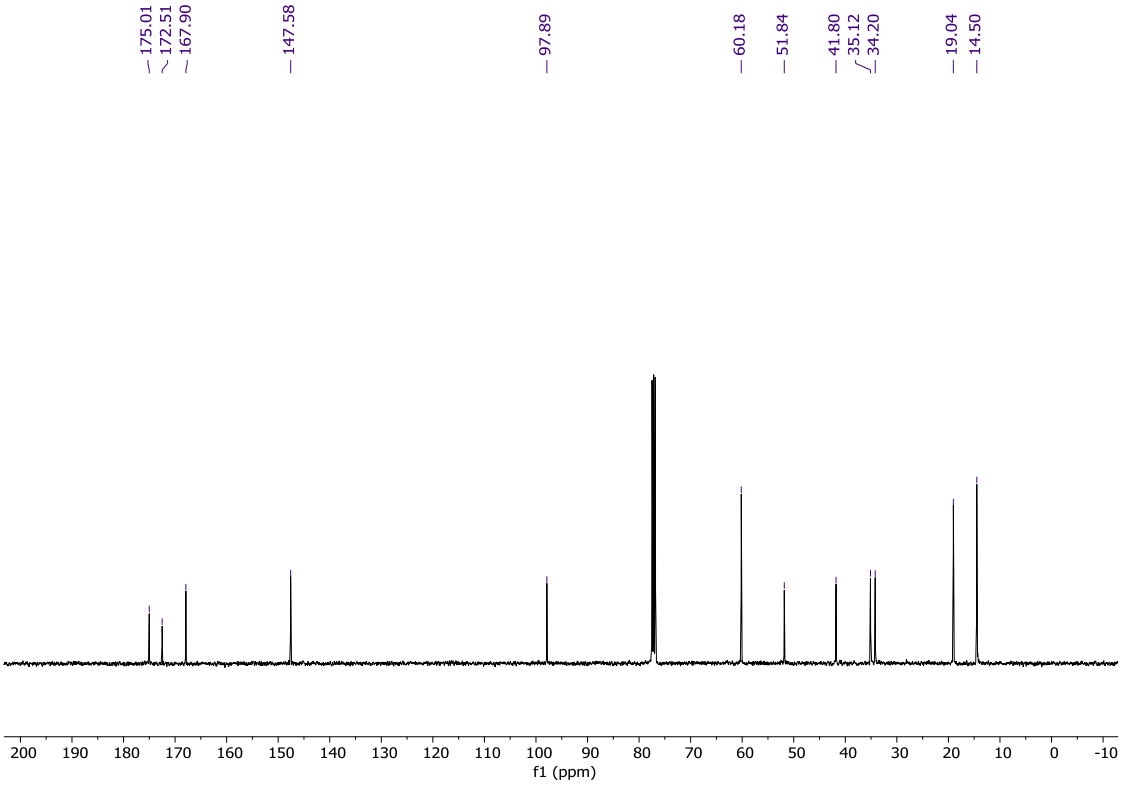

^{13}C NMR (CDCl3, 126 MHz) of 44'.

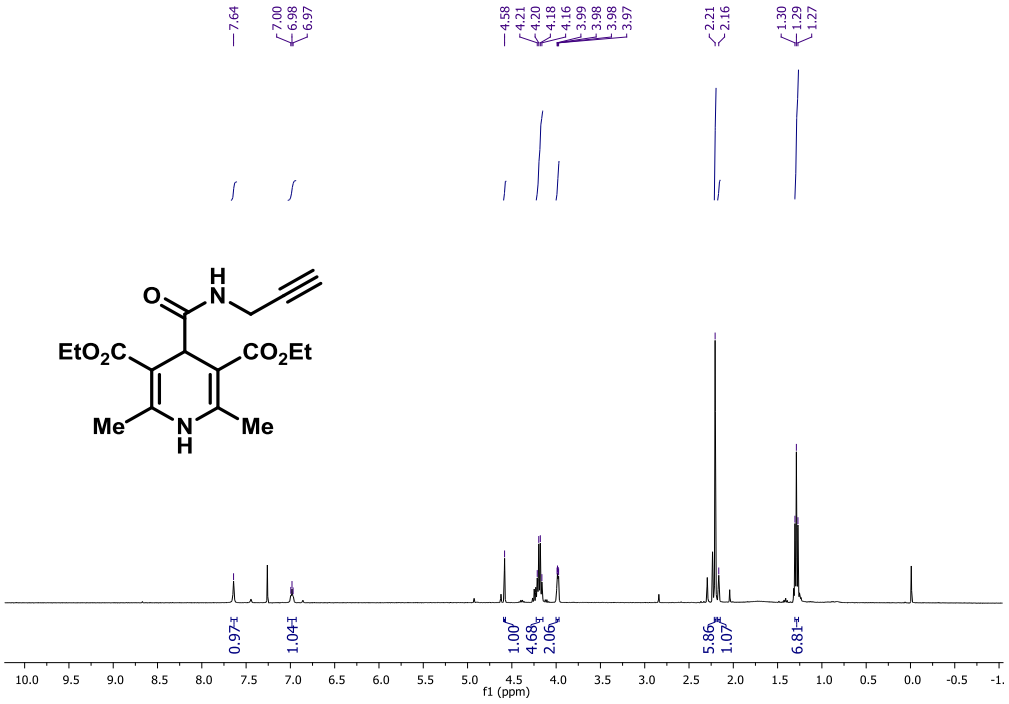

[1]H NMR (CDCl3, 400 MHz) of 45'.

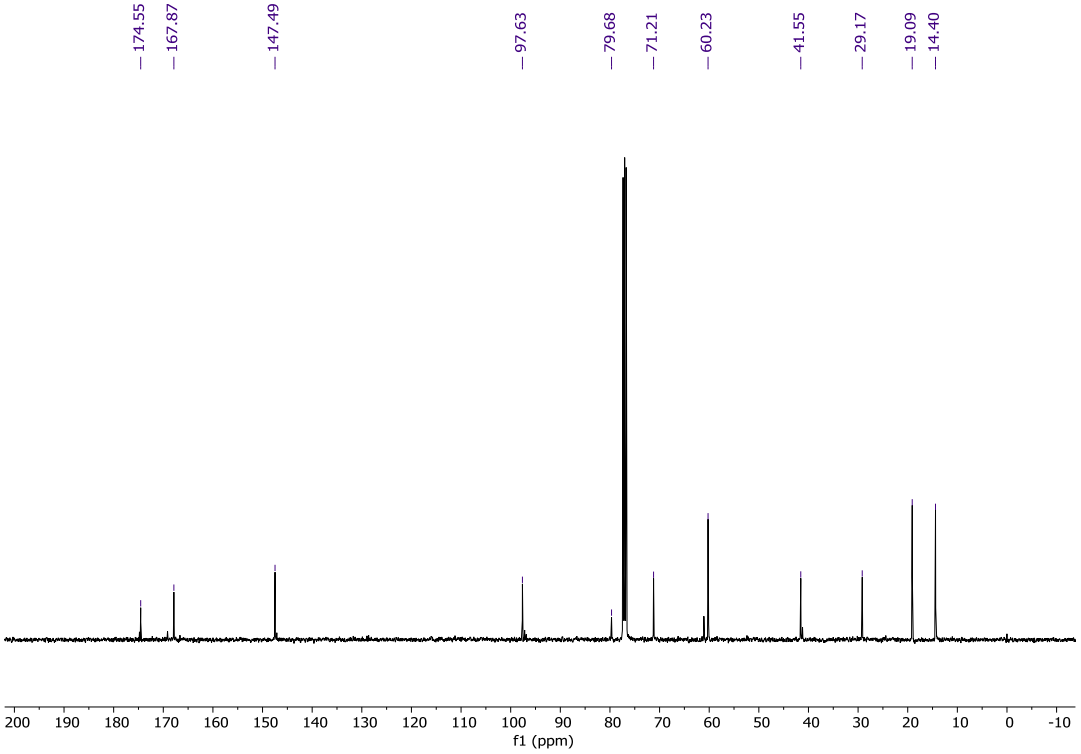

[13]C NMR (CDCl3, 126 MHz) of 45'.

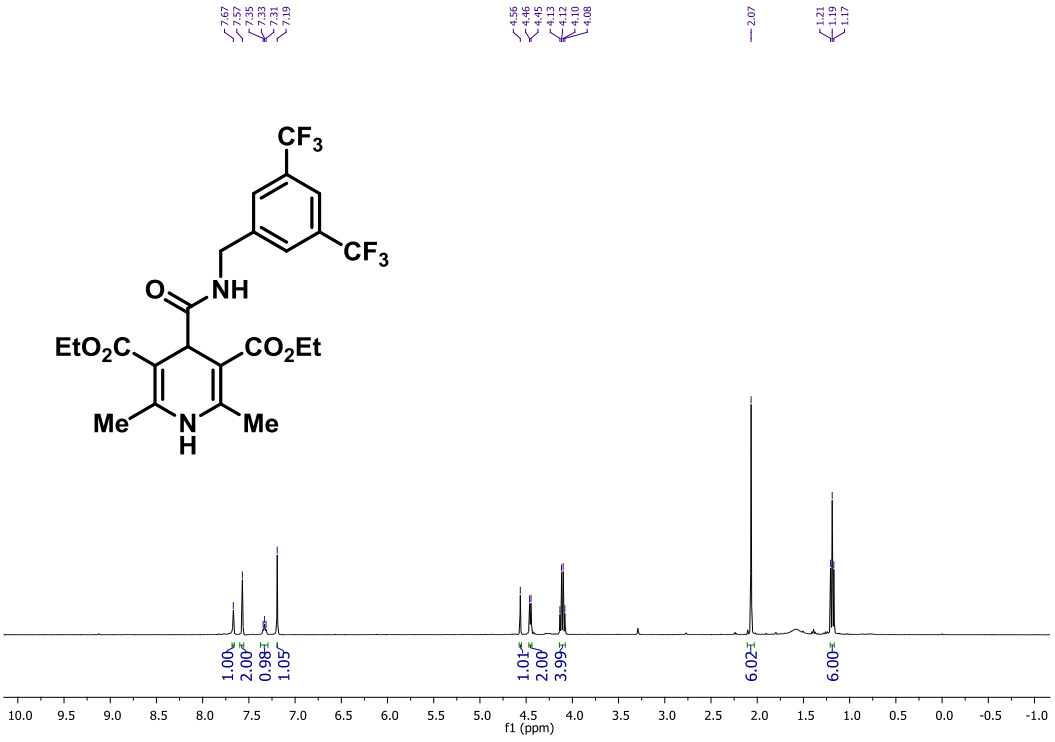

^{1}H NMR (CDCl3, 400 MHz) of 47'.

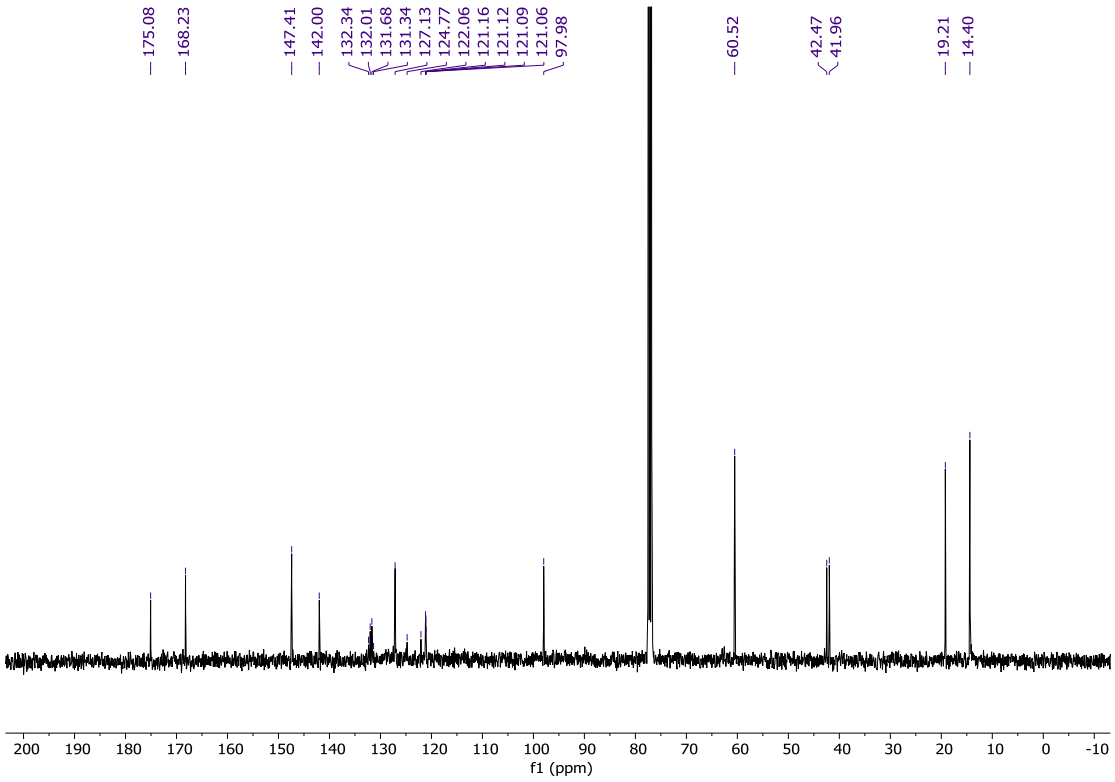

^{13}C NMR (CDCl3, 126 MHz) of 47'.

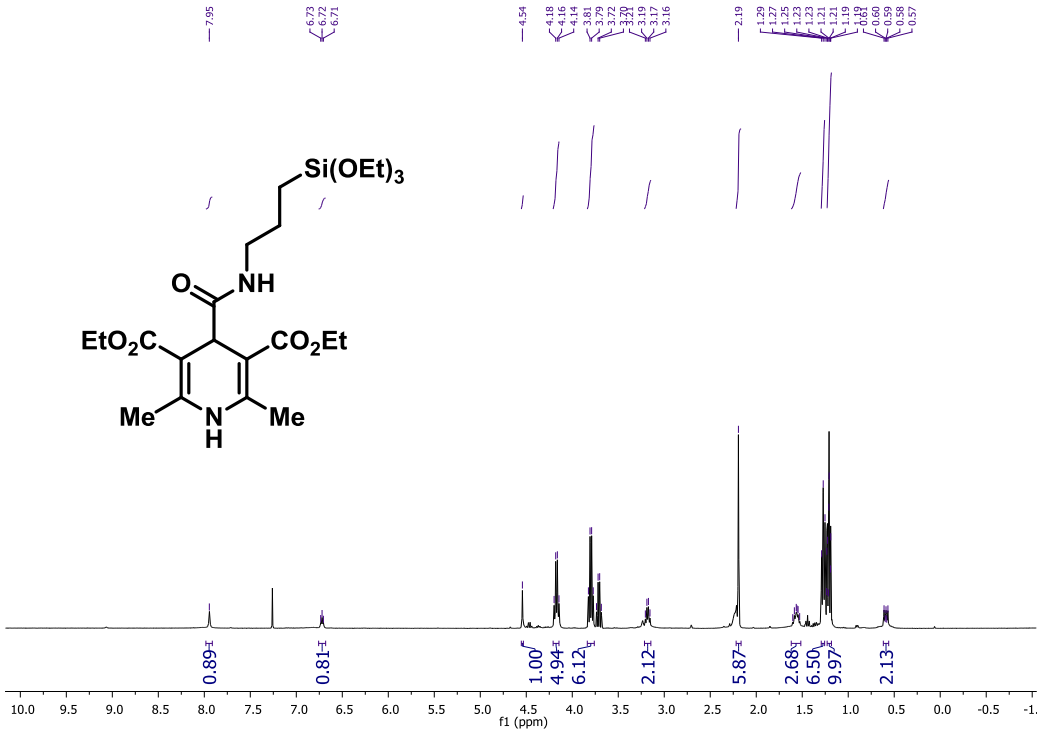

^{1}H NMR (CDCl3, 400 MHz) of 48'.

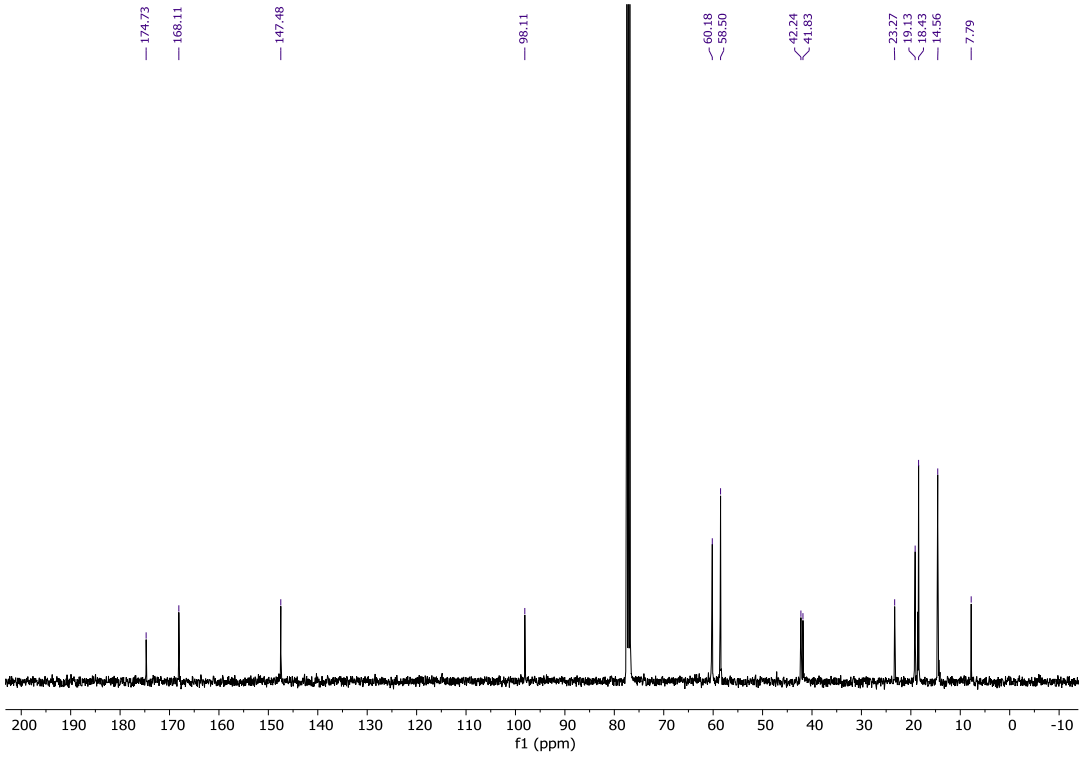

^{13}C NMR (CDCl3, 126 MHz) of 48'.

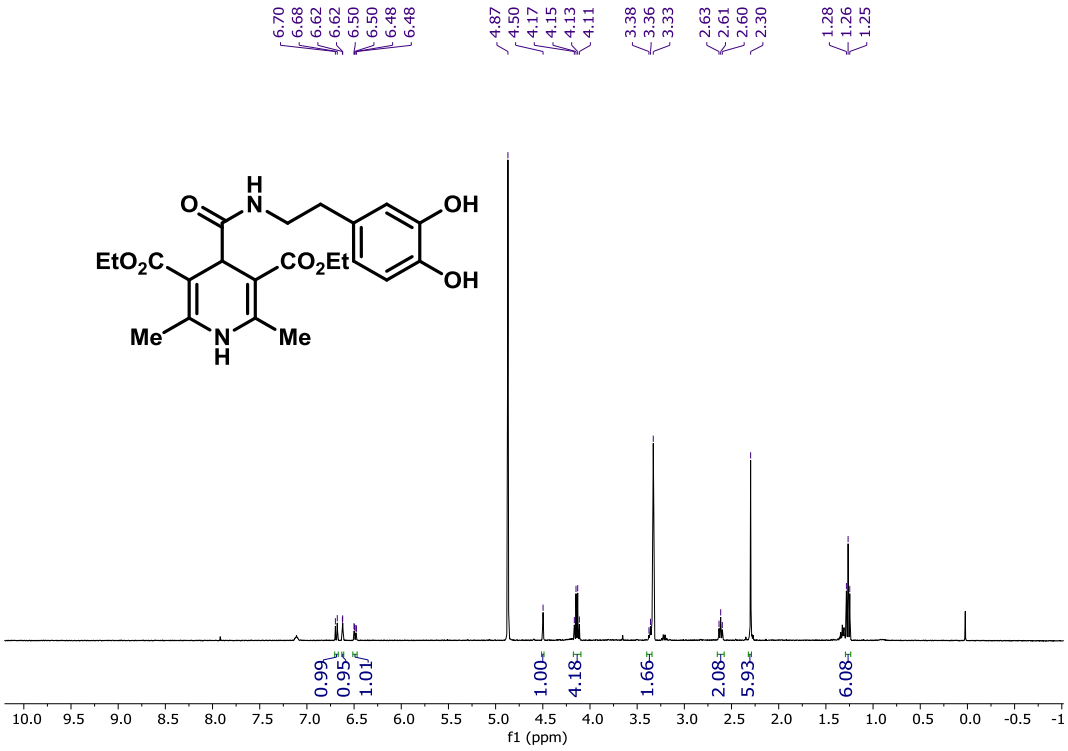

^{1}H NMR (CD_3OD, 400 MHz) of 49'.

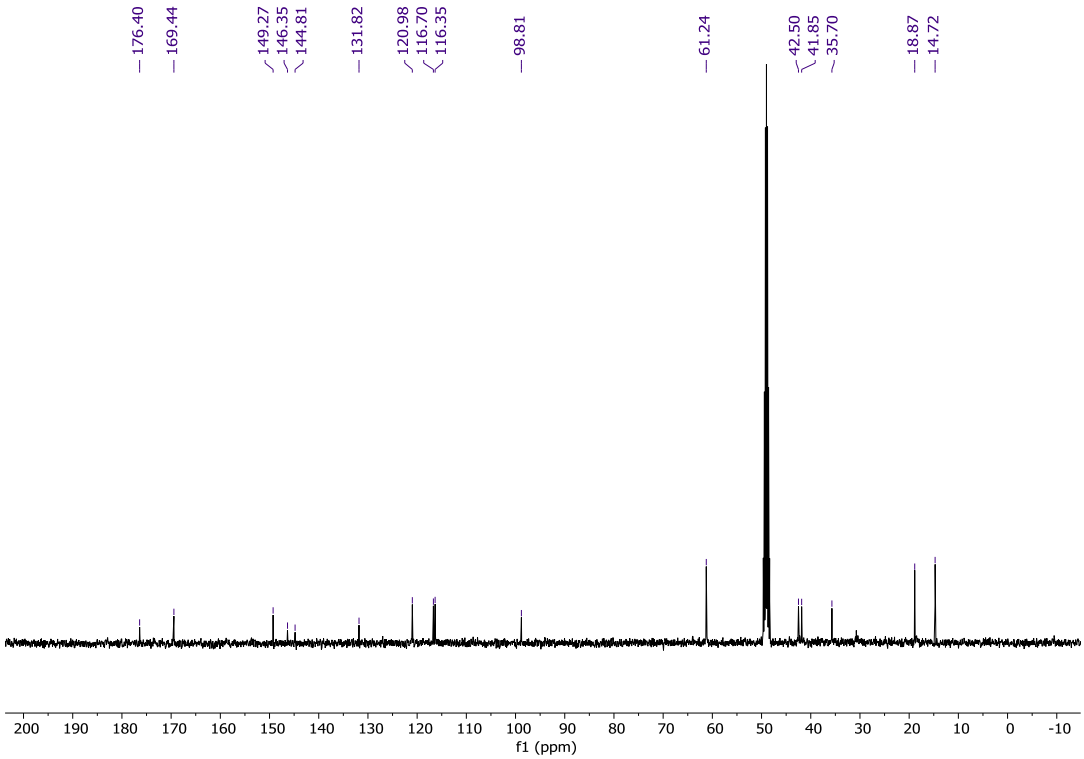

^{13}C NMR (CD_3OD, 126 MHz) of 49'.

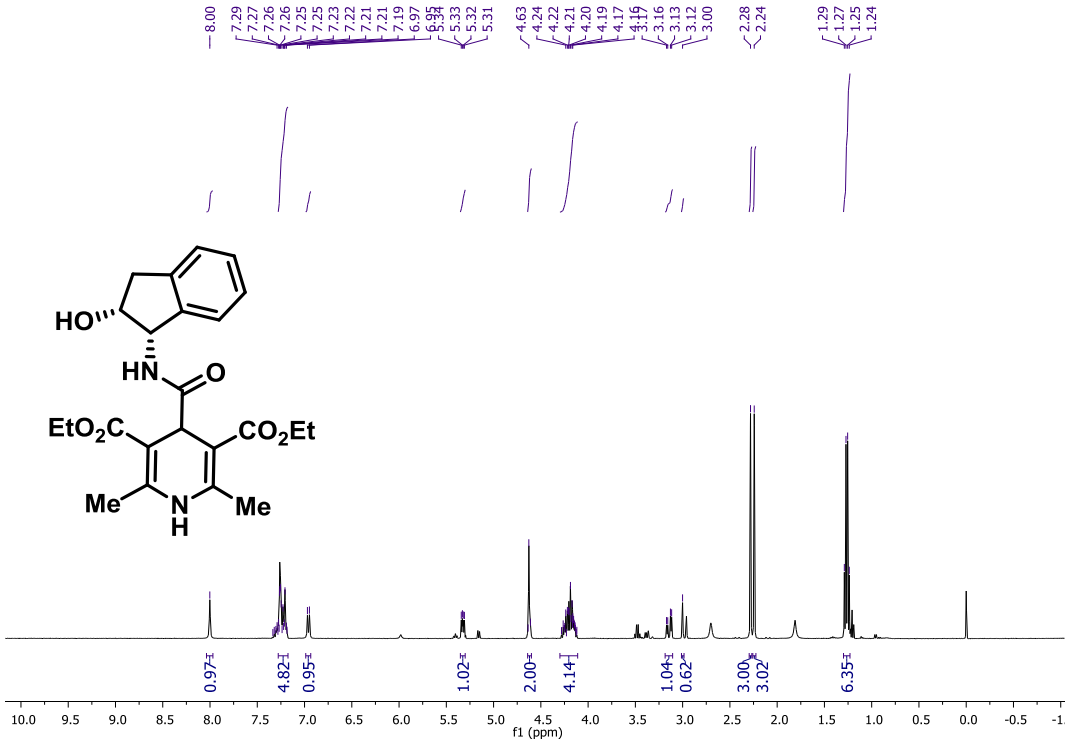

^{1}H NMR (CDCl3, 400 MHz) of 50'.

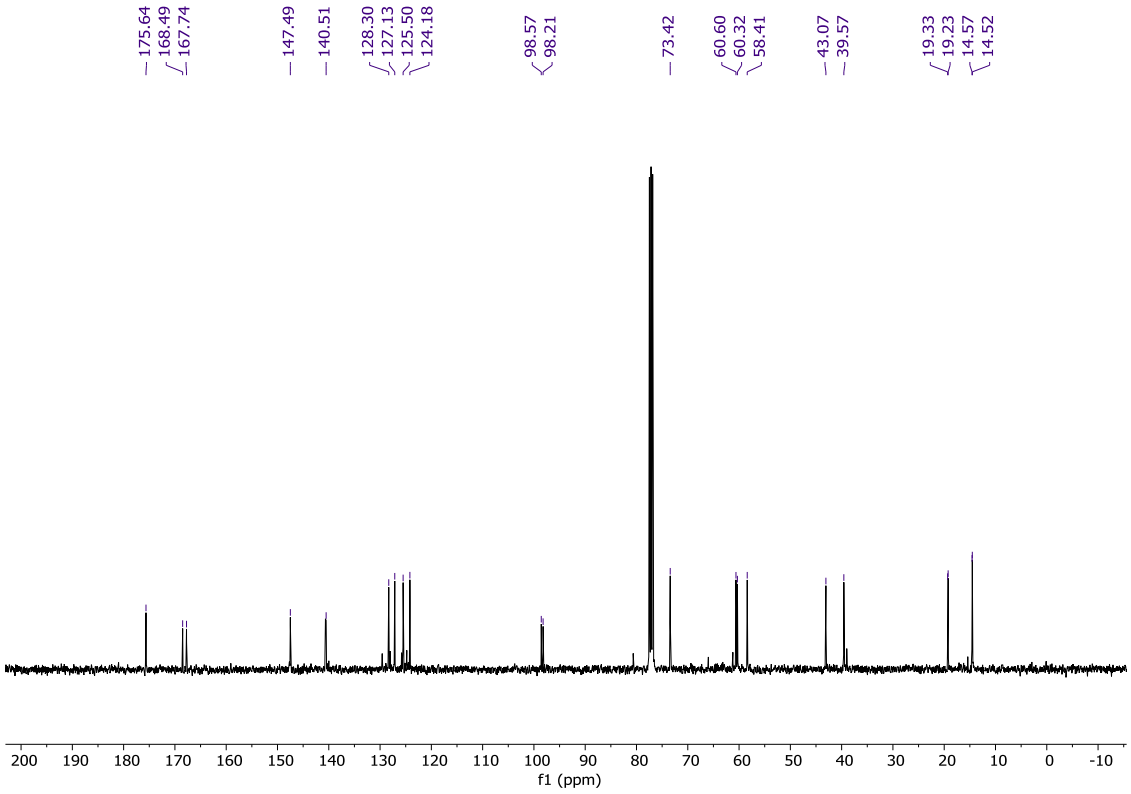

^{13}C NMR (CDCl3, 126 MHz) of 50'.

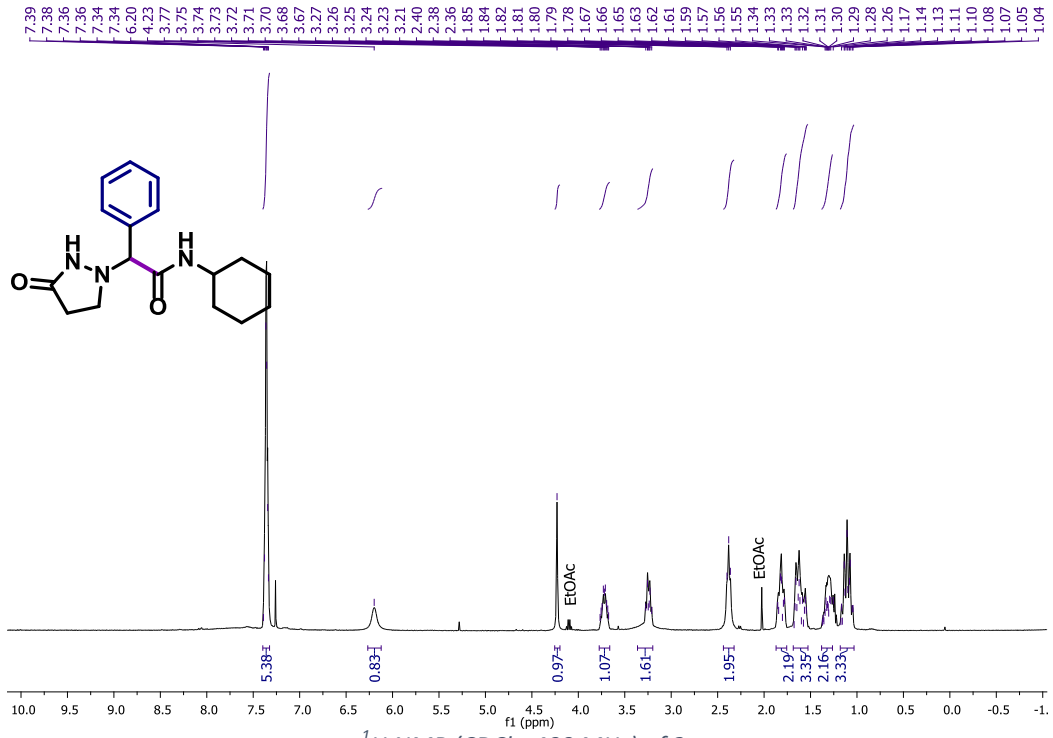

^{1}H NMR ($CDCl_3$, 400 MHz) of 3.

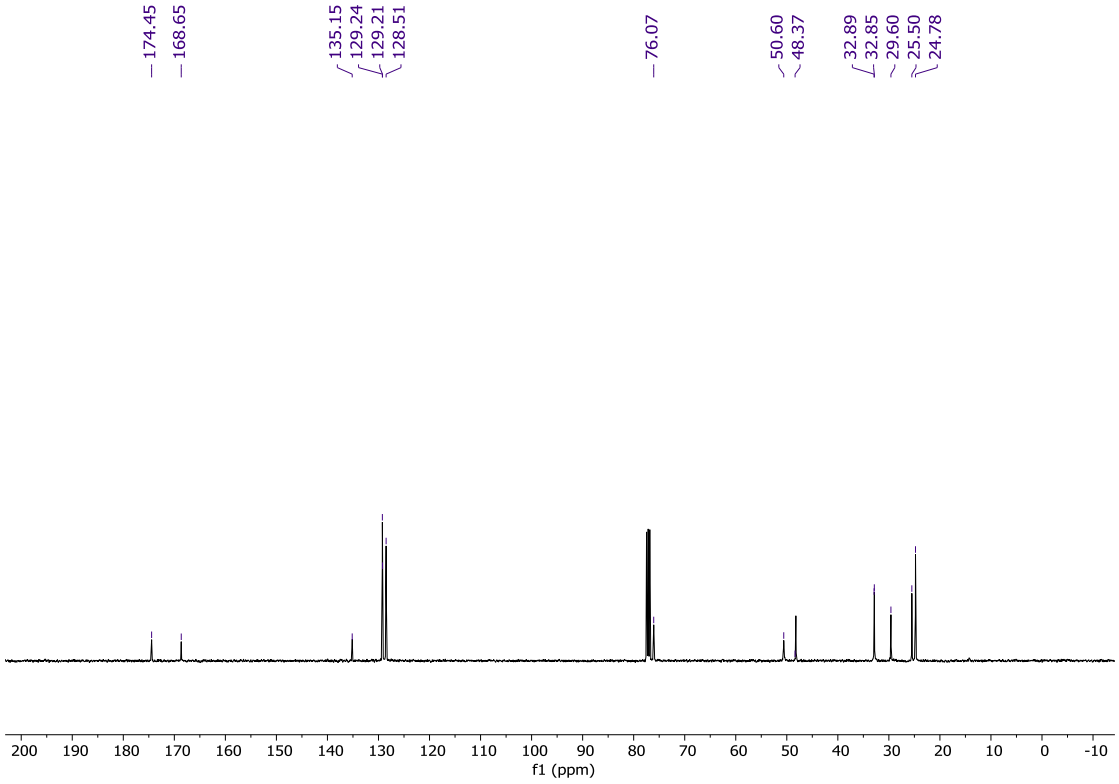

^{13}C NMR ($CDCl_3$, 126 MHz) of 3.

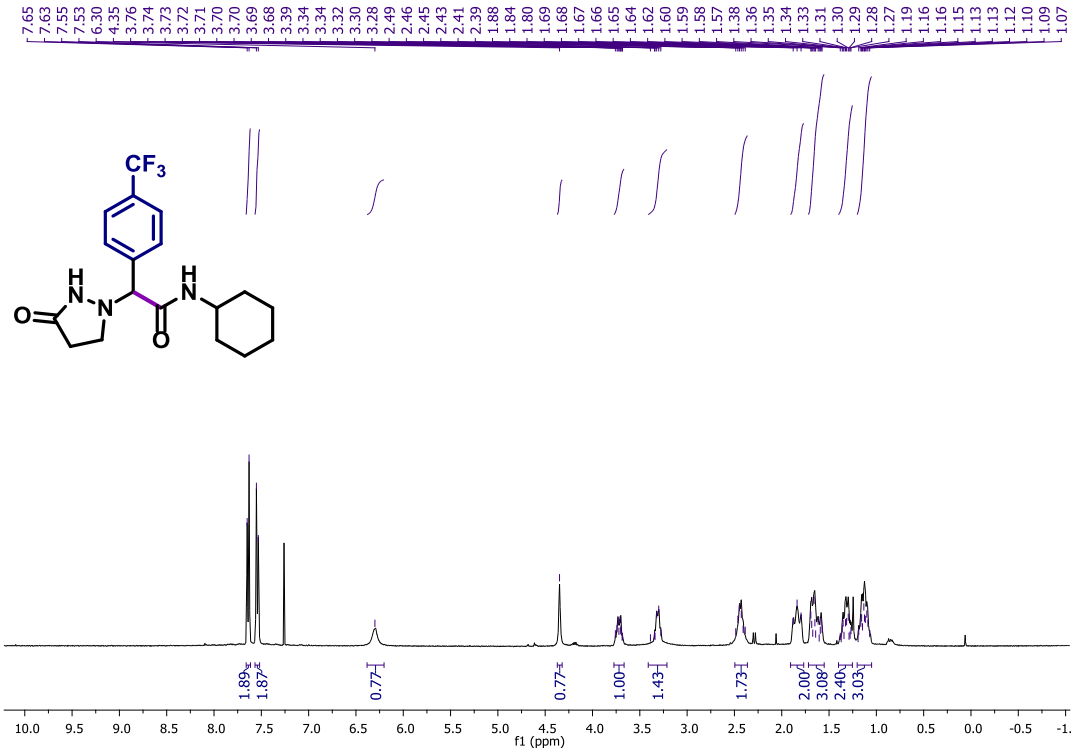

^{1}H NMR ($CDCl_3$, 400 MHz) of 4.

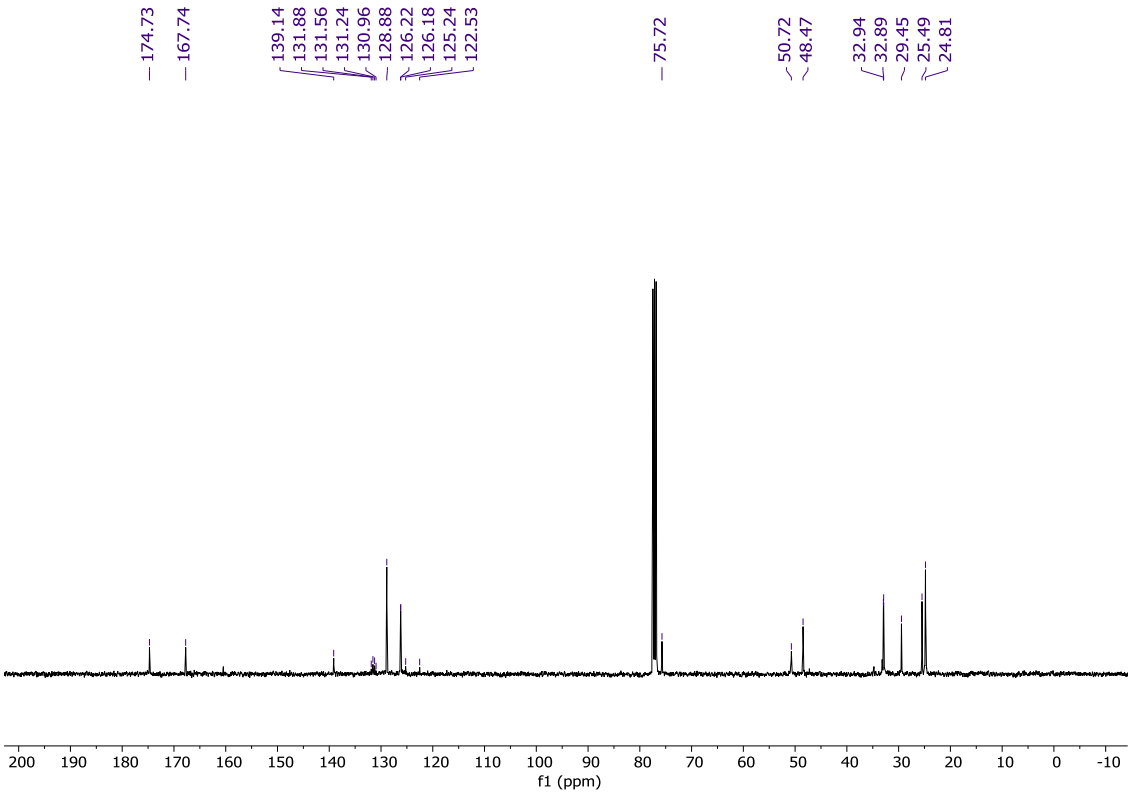

^{13}C NMR ($CDCl_3$, 126 MHz) of 4.

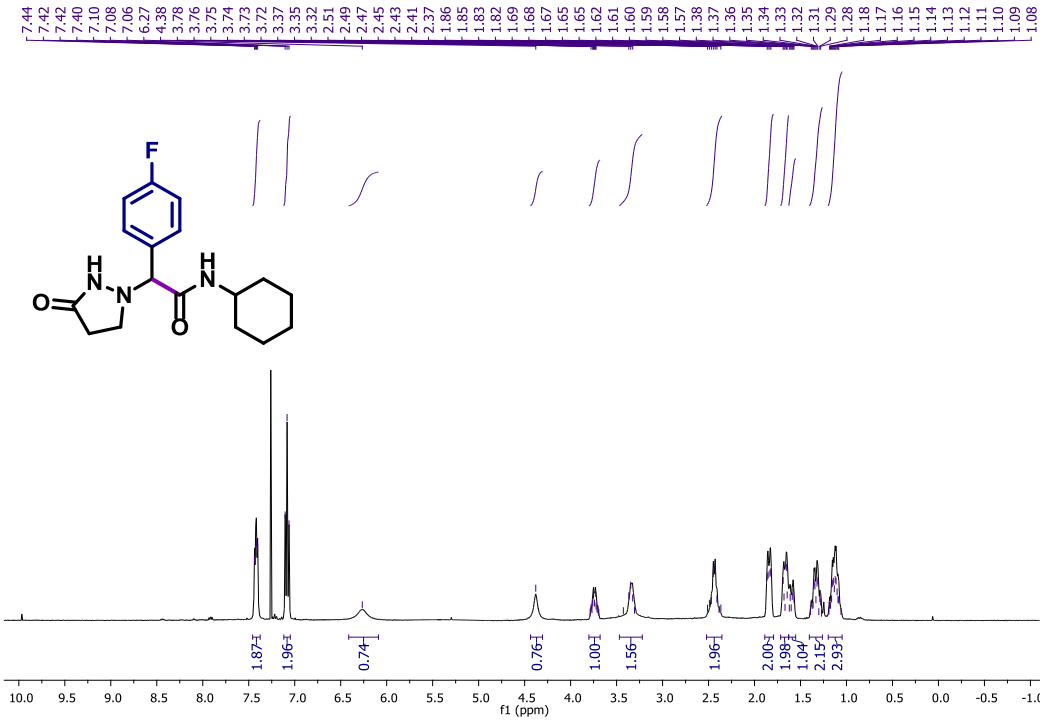

^{1}H NMR ($CDCl_3$, 400 MHz) of 5.

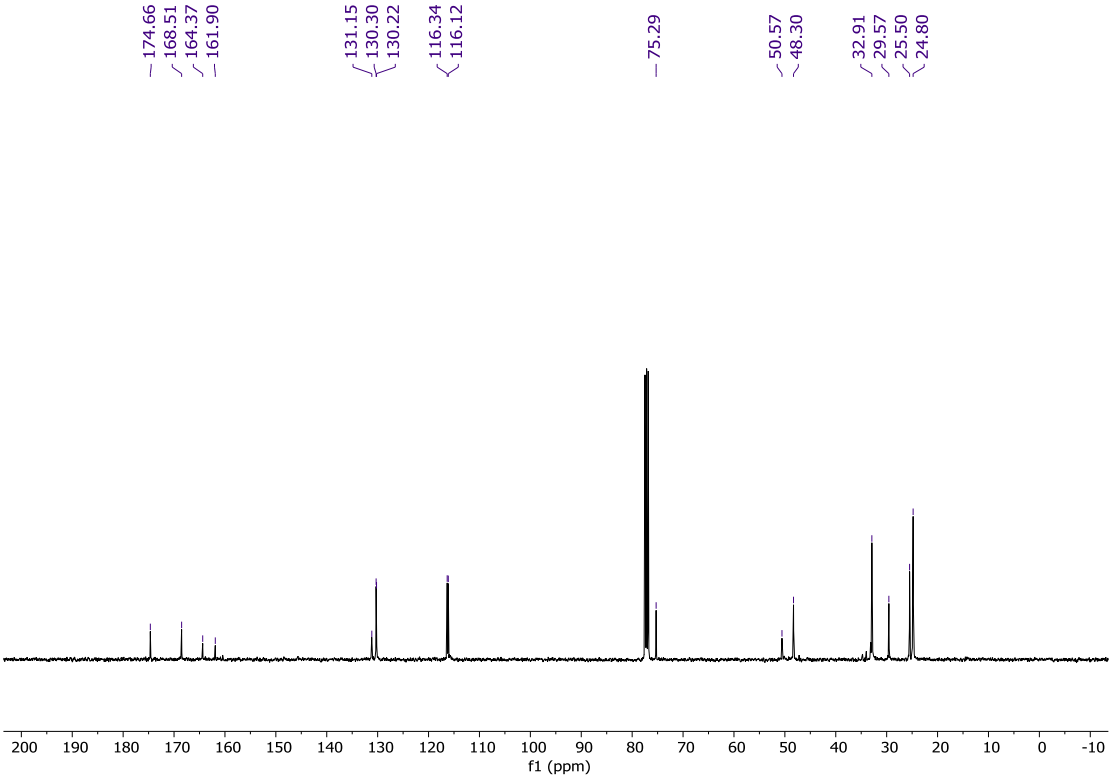

^{13}C NMR ($CDCl_3$, 126 MHz) of 5.

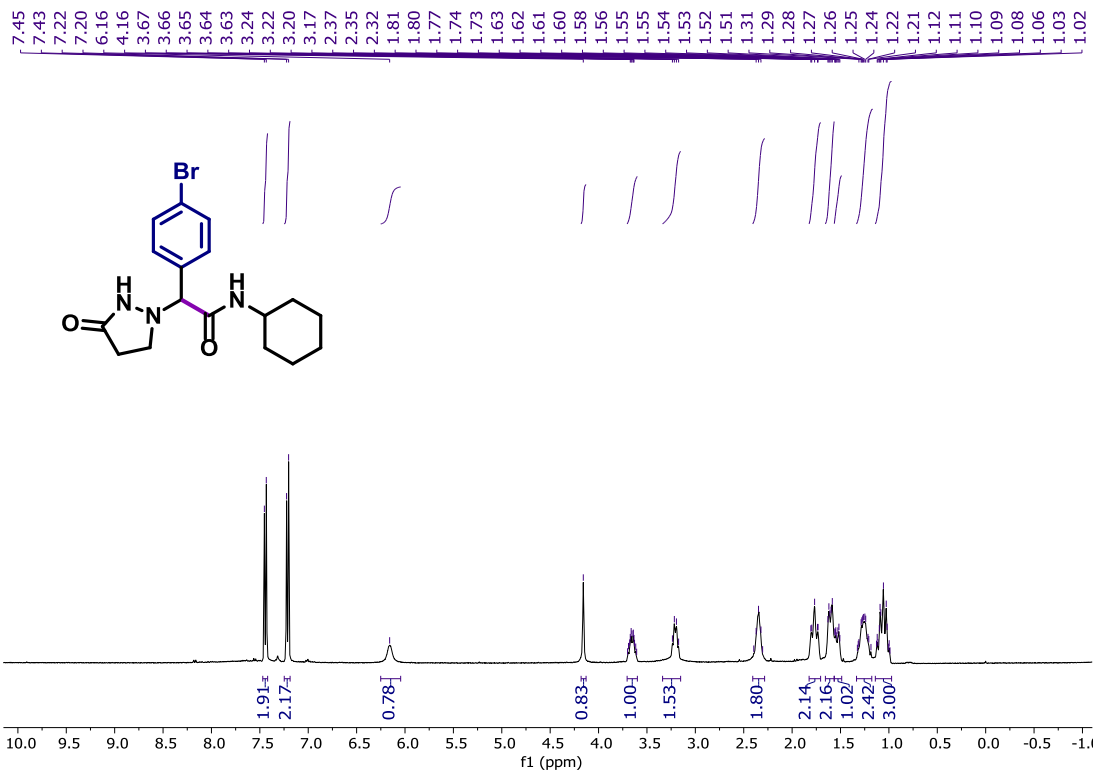

^{1}H NMR ($CDCl_3$, 400 MHz) of 6.

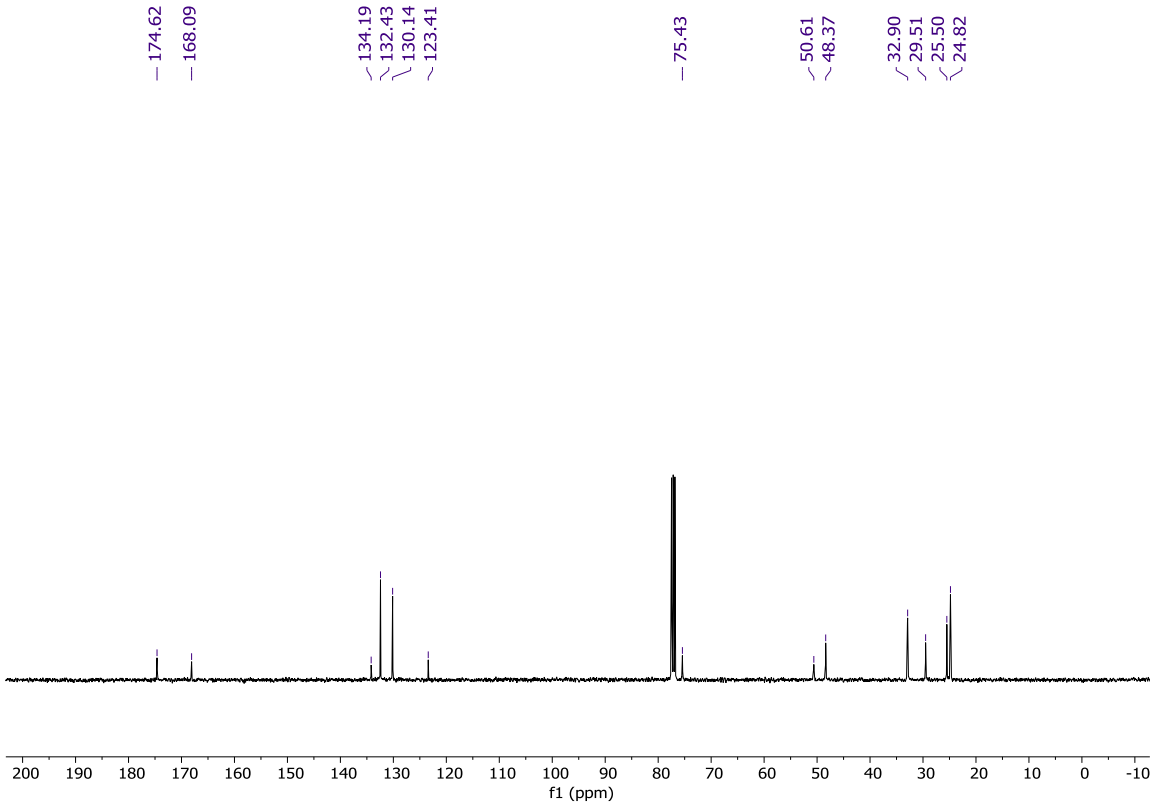

^{13}C NMR ($CDCl_3$, 126 MHz) of 6.

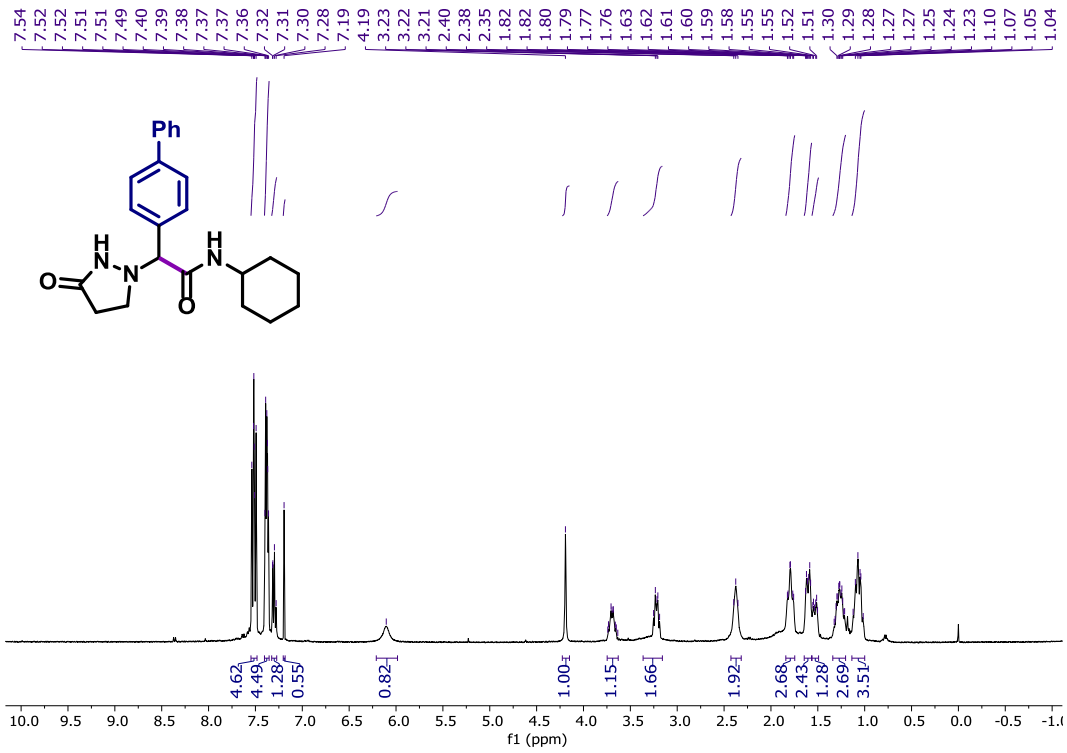

^{1}H NMR ($CDCl_3$, 400 MHz) of 7.

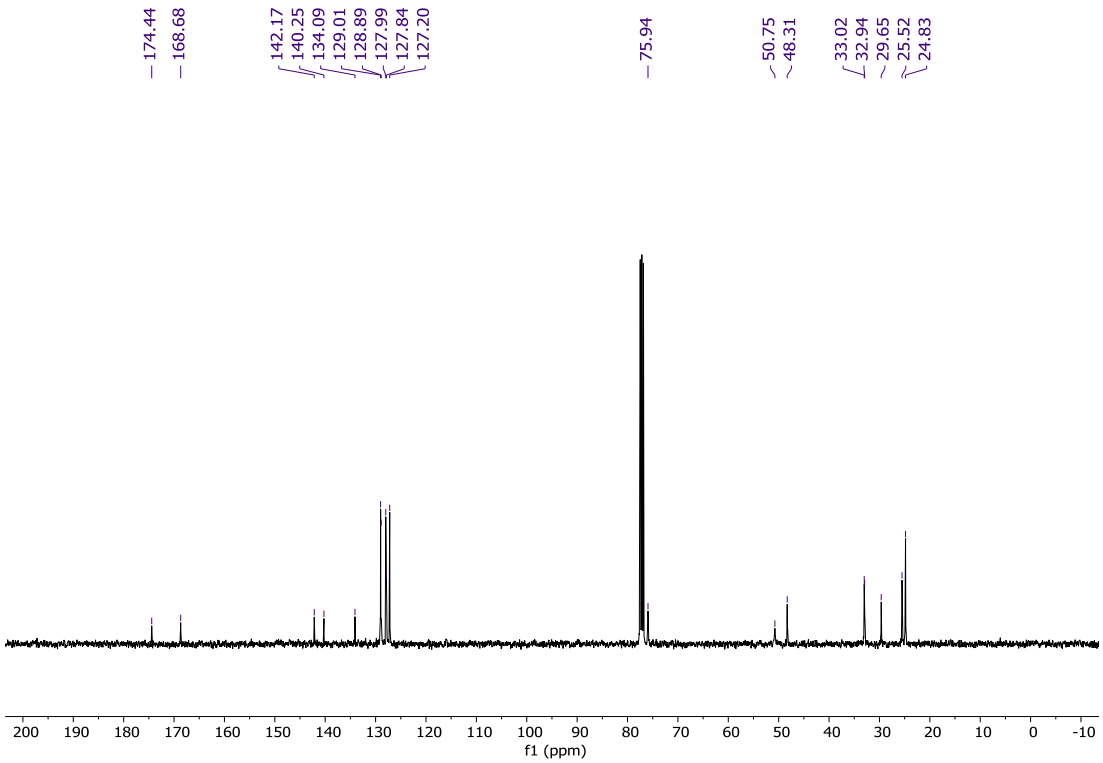

^{13}C NMR ($CDCl_3$, 126 MHz) of 7.

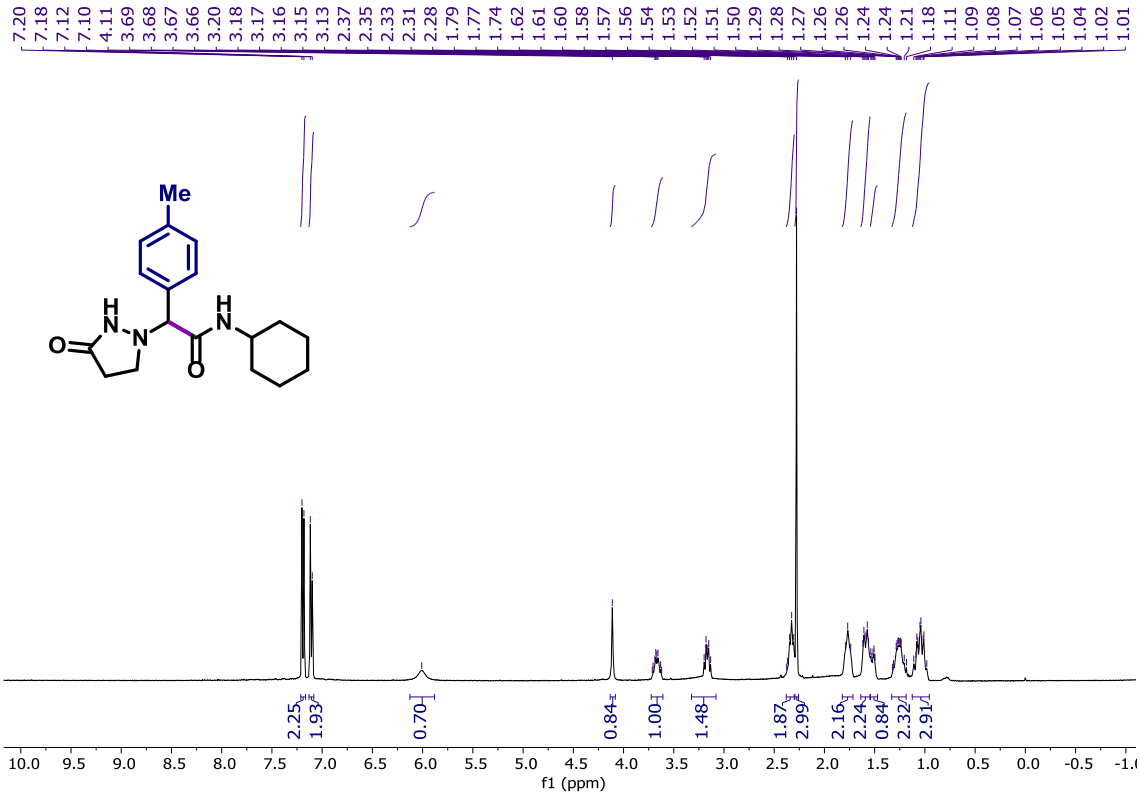

^{1}H NMR ($CDCl_3$, 400 MHz) of 8.

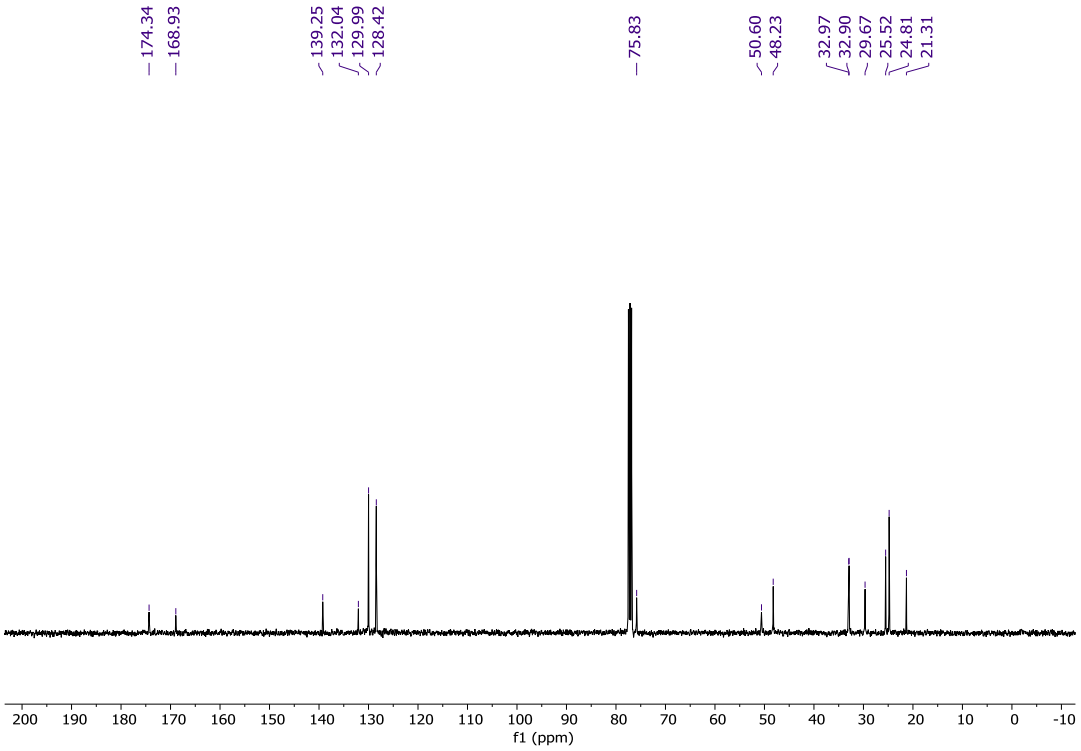

^{13}C NMR ($CDCl_3$, 126 MHz) of 8.

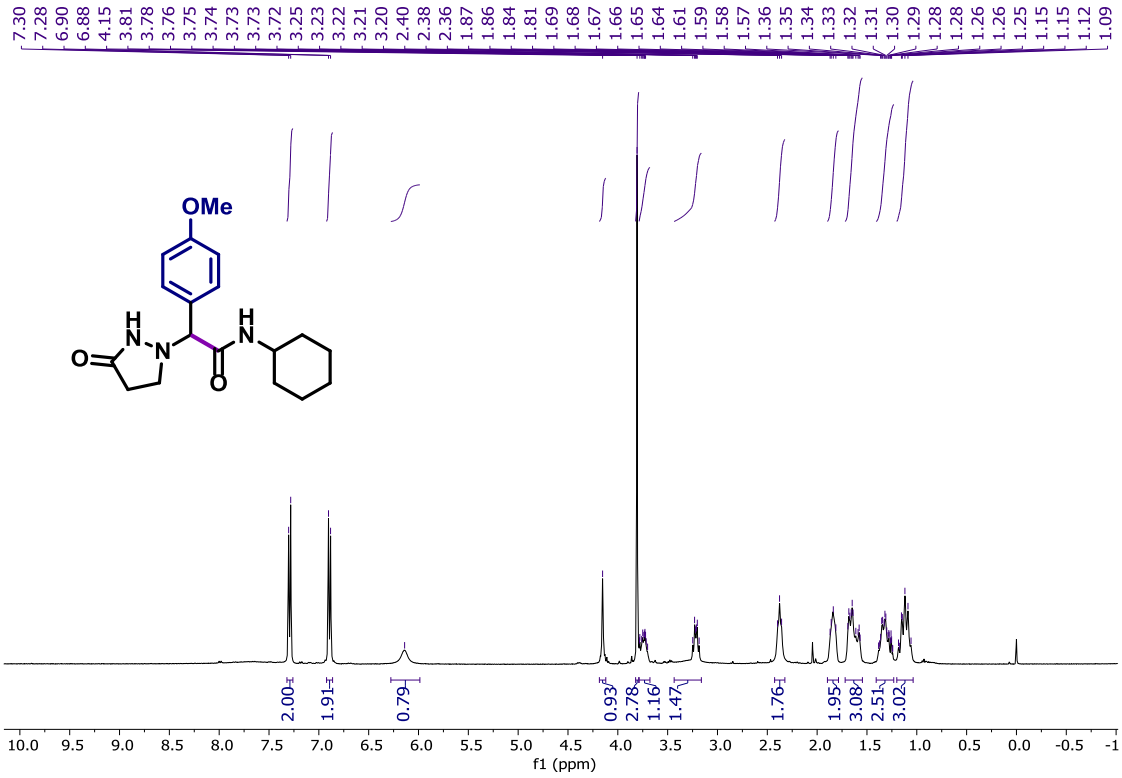

^{1}H NMR ($CDCl_3$, 400 MHz) of 9.

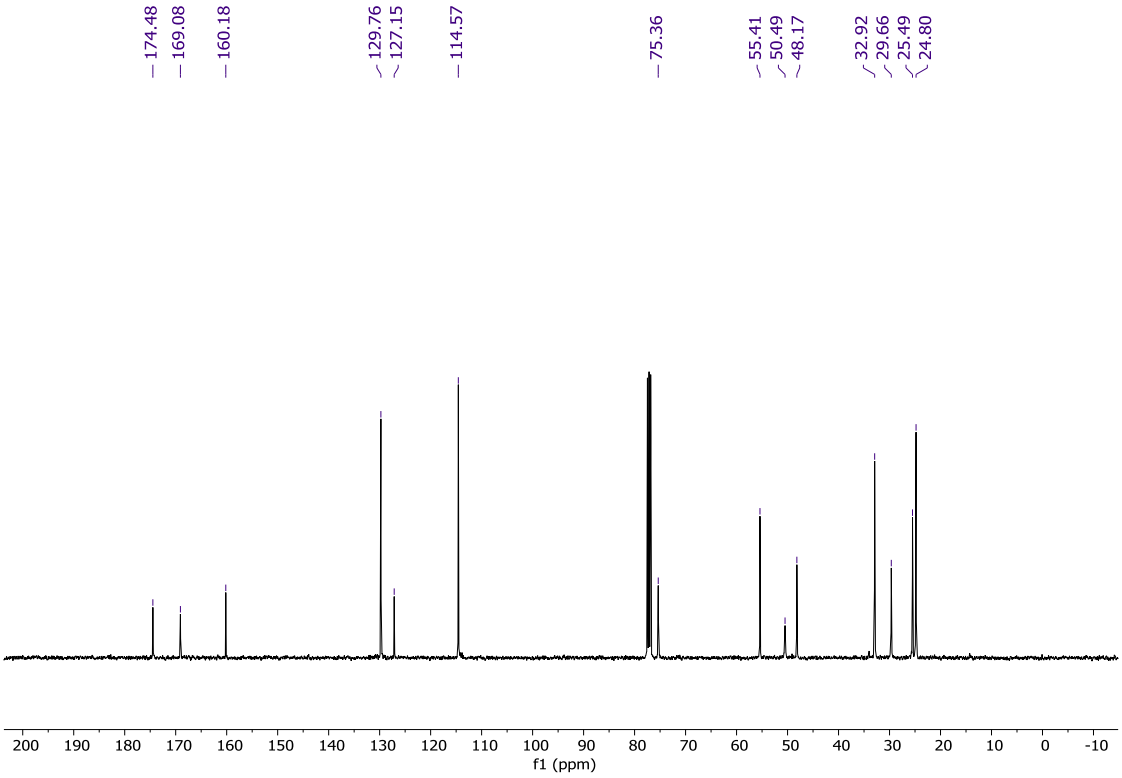

^{13}C NMR ($CDCl_3$, 126 MHz) of 9.

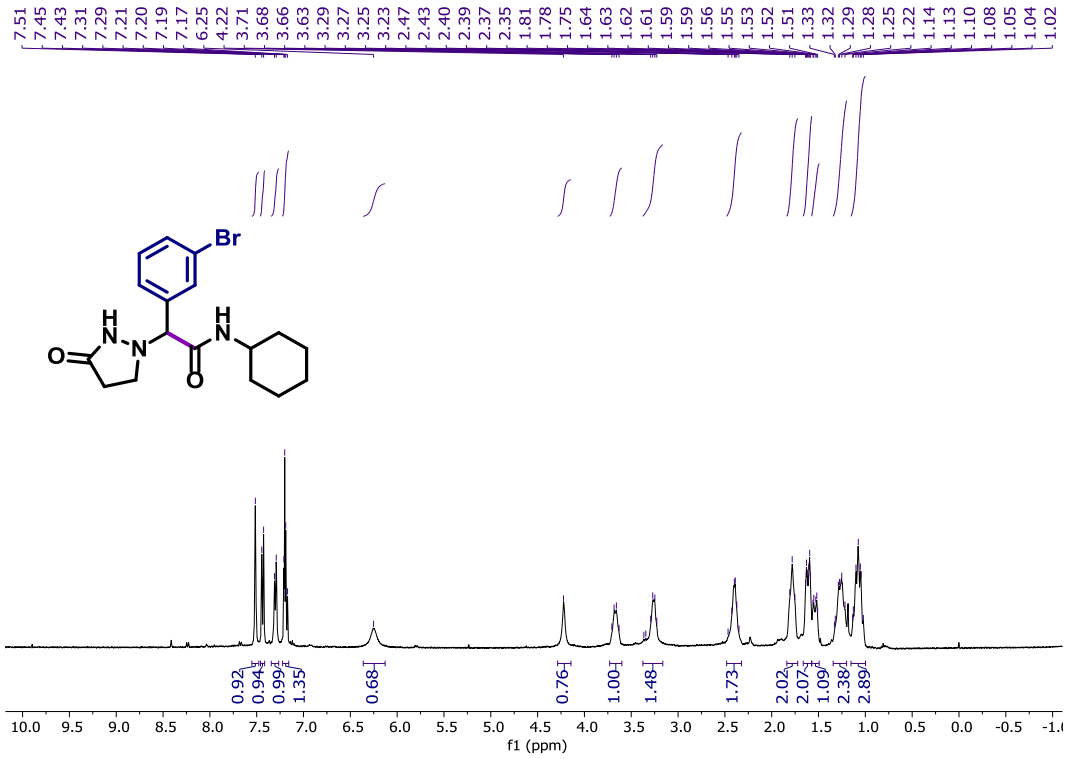

^{1}H NMR ($CDCl_3$, 400 MHz) of 10.

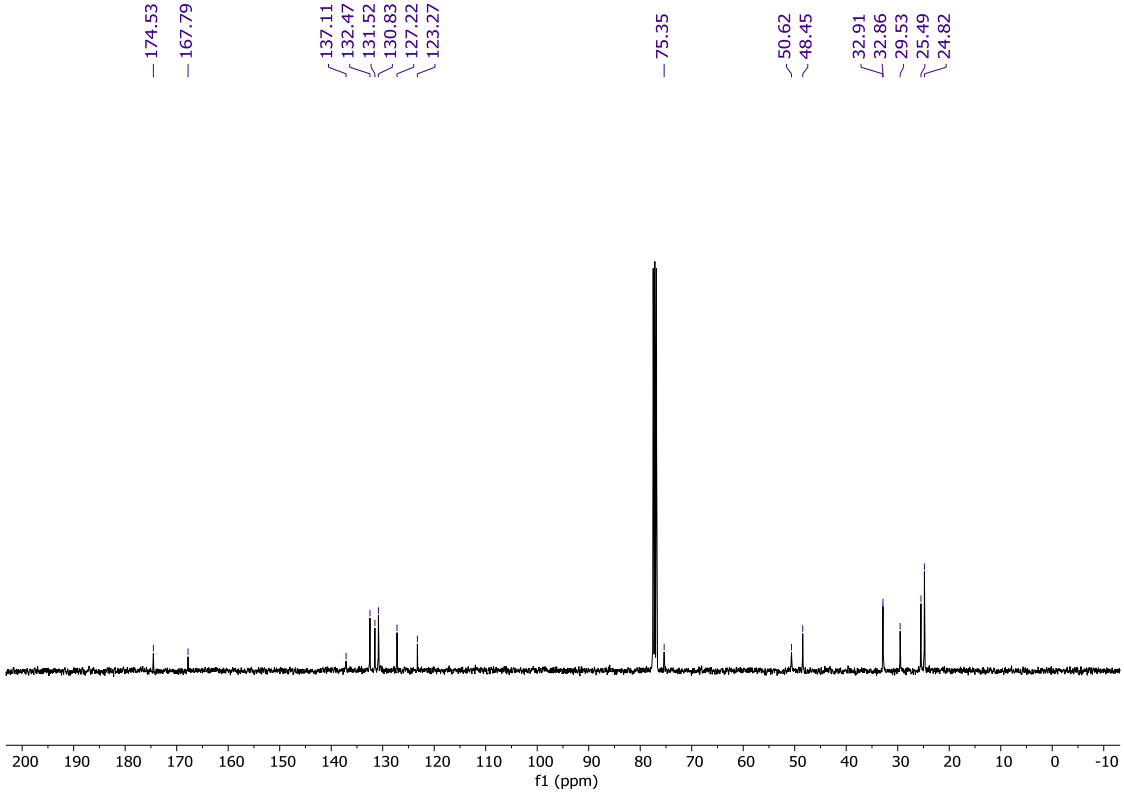

^{13}C NMR ($CDCl_3$, 126 MHz) of 10.

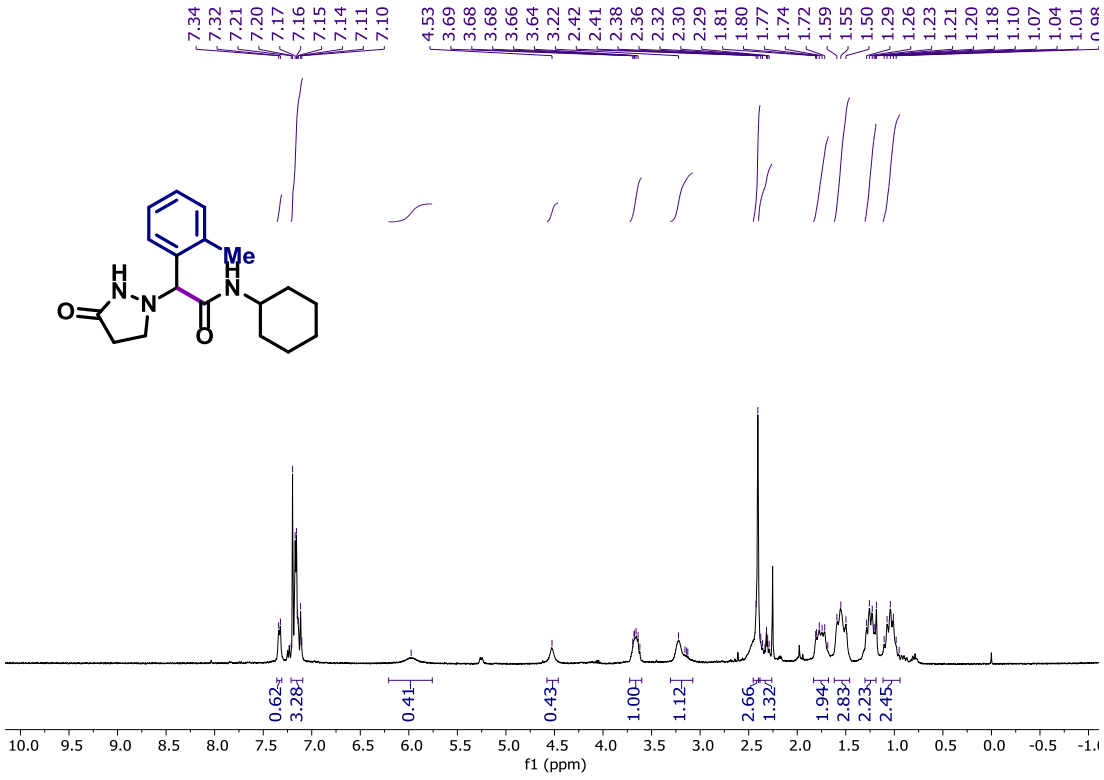

^{1}H NMR ($CDCl_3$, 400 MHz) of 11.

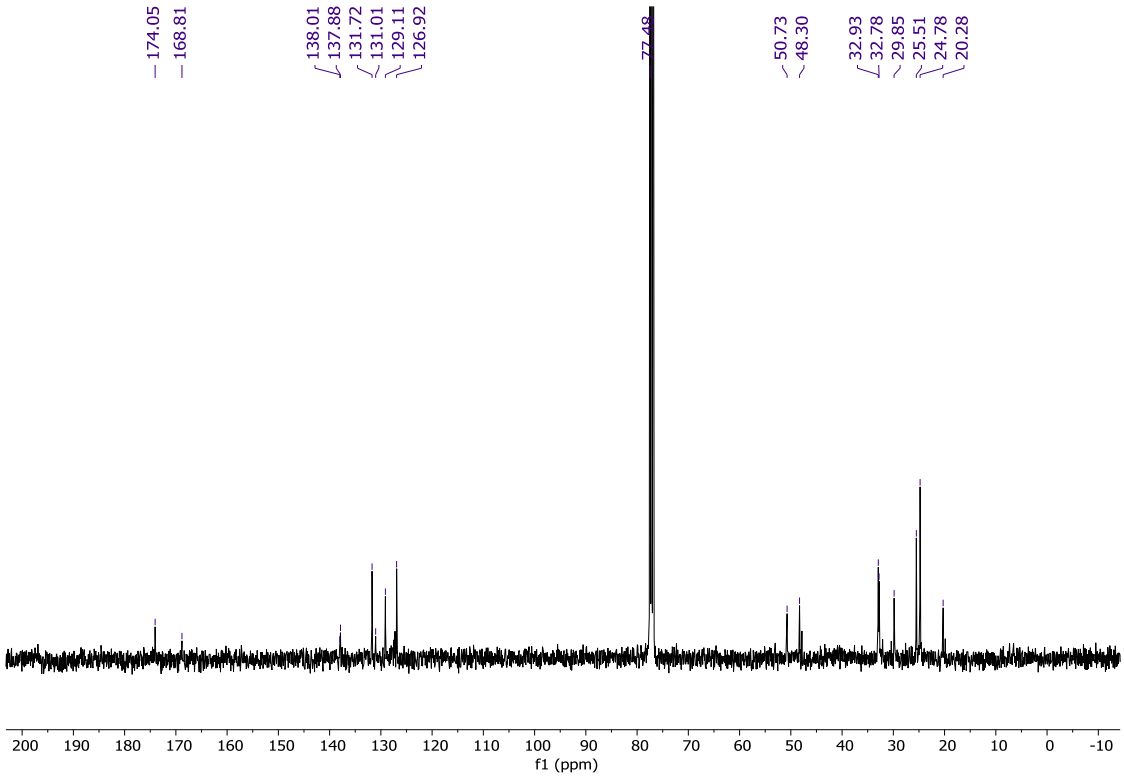

^{13}C NMR ($CDCl_3$, 126 MHz) of 11.

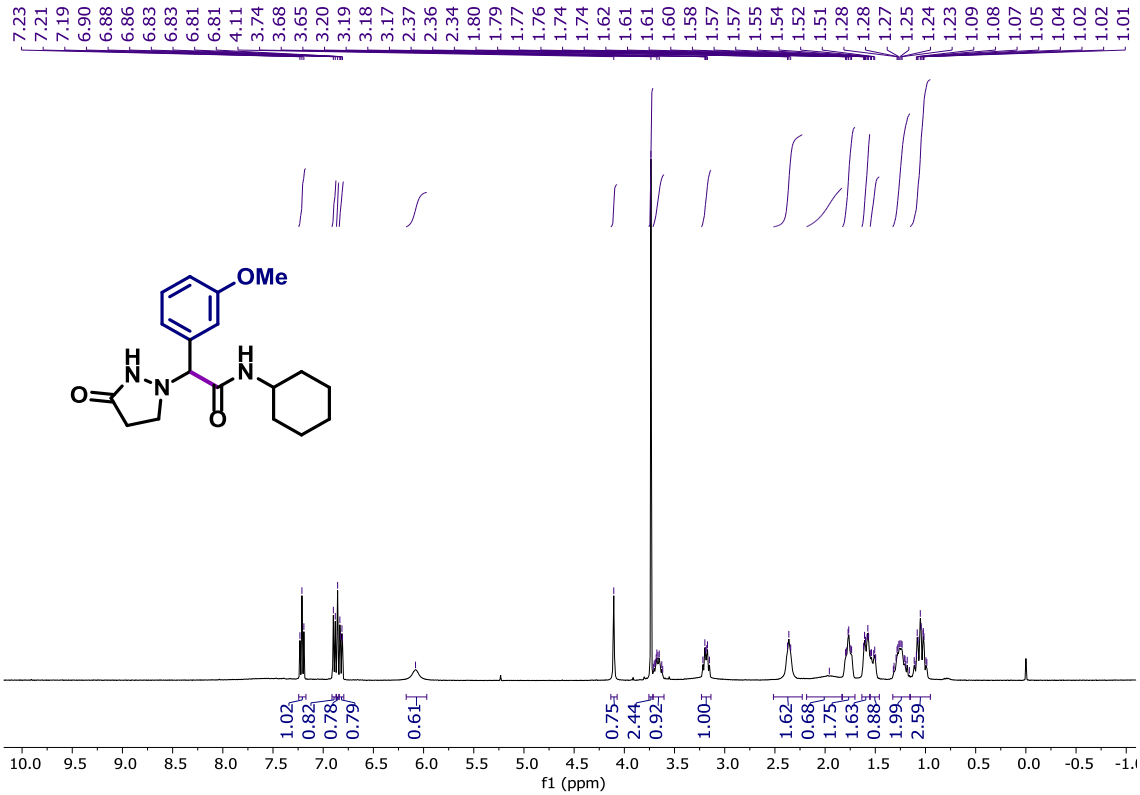

^{1}H NMR ($CDCl_3$, 400 MHz) of 12.

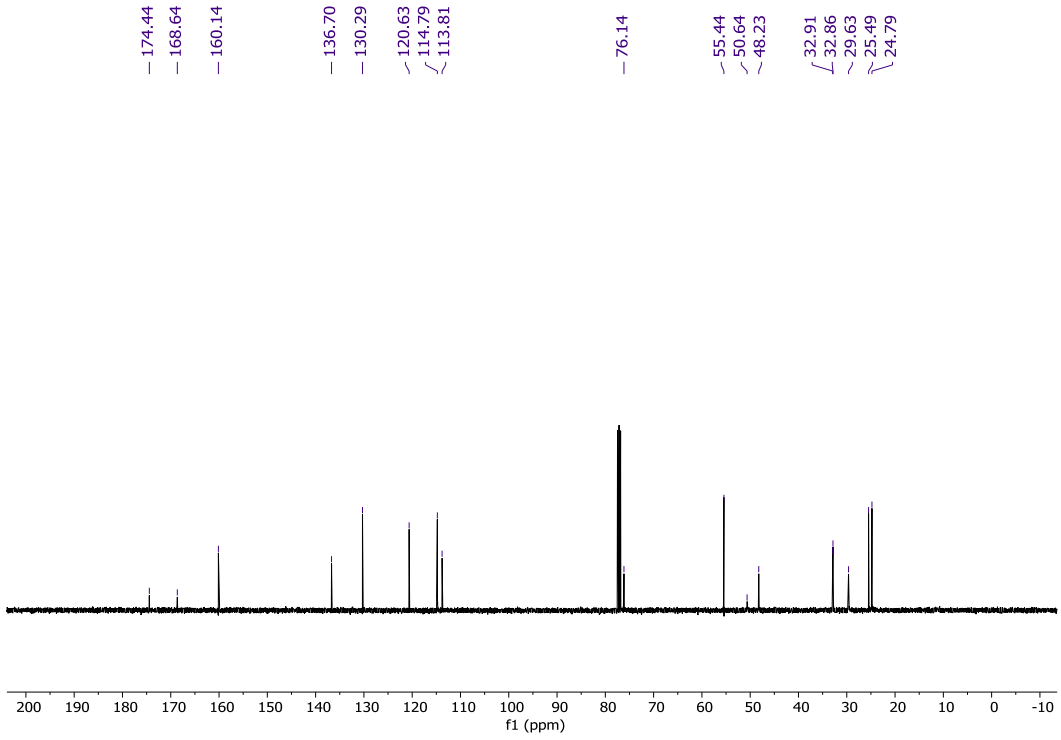

^{13}C NMR ($CDCl_3$, 126 MHz) of 12.

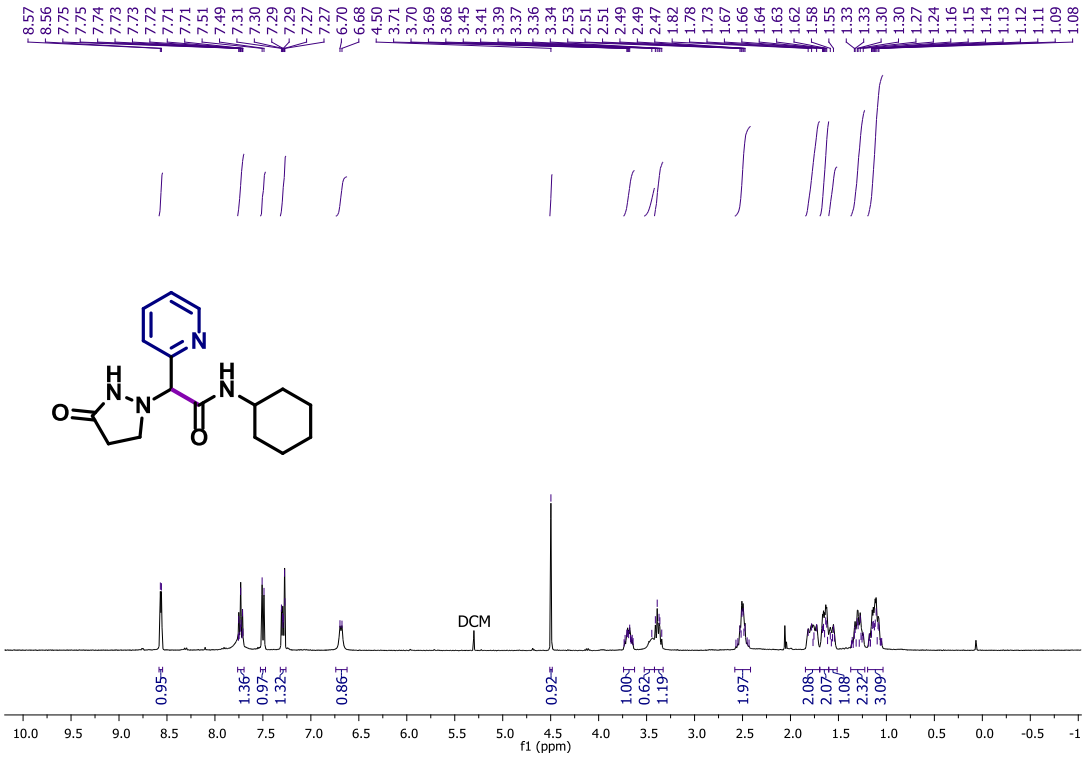

^{1}H NMR ($CDCl_3$, 400 MHz) of 13.

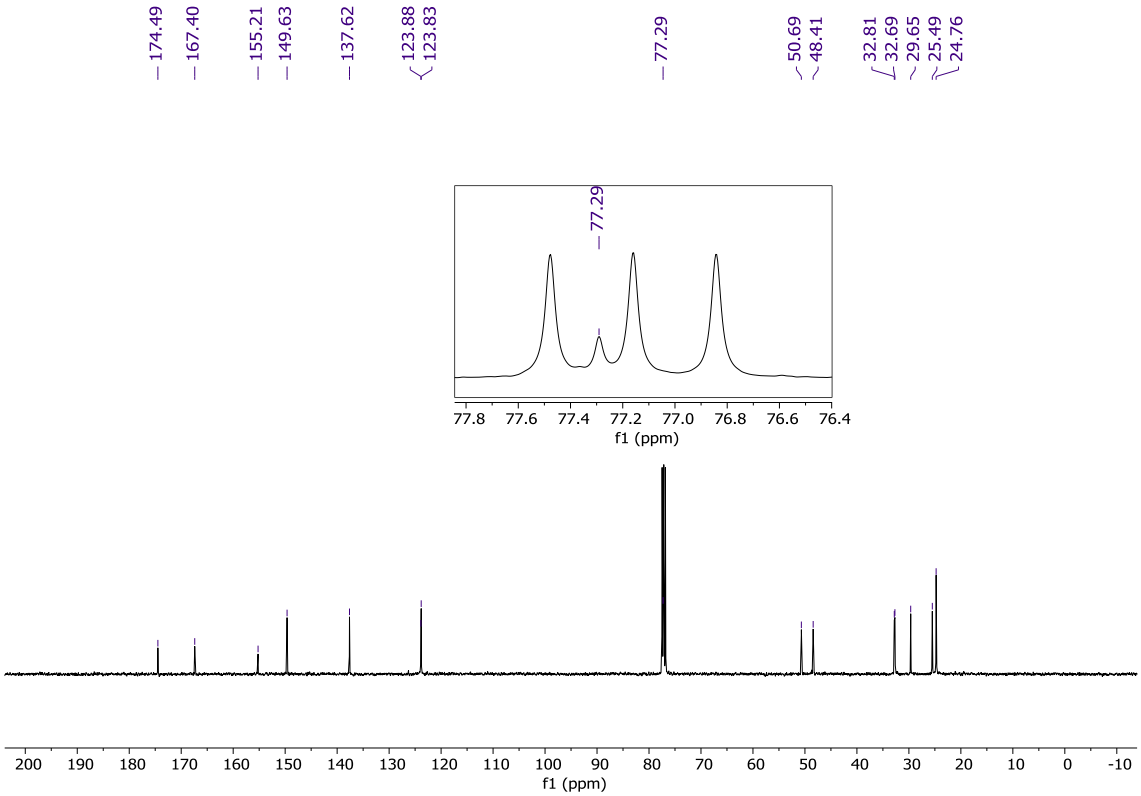

^{13}C NMR ($CDCl_3$, 126 MHz) of 13.

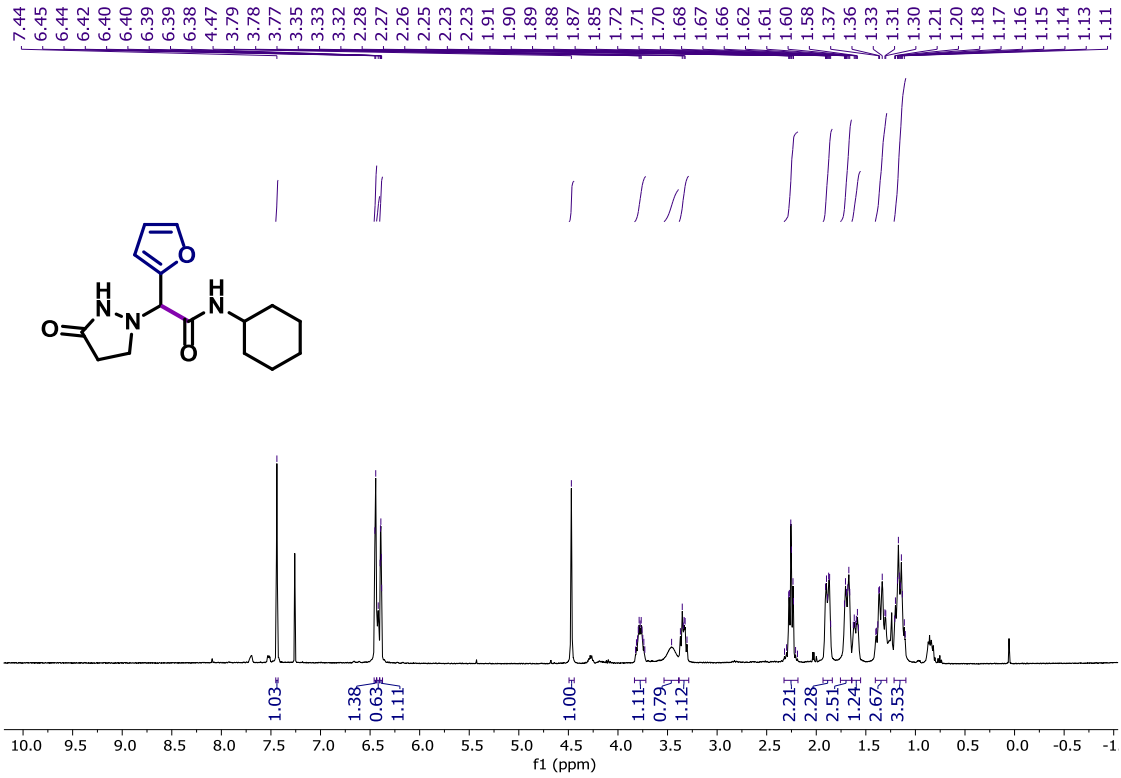

^{1}H NMR ($CDCl_3$, 400 MHz) of 14.

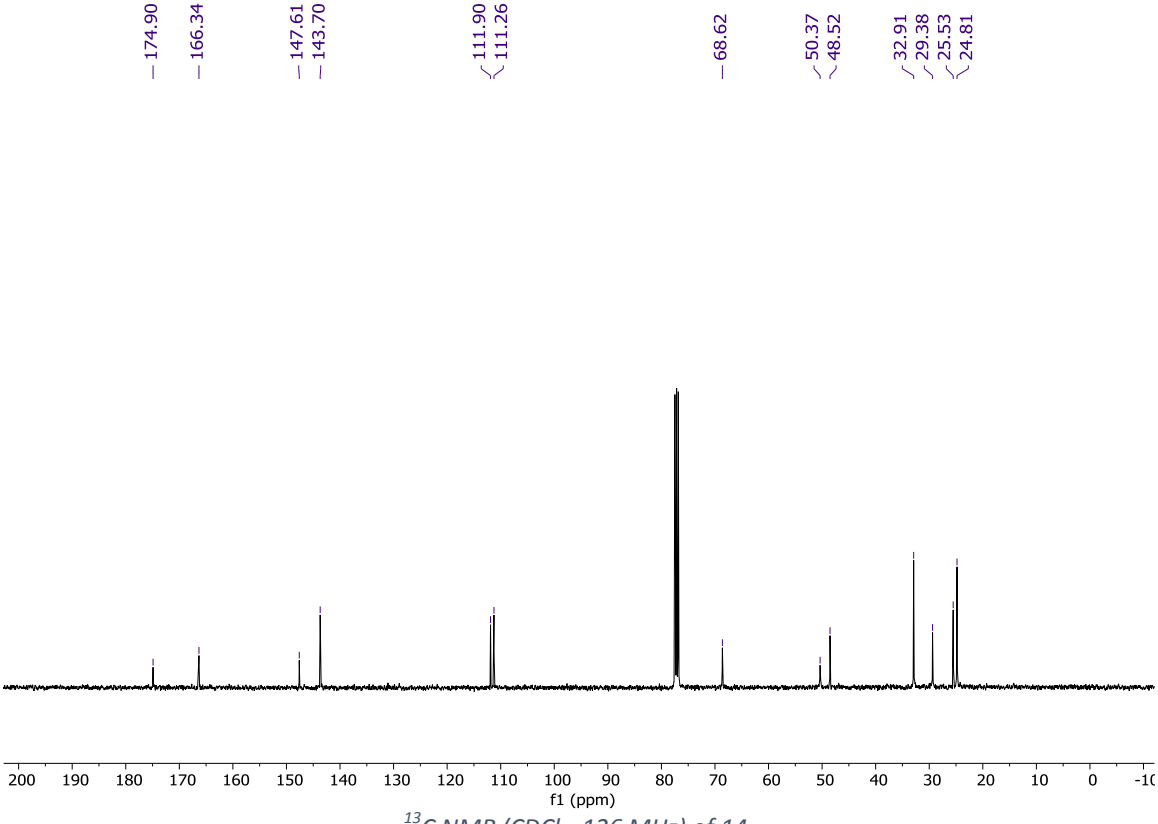

^{13}C NMR ($CDCl_3$, 126 MHz) of 14.

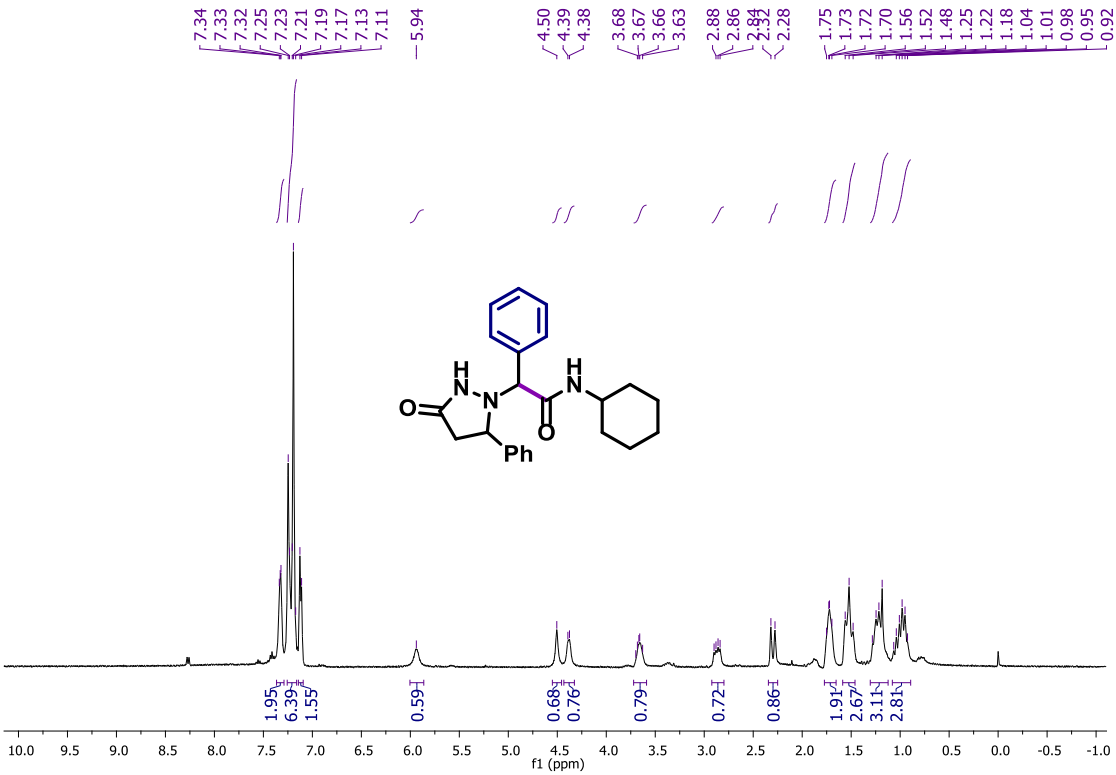

^{1}H NMR ($CDCl_3$, 400 MHz) of 15.

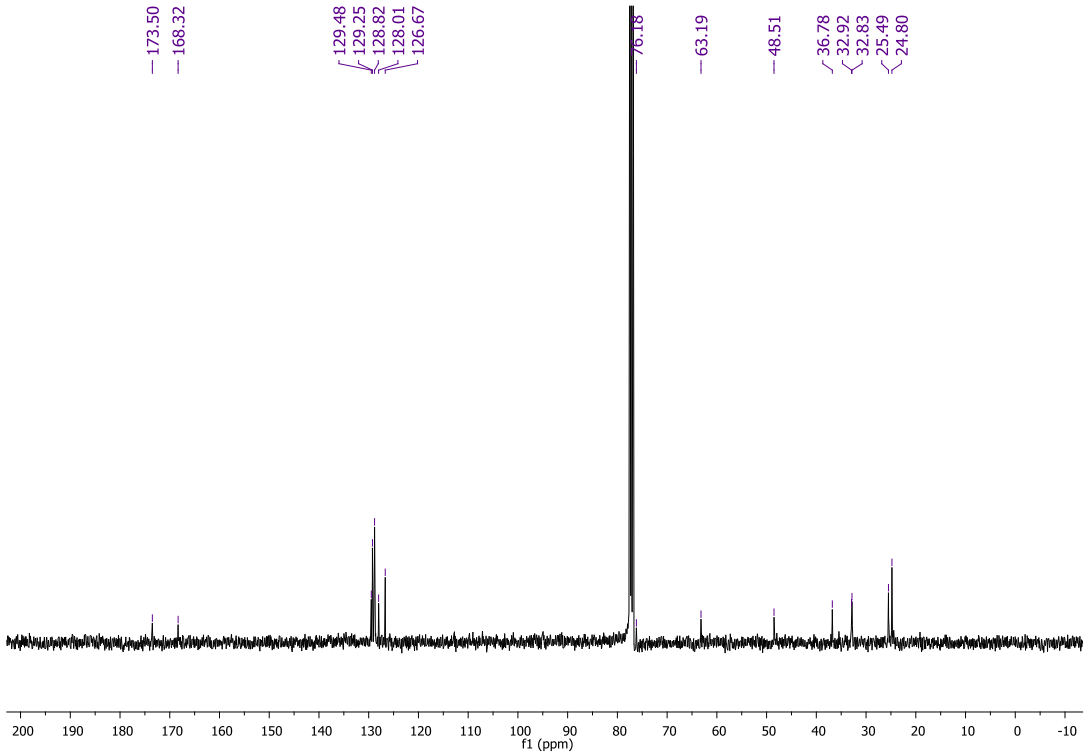

^{13}C NMR ($CDCl_3$, 126 MHz) of 15.

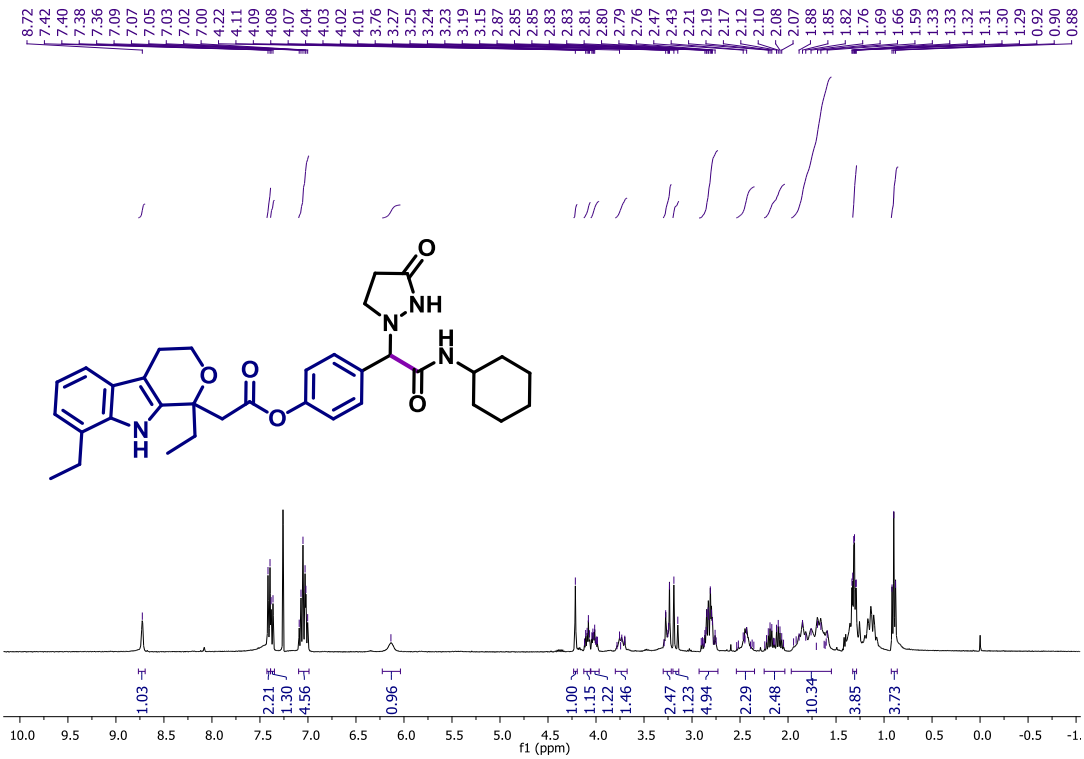

^{1}H NMR ($CDCl_3$, 400 MHz) of 16.

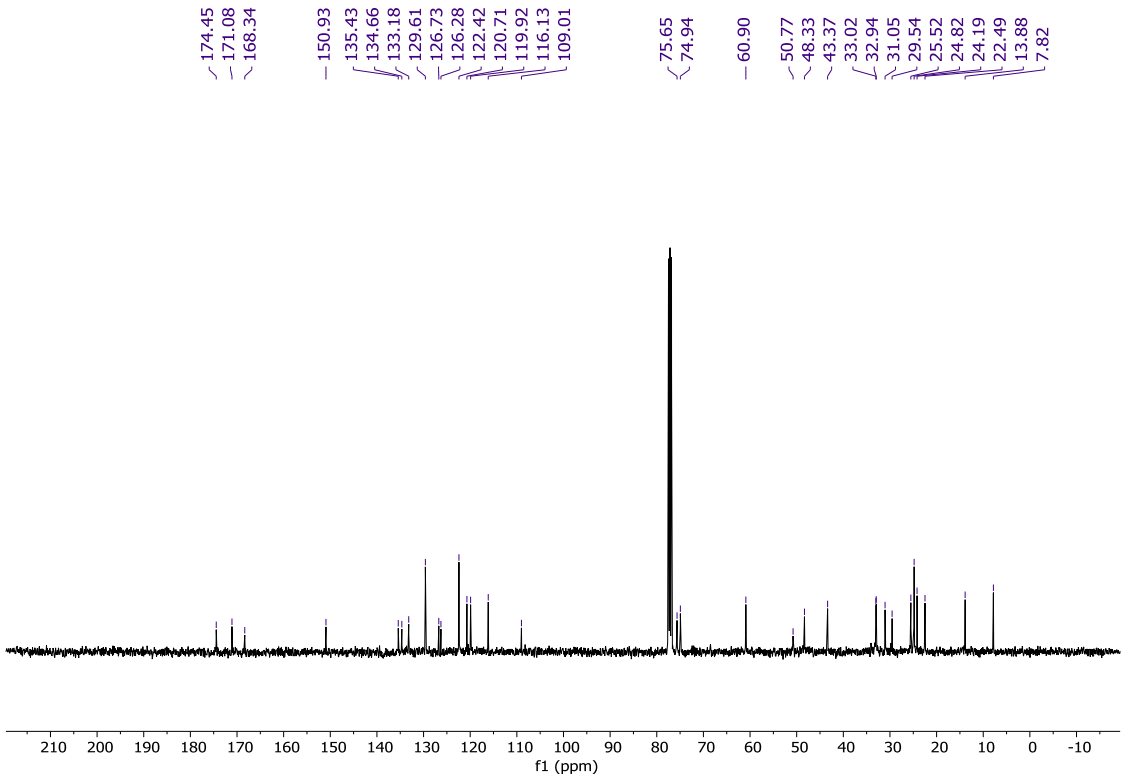

^{13}C NMR ($CDCl_3$, 126 MHz) of 16.

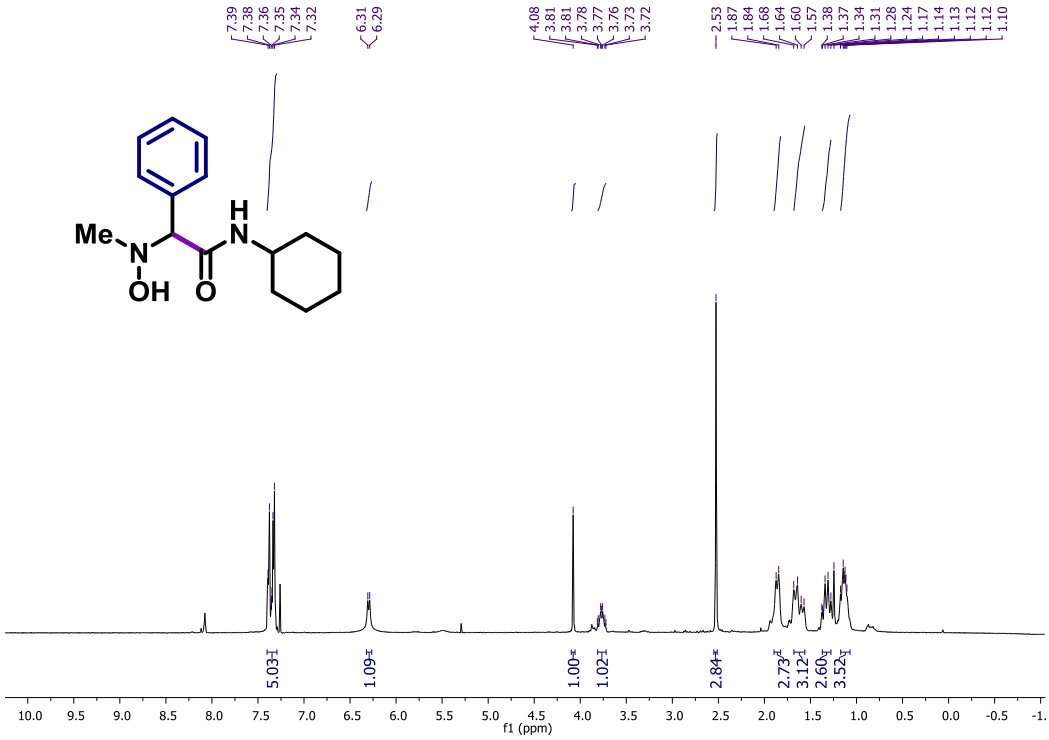

^{1}H NMR ($CDCl_3$, 400 MHz) of 17.

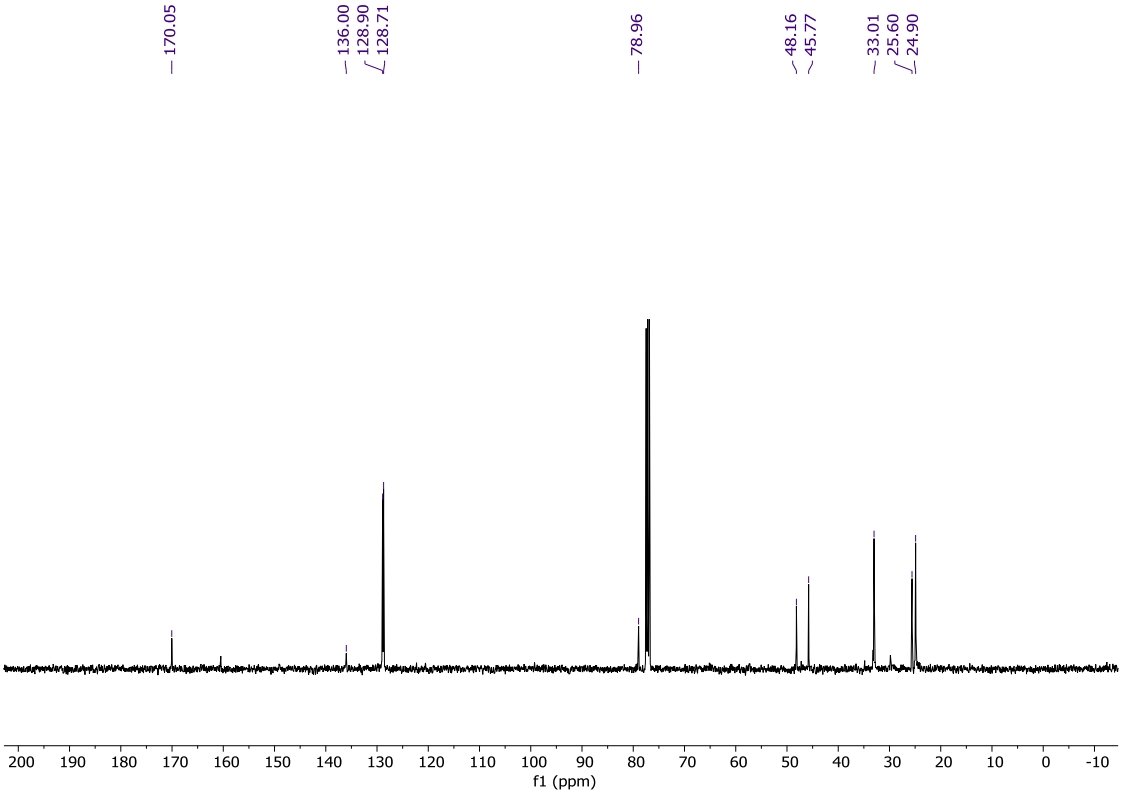

^{13}C NMR ($CDCl_3$, 126 MHz) of 17.

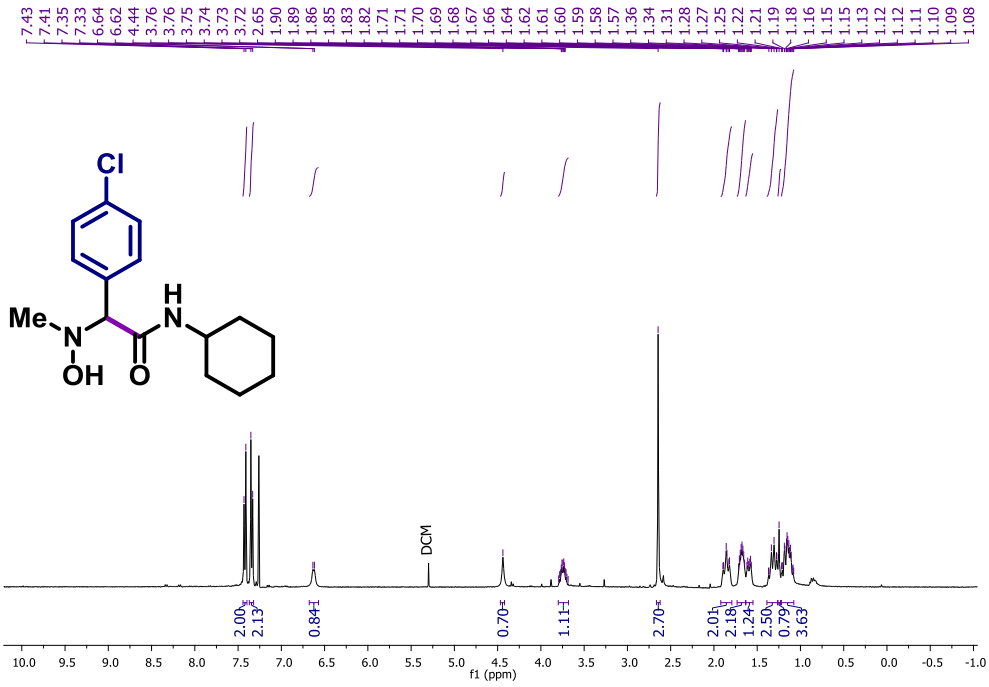

^{1}H NMR ($CDCl_3$, 400 MHz) of 18.

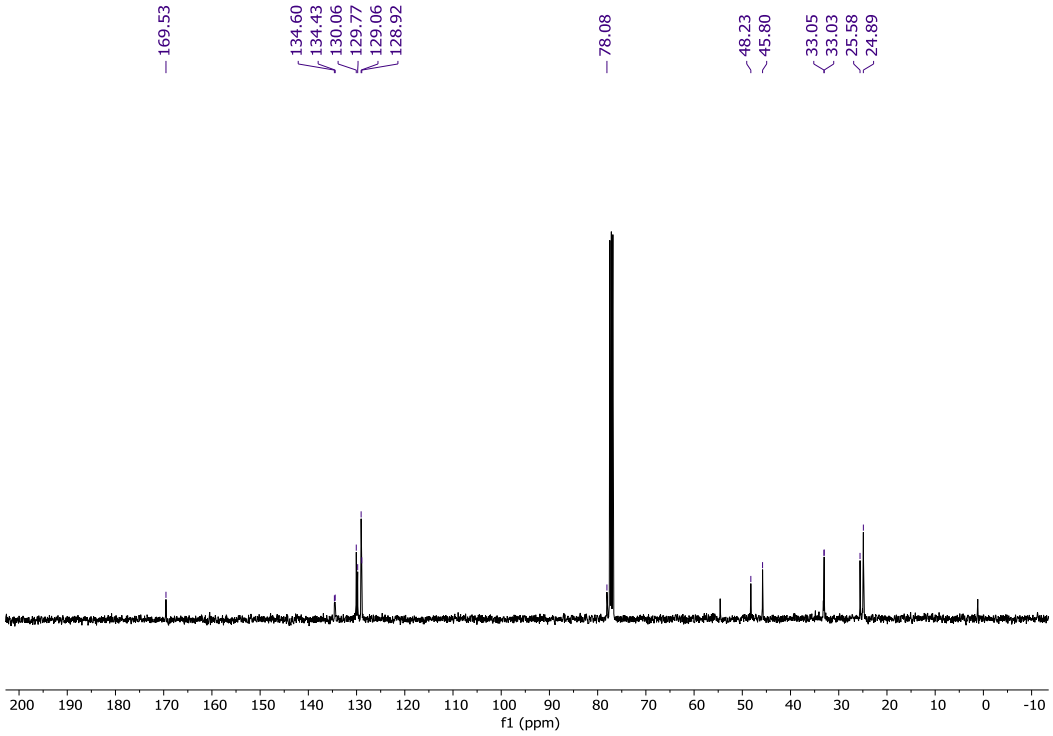

^{13}C NMR ($CDCl_3$, 126 MHz) of 18.

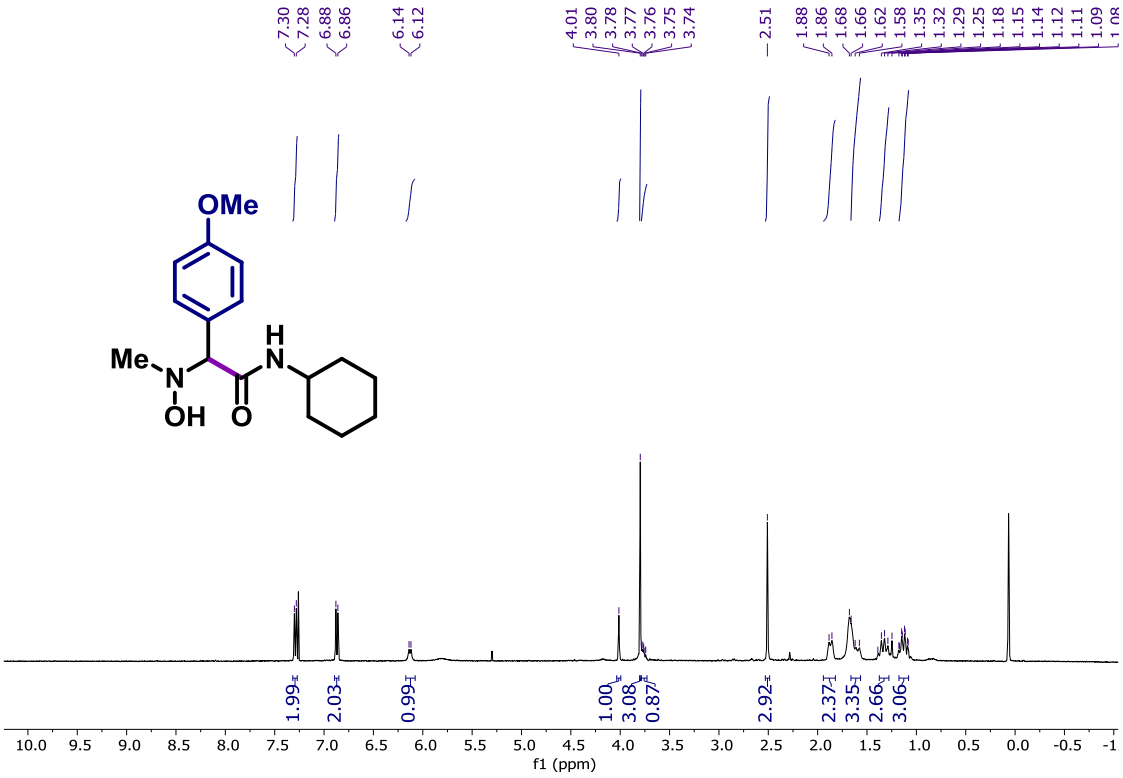

^{1}H NMR ($CDCl_3$, 400 MHz) of 19.

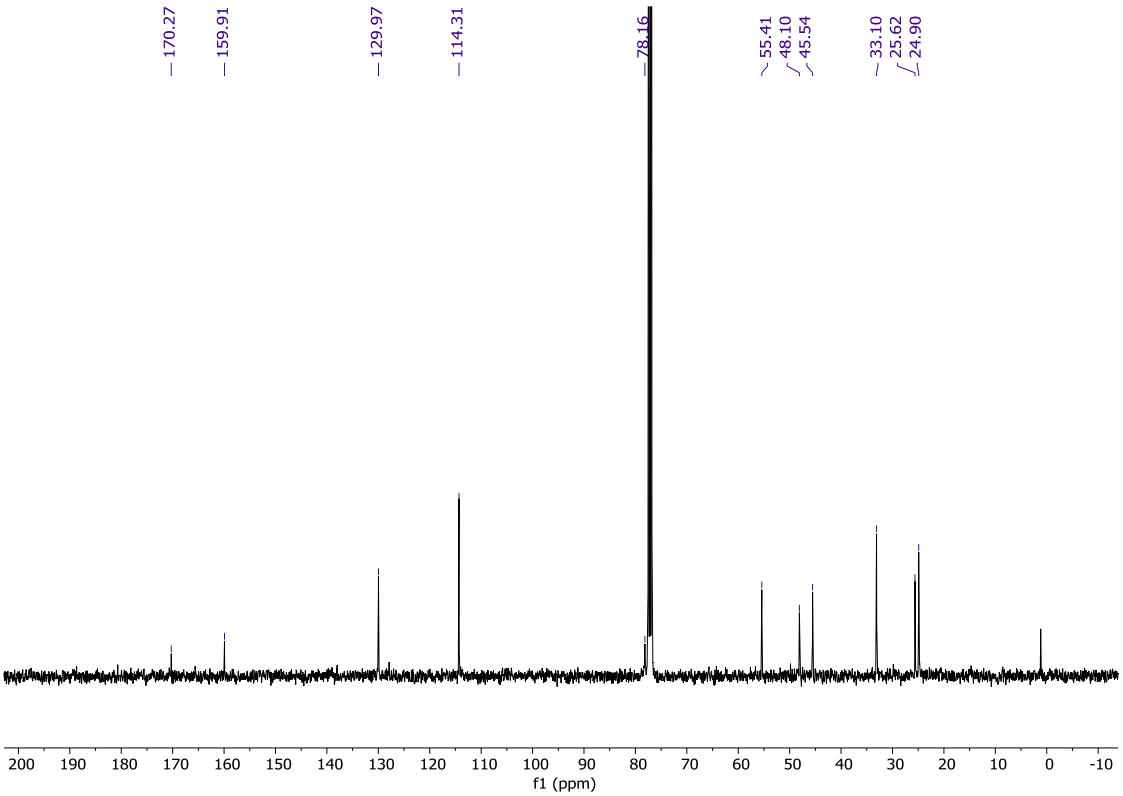

^{13}C NMR ($CDCl_3$, 126 MHz) of 19.

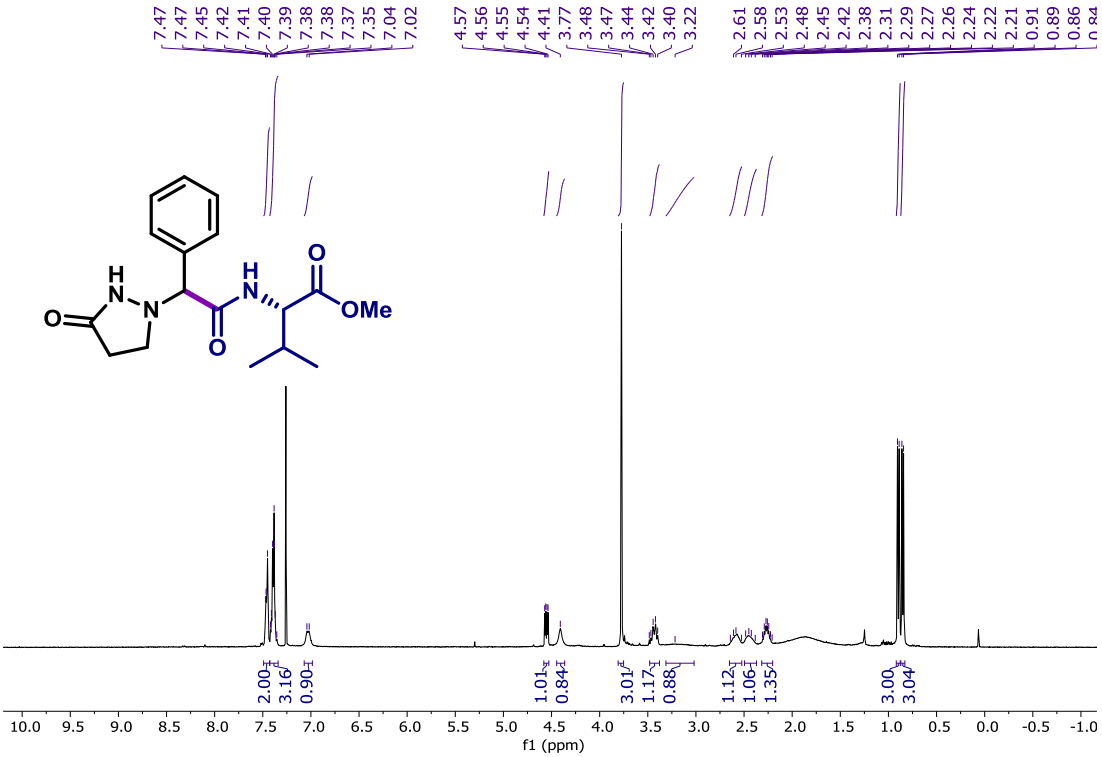

^{1}H NMR ($CDCl_3$, 400 MHz) of 20.

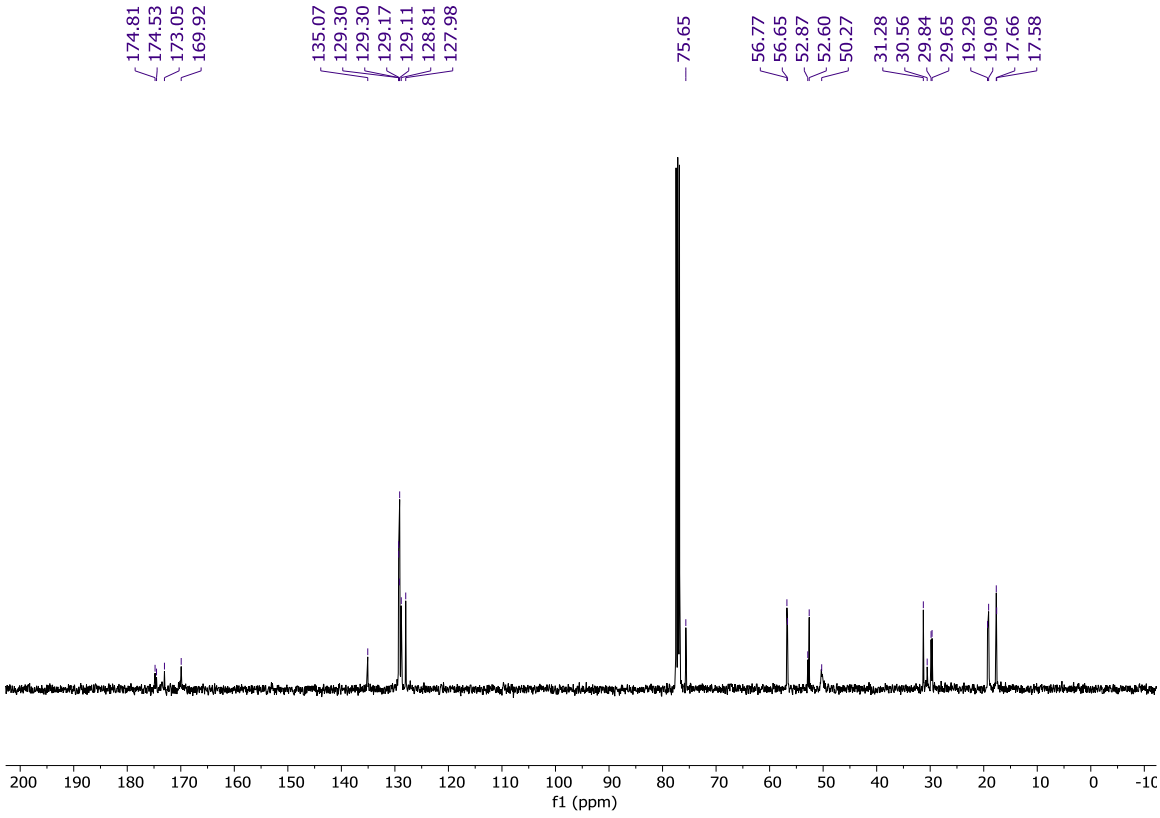

^{13}C NMR ($CDCl_3$, 126 MHz) of 20.

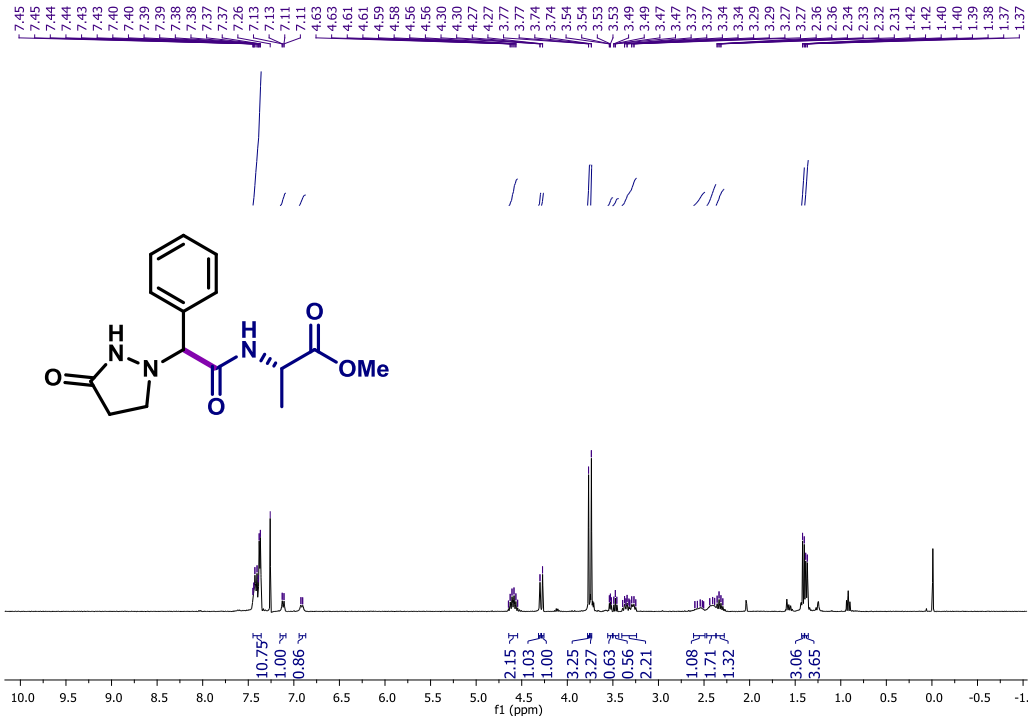

^{1}H NMR ($CDCl_3$, 400 MHz) of 21.

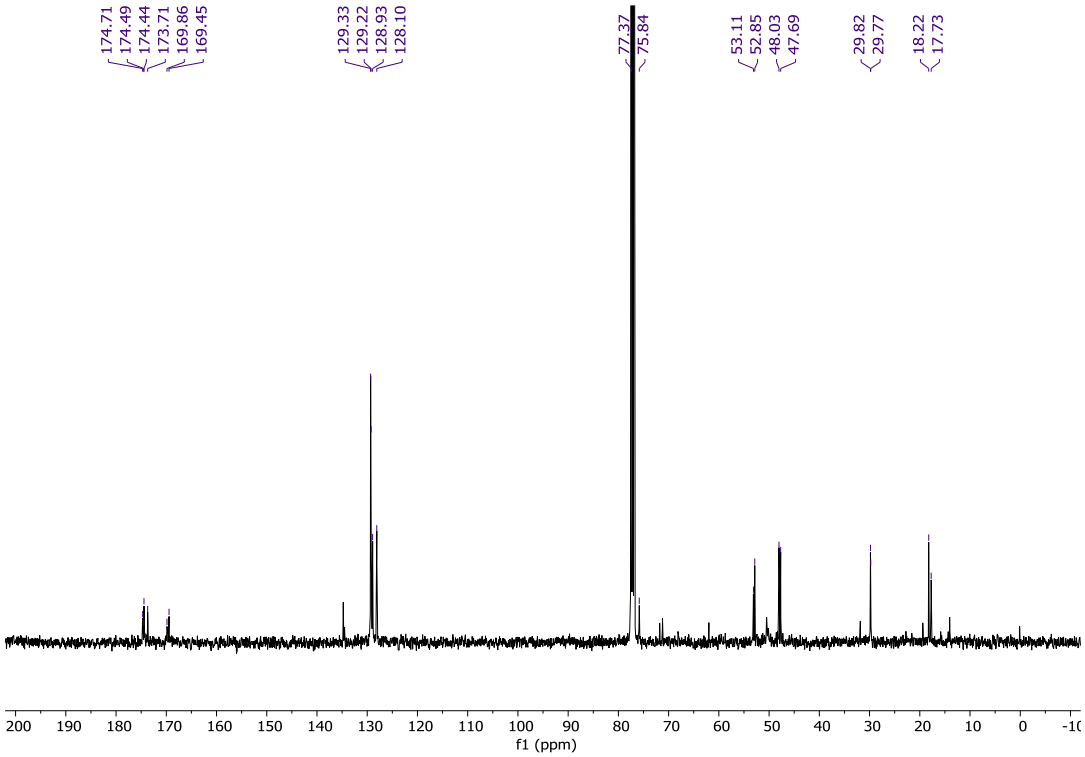

^{13}C NMR ($CDCl_3$, 126 MHz) of 21.

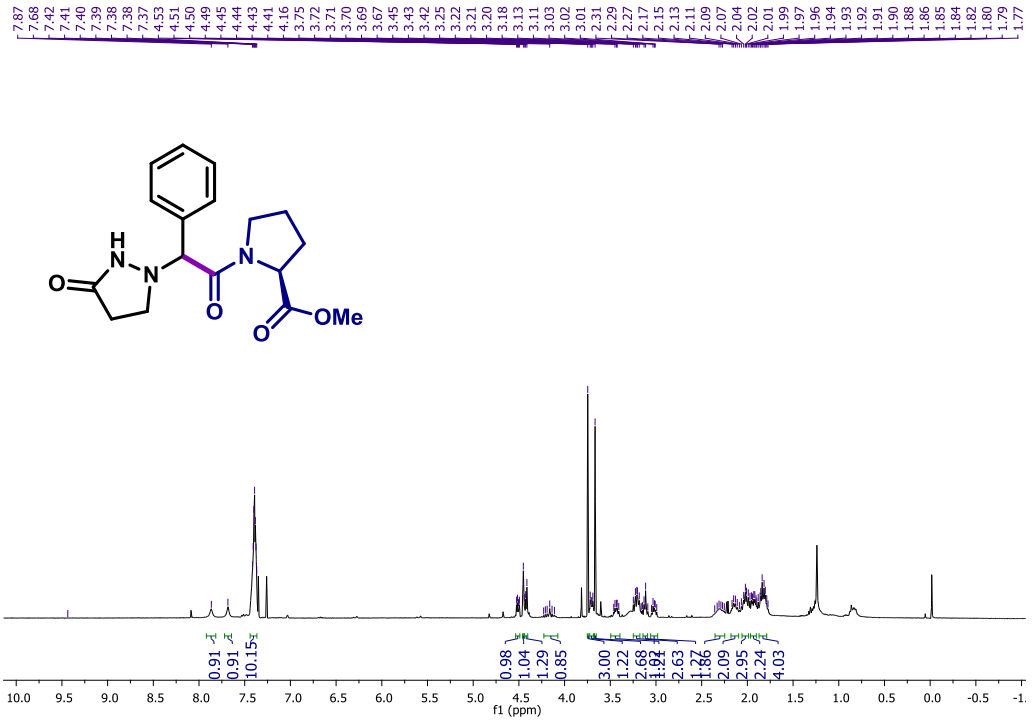

^{1}H NMR ($CDCl_3$, 400 MHz) of 22.

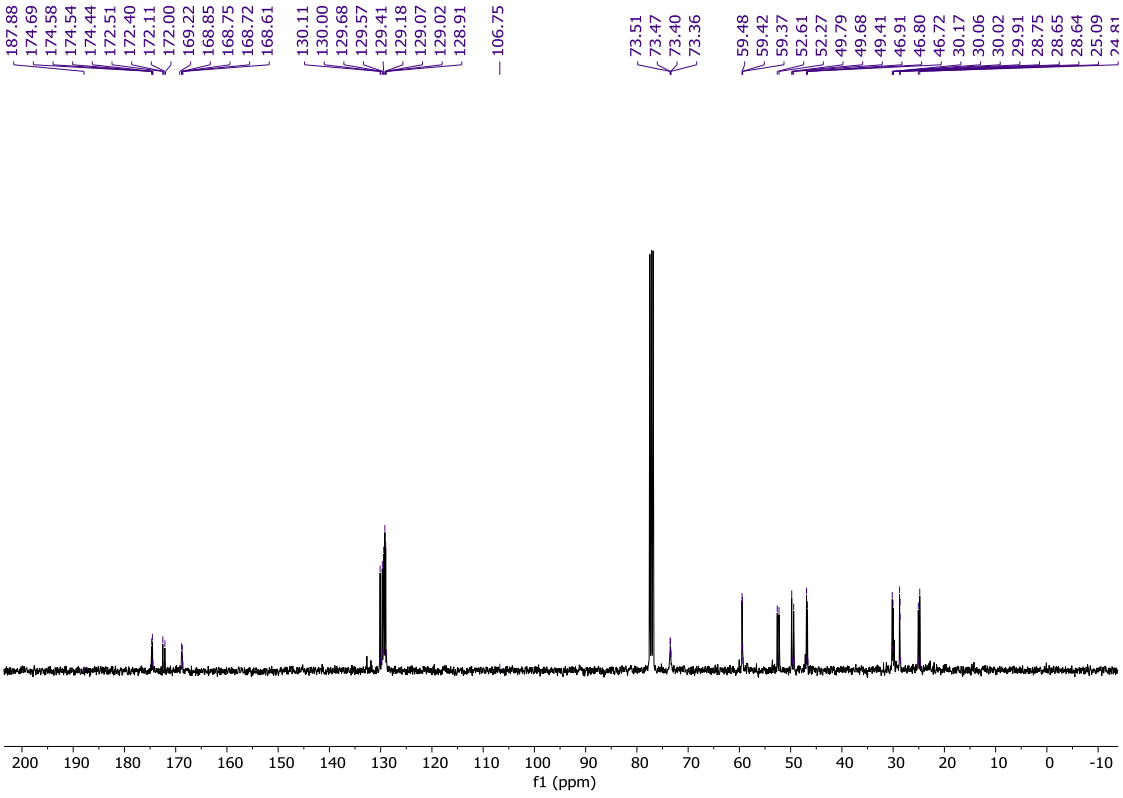

^{13}C NMR ($CDCl_3$, 126 MHz) of 22.

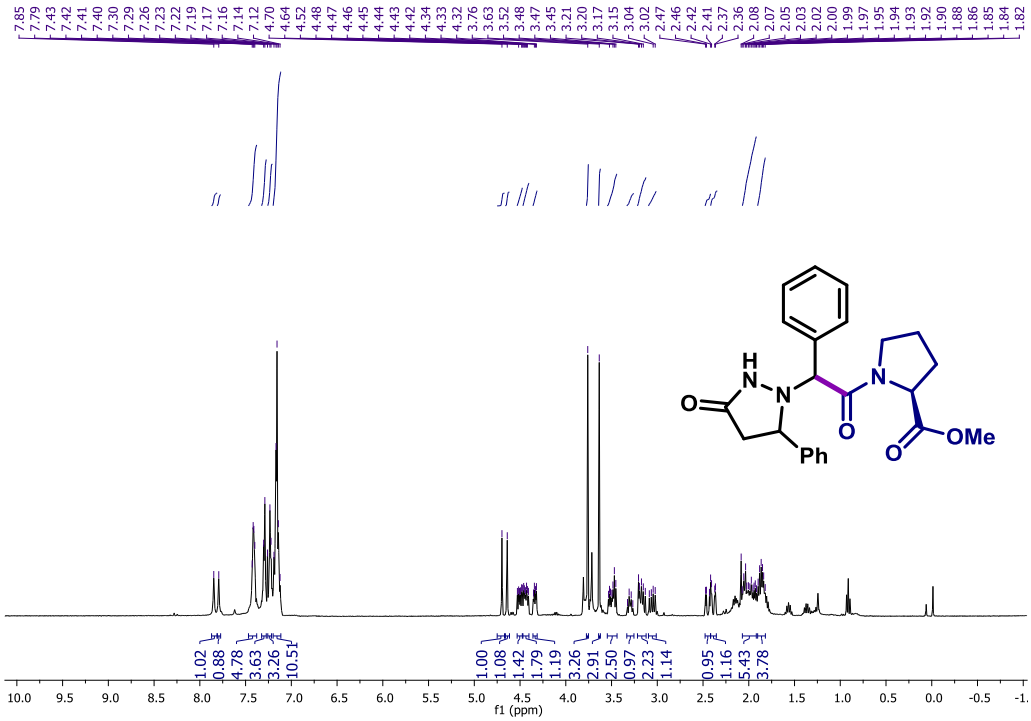

^{1}H NMR ($CDCl_3$, 400 MHz) of 23.

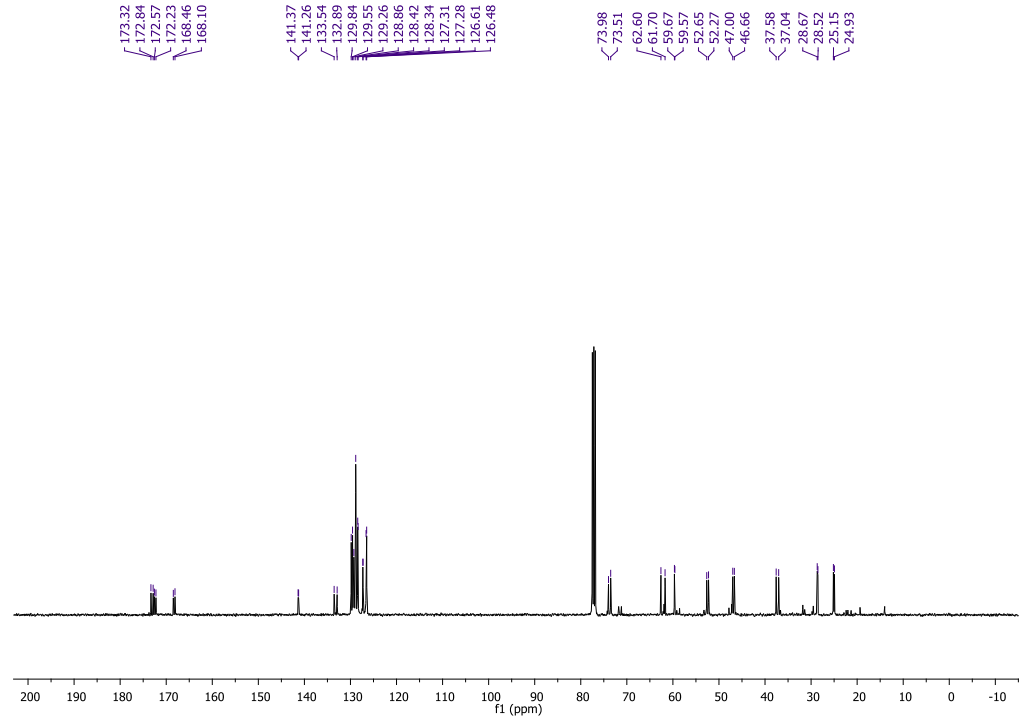

^{13}C NMR ($CDCl_3$, 126 MHz) of 23.

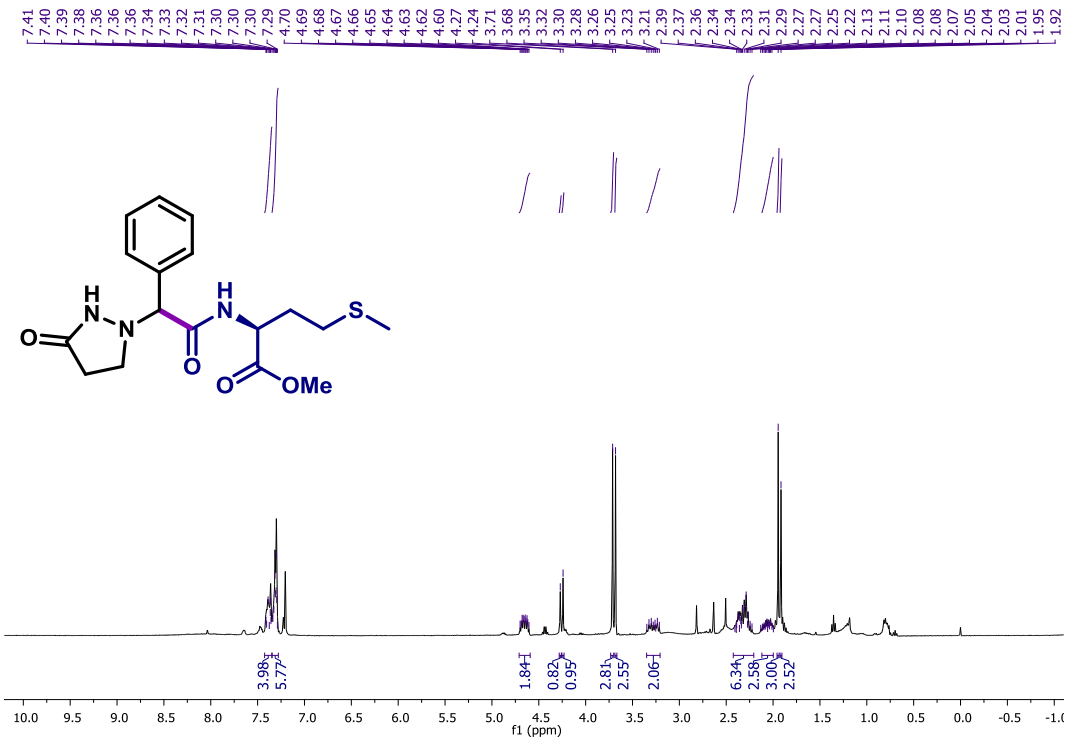

^{1}H NMR ($CDCl_3$, 400 MHz) of 24.

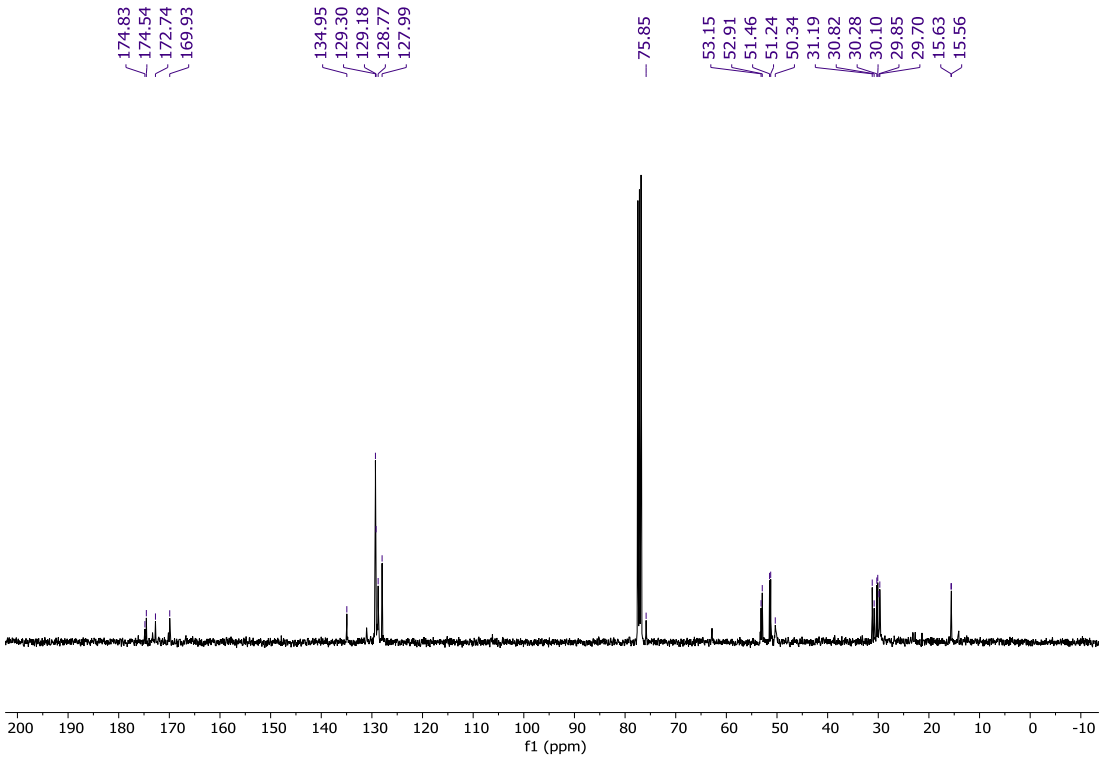

^{13}C NMR ($CDCl_3$, 126 MHz) of 24.

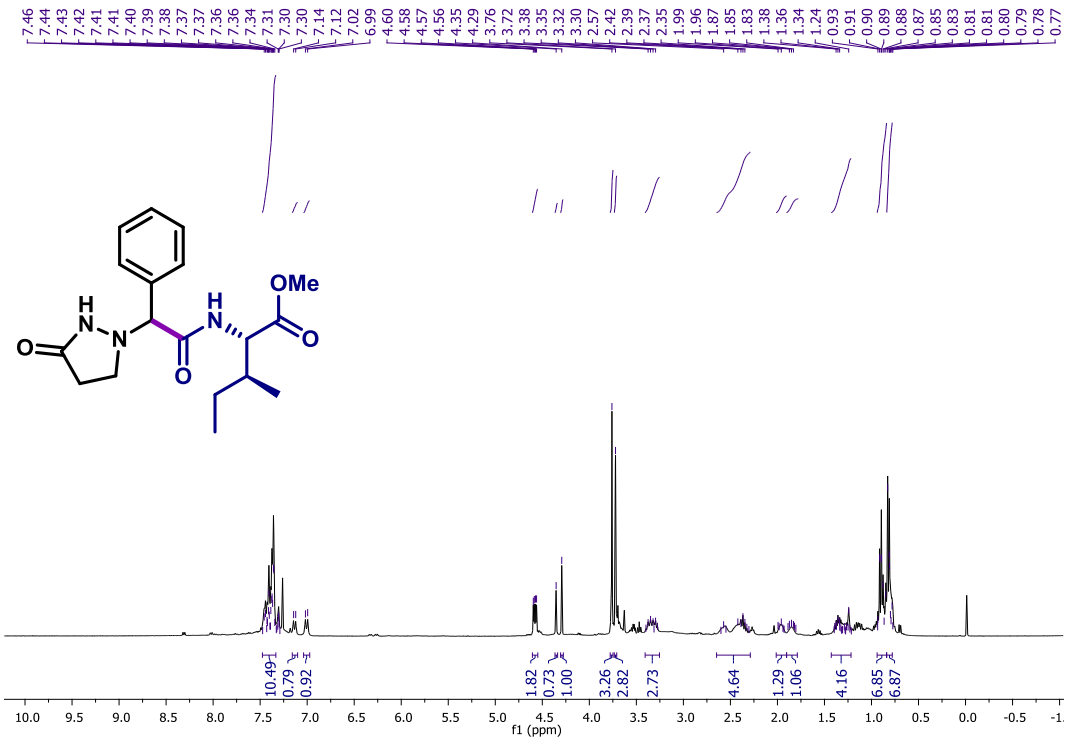

^{1}H NMR ($CDCl_3$, 400 MHz) of 25.

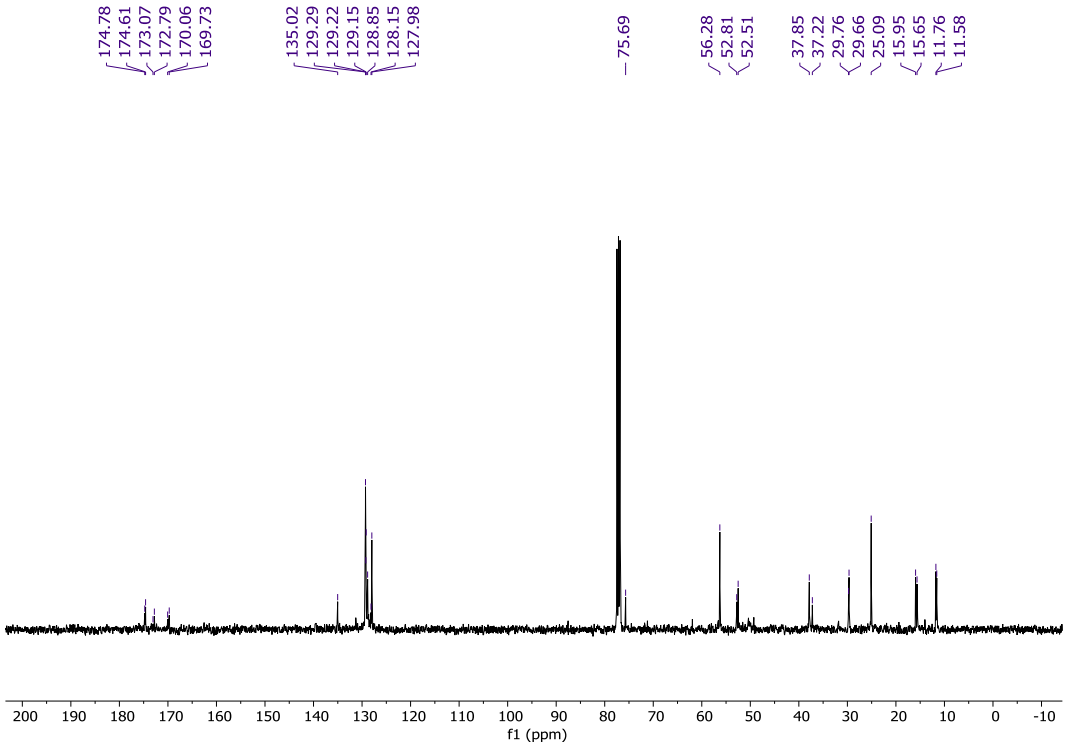

^{13}C NMR ($CDCl_3$, 126 MHz) of 25.

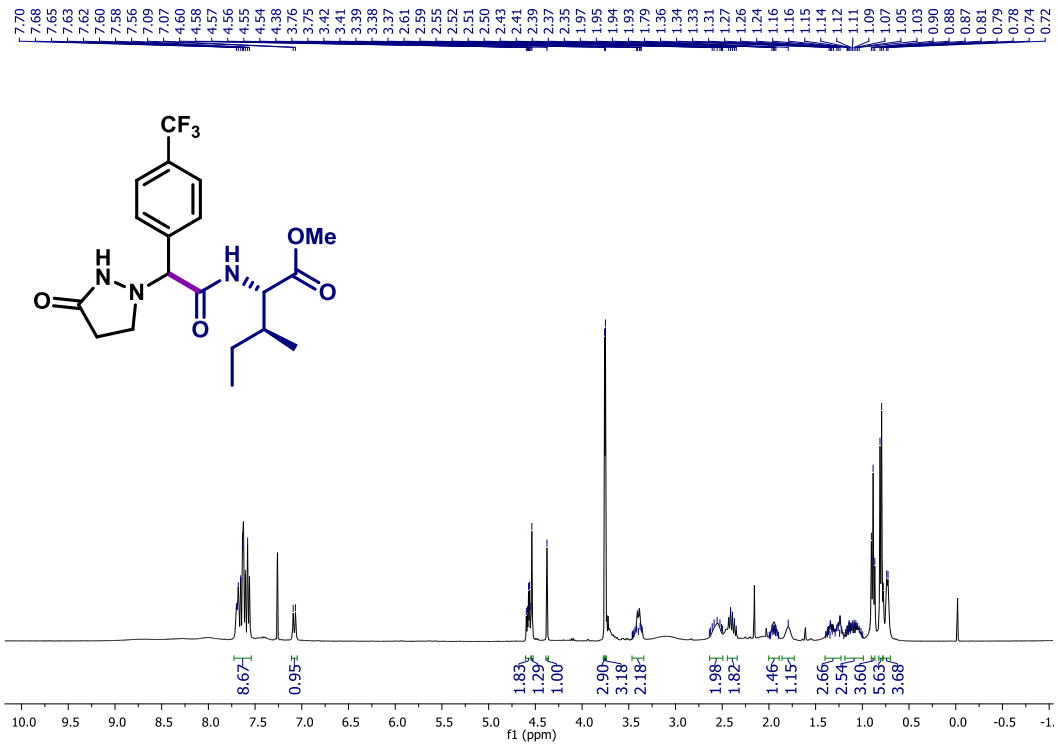

^{1}H NMR ($CDCl_3$, 400 MHz) of 26.

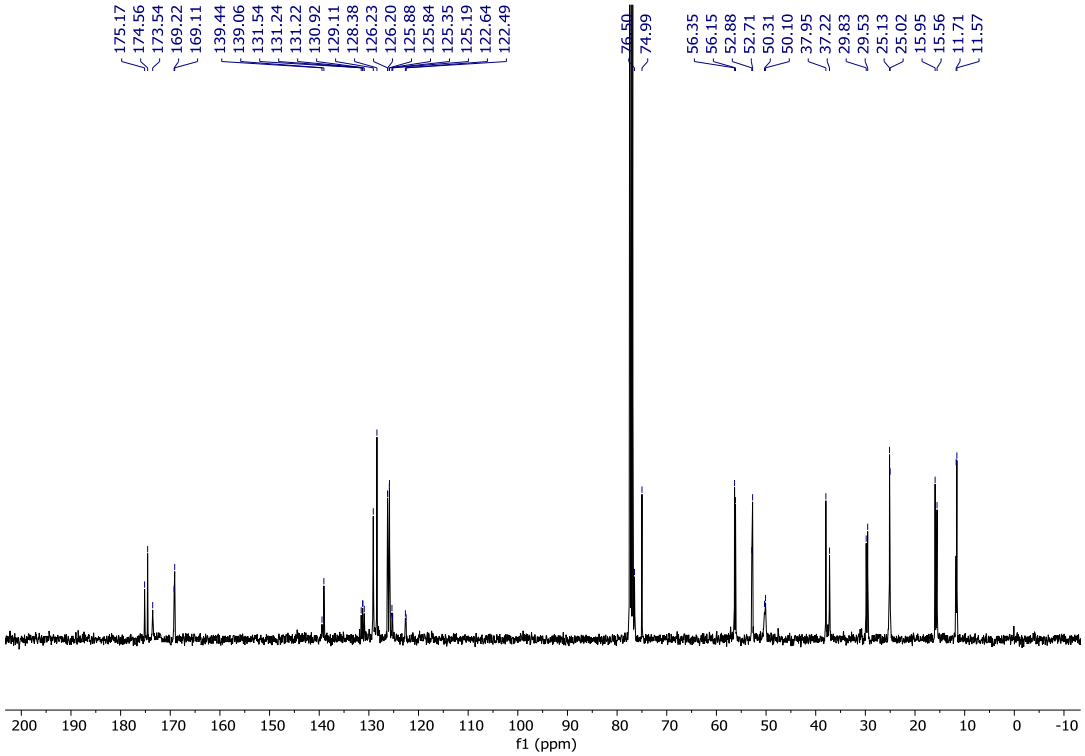

^{13}C NMR ($CDCl_3$, 126 MHz) of 26.

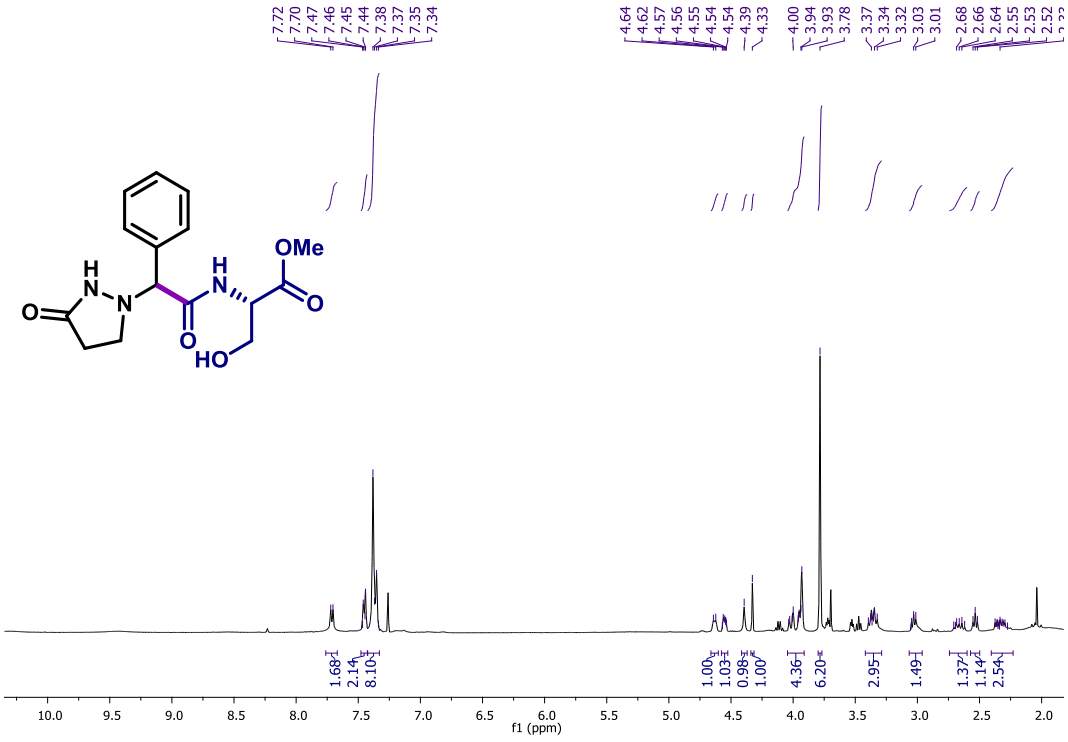

^{1}H NMR ($CDCl_3$, 400 MHz) of 27.

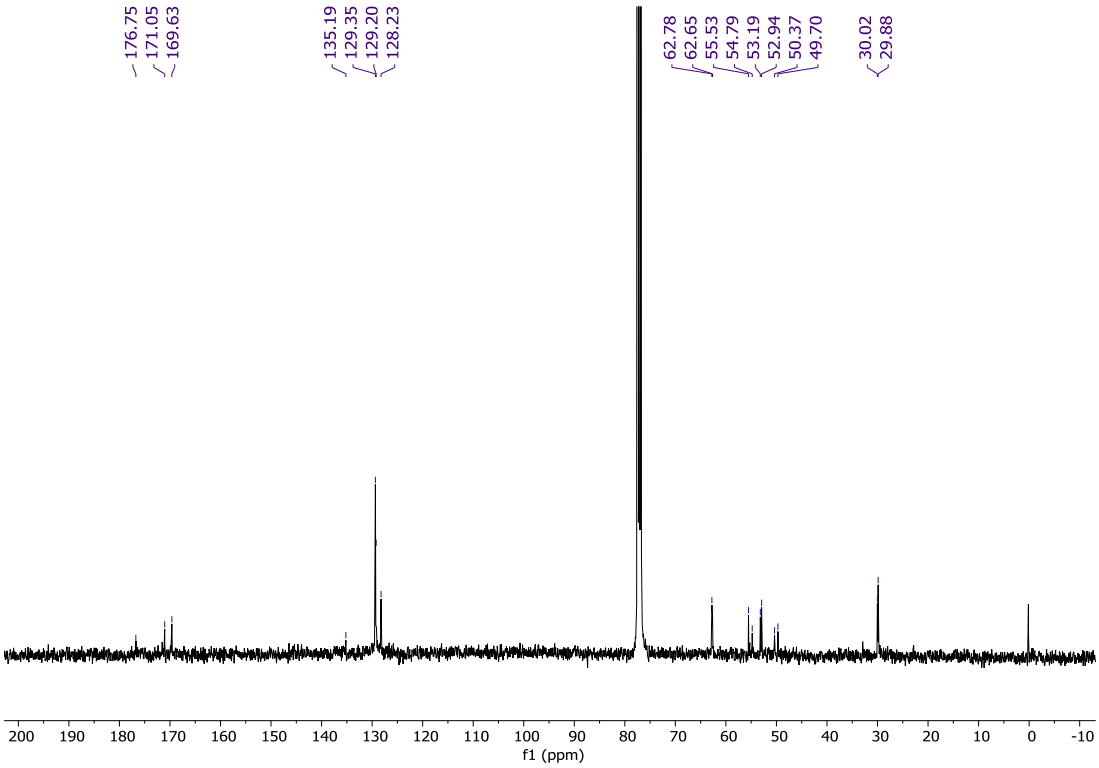

^{13}C NMR ($CDCl_3$, 126 MHz) of 27.

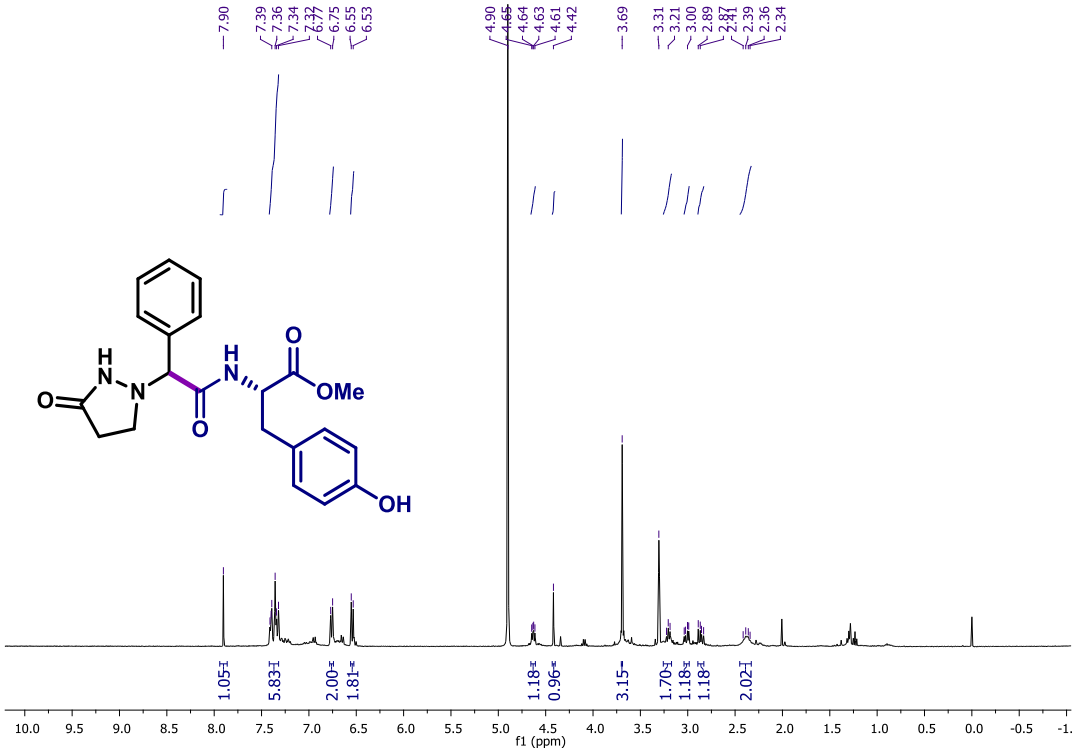

^{1}H NMR (CD_3OD, 400 MHz) of 28.

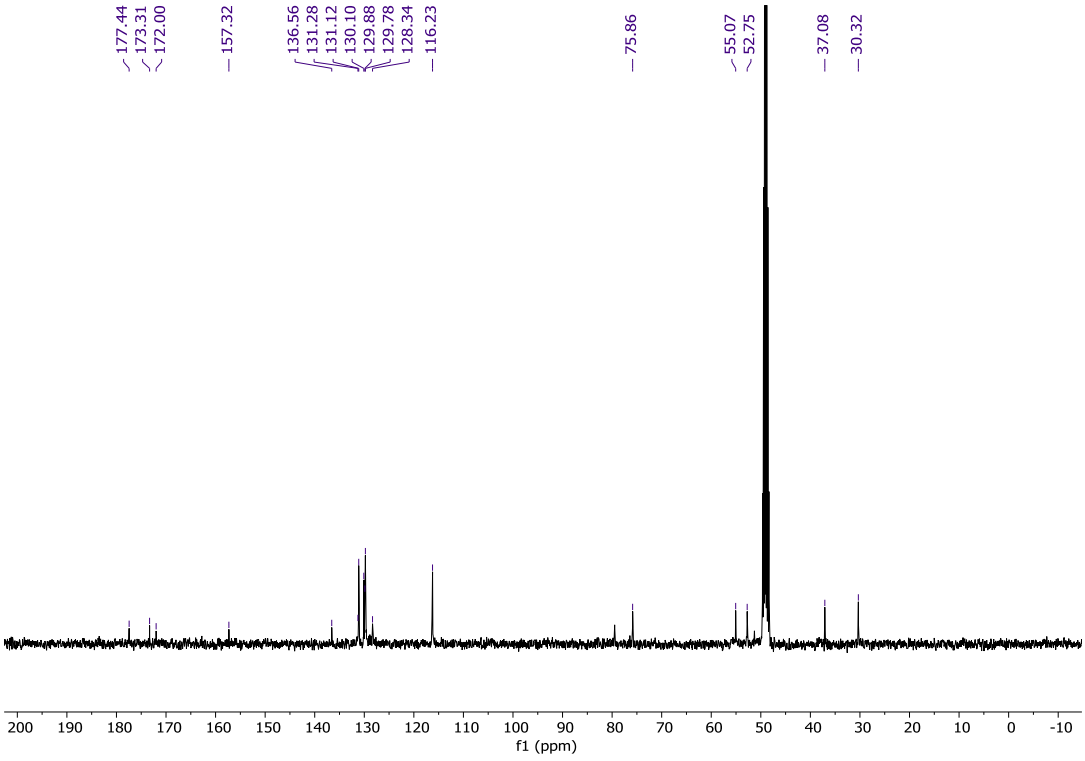

^{13}C NMR (CD_3OD, 126 MHz) of 28.

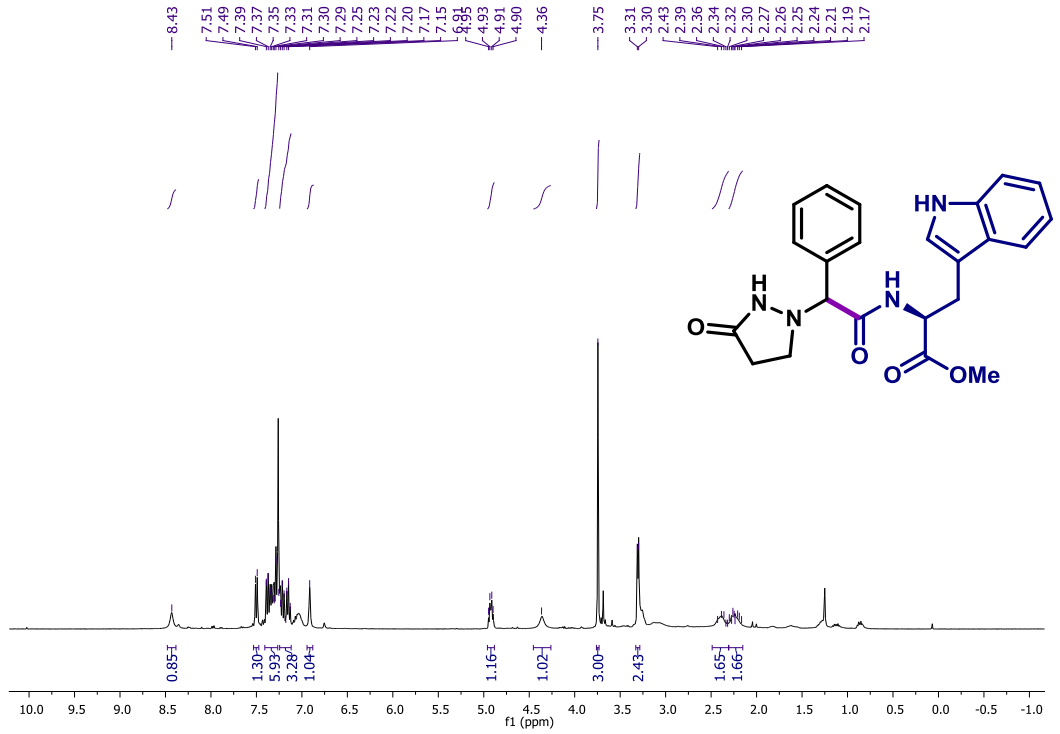

^{1}H NMR ($CDCl_3$, 400 MHz) of 29.

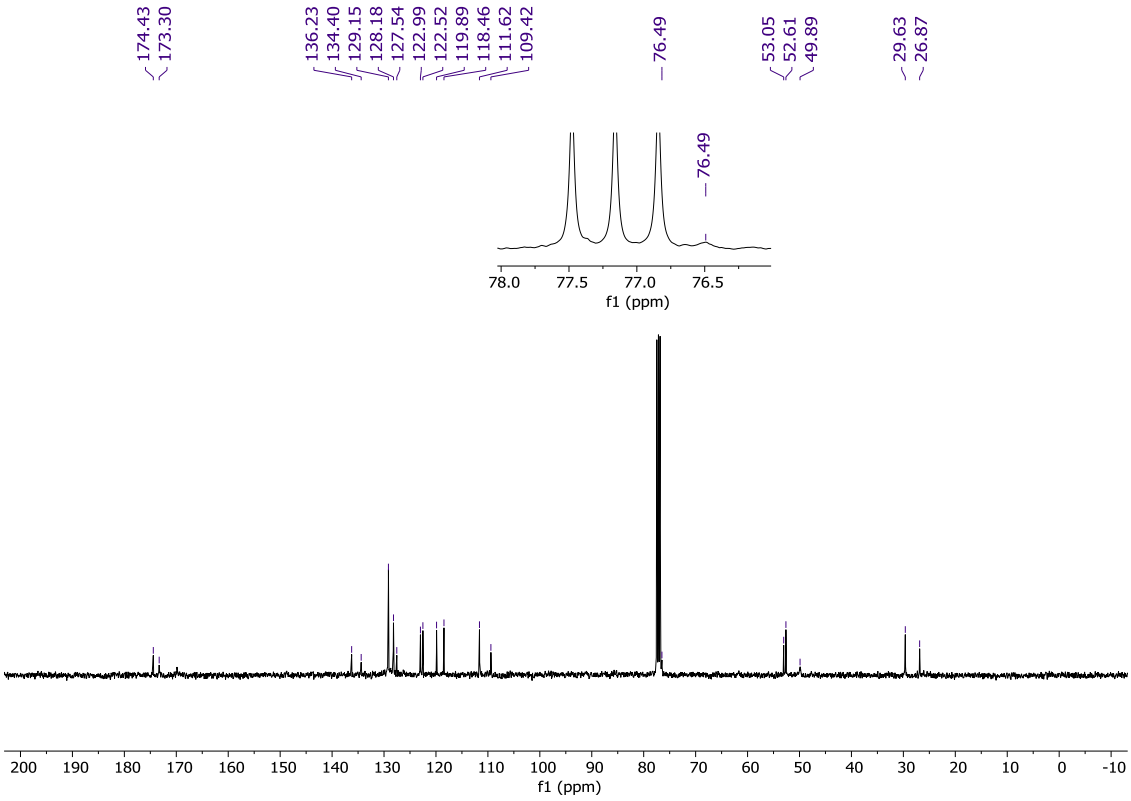

^{13}C NMR ($CDCl_3$, 126 MHz) of 29.

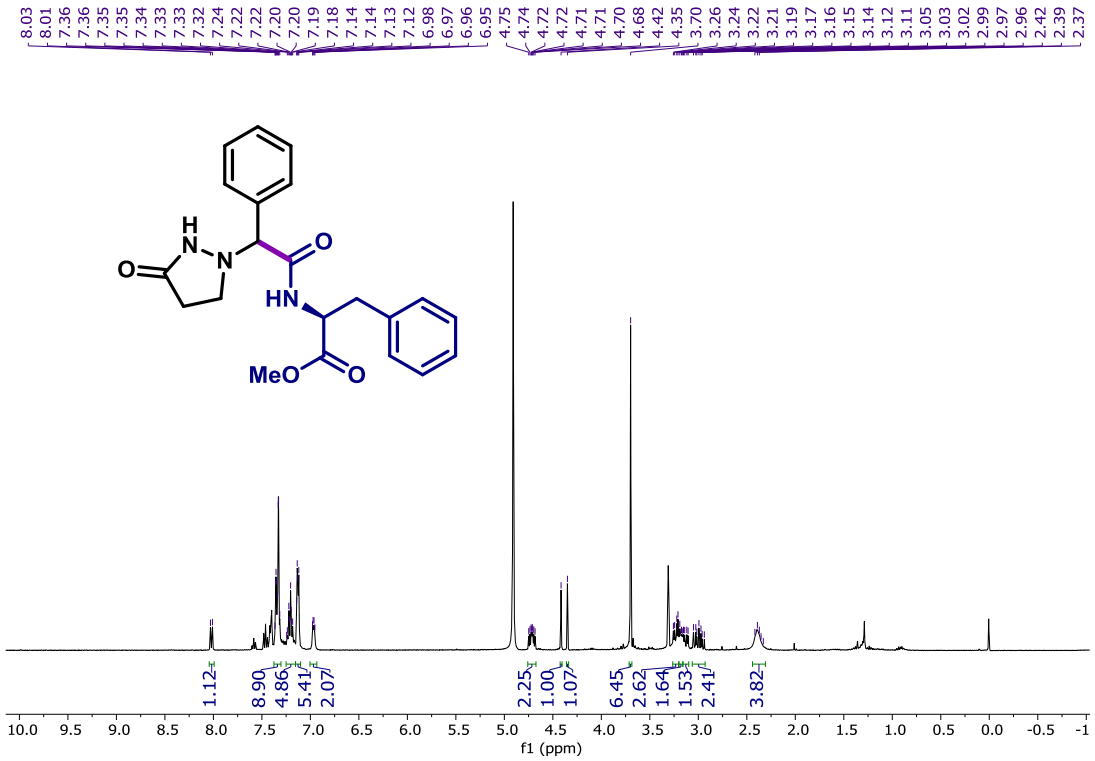

^{1}H NMR (CD_3OD, 400 MHz) of 30.

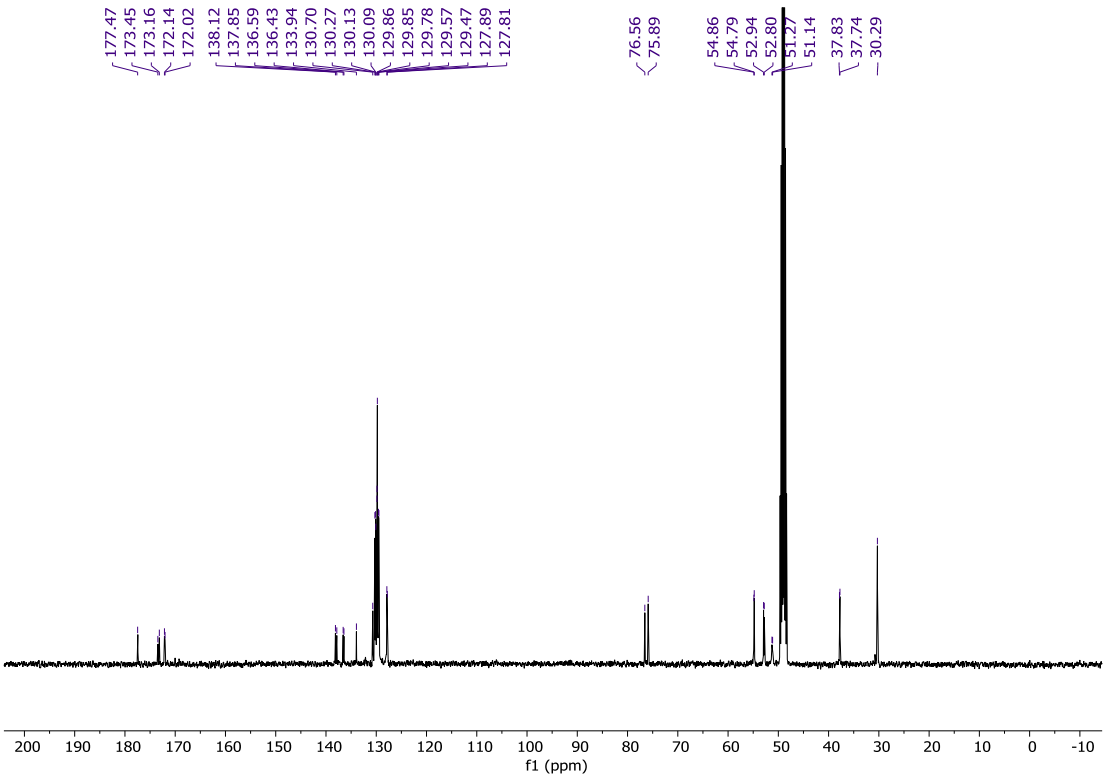

^{13}C NMR (CD_3OD, 126 MHz) of 30.

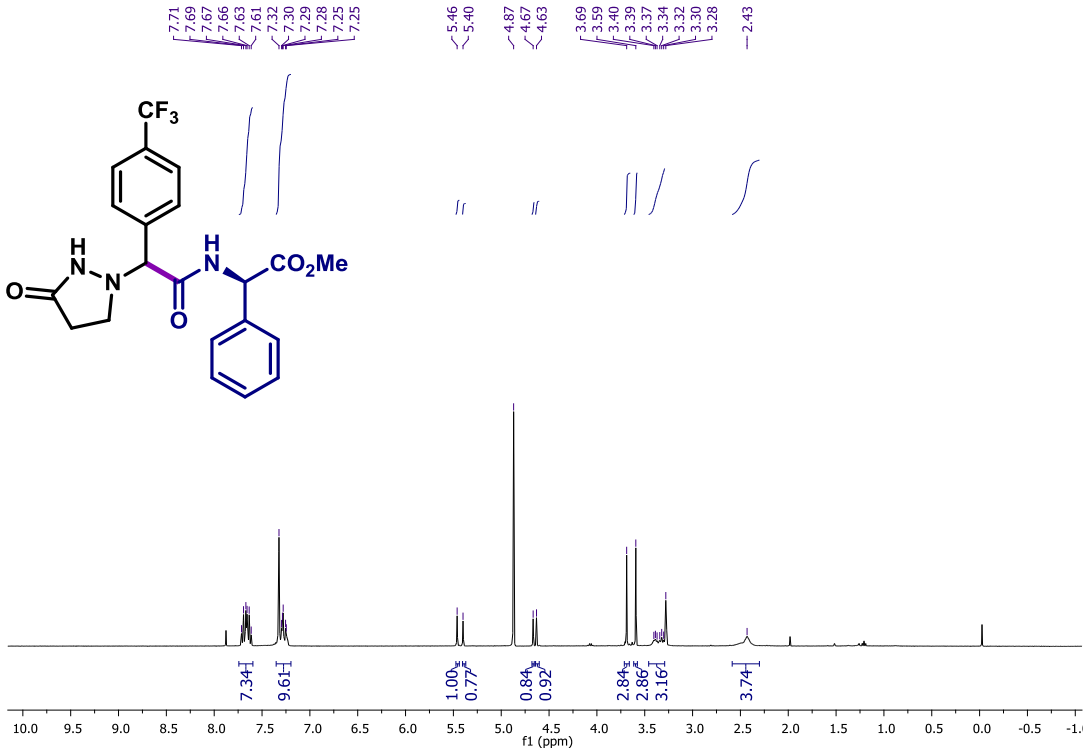

[1]H NMR (CD3OD, 400 MHz) of 31.

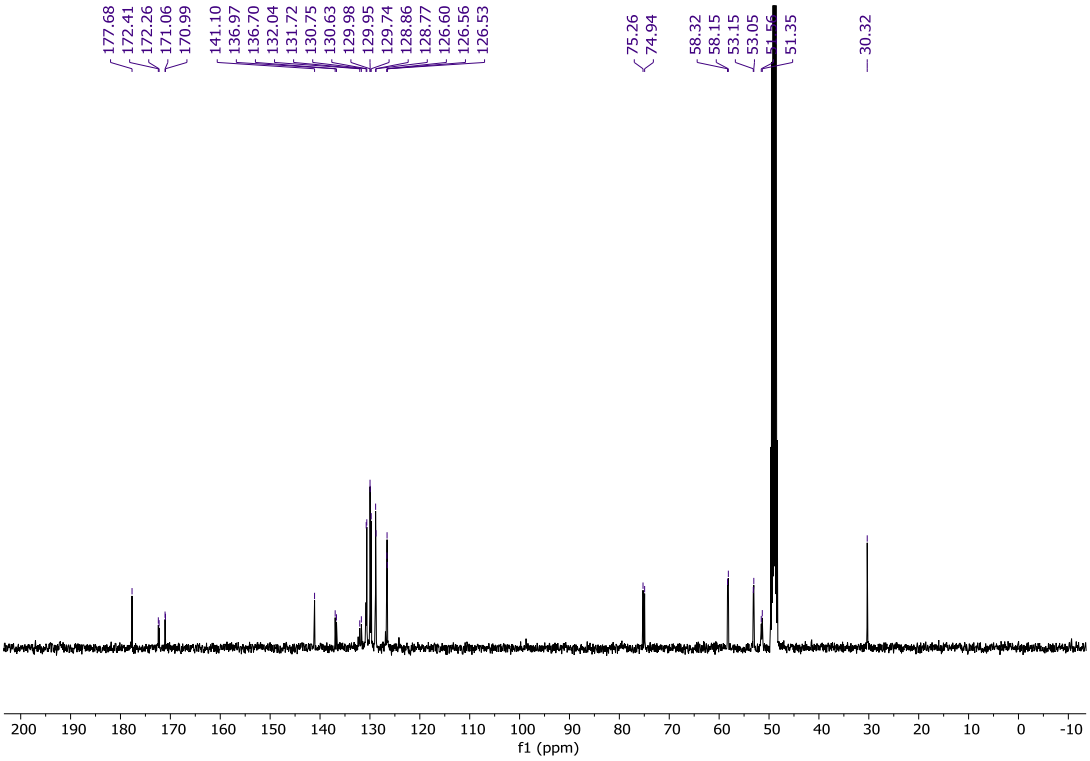

[13]C NMR (CD3OD, 126 MHz) of 31.

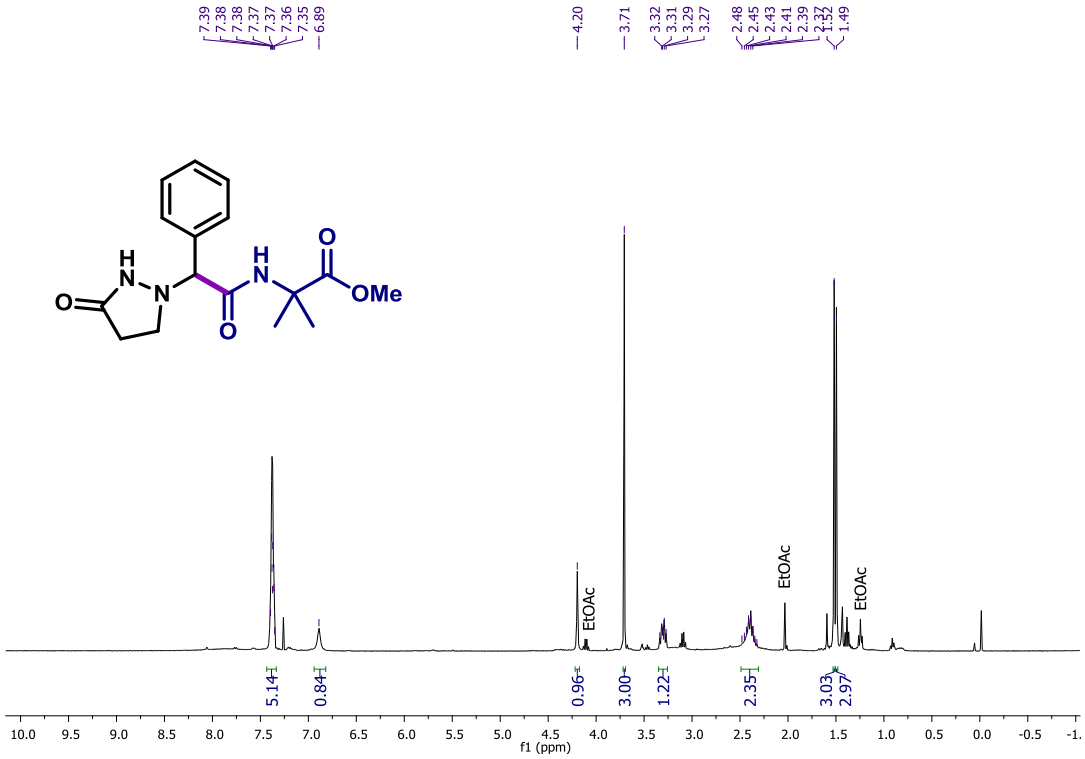

^{1}H NMR ($CDCl_3$, 400 MHz) of 32.

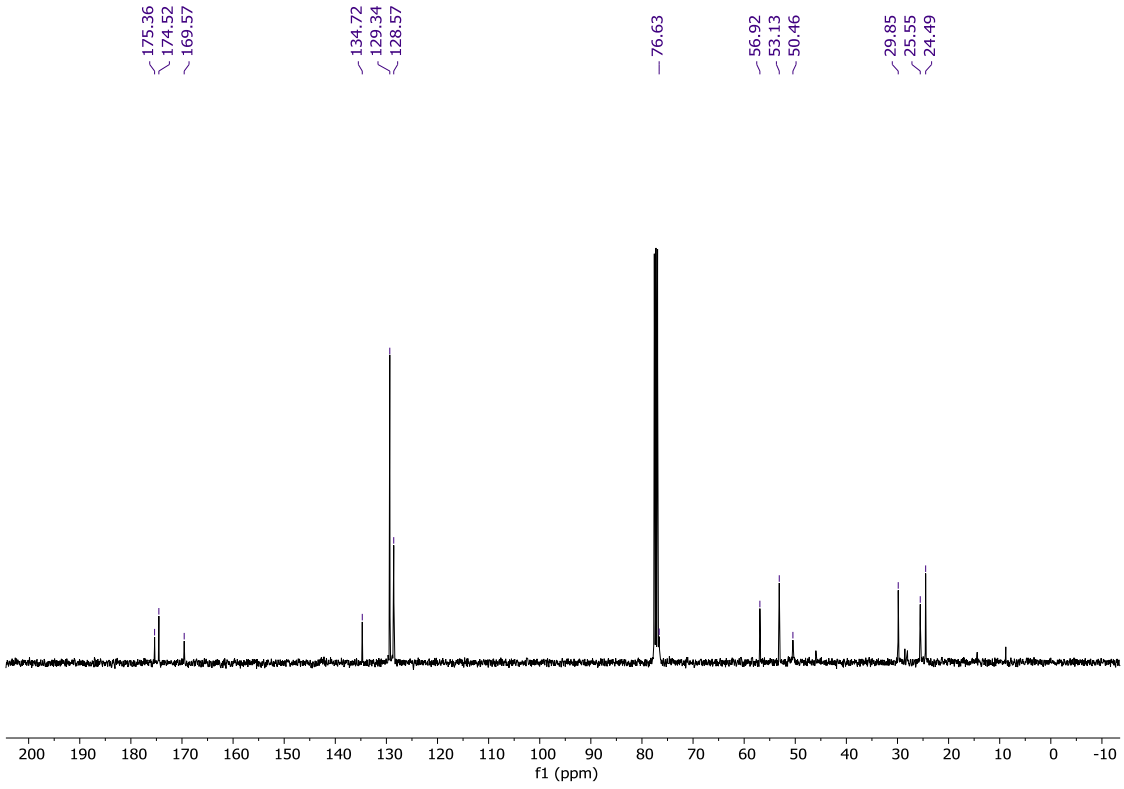

^{13}C NMR ($CDCl_3$, 126 MHz) of 32.

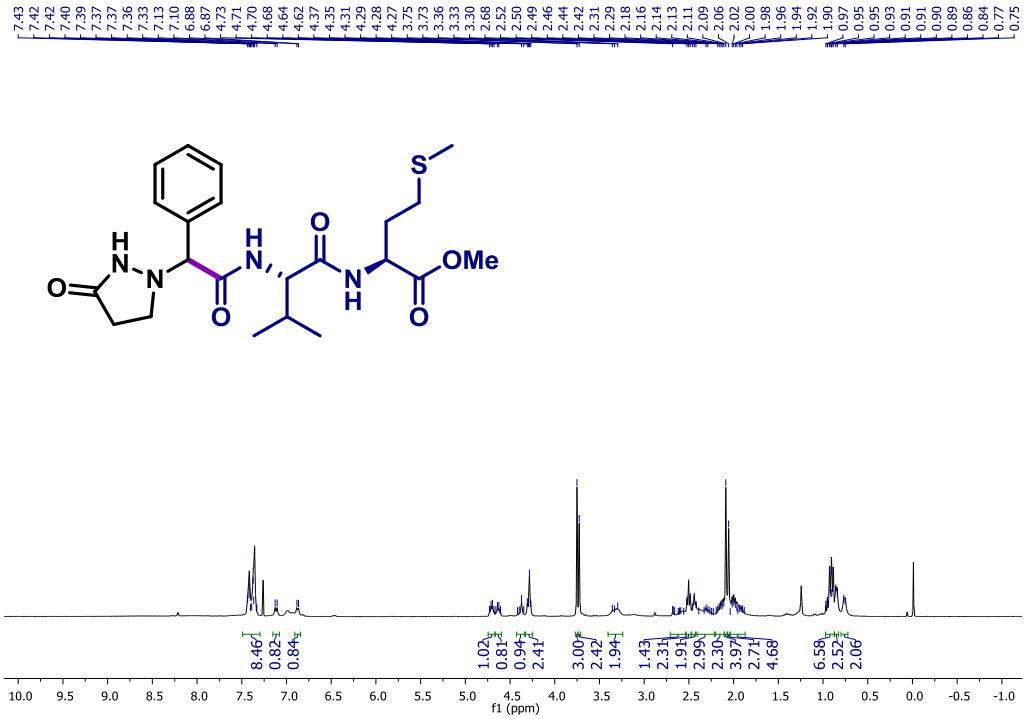

^{1}H NMR ($CDCl_3$, 400 MHz) of 33.

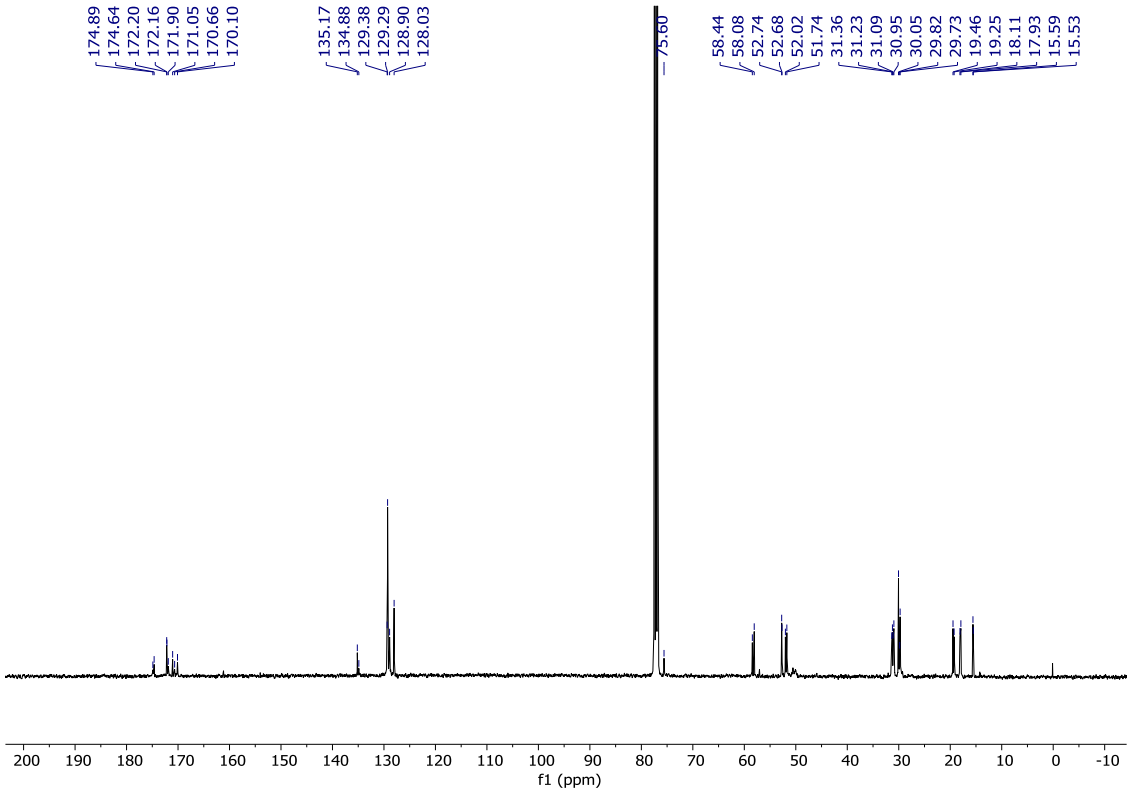

^{13}C NMR ($CDCl_3$, 126 MHz) of 33.

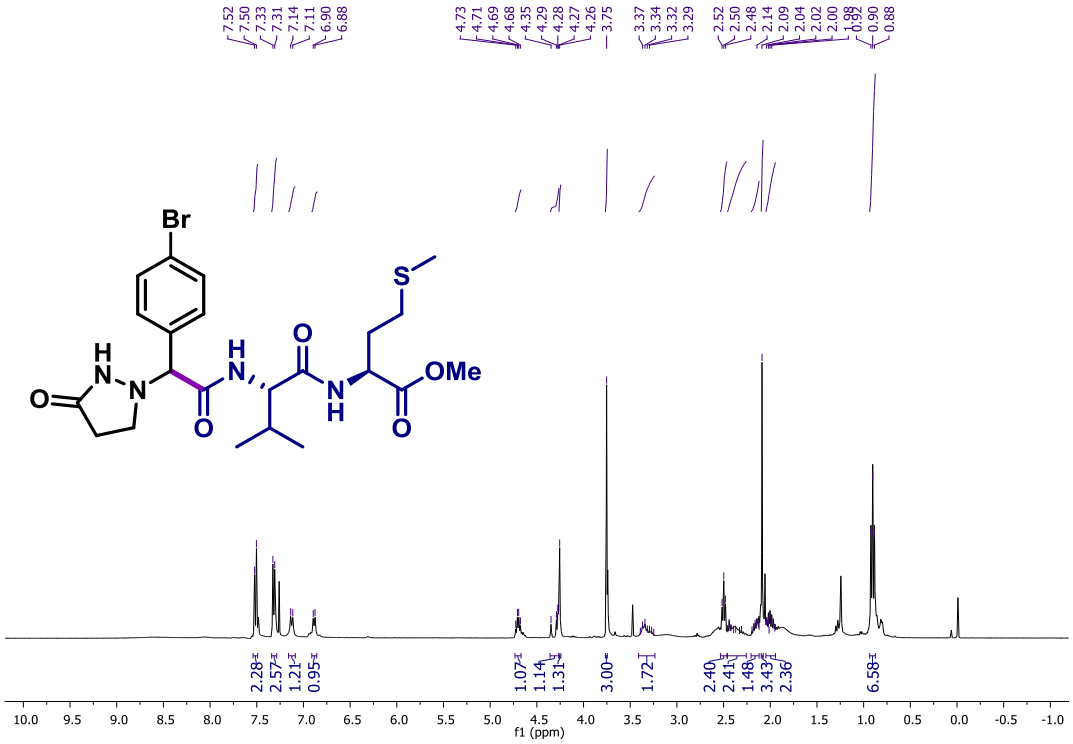

^{1}H NMR ($CDCl_3$, 400 MHz) of 34.

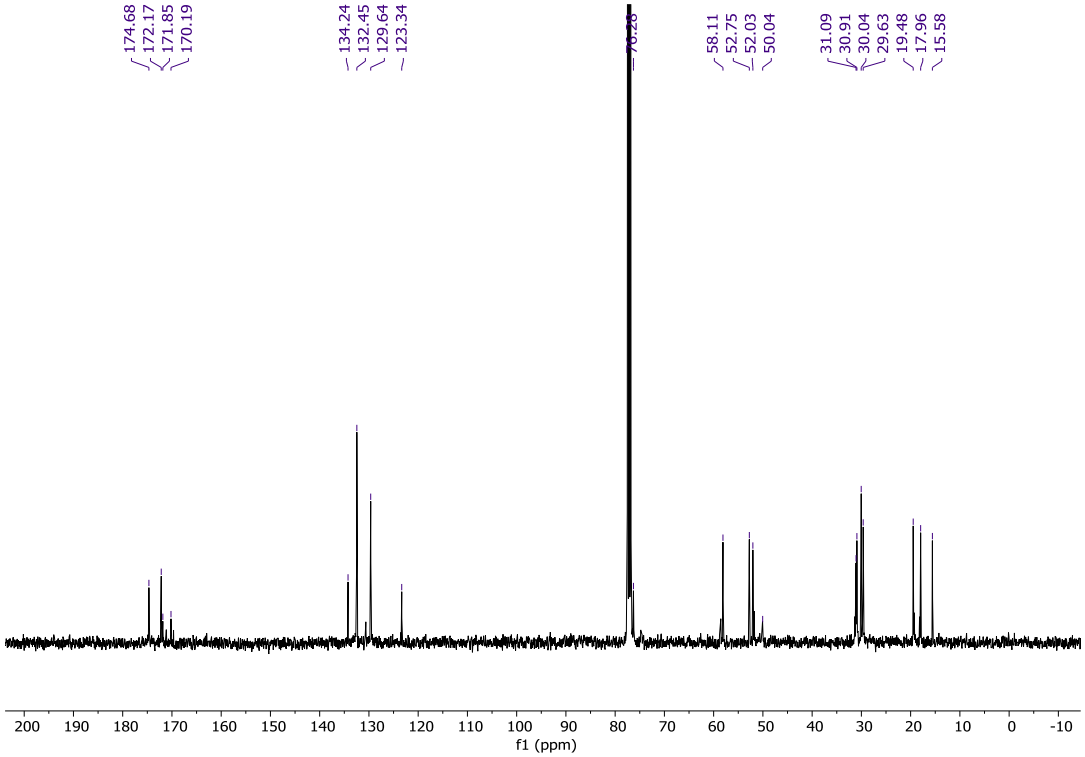

^{13}C NMR ($CDCl_3$, 126 MHz) of 34.

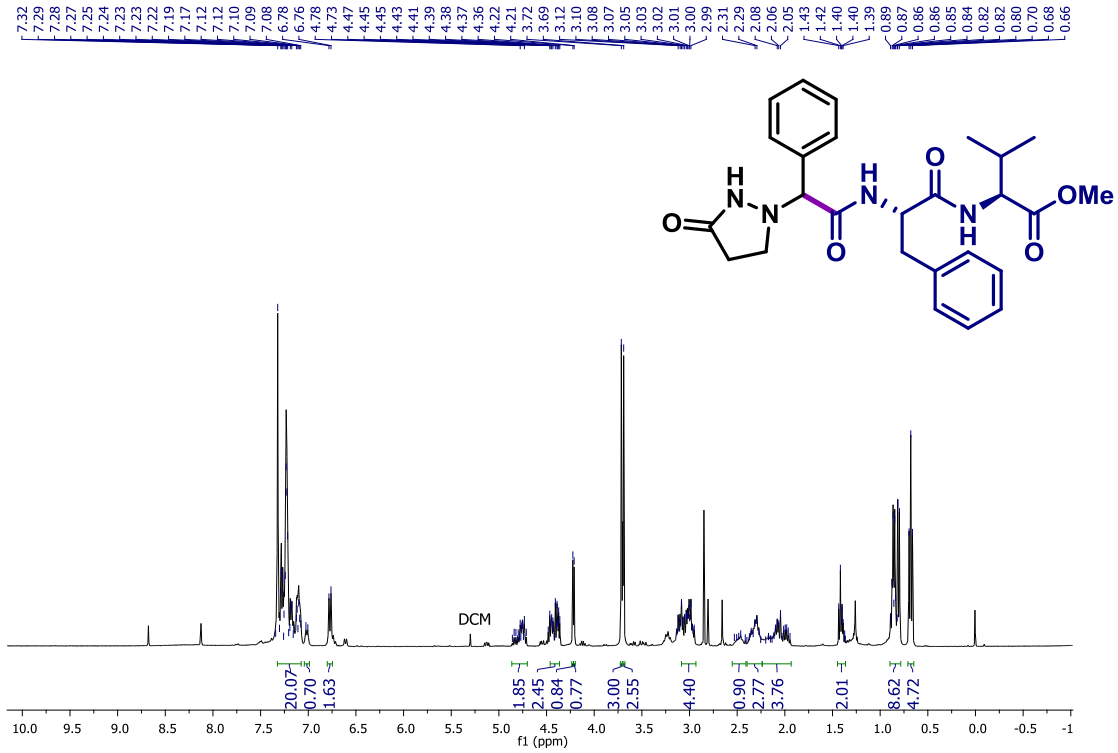

^{1}H NMR ($CDCl_3$, 400 MHz) of 35.

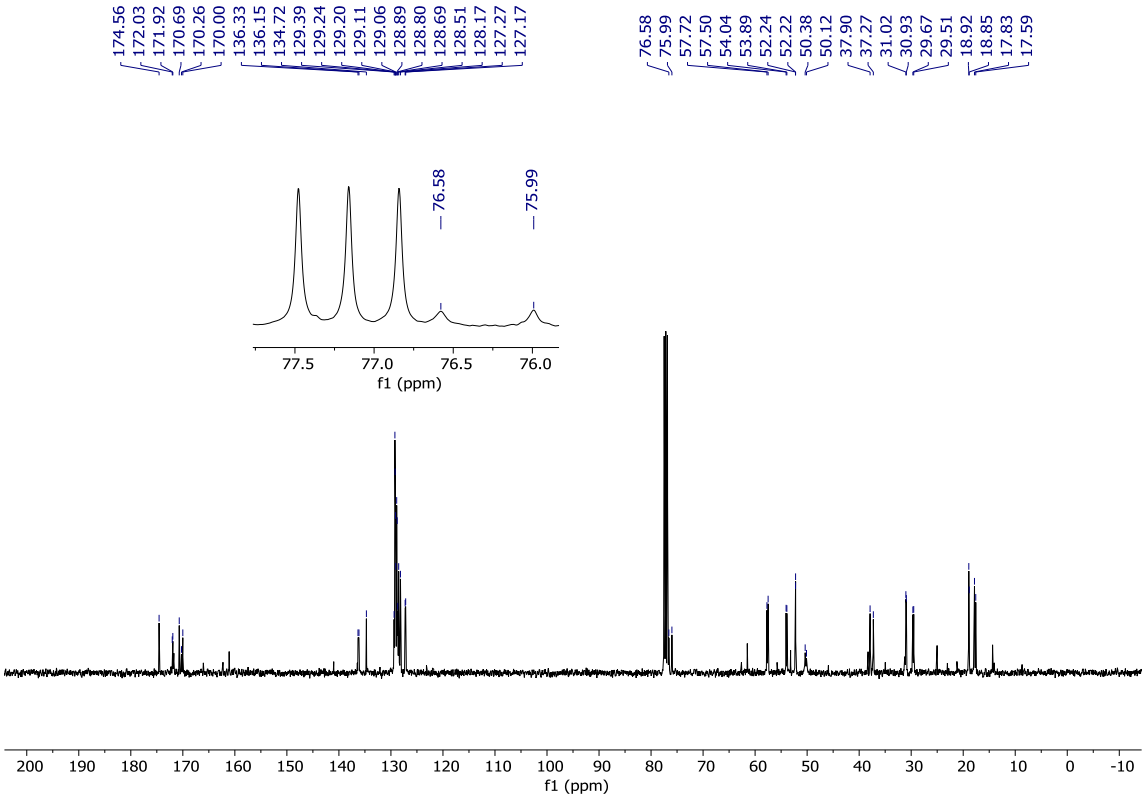

^{13}C NMR ($CDCl_3$, 126 MHz) of 35.

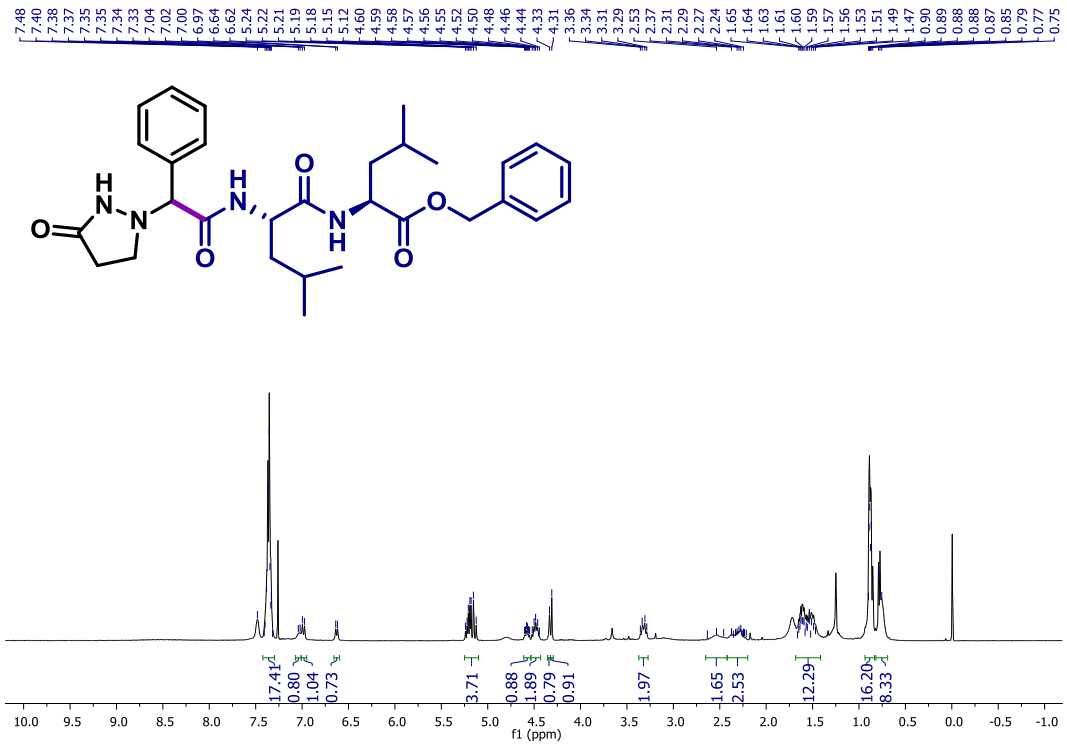

^{1}H NMR ($CDCl_3$, 400 MHz) of 36.

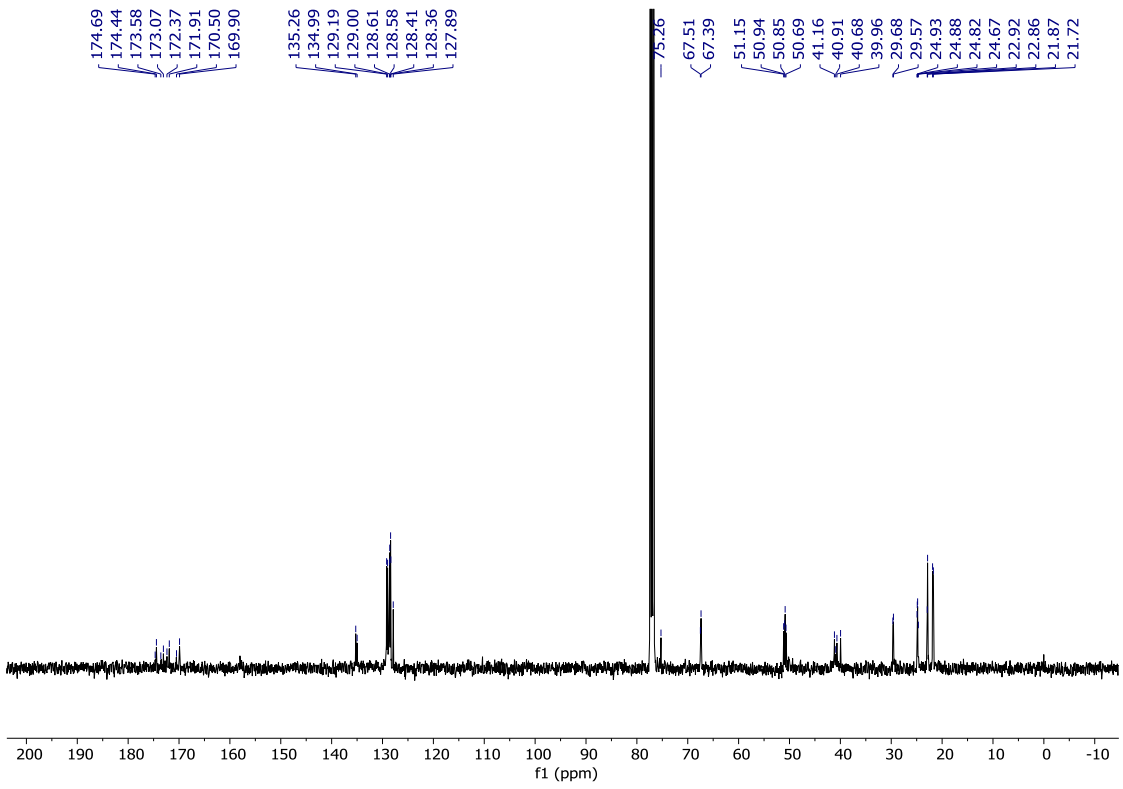

^{13}C NMR ($CDCl_3$, 126 MHz) of 36.

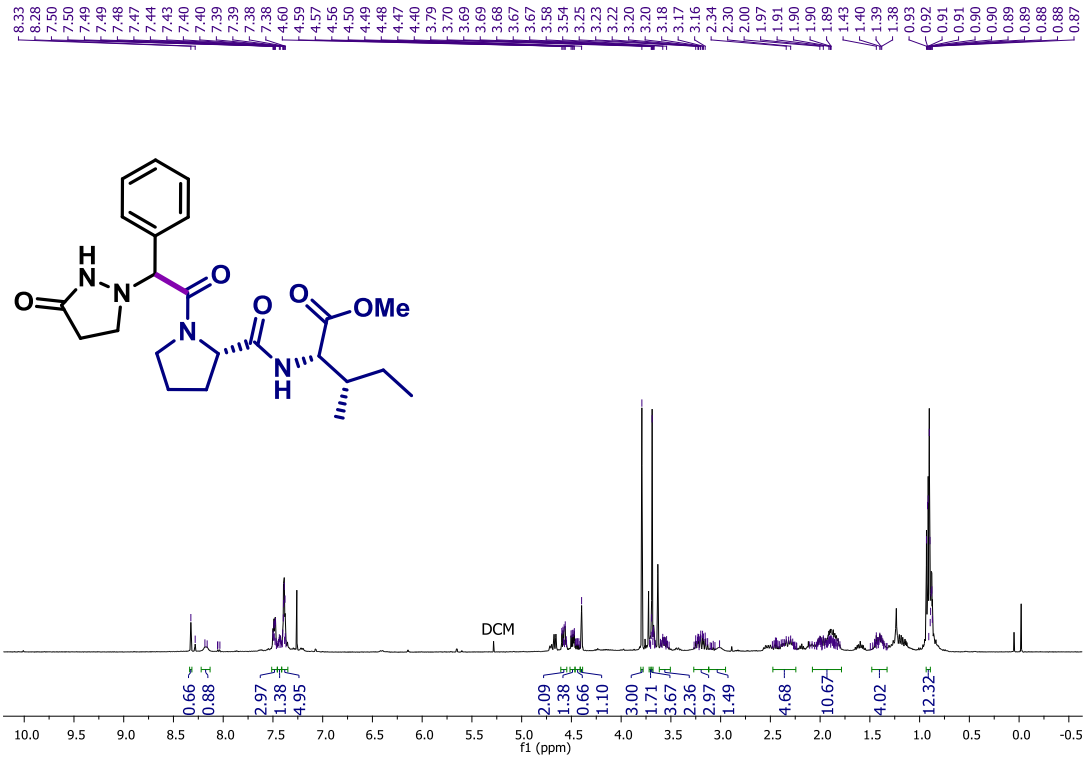

^{1}H NMR ($CDCl_3$, 400 MHz) of 37.

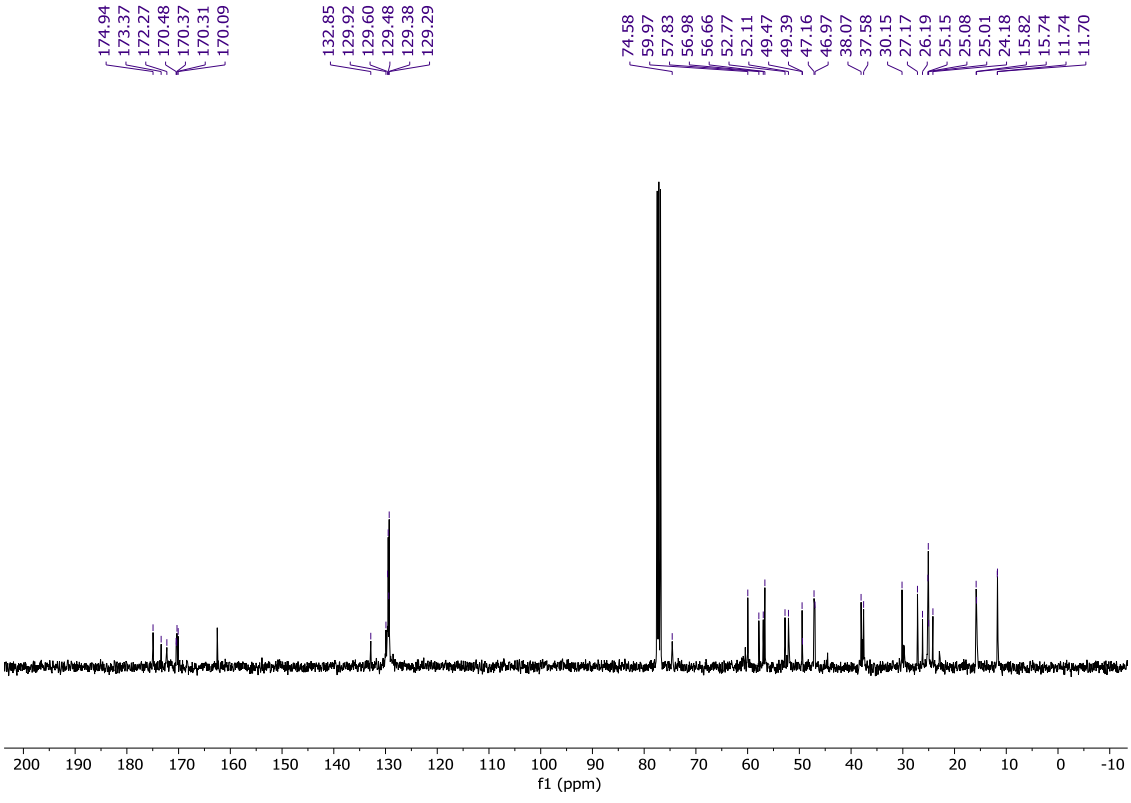

^{13}C NMR ($CDCl_3$, 126 MHz) of 37.

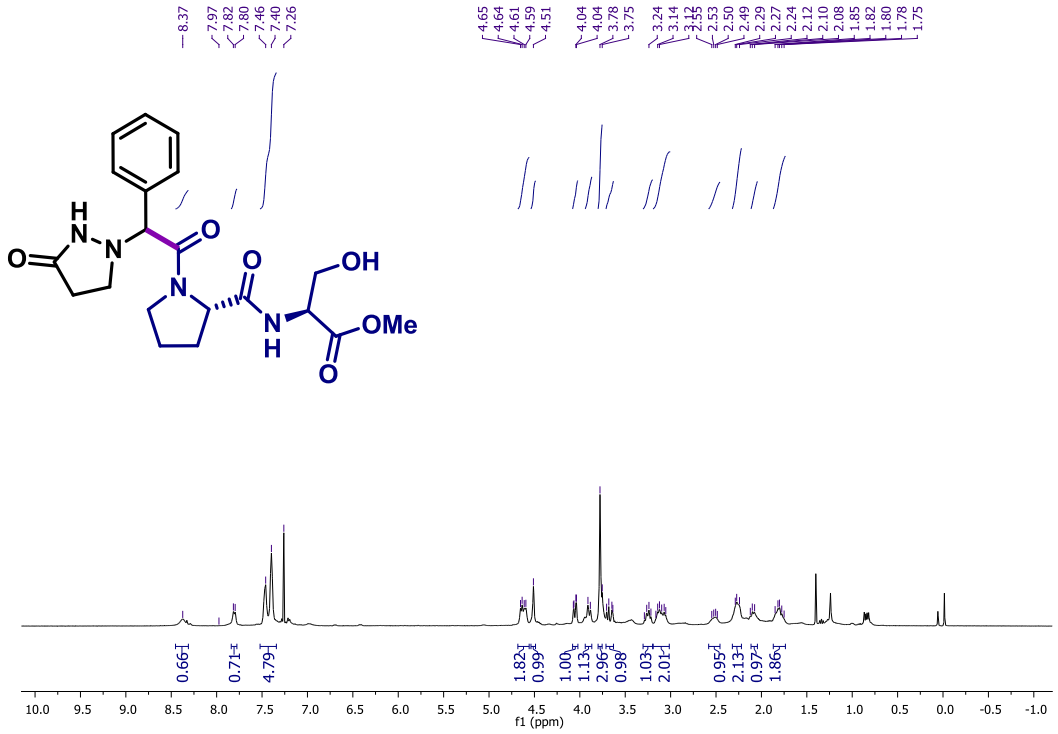

^{1}H NMR ($CDCl_3$, 400 MHz) of 38.

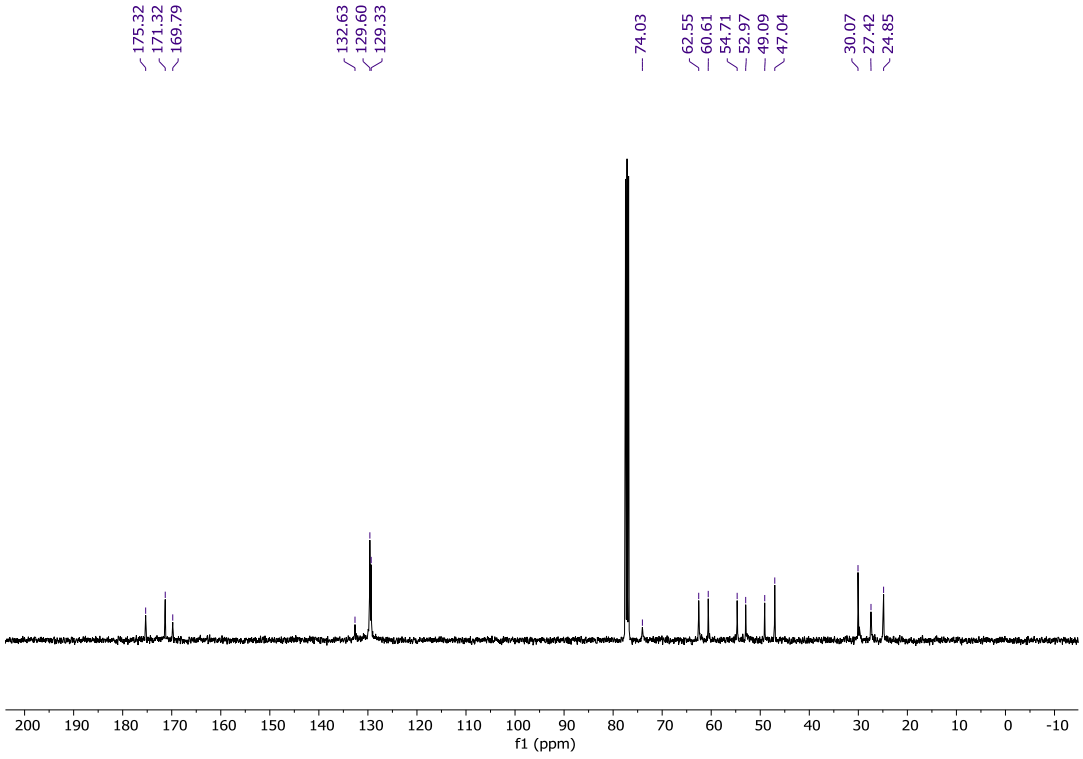

^{3}C NMR ($CDCl_3$, 126 MHz) of 38.

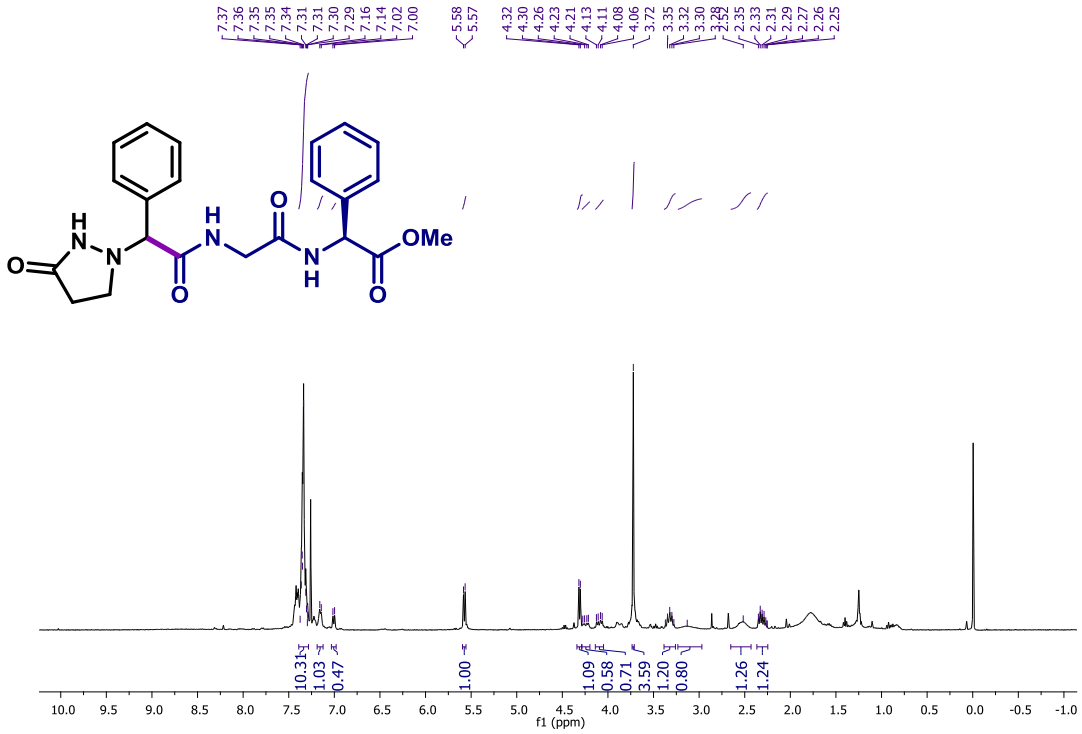

^{1}H NMR ($CDCl_3$, 400 MHz) of 39.

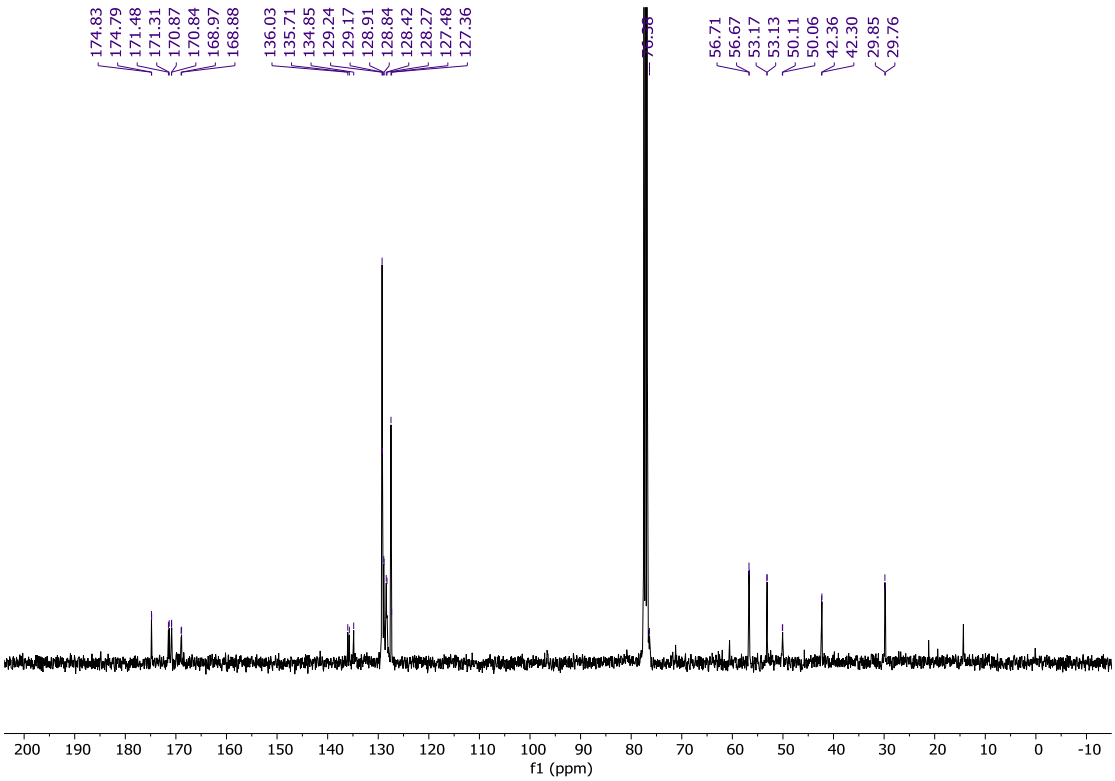

^{13}C NMR ($CDCl_3$, 126 MHz) of 39.

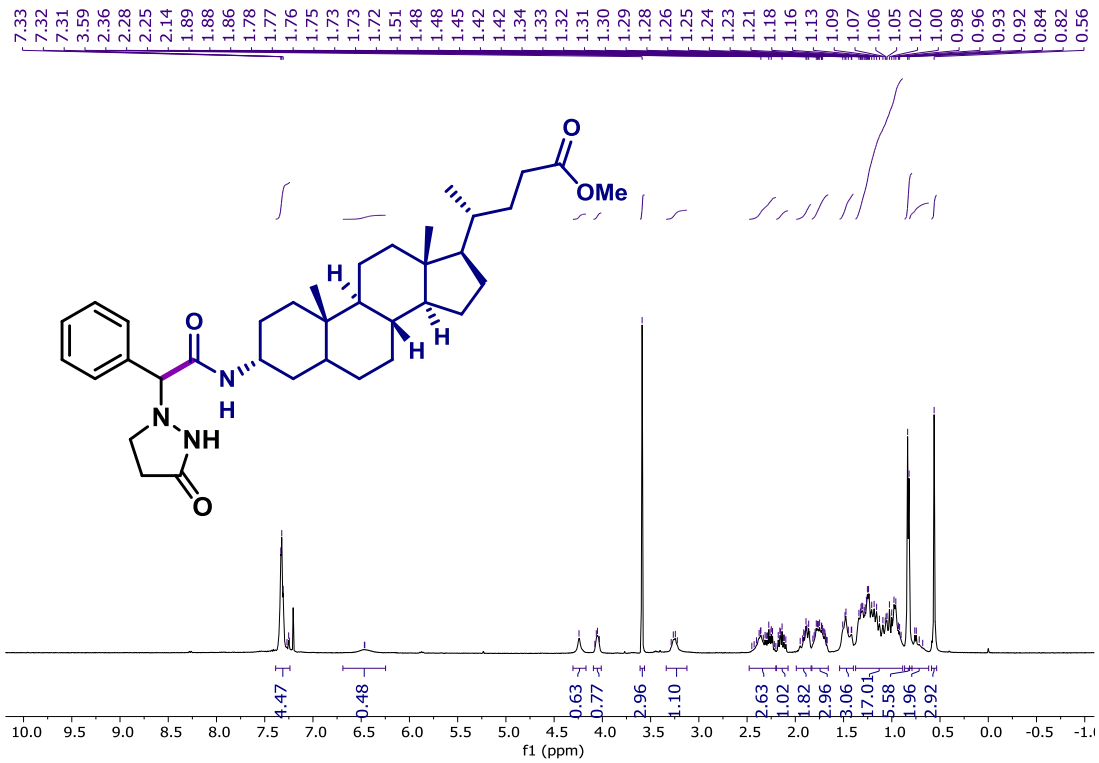

^{1}H NMR ($CDCl_3$, 400 MHz) of 40.

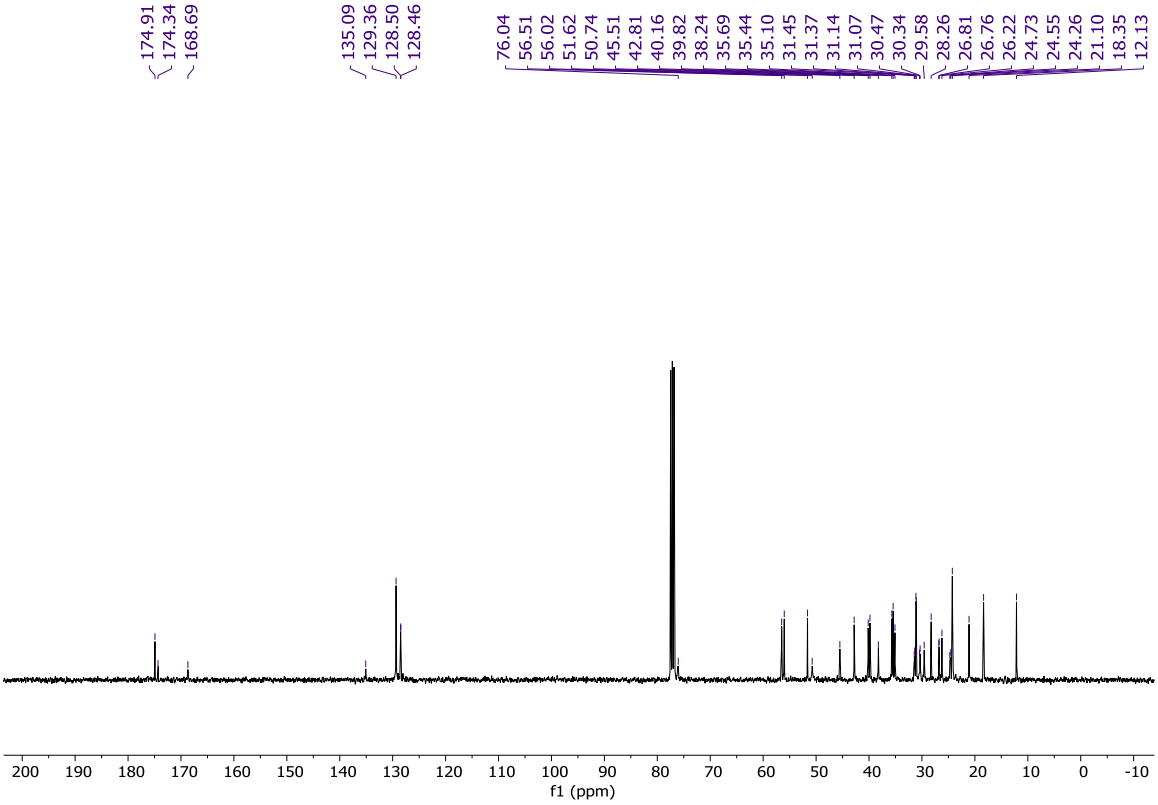

^{13}C NMR (CDCl3, 126 MHz) of 40.

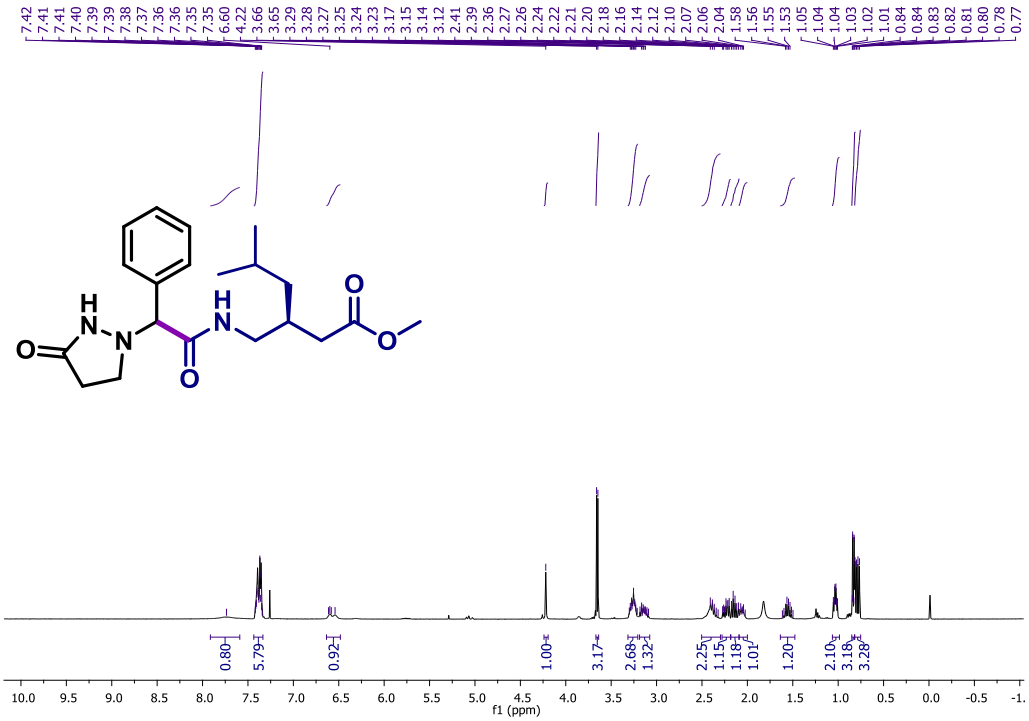

^{1}H NMR ($CDCl_3$, 400 MHz) of 41.

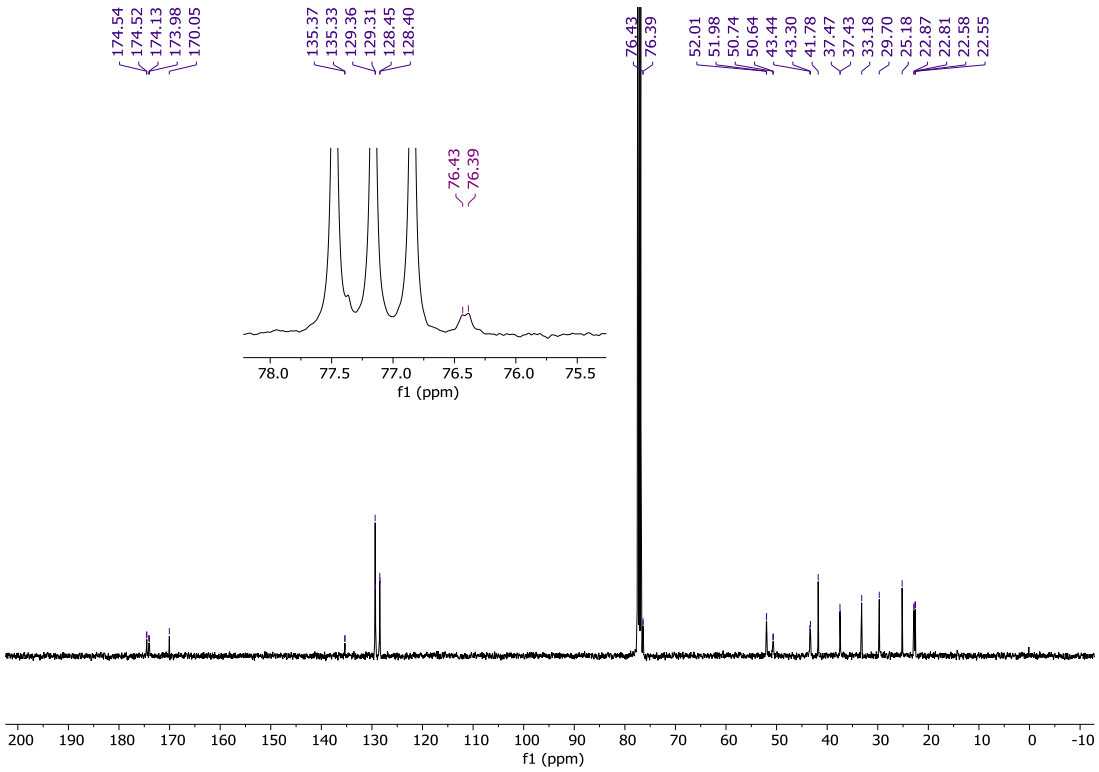

^{13}C NMR (CDCl3, 126 MHz) of 41.

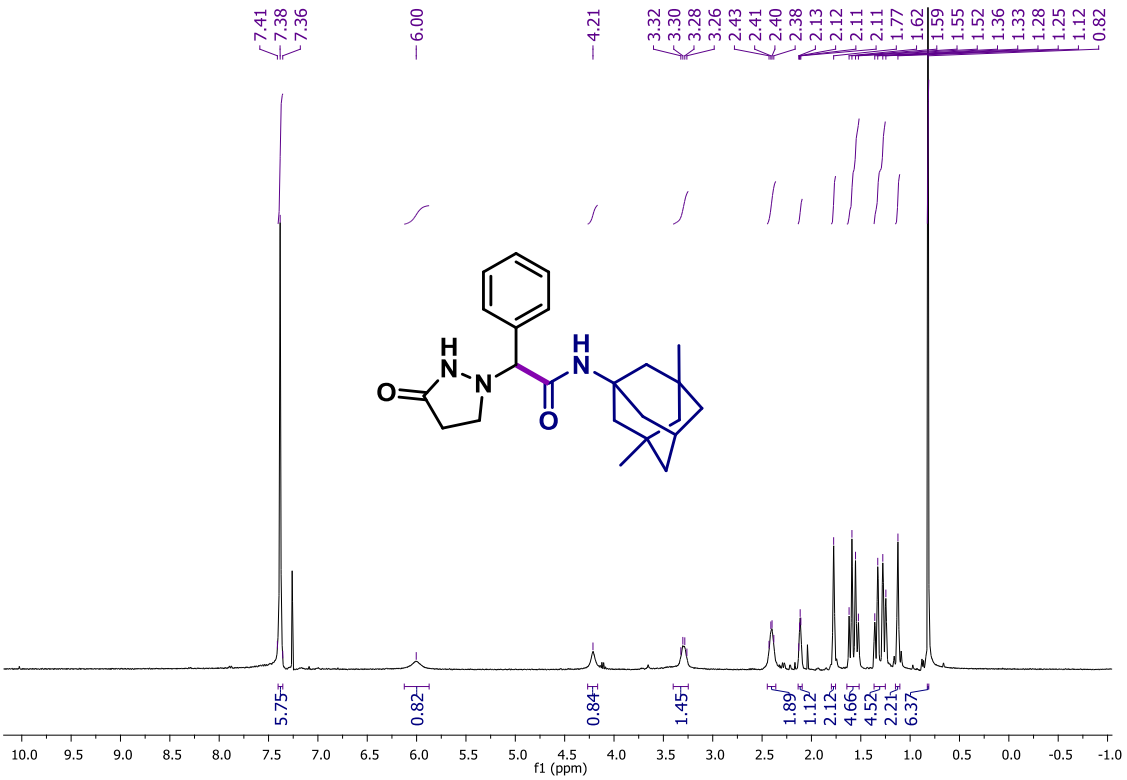

^{1}H NMR ($CDCl_3$, 400 MHz) of 42.

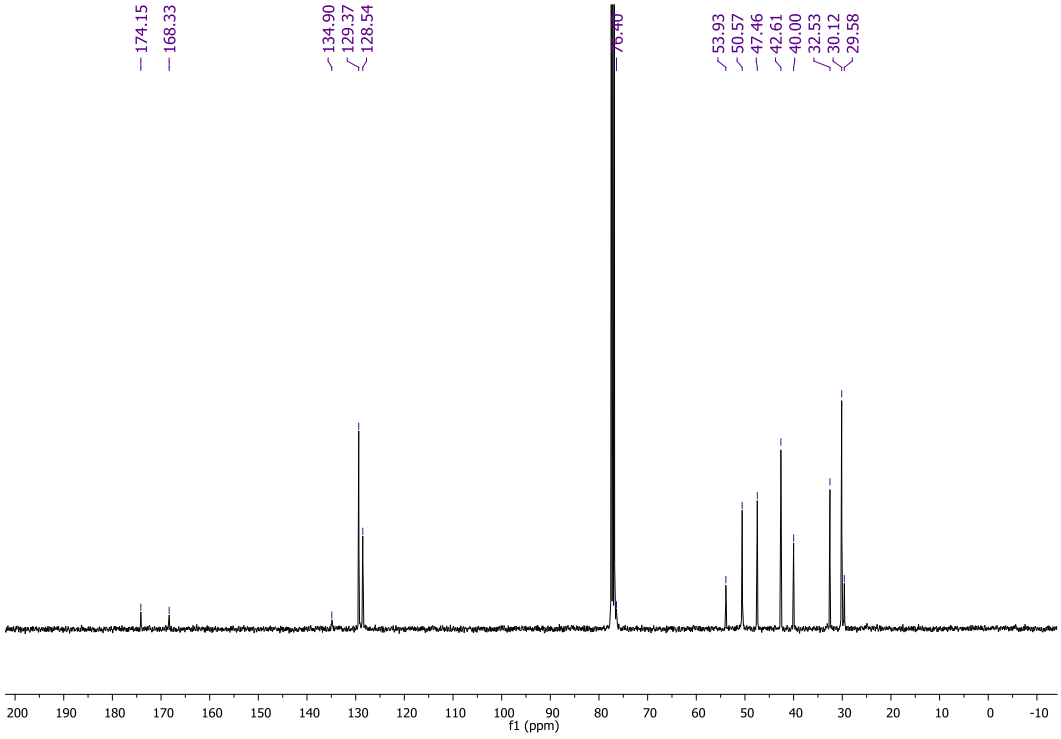

^{13}C NMR (CDCl3, 126 MHz) of 42.

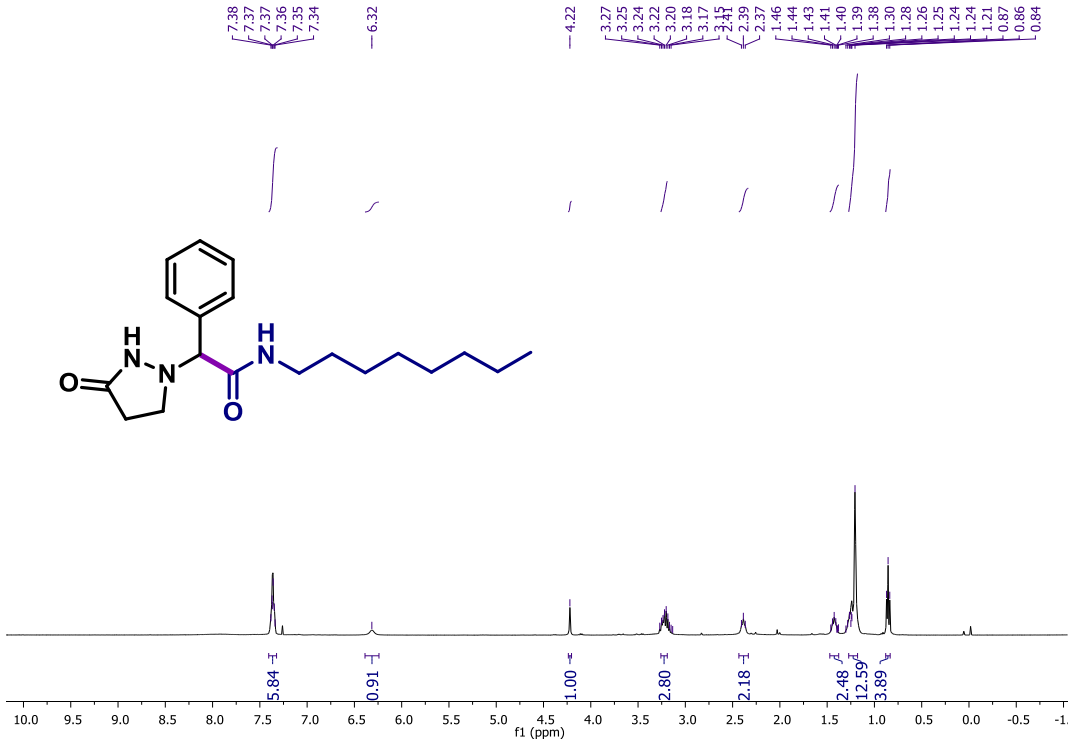

^{1}H NMR ($CDCl_3$, 400 MHz) of 43.

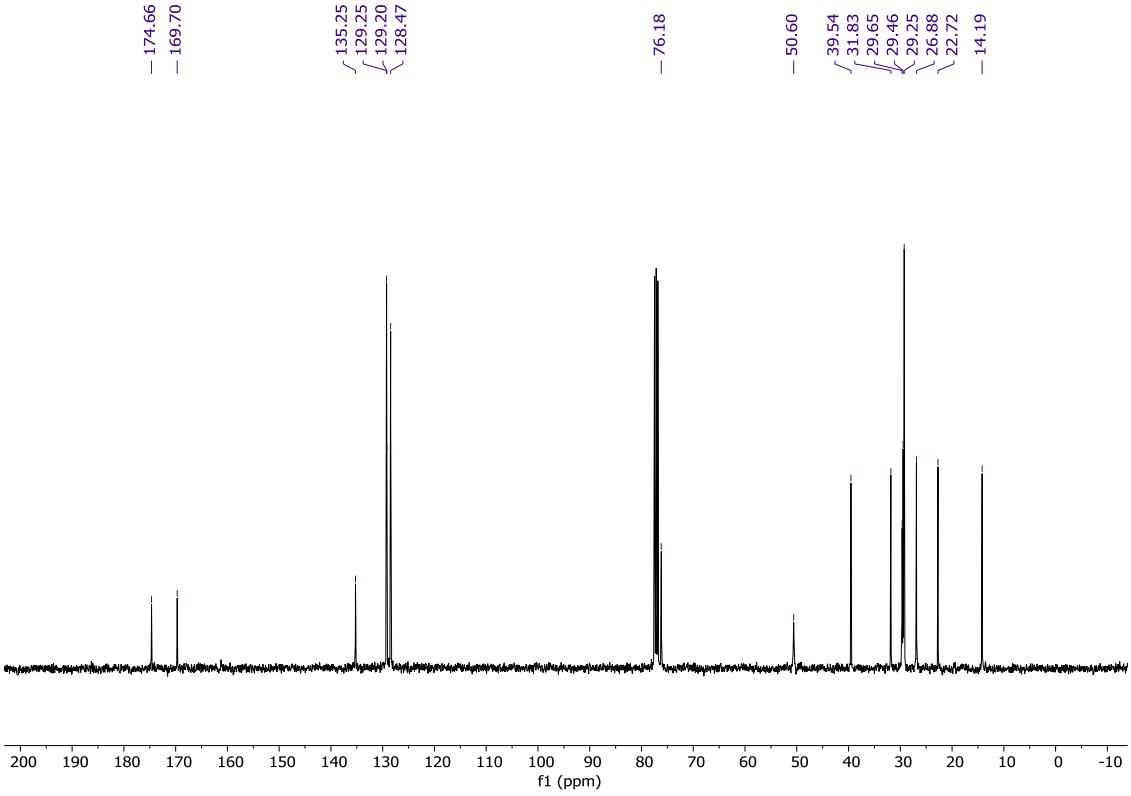

^{1}H NMR ($CDCl_3$, 400 MHz) of 43.

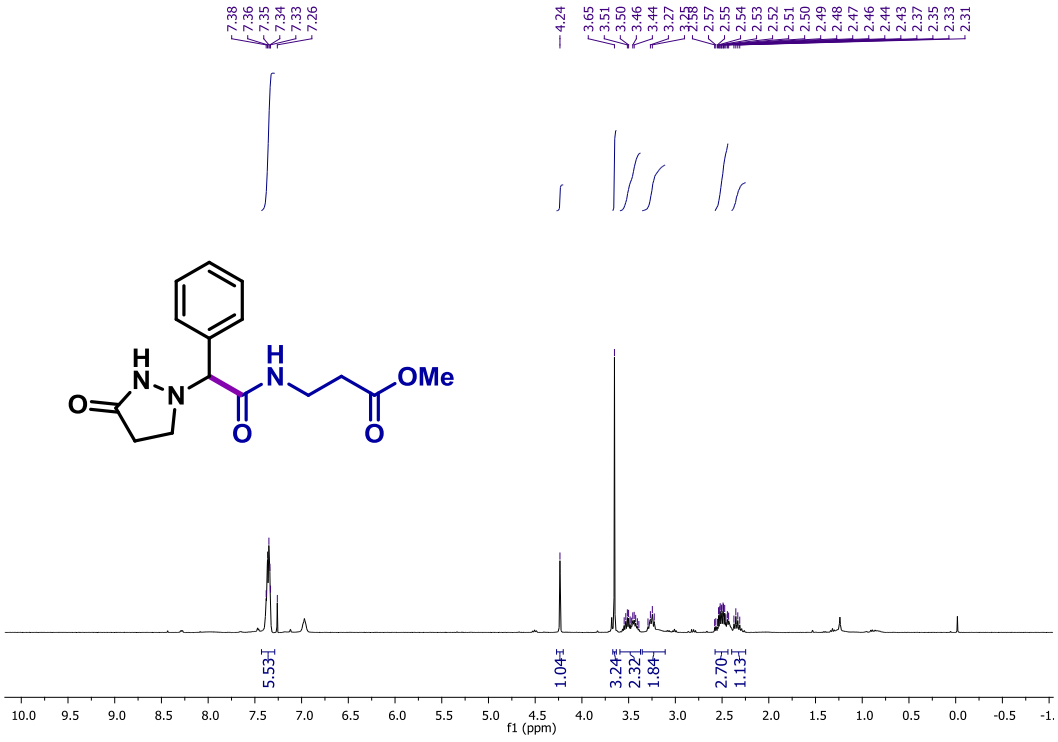

^{1}H NMR ($CDCl_3$, 400 MHz) of 44.

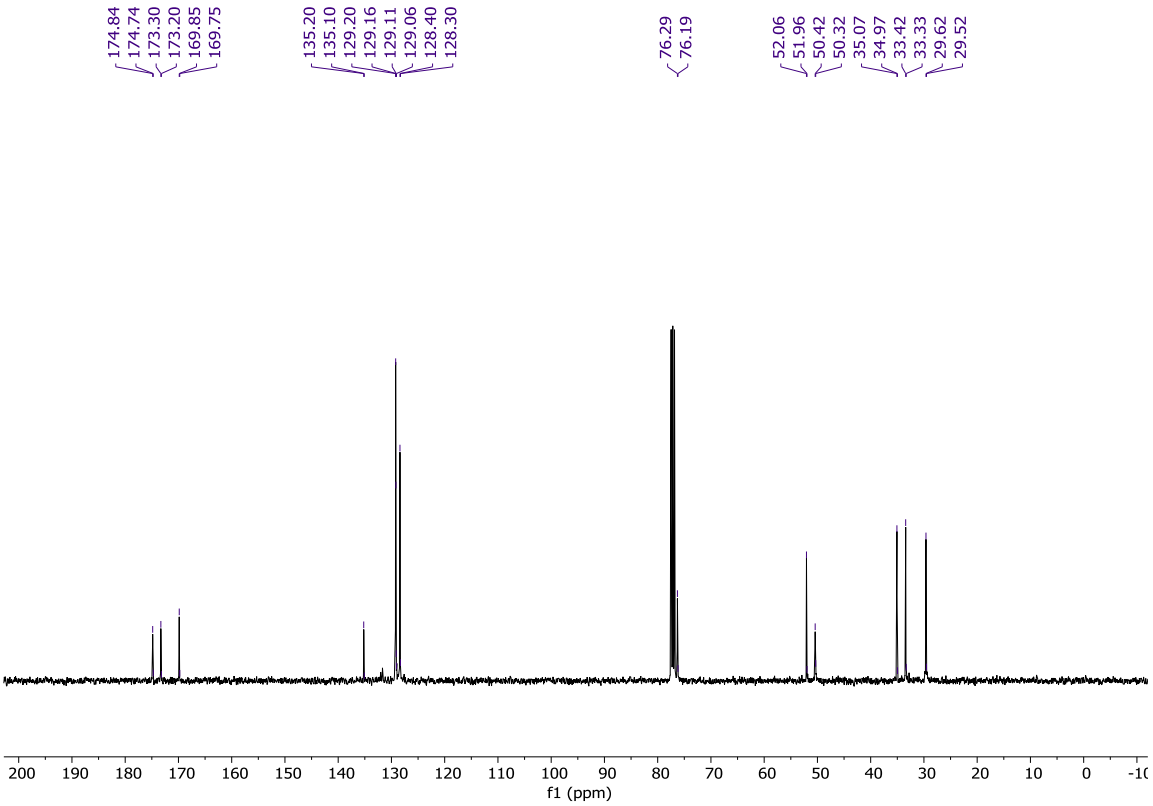

^{13}C NMR ($CDCl_3$, 126 MHz) of 44.

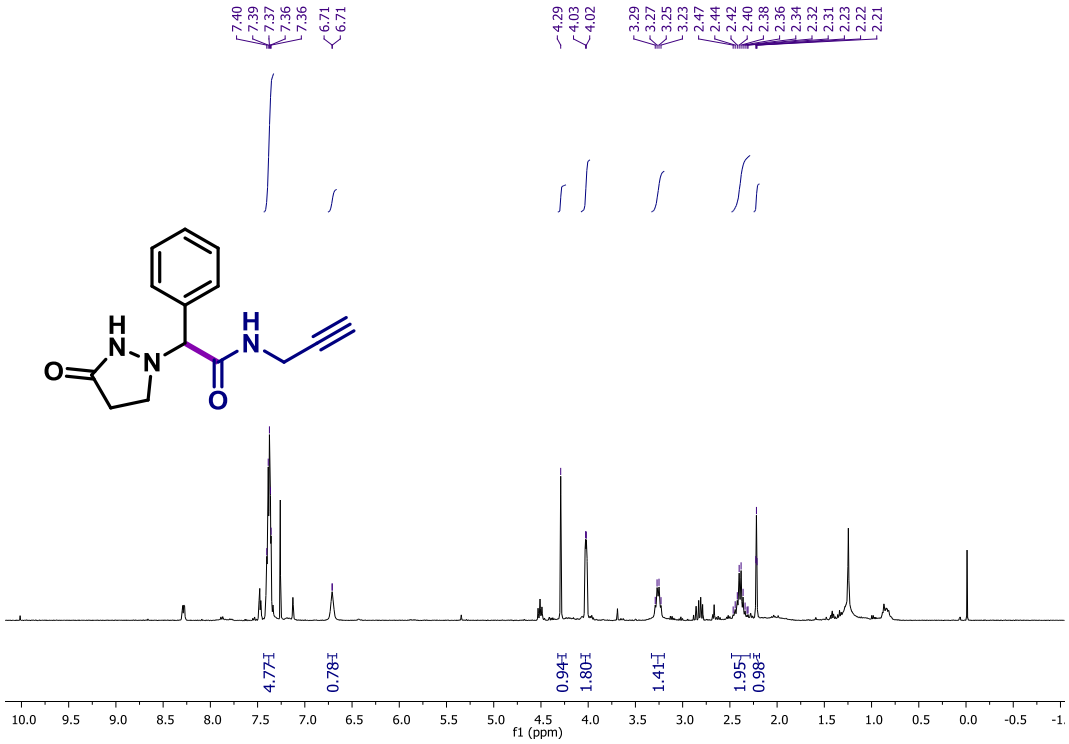

^{1}H NMR ($CDCl_3$, 400 MHz) of 45.

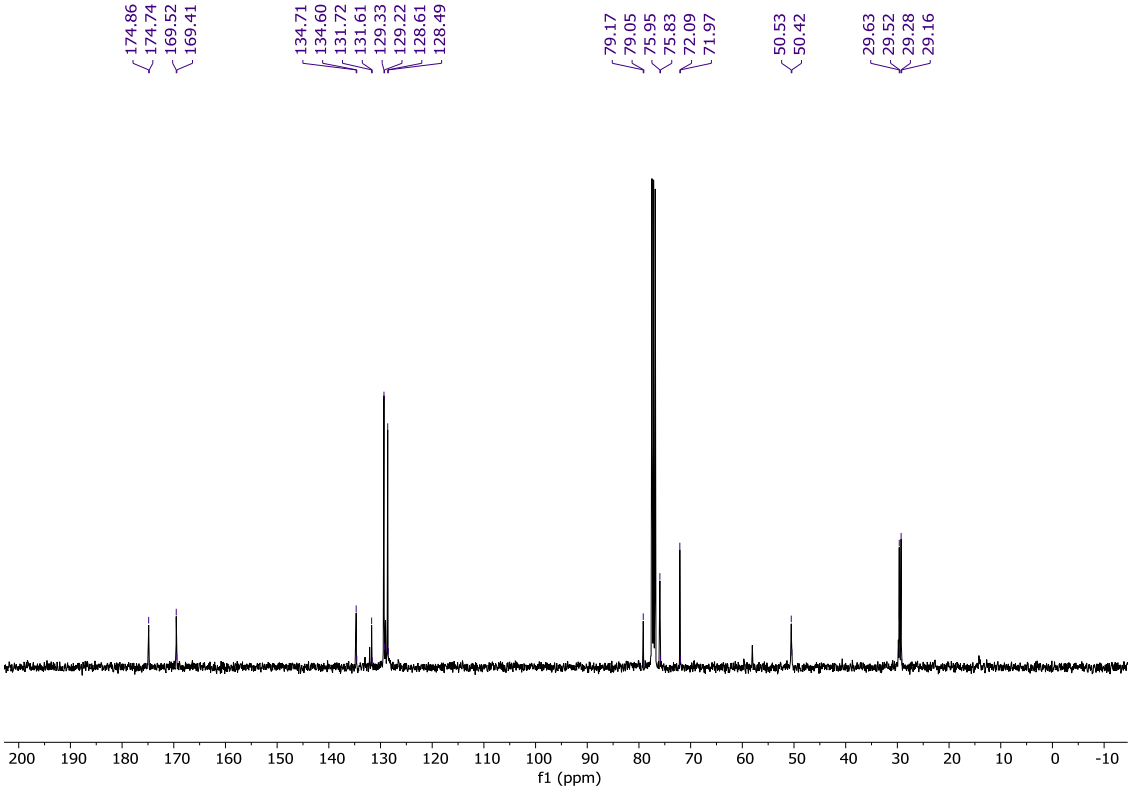

^{13}C NMR ($CDCl_3$, 126 MHz) of 45.

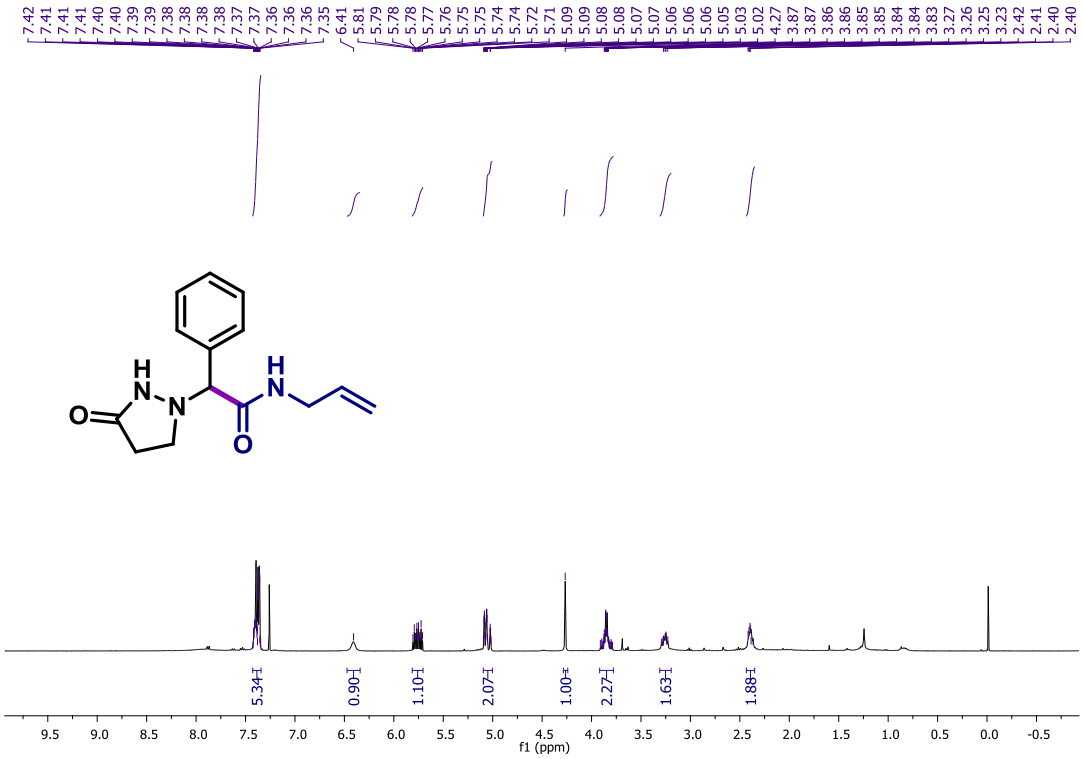

^{1}H NMR ($CDCl_3$, 400 MHz) of 46.

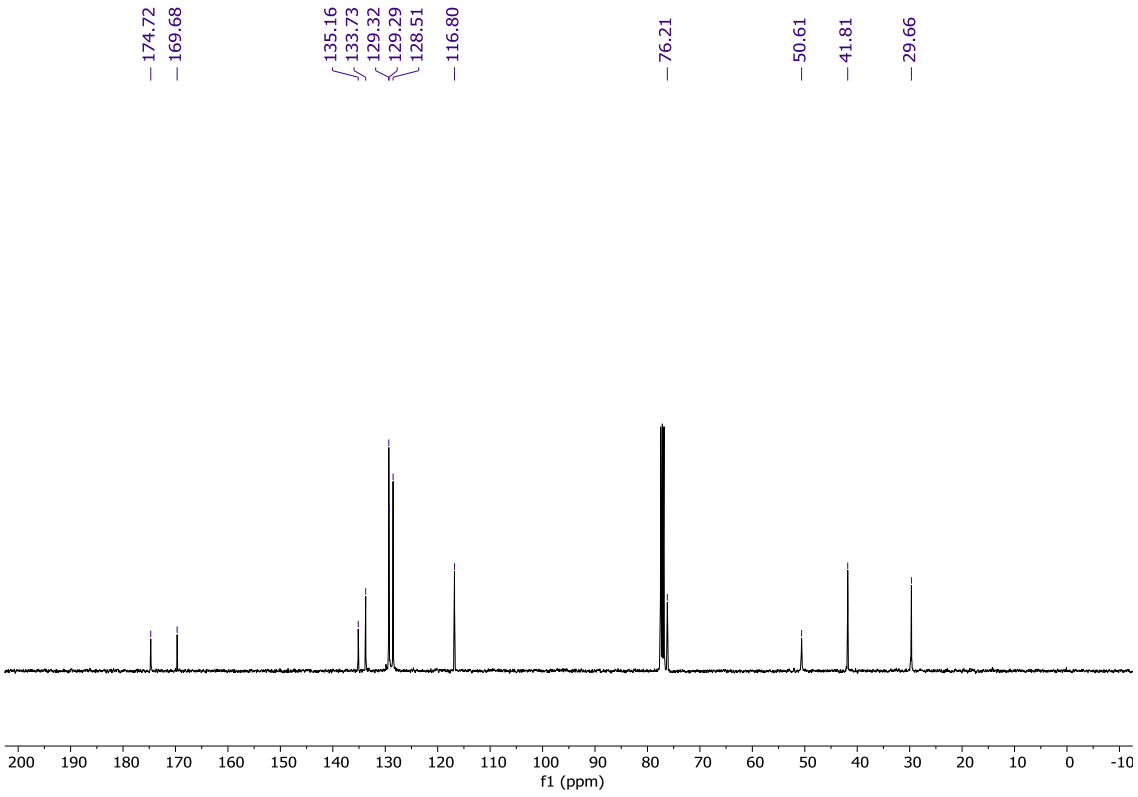

^{13}C NMR ($CDCl_3$, 126 MHz) of 46.

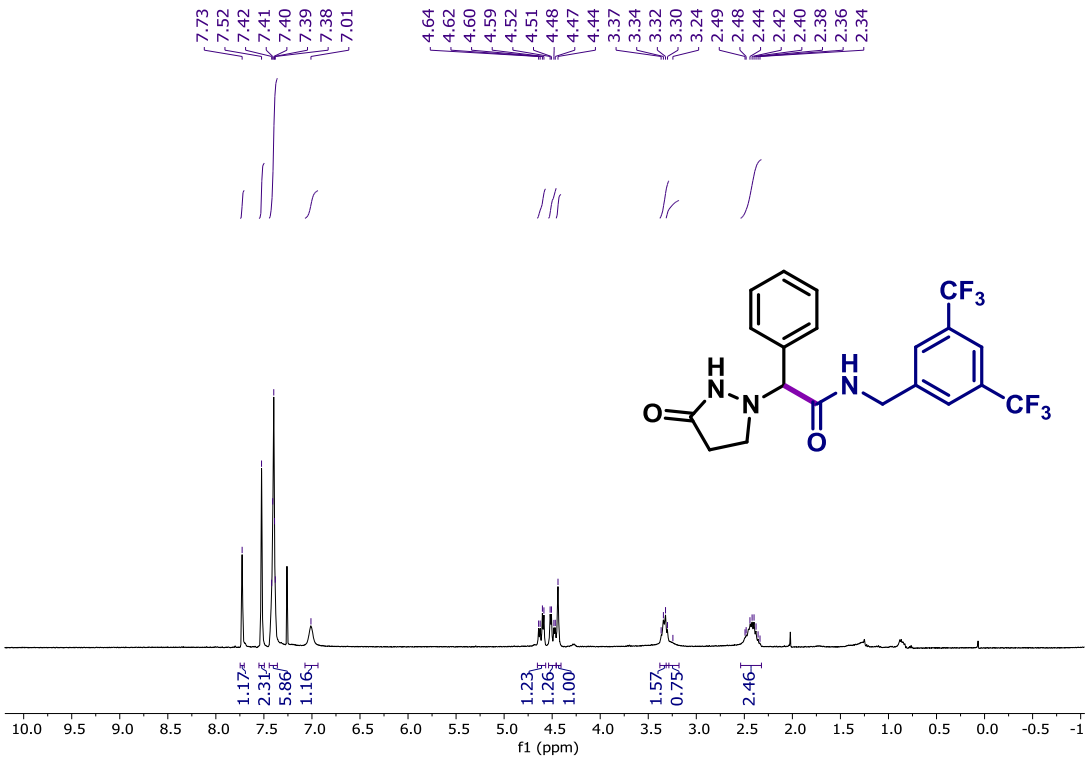

^{1}H NMR ($CDCl_3$, 400 MHz) of 47.

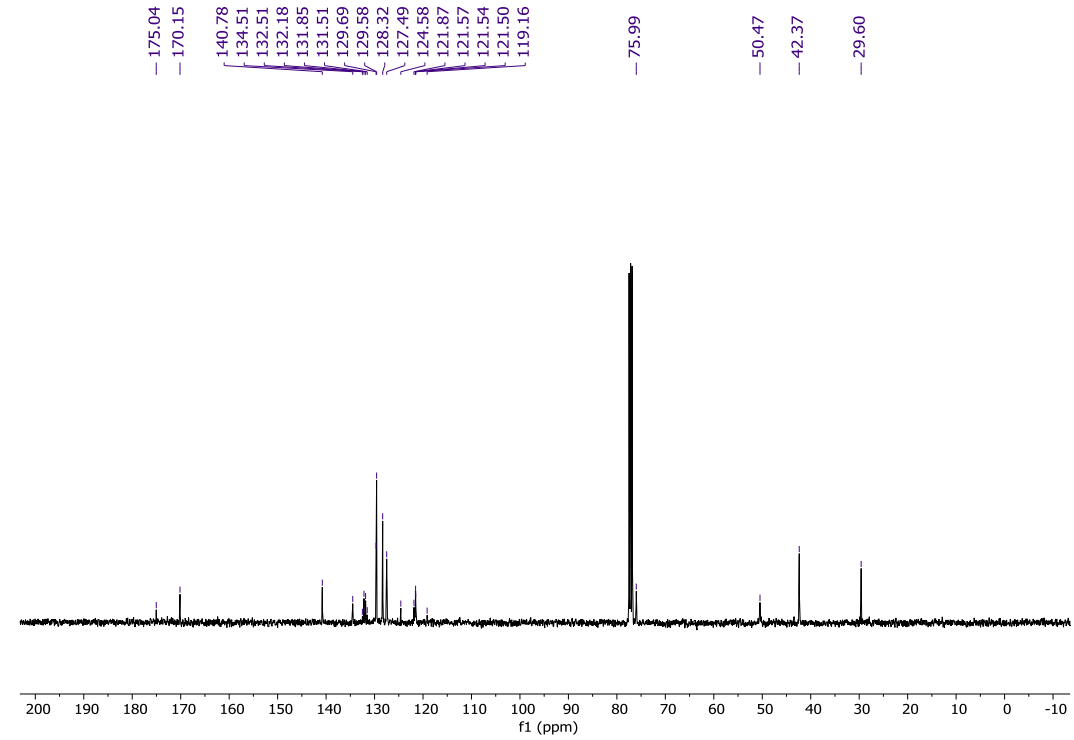

^{13}C NMR ($CDCl_3$, 126 MHz) of 47.

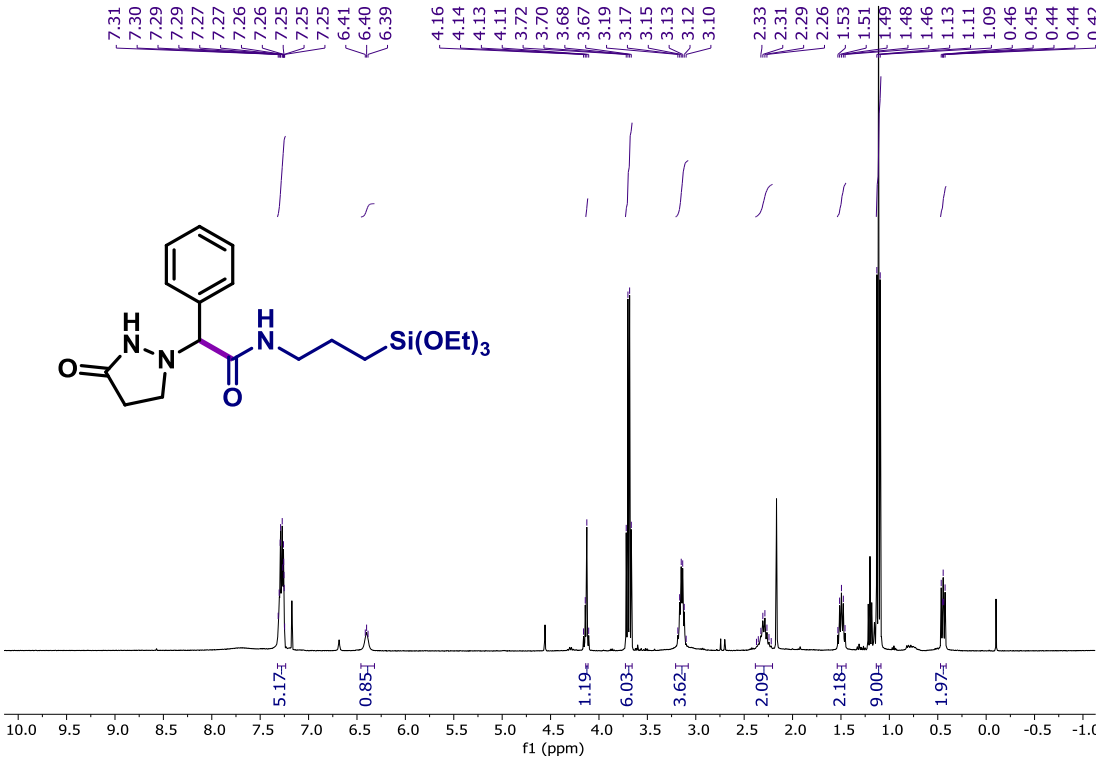

^{1}H NMR ($CDCl_3$, 400 MHz) of 48.

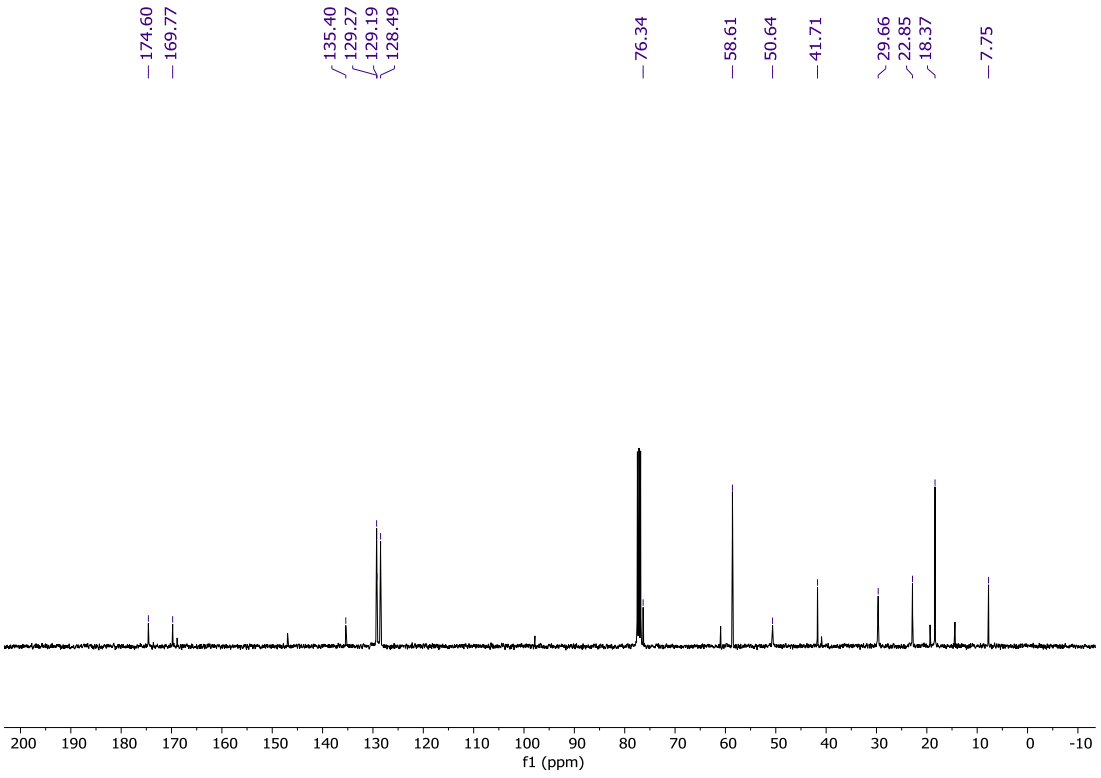

^{13}C NMR ($CDCl_3$, 126 MHz) of 48.

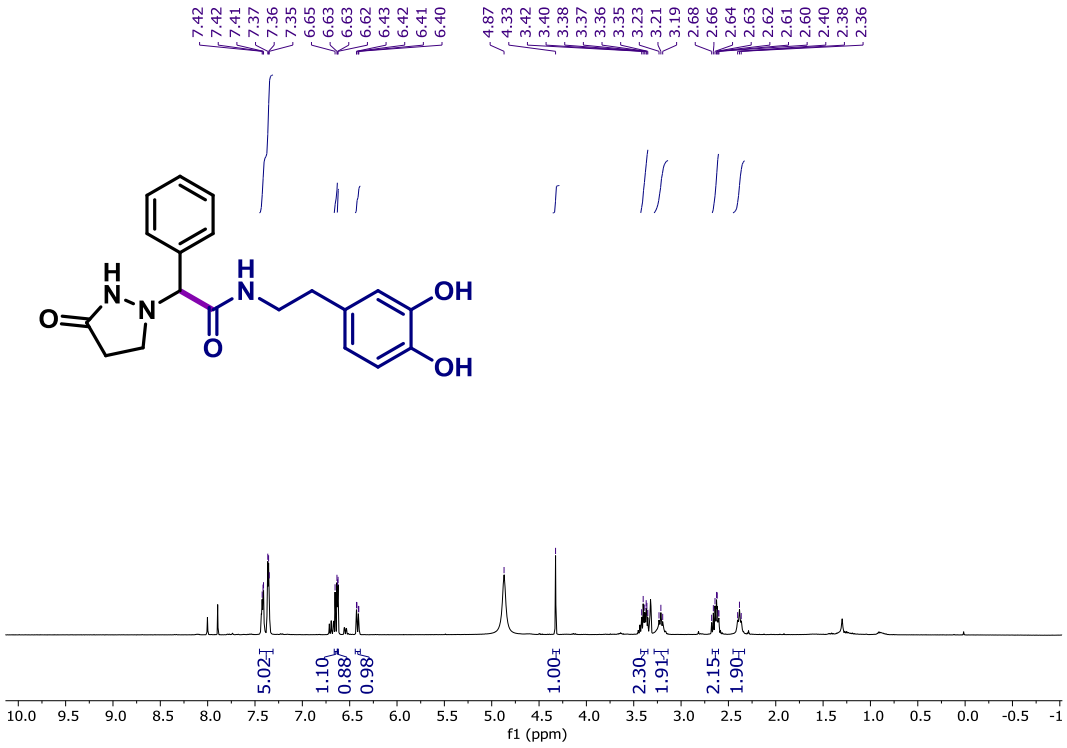

^{1}H NMR (CD_3OD, 400 MHz) of 49.

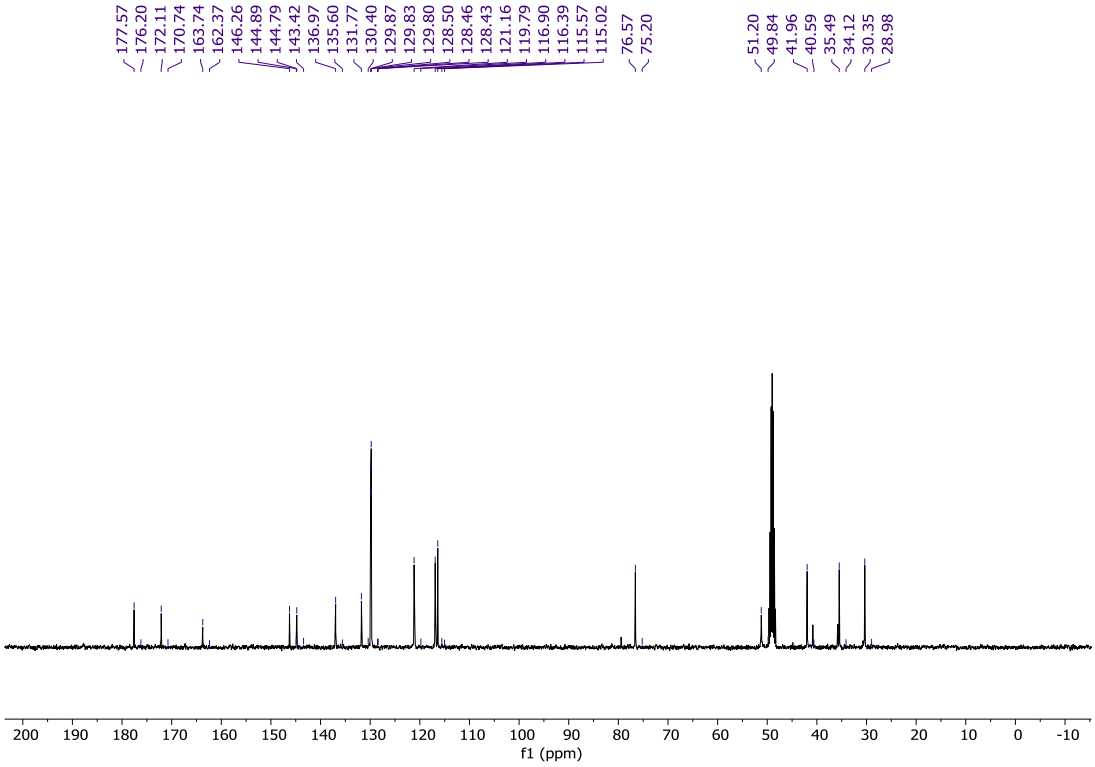

^{13}C NMR (CD_3OD, 126 MHz) of 49.

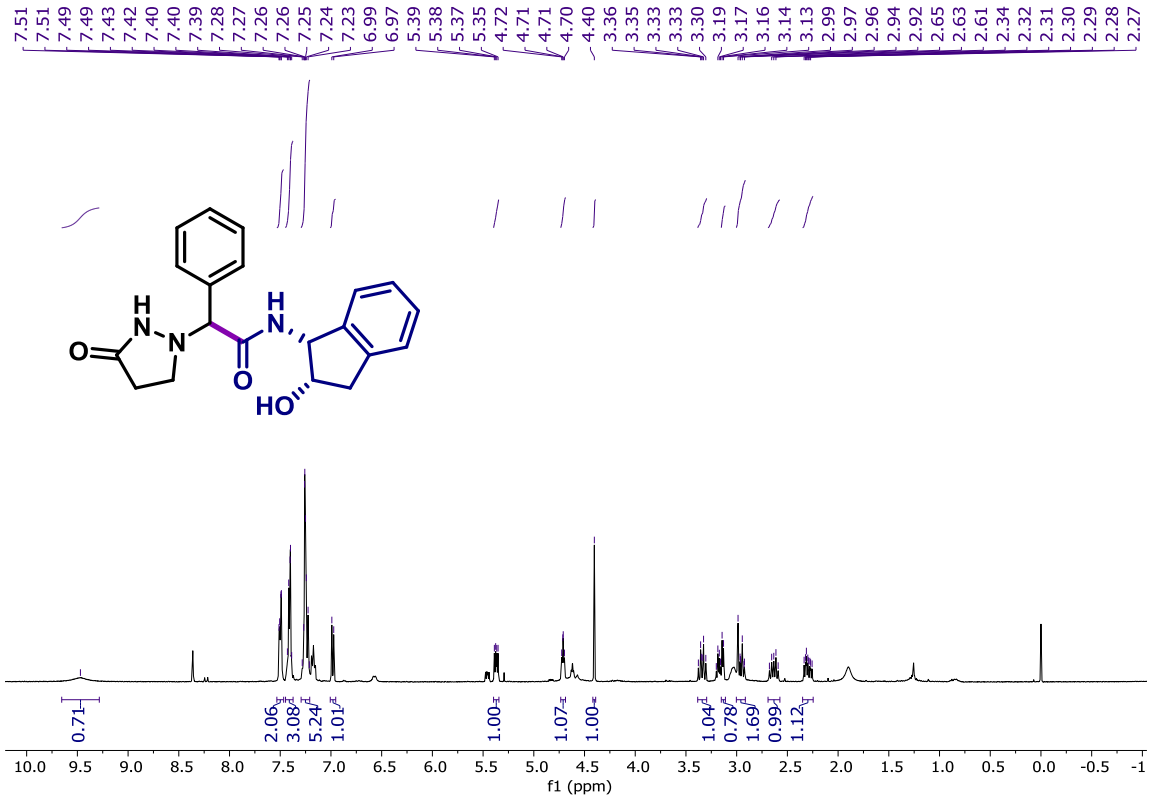

^{1}H NMR ($CDCl_3$, 400 MHz) of 50.

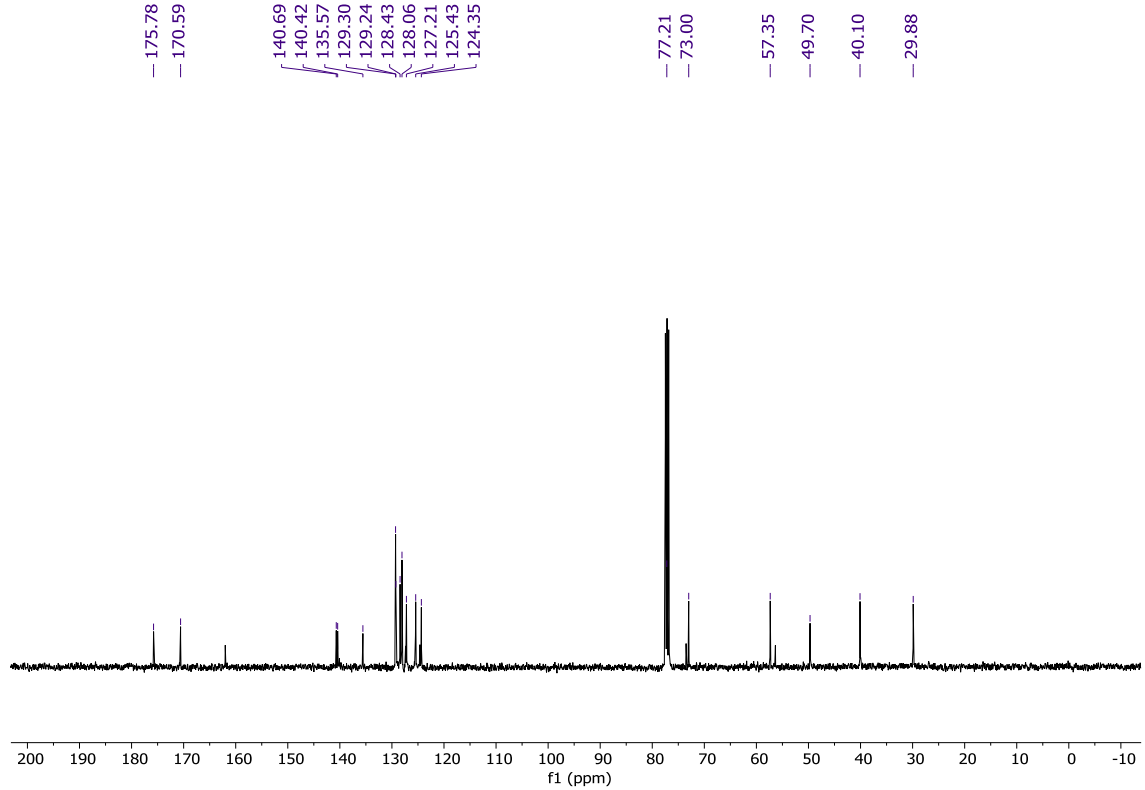

^{13}C NMR ($CDCl_3$, 126 MHz) of 50.

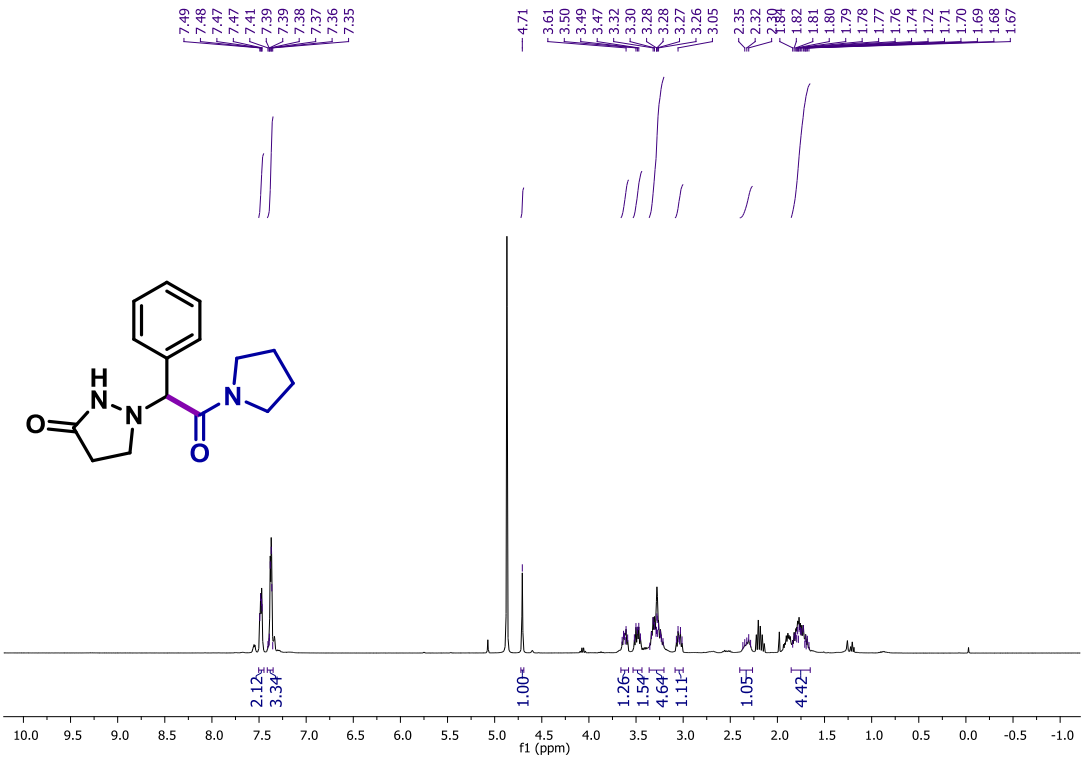

^{1}H NMR ($CDCl_3$, 400 MHz) of 51.

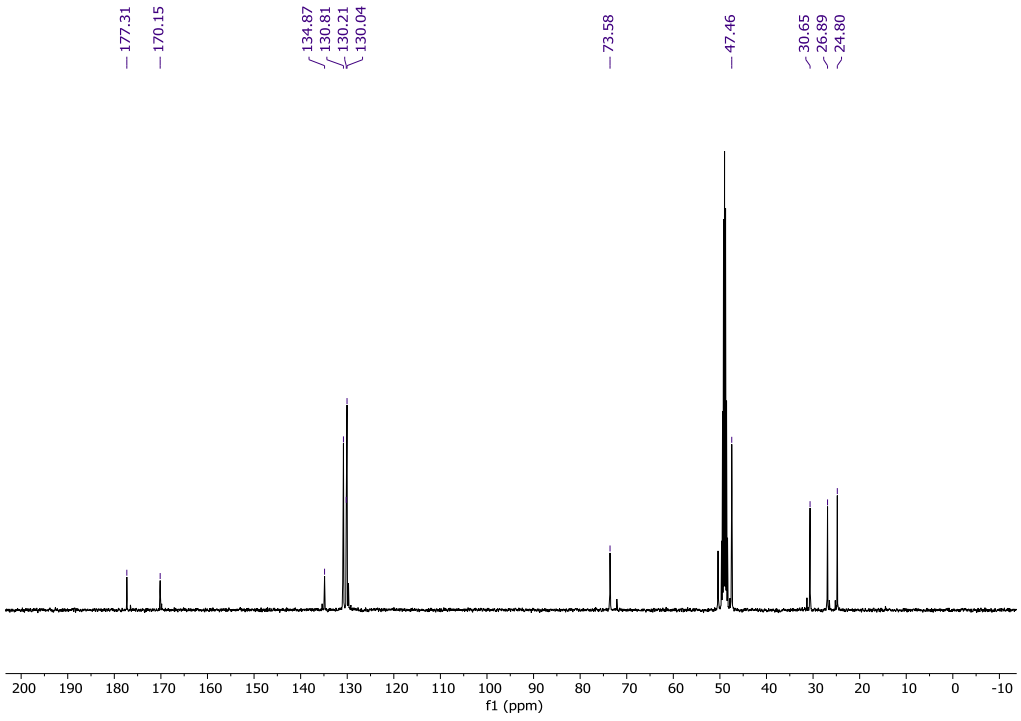

^{13}C NMR ($CDCl_3$, 126 MHz) of 51.

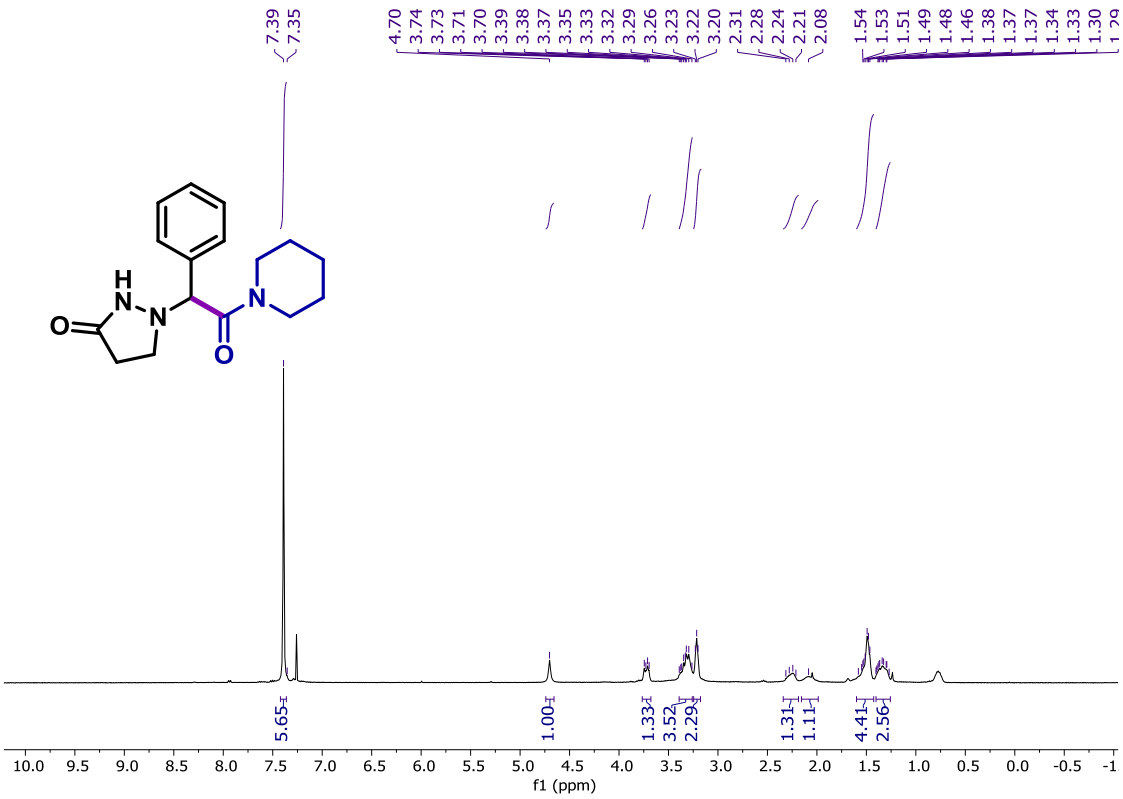

^{1}H NMR ($CDCl_3$, 400 MHz) of 52.

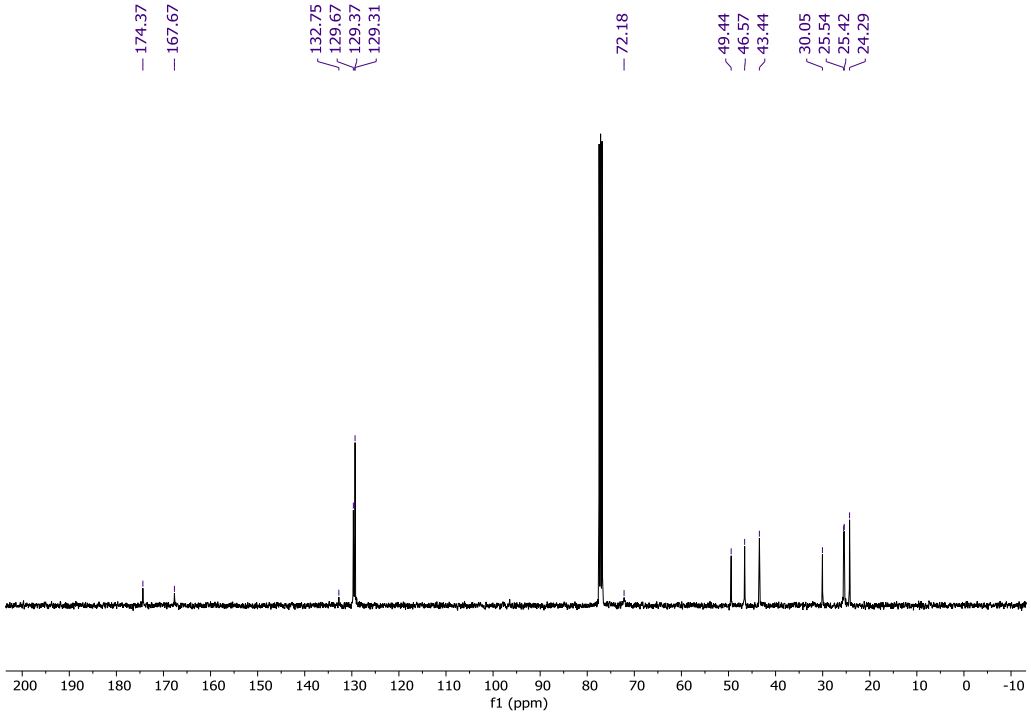

^{13}C NMR ($CDCl_3$, 126 MHz) of 52.

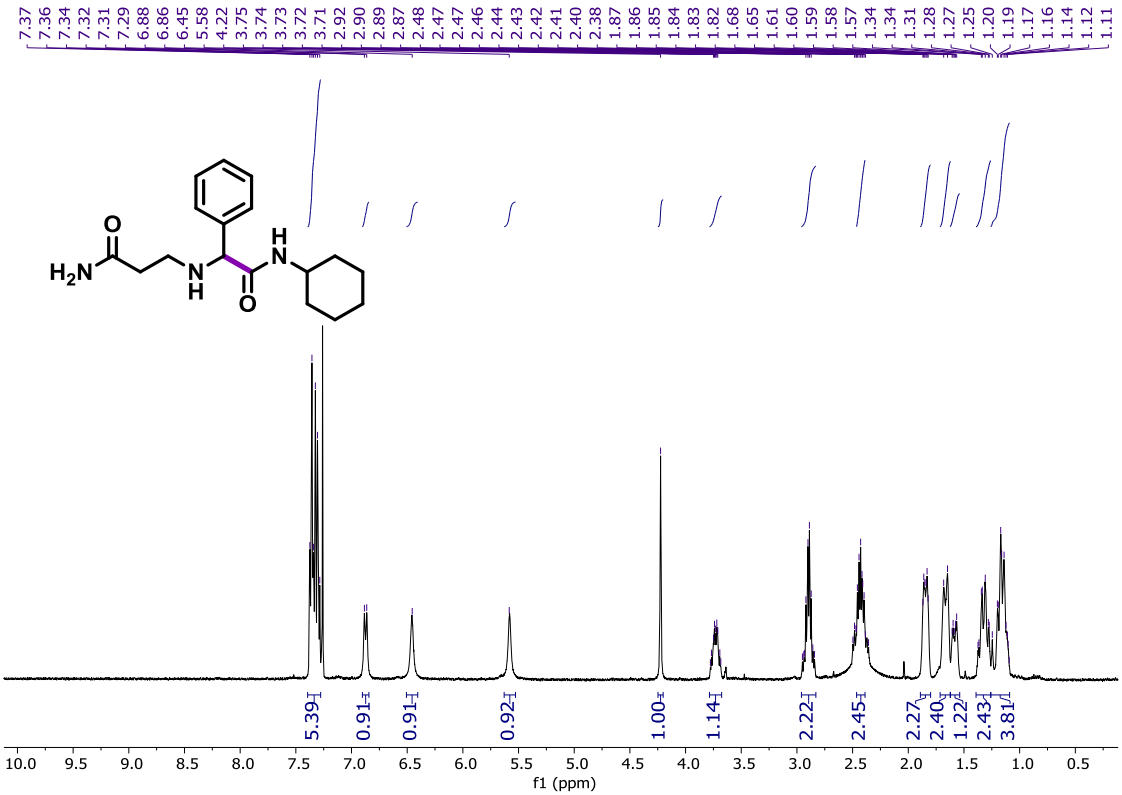

^{1}H NMR ($CDCl_3$, 400 MHz) of 53.

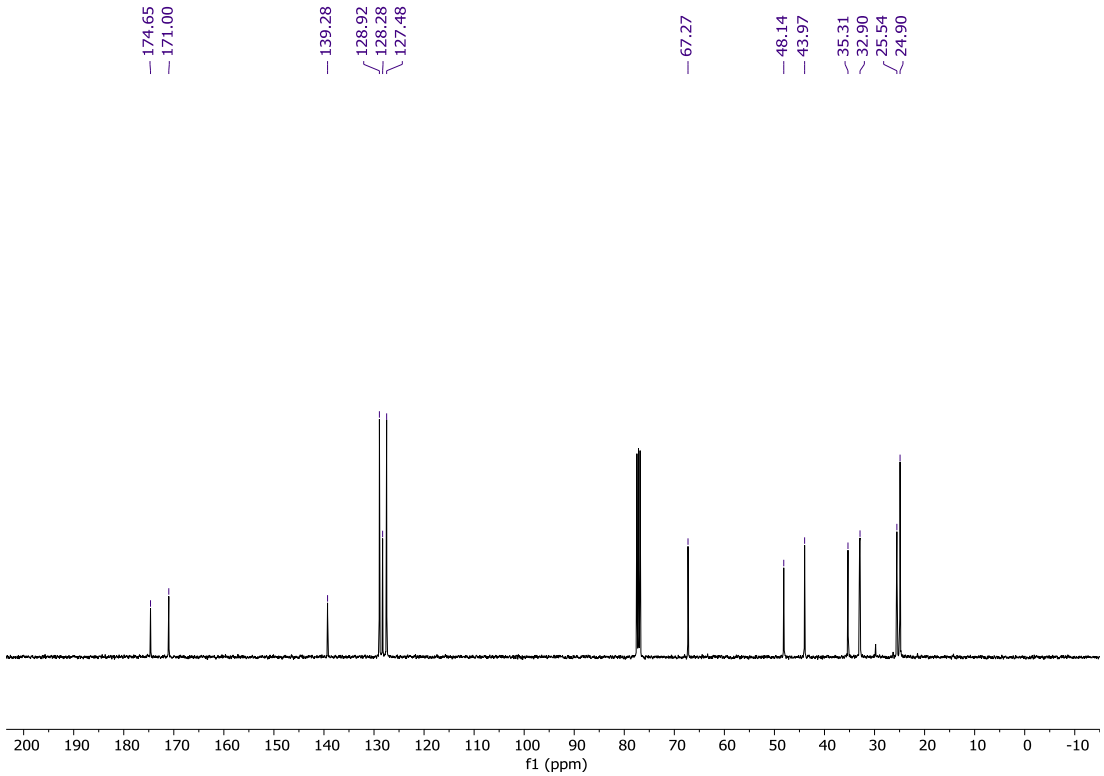

^{13}C NMR ($CDCl_3$, 126 MHz) of 53.

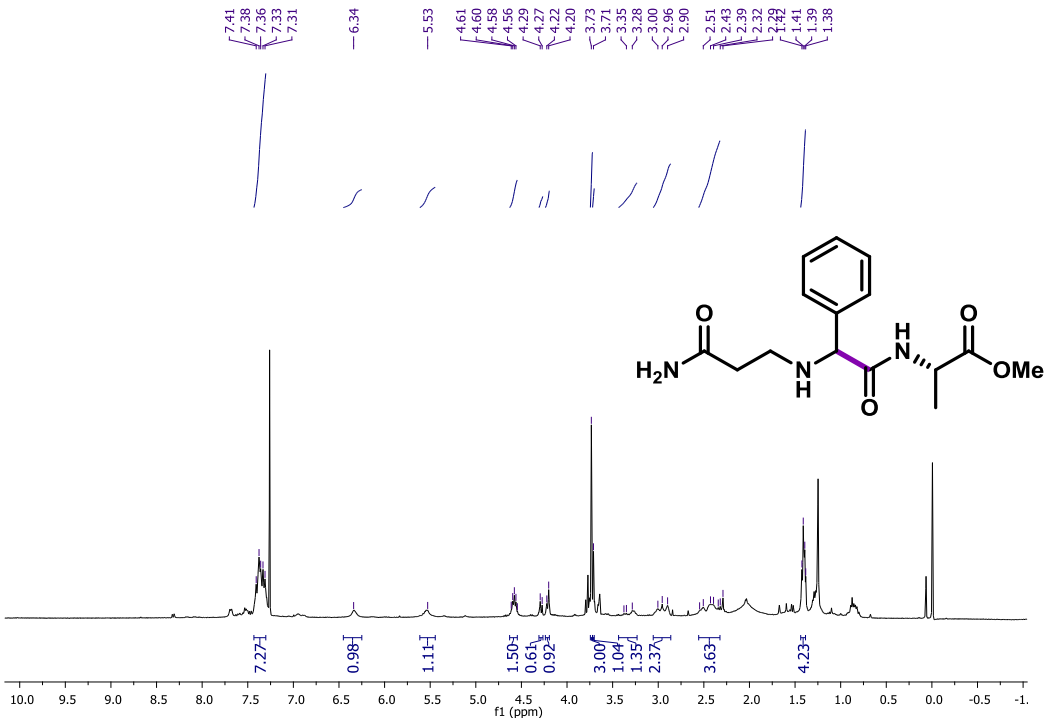

^{1}H NMR ($CDCl_3$, 400 MHz) of 54.

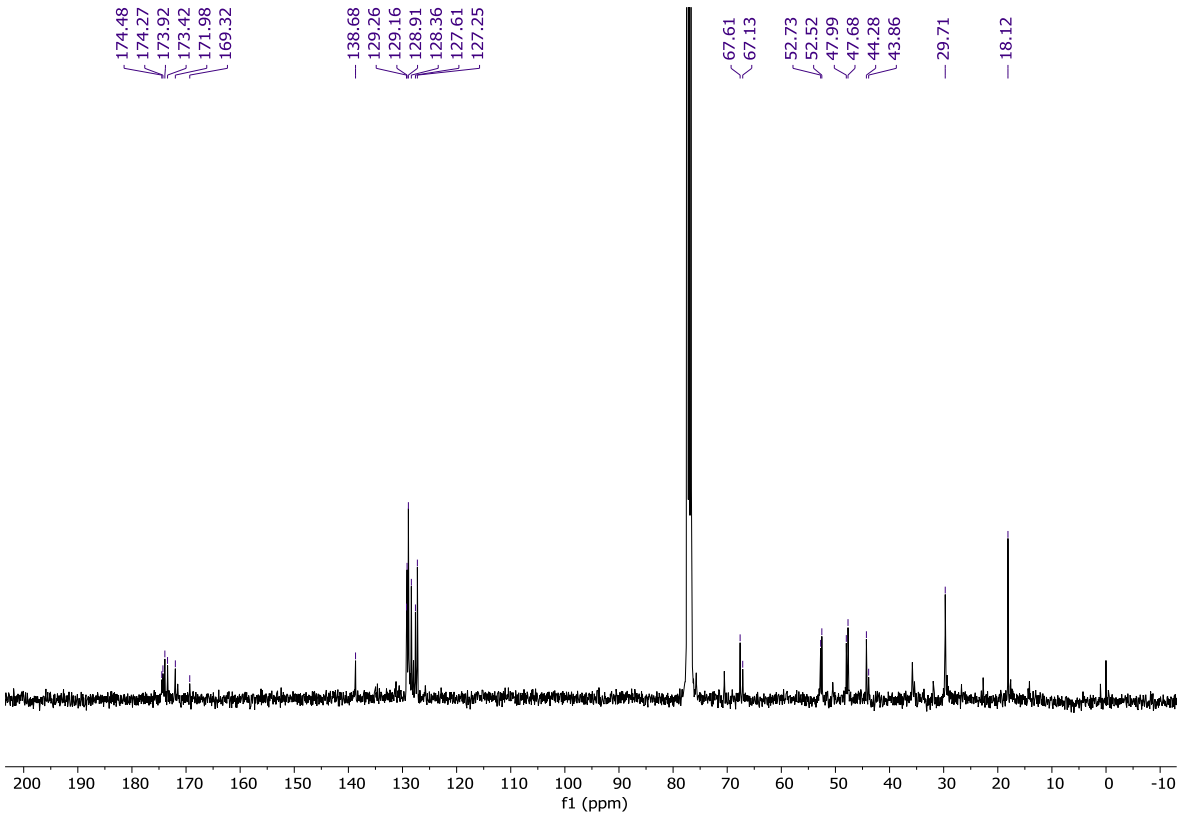

^{13}C NMR ($CDCl_3$, 126 MHz) of 54.

5. References

1 BROWN, D. G. & BOSTRÖM, J. “Analysis of past and present synthetic methodologies on medicinal chemistry: where have all the new reactions gone?”. J. Med. Chem. **59**: 4443, 2016.

2 ROUGHLEY, S. D. & JORDAN, A. M. “The medicinal chemist’s toolbox: an analysis of reactions used in the pursuit of drug candidates”. J. Med. Chem. **54**: 3451, 2011.

3 SEAVILL, P. W. & WILDEN, J. D. “The preparation and applications of amides using electrosynthesis”. Green Chem. **22** : 7737, 2020.

4 PATTABIRAMAN, V. R. & BODE, J. W. “Rethinking amide bond synthesis”. Nature. **480**: 471, 2011.

5 SERRANO, E. & MARTIN, R. “Forging amides through metal-catalyzed C–C coupling with isocyanates”. Eur. J. Org. Chem. **24**: 3051, 2018.

6 SCHÄFER, G.; MATTHEY, C. & BODE, J. W. “Facile synthesis of sterically hindered and electron-deficient secondary amides from isocyanates”. Angew. Chem. Int. Ed. **51**: 9173, 2012.

7 SERRANO, E. & MARTIN, R. “Nickel-catalyzed reductive amidation of unactivated alkyl bromides” Angew. Chem. Int. Ed. **55**: 11207, 2016.

8 ZHENG, S.; PRIMER, D. N. & MOLANDER, G. A. “Nickel/photoredox-catalyzed amidation via alkylsilicates and isocyanates”. ACS Catal. **7**: 7957, 2017.

9 FORNI, J. A.; MICIC, N.; CONNELL, T. U.; WERAGODA, G. & POLYZOS, A. “Tandem photoredox catalysis: enabling carbonylative amidation of aryl and alkylhalides”. Angew. Chem. **59**: 18646, 2020.

10 MIAO, Y.-Q.; KANG, J.-X.; MA, Y.-N. & CHEN, X. “Visible light-mediated synthesis of amides from carboxylic acids and amine-boranes”. Green Chem. **23**: 3595, 2021.

11 SRIVASTAVA, V.; SINGH. P. K. & SINGH, P. P. “Visible light photoredox catalysed amidation of carboxylic acids with amines”. Tetrahedron Lett. **60**: 40, 2019.

12 SONG, W.; DONG, K. & LI, M. “Visible light-induced amide bond formation”. Org. Lett. **22**: 371, 2020.

13 GASPA, S.; FARINA, A.; TILOCCA, M.; PORCHEDDU, A.; PISANO, L.; CARRARO, M.; AZZENA, U. & DE Luca, L. “Visible-light photoredox-catalyzed amidation of benzylic alcohols”. J. Org. Chem. **85**: 11679, 2020.

14 XIAO, Y.; CHUN, Y.-K.; CHENG, S.-C.; NG, C.-O.; TSE, M.-K.; LEI, N.-Y.; LIU, R. & KO, C.-C. “Photocatalytic amidation and esterification with perfluoroalkyl iodide”. Catal. Sci. Technol. **11**: 556, 2021.

15 CORREIA, V. G.; ABREU, J. C.; BARATA, C. A. E. & ANDRADE, L. H. “Iron-catalyzed synthesis of oxindoles: application to the preparation of pyrroloindolines”. Org. Lett. **19**: 1060, 2017.

16 SANABRIA, M. N.; HORNINK, M. M.; CORREIA, V. G. & ANDRADE, L. H. “Nontraditional application of the photo-fenton process: a novel strategy for molecular construction using formamide and flow chemistry”. Org. Process Res. Dev. **24**: 2288, 2020.

17 NASCIMENTO, V. R.; SUENAGA, M. L. S. & ANDRADE, L. H. “An efficient approach for the synthesis of new (±)-coixspirolactams”. Org. Biomol. Chem. **18**: 5458, 2020.

18 HORNINK, M. M.; LOPES, A. U. & ANDRADE, L . H. “Biobased spiroimides from itaconic acid and formamides: molecular targets for a novel synthetic application of renewable chemicals”. Synthesis. **53**: 296, 2021.

19 SACCHELLI, B. A. L.; ROCHA, B. C. & ANDRADE, L. H. “Cascade reactions assisted by microwave irradiation: ultrafast construction of 2-quinolinone-fused γ-lactones from *N*‑(o‑ethynylaryl)acrylamides and formamide”. Org. Lett. **23**: 5071, 2021.

20 PETERSEN, W. F.; TAYLOR, R. J. K. & DONALD, J. R. “Photoredox-catalyzed procedure for carbamoyl radical generation: 3,4-dihydroquinolin-2-one and quinolin-2-one synthesis”. Org. Biomol. Chem. **15**: 5831, 2017.

21 BAI, Q.; JIN, C.; HE, J. & FENG, G. “Carbamoyl radicals via photoredox decarboxylation of oxamic acids in aqueous media: access to 3,4-dihydroquinolin-2(1*H*)-ones”. Org. Lett. **20**: 2172, 2018.

22 PAWAR, G. G.; ROBERT, F.; GRAU, E.; CRAMAIL, H. & LANDAIS, Y. “Visible-light photocatalyzed oxidative decarboxylation of oxamic acids: a green route to urethanes and ureas”. Chem. Commun. **54**: 9337, 2018.

23 JATOI, A. H.; PAWAR, G. G.; ROBERT, F. & LANDAIS, Y. “Visible-light mediated carbamoyl radical addition to heteroarenes”. Chem. Commun. **55**: 466, 2019.

24 (a) WEI, X.; WANG, L.; JIA, W.; DU, S.; WU, L. & LIU, Q. “Metal-free-mediated oxidation aromatization of 1,4-dihydropyridines to pyridines using visible light and air”. Chin. J. Chem. **32** : 1245, 2014; (b) CHENG, J. P.; LU, Y.; ZHU, X. Q.; SUN, Y.; BI, F. & HE, J. “Heterolytic and homolytic N−H bond dissociation energies of 4-substituted hantzsch 2,6-dimethyl-1,4-dihydropyridines and the effect of one-electron transfer on the N−H bond activation”. J. Org. Chem. **65**: 3853, 2000.

25 (a) MILLIGAN, J. A.; PHELAN, J. P.; BADIR, S. O. & Molander, G. A. “Alkyl carbon–carbon bond formation by nickel/photoredox cross-coupling”. Angew. Chem. Int. Ed. **58**: 6152, 2019; (b) WANG, P.-Z.; CHEN, J.-R. & XIAO, W.-J. “Hantzsch esters: an emerging versatile class of reagents in photoredox catalyzed organic synthesis”. Org. Biomol. Chem. **17** : 6936, 2019; (c) HUANGA, W. & CHENG, X. “Hantzsch esters as multifunctional reagents in visible-light photoredox catalysis”. Synlett. **27**: A, 2016; (d) ZHENG, C. & YOU, S. -L. “Transfer hydrogenation with Hantzsch esters and related organic hydride donors”. Chem. Soc. Rev. **41**: 2498, 2012.

26 ALANDINI, N.; BUZZETTI, L.; FAVI, G.; SCHULTE, T.; CANDISH, L.; COLLINS, K. D. & MELCHIORRE, P. “Amide synthesis by nickel/photoredox-catalyzed direct carbamoylation of (hetero)aryl bromides”. Angew. Chem. Int. Ed. **59**: 5248, 2020.

27 CARDINALE, L.; KONEV, M. O. & VON WANGELIN, A. “Photoredox-catalyzed addition of carbamoyl radicals to olefins: a 1,4-dihydropyridine approach”. J. Chem. Eur. J. **26**: 8239, 2020.

28 KIM, I.; PARK, S. & HONG, S. “Functionalization of pyridinium derivatives with 1,4-dihydropyridines enabled by photoinduced charge transfer”. Org. Lett. **22**: 8730, 2020.

29 (a) BOTTECCHIA, C. & NOËL, T. “Photocatalytic modification of amino acids, peptides, and proteins”. Chem. - A Eur. J. **25**: 26, 2019; (b) LIU, J.-Q.; SHATSKIY, A.; MATSUURA, B. S. & KÄRKÄS, M. D. “Recent advances in photoredox catalysis enabled functionalization of *α*-amino acids and peptides: concepts, strategies and mechanisms”. Synthesis (Stuttg). **51**: 2759, 2019.

30 NÁJERA, C.; SANSANO, J. M. & YUS, M. “1,3-Dipolar cycloadditions of azomethine imines”. Org. Biomol. Chem. **13**: 8596, 2015.

31 SHANG, T.-Y.; LU, L.-H.; CAO, Z.; LIU, Y.; HE, W.-M. & YU, B. “Recent advances of 1,2,3,5-tetrakis(carbazol-9-yl)-4,6-dicyanobenzene (4CzIPN) in photocatalytic transformations”. Chem. Commun. **55**: 5408, 2019.

32 MATSUO, B. T.; CORREIA, J. T. M. & PAIXÃO, M. W. “Visible-light-mediated *α*-amino alkylation of azomethine imines: an approach to *N*-(*β*-aminoalkyl)pyrazolidinones”. Org. Lett. **20**: 7891, 2020.

33 (a) HAUN, G.; PANEQUE, A. N.; ALMOND, D. W.; AUSTIN, B. E. & MOURA-LETTS, G. Synthesis of chromenoisoxazolidines from substituted salicylic nitrones via visible-light photocatalysis”. Org. Lett. **21**: 1388, 2019; (b) JANG, G. S.; LEE, J.; SEO, J. & WOO, S. K. “Synthesis of 4-isoxazolines via visible-light photoredox-catalyzed [3 + 2] cycloaddition of oxaziridines with alkynes”. Org. Lett. **19**: 6448, 2017; (c) ZHENG, L.; GAO, F.; YANG, C.; GAO, G.-L.; ZHAO, Y.; GAO, Y. & XIA, W. “Visible-light-mediated anti-regioselective nitrone 1,3-dipolar cycloaddition reaction and synthesis of bisindolylmethanes”. Org. Lett. **19**: 5086, 2017.

34 YE, C.-X.; MELCAMU, Y. Y; LI, H.-H.; CHENG, J.-T.; ZHANG, T.-T.; RUAN, Y.-P.; ZHENG, X.; LU, X. & HUANG, P.-Q. “Dual catalysis for enantioselective convergent synthesis of enantiopure vicinal amino alcohols”. Nat. Commun. **9**: 1, 2018.

35 LIU, Y.-C.; ZHENG, X. & HUANG, P.-Q. “Photoredox catalysis for the coupling reaction of nitrones with aromatic tertiary amines”. Acta Chim. Sinica. **77**: 850, 2019.

36 SUPRANOVICH, V. I.; LEVIN, V. V.; STRUCHKOVA, M. I. & DILMAN, A. D. “Photocatalytic reductive fluoroalkylation of nitrones”. Org. Lett. **20**: 840, 2018.

37 TANG, F.; GUAN, Z. & HE, Y.-H. “Free regioselective carbonylation of imidazo[1,2-*a*]pyridines via photoredox catalysis using nitrones”. Asian J. Org. Chem. **8**: 867, 2019.

38 LI, H.-H.; LI, J.-Q.; ZHENG, X. & HUANG, P.-Q. ‘Photoredox-catalyzed decarboxylative cross-coupling of *α*-amino acids with nitrones”. Org. Lett. **23**: 876, 2021.

39 (a) DEROSA, T. F. Significant Pharmaceuticals Reported in US Patents, Vol. 1; Elsevier Science, 2007; (b) MIRET-CASALS, L.; BAELO, A.; JULIÁN, E.; ASTOLA, J.; LOBO-RUIZ, A.; ALBERICIO, F. & TORRENTS, E. “Hydroxylamine derivatives as a new paradigm in the search of antibacterial agents”. ACS Omega. **12**: 17057, 2018.

40 BUZZETTI, L.; PRIETO, A.; ROY, S. R. & MELCHIORRE, P. “Radical-based C-C bond-forming processes enabled by the photoexcitation of 4-alkyl-1,4-dihydropyridines”. Angew. Chem. Int. Ed. **56**: 15039, 2017.

41 UOYAMA, H.; GOUSHI, K.; SHIZU, K.; NOMURA, H. & ADACHI, C. “Highly efficient organic light-emitting diodes from delayed fluorescence”. Nature. **492**: 234, 2012.

42 LAKOWICZ, J. R. Quenching of Fluorescence. In: Principles of Fluorescence Spectroscopy. Springer, Boston, MA, 1983. p. 277.

43 LUO, J. & ZHANG, J. "Donor–acceptor fluorophores for visible-light-promoted organic synthesis: photoredox/Ni dual catalytic $C(sp^3)$–$C(sp^2)$ cross-coupling". ACS Catal. **6**: 873, 2016.

44 WINTERTON, S. E. & READY, J. M. "[3 + 2]-Cycloadditions of azomethine imines and ynolates". Org. Lett. **18**: 2608, 2016.

45 DU, Q.; NEUDÖRFL, J.-M. & SCHMALZ, H.-G. "Chiral phosphine–phosphite ligands in asymmetric gold catalysis: highly enantioselective synthesis of furo[3,4-*d*]-tetrahydropyridazine derivatives through [3+3]-cycloaddition". Chem. Eur. J. **24**: 2379, 2018.

46 LI, C.; WANG, C. -S.; LI, T.-Z.; MEI, G.-J. & SHI, F. "Brønsted acid-catalyzed (4 + 3) cyclization of *N*,*N*′-cyclic azomethine imines with isatoic anhydrides". Org. Lett. **21**: 598, 2019.

47 SHINTANI, R. & FU, G. C. "A New copper-catalyzed [3 + 2] cycloaddition: enantioselective coupling of terminal alkynes with azomethine imines to generate five-membered nitrogen heterocycles". J. Am. Chem. Soc. **125**: 10778, 2003.

48 SHINTANI, R. & HAYASHI, T. "Palladium-catalyzed [3 + 3] cycloaddition of trimethylenemethane with azomethine imines". J. Am. Chem. Soc. **128**: 6330, 2006.

49 PAGOTI, S.; DUTTA, D. & DASH, J. "A magnetoclick imidazolidinone nanocatalyst for asymmetric 1,3-dipolar cycloadditions". Adv. Synth. Catal. **355**: 3532, 2013.

50 ANDRADE, M. M.; BARROS, M. T. & PINTO, R. C. "Exploiting microwave-assisted neat procedures: synthesis of *N*-aryl and *N*-alkylnitrones and their cycloaddition en route for isoxazolidines". Tetrahedron. **64**: 10521, 2008.

51 DUBUR, G. Y. & ULDRIKIS, Y. R. "Preparation of 3,5-diethoxycarbonyl-2,6-dimethyl-1,4-dihydro-isonicotinic acid and 3,5-diacetyl-2,6-dimethyl-1,4-dihydroisoni-cotinic acid and their salts". Chem. Heterocycl. Compd. **5**: 762, 1972.